JOURNEY TO THE CENTER OF THE BRAIN: CELL PHYSIOLOGY AND INTERCELLULAR COMMUNICATION IN WHITE MATTER

EDITED BY: Maria Kukley and Nicola B. Hamilton-Whitaker
PUBLISHED IN: Frontiers in Cellular Neuroscience

frontiers Research Topics

ISSN 1664-8714
ISBN 978-2-88974-852-5
DOI 10.3389/978-2-88974-852-5

About Frontiers

Frontiers is more than just an open-access publisher of scholarly articles: it is a pioneering approach to the world of academia, radically improving the way scholarly research is managed. The grand vision of Frontiers is a world where all people have an equal opportunity to seek, share and generate knowledge. Frontiers provides immediate and permanent online open access to all its publications, but this alone is not enough to realize our grand goals.

Frontiers Journal Series

The Frontiers Journal Series is a multi-tier and interdisciplinary set of open-access, online journals, promising a paradigm shift from the current review, selection and dissemination processes in academic publishing. All Frontiers journals are driven by researchers for researchers; therefore, they constitute a service to the scholarly community. At the same time, the Frontiers Journal Series operates on a revolutionary invention, the tiered publishing system, initially addressing specific communities of scholars, and gradually climbing up to broader public understanding, thus serving the interests of the lay society, too.

Dedication to Quality

Each Frontiers article is a landmark of the highest quality, thanks to genuinely collaborative interactions between authors and review editors, who include some of the world's best academicians. Research must be certified by peers before entering a stream of knowledge that may eventually reach the public - and shape society; therefore, Frontiers only applies the most rigorous and unbiased reviews.
Frontiers revolutionizes research publishing by freely delivering the most outstanding research, evaluated with no bias from both the academic and social point of view. By applying the most advanced information technologies, Frontiers is catapulting scholarly publishing into a new generation.

What are Frontiers Research Topics?

Frontiers Research Topics are very popular trademarks of the Frontiers Journals Series: they are collections of at least ten articles, all centered on a particular subject. With their unique mix of varied contributions from Original Research to Review Articles, Frontiers Research Topics unify the most influential researchers, the latest key findings and historical advances in a hot research area! Find out more on how to host your own Frontiers Research Topic or contribute to one as an author by contacting the Frontiers Editorial Office: frontiersin.org/about/contact

JOURNEY TO THE CENTER OF THE BRAIN: CELL PHYSIOLOGY AND INTERCELLULAR COMMUNICATION IN WHITE MATTER

Topic Editors:
Maria Kukley, Achucarro Basque Center for Neuroscience, Spain
Nicola B. Hamilton-Whitaker, King's College London, United Kingdom

Citation: Kukley, M., Hamilton-Whitaker, N. B., eds. (2022). Journey to the Center of the Brain: Cell Physiology and Intercellular Communication In White Matter. Lausanne: Frontiers Media SA. doi: 10.3389/978-2-88974-852-5

Table of Contents

frontiers in Cellular Neuroscience

EDITORIAL
published: 14 March 2022
doi: 10.3389/fncel.2022.864368

Editorial: Journey to the Center of the Brain: Cell Physiology and Intercellular Communication in White Matter

Grace Flower[1], *Nicola B. Hamilton*[1*†] *and Maria Kukley*[2,3*†]

[1] Wolfson Centre for Age-Related Diseases, Institute of Psychiatry, Psychology and Neuroscience, King's College London Guy's Campus, London, United Kingdom, [2] Laboratory of Neuronal and Glial Physiology, Achucarro Basque Center for Neuroscience, Leioa, Spain, [3] IKERBASQUE Basque Foundation for Science, Bilbao, Spain

Keywords: central nervous system (CNS), white matter, methods, diseases, omics, myelin, ion channels, neuron-glia interaction

Editorial on the Research Topic

Journey to the Center of the Brain: Cell Physiology and Intercellular Communication in White Matter

OPEN ACCESS

Edited and reviewed by:
Marie-Ève Tremblay,
University of Victoria, Canada

***Correspondence:**
Nicola B. Hamilton
nicola.hamilton-whitaker@kcl.ac.uk
Maria Kukley
maria.kukley@achucarro.org

†These authors have contributed equally to this work and share last authorship

Specialty section:
This article was submitted to Non-Neuronal Cells, a section of the journal Frontiers in Cellular Neuroscience

Received: *28 January 2022*
Accepted: *07 February 2022*
Published: *14 March 2022*

Citation:
Flower G, Hamilton NB and Kukley M (2022) Editorial: Journey to the Center of the Brain: Cell Physiology and Intercellular Communication in White Matter. Front. Cell. Neurosci. 16:864368. doi: 10.3389/fncel.2022.864368

White matter (WM) consists of myelinated axons, which propagate neuronal information over long distances to allow for connectivity between different brain areas. Previously thought to simply assist neuronal transmission, WM structure and function has recently been shown to play a larger role in normal physiology and pathology. These discoveries are the result of the emergence of new, state-of-the-art, imaging, electrophysiological, and omics technologies, allowing us to research WM in humans and animal models (**Figure 1**). For instance, the use of MRI has revealed changes in WM structure during learning (Sampaio-Baptista and Johansen-Berg, 2017) while single-cell electrophysiology helped discover synaptic signaling between axons and oligodendroglial cells in the WM (Kukley et al., 2007; Ziskin et al., 2007), both findings support the idea that cells within the WM respond to neuronal function. Omic approaches that analyze the gene expression profile of WM cells in great detail have revealed heterogeneity within cellular populations and suggested a link between myelination-related genes and decreased WM integrity in psychiatric disorders (Chavarria-Siles et al., 2016; Jakel et al., 2019; Safaiyan et al., 2021; Amor et al., 2022).

The Research Topic "Journey to the Center of the Brain: Cell Physiology and Intercellular Communication In White Matter" encompasses literature reviews and research articles describing recent achievements in WM research at the single-cell level, emphasizing the need for further studies of physiology and the structure of WM cells.

Through an in-depth review, Jakel and Williams present current data from single-cell technologies and indicate which of these approaches will best answer the remaining questions in human WM pathologies. This review hints at an exciting future where we will gain a deeper understanding of disease and create diagnostic and therapeutic tools. To utilize the powerful applications of single-cell technologies, Jahn et al. revisited the myelin proteome of mice, using mass spectrometry to quantitatively measure the most abundant myelin proteins (PLP, MBP, CNP, and MOG) and determine the complexity of the less abundant myelin proteins. Interestingly, they identified that the myelin proteome displays minor changes if assessed 6 h post-mortem. From this, they formed a resourceful dataset for anyone studying CNS myelin, be that in mouse models of demyelination or clinical WM disorders. Taking the myelin and axonal proteome to a structural and mechanical level Shimizu et al. used a unique tension sensor based on fluorescence resonance

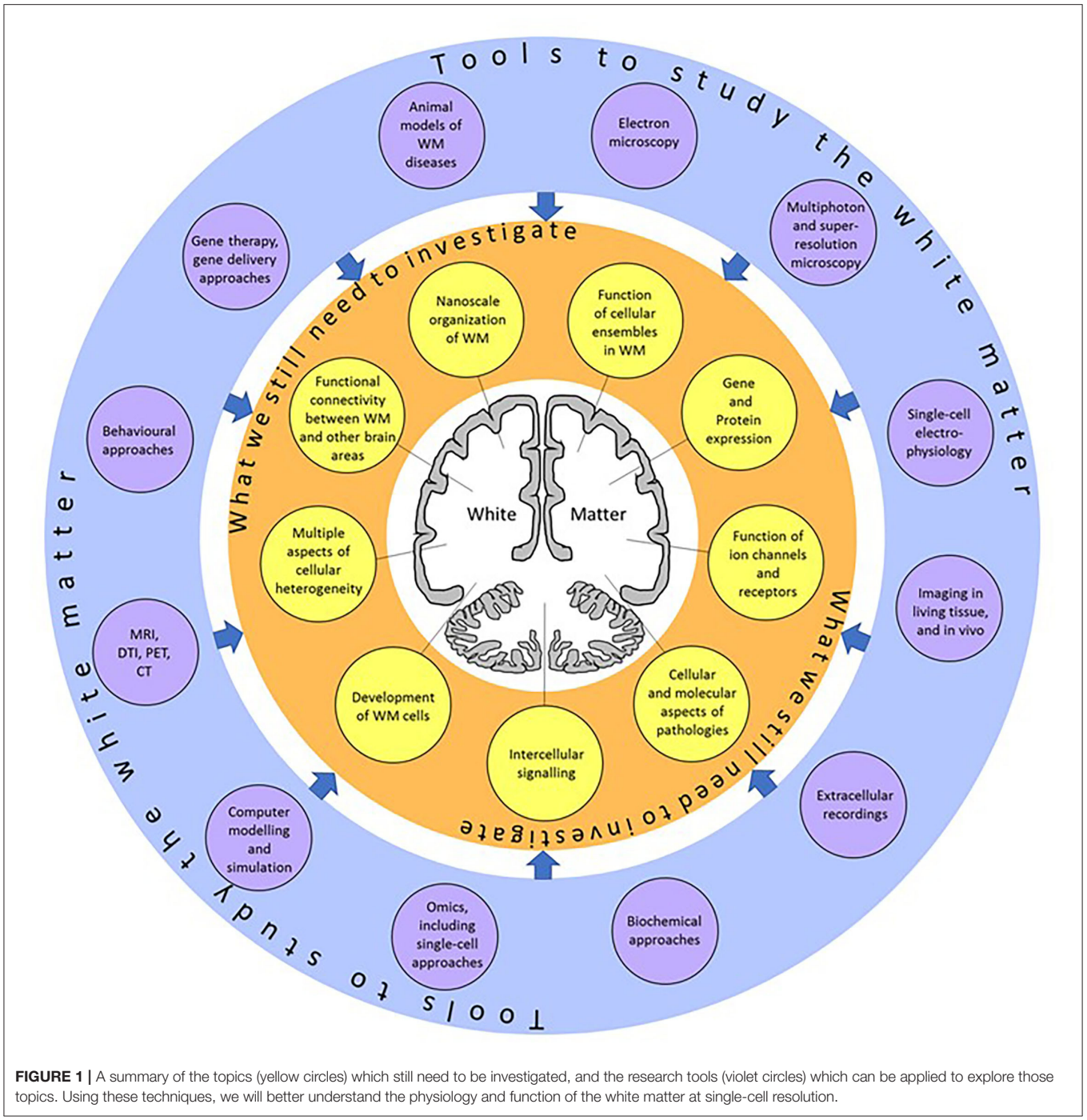

FIGURE 1 | A summary of the topics (yellow circles) which still need to be investigated, and the research tools (violet circles) which can be applied to explore those topics. Using these techniques, we will better understand the physiology and function of the white matter at single-cell resolution.

energy transfer to investigate the physical factors involved in myelin formation in response to axon diameter. The authors observed higher tension at oligodendrocyte processes that contact larger diameter axons and longer oligodendroglial focal adhesions on these axons. These data suggest that oligodendrocytes physically respond to axon diameter by changing their cytoskeletal organization and myelin formation. This is an extremely valuable finding in understanding WM physiology.

Through a comprehensive review of published bulk and single-nuclei RNA-sequencing datasets, Boscia et al. presented the expression levels of ion channels in multiple sclerosis (MS). The authors show there is an upregulation of voltage-gated Na^+ channel genes and downregulation of voltage-gated Cl^- channels in WM lesions. This supports the imbalance of Na^+ homeostasis and the increased excitability observed in progressive MS. On the other hand, there is an upregulation of voltage-gated K^+ channel genes that could be a protective

function in response to the altered Na^+/Cl^- homeostasis. To complement these findings, Serrano-Regal et al. reviewed the role of GABAergic signaling in myelinating cells and its potential for developing therapies in demyelinating disease. They detailed the expression levels of GABA receptors in the myelinating cells with support of functional data demonstrating the involvement of GABAergic signaling in precursor cell development and maturation of myelinating cells. This review supports further study into targeting GABAergic signaling in WM pathology.

Maas and Angulo reviewed the potential therapeutic approach of enhancing neuronal activity to improve remyelination in MS. The authors discussed pre-clinical and clinical evidence that supports the notion that neuronal stimulation induces myelination and behavioral changes. Clinically, non-invasive brain stimulation has been shown to reduce or ameliorate MS symptoms. Maas and Angulo support this attractive therapeutic approach by further discussing the neurobiological basis of enhancing neuronal activity at the single-cell level.

From functional to structural, Dutta and Fields present interesting findings on the myelin membrane protein complex, NF155, which attaches the myelin to the axon in the paranodal region. Using Crispr-Cas9 gene editing, they identified a thrombin binding site of the NF155 complex that is implicated in the plasticity of the myelin sheath. When this site is deleted, there is disruption to myelination, nodal and paranodal organization. Mice with this deletion present tremor and ataxia, demonstrating the importance of this domain for the stability of the protein complex and therefore myelin-axonal integrity. On the note of myelin plasticity, Liu et al. reviewed and developed a model for myelin plasticity in the neural circuits underlying threat and safety learning. These stimuli are a major cause for the emergence of anxiety-related disorders and understanding the circuitry dynamics underlying the response to these stimuli will better inform us on the development of these psychiatric disorders. This review suggests further study is needed to understand myelin plasticity in psychiatric disorders.

Lastly, Cocola et al. share interesting findings on vasculature function in glioblastoma. After recently identifying the transmembrane protein, TMEM230, as a regulator of development associated with angiogenesis in the zebrafish (Carra et al., 2018), the authors further explored its role in the pathogenesis of glioblastomas. They found TMEM230 was necessary for cell growth in a cellular model of human glioblastoma and observed high TMEM230 levels in low-grade gliomas in the patients. These findings suggest that downregulation of TMEM230 expression may inhibit low-grade glioma and glioblastoma tumor progression while supporting the normal formation of blood vessels. As TMEM mRNA is expressed in the WM (according to The Human Protein Atlas) and TMEM230 is necessary for the formation of WM during early development. Future research on the role of TMEM230 in the WM will be of specific interest.

In conclusion, the future looks bright for research into understanding WM structure and function. There is a clear need for further studies of the WM at single-cell resolution in both animal models and human patients but the technologies are becoming more accessible and fast-evolving to enable this research to take place (**Figure 1**). It is becoming more obvious that the WM is more than just passive tissue. The functional properties of the cells forming the WM can influence brain function and may provide therapeutic targets for WM pathologies.

AUTHOR CONTRIBUTIONS

GF, NH, and MK contributed to this editorial by summarizing the findings and content of all scientific manuscripts included in the Research Topic. GF prepared the original draft of the manuscript, MK prepared the figure. All authors approved the submitted version of the manuscript.

FUNDING

Funding of NH and GF was from the European Leukodystrophies Association International (ELA2017-015I4), the Medical Research Council (MR/S003045/1 and MR/V000470/1), and King's College London. GF is supported by the UK Medical Research Council MR/N013700/1 and King's College London member of the MRC Doctoral Training Partnership in Biomedical Sciences. The work of MK was supported by the Ikerbasque (Basque Foundation for Science), the Spanish Ministry of Science and Innovation (grant PID2019-110195RB-I00), and the Basque Government PIBA Project (PIBA 2020_1_0030).

REFERENCES

Amor, S., McNamara, N. B., Gerrits, E., Marzin, M. C., Kooistra, S. M., Miron, V. E., et al. (2022). White matter microglia heterogeneity in the CNS. *Acta Neuropathol.* 143, 125–141. doi: 10.1007/s00401-021-02389-x

Carra, S., Sangiorgio, L., Pelucchi, P., Cermenati, S., Mezzelani, A., Martino, V., et al. (2018). Zebrafish Tmem230a cooperates with the Delta/Notch signaling pathway to modulate endothelial cell number in angiogenic vessels. *J. Cell Physiol.* 233, 1455–1467. doi: 10.1002/jcp.26032

Chavarria-Siles, I., White, T., de Leeuw, C., Goudriaan, A., Lips, E., Ehrlich, S., et al. (2016). Myelination-related genes are associated with decreased white matter integrity in schizophrenia. *Eur. J. Hum. Genet.*. 24, 381–386. doi: 10.1038/ejhg.2015.120

Jakel, S., Agirre, E., Mendanha Falcao, A., van Bruggen, D., Lee, K. W., Knuesel, I., et al. (2019). Altered human oligodendrocyte heterogeneity in multiple sclerosis. *Nature* 566, 543–547. doi: 10.1038/s41586-019-0903-2

Kukley, M., Capetillo-Zarate, E., and Dietrich, D. (2007). Vesicular glutamate release from axons in white matter. *Nat. Neurosci.* 10, 311–320. doi: 10.1038/nn1850

Safaiyan, S., Besson-Girard, S., Kaya, T., Cantuti-Castelvetri, L., Liu, L., Ji, H., et al. (2021). White matter aging drives microglial diversity. *Neuron* 109, 1100–1117.e1110. doi: 10.1016/j.neuron.2021.01.027

Sampaio-Baptista, C., and Johansen-Berg, H. (2017). White matter plasticity in the adult brain. *Neuron* 96, 1239–1251. doi: 10.1016/j.neuron.2017.11.026

Ziskin, J. L., Nishiyama, A., Rubio, M., Fukaya, M., and Bergles, D. E. (2007). Vesicular release of glutamate from unmyelinated axons in white matter. *Nat. Neurosci.* 10, 321–330. doi: 10.1038/nn1854

Conflict of Interest: The authors declare that the research was conducted in the absence of any commercial or financial relationships that could be construed as a potential conflict of interest.

Publisher's Note: All claims expressed in this article are solely those of the authors and do not necessarily represent those of their affiliated organizations, or those of the publisher, the editors and the reviewers. Any product that may be evaluated in this article, or claim that may be made by its manufacturer, is not guaranteed or endorsed by the publisher.

frontiers in Cellular Neuroscience

REVIEW
published: 04 August 2020
doi: 10.3389/fncel.2020.00238

What Have Advances in Transcriptomic Technologies Taught us About Human White Matter Pathologies?

Sarah Jäkel and Anna Williams*

Centre for Regenerative Medicine, Institute for Regeneration and Repair, University of Edinburgh, Edinburgh, United Kingdom

For a long time, post-mortem analysis of human brain pathologies has been purely descriptive, limiting insight into the pathological mechanisms. However, starting in the early 2000s, next-generation sequencing (NGS) and the routine application of bulk RNA-sequencing and microarray technologies have revolutionized the usefulness of post-mortem human brain tissue. This has allowed many studies to provide novel mechanistic insights into certain brain pathologies, albeit at a still unsatisfying resolution, with masking of lowly expressed genes and regulatory elements in different cell types. The recent rapid evolution of single-cell technologies has now allowed researchers to shed light on human pathologies at a previously unreached resolution revealing further insights into pathological mechanisms that will open the way for the development of new strategies for therapies. In this review article, we will give an overview of the incremental information that single-cell technologies have given us for human white matter (WM) pathologies, summarize which single-cell technologies are available, and speculate where these novel approaches may lead us for pathological assessment in the future.

Keywords: single-cell transcriptomics, single-nuclei transcriptomics, human neuropathology, white matter, multiple sclerosis, RNA-sequencing, "omics" approaches

OPEN ACCESS

Edited by:
Maria Kukley,
Achucarro Basque Center for Neuroscience, Spain

Reviewed by:
Sarah Moyon,
CUNY Advanced Science Research Center, United States
Michela Deleidi,
Deutsches Zentrum für Neurodegenerative Erkrankrugen (HZ), Germany
Parras M. Carlos,
Paris Brain Institute, France

****Correspondence:***
Sarah Jäkel
sarah.jaekel@ed.ac.uk

Specialty section:
This article was submitted to Non-Neuronal Cells, a section of the journal Frontiers in Cellular Neuroscience

Received: *24 May 2020*
Accepted: *07 July 2020*
Published: *04 August 2020*

Citation:
Jäkel S and Williams A (2020) What Have Advances in Transcriptomic Technologies Taught us About Human White Matter Pathologies? Front. Cell. Neurosci. 14:238. doi: 10.3389/fncel.2020.00238

INTRODUCTION

Classical Approaches to Study Human White Matter Pathology

Modern neuropathology has its origins in the late 19th and early 20th century when famous neurologists or psychologists such as Santiago Ramon y Cajal, Jean-Martin Charcot, and Alois Alzheimer started to describe and illustrate the central nervous system (CNS) and its pathological changes. These early, but still accurate and detailed illustrations of the brain and individual cells, were all based on histological stains observed through a simple light microscope. It took many years before pathology could reach another level of detail with the common use of antibodies to develop marker-specific immunological stains that are still state-of-the-art in modern research laboratories. Due to the combination with fluorescent labels and the development of better microscopes, this method has become a standard technique to study human pathology and it has helped us to gain a deep understanding of cellular and sub-cellular structures of the brain in health and disease.

Multiple Sclerosis (MS), a chronic inflammatory and demyelinating neurodegenerative disease of the CNS, is a good example of how this descriptive pathology is still used, but it equally applies to other pathologies. The characteristic lesions in white matter (WM) tracts can be classified into active, chronic active, chronic inactive, and remyelinated lesions—so-called shadow plaques (Lassmann et al., 1998). This still highly used classification system is based on the presence of demyelination and the distribution of infiltrating immune cells in and around the lesions and is carried out with simple histological staining on post-mortem human tissue. So far, there are only limited ways of detecting the different lesion stages during the lifetime of a patient using non-invasive imaging techniques (Brück et al., 1997; Hemond and Bakshi, 2018). Specific magnetic resonance imaging sequences enable the detection of chronic active lesions where acute inflammation is happening at the lesion rim (Absinta et al., 2018) and these are associated with disability and ongoing tissue damage (Absinta et al., 2019) aiding prognosis. These new imaging paradigms are exciting but we are still far from a full picture of MS lesions either by pathology or live imaging. Moreover, we still have limited knowledge about molecular or mechanistic changes in MS lesions which are key to understanding the disease.

With the development of new technologies in the 2000s, many labs started to use bulk RNA-sequencing (RNA-seq) or DNA-based microarrays to describe cellular and molecular changes in disease at the transcript level, to gain a deeper insight into functional pathological changes. This was the beginning of a revolution in pathology, helping define molecular markers of disease and raising new hypotheses for disease pathogenesis, to be tested experimentally. This revolution continues with new methods to identify transcripts from single cells or nuclei and to identify these transcripts spatially on the tissue. Here, we describe this revolution, and how this is evolving and will impact our understanding of human WM pathology. Although these techniques apply to a wide range of human WM CNS pathologies, this review will mostly use MS as an exemplar and only touch on other diseases where relevant.

MODERN APPROACHES TO STUDY WM PATHOLOGIES

What Have We Learned From Whole Transcriptomic Approaches?

Bulk RNA-seq is a method to detect the entirety of the transcriptome within a sample of interest, which can either be a whole piece of tissue or sorted cells from a tissue. This can be done in an unbiased way where RNA is isolated, fragments transcribed into cDNA, which is further linked with specific adapters making them compatible with next-generation sequencing (NGS), which is then bioinformatically analyzed (**Figure 1A**). Alternatively, in a more biased way, isolated RNA is loaded onto specific microarray chips containing probes for only predefined gene transcripts. Commercial microarrays contain a large number of probes for the most important gene transcripts spread over the whole genome so that it can still be relatively unbiased. However, early experiments also included home-made arrays with lower numbers of genes.

The hallmark of WM MS pathology is the clearly distinguishable focal demyelinated lesions where myelin is lost. Therefore, due to its ease of detection and separation from the surrounding normal-appearing white matter (NAWM), many groups have performed bulk transcriptome studies on MS tissue comparing these. Besides, probably in part due to its easier accessibility at least in life, many have been performed on body fluids such as blood or cerebrospinal fluid (CSF) but some also used whole-brain or spinal cord tissue samples. Several review articles have already summarized these comparisons and discussed the technical challenges (Comabella and Martin, 2007; Kinter et al., 2008; Dutta and Trapp, 2012). In summary (**Figure 4**), the major findings are that all analyzed tissue sources express high numbers of inflammatory gene transcripts, although the inflammatory pathways differ. Also, it became clear that NAWM is not equal to control WM, suggesting that MS is a more global disease than previously thought. Many other findings of transcript differences across these studies were unique to a specific gene transcript in one study rather than having common ground between studies, providing interesting candidates to be investigated. Most surprisingly and against the common concept in MS that oligodendrocytes are the primary target of the attack, it has been suggested that surviving oligodendrocytes around demyelinating lesions in the NAWM are induced by hypoxia to be neuroprotective and anti-inflammatory and are thus more actively involved in disease and perhaps limiting it (Graumann et al., 2003; Zeis et al., 2008). Very recently, heparan sulfate production by mature oligodendrocytes around demyelinating lesions is one of the mechanisms in limiting demyelinating lesions (Macchi et al., 2020). Lindberg et al. (2004) came to similar conclusions regarding the NAWM and additionally pointed out that the immune response activation is different in the different compartments with a more cellular response in NAWM and a humoral response in lesions. Looking a bit closer into differences between demyelinated lesions, Tajouri et al. (2003) found that although both acute and chronic lesions share the majority of markers that are changed in MS in comparison to control, the fold change of those gene transcripts is however quite different. More recent publications have used bulk RNA-seq on MS tissue in a more complex way to explore either transcriptomic changes of microglia in the initial phase of MS (van der Poel et al., 2019) or transcriptomic changes in a hormonal context of the hypothalamus-pituitary-adrenaline (HPA)-axis (Melief et al., 2019). The first study reported an increase in transcripts related to lipid metabolism in microglia sorted from NAWM that is similar to those found in active demyelinated lesions, however, whilst maintaining their homeostatic functions. The latter study found that gene expression networks in MS tissue correlate with the activity of the HPA axis and/or disease severity, showing that gene expression in a pathological context is not only regulated by the pathology itself but also depends on other environmental factors. Thus, careful consideration of the experimental design and the case selection must be part of planning such an experiment.

Bulk transcriptomic approaches have brought several advantages to the field, but as ever with evolving technology, also some challenges. In contrast to immunohistochemistry (IHC) or quantitative PCR (qPCR) studies of candidate genes, it is unbiased, or relatively unbiased (with microarrays) allowing detection of new mechanisms rather than only digging deeper into already known ones. It is also not dependent on good primers/antibodies or experimenter choice. Long interfering non-coding RNAs are a good example of this, as most of their roles are relatively understudied and one specific RNA was found to play an important region-specific role in a study on Multiple System Atrophy (MSA), another human WM neuropathology, suggesting regional differences of this RNA to control brain function (Mills et al., 2015). Another advantage, at least in theory, is that studies that are performed by different groups in different tissues should be easy to compare, as all capture RNA in an unbiased way. However, disadvantages are plentiful, limiting comparisons as early studies (at least) used low numbers of individuals as input and findings might thus not be representative for a larger MS cohort. Comparisons chosen have varied and have included: (1) Lesions vs. NAWM (Whitney et al., 1999, 2001; Tajouri et al., 2003); (2) Lesions/NAWM vs. Controls (Graumann et al., 2003; Lindberg et al., 2004; Zeis et al., 2008, 2018); and (3) different lesions and/or different regions of lesions (Lock et al., 2002; Mycko et al., 2003; Hendrickx et al., 2017). Furthermore, MS lesions can occur in all WM regions and transcriptional profiling may be different when the lesions from the different studies come from different regions, for example from cerebellar WM and frontal subcortical WM. Many of these studies used non-standardized RNA isolation methods, different types of microarrays (commercial and homemade) with different probe sets (quantity and type), and also different sensitivities for lowly abundant genes, which may explain why different studies found so many different results. Highly abundant genes may mask more subtle effects, and in MS, this often leads to the discovery that MS lesions are associated with demyelination and inflammation (Kinter et al., 2008)—not quite a surprise for the inflammatory demyelinating disease.

A further disadvantage is that bulk transcriptomic studies detect gene expression irrespective of their cellular source within the tissue, so that a signal may be lost if one gene transcript is significantly upregulated in one cell type, but downregulated in another. This becomes especially important when studying a tissue with little cellular heterogeneity, as bulk approaches are generally able to detect a shift in cell-type proportions (e.g., more inflammatory cells in MS lesions), but are less good in detecting changes within similar cells sharing the majority of transcripts.

How Can Complementary Bulk Approaches Help Address WM Pathologies?

Other technologies, such as proteomics and metabolomics may also illuminate human pathologies (**Figures 1B,C**). They are either suitable to help validate hypotheses generated by transcriptomics or to generate new hypotheses themselves. Proteomic approaches using different methods of mass spectrometry have been widely used (as summarized in Farias et al., 2014; Farias and Santos, 2015). Numerous studies have been performed on human blood and CSF samples, which are easier to obtain, and may allow the development of new disease biomarkers in living patients (Del Boccio et al., 2016) as well as elucidating potential mechanisms of pathogenesis. The scarcity of reliable blood or CSF biomarkers for MS has been quite sobering to date, which might also be due to the technical challenges of highly abundant proteins (e.g., albumin) in the samples that mask smaller changes. Few proteomic studies so far have been performed on human brain tissue itself (Han et al., 2008; Broadwater et al., 2011; Ly et al., 2011), perhaps as a full proteomic overview of isolated brain tissue is technically challenging. This is due to the high abundance of proteins that cannot be captured by current technologies, mainly because of their dynamic range and the complexity, a reason why further subsampling of the tissue of interest might be helpful (Werner and Jahn, 2010). One study focussed on mitochondria in gray matter (GM), which suggested dysfunction in the mitochondrial respiratory chain in MS (Broadwater et al., 2011). In line with the findings of bulk transcriptomics data, proteins involved in inflammation and demyelination were upregulated in MS, but to find new disease mechanisms that can be targeted for therapies, more specific and sensitive techniques are needed. However, proteomics has been elaborately applied in mouse models of MS and the results from these studies may be worth trying to validate in humans.

Metabolomics is a relatively newly termed "omics" approach to systemically study metabolites in a sample, and the first metabolomics studies in MS were performed in the 1990s (Lynch et al., 1993). This is useful as metabolites are usually the end product of a biological process allowing us to conclude function. Despite the novelty of this approach, it has already found wide usage in MS and in its animal models, to try to identify biomarkers in body fluids like CSF, blood, and urine. With this, it might also be possible to observe metabolites in different patients and respond to their individual needs by different drugs, which would be the first step to personalized precision medicine (Bhargava and Calabresi, 2016; Del Boccio et al., 2016).

Techniques to study brain WM in bulk have greatly shaped understanding of WM diseases, but we now have the technology to examine pathological changes at a single cell level, gaining even deeper and new insights into these diseases.

How Do Single-Cell Transcriptomic Techniques Work?

Single-cell RNA sequencing (scRNA-seq) is a novel technology using the same principle of capturing and sequencing mRNAs in bulk approaches within a tissue, however with the improvement that individual mRNAs can be associated with each cell of origin. This is particularly important for brain pathologies, where not all cell types are equally affected, for example in MS, where oligodendroglia are primarily lost. Although scRNA-seq is a relatively young technology—the first article was published in 2009 (Tang et al., 2009)—many different commercial techniques are already on the market and new ones are emerging at a rapid speed (Svensson et al., 2018; Chen et al., 2019), possibly

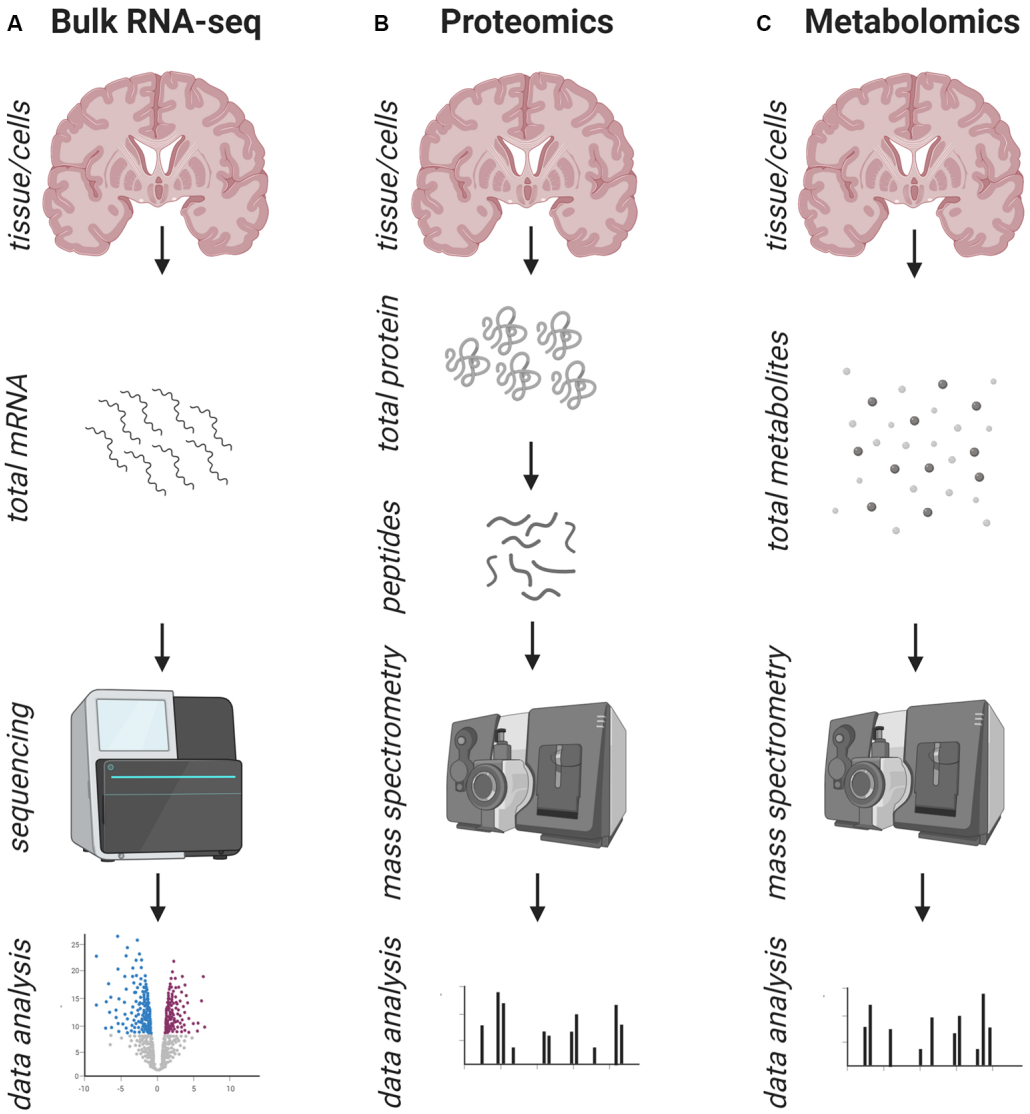

FIGURE 1 | Schematic overview of the workflow of common bulk approaches to address human pathology. **(A)** Standard workflow of bulk RNA-sequencing: the entirety of mRNA/RNA is isolated from a tissue/cell type of interest and prepared for next-generation sequencing (NGS), which is followed by bioinformatics data analysis. **(B)** Standard workflow of bulk proteomics: the entirety of proteins is isolated from a tissue/cell type of interest and prepared for mass spectrometry, which is followed by bioinformatics data analysis. **(C)** Standard workflow of bulk metabolomics: the entirety of metabolites is isolated from a tissue/cell type of interest and prepared for mass spectrometry, which is followed by bioinformatics data analysis. In all approaches **(A–C)** the information about the cell of origin and the spatial distribution is lost.

faster than the publication of this review. Whilst all of them aim to give a snapshot of the transcriptome of individual cells, they are quite different in the technology achieving this. All of them have their advantages and disadvantages depending on the specific scientific question to be answered, so choosing the right technique is an important step in the experimental design. For this, we should consider the number of cells available, the capture efficiency, transcriptome coverage, and cost per cell. Several reviews have summarized and compared single-cell RNA-seq technologies (Haque et al., 2017; Picelli, 2017; Svensson et al., 2018; Chen et al., 2019). Despite the high number of technologies, from an experimental point of view, there are two approaches: studying a high number of cells at a lower resolution (up to tens of thousands of cells) or studying a low number of cells (generally <1,000 cells) at a higher resolution.

The first approach generally uses droplet-based technologies (Macosko et al., 2015; Zheng et al., 2017), whilst the second approach mainly uses well- or device-based technologies (**Figures 2A,B**) to capture single cells (Picelli et al., 2014; Hagemann-Jensen et al., 2020). Droplet-based methods use unique molecular identifiers (UMIs) and/or barcodes to label individual cells and mRNAs during the initial steps, so that the library preparation can be performed in bulk, rather than

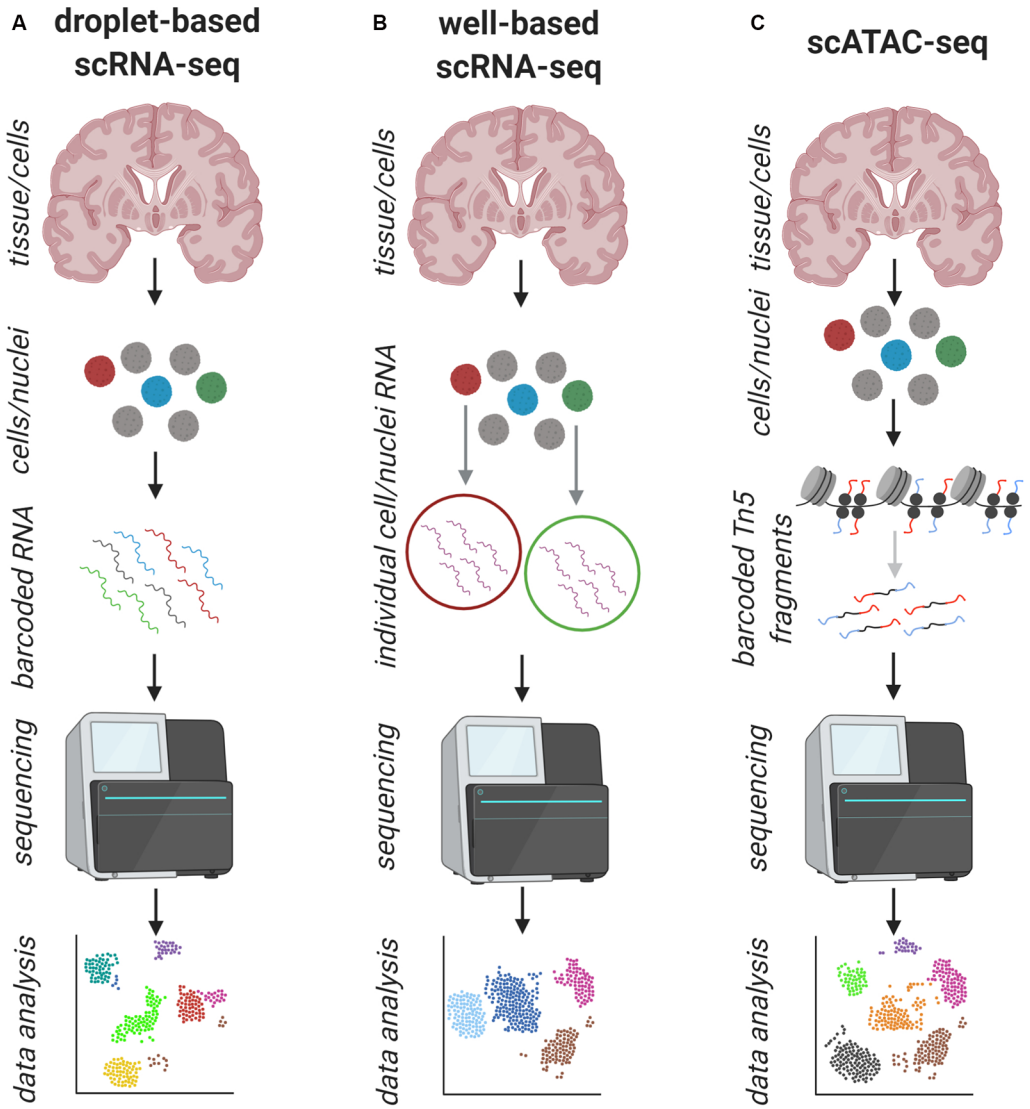

FIGURE 2 | Schematic overview of the workflow of common single-cell/nuclei (sc/sn) approaches to address human pathology. **(A)** Standard workflow of droplet-based sc/sn RNA-sequencing: tissue is dissociated into a single-cell/nuclei suspension and the mRNA of each cell is captured and barcoded individually and prepared for next-generation sequencing (NGS), which is followed by bioinformatics data analysis. This can be done for up to ten thousands of cells. **(B)** Standard workflow of well-based sc/sn RNA-sequencing: tissue is dissociated into a single-cell/nuclei suspension and the cells are captured in individual wells where each cell is prepared for NGS, which is followed by bioinformatics data analysis. This is usually done for less than 1,000 cells. **(C)** Standard workflow of droplet-based Assay for Transposase-Accessible Chromatin using sequencing (ATAC-seq): tissue is dissociated into a single-cell/nuclei suspension and the open chromatin regions of each cell are cut and barcoded individually and prepared for NGS, which is followed by bioinformatics data analysis. This can be done for up to ten thousands of cells. In all approaches **(A–C)** the information about the cell of origin is maintained, but the spatial distribution is lost.

creating individual libraries in wells. As the droplet-based methods are aimed for high throughput, the costs per cell are much cheaper in comparison to well-based technologies. Also with this barcoding approach, copy numbers of mRNAs within a cell can at least in theory directly be measured, without the need of using additional standards such as External RNA Control Consortium (ERCC) spike-ins (Baker et al., 2005). To keep the sequencing costs at a realistic level, usually only the 3' or the 5' ends of the mRNA are amplified and sequenced, which only allows information of whether a gene is expressed or not, with a limited ability to examine splicing variants or SNPs. Conversely, with well- or device-based approaches, it allows the study of splice variants of genes, but the cost per cell is higher.

Sometimes, a combination of both techniques might be useful. Using unbiased droplet-based techniques to look at the entirety of cells in a tissue of interest helps to get an overview of all cells, including rare cell populations, and to find appropriate markers for these. This is especially useful in understudied tissues such as the human brain, as established markers for rodent cells are

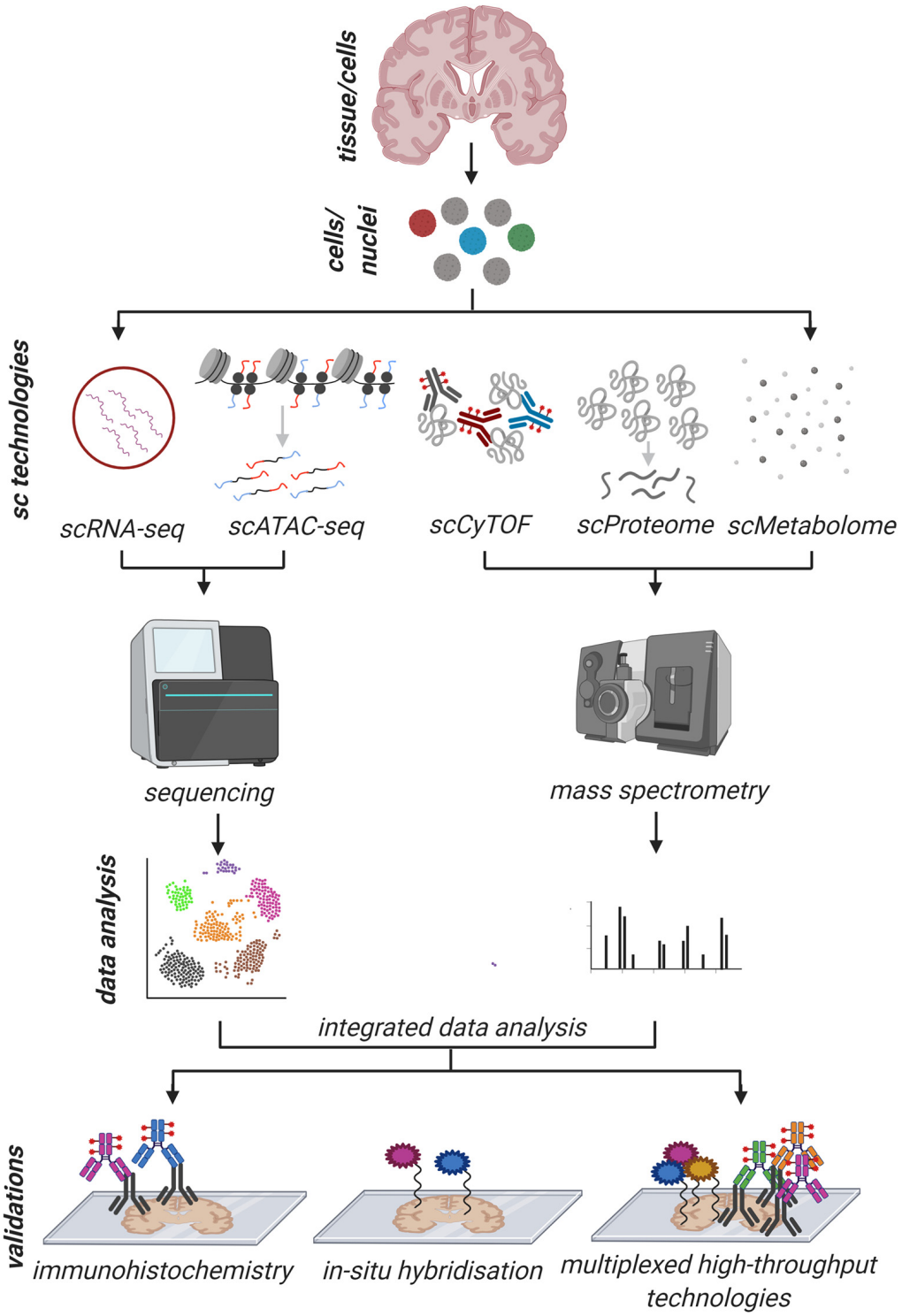

FIGURE 3 | Schematic overview of an imaginative holistic workflow of common single-cell/nuclei (sc/sn) and validation approaches to address human pathology. The tissue is dissociated into a single-cell/nuclei suspension and sc/snRNA-seq, sc/snATAC-seq, scCyTOF, scProteomics, and scMetabolomics are performed in parallel on the same tissue source with their respective workflows. After individual and comparative/integrated bioinformatics data analysis, the results are validated, ideally, on a different tissue source by standard immunohistochemistry (IHC), *in situ* hybridization (ISH) and other high throughput multiplexed techniques (100–1,000 genes/proteins of interest) where IHC and ISH can be combined. With such a possible workflow, first, the information about the cell of origin is maintained, and with the validation techniques, the spatial resolution can be analyzed as well. This holistic approach would allow us to thoroughly exploring human pathology from different angles to gain deeper information.

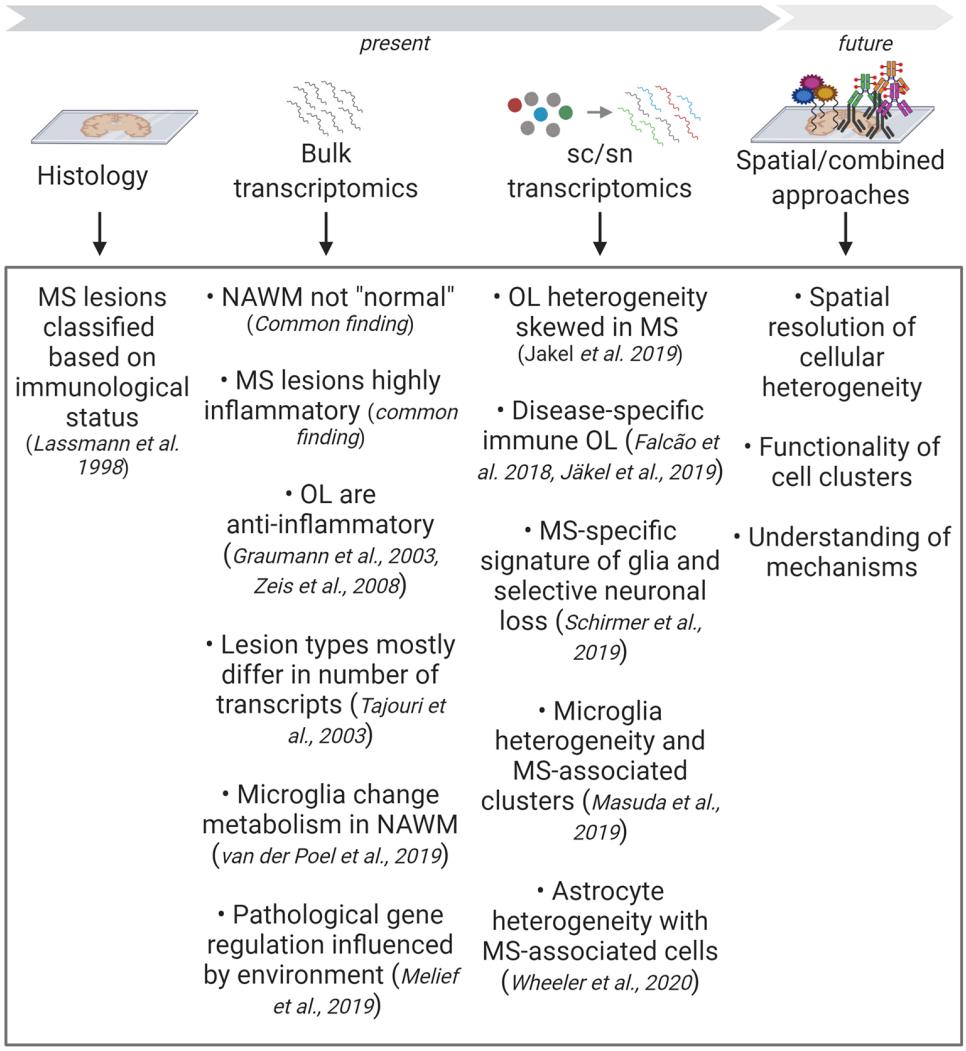

FIGURE 4 | Summary of the biological findings in Multiple Sclerosis (MS) that were gained through advances in technology. Classical histology has helped to classify MS lesions based on their immunological status. The development of bulk transcriptomic approaches has helped to unravel many transcriptional pathways that are changed in MS, with the most important common theme being inflammation. More recent studies using sc/snRNA-seq has started to unravel cellular heterogeneity and changes in the representation of these cells in disease. Combining different sc/sn approaches and using spatial technologies in the future will help to deepen our understanding of the functionality of the heterogeneous clusters and the underlying pathological mechanisms.

not always appropriate in humans. Cell populations of further interest, including rare populations or subpopulations, can then be studied at a deeper resolution using a full-length sequencing approach, after isolation or enrichment using the previously identified markers.

Currently, scRNA-seq experiments are cutting-edge and popular, generating much data and new hypotheses about the heterogeneity of cell function in all tissues with high impact publications. However, it is essential to validate these data and to keep the research question in mind, as sometimes a more classical approach will lead to an answer quicker, more easily, and cheaply. Although bulk approaches seem to be outdated at the moment, these technologies have also improved and are still important tools in studying human pathologies.

What Are the Challenges and Drawbacks of Performing Human Single-Cell RNA-Seq?

All of these single-cell technologies were originally developed for cultured cells or rodent tissue, whilst their application to human tissue has only started to boom in recent years. Besides ethical constraints and the limited availability of human tissue (control equally as pathological tissue), there are more technical challenges that delayed the revolution in this field. Single-cell technologies were developed for viable single-cell suspensions, which is often not possible in WM pathologies, where most tissue is obtained post-mortem and not during biopsies. Hence, cell viability and tissue quality are often already below the

accepted threshold to perform the experiments once the tissue arrives in the hands of the researcher. By this time, surviving cells may be highly selected and their transcriptome likely to have changed dramatically, with degraded RNA resulting in bad data quality and lower biological meaning. Moreover, to reduce confounding factors, all samples should be run ideally together or at least in as small a number of batches as possible (Hicks et al., 2017), which is impossible when using fresh biopsy or autopsy material, as individual tissue samples are sometimes only available months apart. For these reasons, most research so far in the human brain has used single-nuclei (sn) RNAseq using the same technologies from archived and frozen tissue samples instead of fresh viable cells. On comparing cells vs. nuclei, there is now the consensus that although nuclei generally yield a lower number of reads, they can add useful information on the biology. This tissue source may even protect from immediate changes in the transcriptome resulting from cell stress during cell isolation and the proportional representation of the *in vivo* situation may be more preserved, as, during live isolation, vulnerable cells are more likely to die resulting in their underrepresentation (Bakken et al., 2018; Wu et al., 2019). However, a new study suggested that using nuclei is not always a good alternative, as only highly abundant transcripts are detected and the more subtle changes related to the activation state of human microglia could not be distinguished (Thrupp et al., 2020). To get a clear picture of the advantages and disadvantages of using nuclei or cells, more comparative work using the same tissues, experimental setups, and sequencing depth will be helpful. However, given the high number of publications, it is already clear that snRNA-seq is an important tool to resolve biological questions, especially for human pathologies when no other tissue source is available.

More generally, once the decision has been made to use cells or nuclei, other challenges arise. Although at first sight, plentiful rich data is a clear advantage, it can also lead to data overload, that nobody knows what to do with. Especially with droplet-based technologies, individual sc/snRNA-seq experiments generate so many data points that research groups may only process a small part of it: for example, the experimental design might include all unselected nuclei, however, only a certain cell-type may be analyzed. Here is where open access sharing of these data is essential, allowing other groups to use these data to address their research questions and save a lot of time. This also allows for some mitigation of expense, as the rapid development of these technologies comes at a high cost. Although these techniques are becoming cheaper, the costs of commercial kits are still high and the cost per cell must be considered in the experimental plan. Homemade technologies are inevitably cheaper, but require knowledge and time to set up and may not be as robust and comparable between research labs as commercial ones. The costs for the sequencing should not be forgotten, which often equals the cost of the cell capture and cDNA library preparation. The depth of the experimental analysis obtained depends on the depth of sequencing.

A major limitation of sc/snRNA-seq is the number of transcripts that can be detected within a cell. Although the captured transcripts are often treated as representing the entirety of the transcriptome, in reality only about 5–20% of the transcripts are captured depending on the method, leaving about 80% of the biology undiscovered (Islam et al., 2014; Ding et al., 2020). These missing transcripts are usually ones with a low abundance that may represent more subtle changes between cell states. A recent advance is the development of a full-length sequencing method that reaches a significantly deeper transcriptome coverage per cell and thus results in a clearer separation of clusters (Hagemann-Jensen et al., 2020), but unfortunately, this method is not yet suitable for high throughput. Another limitation of these technologies comes from how RNA is captured. Most methods use oligos to capture polyadenylated mRNA only and especially droplet-based methods, additionally only use 3' amplification. Few technologies have been developed to amplify the 5' end of the RNA, however, the libraries are also prepared with the polyA-tail, still only accounting for the same type of RNA (Svensson et al., 2018; Chen et al., 2019). Other forms of biologically interesting RNAs, such as many microRNAs are not identifiable using this capture method and detection of splicing variants of genes is more limited (unless using full-length sequencing).

Once the sequencing data are generated, data storage is another often unconsidered problem. As datasets become bigger, in terms of sample number, cell number, and sequencing depth, the output data files become bigger and too large to be stored on a standard computer, instead of requiring big data servers or cloud storage, which come at a further cost. Data handling capacity challenges go hand in hand with increasing data size and depth, and analysis of these datasets generally requires a high-end workstation or, better, access to a computational cluster with the respective expertise. Associated with the fast development of scRNA-seq technologies, there is a large expansion in the available tools for data analysis, which are evolving all of the time and are generally open source and therefore free. This can give a bewildering variety of options on how to analyze the dataset. The challenge here is to find the right tool that is suitable for the data of interest, as not all available tools are. Helpful comparisons have emerged, for example in an overview of 45 current tools to calculate pseudotime trajectories (Saelens et al., 2019), as not all of them are equally suited for every dataset. Another example would be the availability of different clustering methods, with Seurat (Satija et al., 2015), Monocle (Trapnell et al., 2014), and Conos (Barkas et al., 2019) as highly used examples. Each of them uses a different algorithm and clustering approach, as outlined in Duò et al. (2018), and might thus result in different final clusters of which all may be valid. These are only examples, but every step in the experiment and the analysis part has many options. One study outlined this problem and showed that using only a minimum of options in different steps and combining it differently already results in ∼3,000 different pipelines for analysis (Vieth et al., 2019). This field is as experimental as wet lab work, and it may be useful to use several analysis tools purporting to do the same thing on one dataset, to determine how robust the analysis is. However, ultimately, the only way to discover if the analysis is correct is to validate the results using other methods.

What Have We Learned About WM Pathologies Using Single-Cell/Nuclei Transcriptomic Approaches?

Pioneering scRNA-seq analysis in rodent brain tissue clearly showed the detection of all brain cells that were distinguishable by specific markers (Zeisel et al., 2015). Of interest to MS, a key study in mouse oligodendrocytes (Marques et al., 2016) first used scRNA-seq to report their heterogeneity suggesting different inherent functions of oligodendrocytes not only between the brain and the spinal cord but even in the same region of the brain. The first studies using snRNA-seq on normal human brain tissue were proof of principle that this method was suitable in such tissue and that there is cellular and regional heterogeneity (Habib et al., 2017; Lake et al., 2018) and were the starting point of many following studies. Not surprisingly, it did not take long before this technology was used to study brain pathologies including MS (**Figure 4**).

With this hitherto unreached resolution, cellular heterogeneity in MS tissue was demonstrated in oligodendrocytes, neurons, microglia and astrocytes (Jäkel et al., 2019; Masuda et al., 2019; Schirmer et al., 2019; Wheeler et al., 2020) with disease-specific cell types or different heterogeneous states present in different proportions in MS compared to controls. In their study, Jäkel et al. (2019) found heterogeneous oligodendroglial states in non-pathological brain tissue and contrary to the current idea that all oligodendrocytes in MS lesions are equally vulnerable, reported that some of these states were over- and some underrepresented. Although the functional role of this cellular heterogeneity is not yet clear, this skew in the proportions of different oligodendrocyte states seen in MS was present in both NAWM and in MS lesions, again adding to the evidence that NAWM is indeed not normal, as previously shown for microglia (van der Poel et al., 2019). Furthermore, these data were able to identify a small population of previously unknown oligodendroglia with immunological functions (Falcão et al., 2018; Jäkel et al., 2019) which may influence disease pathogenesis as it suggests that oligodendrocytes may be an active player in the disease as well as a vulnerable target. This is of importance, as therapeutic approaches simply aiming to increase differentiation of oligodendrocytes to improve remyelination may need to be reconsidered, as replacing the "correct" type may be preferred. Another study using a similar approach to address the cellular composition of MS lesions found specific signatures for stressed oligodendrocytes, reactive astrocytes, and activated microglia, especially at the rim of demyelinated lesions. As this study also included cortical GM tissue, the authors reported a selective loss of CUX2-expressing upper layer excitatory projection neurons in the GM both in demyelinated and partially remyelinated lesions (Schirmer et al., 2019). In line with the previous study, they also found that some stressed oligodendrocytes seem to be capable of antigen presentation. This again confirms that damage does not affect all cells equally and that there is still a large gap of knowledge about disease mechanisms in MS. These studies are mostly descriptive, but a recent study in zebrafish has demonstrated that two distinct subgroups of oligodendrocyte precursor cells (OPCs) identified by scRNA-seq are confirmed to be functionally distinct with one primarily making networks and the other primarily differentiating into oligodendrocytes to make myelin (Marisca et al., 2020). Although this study was performed on normal zebrafish, this may also be important as if this is similar in humans, it may again force us to rethink our therapeutic remyelination strategies in MS, aiming to stimulate differentiating OPCs selectively. With a focus on microglia, Masuda et al. (2019) described microglial heterogeneity for the first time in the non-pathological human brain and additionally found clusters of disease-related microglia in MS patients that were similar to rodent animal models of MS, but with high inter-personal variability. A very recent study has directed its focus on astrocytes in MS showing that astrocytes in mice and humans are also heterogeneous. The authors found a clear MS-associated astrocyte cluster actively promoting CNS inflammation by the regulation of gene expression (Wheeler et al., 2020).

These technologies have also reached other human brain pathologies such as Alzheimer's disease (AD; Grubman et al., 2019; Mathys et al., 2019; Zhou et al., 2020), Huntington's disease (Al-Dalahmah et al., 2020) and other psychiatric disorders (Renthal et al., 2018; Velmeshev et al., 2019; Nagy et al., 2020). Although AD is usually considered a neuronal disease most of the GM, it has been surprisingly found that oligodendrocytes in the WM do show a significant transcriptional change in the disease adapting their metabolism to neuronal degeneration (Mathys et al., 2019; Zhou et al., 2020). OPCs also seem involved, as in AD, OPCs repress apolipoprotein E (APOE), which is a genetic risk factor for this disease, strengthening the hypothesis that oligodendroglia actively contribute to pathogenesis (Grubman et al., 2019). This study used the known AD risk genes to study how these contribute to disease in a cell-specific manner, as a relevant strategy to focus on the analysis of the wealth of data. Another recent study found that besides neurons, OPCs are majorly disturbed in major depressive disorder and this seemed to be coupled with their interaction with neurons rather than their ability to differentiate and myelinate (Nagy et al., 2020), which demonstrated that using this technology is important to disentangle the functions of subsets of cells. Most importantly, these new studies have started to shed new light on neurodegenerative and psychiatric diseases, moving away from a neurocentric view of these diseases with new recognition of the importance of glial cells in their pathogenesis—a shift in the research landscape.

What Other Techniques Can We Use to Complement the sc/snRNAseq Approach?

RNA-seq at a single cell/nuclei level is only the start, with the fast development of other single-cell resolution technologies, including epigenetic methods. Assay for Transposase-Accessible Chromatin using sequencing (ATAC-seq) has already long been used to assess the bulk chromatin accessibility and the chromatin signature of cellular DNA (Buenrostro et al., 2013) including the human brain in health and disease (Corces et al., 2017; Bryois et al., 2018; Fullard et al., 2018), but can now also be done at the single-cell/nuclear level (**Figure 2C**). This adds information about the transcriptional regulation of different cell types and has already widely been used on rodents

(Preissl et al., 2018; Sinnamon et al., 2019), but also human brain tissue (Zhong et al., 2020). A very recent study used this method to identify new single nucleotide polymorphisms (SNPs) with a more functional annotation than classically found with GWAS and found new risk-factors for Parkinson's and AD (Corces et al., 2020). Bioinformatics tools are emerging to integrate scRNA-seq with scATAC-seq data to get a deeper understanding of the transcriptional and genomic landscape within one individual cell. Further explorations of the epigenomic landscape at a single cell level include DNA methylation profiling to detect methylation marks identifying regulatory programs in different cell populations (summarized in Fiers et al., 2018). It is already possible to detect epigenetic marks and gene expression in the same cell, not only bioinformatically but also experimentally, as shown with the sc-GEM (single-cell analysis of genotype, expression, and methylation) assay on cultured human fibroblasts (Cheow et al., 2016) and its use on human tissue would be another highly valuable method to understand its pathology.

Clearly, single-cell DNA/RNA changes can imply function but protein detection adds a further level of information to determine a cell's behavior. Single-cell technologies have also entered the protein field with Cytometry by the time of flight (CyTOF), although this is not yet unbiased but requires a selection of markers of interest. This method uses metal-labeled antibodies to detect cellular antigens that are then analyzed by mass cytometry. This approach is similar to classical Fluorescence-activated cell sorting (FACS), but with a broader separation of metals which overcomes the limit of the overlap of fluorophores and allows the use of around 40 antibodies together (up to 100 when considering isotopes as well). With a bioinformatics analysis approach, high numbers of single cells can be thoroughly profiled. This approach has been used to characterize a change in the populations of peripheral immune cells of MS patients (Böttcher et al., 2019a) as well as to characterize multiple different region-dependent populations of microglia in the human brain that are distinguishable from peripheral cells (Böttcher et al., 2019b). CyTOF can also directly be applied to histological tissue sections—called imaging mass cytometry—and can be used to profile individual cells whilst maintaining the spatial information. Although still a fledgling technique at the spatial level, this has already successfully been applied in MS brain tissue to characterize astrocytes and peripheral cells in MS lesions (Park et al., 2019) and to characterize the immune cell landscape within different lesions from an individual MS patient (Ramaglia et al., 2019).

For a disease such as MS, spatial information is very important, due to the focal nature of demyelinated lesions, but there may also be pathological changes in more restricted areas in other neurodegenerative pathologies as well, e.g., in AD. Although not yet at a single-cell resolution, spatial transcriptomics technologies aim to capture the whole transcriptome of each of very small areas of a tissue section in an unbiased way in combination with histological analysis (Ståhl et al., 2016). Using the same principle of capturing and barcoding mRNA as droplet-based methods, this technology allows the location of the origin of an individual mRNA to a defined spot on a predefined grid on which the tissue has been placed, thus maintaining the spatial information. This technology is already being used on human tissue (Maynard et al., 2020), and with an earlier version in ALS (Gregory et al., 2020). With the clear advantage of capturing the transcriptome at a high resolution whilst maintaining spatial information, spatial transcriptomics technologies are clearly at the forefront of development and may in the future be more widely used than current sc/snRNA-seq technologies. They are either based on sequencing the transcripts *in situ* after having been barcoded (Ke et al., 2013; Lee et al., 2014; Wang et al., 2018; Gregory et al., 2020; Lundin et al., 2020; Maynard et al., 2020), or use highly multiplexed single molecular fluorescent *in situ* hybridization probes detectable using confocal microscopy (Lubeck et al., 2014; Shah et al., 2016). The current limitation of sequencing-based methods is the low detection of transcripts. Multiplexed *in situ* methods on the other hand are restricted by the number of probes (hundreds to thousands) due to the limited availability of fluorophores and optical resolution of individual molecules, making them less suitable for an unbiased discovery-driven research approach. However, recent developments have combined the methods, using sequential hybridization with *in situ* sequencing to theoretically cover the whole transcriptome with only a few fluorophores (Shah et al., 2016; Eng et al., 2019). As a result, a higher number of transcripts per cell can be detected. Although these methods have not yet been implemented on human brain tissue, which will be challenging due to its high autofluorescence, this high resolution of individual mRNAs will not only allow the localization of cells within tissue but also will allow the study of the subcellular localization of mRNAs, clear advantages in comparison to scRNA-seq methods. Unfortunately, these methods do only work well on thin tissue sections, limiting the information we gain from a three-dimensional point of view. Sequencing-driven spatial methods in particular are still expensive and are thus tend to be performed on small tissue pieces with few sections from an individual, which may introduce some bias to the biological findings.

Validation of results, preferably on a separate cohort of tissue, is essential by classical immunohistochemistry/fluorescence and *in situ* hybridization, and/or these burgeoning multiplexing technologies, mentioned above. These have allowed spatially detection of 100 different transcripts by *in situ* sequencing (Lundin et al., 2020) or around 100 proteins and 1,000 genes using oligonucleotide labeling in a tissue section (Geiss et al., 2008; Kulkarni, 2011). Although imaging mass cytometry is usually used to characterize novel cell populations, it can clearly serve as a validation method for transcriptomic data as well. These require analysis tools to distinguish signals in different cells, but appear very useful and are likely to become standard to address human pathologies in the future.

What Does the Future Hold?

The outputs of all of these technologies applied to human WM pathologies are still no more than descriptive pathology—although on a much deeper level than was ever possible before and at least implying function. This work, however, is just the start of a new era of single-cell resolution

techniques that will revolutionize human pathology and will most likely become a standard technology for pathological assessment. The richness of these data will allow us to take the next step, which is to address more functional changes to gain a deeper understanding of the diseases. For example, snRNA-seq will allow us to study transcriptomic changes in a high number of cells in many different types of MS lesions which then may allow us to reclassify them on a functional level, namely their regenerative potential rather than using the classical degenerative description. Moreover, these data may allow us to determine lesion markers that can be used for PET-imaging and will thus be an invaluable tool for disease diagnosis, prognosis, and response to therapies. Furthermore, as most of the data are gained similarly and deposited with its metadata on open-source databases, it is then easier to compare many brain regions (such as WM and GM, or brain and spinal cord) or diseases with each other, to gain a much clearer picture of the cellular architecture of our brain. The Human Cell Atlas is a collaborative effort to exactly achieve this aim[1] not only for the brain but for the entire human body.

So far, most of these technologies are used individually by different groups but in the future, complementary but different technologies will be used in the same experimental setup, and their outputs integrated, as recently shown from the Allen Brain Institute (Bakken et al., 2020). Maybe in 10 years from now, it will be possible to look at the transcriptome, the epigenome, the proteome and the metabolome on a single cell level from the same tissue source at once, as suggested in **Figure 3**. Attempts to achieve this have already been made in recent preprint manuscripts where the authors were able to simultaneously study either proteins and mRNA (Vistain et al., 2020) or chromatin accessibility and gene expression (Ma et al., 2020) in single cells. This will allow us to look at the same data from many different perspectives to gain a deeper understanding of individual cells in health and disease and further explore the pathological mechanism. The options here seem endless with money as the only limit!

[1]https://www.humancellatlas.org/

CONCLUSION

Analysis and understanding of human WM pathologies have come a long way from being purely descriptive histological analysis to gaining cell type-specific information at a single-cell resolution (**Figure 4**). This development goes hand in hand with the development of novel technologies, although their use in human tissue is inevitably more challenging than in animal models. We can now sequence the RNA of a cell, examine the state of the chromatin and current proteomic tools will likely become more sensitive as well, which will allow us to explore the proteome of individual cells. Although all of these technologies have developed separately, we will need to link them together to see the full picture in the future. This will allow us to gain a deeper insight into human pathologies and will become important tools not only for basic science, but will also revolutionize diagnostics and may pave the way for developing new therapies. However, even though these technologies are developing at an exciting and rapid speed, it is important to retain a clear focus on the research question to be answered, to avoid distraction by an ocean of data and high costs, and to ensure that we advance biology.

AUTHOR CONTRIBUTIONS

SJ and AW wrote and edited the manuscript. SJ also designed and prepared the figures.

FUNDING

SJ is funded by the European Union, Horizon 2020, Marie-Skodowska Curie Actions EC no. 789492. AW is funded by the UK Multiple Sclerosis Society, Medical Research Council, [Human Cell Atlas (grant number MR/S035915/1)], and F. Hoffmann-La Roche.

ACKNOWLEDGMENTS

All figures created with BioRender.com.

REFERENCES

Absinta, M., Sati, P., Fechner, A., Schindler, M. K., Nair, G., and Reich, D. S. (2018). Identification of chronic active multiple sclerosis lesions on 3T MRI. *Am. J. Neuroradiol.* 39, 1233–1238. doi: 10.3174/ajnr.a5660

Absinta, M., Sati, P., Masuzzo, F., Nair, G., Sethi, V., Kolb, H., et al. (2019). Association of chronic active multiple sclerosis lesions with disability *in vivo*. *JAMA Neurol.* 76, 1474–1483. doi: 10.1001/jamaneurol.2019.2399

Al-Dalahmah, O., Sosunov, A. A., Shaik, A., Ofori, K., Liu, Y., Vonsattel, J. P., et al. (2020). Single-nucleus RNA-seq identifies Huntington disease astrocyte states. *Acta Neuropathol. Commun.* 8:19. doi: 10.1186/s40478-020-0880-6

Baker, S. C., Bauer, S. R., Beyer, R. P., Brenton, J. D., Bromley, B., Burrill, J., et al. (2005). The external RNA controls consortium: a progress report. *Nat. Methods* 2, 731–734. doi: 10.1038/nmeth1005-731

Bakken, T. E., Hodge, R. D., Miller, J. A., Yao, Z., Nguyen, T. N., Aevermann, B., et al. (2018). Single-nucleus and single-cell transcriptomes compared in matched cortical cell types. *PLoS One* 13:e0209648. doi: 10.1371/journal.pone.0209648

Bakken, T. E., Jorstad, N. L., Hu, Q., Lake, B. B., Tian, W., Kalmbach, B. E., et al. (2020). Evolution of cellular diversity in primary motor cortex of human, marmoset monkey, and mouse. *bioRxiv* [Preprint]. doi: 10.1101/2020.03.31.016972

Barkas, N., Petukhov, V., Nikolaeva, D., Lozinsky, Y., Demharter, S., Khodosevich, K., et al. (2019). Joint analysis of heterogeneous single-cell RNA-seq dataset collections. *Nat. Methods* 16, 695–698. doi: 10.1038/s41592-019-0466-z

Bhargava, P., and Calabresi, P. A. (2016). Metabolomics in multiple sclerosis. *Mult. Scler.* 22, 451–460. doi: 10.1177/1352458515622827

Böttcher, C., Fernández-Zapata, C., Schlickeiser, S., Kunkel, D., Schulz, A. R., Mei, H. E., et al. (2019a). Multi-parameter immune profiling of peripheral blood mononuclear cells by multiplexed single-cell mass cytometry in patients with early multiple sclerosis. *Sci. Rep.* 9:19471. doi: 10.1038/s41598-019-55852-x

Böttcher, C., Schlickeiser, S., Sneeboer, M. A. M., Kunkel, D., Knop, A., Paza, E., et al. (2019b). Human microglia regional heterogeneity and phenotypes

determined by multiplexed single-cell mass cytometry. *Nat. Neurosci.* 22, 78–90. doi: 10.1038/s41593-018-0290-2

Broadwater, L., Pandit, A., Clements, R., Azzam, S., Vadnal, J., Sulak, M., et al. (2011). Analysis of the mitochondrial proteome in multiple sclerosis cortex. *Biochim. Biophys. Acta* 1812, 630–641. doi: 10.1016/j.bbadis.2011.01.012

Brück, W., Bitsch, A., Kolenda, H., Brück, Y., Stiefel, M., and Lassmann, H. (1997). Inflammatory central nervous system demyelination: correlation of magnetic resonance imaging findings with lesion pathology. *Ann. Neurol.* 42, 783–793. doi: 10.1002/ana.410420515

Bryois, J., Garrett, M. E., Song, L., Safi, A., Giusti-Rodriguez, P., Johnson, G. D., et al. (2018). Evaluation of chromatin accessibility in prefrontal cortex of individuals with schizophrenia. *Nat. Commun.* 9:3121. doi: 10.1038/s41467-018-05379-y

Buenrostro, J. D., Giresi, P. G., Zaba, L. C., Chang, H. Y., and Greenleaf, W. J. (2013). Transposition of native chromatin for fast and sensitive epigenomic profiling of open chromatin, DNA-binding proteins and nucleosome position. *Nat. Methods* 10, 1213–1218. doi: 10.1038/nmeth.2688

Chen, G., Ning, B., and Shi, T. (2019). Single-cell RNA-seq technologies and related computational data analysis. *Front. Genet.* 10:317. doi: 10.3389/fgene.2019.00317

Cheow, L. F., Courtois, E. T., Tan, Y., Viswanathan, R., Xing, Q., Tan, R. Z., et al. (2016). Single-cell multimodal profiling reveals cellular epigenetic heterogeneity. *Nat. Methods* 13, 833–836. doi: 10.1038/nmeth.3961

Comabella, M., and Martin, R. (2007). Genomics in multiple sclerosis—current state and future directions. *J. Neuroimmunol.* 187, 1–8. doi: 10.1016/j.jneuroim.2007.02.009

Corces, M. R., Shcherbina, A., Kundu, S., Gloudemans, M. J., Frésard, L., Granja, J. M., et al. (2020). Single-cell epigenomic identification of inherited risk loci in Alzheimer's and Parkinson's disease. *bioRxiv* [Preprint]. doi: 10.1101/2020.01.06.896159

Corces, M. R., Trevino, A. E., Hamilton, E. G., Greenside, P. G., Sinnott-Armstrong, N. A., Vesuna, S., et al. (2017). An improved ATAC-seq protocol reduces background and enables interrogation of frozen tissues. *Nat. Methods* 14, 959–962. doi: 10.1038/nmeth.4396

Del Boccio, P., Rossi, C., Di Ioia, M., Cicalini, I., Sacchetta, P., and Pieragostino, D. (2016). Integration of metabolomics and proteomics in multiple sclerosis: from biomarkers discovery to personalized medicine. *Proteomics Clin. Appl.* 10, 470–484. doi: 10.1002/prca.201500083

Ding, J., Adiconis, X., Simmons, S. K., Kowalczyk, M. S., Hession, C. C., Marjanovic, N. D., et al. (2020). Systematic comparison of single-cell and single-nucleus RNA-sequencing methods. *Nat. Biotechnol.* 38, 737–746. doi: 10.1038/s41587-020-0465-8

Duò, A., Robinson, M. D., and Soneson, C. (2018). A systematic performance evaluation of clustering methods for single-cell RNA-seq data. *F1000Res.* 7, 1141–1141. doi: 10.12688/f1000research.15666.2

Dutta, R., and Trapp, B. D. (2012). Gene expression profiling in multiple sclerosis brain. *Neurobiol. Dis.* 45, 108–114. doi: 10.1016/j.nbd.2010.12.003

Eng, C.-H. L., Lawson, M., Zhu, Q., Dries, R., Koulena, N., Takei, Y., et al. (2019). Transcriptome-scale super-resolved imaging in tissues by RNA seqFISH. *Nature* 568, 235–239. doi: 10.1038/s41586-019-1049-y

Falcão, A. M., Van Bruggen, D., Marques, S., Meijer, M., Jäkel, S., Agirre, E., et al. (2018). Disease-specific oligodendrocyte lineage cells arise in multiple sclerosis. *Nat. Med.* 24, 1837–1844. doi: 10.1038/s41591-018-0236-y

Farias, A. S., Pradella, F., Schmitt, A., Santos, L. M., and Martins-De-Souza, D. (2014). Ten years of proteomics in multiple sclerosis. *Proteomics* 14, 467–480. doi: 10.1002/pmic.201300268

Farias, A. S., and Santos, L. M. (2015). How can proteomics elucidate the complexity of multiple sclerosis? *Proteomics Clin. Appl.* 9, 844–847. doi: 10.1002/prca.201400171

Fiers, M., Minnoye, L., Aibar, S., Bravo Gonzalez-Blas, C., Kalender Atak, Z., and Aerts, S. (2018). Mapping gene regulatory networks from single-cell omics data. *Brief. Funct. Genomics* 17, 246–254. doi: 10.1093/bfgp/elx046

Fullard, J. F., Hauberg, M. E., Bendl, J., Egervari, G., Cirnaru, M. D., Reach, S. M., et al. (2018). An atlas of chromatin accessibility in the adult human brain. *Genome Res.* 28, 1243–1252. doi: 10.1101/gr.232488.117

Geiss, G. K., Bumgarner, R. E., Birditt, B., Dahl, T., Dowidar, N., Dunaway, D. L., et al. (2008). Direct multiplexed measurement of gene expression with color-coded probe pairs. *Nat. Biotechnol.* 26, 317–325. doi: 10.1038/nbt1385

Graumann, U., Reynolds, R., Steck, A. J., and Schaeren-Wiemers, N. (2003). Molecular changes in normal appearing white matter in multiple sclerosis are characteristic of neuroprotective mechanisms against hypoxic insult. *Brain Pathol.* 13, 554–573. doi: 10.1111/j.1750-3639.2003.tb00485.x

Gregory, J. M., McDade, K., Livesey, M. R., Croy, I., Marion De Proce, S., Aitman, T., et al. (2020). Spatial transcriptomics identifies spatially dysregulated expression of GRM3 and USP47 in amyotrophic lateral sclerosis. *Neuropathol. Appl. Neurobiol.* doi: 10.1111/nan.12597 [Epub ahead of print]

Grubman, A., Chew, G., Ouyang, J. F., Sun, G., Choo, X. Y., Mclean, C., et al. (2019). A single-cell atlas of entorhinal cortex from individuals with Alzheimer's disease reveals cell-type-specific gene expression regulation. *Nat. Neurosci.* 22, 2087–2097. doi: 10.1038/s41593-019-0539-4

Habib, N., Avraham-Davidi, I., Basu, A., Burks, T., Shekhar, K., Hofree, M., et al. (2017). Massively parallel single-nucleus RNA-seq with DroNc-seq. *Nat. Methods* 14, 955–958. doi: 10.1038/nmeth.4407

Hagemann-Jensen, M., Ziegenhain, C., Chen, P., Ramsköld, D., Hendriks, G.-J., Larsson, A. J. M., et al. (2020). Single-cell RNA counting at allele and isoform resolution using Smart-seq3. *Nat. Biotechnol.* 38, 708–714. doi: 10.1038/s41587-020-0497-0

Han, M. H., Hwang, S.-I., Roy, D. B., Lundgren, D. H., Price, J. V., Ousman, S. S., et al. (2008). Proteomic analysis of active multiple sclerosis lesions reveals therapeutic targets. *Nature* 451, 1076–1081. doi: 10.1038/nature06559

Haque, A., Engel, J., Teichmann, S. A., and Lonnberg, T. (2017). A practical guide to single-cell RNA-sequencing for biomedical research and clinical applications. *Genome Med.* 9:75. doi: 10.1186/s13073-017-0467-4

Hemond, C. C., and Bakshi, R. (2018). Magnetic resonance imaging in multiple sclerosis. *Cold Spring Harb. Perspect. Med.* 8:a028969. doi: 10.1101/cshperspect.a028969

Hendrickx, D.a.E., Van Scheppingen, J., Van Der Poel, M., Bossers, K., Schuurman, K. G., Van Eden, C. G., et al. (2017). Gene expression profiling of multiple sclerosis pathology identifies early patterns of demyelination surrounding chronic active lesions. *Front. Immunol.* 8:1810. doi: 10.3389/fimmu.2017.01810

Hicks, S. C., Townes, F. W., Teng, M., and Irizarry, R. A. (2017). Missing data and technical variability in single-cell RNA-sequencing experiments. *Biostatistics* 19, 562–578. doi: 10.1093/biostatistics/kxx053

Islam, S., Zeisel, A., Joost, S., La Manno, G., Zajac, P., Kasper, M., et al. (2014). Quantitative single-cell RNA-seq with unique molecular identifiers. *Nat. Methods* 11, 163–166. doi: 10.1038/nmeth.2772

Jäkel, S., Agirre, E., Mendanha Falcão, A., Van Bruggen, D., Lee, K. W., Knuesel, I., et al. (2019). Altered human oligodendrocyte heterogeneity in multiple sclerosis. *Nature* 566, 543–547. doi: 10.1038/s41586-019-0903-2

Ke, R., Mignardi, M., Pacureanu, A., Svedlund, J., Botling, J., Wählby, C., et al. (2013). in situ sequencing for RNA analysis in preserved tissue and cells. *Nat. Methods* 10, 857–860. doi: 10.1038/nmeth.2563

Kinter, J., Zeis, T., and Schaeren-Wiemers, N. (2008). RNA profiling of MS brain tissues. *Int. MS J.* 15, 51–58.

Kulkarni, M. M. (2011). Digital multiplexed gene expression analysis using the nanostring ncounter system. *Curr. Protoc. Mol. Biol.* 94, 25B.10.21–25B.10.17. doi: 10.1002/0471142727.mb25b10s94

Lake, B. B., Chen, S., Sos, B. C., Fan, J., Kaeser, G. E., Yung, Y. C., et al. (2018). Integrative single-cell analysis of transcriptional and epigenetic states in the human adult brain. *Nat. Biotechnol.* 36, 70–80. doi: 10.1038/nbt.4038

Lassmann, H., Raine, C. S., Antel, J., and Prineas, J. W. (1998). Immunopathology of multiple sclerosis: report on an international meeting held at the Institute of Neurology of the University of Vienna. *J. Neuroimmunol.* 86, 213–217. doi: 10.1016/s0165-5728(98)00031-9

Lee, J. H., Daugharthy, E. R., Scheiman, J., Kalhor, R., Yang, J. L., Ferrante, T. C., et al. (2014). Highly multiplexed subcellular RNA sequencing in situ. *Science* 343, 1360–1363. doi: 10.1126/science.1250212

Lindberg, R. L., De Groot, C. J., Certa, U., Ravid, R., Hoffmann, F., Kappos, L., et al. (2004). Multiple sclerosis as a generalized CNS disease—comparative microarray analysis of normal appearing white matter and lesions in secondary progressive MS. *J. Neuroimmunol.* 152, 154–167. doi: 10.1016/j.jneuroim.2004.03.011

Lock, C., Hermans, G., Pedotti, R., Brendolan, A., Schadt, E., Garren, H., et al. (2002). Gene-microarray analysis of multiple sclerosis lesions yields new

targets validated in autoimmune encephalomyelitis. *Nat. Med.* 8, 500–508. doi: 10.1038/nm0502-500

Lubeck, E., Coskun, A. F., Zhiyentayev, T., Ahmad, M., and Cai, L. (2014). Single-cell in situ RNA profiling by sequential hybridization. *Nat. Methods* 11, 360–361. doi: 10.1038/nmeth.2892

Lundin, E., Wu, C., Widmark, A., Behm, M., Hjerling-Leffler, J., Daniel, C., et al. (2020). Spatiotemporal mapping of RNA editing in the developing mouse brain using in situ sequencing reveals regional and cell-type-specific regulation. *BMC Biol.* 18:6. doi: 10.1186/s12915-019-0736-3

Ly, L., Barnett, M. H., Zheng, Y. Z., Gulati, T., Prineas, J. W., and Crossett, B. (2011). Comprehensive tissue processing strategy for quantitative proteomics of formalin-fixed multiple sclerosis lesions. *J. Proteome Res.* 10, 4855–4868. doi: 10.1021/pr200672n

Lynch, J., Peeling, J., Auty, A., and Sutherland, G. R. (1993). Nuclear magnetic resonance study of cerebrospinal fluid from patients with multiple sclerosis. *Can. J. Neurol. Sci.* 20, 194–198. doi: 10.1017/s0317167100047922

Ma, S., Zhang, B., Lafave, L., Chiang, Z., Hu, Y., Ding, J., et al. (2020). Chromatin potential identified by shared single cell profiling of RNA and chromatin. *bioRxiv* [Preprint]. doi: 10.1101/2020.06.17.156943

Macchi, M., Magalon, K., Zimmer, C., Peeva, E., El Waly, B., Brousse, B., et al. (2020). Mature oligodendrocytes bordering lesions limit demyelination and favor myelin repair *via* heparan sulfate production. *eLife* 9:e51735. doi: 10.7554/eLife.51735

Macosko, E. Z., Basu, A., Satija, R., Nemesh, J., Shekhar, K., Goldman, M., et al. (2015). Highly parallel genome-wide expression profiling of individual cells using nanoliter droplets. *Cell* 161, 1202–1214. doi: 10.1016/j.cell.2015.05.002

Marisca, R., Hoche, T., Agirre, E., Hoodless, L. J., Barkey, W., Auer, F., et al. (2020). Functionally distinct subgroups of oligodendrocyte precursor cells integrate neural activity and execute myelin formation. *Nat. Neurosci.* 23, 363–374. doi: 10.1038/s41593-019-0581-2

Marques, S., Zeisel, A., Codeluppi, S., Van Bruggen, D., Mendanha Falcao, A., Xiao, L., et al. (2016). Oligodendrocyte heterogeneity in the mouse juvenile and adult central nervous system. *Science* 352, 1326–1329. doi: 10.1126/science.aaf6463

Masuda, T., Sankowski, R., Staszewski, O., Bottcher, C., Amann, L., Sagar, Scheiwe, C., et al. (2019). Spatial and temporal heterogeneity of mouse and human microglia at single-cell resolution. *Nature* 566, 388–392. doi: 10.1038/s41586-019-0924-x

Mathys, H., Davila-Velderrain, J., Peng, Z., Gao, F., Mohammadi, S., Young, J. Z., et al. (2019). Single-cell transcriptomic analysis of Alzheimer's disease. *Nature* 570, 332–337. doi: 10.1038/s41586-019-1195-2

Maynard, K. R., Collado-Torres, L., Weber, L. M., Uytingco, C., Barry, B. K., Williams, S. R., et al. (2020). Transcriptome-scale spatial gene expression in the human dorsolateral prefrontal cortex. *bioRxiv* [Preprint]. doi: 10.1101/2020.02.28.969931

Melief, J., Orre, M., Bossers, K., Van Eden, C. G., Schuurman, K. G., Mason, M. R. J., et al. (2019). Transcriptome analysis of normal-appearing white matter reveals cortisol- and disease-associated gene expression profiles in multiple sclerosis. *Acta Neuropathol. Commun.* 7:60. doi: 10.1186/s40478-019-0705-7

Mills, J. D., Chen, J., Kim, W. S., Waters, P. D., Prabowo, A. S., Aronica, E., et al. (2015). Long intervening non-coding RNA 00320 is human brain-specific and highly expressed in the cortical white matter. *Neurogenetics* 16, 201–213. doi: 10.1007/s10048-015-0445-1

Mycko, M. P., Papoian, R., Boschert, U., Raine, C. S., and Selmaj, K. W. (2003). cDNA microarray analysis in multiple sclerosis lesions: detection of genes associated with disease activity. *Brain* 126, 1048–1057. doi: 10.1093/brain/awg107

Nagy, C., Maitra, M., Tanti, A., Suderman, M., Théroux, J.-F., Davoli, M. A., et al. (2020). Single-nucleus transcriptomics of the prefrontal cortex in major depressive disorder implicates oligodendrocyte precursor cells and excitatory neurons. *Nat. Neurosci.* 23, 771–781. doi: 10.1038/s41593-020-0621-y

Park, C., Ponath, G., Levine-Ritterman, M., Bull, E., Swanson, E. C., De Jager, P. L., et al. (2019). The landscape of myeloid and astrocyte phenotypes in acute multiple sclerosis lesions. *Acta Neuropathol. Commun.* 7:130. doi: 10.1186/s40478-019-0779-2

Picelli, S. (2017). Single-cell RNA-sequencing: the future of genome biology is now. *RNA Biol.* 14, 637–650. doi: 10.1080/15476286.2016.1201618

Picelli, S., Faridani, O. R., Björklund, A. K., Winberg, G., Sagasser, S., and Sandberg, R. (2014). Full-length RNA-seq from single cells using Smart-seq2. *Nat. Protoc.* 9, 171–181. doi: 10.1038/nprot.2014.006

Preissl, S., Fang, R., Huang, H., Zhao, Y., Raviram, R., Gorkin, D. U., et al. (2018). Single-nucleus analysis of accessible chromatin in developing mouse forebrain reveals cell-type-specific transcriptional regulation. *Nat. Neurosci.* 21, 432–439. doi: 10.1038/s41593-018-0079-3

Ramaglia, V., Sheikh-Mohamed, S., Legg, K., Park, C., Rojas, O. L., Zandee, S., et al. (2019). Multiplexed imaging of immune cells in staged multiple sclerosis lesions by mass cytometry. *eLife* 8:e48051. doi: 10.7554/eLife.48051

Renthal, W., Boxer, L. D., Hrvatin, S., Li, E., Silberfeld, A., Nagy, M. A., et al. (2018). Characterization of human mosaic Rett syndrome brain tissue by single-nucleus RNA sequencing. *Nat. Neurosci.* 21, 1670–1679. doi: 10.1038/s41593-018-0270-6

Saelens, W., Cannoodt, R., Todorov, H., and Saeys, Y. (2019). A comparison of single-cell trajectory inference methods. *Nat. Biotechnol.* 37, 547–554. doi: 10.1038/s41587-019-0071-9

Satija, R., Farrell, J. A., Gennert, D., Schier, A. F., and Regev, A. (2015). Spatial reconstruction of single-cell gene expression data. *Nat. Biotechnol.* 33, 495–502. doi: 10.1038/nbt.3192

Schirmer, L., Velmeshev, D., Holmqvist, S., Kaufmann, M., Werneburg, S., Jung, D., et al. (2019). Neuronal vulnerability and multilineage diversity in multiple sclerosis. *Nature* 573, 75–82. doi: 10.1038/s41586-019-1404-z

Shah, S., Lubeck, E., Zhou, W., and Cai, L. (2016). in situ transcription profiling of single cells reveals spatial organization of cells in the mouse hippocampus. *Neuron* 92, 342–357. doi: 10.1016/j.neuron.2016.10.001

Sinnamon, J. R., Torkenczy, K. A., Linhoff, M. W., Vitak, S. A., Mulqueen, R. M., Pliner, H. A., et al. (2019). The accessible chromatin landscape of the murine hippocampus at single-cell resolution. *Genome Res.* 29, 857–869. doi: 10.1101/gr.243725.118

Ståhl, P. L., Salmén, F., Vickovic, S., Lundmark, A., Navarro, J. F., Magnusson, J., et al. (2016). Visualization and analysis of gene expression in tissue sections by spatial transcriptomics. *Science* 353, 78–82. doi: 10.1126/science.aaf2403

Svensson, V., Vento-Tormo, R., and Teichmann, S. A. (2018). Exponential scaling of single-cell RNA-seq in the past decade. *Nat. Protoc.* 13, 599–604. doi: 10.1038/nprot.2017.149

Tajouri, L., Mellick, A. S., Ashton, K. J., Tannenberg, A. E., Nagra, R. M., Tourtellotte, W. W., et al. (2003). Quantitative and qualitative changes in gene expression patterns characterize the activity of plaques in multiple sclerosis. *Mol. Brain Res.* 119, 170–183. doi: 10.1016/j.molbrainres.2003.09.008

Tang, F., Barbacioru, C., Wang, Y., Nordman, E., Lee, C., Xu, N., et al. (2009). mRNA-Seq whole-transcriptome analysis of a single cell. *Nat. Methods* 6, 377–382. doi: 10.1038/nmeth.1315

Thrupp, N., Frigerio, C. S., Wolfs, L., Skene, N. G., Poovathingal, S., Fourne, Y., et al. (2020). Single nucleus sequencing fails to detect microglial activation in human tissue. *bioRxiv* [Preprint]. doi: 10.1101/2020.04.13.035386

Trapnell, C., Cacchiarelli, D., Grimsby, J., Pokharel, P., Li, S., Morse, M., et al. (2014). The dynamics and regulators of cell fate decisions are revealed by pseudotemporal ordering of single cells. *Nat. Biotechnol.* 32, 381–386. doi: 10.1038/nbt.2859

van der Poel, M., Ulas, T., Mizee, M. R., Hsiao, C. C., Miedema, S. S. M., Adelia, Schuurman, K. G., et al. (2019). Transcriptional profiling of human microglia reveals grey-white matter heterogeneity and multiple sclerosis-associated changes. *Nat. Commun.* 10:1139. doi: 10.1038/s41467-019-08976-7

Velmeshev, D., Schirmer, L., Jung, D., Haeussler, M., Perez, Y., Mayer, S., et al. (2019). Single-cell genomics identifies cell type-specific molecular changes in autism. *Science* 364, 685–689. doi: 10.1126/science.aav8130

Vieth, B., Parekh, S., Ziegenhain, C., Enard, W., and Hellmann, I. (2019). A systematic evaluation of single cell RNA-seq analysis pipelines. *bioRxiv* [Preprint]. doi: 10.1038/s41467-019-12266-7

Vistain, L., Phan, H. V., Jordi, C., Chen, M., Reddy, S. T., and Tay, S. (2020). Quantification of proteins, protein complexes and mRNA in single cells by proximity-sequencing. *bioRxiv* [Preprint]. doi: 10.1101/2020.05.15.098780

Wang, X., Allen, W. E., Wright, M. A., Sylwestrak, E. L., Samusik, N., Vesuna, S., et al. (2018). Three-dimensional intact-tissue sequencing of

single-cell transcriptional states. *Science* 361:eaat5691. doi: 10.1126/science.aat5691

Werner, H. B., and Jahn, O. (2010). Myelin matters: proteomic insights into white matter disorders. *Expert Rev. Proteomics* 7, 159–164. doi: 10.1586/epr.09.105

Wheeler, M. A., Clark, I. C., Tjon, E. C., Li, Z., Zandee, S. E. J., Couturier, C. P., et al. (2020). MAFG-driven astrocytes promote CNS inflammation. *Nature* 578, 593–599. doi: 10.1038/s41586-020-1999-0

Whitney, L. W., Becker, K. G., Tresser, N. J., Caballero-Ramos, C. I., Munson, P. J., Prabhu, V. V., et al. (1999). Analysis of gene expression in mutiple sclerosis lesions using cDNA microarrays. *Ann. Neurol.* 46, 425–428. doi: 10.1002/1531-8249(199909)46:3<425::aid-ana22>3.0.co;2-o

Whitney, L. W., Ludwin, S. K., Mcfarland, H. F., and Biddison, W. E. (2001). Microarray analysis of gene expression in multiple sclerosis and EAE identifies 5-lipoxygenase as a component of inflammatory lesions. *J. Neuroimmunol.* 121, 40–48. doi: 10.1016/s0165-5728(01)00438-6

Wu, H., Kirita, Y., Donnelly, E. L., and Humphreys, B. D. (2019). Advantages of single-nucleus over single-cell RNA sequencing of adult kidney: rare cell types and novel cell states revealed in fibrosis. *J. Am. Soc. Nephrol.* 30, 23–32. doi: 10.1681/asn.2018090912

Zeis, T., Graumann, U., Reynolds, R., and Schaeren-Wiemers, N. (2008). Normal-appearing white matter in multiple sclerosis is in a subtle balance between inflammation and neuroprotection. *Brain* 131, 288–303. doi: 10.1093/brain/awm291

Zeis, T., Howell, O. W., Reynolds, R., and Schaeren-Wiemers, N. (2018). Molecular pathology of Multiple Sclerosis lesions reveals a heterogeneous expression pattern of genes involved in oligodendrogliogenesis. *Exp. Neurol.* 305, 76–88. doi: 10.1016/j.expneurol.2018.03.012

Zeisel, A., Muñoz-Manchado, A. B., Codeluppi, S., Lönnerberg, P., La Manno, G., Juréus, A., et al. (2015). Brain structure. Cell types in the mouse cortex and hippocampus revealed by single-cell RNA-seq. *Science* 347, 1138–1142. doi: 10.1126/science.aaa1934

Zheng, G. X., Terry, J. M., Belgrader, P., Ryvkin, P., Bent, Z. W., Wilson, R., et al. (2017). Massively parallel digital transcriptional profiling of single cells. *Nat. Commun.* 8:14049. doi: 10.1038/ncomms14049

Zhong, S., Ding, W., Sun, L., Lu, Y., Dong, H., Fan, X., et al. (2020). Decoding the development of the human hippocampus. *Nature* 577, 531–536. doi: 10.1038/s41586-019-1917-5

Zhou, Y., Song, W. M., Andhey, P. S., Swain, A., Levy, T., Miller, K. R., et al. (2020). Human and mouse single-nucleus transcriptomics reveal TREM2-dependent and TREM2-independent cellular responses in Alzheimer's disease. *Nat. Med.* 26, 131–142. doi: 10.1038/s41591-019-0695-9

Conflict of Interest: The authors declare that the research was conducted in the absence of any commercial or financial relationships that could be construed as a potential conflict of interest.

frontiers in Cellular Neuroscience

ORIGINAL RESEARCH
published: 19 August 2020
doi: 10.3389/fncel.2020.00239

The CNS Myelin Proteome: Deep Profile and Persistence After Post-mortem Delay

*Olaf Jahn[1], Sophie B. Siems[2], Kathrin Kusch[2], Dörte Hesse[1], Ramona B. Jung[2], Thomas Liepold[1], Marina Uecker[1], Ting Sun[2] and Hauke B. Werner[2]**

[1] Proteomics Group, Max Planck Institute of Experimental Medicine, Göttingen, Germany, [2] Department of Neurogenetics, Max Planck Institute of Experimental Medicine, Göttingen, Germany

Myelin membranes are dominated by lipids while the complexity of their protein composition has long been considered to be low. However, numerous additional myelin proteins have been identified since. Here we revisit the proteome of myelin biochemically purified from the brains of healthy c56Bl/6N-mice utilizing complementary proteomic approaches for deep qualitative and quantitative coverage. By gel-free, label-free mass spectrometry, the most abundant myelin proteins PLP, MBP, CNP, and MOG constitute 38, 30, 5, and 1% of the total myelin protein, respectively. The relative abundance of myelin proteins displays a dynamic range of over four orders of magnitude, implying that PLP and MBP have overshadowed less abundant myelin constituents in initial gel-based approaches. By comparisons with published datasets we evaluate to which degree the CNS myelin proteome correlates with the mRNA and protein abundance profiles of myelin and oligodendrocytes. Notably, the myelin proteome displays only minor changes if assessed after a post-mortem delay of 6 h. These data provide the most comprehensive proteome resource of CNS myelin so far and a basis for addressing proteomic heterogeneity of myelin in mouse models and human patients with white matter disorders.

Keywords: oligodendrocyte, myelin proteome, central nervous system (CNS), demyelination, post-mortem delay, autopsy, label-free proteomics, transcriptome

OPEN ACCESS

Edited by:
Nicola B. Hamilton-Whitaker, King's College London, United Kingdom

Reviewed by:
Zsolt Illes, University of Southern Denmark, Denmark
Robert Weissert, University of Regensburg, Germany

****Correspondence:***
Hauke B. Werner
Hauke@em.mpg.de

Specialty section:
This article was submitted to Non-Neuronal Cells, a section of the journal Frontiers in Cellular Neuroscience

Received: *14 May 2020*
Accepted: *07 July 2020*
Published: *19 August 2020*

Citation:
Jahn O, Siems SB, Kusch K, Hesse D, Jung RB, Liepold T, Uecker M, Sun T and Werner HB (2020) The CNS Myelin Proteome: Deep Profile and Persistence After Post-mortem Delay. Front. Cell. Neurosci. 14:239. doi: 10.3389/fncel.2020.00239

INTRODUCTION

In the central nervous system (CNS) of vertebrates, the velocity of nerve conduction is accelerated by the insulation of axons with multiple layers of myelin membrane provided by oligodendrocytes (Nave and Werner, 2014; Snaidero and Simons, 2017). Compared to other cellular membranes myelin is unusually enriched for lipids, in particular cholesterol, galactolipids and plasmalogens (Norton and Poduslo, 1973a; Schmitt et al., 2015; Poitelon et al., 2020). Indeed, the biogenesis of myelin may involve the coalescence of lipid-rich membrane-microdomains in the oligodendroglial secretory pathway (Lee, 2001; Chrast et al., 2011). Notably, the dominant CNS myelin protein, proteolipid protein (PLP), displays a high affinity to cholesterol-rich membrane-microdomains (Simons et al., 2000; Werner et al., 2013). PLP and other cholesterol-associated myelin proteins may thus enhance the coalescence and intracellular traffic of prospective myelin membranes (Schardt et al., 2009). Indeed, both cholesterol and PLP are rate-limiting for myelination, as demonstrated

by the dysmyelination observed in mice lacking oligodendroglial cholesterol synthesis (Saher et al., 2005) or PLP-expression (Yool et al., 2001; Möbius et al., 2008; de Monasterio-Schrader et al., 2013).

As a key stage of myelination, the compaction of adjacent CNS myelin layers requires myelin basic protein (MBP), as evidenced by the complete lack of compact myelin in the CNS of MBP-deficient *shiverer*-mice (Roach et al., 1985). It is now thought that MBP both displaces filamentous actin and cytoskeleton-associated proteins (Nawaz et al., 2015; Zuchero et al., 2015; Snaidero et al., 2017) and saturates negative charges of the headgroups of phosphatidylinositol-4,5-bisphosphate (PIP_2) on the cytoplasmic myelin membrane surfaces (Musse et al., 2008; Nawaz et al., 2009, 2013) thereby pulling together and compacting myelin membranes at the major dense line (Raasakka et al., 2017).

It has been noted already in the early 1970s that PLP and MBP constitute the most abundant CNS myelin proteins. At that time the methods were developed for the enrichment of myelin from nervous tissue by sucrose density gradient centrifugation (Norton and Poduslo, 1973b; Erwig et al., 2019a) separation by one-dimensional (1D)-polyacrylamide gel electrophoresis (SDS-PAGE) and protein staining using Buffalo Black (Morris et al., 1971) Fast Green (Morell et al., 1972) or Coomassie Blue (Magno-Sumbilla and Campagnoni, 1977). Indeed, only few bands were visible that we now know are mainly constituted by PLP, MBP and cyclic nucleotide phosphodiesterase (CNP; Sprinkle et al., 1983). Deficiency of CNP in mice impairs both the ultrastructure of myelin and the long-term preservation of axonal integrity (Lappe-Siefke et al., 2003; Edgar et al., 2009; Patzig et al., 2016; Snaidero et al., 2017).

Evidently, the protein composition of myelin is more complex when considering that various additional myelin proteins have been identified, including myelin associated glycoprotein (MAG; Quarles, 2007; Myllykoski et al., 2018), myelin oligodendrocyte glycoprotein (MOG; Johns and Bernard, 1999; von Büdingen et al., 2015), and claudin 11 (CLDN11; Gow et al., 1999; Denninger et al., 2015). This insight motivated attempts to utilize the emerging mass spectrometric techniques to approach all myelin proteins at once, thereby covering the entire myelin proteome. Indeed, purified myelin is suited for systematic assessment of its molecular constituents (De Monasterio-Schrader et al., 2012; Gopalakrishnan et al., 2013). Most early approaches involved 2D-gels (Taylor et al., 2004; Vanrobaeys et al., 2005; Werner et al., 2007), soon to be complemented by gel-free shotgun-approaches (Vanrobaeys et al., 2005; Roth et al., 2006; Dhaunchak et al., 2010) and hybrid workflows (Ishii et al., 2009). However, first systematic information on the relative abundance of myelin proteins was achieved by label-free quantification involving peptide-separation by liquid chromatography (LC) coupled to detection with quadrupole time-of-flight (QTOF) mass spectrometery (MS) (Jahn et al., 2009) or by chemical peptide labeling with isobaric tags for relative and absolute quantitation (iTRAQ) and subsequent LC-MS-analysis (Manrique-Hoyos et al., 2012). A meta-analysis of the approaches to the myelin proteome published by 2012 is available (De Monasterio-Schrader et al., 2012). Since then, label-free protein quantification by LC-MS has proven useful in the differential analysis of myelin in mouse models including mice lacking PLP, CNP, or MAG (Patzig et al., 2016). For example, this approach allowed identifying cytoskeletal septin filaments to stabilize the ultrastructure of CNS myelin, thereby preventing the formation of pathological myelin outfoldings (Patzig et al., 2016; Erwig et al., 2019b).

The intention of this work was to both establish an updated comprehensive compendium of the proteins associated with CNS myelin and to accurately quantify their relative abundance, as recently achieved for the proteome of myelin in the peripheral nervous system (Siems et al., 2020). To this aim we combined various gel-based and gel-free proteomic techniques. In particular, we used nano-flow ultra-performance liquid chromatography (nanoUPLC) for peptide separation and an ion mobility-enabled QTOF-system for label-free protein quantification by data-independent acquisition (DIA) mass spectrometry in an alternating low and elevated energy mode (MS^E). While the MS^E-mode allows quantifying myelin proteins with the required dynamic range of over four orders of magnitude, an ion mobility-enhanced version thereof [referred to as ultra-definition (UD)-MS^E] covers about twice as many myelin-associated proteins, though at the expense of dynamic range. Our workflow thus facilitates both to reliably quantify the exceptionally abundant PLP, MBP, and CNP and to appreciate the complexity of low-abundant myelin constituents.

MATERIALS AND METHODS

Animals

Male c57BL/6N wild-type mice at postnatal day 75 (P75) were used for all experiments except for the differential analysis of myelin purified from brains immediately frozen after dissection compared to a post-mortem delay of 6 h at room temperature (**Figure 4**), for which female c57BL/6N wild-type mice at P56 were used. Mice were bred and kept in the animal facility of the Max Planck Institute of Experimental Medicine and sacrificed by cervical dislocation. For the procedure of sacrificing mice for subsequent preparation of tissue, all regulations given in the German animal protection law (TierSchG §4) are followed. Since sacrificing of rodents is not an experiment on animals according to §7 Abs. 2 Satz 3 TierSchG, no specific authorization or notification is required for the present work.

Myelin Purification

A myelin-enriched light-weight membrane fraction was biochemically purified from mouse brains by sucrose density centrifugation and osmotic shocks as recently described in detail (Erwig et al., 2019a). Mice were sacrificed by cervical dislocation at the indicated ages as three biological replicates per condition ($n = 3$). Protein concentration was determined using the DC Protein Assay Kit (Bio-Rad). Initial quality control by gel electrophoresis and silver staining of gels was performed as described (de Monasterio-Schrader et al., 2013; Joseph et al., 2019). Briefly, samples were separated on a 12% SDS-PAGE gel

(1 h at 200 V) using the Bio-Rad system, fixated overnight in 10% [v/v] acetic acid and 40% [v/v] ethanol and then washed in 30% ethanol (2 × 20 min) and ddH_2O (1 × 20 min). For sensitization, gels were incubated 1 min in 0.012% [v/v] $Na_2S_2O_3$ and subsequently washed with ddH_2O (3 × 20 s). For silver staining, gels were impregnated for 20 min in 0.2% [w/v] $AgNO_3$/0.04% formaldehyde, washed with ddH_2O (3 × 20 s) and developed in 3% [w/v] Na_2CO_3/0.04% [w/v] formaldehyde. The reaction was stopped by exchanging the solution with 5% [v/v] acetic acid.

Gel-Based Proteome Analysis of Myelin

Gel-electrophoretic separation of myelin proteins with different pre-cast gel systems (Serva) was performed essentially as recently described in detail (Erwig et al., 2019a). Briefly, 1D separations were performed with 5 μg protein load before (pre-wash) or after (post-wash) subjecting myelin to consecutive high-salt and high-pH washing/centrifugation cycles as previously described (Werner et al., 2007; Jahn et al., 2013). Automated tryptic in-gel digestion of proteins in gel bands (Schmidt et al., 2013) and protein identification by LC-MS was performed as described (Ott et al., 2015). For 2D separations, myelin was first delipidated by methanol/chloroform precipitation and 300 μg protein was loaded on a 24 cm immobilized non-linear pH-gradient 3-12 strip (Serva) by active rehydration (Erwig et al., 2019a). Automated tryptic in-gel digestion of proteins in gel spots and protein identification by MALDI-TOF mass spectrometry was performed as described (Jahn et al., 2006; Werner et al., 2007).

Label-Free Quantification of Myelin Proteins

In-solution digestion of myelin proteins according to an automated filter-aided sample preparation (FASP) protocol (Erwig et al., 2019a) and LC-MS-analysis by different MS^E-type data-independent acquisition (DIA) mass spectrometry approaches was performed as recently established for PNS myelin (Siems et al., 2020). Briefly, protein fractions corresponding to 10 μg myelin protein were dissolved in lysis buffer (1% ASB-14, 7 M urea, 2 M thiourea, 10 mM DTT, 0.1 M Tris pH 8.5) and processed according to a CHAPS-based FASP protocol in centrifugal filter units (30 kDa MWCO, Merck Millipore). After removal of the detergents, protein alkylation with iodoacetamide, and buffer exchange to digestion buffer [50 mM ammonium bicarbonate (ABC), 10% acetonitrile], proteins were digested overnight at 37°C with 400 ng trypsin. Tryptic peptides were recovered by centrifugation and extracted with 40 μl of 50 mM ABC and 40 μl of 1% trifluoroacetic acid (TFA), respectively. Combined flow-through were directly subjected to LC-MS-analysis. For quantification according to the TOP3 approach (Silva et al., 2006), aliquots were spiked with 10 fmol/μl of yeast enolase-1 tryptic digest or Hi3 EColi standard (Waters Corporation), the latter containing a set of quantified synthetic peptides derived from *E. coli*. Chaperone protein ClpB.

Nanoscale reversed-phase UPLC separation of tryptic peptides was performed with a nanoAcquity UPLC system equipped with a Symmetry C18 5 μm, 180 μm × 20 mm trap column and a HSS T3 C18 1.8 μm, 75 μm × 250 mm analytical column (Waters Corporation) maintained at 45°C. Peptides were separated over 120 min at a flow rate of 300 nl/min with a gradient comprising two linear steps of 3–35% mobile phase B (acetonitrile containing 0.1% formic acid) in 105 min and 35–60% mobile phase B in 15 min, respectively. Mass spectrometric analysis of tryptic peptides was performed using a Synapt G2-S QTOF mass spectrometer equipped with ion mobility option (Waters Corporation). $UDMS^E$ analysis was performed in the ion mobility-enhanced data-independent acquisition mode with drift time-specific collision energies as described in detail (Distler et al., 2014a, 2016). Continuum LC-MS data were processed using Waters ProteinLynx Global Server (PLGS) and searched against a custom database compiled by adding the sequence information for yeast enolase 1, *E. coli* Chaperone protein ClpB and porcine trypsin to the UniProtKB/Swiss-Prot mouse proteome and by appending the reversed sequence of each entry to enable the determination of false discovery rate (FDR). Precursor and fragment ion mass tolerances were automatically determined by PLGS and were typically below 5 ppm for precursor ions and below 10 ppm (root mean square) for fragment ions. Carbamidomethylation of cysteine was specified as fixed and oxidation of methionine as variable modification. One missed trypsin cleavage was allowed. Minimal ion matching requirements were two fragments per peptide, five fragments per protein, and one peptide per protein. The FDR for protein identification was set to 1% threshold.

For post-identification analysis including TOP3 quantification of proteins, the freely available software ISOQuant[1] was used (Kuharev et al., 2015). Only peptides with a minimum length of seven amino acids that were identified with scores above or equal to 5.5 in at least two runs were considered. FDR for both peptides and proteins was set to 1% threshold and only proteins reported by at least two peptides (one of which unique) were quantified as parts per million (ppm) abundance values (i.e., the relative amount (w/w) of each protein in respect to the sum over all detected proteins). The Bioconductor R packages "limma" and "*q*-value" were used to detect significant changes in protein abundance by moderated t-statistics as described (Ambrozkiewicz et al., 2018; Siems et al., 2020). For proteome profiling of wild-type myelin by MS^E and $UDMS^E$, three independent experiments were performed, each with three biological replicates and sample processing with duplicate digestion and injection, resulting in a total of 12 LC-MS runs per experiment. Abundance values in ppm are given as averages of the four technical replicates per biological replicate and only proteins quantified in at least two out of three experiments are reported in the proteome resource (**Supplementary Table S1**). Proteins identified as contaminants from blood (albumin, hemoglobin) or hair cells (keratins) were removed from the list. Proteome profiling comparing wild-type myelin without and with post-mortem delay (**Figure 4** and **Supplementary Table S2**) was performed with three biological replicates and duplicate digestion, resulting in a total of 6 LC-MS runs per condition. Data acquisition was performed in the DRE-$UDMS^E$ mode

[1] www.isoquant.net

(Siems et al., 2020) i.e., a deflection device was cycled between full (100% for 0.4 s) and reduced (5% for 0.4 s) ion transmission during one 0.8 s full scan, thereby providing a compromise between identification rates and dynamic range.

Interpretation of Single-Cell Resolution Transcriptome Data

Published single-cell RNA-sequencing (scRNA-seq) gene expression matrices from datasets GSE60361 (Zeisel et al., 2015), GSE75330 (Marques et al., 2016), and GSE113973 (Falcão et al., 2018), were obtained from Gene Expression Omnibus (GEO) and analyzed using R package Seurat v3.1.0 (Butler et al., 2018; Stuart et al., 2019). Mature oligodendrocyte cell populations were selected from each dataset as specified in the results section and normalized gene counts were used for calculating average expression profiles across single cells. Bulk proteome and transcriptome datasets specified in the results section were used as supplied in the **Supplementary Tables** to the respective publications.

Deposition, Visualization and Analysis of Proteomic Data

The mass spectrometry proteomics data have been deposited to the ProteomeXchange Consortium via the PRIDE (Perez-Riverol et al., 2019) partner repository with dataset identifier PXD020007. Pie chart, scatter plots, volcano plot and heatmap were prepared in Microsoft Excel 2013 and GraphPad Prism 8. Area-proportional Venn diagrams were prepared using BioVenn (Hulsen et al., 2008)[2]. Trans-membrane domains were predicted using TMHMM Server v. 2.0 (Krogh et al., 2001)[3] and Phobius (Käll et al., 2007)[4].

RESULTS

Proteome Analysis of CNS Myelin

To purify CNS myelin, we applied an established protocol (Erwig et al., 2019a) to prepare a light-weight membrane fraction from the brains of healthy c57Bl/6N-mice at P75. Aiming to systematically identify myelin-associated proteins we used five complementary approaches as summarized in **Figure 1A**. As the most straightforward way of preparing myelin for proteomic analysis, we separated proteins by 1D-SDS-PAGE and sectioned the lane into 24 equally sized slices (**Figure 1B**), which we subjected to automated tryptic in-gel digest followed by LC-MS-analysis, thereby identifying 788 proteins (**Supplementary Table S1**). When we subjected myelin to an additional washing step of high-pH and high-salt conditions (**Figure 1B**) to deplete soluble and peripheral membrane proteins before 1D-SDS-PAGE-separation and mass spectrometry, we identified 521 proteins (**Supplementary Table S1**). To establish a reference map of myelin proteins including proteoforms, we increased the resolving power of protein separation by subjecting myelin to 2D-gel electrophoresis with isoelectric focusing (IEF) in the first and horizontal SDS-PAGE in the second dimension (**Figure 1C**). We stained the comprised proteins with colloidal Coomassie (CBB250), picked CBB250-labeled gel-plugs (i.e., protein spots) for automated tryptic in-gel digestion and identified the proteins by peptide mass fingerprint (PMF) and MS/MS-fragment ion mass spectra, both acquired on a MALDI-TOF mass spectrometer. We identified 181 non-redundant proteins from 352 spots (**Supplementary Table S1**). Thereby we expanded our previous myelin protein map (131 non-redundant proteins from 217 spots, Werner et al., 2007), mainly owing to increased resolution in the first dimension by utilizing longer IEF-strips with a wider pH-range (Erwig et al., 2019a). When comparing the proteins identified using the three gel-based approaches we found a total of 930 proteins with a fair overlap (**Figure 1D**).

Considering that contemporary gel-free, label-free proteomic approaches allow the simultaneous identification and quantification of proteins (Neilson et al., 2011; Distler et al., 2014b) we subjected myelin to a workflow of solubilization using ASB-14 and high-urea conditions, automated tryptic in-solution digest by filter-aided sample preparation (FASP), fractionation of peptides by nanoUPLC, and ESI-QTOF mass spectrometry. This workflow was recently established for peripheral myelin (Siems et al., 2020). Importantly, the utilized data-independent acquisition (DIA)-strategy with data acquisition in the MS^E-mode allows the simultaneous quantification and identification of all peptides entering the mass spectrometer, and thereby, when signal intensities are correlated with a spike protein of known concentration (TOP3 method; Silva et al., 2006; Ahrné et al., 2013) the reliable quantification of proteins based on peptide intensities. When subjecting myelin to LC-MS-analysis using MS^E we quantified 393 proteins (**Supplementary Table S1**; labeled in orange in **Figure 1E**) with a false discovery rate (FDR) of <1% and an average sequence coverage of 38.6%. Notably, MS^E quantitatively covered myelin proteins with a dynamic range of over four orders of magnitude parts per million (ppm), thereby allowing quantification of the exceptionally abundant PLP and MBP. When using the ultra-definition (UD)-MS^E-mode, in which the ion mobility option provides an orthogonal dimension of peptide separation after liquid chromatography and before mass measurement, we identified and quantified 809 proteins (**Supplementary Table S1**; labeled in blue in **Figure 1E**) with an average sequence coverage of 35.0%. $UDMS^E$ thus identified about twice as many proteins as MS^E. However, the larger number of proteins identified by $UDMS^E$ went along with a compressed dynamic range of about three orders of magnitude ppm, which is insufficient to reliably quantify the most abundant myelin constituents including PLP, MBP, and CNP. The data acquisition mode-dependent differences in both numbers of quantified proteins and dynamic range are best explained by $UDMS^E$ achieving more efficient precursor-fragment ion alignment and precursor fragmentation upon ion mobility separation of peptides (Distler et al., 2014a, 2016) which causes a ceiling effect for the detection of exceptionally intense peptide signals and thus a compressed dynamic range as previously observed for PNS myelin (Siems et al., 2020).

[2]https://www.biovenn.nl/

[3]www.cbs.dtu.dk/services/TMHMM

[4]http://phobius.sbc.su.se/

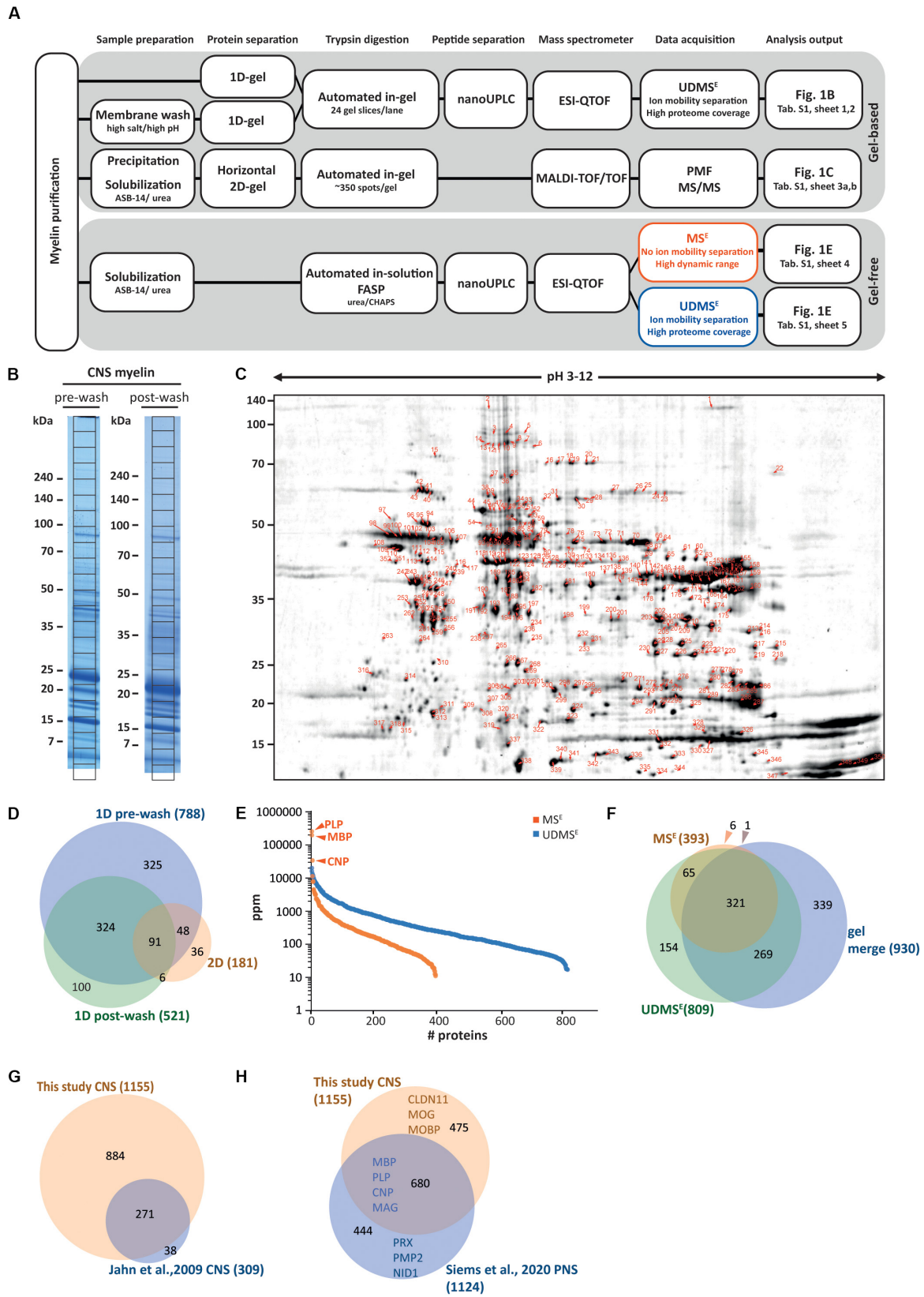

FIGURE 1 | Continued

FIGURE 1 | Proteome analysis of CNS myelin. **(A)** Schematic illustration of the gel-based (top) and gel-free (bottom) proteomic workflow to approach CNS myelin purified from the brains of wild-type c57Bl/6N mice dissected at P75. Note that gel-free proteome analysis enables largely automated sample processing and omits labor-intense gel-electrophoresis, thus reducing hands-on time. **(B)** One-dimensional gel-separation of CNS myelin. Myelin was separated by SDS-PAGE without (pre-wash) or upon (post-wash) depleting soluble and peripheral membrane proteins by an additional step of high-pH and high-salt conditions. Proteins were visualized with colloidal Coomassie (CBB250). The denoted grid subdivides each lane into 24 equally sized slices, which were excised for automated tryptic digest, peptide separation by nanoUPLC and data acquisition using an ESI-QTOF mass spectrometer, thereby identifying 788 (pre-wash) and 521 (post-wash) proteins, respectively (see **Supplementary Table S1**). **(C)** Two-dimensional gel-separation of CNS myelin. Myelin was two-dimensionally separated using a 2D-IEF/SDS-PAGE with isoelectric focusing (IEF) in a 24 cm gel strip with nonlinear pH-gradient (pH 3–12) as the first and 10–15% acrylamide gradient SDS-PAGE (25.5 × 20 cm, gel thickness 0.65 mm) as the second dimension. Proteins were visualized by colloidal Coomassie staining; protein spots were excised, subjected to automated tryptic in-gel digestion and MALDI-TOF mass spectrometry, thereby identifying 181 non-redundant proteins from 352 spots (**Supplementary Table S1**). **(D)** Venn diagram comparing the number of proteins identified in CNS myelin by the three gel-based approaches. **(E)** Number and relative abundance of proteins identified in myelin purified from the brains of wild-type mice using two gel-free data acquisition modes (MS^E, $UDMS^E$). Note that MS^E (orange) identifies comparatively fewer proteins in purified myelin but provides a dynamic range of more than four orders of magnitude. $UDMS^E$ (blue) identifies a larger number of proteins but provides a dynamic range of only about three orders of magnitude. Note that the dynamic range of MS^E is required for the quantification of the exceptionally abundant myelin proteins proteolipid protein (PLP), myelin basic protein (MBP) and cyclic nucleotide phosphodiesterase (CNP). Samples were analyzed in three biological replicates with four technical replicates each (duplicate digestion and injection). For datasets see **Supplementary Table S1**. ppm, parts per million. **(F)** Venn diagram comparing the number of proteins identified in CNS myelin by MS^E, $UDMS^E$ and gel-based approaches. **(G)** Venn diagram of the proteins identified in CNS myelin in this study compared with those identified in a previous approach (Jahn et al., 2009). **(H)** Venn diagram comparing the proteins identified in CNS myelin in this study with those previously identified in PNS myelin (Siems et al., 2020). Selected marker proteins are denoted.

When comparing the proteins identified by MS^E, $UDMS^E$ and gel-based approaches we found a reasonably high overlap (**Figure 1F**). Comparison of the 1155 proteins identified in CNS myelin in the present study with those 309 identified >10 years ago with the methodological standards of that time (Jahn et al., 2009) shows a remarkably high overlap as well as an about three-fold increase in the number of identified proteins (**Figure 1G**). Notwithstanding that a number of the identified proteins will originate from other cellular sources that contaminate purified myelin, we believe that many of them are indeed low-abundant constituents of the non-compact compartments of myelin.

A comparison of the proteins identified in CNS myelin with the recently established PNS myelin proteome (Siems et al., 2020) confirms that numerous proteins are present in both, but also that many proteins were identified exclusively in either CNS or PNS myelin (**Figure 1H**). Together, the evolving technical standards of in-solution sample preparation and MS^E-type DIA mass spectrometry allows to comprehensively identify and quantify proteins in myelin. However, only MS^E (but not $UDMS^E$) provides a dynamic range suited to address the relative abundance of the exceptionally abundant PLP, MBP, and CNP. As importantly, the evolution of gel-free methods shifts the major workload in myelin proteome analysis from manual sample handling to data analysis, with much less hands-on time required when compared to gel-based approaches.

Relative Abundance of CNS Myelin Proteins

As MS^E provides the best possible dynamic range (**Figure 1E**), we evaluated the relative abundance of all 393 proteins identified in myelin by MS^E (**Figure 2** and **Supplementary Table S1**). As per this dataset PLP constitutes 38% of the total myelin protein [±1% relative standard deviation (RSD)]. MBP, CNP, and MOG constitute 30% (±1%), 5% (±0.2%), and 1% (±0.03%) of the total myelin protein, respectively (**Figure 2**). However, the present assessment of CNS myelin by MS^E extends well beyond the most abundant myelin constituents, thus quantifying known myelin proteins including the tetraspan-proteins CLDN11, CD81, TSPAN2, PLLP, CD9, CD82, GPM6B, and GJC3, the immunoglobulin-domain containing cell-surface proteins MAG, NFASC, CNTN1, RTN4, CNTN2, CADM4, HEPACAM, JAM3, CD47, and OMG, the enzymes SIRT2, CA2, and ASPA, the cytoskeletal and cytoskeleton-associated proteins TUBB4, SEPT2, SEPT4, SEPT7, SEPT8, TPPP, ANLN, GSN, CFL1, and PADI2 as well as MOBP, BCAS1, NDRG1, opalin, and CRYAB (**Figure 2**). By MS^E, 46 known myelin proteins account for approximately 80% of the total myelin protein (**Figure 2**). The remaining 27% is constituted by 347 proteins not yet validated as myelin constituents by independent methods.

Comparison to Related Datasets

An increasing number of studies provides mRNA or protein abundance profiles of myelin or oligodendrocytes. To systematically compare the CNS myelin proteome with these profiles, we correlated our MS^E-dataset (**Figure 2** and **Supplementary Table S1**) via the gene name entries with related datasets for which quantitative information is publicly available (**Figure 3**).

We first plotted the present MS^E and $UDMS^E$-datasets (**Supplementary Table S1**) against each other (**Figure 3A**). Considering that the same starting material has been assessed it is not unexpected that the datasets correlate well, as reflected by a correlation coefficient of 0.90 (**Figure 3A**). Most visibly diverging from the linear regression line are the most abundant myelin proteins PLP, MBP, CNP, MOG, and CLDN11, reflecting that the dynamic range of $UDMS^E$ is compressed in the high ppm-range compared to that of MS^E (also see **Figure 1E**). We then compared the present MS^E-dataset with an independent myelin proteome dataset previously established by MS^E (Jahn et al., 2009). We calculated a somewhat lower correlation coefficient of 0.74 (**Figure 3B**), probably owing to the previous use of a predecessor mass spectrometer generation that provided a considerably lower dynamic range. Yet, in conjunction with the high overlap

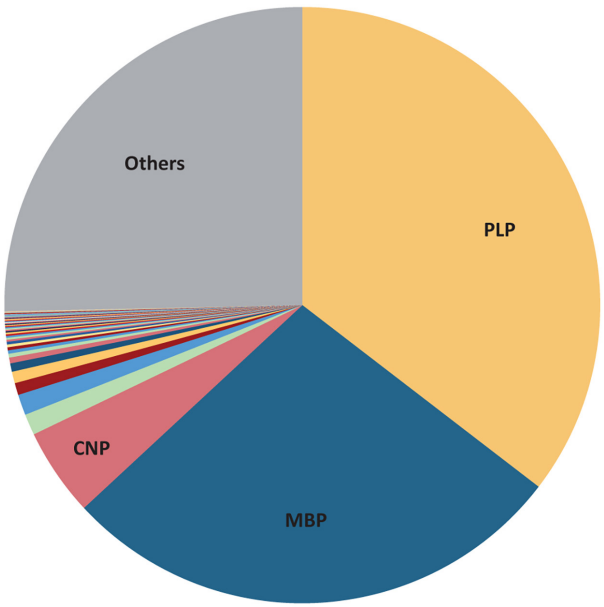

Protein	% (+/- RSD)		Protein	% (+/- RSD)	
PLP1	37,91	0,91	CD9	0,06	0,03
MBP	29,60	0,95	EPB41L2	0,06	0,01
CNP	5,11	0,21	CD82	0,06	0,01
MOG	1,22	0,03	GSN	0,05	0,01
CLDN11	1,20	0,13	CNTN2	0,05	0,00
MOBP	0,70	0,13	CADM4	0,05	0,00
MAG	0,67	0,05	ENPP6	0,05	0,01
SIRT2	0,49	0,03	EPB41L3	0,04	0,00
CD81	0,33	0,073	LGI3	0,04	0,00
TUBB4	0,23	0,051	CFL1	0,04	0,01
BCAS1	0,20	0,02	GPM6B	0,04	0,01
NFASC	0,18	0,01	PADI2	0,04	0,00
CNTN1	0,16	0,02	HEPACAM	0,04	0,01
CA2	0,16	0,03	SEPT2	0,03	0,00
RTN4	0,11	0,02	JAM3	0,03	0,00
SEPT8	0,11	0,02	CD47	0,03	0,01
TSPAN2	0,10	0,02	TPPP3	0,03	0,00
ASPA	0,10	0,07	GPR37	0,03	0,00
SEPT7	0,10	0,01	OPALIN	0,03	0,01
TPPP	0,08	0,01	OMG	0,02	0,01
PLLP	0,08	0,01	GJC3	0,02	0,00
NDRG1	0,08	0,01	CRYAB	0,02	0,00
ANLN	0,07	0,01	Others	27,1	
SEPT4	0,06	0,01			

FIGURE 2 | Relative abundance of CNS myelin proteins. Pie chart of the MS^E dataset shown in **Figure 1E** and **Supplementary Table S1**. The relative abundance of known myelin proteins is given as percent with relative standard deviation (% ±RSD). Note that known myelin proteins constitute approximately 73% of the total myelin protein; proteins so far not independently validated as myelin proteins constitute about 27%.

between the proteins identified in the present and the previous study (Jahn et al., 2009) (**Figure 1G**), myelin proteome analysis emerges as fairly robust across independently purified starting material and different generations of mass spectrometers. We next compared the MS^E-dataset to the proteome of acutely isolated O4-immunopositive oligodendrocytes (**Figure 3C**) as determined by label-free quantification (LFQ) using data-dependent acquisition (DDA) on an orbitrap mass spectrometer and MaxQuant-software (Sharma et al., 2015). The O4-antibody preferentially immunolabels oligodendrocytes at the progenitor (OPC) and pre-myelinating stages (Sommer and Schachner, 1981; Bansal et al., 1989; Goldman and Kuypers, 2015); the correlation coefficient was calculated as 0.16 (**Figure 3C**). A correlation coefficient of 0.02 (**Figure 3D**) was found when comparing the MS^E-dataset with the LFQ-intensity profile of O1-immunopositive primary oligodendrocytes after 4 days *in vitro* (DIV) (Sharma et al., 2015). The myelin proteome as determined here is thus more closely related to the proteome of acutely isolated O4-immunopositive oligodendrocytes than to that of O1-immunopositive primary oligodendrocytes 4 DIV.

We then compared the MS^E-dataset with various available mRNA-abundance profiles. When comparing the MS^E-dataset to the transcriptome of purified CNS myelin as determined by RNA-seq (Thakurela et al., 2016) we calculated a correlation coefficient of 0.27 (**Figure 3E**). Interestingly, the comparison between the MS^E-dataset and the RNA-seq-based transcriptome of oligodendrocytes immunopanned from the cortex using antibodies against MOG (Zhang et al., 2014) revealed a roughly comparable correlation coefficient of 0.31 (**Figure 3F**). Notably, MOG-immunopositivity labels myelinating oligodendrocytes, implying that the stage of oligodendrocyte differentiation must be considered when judging dataset correlations. It is thus not surprising that a somewhat lower correlation coefficient of 0.10 (**Figure 3G**) was calculated when comparing the MS^E-dataset with the RNA-seq-based transcriptome of acutely isolated $O4^+$-oligodendrocytes (Sharma et al., 2015). Finally, we compared the MS^E-dataset to several scRNA-seq-based transcriptome datasets (Zeisel et al., 2015; Marques et al., 2016; Falcão et al., 2018). To this aim we calculated the mean transcript abundance as average count reads per unique molecular identifier (UMI) of the cells in those clusters that reflect mature oligodendrocytes. When comparing the MS^E-dataset to mature oligodendrocytes sorted from the mouse cortex and hippocampus [all 484 cells in clusters Oligo5 and Oligo6 in Zeisel et al. (2015)], we find a correlation coefficient of 0.24 (**Figure 3H**). Importantly, we find a roughly similar correlation coefficient when comparing the MS^E-dataset to mature oligodendrocytes sorted from 10 regions of the mouse CNS [all 2748 cells in clusters MOL1–MOL6 in Marques et al. (2016)] (**Figure 3I**) or to mature oligodendrocytes sorted from the spinal cord of mice [all 617 cells in clusters MOL2-Ct and MOL5/6-Ct in Falcão et al. (2018)] (**Figure 3J**).

Together, when judging correlations between large datasets evaluating mRNA and protein abundance profiles of oligodendrocytes and myelin, aspects to be considered include the method of sample preparation, the stage of oligodendrocyte differentiation and the methodology of analysis. Yet, roughly similar correlation coefficients were calculated when comparing the myelin proteome with various proteomic and transcriptomic approaches to the molecular profiles of oligodendrocytes.

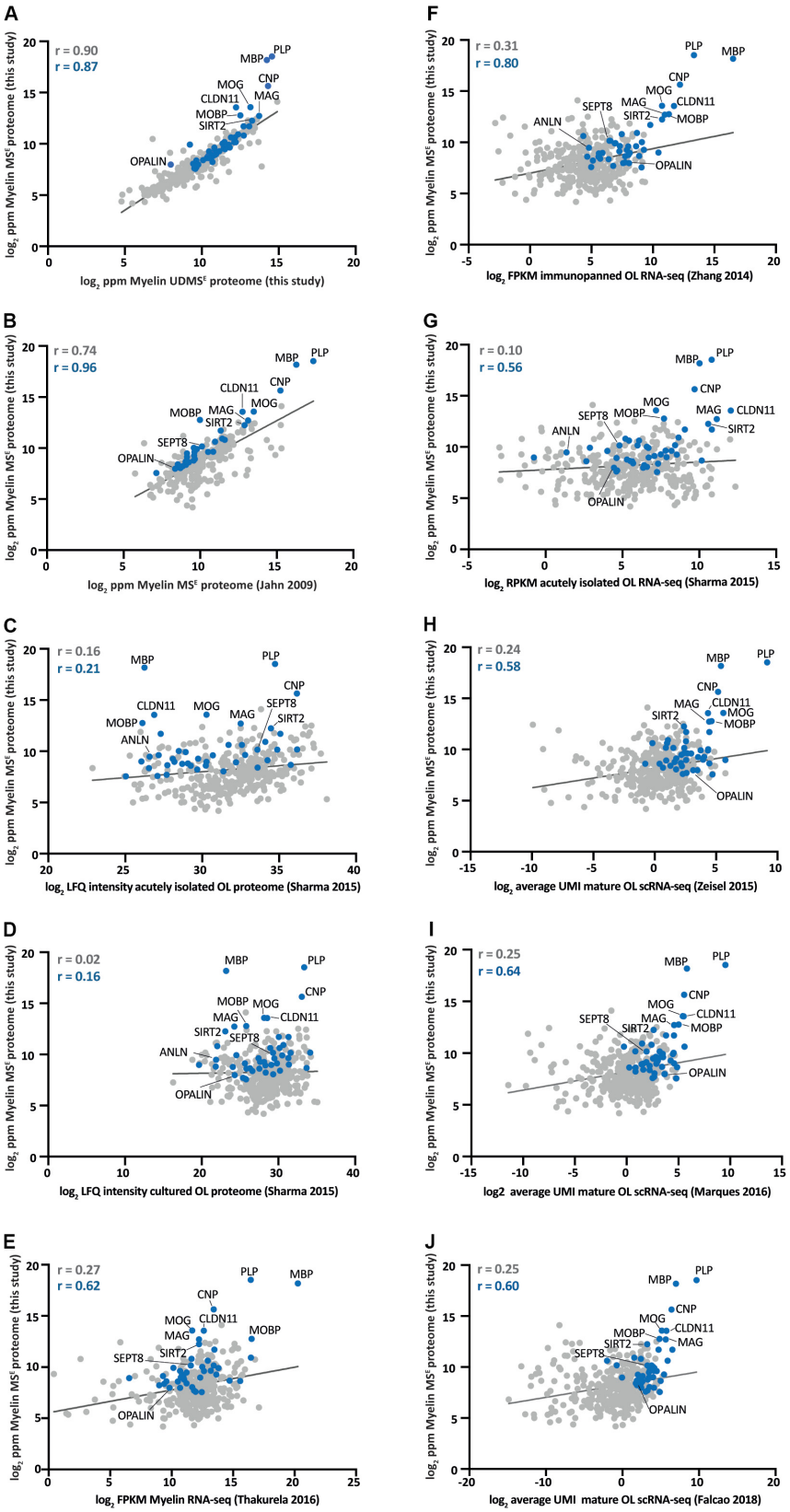

FIGURE 3 | Continued

FIGURE 3 | Comparison of the myelin proteome with proteome and transcriptome profiles of myelin and oligodendrocytes. **(A)** Log_2-transformed relative abundance of the proteins identified in myelin in this study by MS^E plotted against their log_2-transformed relative abundance as quantified by $UDMS^E$. Data points representing known myelin proteins as specified in **Figure 2** are labeled in blue; all other data points in gray. The correlation coefficient (*r*) was calculated for all proteins identified by MS^E (displayed in gray) and specifically for the known myelin proteins (given in blue). The regression line is plotted for orientation. ppm, parts per million. **(B)** Same as **(A)** but plotted against the myelin proteome as previously assessed by MS^E (Jahn et al., 2009). **(C)** Same as **(A)** but plotted against the proteome of acutely isolated O4-immunopositive oligodendrocytes (Sharma et al., 2015). LFQ, label-free quantification. **(D)** Same as **(A)** but plotted against the proteome of O1-immunopositive primary oligodendrocytes cultured for 4 days *in vitro* (DIV) (Sharma et al., 2015). **(E)** Same as **(A)** but plotted against the RNA-seq-based transcriptome of myelin purified from the brains of mice (Thakurela et al., 2016). FPKM, fragments per kilobase of exon model per million reads mapped. **(F)** Same as **(A)** but plotted against the RNA-seq-based transcriptome of oligodendrocytes immunopanned using MOG-specific antibodies (Zhang et al., 2014). **(G)** Same as **(A)** but plotted against the RNA-seq-based transcriptome of acutely isolated O4-immunopositive oligodendrocytes (Sharma et al., 2015). RPKM, reads per kilobase per million mapped reads. **(H)** Same as **(A)** but plotted against the scRNA-seq-based transcriptome of mature oligodendrocytes in the mouse cortex and hippocampus [mean of all 484 cells in clusters Oligo5 and Oligo6 in Zeisel et al. (2015)]. UMI, unique molecular identifiers. **(I)** Same as **(A)** but plotted against the scRNA-seq-based transcriptome of mature oligodendrocytes in 10 regions of the mouse CNS [mean of all 2748 cells in clusters OL1 – OL6 in Marques et al. (2016)]. **(J)** Same as **(A)** but plotted against the scRNA-seq-based transcriptome of mature oligodendrocytes in the mouse spinal cord [mean of all 617 cells in clusters MOL2-Ct and MOL5/6-Ct in Falcão et al. (2018)].

Persistence of the Myelin Proteome Upon Post-mortem Delay

Autopsy material from human patients and healthy-appearing controls is increasingly evaluated by systematic molecular profiling, as exemplified by the recent snRNA-seq-based assessment of oligodendroglial transcriptional profiles in multiple sclerosis patients (Jäkel et al., 2019). Notably, the use of autopsy material involves a post-mortem delay between the death of a subject and the collection of a biopsy. However, post-mortem delay may affect sample integrity and thus data validity. Considering that proteomic analysis of myelin in mice is usually performed upon freezing of samples immediately after dissection, we asked whether the myelin proteome can also be assessed upon post-mortem delay. We thus purified myelin from the brains of c57Bl/6N-mice to compare the myelin proteome between mice after a post-mortem delay of 6 h at room temperature with that of mice upon sample freezing immediately after dissection. Upon SDS-PAGE-separation and silver staining, no signs of major degradation were evident and the band patterns appeared essentially similar (**Figure 4A**). We next subjected myelin to routine differential proteome profiling by $UDMS^E$ with dynamic range enhancement (DRE-$UDMS^E$) (**Supplementary Table S2**). Using this data acquisition mode with intermediate features as to identification rates and dynamic range (for methodological details see Siems et al., 2020) we found that known myelin proteins displayed only minor differences as visualized in a volcano plot (red data points in **Figure 4B**) and a heatmap (**Figure 4C**). Indeed, no known myelin protein exceeded the threshold of a log_2-fold transformed fold-change (FC) of $-1/+1$, i.e., a 2-fold increased or 0.5-fold diminished relative abundance. Together, the myelin proteome displays only minor changes upon a post-mortem delay of 6 h, implying that proteomic assessment of myelin purified from autopsy samples appears feasible.

DISCUSSION

Understanding the molecular complexity of the nervous system involves molecular profiling of cells and cellular specializations including myelin. Here we combined various proteomic approaches for comprehensive coverage of the CNS myelin proteome and identified 1155 proteins in myelin biochemically purified from the brains of mice. We note that gel-based methods involving separation at the protein level facilitated a slightly higher identification rate compared to gel-free methods comprising *in situ*-digestion of the entire proteome, likely because of the pre-fractionation effect inherent to the former. On the other hand, gel-free data acquisition by $UDMS^E$ also enabled deep qualitative coverage while necessitating considerably less input material and manual sample handling.

Importantly, the MS^E-data acquisition mode covered a dynamic range of over four orders of magnitude of protein abundance. Indeed, compared to a previous approach (Jahn et al., 2009) the technical advancements implemented in the current mass spectrometer generation now allow reliable quantification of myelin proteins spanning from the exceptionally abundant PLP and MBP to low-abundant constituents including oligodendrocyte myelin glycoprotein (OMG) (Wang et al., 2002), oligodendrocytic myelin paranodal and inner loop protein (OPALIN) (Golan et al., 2008; Kippert et al., 2008) and the G-protein coupled receptor GPR37 (Yang et al., 2016). For PLP, MBP and CNP our quantification is in accordance with but specifies prior estimates based on 1D-gel separation and various protein staining techniques, in which they were proposed to constitute 30–45%, 22–35%, and 4–15% of the total myelin protein, respectively (Morell et al., 1972, 1973; Banik and Smith, 1977; Deber and Reynolds, 1991). Notably, it also shifts our previous MS^E-based estimates for PLP and MBP (Jahn et al., 2009) toward higher relative abundance, with the lower dynamic range of the mass spectrometers at that time being the most likely reason for the former under-quantification. It is not surprising that PLP, MBP, and CNP have overshadowed less abundant myelin constituents in initial gel-based approaches when considering the exceptional dynamic range of the relative abundance of myelin proteins. Together, the myelin proteome provided here provides an updated comprehensive compendium and re-adjusts the relative abundance of CNS myelin proteins.

Do true myelin proteins exist that escape proteomic identification? As exemplified by myelin and lymphocyte protein (MAL) (Schaeren-Wiemers et al., 2004), the tryptic digest of

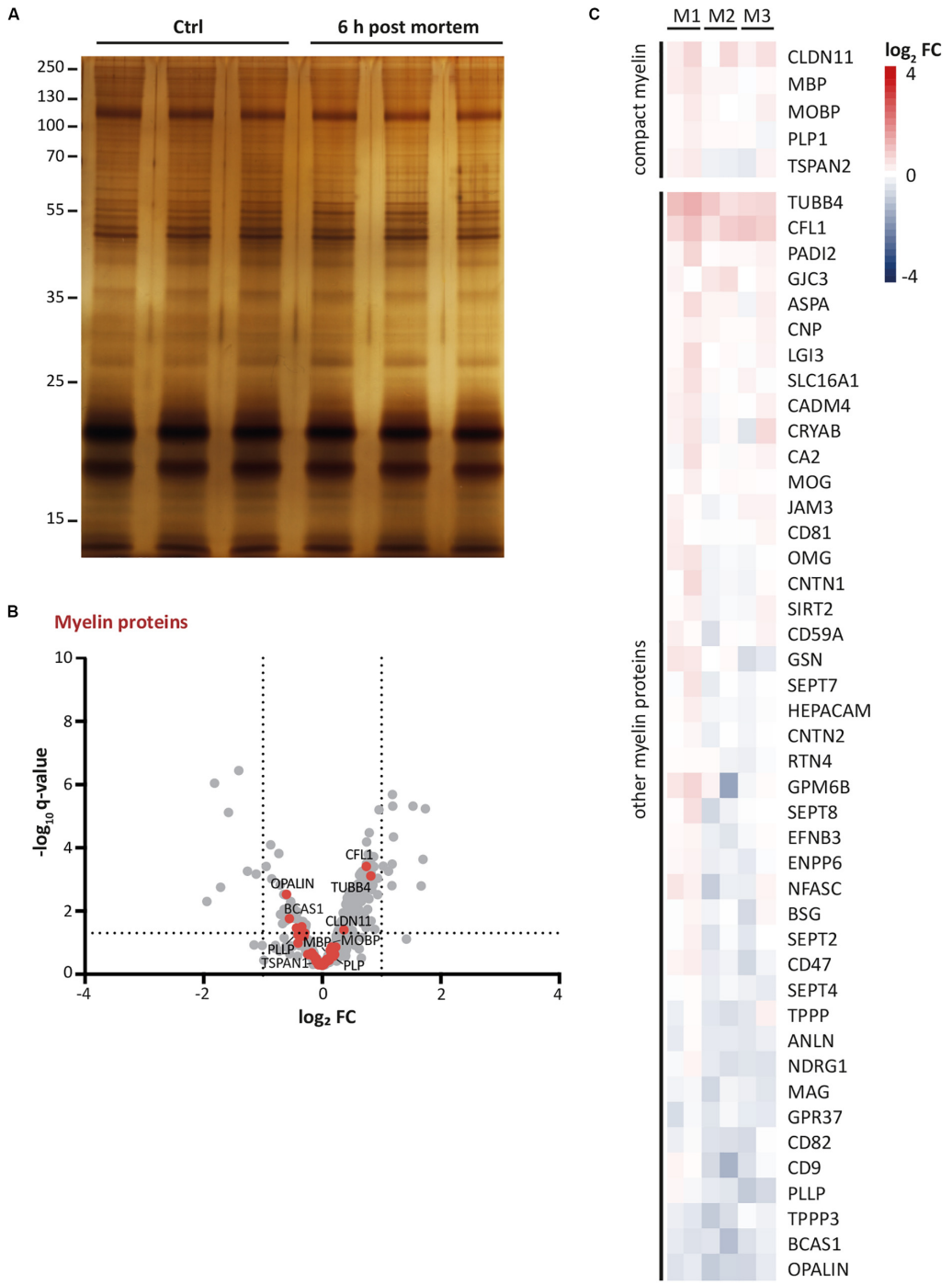

FIGURE 4 | Persistence of myelin proteins upon post-mortem delay. **(A)** Myelin purified from the brains of mice at P56 was separated by SDS-PAGE (0.5 µg protein load) and proteins were visualized by silver staining. Myelin of brains frozen upon a post-mortem delay of 6 h at room temperature was compared with myelin of brains frozen immediately upon dissection (Ctrl). Note the similar band pattern. Gel shows $n = 3$ biological replicates per condition. **(B)** Volcano plot representing differential proteome analysis by DRE-UDMS^E to compare myelin purified from brains upon post-mortem delay with myelin of brains immediately frozen upon dissection. For entire dataset see **Supplementary Table S1**. Data points represent proteins quantified in myelin purified from mouse brains frozen after a post-mortem delay of 6 h at room temperature compared to immediately frozen brains and are plotted as the $\log_2$-transformed fold-change (FC) on the *x*-axis against the $-\log_{10}$-transformed *q*-value on the *y*-axis. Vertical stippled lines mark a 2-fold/0.5-fold change (FC) as significance threshold. Horizontal stippled line represents a $-\log_{10}$-transformed *q*-value of 1.301, reflecting a *q*-value of 0.05 as significance threshold. Data points highlighted in red represent known myelin proteins as specified in **Figure 4C**. Note that no known myelin protein exceeds the fold-change significance threshold. **(C)** Heatmap displaying known myelin proteins as highlighted by the red data points in **Figure 4B**. Heatmap shows reduced (blue) or increased (red) abundance in myelin purified from brains after post-mortem delay. Each horizontal line corresponds to the fold-change (FC) of a distinct myelin protein compared to its average abundance in control myelin plotted on a $\log_2$ color scale. Heatmap displays 6 replicates, i.e., three biological replicates per condition (M1, M2, M3) with two technical replicates each.

TABLE 1 | Comparison of proteins identified in CNS myelin and disease genes associated with white matter pathology.

Protein name	Gene symbol	OMIM#	Gene Locus	Disease
Aldehyde dehydrogenase 3a2	*ALDH3A2*	609523	17p11.2	Sjogren-Larsson Syndrome
Aspartoacylase	*ASPA*	608034	17p13.2	Canavan disease
Atlastin GTPase 1	*ATL1*	606439	14q22.1	SPG 3A
Cathepsin *D*	*CTSD*	610127	11p15.5	Ceroid lipofuscinosis
Contactin-associated protein 1	*CNTNAP1*	602346	17q21.2	LCCS 7
Cyclic nucleotide phosphodiesterase	*CNP*	123830	17q21.2	HLD
Dynamin 2	*DNM2*	602378	19p13.2	LCCS 5
Endoplasmic reticulum lipid raft-associated protein 2	*ERLIN2*	611605	8p11.23	SPG 18
Glial fibrillary acidic protein	*GFAP*	137780	17q21.31	Alexander disease
Glutamate-Ammonia ligase	*GLUL*	138290	1q25.3	Glutamine-deficiency, congenital
Heat-shock 60-kD protein 1	*HSPD1*	118190	2q33.1	HLD 4, SPG 13
Hepatocyte cell adhesion molecule	*HEPACAM*	611642	11q24.2	MLC 2
Junctional adhesion molecule 3	*JAM3*	613730	11q25	HDBSCC
Magnesium transporter NIPA1	*NIPA1*	608145	15q11.2	SPG 6
Monoacylglycerol lipase ABHD12	*ABHD12*	613599	20p11.21	PHARC
Myelin basic protein	*MBP*	159430	18q23	18q deletion syndrome
Myelin-associated glycoprotein	*MAG*	159460	19q13.12	SPG 75
Myelin-oligodendrocyte glycoprotein	*MOG*	159465	6p22.1	Narcolepsy 7
Neurofascin	*NFASC*	609145	1q32.1	NEDCPMD
Phosphoglycerate dehydrogenase	*PHGDH*	606879	1p12	PHGDH deficiency, NLS 1
Phosphoserine aminotransferase 1	*PSAT1*	610936	9q21.2	PSAT deficiency, NLS 2
Prosaposin	*PSAP*	176801	10q22.1	Metachromatic Leukodystrophy
Proteolipid protein	*PLP1*	300401	Xq22.2	Pelizaeus-Merzbacher disease, SPG 2
Transmembrane protein 63a	*TMEM63A*	618685	1q42.12	HLD 19
Tubulin beta 4a	*TUBB4A*	602662	19p13.3	Dystonia 4, HLD 6

Proteins listed fulfill three criteria: (1) mass spectrometric identification in purified CNS myelin, (2) transcript expression in oligodendrocytes and (3) gene mutations associated with diseases involving pathology of myelin or the white matter. For some of the proteins with additional expression in astrocytes, microglia or neurons it is presently unknown whether loss/gain of function in oligodendrocytes is causative of the disease. HLD, Hypomyelinating Leukodystrophy; SPG, Spastic Paraplegia; LCCS, Lethal Congenital Contracture Syndrome; MLC, Megalencephalic leukoencephalopathy with subcortical cysts; NLS, Neu-Laxova syndrome; HDBSCC, Hemorrhagic destruction of the brain, subependymal calcification and cataracts; PHARC, polyneuropathy, hearing loss, ataxia, retinitis pigmentosa and cataract; NEDCPMD, neurodevelopmental disorder with central and peripheral motor dysfunction.

some myelin proteins may result in peptides incompatible with mass spectrometric detection; their identification would require the use of proteases other than trypsin. We also note that some low-abundant signaling proteins with potent functions in regulating myelination may be assumed to localize to myelin *in vivo* but were not mass spectrometrically identified, as exemplified by the G-protein coupled receptors GPR17 (Chen et al., 2009) and GPR56/ADGRG1 (Ackerman et al., 2015; Giera et al., 2015) and the Ig-domain containing LINGO1 (Mi et al., 2005). It is currently speculative if these proteins are preferentially expressed in oligodendroglial cell bodies rather than myelin membranes or during the stages of oligodendrocyte differentiation that precede myelination. It is also speculative if enhanced mass spectrometric sensitivity would facilitate their identification in myelin. Indeed, we can not formally exclude that these proteins may be identified if less rigorous criteria were applied (e.g., demanding only one peptide per protein), which may be sufficient for identification but not for the reliable quantification of proteins as aimed at in the present study. Importantly, however, lower stringency may not only identify more true myelin constituents but also false-positive hits. This is a concern, in particular when considering that the myelin-enriched fraction may comprise up to 5% contaminants from other cellular sources (De Monasterio-Schrader et al., 2012). We note that currently no biochemical method is available that allows preventing this limitation. Yet, comparing various datasets yields systematic information, for example on the presence of a transcript in oligodendrocytes as expected for a CNS myelin protein.

Mutations affecting genes that encode classical myelin proteins including PLP, CNP, MAG, TUBB4, and ASPA cause severe neurological disorders including hypomyelinating leukodystrophies (HLD) and spastic paraplegias (SPG) (Kaul et al., 1993; Saugier-Veber et al., 1994; Simons et al., 2013; Lossos et al., 2015; Al-Abdi et al., 2020) (**Table 1**). However, current sequencing efforts also identify disease-causing genes that encode less well-characterized proteins. Notably, most types of leukodystrophies and spastic paraplegias are caused by mutations affecting genes of which the transcripts are enriched in neurons, astrocytes or microglia rather than oligodendrocytes (Nave and Werner, 2014; van der Knaap et al., 2019). For newly identified disease genes, thus, evaluating mRNA-expression using transcriptome datasets and presence of the protein in myelin using the present myelin proteome resource may serve as a useful entry point into identifying the primarily affected cell type. For example, mutations of the *HSPD1* gene cause

HLD4 or SPG13 (Hansen et al., 2002; Magen et al., 2008) and mutations of the *TMEM63A* gene cause HLD19 (Yan et al., 2019) (**Table 1**). Considering that both transcripts are expressed in oligodendrocytes as per transcriptome datasets and both proteins are comprised in the myelin proteome, the disease mechanisms may involve primary impairment of the biogenesis, maintenance or functions of myelin.

Dysfunctions of oligodendrocytes and myelin contribute to the neuropathology in a growing number of neurodegenerative disorders and their respective mouse models, including Rett syndrome (Nguyen et al., 2013), amyotrophic lateral sclerosis (Kang et al., 2013), Down syndrome (Olmos-Serrano et al., 2016), Alzheimer's disease (Nasrabady et al., 2018) and multiple sclerosis (Factor et al., 2020). Considering that molecular assessments now frequently involve autopsy material, it is motivating that our data imply that myelin proteome analysis appears well possible post-mortem, at least up to a 6 h delay. A systematic understanding of the abundance profiles of all myelin proteins in the healthy brain and in myelin-related disorders may contribute to comprehending myelin-related physiology and pathophysiology. Myelin proteome analysis as pursued here provides a basis for addressing possible proteomic heterogeneity of myelin in dependence of CNS region, age and species, as well as in mouse models and human patients with white matter disorders.

DATA AVAILABILITY STATEMENT

The mass spectrometry proteomics data have been deposited to the ProteomeXchange Consortium via the PRIDE (Perez-Riverol et al., 2019) partner repository with dataset identifier, PXD020007.

ETHICS STATEMENT

Ethical review and approval was not required for the animal study because for the procedure of sacrificing mice for subsequent preparation of tissue, all regulations given in the German animal protection law (TierSchG §4) are followed. Since sacrificing of rodents is not an experiment on animals according to §7 Abs. 2 Satz 3 TierSchG, no specific authorization or notification is required for the present work.

AUTHOR CONTRIBUTIONS

KK, DH, RJ, TL, and MU performed the experiments. SS analyzed the data and performed the statistical analysis. TS wrote the code to interpret single cell resolution transcriptome data. OJ and HW conceived, designed, and directed the study. HW wrote the manuscript with major contributions by SS and OJ. All the authors contributed to revising the manuscript and approved the submitted version.

FUNDING

Our work was supported by the Deutsche Forschungsgemeinschaft (DFG; Grants WE 2720/2-2, WE 2720/4-1, and WE 2720/5-1 to HW).

ACKNOWLEDGMENTS

We thank G. Castelo-Branco and D. van Bruggen for providing dataset metadata information, S. Tenzer, M. Eichel, and T. Buscham for discussions, L. Piepkorn for support in data analysis, K.-A. Nave for support made possible by a European Research Council Advanced Grant ('MyeliNano' to K.-A. Nave), and the International Max Planck Research School for Genome Science (IMPRS-GS) for supporting SS.

SUPPLEMENTARY MATERIAL

The Supplementary Material for this article can be found online at: https://www.frontiersin.org/articles/10.3389/fncel.2020.00239/full#supplementary-material

TABLE S1 | Compendium of the mouse CNS myelin proteome. **(Sheet 1)** 1D gel separation of proteins followed by in-gel digestion and LC-MS analysis (788 proteins). **(Sheet 2)** 1D gel separation of proteins after membrane wash followed by in-gel digestion and LC-MS analysis (521 proteins). **(Sheet 3a)** 2D gel separation of proteins followed by in-gel digestion and MALDI-TOF-MS: spot annotation of the master gel shown in **Figure 3C** (352 gel spots). **(Sheet 3b)** 2D gel separation of proteins followed by in-gel digestion and MALDI-TOF-MS: non-redundant protein list (181 proteins). **(Sheet 4)** In-solution digestion of proteins and label-free quantification by MS^E (393 proteins). **(Sheet 5)** In-solution digestion of proteins and label-free quantification by $UDMS^E$ (809 proteins). **(Sheet 6)** Compendium providing information on the approach by which a myelin-associated protein was identified and on predicted transmembrane domains (1155 proteins).

TABLE S2 | Label-free quantification of proteins in CNS myelin purified from mouse brains without (Ctrl) and after 6 h post-mortem delay (PMD6h) by DRE-$UDMS^E$. Related to **Figure 4**. **(Sheet 1)** Dataset.

REFERENCES

Ackerman, S. D., Garcia, C., Piao, X., Gutmann, D. H., and Monk, K. R. (2015). The adhesion GPCR Gpr56 regulates oligodendrocyte development via interactions with Gα12/13 and RhoA. *Nat. Commun.* 6:6122. doi: 10.1038/ncomms7122

Ahrné, E., Molzahn, L., Glatter, T., and Schmidt, A. (2013). Critical assessment of proteome-wide label-free absolute abundance estimation strategies. *Proteomics* 13, 2567–2578. doi: 10.1002/pmic.201300135

Al-Abdi, L., Al Murshedi, F., Elmanzalawy, A., Al Habsi, A., Helaby, R., Ganesh, A., et al. (2020). CNP deficiency causes severe hypomyelinating leukodystrophy in humans. *Hum. Genet.* 139, 615–622. doi: 10.1007/s00439-020-02144-4

Ambrozkiewicz, M. C., Schwark, M., Kishimoto-Suga, M., Borisova, E., Hori, K., Salazar-Lázaro, A., et al. (2018). Polarity Acquisition in Cortical Neurons Is Driven by Synergistic Action of Sox9-Regulated Wwp1 and Wwp2 E3 Ubiquitin Ligases and Intronic miR-140. *Neuron* 100:1097-1115.e15. doi: 10.1016/j.neuron.2018.10.008

Banik, N. L., and Smith, M. E. (1977). Protein determinants of myelination in different regions of developing rat central nervous system. *Biochem. J.* 162, 247–255. doi: 10.1042/bj1620247

Bansal, R., Warrington, A. E., Gard, A. L., Ranscht, B., and Pfeiffer, S. E. (1989). Multiple and novel specificities of monoclonal antibodies O1, O4, and R-mAb used in the analysis of oligodendrocyte development. *J. Neurosci. Res.* 24, 548–557. doi: 10.1002/jnr.490240413

Butler, A., Hoffman, P., Smibert, P., Papalexi, E., and Satija, R. (2018). Integrating single-cell transcriptomic data across different conditions, technologies, and species. *Nat. Biotechnol.* 36, 411–420. doi: 10.1038/nbt.4096

Chen, Y., Wu, H., Wang, S., Koito, H., Li, J., Ye, F., et al. (2009). The oligodendrocyte-specific G protein-coupled receptor GPR17 is a cell-intrinsic timer of myelination. *Nat. Neurosci.* 12, 1398–1406. doi: 10.1038/nn.2410

Chrast, R., Saher, G., Nave, K. A., and Verheijen, M. H. G. (2011). Lipid metabolism in myelinating glial cells: Lessons from human inherited disorders and mouse models. *J. Lipid Res.* 52, 419–434. doi: 10.1194/jlr.R009761

De Monasterio-Schrader, P., Jahn, O., Tenzer, S., Wichert, S. P., Patzig, J., and Werner, H. B. (2012). Systematic approaches to central nervous system myelin. *Cell. Mol. Life Sci.* 69, 2879–2894. doi: 10.1007/s00018-012-0958-9

de Monasterio-Schrader, P., Patzig, J., Möbius, W., Barrette, B., Wagner, T. L., Kusch, K., et al. (2013). Uncoupling of neuroinflammation from axonal degeneration in mice lacking the myelin protein tetraspanin-2. *Glia* 61, 1832–1847. doi: 10.1002/glia.22561

Deber, C. M., and Reynolds, S. J. (1991). Central nervous system myelin: structure, function, and pathology. *Clin. Biochem.* 24, 113–134. doi: 10.1016/0009-9120(91)90421-A

Denninger, A. R., Breglio, A., Maheras, K. J., Leduc, G., Cristiglio, V., Demé, B., et al. (2015). Claudin-11 tight junctions in myelin are a barrier to diffusion and lack strong adhesive properties. *Biophys. J.* 109, 1387–1397. doi: 10.1016/j.bpj.2015.08.012

Dhaunchak, A. S., Huang, J. K., De Faria, O., Roth, A. D., Pedraza, L., Antel, J. P., et al. (2010). A proteome map of axoglial specializations isolated and purified from human central nervous system. *Glia* 58, 1949–1960. doi: 10.1002/glia.21064

Distler, U., Kuharev, J., Navarro, P., Levin, Y., Schild, H., and Tenzer, S. (2014a). Drift time-specific collision energies enable deep-coverage data-independent acquisition proteomics. *Nat. Methods* 11, 167–170. doi: 10.1038/nmeth.2767

Distler, U., Kuharev, J., and Tenzer, S. (2014b). Biomedical applications of ion mobility-enhanced data-independent acquisition-based label-free quantitative proteomics. *Expert Rev. Proteomics* 11, 675–684. doi: 10.1586/14789450.2014.971114

Distler, U., Kuharev, J., Navarro, P., and Tenzer, S. (2016). Label-free quantification in ion mobility–enhanced data-independent acquisition proteomics. *Nat. Protoc.* 11, 795–812. doi: 10.1038/nprot.2016.042

Edgar, J. M., McLaughlin, M., Werner, H. B., McCulloch, M. C., Barrie, J. A., Brown, A., et al. (2009). Early ultrastructural defects of axons and axon-glia junctions in mice lacking expression of Cnp1. *Glia* 57, 1815–1824. doi: 10.1002/glia.20893

Erwig, M. S., Hesse, D., Jung, R. B., Uecker, M., Kusch, K., Tenzer, S., et al. (2019a). 'Myelin: Methods for Purification and Proteome Analysis'. *Methods Mol. Biol.* 1936, 37–63. doi: 10.1007/978-1-4939-9072-6_3

Erwig, M. S., Patzig, J., Steyer, A. M., Dibaj, P., Heilmann, M., Heilmann, I., et al. (2019b). Anillin facilitates septin assembly to prevent pathological outfoldings of central nervous system myelin. *eLife* 8:e43888. doi: 10.7554/eLife.43888

Factor, D. C., Barbeau, A. M., Allan, K. C., Hu, L. R., Madhavan, M., Hoang, A. T., et al. (2020). Cell type-specific intralocus interactions reveal oligodendrocyte mechanisms in MS. *Cell* 181:382-395.e21. doi: 10.1016/j.cell.2020.03.002

Falcão, A. M., van Bruggen, D., Marques, S., Meijer, M., Jäkel, S., Agirre, E., et al. (2018). Disease-specific oligodendrocyte lineage cells arise in multiple sclerosis. *Nat. Med.* 24, 1837–1844. doi: 10.1038/s41591-018-0236-y

Giera, S., Deng, Y., Luo, R., Ackerman, S. D., Mogha, A., Monk, K. R., et al. (2015). The adhesion G protein-coupled receptor GPR56 is a cell-autonomous regulator of oligodendrocyte development. *Nat. Commun.* 6:6121. doi: 10.1038/ncomms7121

Golan, N., Adamsky, K., Kartvelishvily, E., Brockschnieder, D., Möbius, W., Spiegel, I., et al. (2008). Identification of Tmem10/Opalin as an oligodendrocyte enriched gene using expression profiling combined with genetic cell ablation. *Glia* 56, 1176–1186. doi: 10.1002/glia.20688

Goldman, S. A., and Kuypers, N. J. (2015). How to make an oligodendrocyte. *Development* 142, 3983–3995. doi: 10.1242/dev.126409

Gopalakrishnan, G., Awasthi, A., Belkaid, W., De Faria, O., Liazoghli, D., Colman, D. R., et al. (2013). Lipidome and proteome map of myelin membranes. *J. Neurosci. Res.* 91, 321–334. doi: 10.1002/jnr.23157

Gow, A., Southwood, C. M., Li, J. S., Pariali, M., Riordan, G. P., Brodie, S. E., et al. (1999). CNS Myelin and sertoli cell tight junction strands are absent in OSP/claudin-11 null mice. *Cell* 99, 649–659. doi: 10.1016/S0092-8674(00)81553-6

Hansen, J. J., Dürr, A., Cournu-Rebeix, I., Georgopoulos, C., Ang, D., Nielsen, M. N., et al. (2002). Hereditary spastic paraplegia SPG13 is associated with a mutation in the gene encoding the mitochondrial chaperonin Hsp60. *Am. J. Hum. Genet.* 70, 1328–1332. doi: 10.1086/339935

Hulsen, T., de Vlieg, J., and Alkema, W. (2008). BioVenn – a web application for the comparison and visualization of biological lists using area-proportional Venn diagrams. *BMC Genomics* 9:488. doi: 10.1186/1471-2164-9-488

Ishii, A., Dutta, R., Wark, G. M., Hwang, S. II, Han, D. K., Trapp, B. D., et al. (2009). Human myelin proteome and comparative analysis with mouse myelin. *Proc. Natl. Acad. Sci. U.S.A.* 106, 14605–14610. doi: 10.1073/pnas.0905936106

Jahn, O., Hesse, D., Reinelt, M., and Kratzin, H. D. (2006). Technical innovations for the automated identification of gel-separated proteins by MALDI-TOF mass spectrometry. *Anal. Bioanal. Chem.* 386, 92–103. doi: 10.1007/s00216-006-0592-1

Jahn, O., Tenzer, S., Bartsch, N., Patzig, J., and Werner, H. B. (2013). "Myelin proteome analysis: methods and implications for the myelin cytoskeleton," in *The Cytoskeleton. Neuromethods*, Vol. 79, ed. R. Dermietzel, (Totowa, NJ: Humana Press), doi: 10.1007/978-1-62703-266-7_15

Jahn, O., Tenzer, S., and Werner, H. B. (2009). Myelin proteomics: Molecular anatomy of an insulating sheath. *Mol. Neurobiol.* 40, 55–72. doi: 10.1007/s12035-009-8071-2

Jäkel, S., Agirre, E., Mendanha Falcão, A., van Bruggen, D., Lee, K. W., Knuesel, I., et al. (2019). Altered human oligodendrocyte heterogeneity in multiple sclerosis. *Nature* 566, 543–547. doi: 10.1038/s41586-019-0903-2

Johns, T. G., and Bernard, C. C. A. (1999). The structure and function of myelin oligodendrocyte glycoprotein. *J. Neurochem.* 72, 1–9. doi: 10.1046/j.1471-4159.1999.0720001.x

Joseph, S., Werner, H., and Stegmüller, J. (2019). Gallyas silver impregnation of myelinated nerve fibers. *Bio-Protocol* 9:e3436. doi: 10.21769/bioprotoc.3436

Käll, L., Krogh, A., and Sonnhammer, E. L. L. (2007). Advantages of combined transmembrane topology and signal peptide prediction-the Phobius web server. *Nucleic Acids Res.* 35, W429–W432. doi: 10.1093/nar/gkm256

Kang, S. H., Li, Y., Fukaya, M., Lorenzini, I., Cleveland, D. W., Ostrow, L. W., et al. (2013). Degeneration and impaired regeneration of gray matter oligodendrocytes in amyotrophic lateral sclerosis. *Nat. Neurosci.* 16, 571–579. doi: 10.1038/nn.3357

Kaul, R., Gao, G. P., Balamurugan, K., and Matalon, R. (1993). Cloning of the human aspartoacylase cDNA and a common missense mutation in Canavan disease. *Nat. Genet.* 5, 118–123. doi: 10.1038/ng1093-118

Kippert, A., Trajkovic, K., Fitzner, D., Opitz, L., and Simons, M. (2008). Identification of tmem10/opalin as a novel marker for oligodendrocytes using gene expression profiling. *BMC Neurosci.* 9:40. doi: 10.1186/1471-2202-9-40

Krogh, A., Larsson, B., Von Heijne, G., and Sonnhammer, E. L. L. (2001). Predicting transmembrane protein topology with a hidden Markov model: Application to complete genomes. *J. Mol. Biol.* 305, 567–580. doi: 10.1006/jmbi.2000.4315

Kuharev, J., Navarro, P., Distler, U., Jahn, O., and Tenzer, S. (2015). In-depth evaluation of software tools for data-independent acquisition based label-free quantification. *Proteomics* 15, 3140–3151. doi: 10.1002/pmic.201400396

Lappe-Siefke, C., Goebbels, S., Gravel, M., Nicksch, E., Lee, J., Braun, P. E., et al. (2003). Disruption of Cnp1 uncouples oligodendroglial functions in axonal support and myelination. *Nat. Genet.* 33, 366–374. doi: 10.1038/ng1095

Lee, A. G. (2001). Myelin: delivery by raft. *Curr. Biol.* 11, R60–R62. doi: 10.1016/S0960-9822(01)00008-2

Lossos, A., Ponger, P., Newman, J. P., Elazar, N., Mor, N., Eshed-Eisenbach, Y., et al. (2015). Myelin-associated glycoprotein gene mutation causes Pelizaeus-Merzbacher disease-like disorder. *Brain* 138, 2521–2536. doi: 10.1093/brain/awv204

Magen, D., Georgopoulos, C., Bross, P., Ang, D., Segev, Y., Goldsher, D., et al. (2008). Mitochondrial Hsp60 chaperonopathy causes an autosomal-recessive neurodegenerative disorder linked to brain hypomyelination and leukodystrophy. *Am. J. Hum. Genet.* 83, 30–42. doi: 10.1016/j.ajhg.2008.05.016

Magno-Sumbilla, C., and Campagnoni, A. T. (1977). Factors affecting the electrophoretic analysis of myelin proteins: Application to changes occurring during brain development. *Brain Res.* 126, 131–148. doi: 10.1016/0006-8993(77)90220-7

Manrique-Hoyos, N., Jürgens, T., Grønborg, M., Kreutzfeldt, M., Schedensack, M., Kuhlmann, T., et al. (2012). Late motor decline after accomplished remyelination: Impact for progressive multiple sclerosis. *Ann. Neurol.* 71, 227–244. doi: 10.1002/ana.22681

Marques, S., Zeisel, A., Codeluppi, S., van Bruggen, D., Mendanha Falcao, A., Xiao, L., et al. (2016). Oligodendrocyte heterogeneity in the mouse juvenile and adult central nervous system. *Science* 352, 1326–1329. doi: 10.1126/science.aaf6463

Mi, S., Miller, R. H., Lee, X., Scott, M. L., Shulag-Morskaya, S., Shao, Z., et al. (2005). LINGO-1 negatively regulates myelination by oligodendrocytes. *Nat. Neurosci.* 8, 745–751. doi: 10.1038/nn1460

Möbius, W., Patzig, J., Nave, K. A., and Werner, H. B. (2008). Phylogeny of proteolipid proteins: Divergence, constraints, and the evolution of novel functions in myelination and neuroprotection. *Neuron Glia Biol.* 4, 111–127. doi: 10.1017/S1740925X0900009X

Morell, P., Greenfield, S., Costantino-Ceccarini, E., and Wisniewski, H. (1972). Changes in the protein composition of mouse brain myelin during development. *J. Neurochem.* 19, 2545–2554. doi: 10.1111/j.1471-4159.1972.tb01313.x

Morell, P., Lipkind, R., and Greenfield, S. (1973). Protein composition of myelin from brain and spinal cord of several species. *Brain Res.* 58, 510–514. doi: 10.1016/0006-8993(73)90023-1

Morris, S. J., Louis, C. F., and Shooter, E. M. (1971). Separation of myelin proteins on two different polyacrylamide gel systems. *Neurobiology* 1, 64–67.

Musse, A. A., Gao, W., Homchaudhuri, L., Boggs, J. M., and Harauz, G. (2008). Myelin basic protein as a 'PI(4,5)P2-modulin': A new biological function for a major central nervous system protein. *Biochemistry* 47, 10372–10382. doi: 10.1021/bi801302b

Myllykoski, M., Eichel, M. A., Jung, R. B., Kelm, S., Werner, H. B., and Kursula, P. (2018). High-affinity heterotetramer formation between the large myelin-associated glycoprotein and the dynein light chain DYNLL1. *J. Neurochem.* 147, 764–783. doi: 10.1111/jnc.14598

Nasrabady, S. E., Rizvi, B., Goldman, J. E., and Brickman, A. M. (2018). White matter changes in Alzheimer's disease: a focus on myelin and oligodendrocytes. *Acta Neuropathol. Commun.* 6:22. doi: 10.1186/s40478-018-0515-3

Nave, K.-A., and Werner, H. B. (2014). Myelination of the Nervous System: Mechanisms and Functions. *Annu. Rev. Cell Dev. Biol.* 30, 503–533. doi: 10.1146/annurev-cellbio-100913-013101

Nawaz, S., Kippert, A., Saab, A. S., Werner, H. B., Lang, T., Nave, K. A., et al. (2009). Phosphatidylinositol 4,5-bisphosphate-dependent interaction of myelin basic protein with the plasma membrane in oligodendroglial cells and its rapid perturbation by elevated calcium. *J. Neurosci.* 29, 4794–4807. doi: 10.1523/JNEUROSCI.3955-08.2009

Nawaz, S., Sánchez, P., Schmitt, S., Snaidero, N., Mitkovski, M., Velte, C., et al. (2015). Actin filament turnover drives leading edge growth during myelin sheath formation in the central nervous system. *Dev. Cell.* 34, 139–151. doi: 10.1016/j.devcel.2015.05.013

Nawaz, S., Schweitzer, J., Jahn, O., and Werner, H. B. (2013). Molecular evolution of myelin basic protein, an abundant structural myelin component. *Glia* 61, 1364–1377. doi: 10.1002/glia.22520

Neilson, K. A., Ali, N. A., Muralidharan, S., Mirzaei, M., Mariani, M., Assadourian, G., et al. (2011). Less label, more free: Approaches in label-free quantitative mass spectrometry. *Proteomics* 11, 535–553. doi: 10.1002/pmic.201000553

Nguyen, M. V. C., Felice, C. A., Du, F., Covey, M. V., Robinson, J. K., Mandel, G., et al. (2013). Oligodendrocyte lineage cells contribute unique features to rett syndrome neuropathology. *J. Neurosci.* 33, 18764–18774. doi: 10.1523/JNEUROSCI.2657-13.2013

Norton, W. T., and Poduslo, S. E. (1973a). Myelination in rat brain: changes in myelin composition during brain maturation. *J. Neurochem.* 21, 759–773. doi: 10.1111/j.1471-4159.1973.tb07520.x

Norton, W. T., and Poduslo, S. E. (1973b). Myelination in rat brain: method of myelin isolation. *J. Neurochem.* 21, 749–757. doi: 10.1111/j.1471-4159.1973.tb07519.x

Olmos-Serrano, J. L., Kang, H. J., Tyler, W. A., Silbereis, J. C., Cheng, F., Zhu, Y., et al. (2016). Down syndrome developmental brain transcriptome reveals defective oligodendrocyte differentiation and myelination. *Neuron* 89, 1208–1222. doi: 10.1016/j.neuron.2016.01.042

Ott, C., Martens, H., Hassouna, I., Oliveira, B., Erck, C., Zafeiriou, M. P., et al. (2015). Widespread expression of erythropoietin receptor in brain and its induction by injury. *Mol. Med.* 21, 803–815. doi: 10.2119/molmed.2015.00192

Patzig, J., Erwig, M. S., Tenzer, S., Kusch, K., Dibaj, P., Möbius, W., et al. (2016). Septin/anillin filaments scaffold central nervous system myelin to accelerate nerve conduction. *eLife* 5:e17119. doi: 10.7554/eLife.17119.001

Perez-Riverol, Y., Csordas, A., Bai, J., Bernal-Llinares, M., Hewapathirana, S., Kundu, D. J., et al. (2019). The PRIDE database and related tools and resources in 2019: Improving support for quantification data. *Nucleic Acids Res.* 47, D442–D450. doi: 10.1093/nar/gky1106

Poitelon, Y., Kopec, A. M., and Belin, S. (2020). Myelin fat facts: an overview of lipids and fatty acid metabolism. *Cells* 9:812. doi: 10.3390/cells9040812

Quarles, R. H. (2007). Myelin-associated glycoprotein (MAG): Past, present and beyond. *J. Neurochem.* 100, 1431–1448. doi: 10.1111/j.1471-4159.2006.04319.x

Raasakka, A., Ruskamo, S., Kowal, J., Barker, R., Baumann, A., Martel, A., et al. (2017). Membrane association landscape of myelin basic protein portrays formation of the myelin major dense line. *Sci. Rep.* 7:4974. doi: 10.1038/s41598-017-05364-3

Roach, A., Takahashi, N., Pravtcheva, D., Ruddle, F., and Hood, L. (1985). Chromosomal mapping of mouse myelin basic protein gene and structure and transcription of the partially deleted gene in shiverer mutant mice. *Cell* 42, 149–155. doi: 10.1016/S0092-8674(85)80110-0

Roth, A. D., Ivanova, A., and Colman, D. R. (2006). New observations on the compact myelin proteome. *Neuron Glia Biol.* 2, 15–21. doi: 10.1017/S1740925X06000068

Saher, G., Brügger, B., Lappe-Siefke, C., Möbius, W., Tozawa, R. I., Wehr, M. C., et al. (2005). High cholesterol level is essential for myelin membrane growth. *Nat. Neurosci.* 8, 468–475. doi: 10.1038/nn1426

Saugier-Veber, P., Munnich, A., Bonneau, D., Rozet, J. M., le Merrer, M., Gil, R., et al. (1994). X-linked spastic paraplegia and Pelizaeus-Merzbacher disease are allelic disorders at the proteolipid protein locus. *Nat. Genet.* 6, 257–262. doi: 10.1038/ng0394-257

Schaeren-Wiemers, N., Bonnet, A., Erb, M., Erne, B., Bartsch, U., Kern, F., et al. (2004). The raft-associated protein MAL is required for maintenance of proper axon–glia interactions in the central nervous system. *J. Cell Biol.* 166, 731–742. doi: 10.1083/jcb.200406092

Schardt, A., Brinkmann, B. G., Mitkovski, M., Sereda, M. W., Werner, H. B., and Nave, K.-A. (2009). The SNARE protein SNAP-29 interacts with the GTPase Rab3A: implications for membrane trafficking in myelinating glia. *J. Neurosci. Res.* 87, 3465–3479. doi: 10.1002/jnr.22005

Schmidt, C., Hesse, D., Raabe, M., Urlaub, H., and Jahn, O. (2013). An automated in-gel digestion/iTRAQ-labeling workflow for robust quantification of gel-separated proteins. *Proteomics* 13, 1417–1422. doi: 10.1002/pmic.201200366

Schmitt, S., Cantuti Castelvetri, L., and Simons, M. (2015). Metabolism and functions of lipids in myelin. *Biochim. Biophys. Acta Mol. Cell Biol. Lipids.* 1851, 999–1005. doi: 10.1016/j.bbalip.2014.12.016

Sharma, K., Schmitt, S., Bergner, C. G., Tyanova, S., Kannaiyan, N., Manrique-Hoyos, N., et al. (2015). Cell type– and brain region–resolved mouse brain proteome. *Nat. Neurosci.* 18, 1819–1831. doi: 10.1038/nn.4160

Siems, S. B., Jahn, O., Eichel, M. A., Kannaiyan, N., Wu, L. M. N., Sherman, D. L., et al. (2020). Proteome profile of peripheral myelin in healthy mice and in a neuropathy model. *eLife* 9:e51406. doi: 10.7554/eLife.51406

Silva, J. C., Gorenstein, M. V., Li, G.-Z., Vissers, J. P. C., and Geromanos, S. J. (2006). Absolute Quantification of Proteins by LCMS E. *Mol. Cell. Proteomics* 5, 144–156. doi: 10.1074/mcp.M500230-MCP200

Simons, C., Wolf, N. I., McNeil, N., Caldovic, L., Devaney, J. M., Takanohashi, A., et al. (2013). A de novo mutation in the β-tubulin gene TUBB4A results in the leukoencephalopathy hypomyelination with atrophy of the basal ganglia and cerebellum. *Am. J. Hum. Genet.* 92, 767–773. doi: 10.1016/j.ajhg.2013.03.018

Simons, M., Krämer, E. M., Thiele, C., Stoffel, W., and Trotter, J. (2000). Assembly of myelin by association of proteolipid protein with cholesterol- and galactosylceramide-rich membrane domains. *J. Cell Biol.* 151, 143–154. doi: 10.1083/jcb.151.1.143

Snaidero, N., and Simons, M. (2017). The logistics of myelin biogenesis in the central nervous system. *Glia* 65, 1021–1031. doi: 10.1002/glia.23116

Snaidero, N., Velte, C., Myllykoski, M., Raasakka, A., Ignatev, A., Werner, H. B., et al. (2017). Antagonistic Functions of MBP and CNP establish cytosolic channels in CNS myelin. *Cell Rep.* 18, 314–323. doi: 10.1016/j.celrep.2016.12.053

Sommer, I., and Schachner, M. (1981). Monoclonal antibodies (O1 to O4) to oligodendrocyte cell surfaces: An immunocytological study in the central nervous system. *Dev. Biol.* 83, 311–327. doi: 10.1016/0012-1606(81)90477-2

Sprinkle, T. J., Sheedlo, H. J., Buxton, T. B., and Rissing, J. P. (1983). Immunochemical Identification of 2', 3'-Cyclic Nucleotide 3'-Phosphodiesterase in Central and Peripheral Nervous System Myelin, the Wolfgram Protein Fraction, and Bovine Oligodendrocytes. *J. Neurochem.* 41, 1664–1671. doi: 10.1111/j.1471-4159.1983.tb00878.x

Stuart, T., Butler, A., Hoffman, P., Hafemeister, C., Papalexi, E., Mauck, W. M., et al. (2019). Comprehensive integration of single-cell data. *Cell* 177:1888-1902.e21. doi: 10.1016/j.cell.2019.05.031

Taylor, C. M., Marta, C. B., Claycomb, R. J., Han, D. K., Rasband, M. N., Coetzee, T., et al. (2004). Proteomic mapping provides powerful insights into functional myelin biology. *Proc. Natl. Acad. Sci. U.S.A.* 101, 4643–4648. doi: 10.1073/pnas.0400922101

Thakurela, S., Garding, A., Jung, R. B., Müller, C., Goebbels, S., White, R., et al. (2016). The transcriptome of mouse central nervous system myelin. *Sci. Rep.* 6:25828. doi: 10.1038/srep25828

van der Knaap, M. S., Schiffmann, R., Mochel, F., and Wolf, N. I. (2019). Diagnosis, prognosis, and treatment of leukodystrophies. *Lancet Neurol.* 18, 962–972. doi: 10.1016/S1474-4422(19)30143-7

Vanrobaeys, F., Van Coster, R., Dhondt, G., Devreese, B., and Van Beeumen, J. (2005). Profiling of myelin proteins by 2D-gel electrophoresis and multidimensional liquid chromatography coupled to MALDI TOF-TOF mass spectrometry. *J. Proteome Res.* 4, 2283–2293. doi: 10.1021/pr050205c

von Büdingen, H. C., Mei, F., Greenfield, A., Jahn, S., Shen, Y. A. A., Reid, H. H., et al. (2015). The myelin oligodendrocyte glycoprotein directly binds nerve growth factor to modulate central axon circuitry. *J. Cell Biol.* 210, 891–898. doi: 10.1083/jcb.201504106

Wang, K. C., Koprivica, V., Kim, J. A., Sivasankaran, R., Guo, Y., Neve, R. L., et al. (2002). Oligodendrocyte-myelin glycoprotein is a Nogo receptor ligand that inhibits neurite outgrowth. *Nature* 417, 941–944. doi: 10.1038/nature00867

Werner, H. B., Krämer-Albers, E. M., Strenzke, N., Saher, G., Tenzer, S., Ohno-Iwashita, Y., et al. (2013). A critical role for the cholesterol-associated proteolipids PLP and M6B in myelination of the central nervous system. *Glia* 61, 567–586. doi: 10.1002/glia.22456

Werner, H. B., Kuhlmann, K., Shen, S., Uecker, M., Schardt, A., Dimova, K., et al. (2007). Proteolipid Protein Is Required for Transport of Sirtuin 2 into CNS Myelin. *J. Neurosci.* 27, 7717–7730. doi: 10.1523/JNEUROSCI.1254-07.2007

Yan, H., Helman, G., Murthy, S. E., Ji, H., Crawford, J., Kubisiak, T., et al. (2019). Heterozygous Variants in the Mechanosensitive Ion Channel TMEM63A Result in Transient Hypomyelination during Infancy. *Am. J. Hum. Genet.* 105, 996–1004. doi: 10.1016/j.ajhg.2019.09.011

Yang, H. J., Vainshtein, A., Maik-Rachline, G., and Peles, E. (2016). G protein-coupled receptor 37 is a negative regulator of oligodendrocyte differentiation and myelination. *Nat. Commun.* 7:10884. doi: 10.1038/ncomms10884

Yool, D. A., Klugmann, M., McLaughlin, M., Vouyiouklis, D. A., Dimou, L., Barrie, J. A., et al. (2001). Myelin proteolipid proteins promote the interaction of oligodendrocytes and axons. *J. Neurosci. Res.* 63, 151–164. doi: 10.1002/1097-4547(20010115)63:2<151::AID-JNR1007>3.0.CO;2-Y

Zeisel, A., Muñoz-Manchado, A. B., Codeluppi, S., Lönnerberg, P., Manno, G. L., Juréus, A., et al. (2015). Cell types in the mouse cortex and hippocampus revealed by single-cell RNA-seq. *Science* 347, 1138–1142. doi: 10.1126/science.aaa1934

Zhang, Y., Chen, K., Sloan, S. A., Bennett, M. L., Scholze, A. R., O'Keeffe, S., et al. (2014). An RNA-Sequencing Transcriptome and Splicing Database of Glia, Neurons, and Vascular Cells of the Cerebral Cortex. *J. Neurosci.* 34, 11929–11947. doi: 10.1523/JNEUROSCI.1860-14.2014

Zuchero, J. B., Fu, M. M., Sloan, S. A., Ibrahim, A., Olson, A., Zaremba, A., et al. (2015). CNS myelin wrapping is driven by actin disassembly. *Dev. Cell.* 34, 152–167. doi: 10.1016/j.devcel.2015.06.011

Conflict of Interest: The authors declare that the research was conducted in the absence of any commercial or financial relationships that could be construed as a potential conflict of interest.

frontiers in Cellular Neuroscience

REVIEW
published: 21 August 2020
doi: 10.3389/fncel.2020.00256

Expression and Function of GABA Receptors in Myelinating Cells

Mari Paz Serrano-Regal[1,2,3†], Laura Bayón-Cordero[1,2,3], Rainald Pablo Ordaz[4], Edith Garay[4], Agenor Limon[5], Rogelio O. Arellano[4], Carlos Matute[1,2,3] and María Victoria Sánchez-Gómez[1,2,3]**

[1]Laboratory of Neurobiology, Achucarro Basque Center for Neuroscience, Leioa, Spain, [2]Department of Neurosciences, University of the Basque Country (UPV/EHU), Leioa, Spain, [3]Centro de Investigación Biomédica en Red de Enfermedades Neurodegenerativas (CIBERNED), Leioa, Spain, [4]Laboratorio de Neurofisiología Celular, Instituto de Neurobiología, Universidad Nacional Autónoma de México, Juriquilla, Mexico, [5]Department of Neurology, Mitchell Center for Neurodegenerative Diseases, University of Texas Medical Branch, Galveston, TX, United States

OPEN ACCESS

Edited by:
Nicola B. Hamilton-Whitaker, King's College London, United Kingdom

Reviewed by:
Åsa Fex-Svenningsen, University of Southern Denmark, Denmark
Beatriz Garcia-Diaz, INSERM U1127 Institut du Cerveau et de la Moelle épinière (ICM), France
Maria Cecilia Angulo, Centre National de la Recherche Scientifique (CNRS), France

***Correspondence:**
Carlos Matute
carlos.matute@ehu.eus
María Victoria Sánchez-Gómez
vicky.sanchez@ehu.eus

†ORCID:
Mari Paz Serrano-Regal
orcid.org/0000-0002-1133-7261

Specialty section:
This article was submitted to Non-Neuronal Cells, a section of the journal Frontiers in Cellular Neuroscience

Received: 25 May 2020
Accepted: 24 July 2020
Published: 21 August 2020

Citation:
Serrano-Regal MP, Bayón-Cordero L, Ordaz RP, Garay E, Limon A, Arellano RO, Matute C and Sánchez-Gómez MV (2020) Expression and Function of GABA Receptors in Myelinating Cells. Front. Cell. Neurosci. 14:256. doi: 10.3389/fncel.2020.00256

Myelin facilitates the fast transmission of nerve impulses and provides metabolic support to axons. Differentiation of oligodendrocyte progenitor cells (OPCs) and Schwann cell (SC) precursors is critical for myelination during development and myelin repair in demyelinating disorders. Myelination is tightly controlled by neuron-glia communication and requires the participation of a wide repertoire of signals, including neurotransmitters such as glutamate, ATP, adenosine, or γ-aminobutyric acid (GABA). GABA is the main inhibitory neurotransmitter in the central nervous system (CNS) and it is also present in the peripheral nervous system (PNS). The composition and function of GABA receptors (GABARs) are well studied in neurons, while their nature and role in glial cells are still incipient. Recent studies demonstrate that GABA-mediated signaling mechanisms play relevant roles in OPC and SC precursor development and function, and stand out the implication of GABARs in oligodendrocyte (OL) and SC maturation and myelination. In this review, we highlight the evidence supporting the novel role of GABA with an emphasis on the molecular identity of the receptors expressed in these glial cells and the possible signaling pathways involved in their actions. GABAergic signaling in myelinating cells may have potential implications for developing novel reparative therapies in demyelinating diseases.

Keywords: GABA, GABA receptor, oligodendrocyte, Schwann cell, differentiation, myelination

INTRODUCTION

Glial cells express a vast repertoire of receptors and transporters for neurotransmitters and neuromodulators and respond to axonal signals, being key and active elements of the nervous system (Allen and Lyons, 2018). In vertebrates, oligodendrocytes (OLs) and Schwann cells (SCs) are the myelin-forming glia of the central nervous system (CNS) and peripheral nervous system (PNS), respectively. These cells are responsible for myelin building and maintenance, a function highly regulated by neuronal activity (Gibson et al., 2014; Mitew et al., 2018). Myelin speeds up nerve impulse propagation and provides metabolic and trophic support to axons (Nave and Trapp, 2008; Kidd et al., 2013; Philips and Rothstein, 2017). Thus, myelination represents the major function of these cells, although they carry it out with some differences; while OLs can myelinate multiple axons simultaneously, each SC

wraps one single axon (Jessen and Mirsky, 2005; Nave and Trapp, 2008). Regarding their specific characteristics, oligodendroglial cells represent a highly diverse and specialized cell population (Marques et al., 2016). Mature myelinating OLs develop from glial precursors named oligodendrocyte progenitor cells (OPCs), which constitute the main proliferating cell type in the adult CNS (Dawson et al., 2003). On the other hand, SCs derive from SC precursors, which differentiate into immature SCs. These immature SCs can generate both myelinating and non-myelinating SCs (or Remak glia) according to PNS requirements, like the presence of specific signals in the microenvironment and the diameter of axons in their vicinity (Jessen and Mirsky, 2005, 2019; Kidd et al., 2013).

Differentiation of OPCs and SC precursors is necessary for remyelination in demyelinating diseases like multiple sclerosis (MS) and myelin formation in dysmyelinating diseases such as leukodystrophies in the CNS or Charcot-Marie Tooth in the PNS. In this regard, understanding the mechanisms of action involved in this complex neuron-glia crosstalk will help us in the search for new therapeutic approaches in these pathologies.

Neuronal activity and several signals such as transcriptional and growth factors, axonal ligands, hormones, extracellular matrix components or neurotransmitters regulate OPC/SC precursor differentiation and myelination. Among them, GABAergic signaling has attracted great interest in the last years (Procacci et al., 2013; Zonouzi et al., 2015; Arellano et al., 2016; Hamilton et al., 2017; Serrano-Regal et al., 2020).

GABA, which is present both in the CNS and PNS, exerts an excitatory role during development to modulate neuronal growth and synapse formation (Ben-Ari, 2002). It acts mostly through ionotropic $GABA_A$ ($GABA_A$Rs) and metabotropic $GABA_B$ receptors ($GABA_B$Rs) that are well described in neurons but not yet fully characterized in myelinating cells. Although the expression of GABA receptors (GABARs) in OL/SC precursor lineages is widely documented (von Blankenfeld et al., 1991; Williamson et al., 1998; Magnaghi et al., 2004; Luyt et al., 2007; Arellano et al., 2016; Serrano-Regal et al., 2020), their role in differentiation and myelination is a matter of ongoing research.

In this review, we recapitulate recent evidence about $GABA_A$ and $GABA_B$ receptor expression and function in oligodendroglial and SCs, together with the implication of the GABAergic signaling in OPC/SC differentiation and myelination. Furthermore, we discuss possible signaling pathways involved in these events and their relevance to develop new therapies to treat demyelinating and dysmyelinating diseases.

EXPRESSION OF GABARs IN OLIGODENDROGLIAL AND SCHWANN CELLS

$GABA_A$ Receptors

$GABA_A$Rs are integral membrane ion channels—permeable to Cl^- and HCO_3^- anions—composed of five subunits that mediate the major form of fast inhibitory neurotransmission in the CNS (Olsen and Sieghart, 2008; Doyon et al., 2016). There are, at least, 19 distinct $GABA_A$R subunit genes, which include 6 α (α1-α6), 3 β (β1-β3), 3 γ (γ1-γ3), 3 ρ (ρ1-ρ3), and 1 gene of the respective δ, ε, θ, and π subunits (Sieghart and Savić, 2018). This diversity results in different homomeric or heteromeric subunit combinations that may have specific locations in the CNS, particular pharmacology, and, consequently, distinctive functional characteristics (Vogt, 2015). The subunit profile that forms $GABA_A$Rs depends on several factors including brain region, cell type, developmental stage, and physiological or pathophysiological conditions (Levitan et al., 1988; Seeburg et al., 1990; Waldvogel and Faull, 2015). Currently, 11 $GABA_A$R subtypes with different subunit combinations have been identified, being most of them heteromeric receptors formed by $\alpha x\beta x\gamma x$ or $\alpha x\beta x\delta$ (where *x* represents any subtype of a given subunit; **Figure 1A**), whereas others are homomeric receptors formed by ρ subunits (Barnard et al., 1998).

Oligodendroglial Cells

Activation of $GABA_A$Rs is relevant for the modulation of myelinating cell physiology (Magnaghi, 2007; Vélez-Fort et al., 2012), however, the specific subunit composition of $GABA_A$Rs expressed in these cells remains unknown. Electrophysiological recordings in OPCs and OLs reveal differences between the response of the $GABA_A$R expressed in these cells and those expressed in neurons and astrocytes (**Table 1**), suggesting the presence of a novel $GABA_A$R subtype with unique stoichiometry in the oligodendroglial lineage (von Blankenfeld et al., 1991; Williamson et al., 1998; Vélez-Fort et al., 2012; Arellano et al., 2016).

von Blankenfeld et al. (1991) suggested that $GABA_A$Rs in murine OPCs and OLs carry a γ subunit required to form the benzodiazepine binding site, as they observed potentiation of the GABA response in these cells with classic benzodiazepines. Moreover, the inverse agonist β-carboline methyl 4-ethyl-6,7-dimethoxy-9H-β-carboline-3-carboxylate (DMCM) reduced the GABA-induced current responses in oligodendroglial cells, unlike what happens in astrocytes. Contrary to that, Williamson et al. (1998) reported no influence of flunitrazepam or DMCM in the response elicited by GABA in rat-derived OPCs, indicating an absence of the γ subunit in the $GABA_A$Rs expressed by these cells. This observation was supported by the inhibitory effect of Zn^{2+}, which is characteristic of receptors that lack the γ2 subunit. RT-PCR analyses conducted in the same study did not find expression of γ2, α1, α6, and δ subunit mRNAs in OPCs. Although amplification of other subunits was demonstrated, the results were interpreted with caution since the preparation was 85% pure for OPCs and the presence of $GABA_A$Rs from other cell types could not be excluded. In a third study conducted by Bronstein et al. (1998), the GABA response of an immortalized murine glial cell line that expresses mature myelin proteins was insensitive to diazepam and sensitive to Zn^{2+}, reinforcing the idea of γ-subunit absence.

Later, Passlick et al. (2013) reported the expression of two types of $GABA_A$Rs in hippocampal NG2 cells from juvenile mice by functional and pharmacological analyses and single-cell RT-PCR. NG2 cells from this brain area express, on the one hand, postsynaptic $GABA_A$Rs comprised of a combination of α1, α2, β3, γ1, and γ2 subunits and, on the other hand, they

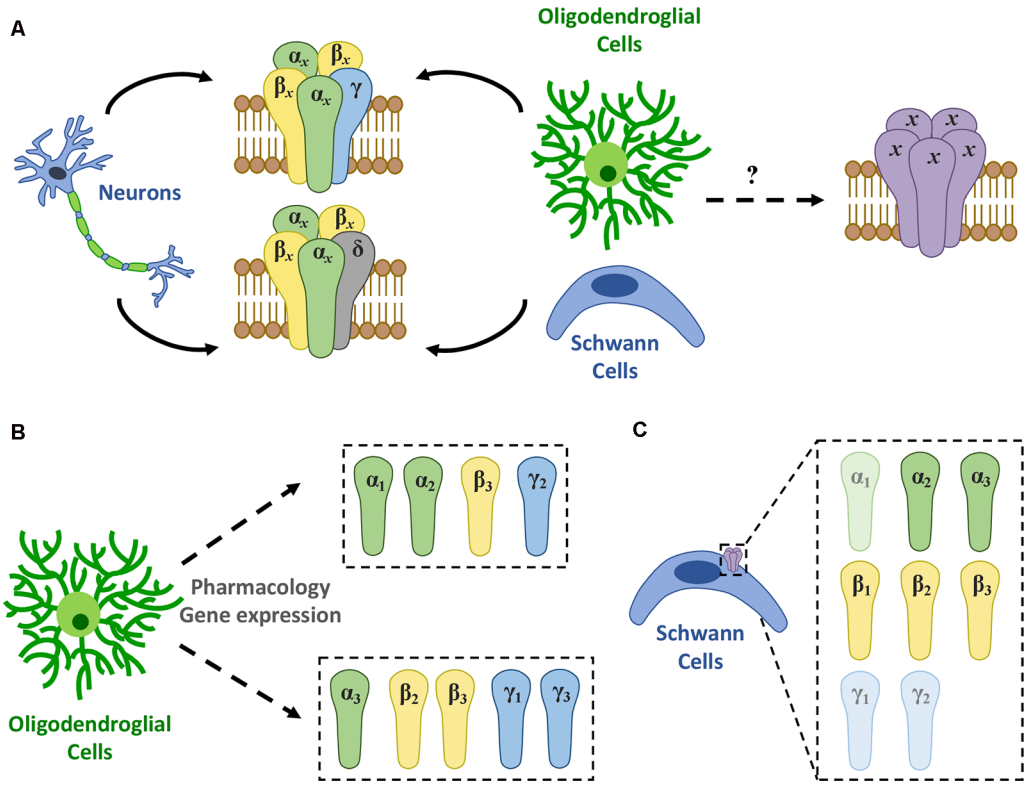

FIGURE 1 | $GABA_AR$ expression in myelinating cells. **(A)** There are 11 different $GABA_AR$ subtypes described, mainly heteromeric receptors with $\alpha x\beta x\gamma x$ or $\alpha x\beta x\delta$ (where *x* represents any subtype of a given subunit) stoichiometry (Olsen and Sieghart, 2008). Among them, a single type of $GABA_AR$ appears to be present in oligodendrocytes though its molecular nature remains elusive. **(B)** Recent evidence using gene expression and pharmacology shows that $GABA_ARs$ in oligodendroglia are heterogeneous and may change in subunit composition during differentiation. Thus, at least two novel subtypes were identified: one formed by a combination of α1 or α2, β3, and γ2 subunits (Passlick et al., 2013) and another made up by α3, β2 or β3, and γ1 or γ3 subunits (Arellano et al., 2016). **(C)** In turn, studies using RT-PCR and/or immunohistochemistry conclude that SCs express high levels of α2, α3, β1, β2, and β3, while α1, γ1, and γ2 levels are relatively low in these cells (Magnaghi et al., 2006).

have extrasynaptic $GABA_ARs$ mostly lacking the γ2 subunit (**Figure 1B**).

Our studies of $GABA_AR$ responses conducted in cultured immature OLs from the rat forebrain and mature OLs from the optic nerve showed that these cells are diazepam-sensitive, suggesting once more the presence of a γ subunit (Arellano et al., 2016). This positive modulation by benzodiazepines was observed when using low GABA concentrations ($\leq EC_{30}$), which may explain the discrepancies with previous studies. Concerning the specific subtype of γ subunit, two observations indicate that γ2 may not contribute to oligodendroglial $GABA_ARs$: (1) Zn^{2+} blocks GABA responses; and (2) indiplon, a positive allosteric modulator acting on γ2 subunit-containing receptors, does not modulate GABA currents. Therefore, these receptors likely contain either γ1 or γ3 subunit (Arellano et al., 2016).

Regarding β subunits, potentiation of the GABA response by loreclezole suggests the presence of β2 or β3 subunits, since β1 subunit-containing receptors are insensitive to this drug (Arellano et al., 2016). Finally, concerning α subunits, α3 is the most likely candidate because it forms receptors with low sensitivity to GABA (Karim et al., 2013), as it is the case of OLs (EC_{50} between 70 and 100 μM).

Together, these pharmacological studies suggest that the composition of the $GABA_AR$ expressed in rat-derived oligodendroglial cells is a combination of the α3, β2 or β3, and γ1 or γ3 subunits (**Figure 1B**). Also, we confirmed the expression of the α3 subunit by immunocytochemistry in cultured OLs (Arellano et al., 2016). These observations are supported by previous functional genomic analyses performed in OLs (Cahoy et al., 2008). Moreover, RNA sequencing (RNA-Seq) transcriptional analyses of purified NG2 cells obtained from P17 mice revealed that the α3 subunit is the most expressed α-subtype, while among β subunits, β3 and β2 are much more abundant than β1. Lastly, γ1 is expressed at much higher levels than γ2 and γ3 (Larson et al., 2016).

An important factor for the diversity of $GABA_ARs$ expressed and the subunits involved in their conformation will undoubtedly be the species. For example, regarding humans, a recent study of the $GABA_AR$-subunit expression in OPCs isolated from the middle temporal gyrus of healthy adults—based on the single-nucleus RNA-Seq analysis by Hodge

TABLE 1 | Pharmacological properties of neuronal and oligodendroglial $GABA_A$Rs.

	Neurons		
Drug	**Synaptic ($\alpha x\beta x\gamma 2$)**	**Extrasynaptic ($\alpha x\beta x\delta$)**	**Oligodendroglial cells**
GABA	Low EC_{50} 1–30 μM (Gibbs et al., 1996; Baur and Sigel, 2003; Mortensen et al., 2012)	Low EC_{50} 0.5 nM–10 μM (Brown et al., 2002; Wallner et al., 2003; Mortensen et al., 2012)	High EC_{50} 70–100 μM (Williamson et al., 1998; Arellano et al., 2016)
THIP	No effect (Mortensen et al., 2010)	+ (Brown et al., 2002; Meera et al., 2011)	No effect (Arellano et al., 2016)
Zn^{2+}	Low or No effect (Hosie et al., 2003)	– (Carver et al., 2016)	– (Bronstein et al., 1998; Passlick et al., 2013; Arellano et al., 2016)
β-CCB	– or No effect (Peña et al., 1986; Cisneros-Mejorado et al., 2020)	No effect (Jiménez-González et al., 2011)	+ (Arellano et al., 2016; Cisneros-Mejorado et al., 2020)
DMCM	– (Peña et al., 1986)	– (Brown et al., 2002)	– (von Blankenfeld et al., 1991; Arellano et al., 2016)
Diazepam	+ (Walters et al., 2000; Goodkin and Kapur, 2009)	No effect (Goodkin and Kapur, 2009)	+ (von Blankenfeld et al., 1991; Passlick et al., 2013; Arellano et al., 2016)
Indiplon	+ (Petroski et al., 2006)	No effect (Michelsen et al., 2007)	No effect (Arellano et al., 2016)
Flunitrazepam	+ (Goodkin and Kapur, 2009)	No effect (Goodkin and Kapur, 2009)	+ (von Blankenfeld et al., 1991; Arellano et al., 2016)
Loreclezole	+* (Wingrove et al., 1994)	+* (Wingrove et al., 1994)	+ (Arellano et al., 2016)

(+) Potentiator/agonist; (–) Inhibitor; (*) β2 or β3 subunit required.

et al. (2019)—showed that OPCs from this brain area express high mRNA levels of α3, all β subunits, γ2 and, interestingly, the ε subunit (**Figure 2**). These mRNAs, if translated and incorporated into functional receptors, would increase the variety of potential configurations and may have important functional and pharmacological consequences (Jones and Henderson, 2007; Bollan et al., 2008; Belujon et al., 2009).

Schwann Cells

$GABA_A$-type receptors are relevant to SC physiology (Magnaghi et al., 2001, 2006). However, their pharmacological and functional properties, as well as their molecular identity, are not clear. $GABA_A$R subunit composition in rat-derived cultured SCs includes α2 and α3, as well as the three β subunits, while mRNAs of α1 and γ2 subunits have been found at much lower levels (Magnaghi et al., 2006; **Figure 1C**). Moreover, the presence of α2, α3, and β3 proteins were confirmed by immunocytochemistry. Alpha-2 and β3 subunits are also expressed in SC-like adult stem cells derived from bone marrow or adipose tissue, as their levels are upregulated following SC differentiation *in vitro* (Faroni et al., 2012). Also, $GABA_A$R stimulation with muscimol increases the proliferation rate of SCs, meaning that GABAergic signaling has an important role in these cells (Magnaghi et al., 2006). However, despite these important findings, there is still little knowledge about the specific composition of $GABA_A$Rs expressed in differentiated SCs.

$GABA_B$ Receptors

$GABA_B$Rs are G-protein coupled receptors (GPCRs) responsible for the slower and prolonged GABA-mediated inhibitory transmission. They were first described pharmacologically as bicuculline-insensitive metabotropic receptors that were activated by the GABA analog baclofen (Bowery and Hudson, 1979; Hill and Bowery, 1981). Functional $GABA_B$Rs are heterodimers constituted by two receptor subunits, $GABA_{B1}$ and $GABA_{B2}$, that cooperate to perform signal activation (Kaupmann et al., 1998; Kuner et al., 1999). $GABA_{B1}$ is responsible for ligand binding, while $GABA_{B2}$ contains binding sites for allosteric modulators (Galvez et al., 2001; Binet et al., 2004), couples with $G_{i/o}$-protein, and is necessary for trafficking the heterodimer to the cell surface, where the receptor becomes active (Calver et al., 2000; Couve et al., 2000). Among the effector elements involved in $GABA_B$R signaling pathways in neurons are voltage-gated Ca^{2+} channels (VGCC), inwardly-rectifying potassium channels (Kir) and adenylyl cyclase (AC; Bowery et al., 2002; Bettler et al., 2004; **Figure 3**). However, the specific coupling of $GABA_B$Rs to the molecular effector may differ depending on the cell type and region analyzed (Booker et al., 2018).

Oligodendroglial Cells

Myelinating cells express both subunits of $GABA_B$Rs, which are negatively-coupled to AC (Magnaghi et al., 2004; Luyt et al., 2007). However, their functional characteristics are not as well known as in the case of neurons. Regarding oligodendroglial cells, we recently confirmed by immunocytochemistry and RT-qPCR the expression of $GABA_{B1}$ and $GABA_{B2}$ subunits in OPCs and OLs from the rat cerebral cortex and in OLs from the optic nerve (Serrano-Regal et al., 2020). We also performed calcium imaging assays and electrophysiological

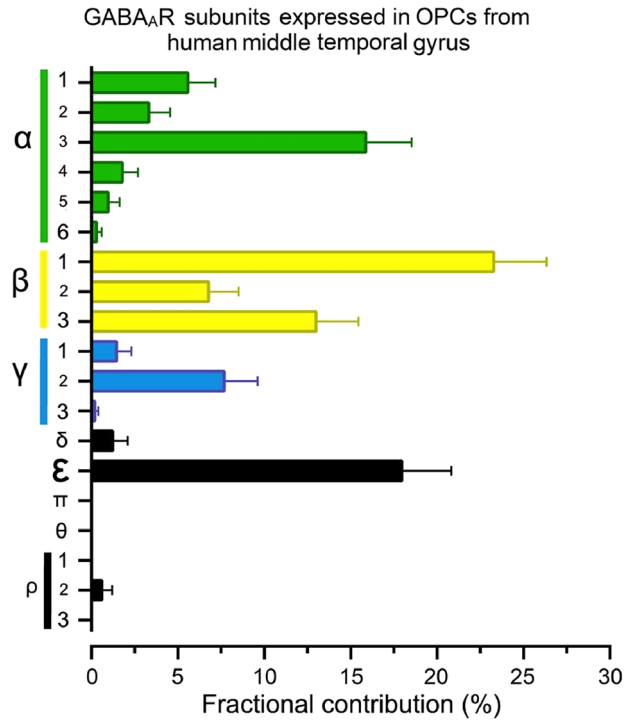

FIGURE 2 | The fractional contribution (FC) of GABA$_A$R subunits in human oligodendrocyte progenitor cells (OPCs). Normalized gene expression levels for all 19 GABA$_A$R subunits expressed as a percentage (mean ± S.E.M.) of the total available pool of mRNA for GABA$_A$Rs in OPCs (PDGFRα$^+$ cells) from human brains, estimated from publicly available datasets (Hodge et al., 2019; https://celltypes.brain-map.org/rnaseq). The single-nucleus analysis used normalized RNA-Seq datasets from the middle temporal gyrus isolated from six subjects with no known neuropsychiatry or neuropathological history (three males and three females; 35–66 years old). Gene expression level in each dataset was transformed into FC (Sequeira et al., 2019). FC is defined as the percentage of the expression level of each subunit gene (signaled in the "y" axis) to the sum of the 19 genes for GABA$_A$Rs subunits within each human/cell. Detailed demographic characteristics, as well as technical white papers for data processing and quality control, can be downloaded from the same site. Confirmatory analysis of OPC markers enrichment and lack of neuronal markers were performed for all datasets.

recordings in these cells and observed that baclofen does not modify their response to KCl 50 mM, calcium influx, and Kir currents. These results strongly suggest that GABA$_B$Rs in oligodendroglial cells are not coupled to Ca^{2+} and Kir channels in the same manner as in other cell types (Serrano-Regal et al., 2020). Likewise, GABA$_B$Rs from CA1 somatostatin interneurons, unlike pyramidal neurons, are not coupled to the canonical Kir3 signaling cascade (Booker et al., 2018), which suggests a functional diversity of downstream effectors depending on cell type and location, and warrants the need of exploring these features in OLs as well as in SCs.

Charles et al. (2003) did not find any colocalization of GABA$_{B1}$ subunit and MBP expression in myelinating OLs in the white matter of the rat spinal cord and suggested that GABA$_B$R expression in developing OLs decreases during differentiation. Following this, Luyt et al. (2007) observed downregulation of the GABA$_{B1}$ subunit in mature OLs from the mouse periventricular white matter, while the expression of GABA$_{B2}$ remained constant. As they reported changes in GABA$_{B1}$/GABA$_{B2}$ ratios in mature OLs, they raised the possibility that one subunit alone or in combination with another protein could make GABA$_B$R functional in different cell types (Calver et al., 2000; Luyt et al., 2007). In contrast, our recent results show that cultured oligodendroglial cells from the rat forebrain and mature OLs from the optic nerve express GABA$_{B1}$ and GABA$_{B2}$ subunits at different stages of maturation, as well as mature OLs from the juvenile and adult rodent *corpus callosum in vivo* (Serrano-Regal et al., 2020). These discrepancies can be explained by the different regions analyzed, as GABA$_{B1}$/GABA$_{B2}$ expression exhibits important regional variations (Luyt et al., 2007). Since oligodendroglial cells are extremely diversified, the different cells targeted in these studies may correspond to distinct oligodendroglial and OPC subpopulations (Marques et al., 2016; Spitzer et al., 2019; Marisca et al., 2020).

Schwann Cells

SCs also express different isoforms of the GABA$_B$R, such as -1a, -1b, -1c, and -2 (Magnaghi et al., 2004, 2006).

Downregulation of GABA$_B$R expression occurs in pre- and non-myelinating SCs (Corell et al., 2015). Neurosteroids modulate the expression of GABA$_B$R subunits in cultured SCs and, as GABA$_B$R is downregulated with age in the PNS, the GABA synthesized in the adult sciatic nerve acts through the ionotropic GABA$_A$R, present both in neurons and SCs (Magnaghi et al., 2006). Interestingly, the conditional knockout of the GABA$_{B1}$ subunit in SCs changes the expression of GABA$_A$R subunits α3, α4, β1, and δ (Faroni et al., 2019), suggesting that GABA$_B$Rs in these cells regulate somehow the expression of GABA$_A$Rs and/or their subunits.

Overall, more detailed analyses such as single-cell RNA-seq would help to better figure out the expression of GABA$_{B1}$ and GABA$_{B2}$ subunits along the oligodendroglial and SC lineages.

POTENTIAL GABA SYNTHESIS AND RELEASE IN MYELINATING CELLS

Although GABAergic neurons are the main source of GABA (especially in the CNS), GABA synthesis also occurs in glial cells (Seiler et al., 1979; Angulo et al., 2008; Héja et al., 2012). Two potential pathways for GABA synthesis have been described in brain-derived glial cells. GABA is mainly produced through the classical pathway as a result of glutamate decarboxylation by the glutamic acid decarboxylase (GAD) enzymes (Roberts and Frankel, 1950). In neurons, the two isoforms of GAD—GAD$_{65}$ and GAD$_{67}$—differ in their catalytic and kinetic properties and their subcellular distribution (Kaufman et al., 1991). Also, GABA can be synthesized from the monoacetylation of putrescine with the participation of the monoamine oxidase B (MAO$_B$) enzyme in the non-classical pathway (Seiler et al., 1973).

Consistent with an RNA-seq transcriptome and splicing database (Zhang et al., 2014), oligodendroglial cells express *gad1*, *gad2*, and *maob* mRNAs. GAD$_{67}$ mRNA (*gad1*) is greatly expressed by OPCs, although its levels decrease notably as they

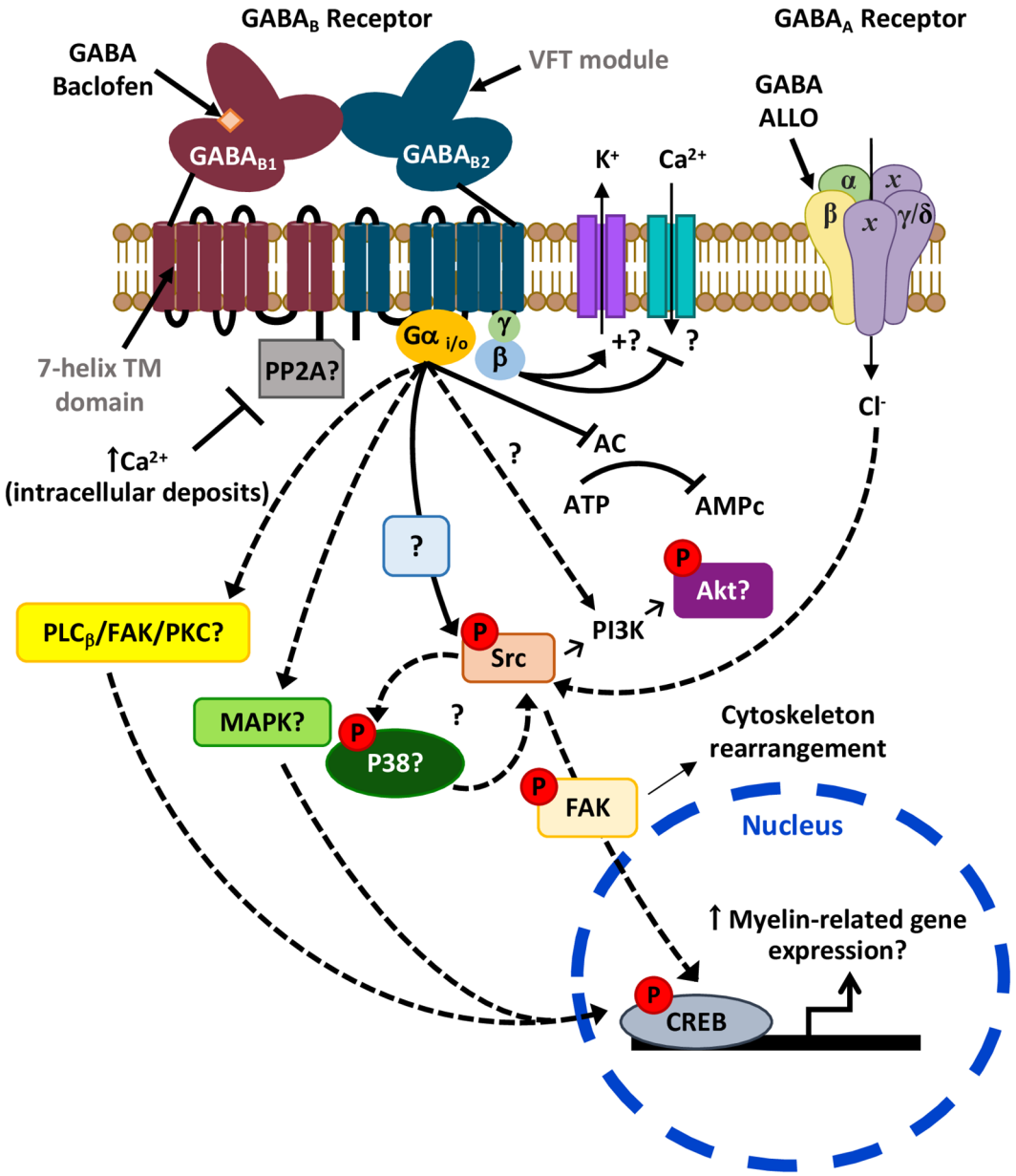

FIGURE 3 | Possible signaling pathways downstream GABARs leading to myelination. Activation of the Gi/o-linked $GABA_BR$ may reduce CREB phosphorylation as it is negatively coupled to adenylyl cyclase (AC; Luyt et al., 2007). Alternatively, it may also induce CREB phosphorylation possibly *via* activation of $PLC_β$/FAK/PKC or MAPK cascades, as observed in neurons (Carlezon et al., 2005; Zhang et al., 2015). Moreover, activation of $GABA_BR$ leads to Src phosphorylation (Serrano-Regal et al., 2020) that could ultimately induce CREB activation. Phosphorylation of Src may also lead to Akt phosphorylation *via* PI3K as observed earlier (Barati et al., 2015), and contribute to a positive feedback loop with p38MAPK (Mugabe et al., 2010; Lin et al., 2015), which is involved in myelination (Fragoso et al., 2003, 2007). On the other hand, the $GABA_{B1}$ subunit of $GABA_BR$ might be sequestered by phosphatases like PP2A (as occurs in some neurons), a mechanism that blocks its activity and can be reverted by high intracellular Ca^{2+} levels (Li et al., 2020). Finally, the $GABA_AR$ allosteric modulator ALLO regulates Schwann cell (SC) myelination *via* Src-FAK signaling, involving cytoskeleton reorganization (Melfi et al., 2017).

differentiate into mature myelinating OLs. However, *gad2* is expressed to a lesser extent throughout the oligodendroglial lineage. Regarding *maob*, OPCs and myelinating OLs express higher levels than newly formed or immature OLs (Zhang et al., 2014). Accordingly, we confirmed the presence of $GAD_{65/67}$ by immunocytochemistry and western blot in rat-derived cortical oligodendroglial cells at 1, 3, and 6 days *in vitro* (Serrano-Regal et al., 2020). Similarly, we verified the expression of the MAO_B enzyme in these cells at the same time points. These results indicate that cultured oligodendroglial cells may synthesize GABA by the two alternative pathways mentioned above. Indeed, we found GABA immunostaining in cortical and optic-nerve

derived oligodendroglial cells at different stages of maturation (Serrano-Regal et al., 2020). Possibly, GABA is synthesized by one pathway or another depending on the stage of maturation of the cells, as GABA may have different roles in OPCs vs. mature OLs.

GAD_{67} is present in SCs and its levels increase in the presence of the progesterone metabolite allopregnanolone (ALLO; Magnaghi et al., 2010). Moreover, Corell et al. (2015) demonstrated the presence of GABA and $GAD_{65/67}$ in premyelinating and non-myelinating SCs. These findings show that SCs both produce and store GABA.

Together, these observations indicate that OLs and SCs synthesize and store GABA, which could be released by reversal operation of GABA transporters including GAT-1 and GAT-3, that are expressed by OLs (Fattorini et al., 2017; Serrano-Regal et al., 2020). Also, SCs are capable to take up ambient GABA at concentrations above 1 μM (Brown et al., 1979), though the nature of the transporters involved is still unknown.

GABA RECEPTORS IN OPC/SC PRECURSOR DIFFERENTIATION AND MYELINATION

In the CNS, OPCs are the main (but not unique) source of remyelination, since they respond to white matter injury, migrate to the lesioned area and differentiate into mature OLs to produce new myelin sheaths (Franklin et al., 1997; Nait-Oumesmar et al., 1999; Hesp et al., 2015). Moreover, surviving mature OLs are also a source of remyelination (Duncan et al., 2018). SCs may also participate, although to a lesser extent, in restoring myelin in the CNS (Zawadzka et al., 2010; García-Díaz and Baron-Van Evercooren, 2020).

Differentiation of OPCs/SCs and myelination are exquisitely coordinated processes mediated by a deep dialogue between neuronal and glial cells that entail the participation of a variety of signals and intercellular communication systems, including ATP, glutamate or GABA neurotransmitter signaling (Li et al., 2013; Faroni et al., 2014; Salzer, 2015; Zonouzi et al., 2015; Arellano et al., 2016; Hamilton et al., 2017; Serrano-Regal et al., 2020), as well as neuronal activity (Wake et al., 2011; Gibson et al., 2014; Fannon et al., 2015). Specifically, GABAergic neurons establish direct synapses with OPCs throughout the CNS, indicating that this communication may control proliferation, migration, differentiation, the establishment of axonal contacts and their wrapping, OPC survival in the adult brain or myelin maintenance (Lin and Bergles, 2004; Kukley et al., 2008; Vélez-Fort et al., 2010; Orduz et al., 2015; Zonouzi et al., 2015; Balia et al., 2017; Mount et al., 2019). However, the precise function of GABA in OPC differentiation and myelination remains controversial.

$GABA_A$ Receptors

Contrary to mature neurons, activation of $GABA_A$Rs in OPCs leads to depolarization and an increase in cytosolic Ca^{2+} levels (Kirchhoff and Kettenmann, 1992), resulting from Ca^{2+} influx through activated VGCC (Paez and Lyons, 2020). Thus, a rise in Ca^{2+} in the cytosol may regulate OPC proliferation, migration and maturation and, consequently, OL (re)myelination (Cheli et al., 2016; Santiago-González et al., 2017; Baraban et al., 2018; Krasnow et al., 2018; Marisca et al., 2020).

As oligodendroglial cells constitute a highly dynamic and heterogeneous population, the expression of $GABA_A$Rs and their different subunits changes as these cells progress along their lineage, as occurs with the expression of certain ion-channels (Spitzer et al., 2019), and these changes can affect their intercellular relationship and differentiation. In line with this, we observed that oligodendroglial $GABA_A$R expression *in vitro* is dependent on the close interaction between axons and OLs, as OLs cultured alone lose GABA responses with differentiation (Arellano et al., 2016). Moreover, the presence of the γ2 subunit, which is associated with a possible role in neuron-OPC synapse formation, decreases with age along with the density of GABAergic synaptic contacts in cortical NG2 cells of mature mice (Balia et al., 2015). Thus, NG2 cells may switch the expression of $GABA_A$Rs from synaptic (with γ2 subunit) to extrasynaptic (without γ2 subunit) during development (Vélez-Fort et al., 2010). Surprisingly, genetic inactivation of oligodendroglial γ2 does not affect OPC proliferation and differentiation, while it causes progressive and specific depletion of the OPC pool that lacks γ2-mediated synaptic activity without affecting the oligodendrocyte production (Balia et al., 2017). These observations indicate that GABAergic communication in cortical OPCs through γ2-containing $GABA_A$Rs does not play a role in oligodendrogenesis but rather modulates OPC maintenance.

GABAergic signaling regulates OPC population and OPC differentiation and myelination in the cerebellar white matter *in vivo* (Zonouzi et al., 2015). In turn, hypoxia causes a strong downregulation of the GABAergic synaptic input from local interneurons to OPCs (NG2 cells) as well as an increase in the proliferation of these cells and a delay in their maturation, which limits myelination. These effects are mimicked in control animals when blocking $GABA_A$Rs with their antagonist bicuculline. However, they are reverted when applying tiagabine, a selective inhibitor of the GABA transporter GAT-1 that increases GABA availability in the extracellular space. Treatment with tiagabine results in a decrease of NG2 cell proliferation and an increase of myelinating OLs, reverting the hypomyelinating effect caused by perinatal hypoxia (Zonouzi et al., 2015). These findings strongly suggest that GABAergic signaling (either neuronal activity-dependent or independent) influences OPC development and differentiation and, therefore, it may help to develop novel therapies to improve OPC differentiation into damaged brain areas.

GABAergic signaling through $GABA_A$Rs may also be relevant for the stronger remyelination that occurs following focal demyelination in the *corpus callosum* of late pregnant rats compared to virgin and postpartum ones (Kalakh and Mouihate, 2019). This pregnancy-associated promyelinating effect was lost when either the $GABA_A$R was blocked or when 5α-reductase, the rate-limiting enzyme for the endogenous $GABA_A$R activator ALLO, was inhibited (Kalakh and Mouihate, 2019). Moreover,

N-butyl-β-carboline-3-carboxylate (β-CCB), a selective drug activating preferentially oligodendroglial $GABA_AR$s, promotes remyelination in a model of gliotoxin-induced demyelination in the rat cerebellar caudal peduncle as assessed using magnetic resonance imaging (MRI) together with myelin staining (Cisneros-Mejorado et al., 2020). Together, these results strongly suggest that $GABA_AR$-mediated signaling promotes myelination and remyelination in OLs either directly or indirectly. However, at odds with these data, activation of $GABA_AR$s by endogenous GABA in cortical organotypic cultures reduces the number of oligodendroglial cells and myelination whereas enlarges internode length, influencing the velocity of the nerve impulse propagation (Hamilton et al., 2017). These effects may be due to GABA released by glial cells. However, we could not assess this idea as gabazine treatment of OPC cultures had no significant effect on myelin protein production (Serrano-Regal et al., 2020).

Neurosteroid therapy is another pharmacological approach to modulate $GABA_AR$ activity in the nervous system, as they act as allosteric modulators of these receptors in the nanomolar concentration range (Lambert et al., 2009). Indeed, progestin ALLO increases myelin basic protein (MBP) production in rat-derived cerebellar organotypic slices, an effect that requires $GABA_AR$s (Ghoumari et al., 2003). This observation points to these receptors as mediators of myelination. The effects of neurosteroids are of special interest in postnatal development, as they may help to prevent neurodevelopmental disorders associated with preterm birth (Shaw et al., 2019). ALLO, which is mainly synthesized in the placenta, has an important role during nervous system development. In premature neonates, ALLO concentration decreases abruptly and this decrease is associated, in part, with hypomyelination (Shaw et al., 2015). Consequently, experimental administration of the ALLO analog ganaxolone as replacement therapy in guinea pig-preterm neonates showed positive effects on myelination, through its interaction with $GABA_AR$s. Therefore, neurosteroid replacement could be a good therapeutic option to improve myelination in this condition (Shaw et al., 2019).

Neurosteroids may also enhance $GABA_AR$ function in SCs. Thus, ALLO acting *via* $GABA_A$ receptor can influence peripheral myelin protein 22 (PMP22) synthesis (Magnaghi et al., 2006). Moreover, ALLO modulates SC morphology, motility, and myelination in SC/dorsal root ganglia neuron (DRG) co-cultures *via* the Src/focal adhesion kinase (FAK) pathway, a signaling cascade that involves $GABA_AR$s and relies on actin rearrangements (Melfi et al., 2017). Therefore, neurosteroids represent a promising molecular approach for the treatment of peripheric pathologies. Together, the studies discussed in this section connect $GABA_AR$ signaling with OPC/SC differentiation and/or myelination using pharmacological approaches. However, the results observed cannot be solely attributed to the action of GABA on $GABA_AR$s. Although pharmacology may be a good strategy to enhance OPC/SC differentiation and myelination in pathological conditions, potential side-effects must also be considered. To minimize them, it would be of great interest to use more specific drugs acting on myelinating cell $GABA_AR$s and/or to use genetic approaches to specifically target the different $GABA_AR$ subunits expressed in these cells.

$GABA_B$ Receptors

An early study suggests that $GABA_BR$s may be relevant for OPC development as baclofen increases migration and proliferation in cultured OPCs derived from periventricular white matter (Luyt et al., 2007). However, more recent studies could not confirm those findings as baclofen did not change OPC proliferation or total OPC number in dissociated and organotypic cultures derived from the cortex (Hamilton et al., 2017; Serrano-Regal et al., 2020). This discrepancy could reflect the different brain areas studied. Thus, different subpopulations of OPCs may exist in white and gray matter that behave differently or have different responses to baclofen, as proposed by Luyt et al. (2007). In contrast, baclofen reduced cell proliferation of SC cultures (Magnaghi et al., 2004). However, in dissociated developing DRG primary cultures, in which SCs proliferate spontaneously *in vitro*, baclofen did not affect (Corell et al., 2015).

On the other hand, GABA and baclofen modulate OPC differentiation, as well as the myelination capacity of mature OLs cultured with DRG neurons, pointing out $GABA_BR$s as relevant modulators of OL maturation and myelination (Serrano-Regal et al., 2020). Consistent with these observations, $GABA_BR$s also regulate SC differentiation both in the myelinating and non-myelinating phenotypes. Thus, forskolin-induced SC differentiation *in vitro* correlates with a redistribution of $GABA_{B1}$ and $GABA_{B2}$ subunits of $GABA_BR$s. Indeed, in the cytoskeleton rearrangement that takes place during differentiation, $GABA_BR$s colocalize with f-actin on the SC elongated processes (Procacci et al., 2013).

Apart from being essential for SC commitment to a non-myelinating phenotype during development, $GABA_BR$s are key modulators of neuronal-SC interactions regarding myelination, as $GABA_{B1}$ receptor total null mice showed altered levels of PMP22 and myelin protein zero (P0) as well as thinner myelin sheaths. These mice also presented fiber alterations, which causes changes in pain behavior, gait abnormalities, and motor coordination disturbances (Magnaghi et al., 2008). Together, these findings suggest a role for $GABA_BR$s in the control of SC myelination. Moreover, both $GABA_BR$ subunits in addition to GABA and $GAD_{65/67}$ were found at the node of Ranvier in a sub-population of myelinated sensory fibers (Corell et al., 2015). Surprisingly, $GABA_BR$ expression is upregulated in SCs of injured nerves, which may be interpreted as an adaptive response for stimulating the neighboring axons to re-grow distally to the injury (Corell et al., 2015).

Finally, conditional deletion of the $GABA_{B1}$ subunit in SCs altered their proliferation, migration, and myelination capacities, as well as reduced neurite length of co-cultured DRGs (Faroni et al., 2019). Furthermore, molecular and transcriptomic changes were also observed both in SCs and DRGs derived from mice lacking $GABA_{B1}$ subunit in SCs (P0-GABA-$B1^{fl/fl}$). Interestingly, the expression of some $GABA_AR$ subunits by SCs and DRGs was also altered, indicating a possible role of $GABA_BR$s in regulating the expression of $GABA_AR$s in these cells (Faroni et al., 2019). Similar studies using conditional deletion of $GABA_BR$

subunits in oligodendroglia will help to understand the role of these receptors and their impact on myelination and pain and motor behavior.

POSSIBLE SIGNALING PATHWAYS DOWNSTREAM GABARs RELATED TO MYELINATION

Myelination, either by OLs or SCs, involves the participation of several intracellular signaling pathways. Indeed, some of those pathways are common in the CNS and PNS. For instance, binding of neuregulins (NRGs) to ErbB receptors activates a sequence of canonical intracellular pathways downstream from many receptor tyrosine kinases (RTKs), such as phosphatidylinositol-3-kinase (PI3K)/Akt/mammalian target of rapamycin (mTOR) or mitogen-activated protein kinases (MAPK; Newbern and Birchmeier, 2010).

Intracellular 3′,5′-cyclic adenosine monophosphate (cAMP) induces cell differentiation and myelination requiring the participation of the cAMP response element-binding protein (CREB). CREB mediates the stimulation of MBP expression by cAMP in OLs (Afshari et al., 2001). Moreover, in mouse-derived cultured SCs, the combined action of cAMP/NRG1 increases the expression of myelin proteins Krox-20 and P0, through a mechanism that relies on the activity of transcription factors from the CREB family (Arthur-Farraj et al., 2011).

The Src family kinases (SFKs) are nonreceptor tyrosine kinases that integrate external signals from both integrin and growth factor receptors and transduce signals related to OL and SC development and myelination (Colognato et al., 2004; Melfi et al., 2017). In particular, signaling pathways downstream the Src-family member Fyn regulate morphological differentiation of OLs, the recruitment of cytoskeleton components, and local translation of MBP (see White and Krämer-Albers, 2014; Quintela-López et al., 2019). $GABA_BR$ specific activation with baclofen induces Akt phosphorylation, which is dependent on PI3K and Src kinases, promoting chemotaxis and cytoskeletal rearrangement in rat basophilic leukemic cells (Barati et al., 2015). Accordingly, we found that Src-family kinases inhibition abrogates $GABA_BR$-induced OL differentiation (Serrano-Regal et al., 2020). This observation corroborates the role of the Src family in OL differentiation through a mechanism dependent on $GABA_BR$ activation (**Figure 3**).

$GABA_AR$s are also linked to Src and FAK signaling. The modulation of SC development and myelination by the neurosteroid ALLO in SC/DRG co-cultures occurs *via* Src and FAK signaling activation, which depends on $GABA_AR$s and actin reorganization (Melfi et al., 2017). Besides, Src-family members can interact reciprocally with kinases from the MAPK family, like the serine/threonine-protein kinase p38 MAPK, as c-Src elicits p38 MAPK phosphorylation and the opposite (Mugabe et al., 2010; Lin et al., 2015; Wu et al., 2015). Therefore, it would be of great interest to investigate this kind of interactions in myelinating cells, as p38 MAPK is a key element in the initial steps of myelination in SCs (Fragoso et al., 2003), as well as in OL maturation and myelination since specific p38 inhibitors block *in vitro* myelination of DRGs by OLs (Fragoso et al., 2007). Also, conditional knockout of p38 in oligodendroglial cells leads to defects in myelination early in development (Chung et al., 2015). At odds with those findings, deletion of p38 in the same mouse model increases remyelination after cuprizone-induced demyelination (Chung et al., 2015), while selective deletion of p38α MAPK in OLs did not compromise myelination in a mouse model of periventricular leukomalacia (PVL; Chung et al., 2018). These conflicting pieces of evidence indicate that the precise role of p38 MAPK in SC/OL differentiation and myelination and its relation with GABARs remains to be elucidated (**Figure 3**).

Since $GABA_BR$s couple negatively to AC in OLs (Luyt et al., 2007), activation of CREB downstream these receptors is not expected due to decreased cAMP levels. However, other intracellular signaling cascades activated downstream G-protein coupled receptors, such as MAPK cascades, may phosphorylate CREB (see Carlezon et al., 2005). Thus, $GABA_BR$ stimulation in cultured mouse cerebellar granule neurons with baclofen activates CREB *via* PLCβ/FAK/PKC (Zhang et al., 2015). Further clarification of the link between $GABA_BR$ activation and CREB specifically in myelinating cells is a matter of ongoing study and could contribute to a better understanding of the signaling routes that control myelination and remyelination (**Figure 3**).

Finally, $GABA_BR$ function may be modulated by its direct association to protein phosphatase 2A (PP2A), as observed in GABAergic neurons from the rodent ventral tegmental area (Li et al., 2020). Therefore, PP2A-$GABA_BR$ interaction results in an increase of $GABA_BR$ dephosphorylation and its subsequent internalization, an effect reverted with high intracellular Ca^{2+} levels. Again, it is worth exploring if these mechanisms also occur in myelinating cells and whether they are relevant to myelin pathology (**Figure 3**).

DISCUSSION

GABA is among the signals that drive OLs and SCs to axon interactions. The fact that GABA acts mainly on two different types of receptors—ionotropic $GABA_AR$s and metabotropic $GABA_BR$s—makes it difficult to understand the role of this neurotransmitter in myelinating cell physiology. Moreover, OLs and SCs are highly dynamic cell lineages with different stages of maturation.

While the molecular composition of both GABARs and their mechanisms of action are well described in neurons, their properties in myelinating glial cells remain elusive. Native $GABA_AR$s are composed of multiple subunit combinations with diverse pharmacology, both of which vary regionally, adding a huge heterogeneity to their properties and functions. This diversity is also reflected somehow in $GABA_AR$s in OLs and SCs. Thus, SCs express extra-synaptic subunits (in particular the δ subunit, which is key for neurosteroid affinity), while OLs express subunits commonly found at postsynaptic densities, meaning that $GABA_AR$s of OLs and SCs have different subunit composition and, consequently, different pharmacological profiles and functional behaviors (Faroni et al., 2019). Also, there is a switch in the expression of synaptic to extrasynaptic $GABA_AR$s as OPCs progress in the lineage (Vélez-Fort et al., 2010; Balia et al., 2017).

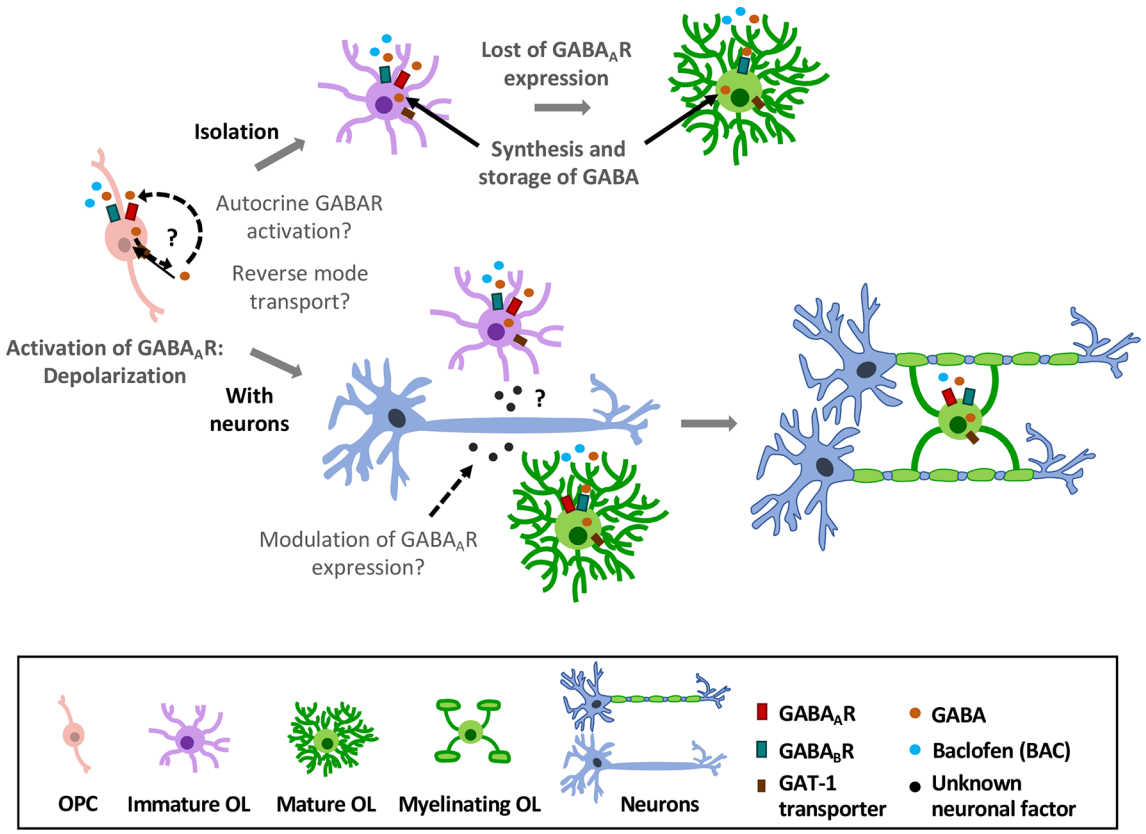

FIGURE 4 | Effects of GABAergic signaling in oligodendroglial differentiation and myelination. OPCs express $GABA_A$ and $GABA_B$Rs. Activation of $GABA_A$Rs causes depolarization in these cells (Kirchhoff and Kettenmann, 1992; Baraban et al., 2018). In absence of axons (top), they lose $GABA_A$R expression as they differentiate into mature OLs (Berger et al., 1992; Arellano et al., 2016); however, expression of $GABA_B$Rs is largely stable over time (Serrano-Regal et al., 2020). In the presence of axons (low), $GABA_A$R expression is modulated by neurons, as OPCs maintain their expression towards the myelinating stage (Arellano et al., 2016). Moreover, oligodendroglial cells express GAT-1 transporter and synthesize GABA, which may be released by reverse GAT-1 operation and activate GABA receptors (GABARs) in an autocrine manner. Exogenous GABA or baclofen promotes oligodendroglial differentiation and myelination *in vitro* (Serrano-Regal et al., 2020).

In oligodendroglial cells, $GABA_A$R expression goes down as they mature and acquire a myelinating phenotype (Berger et al., 1992; Arellano et al., 2016). In contrast, $GABA_B$R expression is quite stable at all stages (Serrano-Regal et al., 2020). Sustained $GABA_A$R expression in oligodendroglial cells depends on the presence of axons, though the mechanisms driving $GABA_A$R stabilization remain still unknown. Thus, it is likely that molecules released from neurons in an activity-independent manner may drive $GABA_A$R expression (Arellano et al., 2016; Hamilton et al., 2017; **Figure 4**).

Also, OLs and SCs can synthesize and store GABA, and to take it up from the extracellular fluid through specific GABA transporters (Fattorini et al., 2017). It is therefore conceivable that these cells may release GABA by mechanisms including reverse functioning of the transporters, as observed in other glial cell types (Barakat and Bordey, 2002). Early experiments demonstrated that cultured satellite glial cells from DRG can release [^{3}H]GABA in response to a depolarizing stimulus (Minchin and Iversen, 1974). Thus, GABA released by myelinating cells might act in a paracrine or autocrine way (as suggested by Magnaghi, 2007) to, ultimately, modulate their differentiation and/or their myelination capacity (**Figure 4**). Interestingly, this mechanism operates for instance in polysialylated forms of neural cell-adhesion molecule (PSA-NCAM) progenitor cells in the CNS, which eventually differentiate into glial cells. Thus, autocrine/paracrine loops involving neurosteroids and GABA signaling in these progenitors modulate their proliferation and differentiation (Gago et al., 2004). Synthesis of neurosteroids occurs in SCs (Chan et al., 2000), and may stimulate GABA synthesis in these cells *via* a rapid protein kinase A (PKA)-dependent autocrine loop (Magnaghi et al., 2010). In this way, neurosteroids provide the specific ligand for $GABA_A$R activation (Magnaghi et al., 2010). As neurosteroids are involved in promoting SC differentiation and myelination acting through $GABA_A$Rs, a possible paracrine/autocrine mechanism could underlie these processes.

$GABA_A$ and $GABA_B$ receptors may exert opposite roles on myelinating cells, as proposed for SCs in pathological conditions (Faroni and Magnaghi, 2011). Both central and peripheral myelinating cells express $GABA_A$ and $GABA_B$ receptors, however, this expression depends on the presence

of surrounding axons and, as occurs with other receptors and transporters, may vary along the lineage or even depending on the nervous system area (Marques et al., 2016; Spitzer et al., 2019). Thus, depending on the developmental stage of these cells and the GABAR involved, the neurotransmitter GABA may play different physiological functions. Moreover, GABAergic signaling could potentially regulate specific subgroups of cells from the OL/SC lineages in different ways, either action-potential dependently or independently. Thus, it appears that in OPCs GABA acts mostly through $GABA_A$Rs to carry out some important functions at the progenitor level (as regulation of the population size, OPC maintenance, axon-glia recognition, differentiation or myelination initiation; Zonouzi et al., 2015; Arellano et al., 2016; Balia et al., 2017; Hamilton et al., 2017; Marisca et al., 2020).

Finally, $GABA_B$Rs may contribute to myelin maintenance (**Figure 4**). In this regard, GABARs may parallel somehow the various functions played by glutamate receptors, as AMPARs are crucial for the early stages of remyelination while NMDARs are relevant for myelin maintenance and to fuel axonal function (Lundgaard et al., 2013; Gautier et al., 2015; Saab et al., 2016).

In sum, understanding the contribution of the GABAergic signaling to OL and SC physiology may be critical to find therapeutic tools to improve remyelination in demyelinating diseases. Meanwhile, it is necessary to clarify in detail the role of GABA in OL and SC differentiation and myelination, and the mechanisms that mediate these responses. To that aim, it will be important to specifically target $GABA_A$Rs and $GABA_B$Rs either at the progenitor stage or the more mature stages of the myelinating cells. Drugs preferentially acting on GABARs in OLs and SCs will certainly help to successfully tackle these tasks.

AUTHOR CONTRIBUTIONS

MS-R and RA wrote the manuscript, designed its content, and prepared the figures and table. LB-C, RO, and AL wrote the manuscript and prepared the figures and table. EG wrote the manuscript. CM and MS-G wrote the manuscript and designed its content.

FUNDING

This work was supported by CIBERNED (CB06/05/0076; CM) and by grants from the Ministry of Economy and Competitiveness, Government of Spain (SAF2016-75292-R and PID2019-109724RB-I00; CM), Basque Government (IT1203-19; CM), CONACYT-México (No. 252121; RA), PAPIIT-UNAM-México (IN203519; RA) and NIH (R21AG053740 and R21MH113177; AL). MS-R was hired thanks to the Gangoiti Foundation (Bilbao). LB-C and RO hold fellowships from Basque Government and CONACYT-México, respectively.

REFERENCES

Afshari, F. S., Chu, A. K., and Sato-Bigbee, C. (2001). Effect of cyclic AMP on the expression of myelin basic protein species and myelin proteolipidprotein in committed oligodendrocytes: differential involvement of the transcription factor CREB. *J. Neurosci. Res.* 66, 37–45. doi: 10.1002/jnr.1195

Allen, N. J., and Lyons, D. A. (2018). Glia as architects of central nervous system formation and function. *Science* 362, 181–185. doi: 10.1126/science.aat0473

Angulo, M. C., Le Meur, K., Kozlov, A. S., Charpak, S., and Audinat, E. (2008). GABA, a forgotten gliotransmitter. *Prog. Neurobiol.* 86, 297–303. doi: 10.1016/j.pneurobio.2008.08.002

Arellano, R. O., Sánchez-Gómez, M. V., Alberdi, E., Canedo-Antelo, M., Chara, J. C., Palomino, A., et al. (2016). Axon-to-glia interaction regulates $GABA_A$ receptor expression in oligodendrocytes. *Mol. Pharmacol.* 89, 63–74. doi: 10.1124/mol.115.100594

Arthur-Farraj, P., Wanek, K., Hantke, J., Davis, C. M., Jayakar, A., Parkinson, D. B., et al. (2011). Mouse Schwann cells need both NRG1 and cyclic AMP to myelinate. *Glia* 59, 720–733. doi: 10.1002/glia.21144

Balia, M., Benamer, N., and Angulo, M. C. (2017). A specific GABAergic synapse onto oligodendrocyte precursors does not regulate cortical oligodendrogenesis. *Glia* 65, 1821–1832. doi: 10.1002/glia.23197

Balia, M., Vélez-Fort, M., Passlick, S., Schäfer, C., Audinat, E., Steinhäuser, C., et al. (2015). Postnatal down-regulation of the $GABA_A$ receptor γ2 subunit in neocortical NG2 cells accompanies synaptic-to-extrasynaptic switch in the GABAergic transmission mode. *Cereb. Cortex* 25, 1114–1123. doi: 10.1093/cercor/bht309

Baraban, M., Koudelka, S., and Lyons, D. A. (2018). Ca^{2+} activity signatures of myelin sheath formation and growth *in vivo*. *Nat. Neurosci.* 21, 19–23. doi: 10.1038/s41593-017-0040-x

Barakat, L., and Bordey, A. (2002). GAT-1 and reversible GABA transport in Bergmann glia in slices. *J. Neurophysiol.* 88, 1407–1419. doi: 10.1152/jn.2002.88.3.1407

Barati, M. T., Lukenbill, J., Wu, R., Rane, M. J., and Klein, J. B. (2015). Cytoskeletal rearrangement and Src and PI-3K-dependent Akt activation control $GABA_B$R-mediated chemotaxis. *Cell. Signal.* 27, 1178–1185. doi: 10.1016/j.cellsig.2015.02.022

Barnard, E. A., Skolnick, P., Olsen, R. W., Mohler, H., Sieghart, W., Biggio, G., et al. (1998). International Union of Pharmacology. XV. Subtypes of gamma-aminobutyric acid A receptors: classification on the basis of subunit structure and receptor function. *Pharmacol. Rev.* 50, 291–313.

Baur, R., and Sigel, E. (2003). On high- and low-affinity agonist sites in $GABA_A$ receptors. *J. Neurochem.* 87, 325–332. doi: 10.1046/j.1471-4159.2003.01982.x

Belujon, P., Baufreton, J., Grandoso, L., Boué-Grabot, E., Batten, T. F., Ugedo, L., et al. (2009). Inhibitory transmission in locus coeruleus neurons expressing $GABA_A$ receptor epsilon subunit has a number of unique properties. *J. Neurophysiol.* 102, 2312–2325. doi: 10.1152/jn.00227.2009

Ben-Ari, Y. (2002). Excitatory actions of gaba during development: the nature of the nurture. *Nat. Rev. Neurosci.* 3, 728–739. doi: 10.1038/nrn920

Berger, T., Walz, W., Schnitzer, J., and Kettenmann, H. (1992). GABA-and glutamate-activated currents in glial cells of the mouse corpus callosum slice. *J. Neurosci. Res.* 31, 21–27. doi: 10.1002/jnr.490310104

Bettler, B., Kaupmann, K., Mosbacher, J., and Gassmann, M. (2004). Molecular structure and physiological functions of $GABA_B$ receptors. *Physiol. Rev.* 84, 835–867. doi: 10.1152/physrev.00036.2003

Binet, V., Brajon, C., Le Corre, L., Acher, F., Pin, J. P., and Prézeau, L. (2004). The heptahelical domain of $GABA_{B2}$ is activated directly by CGP7930, a positive allosteric modulator of the $GABA_B$ receptor. *J. Biol. Chem.* 279, 29085–29091. doi: 10.1074/jbc.m400930200

Bollan, K. A., Baur, R., Hales, T. G., Sigel, E., and Connolly, C. N. (2008). The promiscuous role of the epsilon subunit in $GABA_A$ receptor biogenesis. *Mol. Cell. Neurosci.* 37, 610–621. doi: 10.1016/j.mcn.2007.12.011

Booker, S. A., Loreth, D., Gee, A. L., Watanabe, M., Kind, P. C., Wyllie, D. J. A., et al. (2018). Postsynaptic $GABA_B$Rs inhibit L-type calcium channels and abolish long-term potentiation in hippocampal somatostatin interneurons. *Cell. Rep.* 22, 36–43. doi: 10.1016/j.celrep.2017.12.021

Bowery, N. G., Bettler, B., Froestl, W., Gallagher, J. P., Marshall, F., Raiteri, M., et al. (2002). International Union of Pharmacology. XXXIII. Mammalian gamma-aminobutyric $Acid_B$ receptors: structure and function. *Pharmacol. Rev.* 54, 247–264. doi: 10.1124/pr.54.2.247

Bowery, N. G., and Hudson, A. L. (1979). γ-aminobutyric acid reduces the evoked release of [3H]-noradrenaline from sympathetic nerve therminals [proceedings]. *Br. J. Pharmacol.* 66:108P.

Bronstein, J. M., Hales, T. G., Tyndale, R. F., and Charles, A. C. (1998). A conditionally immortalized glial cell line that expresses mature myelin proteins and functional $GABA_A$ receptors. *J. Neurochem.* 70, 483–491. doi: 10.1046/j.1471-4159.1998.70020483.x

Brown, D. A., Adams, P. R., Higgins, A. J., and Marsh, S. (1979). Distribution of gaba-receptors and gaba-carriers in the mammalian nervous system. *J. Physiol.* 75, 667–671.

Brown, N., Kerby, J., Bonnert, T. P., Whiting, P. J., and Wafford, K. A. (2002). Pharmacological characterization of a novel cell line expressing human $\alpha_4\beta_3\delta$ $GABA_A$ receptors. *Br. J. Pharmacol.* 136, 965–974. doi: 10.1038/sj.bjp.0704796

Cahoy, J. D., Emery, B., Kaushal, A., Foo, L. C., Zamanian, J. L., Christopherson, K. S., et al. (2008). A transcriptome database for astrocytes, neurons and oligodendrocytes: a new resource for understanding brain development and function. *J. Neurosci.* 28, 264–278. doi: 10.1523/JNEUROSCI.4178-07.2008

Calver, A. R., Medhurst, A. D., Robbins, M. J., Charles, K. J., Evans, M. L., Harrison, D. C., et al. (2000). The expression of $GABA_{B1}$ and $GABA_{B2}$ receptor subunits in the CNS differs from that in peripheral tissues. *Neuroscience* 100, 155–170. doi: 10.1016/s0306-4522(00)00262-1

Carlezon, W. A. Jr., Duman, R. S., and Nestler, E. J. (2005). The many faces of CREB. *Trends Neurosci.* 28, 436–445. doi: 10.1016/j.tins.2005.06.005

Carver, C. M., Chuang, S., and Reddy, D. S. (2016). Zinc selectively blocks neurosteroid-sensitive extrasynaptic δGABA A receptors in the hippocampus. *J. Neurosci.* 36, 8070–8077. doi: 10.1523/jneurosci.3393-15.2016

Chan, J. R., Rodriguez-Waitkus, P. M., Ng, B. K., Liang, P., and Glaser, M. (2000). Progesterone synthesized by Schwann cells during myelin formation regulates neuronal gene expression. *Mol. Biol. Cell.* 11, 2283–2295. doi: 10.1091/mbc.11.7.2283

Charles, K. J., Deuchars, J., Davies, C. H., and Pangalos, M. N. (2003). $GABA_B$ receptor subunit expression in glia. *Mol. Cell. Neurosci.* 24, 214–223. doi: 10.1016/s1044-7431(03)00162-3

Cheli, V. T., Sántiago-González, D. A., Namgyal-Lama, T., Spreuer, V., Handley, V., Murphy, G. G., et al. (2016). Conditional deletion of the L-type calcium channel Cav1.2 in oligodendrocyte progenitor cells affects postnatal myelination in mice. *J. Neurosci.* 36, 10853–10869. doi: 10.1523/jneurosci.1770-16.2016

Chung, S. H., Biswas, S., Selvaraj, V., Liu, X. B., Sohn, J., Jiang, P., et al. (2015). The p38α mitogen-activated protein kinase is a key regulator of myelination and remyelination in the CNS. *Cell Death Dis.* 6:e1748. doi: 10.1038/cddis.2015.119

Chung, S. H., Biswas, S., Sohn, J., Jiang, P., Dehghan, S., Marzban, H., et al. (2018). The p38α MAPK deletion in oligodendroglia does not attentuate myelination defects in a mouse model of periventricular leukomalacia. *Neuroscience* 386, 175–181. doi: 10.1016/j.neuroscience.2018.06.037

Cisneros-Mejorado, A. J., Garay, E., Ortiz-Retana, J., Concha, L., Moctezuma, J. P., Romero, S., et al. (2020). Demyelination-remyelination of the rat caudal cerebellar peduncle evaluated with magnetic resonance imaging. *Neuroscience* 439, 255–267. doi: 10.1016/j.neuroscience.2019.06.042

Colognato, H., Ramachandrappa, S., Olsen, I. M., and ffrench-Constant, C. (2004). Integrins direct Src family kinases to regulate distinct phases of oligodendrocyte development. *J. Cell Biol.* 167, 365–375. doi: 10.1083/jcb.200404076

Corell, M., Wicher, G., Radomska, K. J., Daglikoca, E. D., Godskesen, R. E., Fredriksson, R., et al. (2015). GABA and its B-receptor are present at the node of Ranvier in a small population of sensory fibers, implicating a role in myelination. *J. Neurosci. Res.* 93, 285–295. doi: 10.1002/jnr.23489

Couve, A., Moss, S. J., and Pangalos, M. N. (2000). $GABA_B$ receptors: a new paradigm in G protein signaling. *Mol. Cell. Neurosci.* 16, 296–312. doi: 10.1006/mcne.2000.0908

Dawson, M. R., Polito, A., Levine, J. M., and Reynolds, R. (2003). NG2-expressing glial progenitor cells: an abundant and widespread population of cycling cells in the adult rat CNS. *Mol. Cell. Neurosci.* 24, 476–488. doi: 10.1016/s1044-7431(03)00210-0

Doyon, N., Vinay, L., Prescott, S. A., and De Koninck, Y. (2016). Chloride regulation: a dynamic equilibrium crucial for synaptic inhibition. *Neuron* 89, 1157–1172. doi: 10.1016/j.neuron.2016.02.030

Duncan, I. D., Radcliff, A. B., Heidari, M., Kidd, G., August, B. K., and Wierenga, L. A. (2018). The adult oligodendrocyte can participate in remyelination. *Proc. Natl. Acad. Sci. U S A* 115, E11807–E11816. doi: 10.1073/pnas.1808064115

Fannon, J., Tarmier, W., and Fulton, D. (2015). Neuronal activity and AMPA-type glutamate receptor activation regulates the morphological development of oligodendrocyte precursor cells. *Glia* 63, 1021–1035. doi: 10.1002/glia.22799

Faroni, A., and Magnaghi, V. (2011). The neurosteroid allopregnanolone modulates specific functions in central al peripheral glial cells. *Front. Endocrinol.* 2:103. doi: 10.3389/fendo.2011.00103

Faroni, A., Melfi, S., Castelnovo, L. F., Bonalume, V., Colleoni, D., Magni, P., et al. (2019). GABA-B1 receptor-null Schwann cells exhibit compromised *in vitro* myelination. *Mol. Neurobiol.* 56, 1461–1474. doi: 10.1007/s12035-018-1158-x

Faroni, A., Smith, R. J., Procacci, P., Castelnovo, L. F., Puccianti, E., Reid, A. J., et al. (2014). Purinergic signaling mediated by P2X7 receptors controls myelination in sciatic nerves. *J. Neurosci. Res.* 92, 1259–1269. doi: 10.1002/jnr.23417

Faroni, A., Terenghi, G., and Magnaghi, V. (2012). Expression of functional γ-aminobutyric acid type A receptors in Schwann-like adult stem cells. *J. Mol. Neurosci.* 47, 619–630. doi: 10.1007/s12031-011-9698-9

Fattorini, G., Melone, M., Sánchez-Gómez, M. V., Arellano, R. O., Bassi, S., Matute, C., et al. (2017). GAT-1 mediated GABA uptake in rat oligodendrocytes. *Glia* 65, 514–522. doi: 10.1002/glia.23108

Fragoso, G., Haines, J. D., Robertson, J., Pedraza, L., Mushynski, W. E., and Almazan, G. (2007). p38 mitogen-activated protein kinase is required for central nervous system myelination. *Glia* 55, 1531–1541. doi: 10.1002/glia.20567

Fragoso, G., Robertson, J., Athlan, E., Tam, E., Almazan, G., and Mushynski, W. E. (2003). Inhibition of p38 mitogen-activated protein kinase interferes with cell shape changes and gene expression associated with Schwann cell myelination. *Exp. Neurol.* 183, 34–46. doi: 10.1016/s0014-4886(03)00101-8

Franklin, R. J., Gilson, J. M., and Blakemore, W. F. (1997). Local recruitment of remyelinating cells in the repair of demyelination in the central nervous system. *J. Neurosci. Res.* 50, 337–344. doi: 10.1002/(sici)1097-4547(19971015)50:2<337::aid-jnr21>3.0.co;2-3

Gago, N., El-Etr, M., Sananès, N., Cadepond, F., Samuel, D., Avellana-Adalid, V., et al. (2004). 3alpha,5alpha-Tetrahydroprogesterone (allopregnanolone) and gamma-aminobutyric acid: autocrine/paracrine interactions in the control of neonatal PSA-NCAM+ progenitor proliferation. *J. Neurosci. Res.* 78, 770–783. doi: 10.1002/jnr.20348

Galvez, T., Duthey, B., Kniazeff, J., Blahos, J., Rovelli, G., Bettler, B., et al. (2001). Allosteric interactions between GB1 and GB2 subunits are required for optimal $GABA_B$ receptor function. *EMBO J.* 20, 2152–2159. doi: 10.1093/emboj/20.9.2152

García-Díaz, B., and Baron-Van Evercooren, A. (2020). Schwann cells: recuers of central demyelination. *Glia* doi: 10.1002/glia.23788 [Epub ahead of print].

Gautier, H. O., Evans, K. A., Volbracht, K., James, R., Sitnikov, S., Lundgaard, I., et al. (2015). Neuronal activity regulates remyelination *via* glutamate signalling to oligodendrocyte protenitors. *Nat. Commun.* 6:8518. doi: 10.1038/ncomms9518

Ghoumari, A. M., Ibanez, C., El-Etr, M., Leclerc, P., Eychenne, B., O'Malley, B. W., et al. (2003). Progesterone and its metabolites increase myelin basic protein expression in organotypic slice cultures of rat cerebellum. *J. Neurochem.* 86, 848–859. doi: 10.1046/j.1471-4159.2003.01881.x

Gibbs, J. W., Zhang, Y. F., Kao, C. Q., Holloway, K. L., Oh, K. S., and Coulter, D. A. (1996). Characterization of $GABA_A$ receptor function in human temporal cortical neurons. *J. Neurophysiol.* 75, 1458–1471. doi: 10.1152/jn.1996.75.4.1458

Gibson, E. M., Purger, D., Mount, C. W., Goldstein, A. K., Lin, G. L., Wood, L. S., et al. (2014). Neuronal activity promotes oligodendrogenesis and adaptive myelination in the mammalian brain. *Science* 344:1252304. doi: 10.1126/science.1252304

Goodkin, H. P., and Kapur, J. (2009). The impact of diazepam's discovery on the treatment and understanding of status epilepticus. *Epilepsia* 50, 2011–2018. doi: 10.1111/j.1528-1167.2009.02257.x

Hamilton, N. B., Clarke, L. E., Arancibia-Carcamo, I. L., Kougioumtzidou, E., Matthey, M., Karadottir, R., et al. (2017). Endogenous GABA controls oligodendrocyte lineage cell number, myelination and CNS internode length. *Glia* 65, 309–321. doi: 10.1002/glia.23093

Héja, L., Nyitrai, G., Kékesi, O., Dobolyi, A., Szabó, P., Fiáth, R., et al. (2012). Astrocytes convert network excitation to tonic inhibition of neurons. *BMC Biol.* 10:26. doi: 10.1186/1741-7007-10-26

Hesp, Z. C., Goldstein, E. A., Miranda, C. J., Kaspar, B. K., McTigue, D. M., Kaspar, B. K., et al. (2015). Chronic oligodendrogenesis and remyelination after spinal cord injury in mice and rats. *J. Neurosci.* 35, 1274–1290. doi: 10.1523/jneurosci.1414-15.2015

Hill, D. R., and Bowery, N. G. (1981). ^{3}H-Baclofen and ^{3}H-GABA bind to bicuculline-insensitive $GABA_B$ sites in rat brain. *Nature* 290, 149–152. doi: 10.1038/290149a0

Hodge, R. D., Bakken, T. E., Miller, J. A., Smith, K. A., Barkan, E. R., Graybuck, L. T., et al. (2019). Conserved cell types with divergent features in human versus mouse cortex. *Nature* 573, 61–68. doi: 10.1038/s41586-019-1506-7

Hosie, A. M., Dunne, E. L., Harvey, R. J., and Smart, T. G. (2003). Zinc-mediated inhibition of $GABA_A$ receptors: discrete binding sites underlie subtype specificity. *Nat. Neurosci.* 6, 362–369. doi: 10.1038/nn1030

Jessen, K. R., and Mirsky, R. (2005). The origin and development of glial cells in peripheral nerves. *Nat. Rev. Neurosci.* 6, 671–682. doi: 10.1038/nrn1746

Jessen, K. R., and Mirsky, R. (2019). The success and failure of the Schwann cell response to nerve injury. *Front. Cell. Neurosci.* 13:33. doi: 10.3389/fncel.2019.00033

Jiménez-González, C., Pirttimaki, T., Cope, D. W., and Parri, H. R. (2011). Non-neuronal, slow GABA signalling in the ventrobasal thalamus targets δ-subunit-containing $GABA_A$ receptors. *Eur. J. Neurosci.* 33, 1471–1482. doi: 10.1111/j.1460-9568.2011.07645.x

Jones, B. L., and Henderson, L. P. (2007). Trafficking and potential assembly patterns of epsilon-containing $GABA_A$ receptors. *J. Neurochem.* 103, 1258–1271. doi: 10.1111/j.1471-4159.2007.04833.x

Kalakh, S., and Mouihate, A. (2019). Enhanced remyelination during late pregnancy: involvement of the GABAergic system. *Sci. Rep.* 9:7728. doi: 10.1038/s41598-019-44050-4

Karim, N., Wellendorph, P., Absalom, N., Johnston, G. A., Hanrahan, J. R., and Chebib, M. (2013). Potency of GABA at human recombinant $GABA_A$ receptors expressed in Xenopus oocytes: a mini review. *Amino Acids* 44, 1139–1149. doi: 10.1007/s00726-012-1456-y

Kaufman, D. L., Houser, C. R., and Tobin, A. J. (1991). Two forms of the gamma-aminobutyric acid synthetic enzyme glutamate decarboxylase have distinct intraneuronal distributions and cofactor interactions. *J. Neurochem.* 56, 720–723. doi: 10.1111/j.1471-4159.1991.tb08211.x

Kaupmann, K., Malitschek, B., Schuler, V., Heid, J., Froestl, W., Beck, P., et al. (1998). $GABA_B$-receptor subtypes assemble into functional heteromeric complexes. *Nature* 396, 683–687. doi: 10.1038/25360

Kidd, G. J., Ohno, N., and Trapp, B. D. (2013). Biology of Schwann cells. *Handb. Clin. Neurol.* 115, 55–79. doi: 10.1016/B978-0-444-52902-2.00005-9

Kirchhoff, F., and Kettenmann, H. (1992). GABA triggers a $[Ca^{2+}]_i$ increase in murine precursor cells of the oligodendrocyte lineage. *Eur. J. Neurosci.* 4, 1049–1058. doi: 10.1111/j.1460-9568.1992.tb00131.x

Krasnow, A. M., Ford, M. C., Valdivia, L. E., Wilson, S. W., and Attwell, D. (2018). Regulation of developing myelin sheath elongation by oligodendrocyte calcium transients *in vivo*. *Nat. Neurosci.* 21, 24–30. doi: 10.1038/s41593-017-0031-y

Kukley, M., Kiladze, M., Tognatta, R., Hans, M., Swandulla, D., Schramm, J., et al. (2008). Glial cells are born with synapses. *FASEB J.* 22, 2957–2969. doi: 10.1096/fj.07-090985

Kuner, R., Köhr, G., Grünewald, S., Eisenhardt, G., Bach, A., and Kornau, H. C. (1999). Role of the heteromer formation in $GABA_B$ receptor function. *Science* 283, 74–77. doi: 10.1126/science.283.5398.74

Lambert, J. J., Cooper, M. A., Simmons, R. D., Weir, C. J., and Belelli, D. (2009). Neurosteroids: endogenous allosteric modulators of $GABA_A$ receptors. *Psychoneuroendocrinology* 34, S48–S58. doi: 10.1016/j.psyneuen.2009.08.009

Larson, V. A., Zhang, Y., and Bergles, D. E. (2016). Electrophysiological properties of $NG2^+$ cells: matching physiological studies with gene expression profiles. *Brain Res.* 1638, 138–160. doi: 10.1016/j.brainres.2015.09.010

Levitan, E. S., Schofieldh, P. R., Burt, D. R., Rhee, L. M., Wisden, W., Kohler, M., et al. (1988). Structural and functional basis for $GABA_A$ receptor heterogeneity. *Nature* 335, 76–79. doi: 10.1038/335076a0

Li, C., Xiao, L., Liu, X., Yang, W., Shen, W., Hu, C., et al. (2013). A functional role of NMDA receptor in regulating the differentiation of oligodendrocyte precursor cells and remyelination. *Glia* 61, 732–749. doi: 10.1002/glia.22469

Li, X., Terunuma, M., Deeb, T. G., Wiseman, S., Pangalos, M. N., Nairn, A. C., et al. (2020). Direct interaction of PP2A phosphatase with $GABA_B$ receptors alters functional signaling. *J. Neurosci.* 40, 2808–2816. doi: 10.1523/JNEUROSCI.2654-19.2020

Lin, S. C., and Bergles, D. E. (2004). Synaptic signaling between GABAergic interneurons and oligodendrocyte precursor cells in the hippocampus. *Nat. Neurosci.* 7, 24–32. doi: 10.1038/nn1162

Lin, C. C., Lee, I. T., Hsu, C. H., Hsu, C. K., Chi, P. L., Hsiao, L. D., et al. (2015). Sphingosine-1-phosphate mediates ICAM-1-dependent monocyte adhesion through p38 MAPK and p42/p44 MAPK-dependent Akt activation. *PLoS One* 10:e0118473. doi: 10.1371/journal.pone.0118473

Lundgaard, I., Luzhynskaya, A., Stockley, J. H., Wang, Z., Evans, K. A., Swire, M., et al. (2013). Neuregulin and BDNF induce a switch to NMDA receptor-dependent myelination by oligodendrocytes. *PLoS Biol.* 11:e1001743. doi: 10.1371/journal.pbio.1001743

Luyt, K., Slade, T. P., Dorward, J. J., Durant, C. F., Wu, Y., Shigemoto, R., et al. (2007). Developing oligodendrocytes express functional $GABA_B$ receptors that stimulate cell proliferation and migration. *J. Neurochem.* 100, 822–840. doi: 10.1111/j.1471-4159.2006.04255.x

Magnaghi, V. (2007). GABA and neuroactive steroid interactions in glia: new roles for old players? *Curr. Neuropharmacol.* 5, 47–64. doi: 10.2174/157015907780077132

Magnaghi, V., Ballabio, M., Camozzi, F., Colleoni, M., Consoli, A., Gassmann, M., et al. (2008). Altered peripheral myelination in mice lacking $GABA_B$ receptors. *Mol. Cell. Neurosci.* 37, 599–609. doi: 10.1016/j.mcn.2007.12.009

Magnaghi, V., Ballabio, M., Cavarretta, I. T., Froestl, W., Lambert, J. J., Zucchi, I., et al. (2004). $GABA_B$ receptors in Schwann cells influence proliferation and myelin protein expression. *Eur. J. Neurosci.* 19, 2641–2649. doi: 10.1111/j.0953-816x.2004.03368.x

Magnaghi, V., Ballabio, M., Consoli, A., Lambert, J. J., Roglio, I., and Melcangi, R. C. (2006). GABA receptor-mediated effects in the peripheral nervous system: a cross-interaction with neuroactive steroids. *J. Mol. Neurosci.* 28, 89–102. doi: 10.1385/jmn:28:1:89

Magnaghi, V., Cavarretta, I., Galbiati, M., Martini, L., and Melcangi, R. C. (2001). Neuroactive steroids and peripheral myelin proteins. *Brain Res. Rev.* 37, 360–371. doi: 10.1016/s0165-0173(01)00140-0

Magnaghi, V., Parducz, A., Frasca, A., Ballabio, M., Procacci, P., Racagni, G., et al. (2010). GABA synthesis in Schwann cells is induced by the neuroactive steroid allopregnanolone. *J. Neurochem.* 112, 980–990. doi: 10.1111/j.1471-4159.2009.06512.x

Marisca, R., Hoche, T., Agirre, E., Jane Hoodless, L., Barkey, W., Auer, F., et al. (2020). Functionally distinct subgroups of oligodendrocyte precursor cells integrate neural activity and execute myelin formation. *Nat. Neurosci.* 23, 363–374. doi: 10.1038/s41593-019-0581-2

Marques, S., Zeisel, A., Codeluppi, S., van Bruggen, D., Mendanha Falcão, A., Xiao, L., et al. (2016). Oligodendrocyte heterogeneity in the mouse juvenile and adult central nervous system. *Science* 352, 1326–1329. doi: 10.1126/science.aaf6463

Meera, P., Wallner, M., and Otis, T. S. (2011). Molecular basis for the high THIP/gaboxadol sensitivity of extrasynaptic $GABA_A$ receptors. *J. Neurophysiol.* 106, 2057–2064. doi: 10.1152/jn.00450.2011

Melfi, S., Montt Guevara, M. M., Bonalume, V., Ruscica, M., Colciago, A., Simoncini, T., et al. (2017). Src and phosphor-FAK kinases are activated by allopregnanolone promoting Schwann cell motility, morphology and myelination. *J. Neurochem.* 141, 165–178. doi: 10.1111/jnc.13951

Michelsen, S., Sánchez, C., and Ebert, B. (2007). Lack of generalisation between the $GABA_A$ receptor agonist, gaboxadol and allosteric modulators of the benzodiazepine binding site in the rat drug discrimination procedure. *Psychopharmacology* 193, 151–157. doi: 10.1007/s00213-007-0750-y

Minchin, M. C., and Iversen, L. L. (1974). Release of (3H)gamma-aminobutyric acid from glial cells in rat dorsal root ganglia. *J. Neurochem.* 23, 533–540. doi: 10.1111/j.1471-4159.1974.tb06056.x

Mitew, S., Gobius, I., Fenlon, L. R., McDougall, S. J., Hawkes, D., Xing, Y. L., et al. (2018). Pharmacogenetic stimulation of neuronal activity increases myelination in an axon-specific manner. *Nat. Commun.* 9:306. doi: 10.3410/f.732542465.793542118

Mortensen, M., Ebert, B., Wafford, K., and Smart, T. G. (2010). Distinct activities of GABA agonists at synaptic- and extrasynaptic-type $GABA_A$ receptors. *J. Physiol.* 588, 1251–1268. doi: 10.1113/jphysiol.2009.182444

Mortensen, M., Patel, B., and Smart, T. G. (2012). GABA potency at $GABA_A$receptors found in synaptic and extrasynaptic zones. *Front. Cell. Neurosci.* 6:1. doi: 10.3389/fncel.2012.00001

Mount, C. W., Yalçın, B., Cunliffe-Koehler, K., Sundaresh, S., and Monje, M. (2019). Monosynaptic tracing maps brain-wide afferent oligodendrocyte precursor cell connectivity. *Elife* 8:e49291. doi: 10.7554/eLife.49291

Mugabe, B. E., Yaghini, F. A., Song, C. Y., Buharalioglu, C. K., Waters, C. M., and Malik, K. U. (2010). Angiotensin II-induced migration of vascular smooth muscle cells is mediated by p38 mitogen-activated protein kinase-activated c-Src through spleen tyrosine kinase and epidermal growth factor receptor transactivation. *J. Pharmacol. Exp. Ther.* 332, 116–124. doi: 10.1124/jpet.109.157552

Nait-Oumesmar, B., Decker, L., Lachapelle, F., Avellana-Adalid, V., Bachelin, C., and Baron-Van Evercooren, A. (1999). Progenitor cells of the adult mouse subventricular zone proliferate, migrate and differentiate into oligodendrocytes after demyelination. *Eur. J. Neurosci.* 11, 4357–4366. doi: 10.1046/j.1460-9568.1999.00873.x

Nave, K. A., and Trapp, B. D. (2008). Axon-glial signaling and the glial support of axon function. *Annu. Rev. Neurosci.* 31, 535–561. doi: 10.1146/annurev.neuro.30.051606.094309

Newbern, J., and Birchmeier, C. (2010). Nrg1/ErbB signaling networks in Schwann cell development and myelination. *Semin. Cell. Dev. Biol.* 21, 922–928. doi: 10.1016/j.semcdb.2010.08.008

Olsen, R. W., and Sieghart, W. (2008). International Union of Pharmacology. LXX. Subtypes of gamma-aminobutyric $Acid_A$ receptors: classification on the basis of subunit composition, pharmacology and function. Update. *Pharmacol. Rev.* 60, 243–260. doi: 10.1124/pr.108.00505

Orduz, D., Maldonado, P. P., Balia, M., Vélez-Fort, M., de Sars, V., Yanagawa, Y., et al. (2015). Interneurons and oligodendrocyte progenitors form a structured synaptic network in the developing neocortex. *Elife* 4:e06953. doi: 10.7554/eLife.06953.021

Paez, P. M., and Lyons, D. (2020). Calcium signaling in the oligodendrocyte lineage: regulators and consequences. *Annu. Rev. Neurosci.* 43, 163–186. doi: 10.1146/annurev-neuro-100719-093305

Passlick, S., Grauer, M., Schafer, C., Jabs, R., Seifert, G., and Steinhauser, C. (2013). Expression of the 2-subunit distinguishes synaptic and extrasynaptic $GABA_A$ receptors in NG2 cells of the hippocampus. *J. Neurosci.* 33, 12030–12040. doi: 10.1523/JNEUROSCI.5562-12.2013

Peña, C., Medina, J. H., Novas, M. L., Paladini, A. C., and De Robertis, E. (1986). Isolation and identification in bovine cerebral cortex of n-butyl β-carboline-3-carboxylate, a potent benzodiazepine binding inhibitor. *Proc. Natl. Acad. Sci. U S A* 83, 4952–4956. doi: 10.1073/pnas.83.13.4952

Petroski, R. E., Pomeroy, J. E., Das, R., Bowman, H., Yang, W., Chen, A. P., et al. (2006). Indiplon is a high-affinity positive allosteric modulator with selectivity for alpha1 subunit-containing $GABA_A$ receptors. *J. Pharmacol. Exp. Ther.* 317, 369–377. doi: 10.1124/jpet.105.096701

Philips, T., and Rothstein, J. D. (2017). Oligodendroglia: metabolic supporters of neurons. *J. Clin. Invest.* 127, 3271–3280. doi: 10.1172/JCI90610

Procacci, P., Ballabio, M., Castelnovo, L. F., Mantovani, C., and Magnaghi, V. (2013). GABA-B receptors in the PNS have a role in Schwann cells differentiation? *Front. Cell. Neurosci.* 6:68. doi: 10.3389/fncel.2012.00068

Quintela-López, T., Ortiz-Sanz, C., Serrano-Regal, M. P., Gaminde-Blasco, A., Valero, J., Baleriola, J., et al. (2019). Aβ oligomers promote oligodendrocyte differentiation and maturation via integrin β1 and Fyn kinase signaling. *Cell Death Dis.* 10:445. doi: 10.1038/s41419-019-1636-8

Roberts, E., and Frankel, S. (1950). γ-aminobutyric acid in brain: its formation from glutamic acid. *J. Biol. Chem.* 187, 55–63.

Saab, A. S., Tzvetavona, I. D., Trevisiol, A., Baltan, S., Dibaj, P., Kusch, K., et al. (2016). Oligodendroglial NMDA receptors regulate glucose import and axonal energy metabolism. *Neuron* 91, 119–132. doi: 10.1016/j.neuron.2016.05.016

Salzer, J. (2015). Schwann cell myelination. *Cold Spring Harb. Perspect. Biol.* 7:a020529. doi: 10.1101/cshperspect.a020529

Santiago-González, D. A., Cheli, V. T., Zamora, N. N., Lama, T. N., Spreuer, V., Murphy, G. G., et al. (2017). Conditional deletion of the L-type calcium channel Cav1.2 in NG2-positive cells impairs remyelination in mice. *J. Neurosci.* 37, 10038–10051. doi: 10.1523/JNEUROSCI.1787-17.2017

Seeburg, P. H., Wisden, W., Verdoorn, T. A., Pritchett, D. B., Werner, P., Herb, A., et al. (1990). The $GABA_A$ receptor family: molecular and functional diversity. *Cold Spring Harb. Symp. Quant. Biol.* 55, 29–40. doi: 10.1101/sqb.1990.055.01.006

Seiler, N., al-Therib, M. J., and Kataola, K. (1973). Formation of GABA from putrescine in the brain of fish (Salmo irideus Gibb.). *J. Neurochem.* 20, 699–708. doi: 10.1111/j.1471-4159.1973.tb00030.x

Seiler, N., Schmidt-Glenewinkel, T., and Sarhan, S. (1979). On the formation of gamma-aminobutyric acid from putrescine in brain. *J. Biochem.* 86, 277–279. doi: 10.1093/oxfordjournals.jbchem.a132515

Sequeira, A., Shen, K., Gottlieb, A., and Limon, A. (2019). Human brain transcriptome analysis finds region- and subject-specific expression signatures of $GABA_A$R subunits. *Commun. Biol.* 2:153. doi: 10.1038/s42003-019-0413-7

Serrano-Regal, M. P., Luengas-Escuza, I., Bayón-Cordero, L., Ibarra-Aizpurua, N., Alberdi, E., Pérez-Samartín, A., et al. (2020). Oligodendrocyte differentiation and myelination is potentiated via $GABA_B$ receptor activation. *Neuroscience* 439, 163–180. doi: 10.1016/j.neuroscience.2019.07.014

Shaw, J. C., Berry, M. J., Dyson, R. M., Crombie, G. K., Hirst, J. J., and Palliser, H. K. (2019). Reduced neurosteroid exposure following preterm birth and its' contribution to neurological impairment: a novel avenue for preventative therapies. *Front. Physiol.* 10:599. doi: 10.3389/fphys.2019.00599

Shaw, J. C., Dyson, R. M., Palliser, H. K., Gray, C., Berry, M. J., and Hirst, J. J. (2019). Neurosteroid replacement therapy using the allopregnanolone-analogue ganaxolone following preterm birth in male guinea pigs. *Pediatr. Res.* 85, 86–96. doi: 10.1038/s41390-018-0185-7

Shaw, J. C., Palliser, H. K., Walker, D. W., and Hirst, J. J. (2015). Preterm birth affects $GABA_A$ receptor subunit mRNA levels during the foetal-to-neonatal transition in guinea pigs. *J. Dev. Orig. Health Dis.* 6, 250–260. doi: 10.1017/S2040174415000069

Sieghart, W., and Savić, M. M. (2018). International Union of Basic and Clinical Pharmacology. CVI: $GABA_A$ receptor subtype- and function-selective ligands: key issues in translation to humans. *Pharmacol. Rev.* 70, 836–878. doi: 10.1124/pr.117.014449

Spitzer, S. O., Sitnikov, S., Kamen, Y., Evans, K. A., Kronenberg-Versteeg, D., Dietmann, S., et al. (2019). Oligodendrocyte progenitor cells become regionally diverse and heterogeneous with age. *Neuron* 101, 459–471. doi: 10.1016/j.neuron.2018.12.020

Vélez-Fort, M., Audinat, E., and Angulo, M. C. (2012). Central role of GABA in neuron-glia interactions. *Neuroscientist* 18, 237–250. doi: 10.1177/1073858411403317

Vélez-Fort, M., Maldonado, P. P., Butt, A. M., Audinat, E., and Angulo, M. C. (2010). Postnatal switch from synaptic to extrasynaptic transmission between interneurons and NG2 cells. *J. Neurosci.* 30, 6921–6929. doi: 10.1523/JNEUROSCI.0238-10.2010

Vogt, K. (2015). "Diversity in GABAergic signaling," in *Diversity and Functions of GABA Receptors: a Tribute to Hanns Möhler, Part B*, ed. U. Rudolph (Waltham and San Diego, USA; London and Oxford, UK: Elsevier Inc.), 203–222.

von Blankenfeld, G., Trotter, J., and Kettenmann, H. (1991). Expression and developmental regulation of a $GABA_A$ receptor in cultured murine cells of the oligodendrocyte lineage. *Eur. J. Neurosci.* 3, 310–316. doi: 111/j.1460-9568.1991.tb00817.x

Wake, H., Lee, P. R., and Fields, R. D. (2011). Control of local protein synthesis and initial events in myelination by action potentials. *Science* 333, 1647–1651. doi: 10.1126/science.1206998

Waldvogel, H. J., and Faull, R. L. M. (2015). "The diversity of $GABA_A$ receptor subunit distribution in the normal and Huntington's disease human brain[1]," in *Diversity and Functions of GABA Receptors: a Tribute to Hanns Möhler, Part B*, ed. U. Rudolph (London and Oxford, UK: Elsevier Inc.), 223–264.

Wallner, M., Hanchar, H. J., and Olsen, R. W. (2003). Ethanol enhances alpha 4 beta 3 delta and alpha 6 beta 3 delta gamma-aminobutyric acid type A receptors at low concentrations known to affect humans. *Proc. Natl. Acad. Sci. U S A* 100, 15218–15223. doi: 10.1073/pnas.2435171100

Walters, R. J., Hadley, S. H., Morris, K. D. W., and Amin, J. (2000). Benzodiazepines act on $GABA_A$receptors *via* two distinct and separable mechanisms. *Nat. Neurosci.* 3, 1274–1281. doi: 10.1038/81800

White, R., and Krämer-Albers, E. M. (2014). Axon-glia interaction and membrane traffic in myelin formation. *Front. Cell. Neurosci.* 7:284. doi: 10.3389/fncel.2013.00284

Williamson, A. V., Mellor, J. R., Grant, A. L., and Randall, A. D. (1998). Properties of $GABA_A$ receptors in cultured rat oligodendrocyte progenitor cells. *Neuropharmacology* 37, 859–873. doi: 10.1016/s0028-3908(98)00016-1

Wingrove, P. B., Wafford, K. A., Bain, C., and Whiting, P. J. (1994). The modulatory action of loreclezole at the gamma-aminobutyric acid type A receptor is determined by a single amino acid in the beta2 and beta3 subunit. *Proc. Natl. Acad. Sci. U S A* 91, 4569–4573. doi: 10.1073/pnas.91.10.4569

Wu, H., Shi, Y., Deng, X., Su, Y., Du, C., Wei, J., et al. (2015). Inhibition of c-Src/p38 MAPK pathway ameliorates renal tubular epithelial cells apoptosis in db/db mice. *Mol. Cell. Endocrinol.* 417, 27–35. doi: 10.1016/j.mce.2015.09.008

Zawadzka, M., Rivers, L. E., Fancy, S. P., Zhao, C., Tripathi, R., Jamen, F., et al. (2010). CNS-resident glial progenitors/stem cells produce Schwann cells as well as oligodendrocytes during repair of CNS demyelination. *Cell Stem Cell* 6, 578–590. doi: 10.1016/j.stem.2010.04.002

Zhang, Y., Chen, K., Sloan, S. A., Bennett, M. L., Scholze, A. R., O' Keeffe, S., et al. (2014). An RNA-sequencing transcriptome and splicing database of glia, neurons and vascular cells of the cerebral cortex. *J. Neurosci.* 34, 11929–11947. doi: 10.1523/JNEUROSCI.1860-14.2014

Zhang, W., Xu, C., Tu, H., Wang, Y., Sun, Q., Hu, P., et al. (2015). $GABA_B$ receptor upregulates Fragile X mental retardation protein expression in neurons. *Sci. Rep.* 5:10468. doi: 10.1038/srep10468

Zonouzi, M., Scafidi, J., Li, P., McEllin, B., Edwards, J., Dupree, J. L., et al. (2015). GABAergic regulation of cerebellar NG2 cell development is altered in perinatal white matter injury. *Nat. Neurosci.* 18, 674–682. doi: 10.1038/nn.3990

Conflict of Interest: The authors declare that the research was conducted in the absence of any commercial or financial relationships that could be construed as a potential conflict of interest.

frontiers in Cellular Neuroscience

PERSPECTIVE
published: 05 November 2020
doi: 10.3389/fncel.2020.587053

White Matter Plasticity in Anxiety: Disruption of Neural Network Synchronization During Threat-Safety Discrimination

Jia Liu[1]*, *Ekaterina Likhtik*[2,3], *A. Duke Shereen*[1], *Tracy A. Dennis-Tiwary*[4,5] and *Patrizia Casaccia*[1,3,6,7]*

[1]Advanced Science Research Center at the Graduate Center, Neuroscience Initiative, City University of New York, New York, NY, United States, [2]Department of Biology, Hunter College, City University of New York, New York, NY, United States, [3]Graduate Program in Biology at the Graduate Center, City University of New York, New York, NY, United States, [4]Department of Psychology, Hunter College, City University of New York, New York, NY, United States, [5]Graduate Program in Psychology and Behavioral and Cognitive Neuroscience at the Graduate Center, City University of New York, New York, NY, United States, [6]Graduate Program in Biochemistry at the Graduate Center, City University of New York, New York, NY, United States, [7]Department of Neuroscience, Icahn School of Medicine at Mount Sinai, New York, NY, United States

OPEN ACCESS

Edited by:
Nicola B. Hamilton-Whitaker, King's College London, United Kingdom

Reviewed by:
Hermona Soreq, Hebrew University of Jerusalem, Israel
Lauren Jantzie, Johns Hopkins University, United States
Michelle Monje, Stanford University, United States

***Correspondence:**
Jia Liu
jliu1@gc.cuny.edu
Patrizia Casaccia
pcasaccia@gc.cuny.edu

Specialty section:
This article was submitted to Non-Neuronal Cells, a section of the journal Frontiers in Cellular Neuroscience

Received: 24 July 2020
Accepted: 02 October 2020
Published: 05 November 2020

Citation:
Liu J, Likhtik E, Shereen AD, Dennis-Tiwary TA and Casaccia P (2020) White Matter Plasticity in Anxiety: Disruption of Neural Network Synchronization During Threat-Safety Discrimination. Front. Cell. Neurosci. 14:587053. doi: 10.3389/fncel.2020.587053

Recent evidence highlighted the importance of white matter tracts in typical and atypical behaviors. White matter dynamically changes in response to learning, stress, and social experiences. Several lines of evidence have reported white matter dysfunction in psychiatric conditions, including depression, stress- and anxiety-related disorders. The mechanistic underpinnings of these associations, however, remain poorly understood. Here, we outline an integrative perspective positing a link between aberrant myelin plasticity and anxiety. Drawing on extant literature and emerging new findings, we suggest that in anxiety, unique changes may occur in response to threat and to safety learning and the ability to discriminate between both types of stimuli. We propose that altered myelin plasticity in the neural circuits underlying these two forms of learning relates to the emergence of anxiety-related disorders, by compromising mechanisms of neural network synchronization. The clinical and translational implications of this model for anxiety-related disorders are discussed.

Keywords: myelin, synchrony, oligodendroccyte, connectivity, interneuron

INTRODUCTION

Myelination in vertebrates, represents a successful mechanism of adaptation to the development of complex behaviors, requiring increased speed of axonal conduction. While in some invertebrates fast transmission is achieved by decreasing resistance due to axonal expansion, in craniates and jawed fish the insulation provided by myelin allows axons of similar caliber to increase their speed of communication by several hundred folds (Tomassy et al., 2016). Oligodendrocytes (OLs) are the myelin-forming cells of the central nervous system (CNS). They derive from oligodendrocyte progenitor cells (OPCs), which continue to proliferate and differentiate into new OLs throughout life (Dimou et al., 2008; Zhu et al., 2011; Young et al., 2013; Hill et al., 2018).

The insulating properties of myelin are essential for saltatory axonal conduction. However, in higher-order organisms, the myelin sheath is not a static cellular compartment but is rather a dynamic membrane, capable of providing metabolic supports to axons in conditions of elevated energetic demands (Nave, 2010; Saab and Nave, 2017). Finally, recent findings have defined the formation and remodeling of new myelin in response to experience and learning as key contributors to physiological brain function and behavior (Liu et al., 2012; Makinodan et al., 2012; Gibson et al., 2014; Mckenzie et al., 2014; Hughes et al., 2018; Mitew et al., 2018; Bonnefil et al., 2019; Geraghty et al., 2019; Swire et al., 2019; Pan et al., 2020; Steadman et al., 2020). Yet, the functional significance of myelinating OLs concerning psychological adaptation remains poorly understood. Here, we first discuss the concept of myelin plasticity and review evidence that it occurs in response to social experiences and in the context of learning of motor and non-motor skills, including learning about threat. We then review literature related to white matter alterations in psychiatric disorders, with a focus on stress- and anxiety-related disorders. Finally, we discuss emerging evidence supporting associations between altered myelin plasticity in circuits regulating threat and safety learning and the ability to discriminate between threat and safety stimuli as purported anxiogenic mechanisms and outline key clinical and translational implications.

WHITE MATTER AND MYELIN PLASTICITY IN RESPONSE TO SOCIAL EXPERIENCE OR LEARNING

The concept of myelin plasticity includes diverse types of cellular processes such as *de novo* myelin formation and remodeling of pre-existing myelin. *De novo* myelination refers to the differentiation of local resident OPCs into myelin-forming OLs and/or wrapping of previously unmyelinated axons or axonal segments (Tomassy et al., 2014; Hill et al., 2018). Myelin remodeling refers to changes in the number of wraps around myelinated axons or in the length of myelinated segments between two nodes of Ranvier (i.e., internodal length).

Myelin plasticity was initially reported in studies addressing exposure to social stressors both in humans and in animal models. One of the initial studies conducted in human children exposed to severe childhood neglect identified reduced thickness of the corpus callosum area in these individuals compared to controls (Teicher et al., 2004; Mehta et al., 2009). Maternal deprivation in rodents, early weaning, and social deprivation during the critical period of adolescence also resulted in defective myelination detected in juvenile mice (Kodama et al., 2008; Makinodan et al., 2012; Yang et al., 2017). The effect of social stress was not limited to a critical developmental period, as adult mice exposed to chronic variable stress, social isolation or social defeat, also altered the OL transcriptome, and decreased myelin thickness in the medial prefrontal cortex (mPFC; Liu et al., 2012, 2018; Bonnefil et al., 2019). Together, these studies provide clear evidence of a link between myelination of specific brain regions and social experience.

White matter plasticity was reported to be modulated also in response to motor and non-motor learning. Myelination of distinct neural pathways in children, for instance, follows a stereotyped sequence that coincides with the development of important motor milestones, such as sitting, crawling, and then walking (Aubert-Broche et al., 2008; Tomassy et al., 2016). Learning how to juggle in adulthood increased myelination of subcortical white matter at the right posterior intraparietal sulcus, which was detected as increased fractional anisotropy (FA) in MRI (Scholz et al., 2009). The inverse relationship between the extent of white matter changes and age of training was assessed by the analysis of FA at the posterior midbody/isthmus of the corpus callosum in piano players, which revealed greater connectivity and sensorimotor synchronization performance in those who learned earlier rather than later in life (Steele et al., 2013). Non-motor learning was similarly associated with changes in white matter. For example, in children aged 3 months to 4 years, the myelin volume fraction in the frontal and temporal cortices showed a positive correlation with predicted language abilities, which strengthened with age (O'Muircheartaigh et al., 2014). In subjects learning a second language as adults, systematic, learning-dependent changes were also observed in the white matter tracts associated with traditional left hemisphere language areas and their right hemisphere analogs (Schlegel et al., 2012).

Animal studies repeatedly demonstrate life-long myelin plasticity in response to motor and non-motor learning. For instance, learning a novel motor skill in rats resulted in higher FA in the subcortical white matter of the sensorimotor cortex and increased myelin protein expression after training (Sampaio-Baptista et al., 2013). The necessity of myelin plasticity for skill acquisition and memory consolidation was further demonstrated using transgenic mice. Impairing new myelin synthesis by conditional ablation of the lineage-specific transcription factor *Myrf*, prevented *de novo* myelination during training and impaired new motor skill acquisition while retaining intact general motor function (Mckenzie et al., 2014). Similarly, preventing the formation of new OLs and myelin impaired spatial memory formation and water maze performance (Pan et al., 2020; Steadman et al., 2020).

Additional studies support a role for OL lineage cells in memory consolidation. Impaired formation of new myelin *via* lineage-specific ablation of the transcription factor *Myrf* did not affect contextual freezing immediately after learning, but rather impaired memory retrieval (Pan et al., 2020; Steadman et al., 2020), thereby suggesting that generation of new OLs was required for fear memory consolidation. It was also reported that memory consolidation required the occurrence of rhythmic oscillatory communication to synchronize activity across brain regions (Pajevic et al., 2014), which was impaired in the *Myrf* conditional knockout mice (Steadman et al., 2020), thereby highlighting the functional relevance of myelination for learning-induced synchronized activity.

MYELIN AND WHITE MATTER ALTERATIONS IN STRESS- AND ANXIETY-RELATED DISORDERS

The importance of myelin plasticity in response to external conditions and shaping behavioral consequences led to the concept that myelination of white matter tracts regulating learning about threat may be altered in pathologies characterized by behavioral maladaptation and are associated with changes in brain function. Magnetic resonance imaging (MRI) allows for the indirect measurement of brain connectivity, both functionally (fMRI) and structurally (diffusion MRI; **Figure 1**). Parameters that are characteristically measured are FA, which indicates the degree to which water molecules preferentially diffuse along one direction. Because myelin restricts water molecules to diffuse mainly along the direction of axonal bundles, higher FA values are often interpreted as indicating greater myelination or organization of white matter tracts (Thomason and Thompson, 2011). Complementary diffusion values, such as radial, axial, and mean diffusivities, provide additional information related to the integrity, caliber, and myelination of white matter (Song et al., 2003).

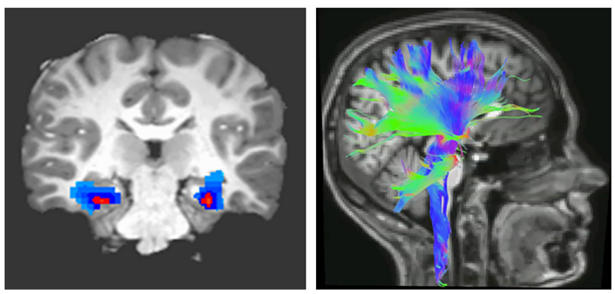

FIGURE 1 | Imaging brain connectivity. Two widely used imaging techniques to assess connectivity are functional magnetic resonance (fMRI; left) and diffusion tensor imaging (DTI; right). fMRI indirectly measures neural activity between two or more regions through statistical analysis of correlated changes in the blood oxygen level-dependent MRI signal (Buxton, 2009). In contrast, DTI measures structural connectivity or the organization of white matter tracts running between neural regions. Fractional anisotropy (FA), derived from DTI, indicates the degree to which water molecules preferentially diffuse along one direction. Because myelin restricts water molecules to diffuse mainly along the direction of axonal bundles, higher FA values are often interpreted as indicating greater myelination or organization of white matter tracts (Thomason and Thompson, 2011).

The uncinate fasciculus is an important white matter tract connecting brain regions regulating the threat response (e.g., amygdala) with those regulating behavior (e.g., PFC; **Figure 2**), and its myelination follows a characteristic developmental trajectory during adolescence, reaching stability in young adulthood (Lebel and Beaulieu, 2011; Thomason and Thompson, 2011). Early in life, excitatory signals have been shown to emerge from the amygdala directed to the PFC, while later in life, inhibitory signaling from the PFC to the amygdala favors emotional regulation (Ghashghaei et al., 2007; Cressman et al., 2010). While functional connectivity studies do not indicate the direction of influence, a valence switch from positive to negative PFC-amygdala fMRI correlations during normal development supports the existence of this developmental pattern (Gee et al., 2013).

The progressive increase of FA in the uncinate fasciculus, in young healthy subjects, reflects effective myelination of this tract and results in facilitated communication between PFC and amygdala (Kim and Whalen, 2009; Tromp et al., 2012). In contrast, decreased FA in the uncinate fasciculus was reported in subjects with anxiety-related traits and was suggestive of disrupted or inefficient myelination (Westlye et al., 2011). Importantly, a reduction in structural connectivity, as indicated by reduced bilateral FA in both uncinate fasciculi was consistently detected among individuals with a generalized anxiety disorder (Tromp et al., 2012), and also in children

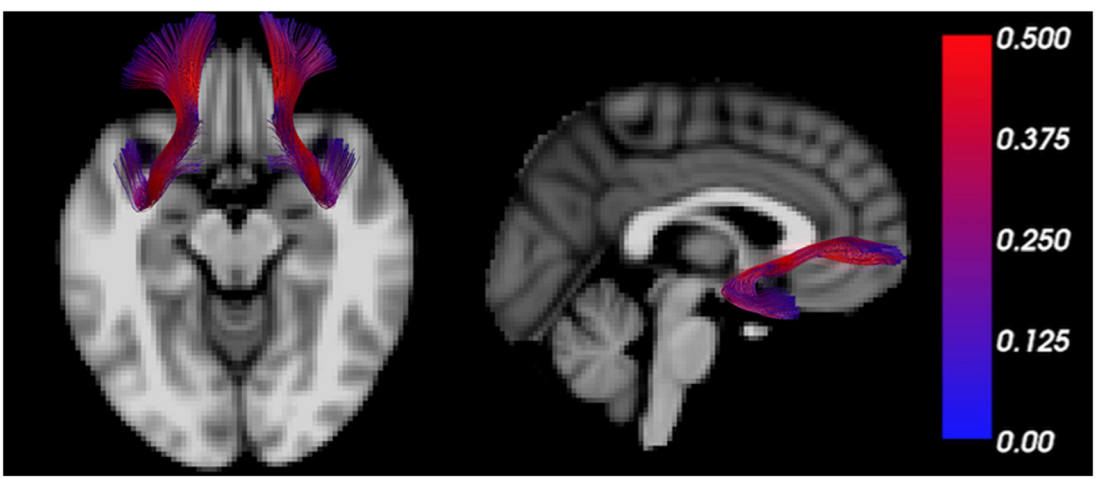

FIGURE 2 | The uncinate fasciculus is a characteristic trajectory connecting the prefrontal cortex (PFC) and amygdala. MRI tractography depicts the uncinate fasciculus overlain on transverse (left) and sagittal (right) T1 weighted sections. The color bar scales the tract by fractional anisotropy (FA) values.

exposed to socioemotional deprivation (Eluvathingal et al., 2006). Decreased FA and radial diffusivity were also detected in the left uncinate fasciculus of affected monozygotic adolescent twins with anxiety disorders compared to unaffected siblings (Adluru et al., 2017), collectively suggesting compromised communication between PFC and amygdala in such individuals (Yavas et al., 2019).

While altered connectivity between the amygdala and PFC has been well documented in several stress and anxiety-related disorders (Tromp et al., 2012), pathological inflammatory demyelination of the septo-fornical area, has also been reported in multiple sclerosis patients with high anxiety, and suggested to contribute to its pathogenesis (Palotai et al., 2018).

However, the alteration of white matter microstructure involved in anxiety-related personality traits is not restricted to corticolimbic pathways. For example, harm avoidance in adult subjects was positively associated with radial and mean diffusivity, not only in the uncinate fasciculus but also in the anterior thalamic radiation, corpus callosum, parahippocampal cingulum, corticospinal tract, and inferior and superior longitudinal fasciculi (Westlye et al., 2011; Lu et al., 2018). Reduced FA was also detected in the medial and posterior portions of the corpus callosum of children with post-traumatic stress disorder (PTSD; Jackowski et al., 2008), and altered inter-hemispheric frontal, frontal-limbic, or frontal-temporal connectivity was identified as a potential marker of vulnerability to anxiety in young healthy subjects (Yang et al., 2019) and symptomatic anxiety in patients with late-life depression (Li et al., 2020). Finally, it is conceivable that anxiety may lead to elevated blood pressure, a condition that has been associated with scattered ischemic or micro-hemorrhagic white matter lesions occurring in bloodshed regions in older subjects (Iadecola et al., 2016). While this association is unlikely to account for the changes in FA as discussed above, it is worth mentioning that hypertensive patients with dislipidemia showed decreased spectroscopic signal for N-acetylaspartic-acid (NAA), thereby suggesting that associated comorbidities may interfere with the process of new myelin synthesis in white matter tracts (Chiappelli et al., 2019).

THE IMPORTANCE OF THREAT AND SAFETY DISCRIMINATION IN ANXIOGENIC MECHANISMS OF STRESS- AND ANXIETY-RELATED DISORDERS

In addition to disruptions in threat learning, growing evidence suggests that anxiety disorders are characterized by impaired threat/safety discrimination, resulting in generalized fear that is typically associated with a proliferation of avoidance behaviors that incapacitate daily function and have a negative impact on mental health (Lissek et al., 2009; Sep et al., 2019). Disrupted discrimination derives from several learning processes gone awry: overly strong conditioning to threat, as well as underdeveloped defensive response suppression to non-threatening stimuli. Combined, overactive communication patterns characteristic of making associations between cues and threatening outcomes, and underactive patterns of communication that are characteristic of fear suppression towards non-threatening cues, leads to generalized fear and anxiety (Jovanovic et al., 2010, 2012). Therefore, proper discrimination learning depends on the development and maintenance of connected functional circuits that can support both fear acquisition and fear suppression.

Safety learning is integrally linked to fear learning. Non-threatening neutral cues or safety cues that signal the explicit absence of threat, when learned, become conditioned inhibitors of fear (Pavlov, 1927; Rescorla, 1988). An effective safety cue can also be positively reinforcing because it signals the active lack of threat, and therefore carries motivational and rewarding properties. For example, when presented with a safety cue, animals show increased instrumental responding, such as more vigorous bar pressing for a reward (Hendry, 1967), and stronger conditioned place preference for the area where the safety cue was presented (Rogan et al., 2005). Therefore, learning about non-threatening or safe stimuli is likely to engage a set of regions that are overlapping but distinct from those involved in fear conditioning, and can include circuits that engage the processing of reward (Luo et al., 2018). Although the hippocampal-amygdala-prefrontal network is active during threatening and non-threatening cues, the cell populations involved and modes of communication between these regions are different during these two types of learning (Sangha et al., 2013, 2014; Mayer et al., 2018; Ng et al., 2018). Therefore, encoding modes within and communication between areas are both crucial to maintain accurate and updated information to appropriately dial anxiety, and myelin dysregulation in this circuit has been associated with fear generalization and PTSD (Jovanovic et al., 2010; Fani et al., 2012).

CIRCUIT-LEVEL COMMUNICATION THAT SCULPTS THREAT-SAFETY DISCRIMINATION LEARNING

At the circuit level, inter-regional communication underlies the ability to discriminate between threat and safety and is manifested by oscillations that reflect fluctuating membrane potentials in groups of neurons due to incoming inputs from distal sites and local firing (Buzsáki et al., 2013; Akam and Kullmann, 2014; Pesaran et al., 2018). Theta (4–12 Hz) and gamma (30–120 Hz) rhythms are the two main types of oscillations related to discrimination learning. The oscillatory communication patterns between distal sites shift as different regions are exposed to cues that are paired or unpaired with aversive experience (Lesting et al., 2011; Likhtik et al., 2014; Stujenske et al., 2014; Ciocchi et al., 2015; Karalis et al., 2016; Padilla-Coreano et al., 2019).

For instance, during retrieval of differential fear conditioning, presentations of aversive stimuli lead to increased strength and theta synchrony in the basolateral amygdala (BLA) and in the PFC, relative to presentations of the non-threatening stimulus (Likhtik et al., 2014; Karalis et al., 2016). Furthermore, when fear is suppressed during retrieval of non-aversive stimuli,

theta oscillations in the PFC predict BLA theta rhythms, suggesting that information from PFC to BLA is transferred *via* oscillatory theta band activity (Likhtik et al., 2014; **Figure 3**). Likewise, when a fear-conditioned cue becomes less aversive after extinction learning, communication in the theta band decreases between these regions, and PFC theta oscillations organize BLA activity (Lesting et al., 2011; Davis et al., 2017; Rahman et al., 2018), suggesting that theta-encoded information transfer from the PFC to the BLA (carried by the uncinate fasciculus) may be a common signature of fear inhibition across

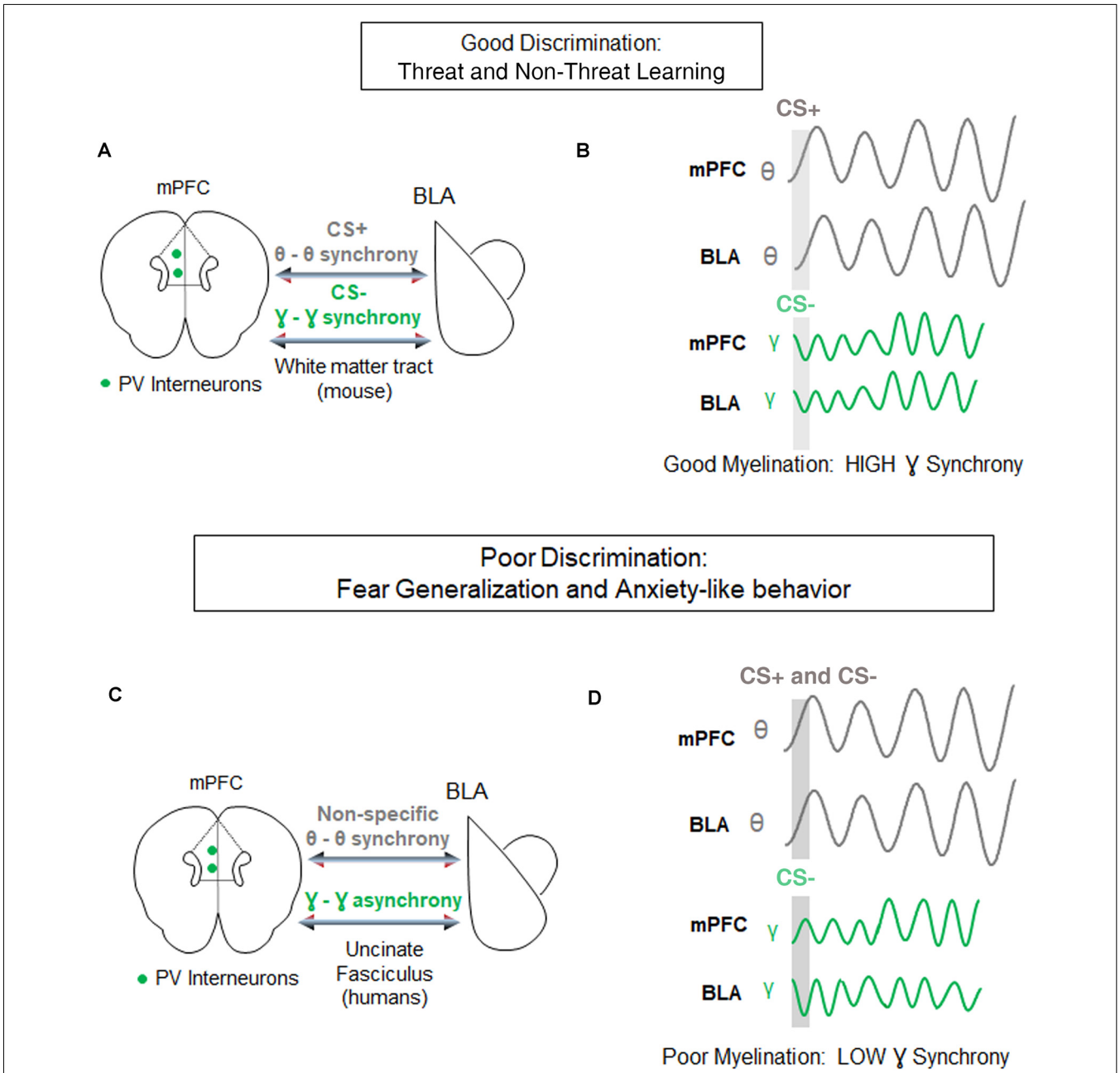

FIGURE 3 | Circuit-level synchrony is required for discrimination of threat from non-threat. **(A)** Under conditions of well-myelinated tracts, medial prefrontal cortex (mPFC)-basolateral amygdala (BLA) communication *via* white matter tracts during successful discrimination of threat from non-threat is characterized by high theta-range synchrony selectively during the aversive CS+ (gray), and high gamma-range synchrony selectively during the discriminated non-aversive CS− (green). Parvalbumin positive (PV) interneurons in the mPFC are posited to contribute to gamma oscillations-based, fast communication during discrimination. **(B)** *Top*, Examples of synchrony in CS+ evoked (gray bar) theta signals of the mPFC and BLA (gray lines). *Bottom*, examples of synchrony in CS− evoked gamma signals of the mPFC and BLA (green lines). **(C)** During poor fear discrimination and compromised myelination, theta synchrony in the mPFC-BLA circuit increases non-selectively to threatening and non-threatening cues (gray), and gamma-synchrony during the non-threatening cues is diminished. The direct communication between these circuits occurs *via* the Uncinate Fasciculus tract in humans. **(D)** The same as in **(C)** but demonstrating non-specific theta-synchrony, and lower gamma synchrony in this circuit during poor discrimination of the CS−.

several learning paradigms. Notably, in animals that generalize fear after discrimination learning, theta oscillations remain high in the PFC-BLA pathway during aversive and non-aversive stimuli, without a predominance of theta-information transfer from the PFC to the BLA (Likhtik et al., 2014). Thus, similar PFC-BLA processing of threat and non-threat are signature characteristics of fear generalization.

Gamma oscillations develop along with the maturation of inhibitory signaling and depend on the myelination of Parvalbumin (PV+) GABAergic inhibitory interneurons (Traub et al., 1996; Fries, 2009; Sohal et al., 2009; Hu et al., 2014; Strüber et al., 2015), which are extensively myelinated in an activity-dependent manner (Stedehouder and Kushner, 2017; Stedehouder et al., 2018, 2019). GABAergic activity and gamma oscillations in the PFC are crucial for cue detection and encoding (Courtin et al., 2014; Piantadosi and Floresco, 2014; Howe et al., 2017). While the role of gamma rhythm in fear learning is still the subject of active investigation (Headley and Paré, 2013), fear suppression to non-threat is associated with an increase in gamma-range synchrony in communication among cortical and subcortical regions (**Figure 3**; Stujenske et al., 2014; Concina et al., 2018). We, therefore, propose that good discrimination between threat and non-threat requires optimal myelination of PV+ interneurons, manifesting in regional gamma synchrony. We further posit that aberrant myelination coupled with impaired white matter integrity of the PFC-BLA connection may result in decreased gamma rhythm, loss of discrimination, and lead to fear generalization.

Furthermore, temporal precision is necessary for inter-regional communication, when BLA gamma oscillations are coupled to PFC theta oscillations during a successfully discriminated non-threat (Stujenske et al., 2014), suggesting that prefrontal input has a direct or indirect role in driving gamma activity in the BLA (Rosenkranz and Grace, 2001; Amano et al., 2010; Bukalo et al., 2015; Strobel et al., 2015; Bloodgood et al., 2018). This faster oscillatory mode of cross-regional communication is shaped by excitatory-inhibitory interactions that require millisecond range timing of inhibitory activity (Buzsáki and Wang, 2012; Courtin et al., 2014). Given its role in speeding up communication, new myelin formation, sheath integrity, and effective remodeling are likely to play an integral role in sculpting inhibitory-excitatory dialogue during discrimination learning.

MYELIN PLASTICITY AND OLIGODENDROCYTE LINEAGE CELLS AS REGULATORY MECHANISMS OF CIRCUIT CONNECTIVITY

Based on the previously discussed evidence of changes in white matter tracts in anxiety disorders, we posit that

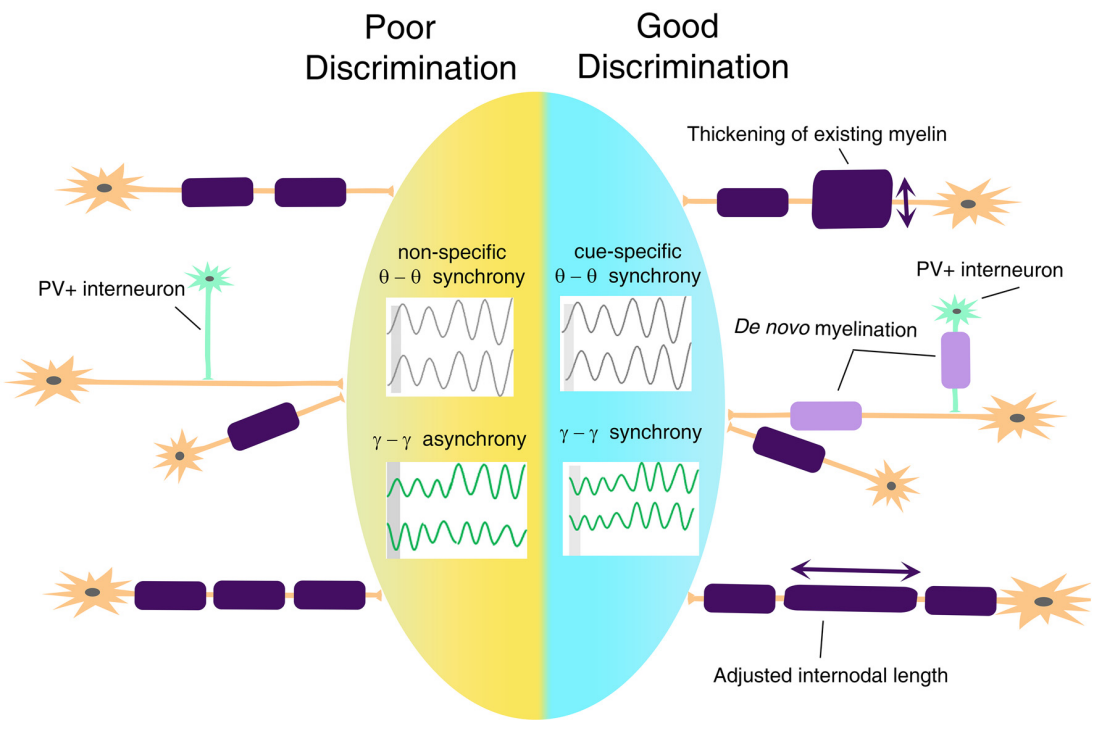

FIGURE 4 | A proposed model for myelin plasticity in discrimination between threat and safety. Myelin remodeling mechanisms include thickening of existing myelin, *de novo* myelination on unmyelinated axons, and adjusted internodal length, which could occur both on excitatory neurons and parvalbumin-positive (PV+) interneurons. Such experience-dependent myelin remodeling allows inter-regional cue-specific theta-range synchrony and gamma-range synchrony to establish, which is essential for successful threat and safety discrimination.

disruptions in threat and safety discrimination are related to defective mechanisms of cortical synchronization. Connectivity determines the speed and timing of electrical activity transmitted between relay points, leading to synchronous activation of neural networks and rhythmic oscillations. A mathematical model has predicted that a 1-ms conduction delay would interrupt the phase by 30°, significantly affecting signal amplitude and phase coherence (Pajevic et al., 2014). Besides, myelination may be the most effective way not only of modulating conduction velocity, but also impacting self-organization of brain oscillation and affecting cognitive performance (Mabbott et al., 2006; Scantlebury et al., 2014; Bells et al., 2019; Noori et al., 2020). In terms of threat and safety learning, it will be important to take into consideration the fact that myelination of glutamatergic neurons and PV+ GABAergic interneurons (Stedehouder and Kushner, 2017; Stedehouder et al., 2018, 2019) might bear important and unique functional consequences on the overall activity of the neural networks and consequent oscillations (**Figure 4**), with altered myelination of PV+ interneurons, likely impacting gamma oscillations and myelination of BLA-mPFC pyramidal tracts impacting theta rhythms.

It is also important to notice that OL lineage cells are capable of influencing neural activity and regulating circuit function in manners that are independent of canonical models of myelin plasticity and myelin remodeling. One example is the role of transmembrane proteoglycan nerve-glia antigen 2 (NG2), which is expressed on the surface of OPCs and has been proposed to act as a neuro-glial signal (Sakry et al., 2014) by being cleaved in an activity-dependent manner and modulating glutamate receptor activity in neighboring neurons (Sakry et al., 2014). Myelinating OLs also regulate K+ homeostasis, due to the expression of inward rectifying K+ channel, $K_{ir}4.1$, and OL-specific conditional ablation of this channel has been linked to delayed recovery of white matter axons from repetitive stimulation (Larson et al., 2018).

Taken together, we, therefore, posit that discrimination between threatening and safe cues may rely on distinct modalities of white matter plasticity or regulation of OL lineage cell function to favor neuronal synchronization across neural networks. We further predict that specific alterations of these mechanisms may be related to the development of anxiety disorders.

CONCLUDING REMARKS

As reviewed above, studying myelination mechanisms in circuits underlying anxious behavior and discrimination learning represents an intriguing approach to understanding the development of anxiety disorders and clarifying novel treatment approaches. To test this framework, it will be important to determine the effectiveness of interventions targeting learning and discrimination processes and their underlying circuit functioning in the treatment of stress- and anxiety-related disorders. The key to this approach will be to understand the multiple ways in which myelin and OL functioning and plasticity contribute to these effects to inform the development of more targeted behavioral interventions that reverse disruptions in circuit-level functioning and ultimately improve management of anxiety symptoms.

DATA AVAILABILITY STATEMENT

The original contributions presented in the study are included in the article, further inquiries can be directed to the corresponding author/s.

AUTHOR CONTRIBUTIONS

All authors conceived the concept and wrote the manuscript. All authors contributed to the article and approved the submitted version.

FUNDING

This work was supported by PSC-CUNY awards to JL and EL, by NIH-National Institute of Neurological Disorders and Stroke (NINDS) award no. R35 NS111604 to PC, by NIH-National Institute of Mental Health R56MH111700 and RF1MH120846 to TD-T, and R01MH118441 to EL.

ACKNOWLEDGMENTS

We would like to thank Dr. Do Tromp for her contribution to the uncinate tractography image in **Figure 2**.

REFERENCES

Adluru, N., Luo, Z., Van Hulle, C. A., Schoen, A. J., Davidson, R. J., Alexander, A. L., et al. (2017). Anxiety-related experience-dependent white matter structural differences in adolescence: a monozygotic twin difference approach. *Sci. Rep.* 7:8749. doi: 10.1038/s41598-017-08107-6

Akam, T., and Kullmann, D. M. (2014). Oscillatory multiplexing of population codes for selective communication in the mammalian brain. *Nat. Rev. Neurosci.* 15, 111–122. doi: 10.1038/nrn3668

Amano, T., Unal, C. T., and Paré, D. (2010). Synaptic correlates of fear extinction in the amygdala. *Nat. Neurosci.* 13, 489–494. doi: 10.1038/nn.2499

Aubert-Broche, B., Fonov, V., Leppert, I., Pike, G. B., and Collins, D. L. (2008). Human brain myelination from birth to 4.5 years. *Med. Image Comput. Comput. Assist. Interv.* 11, 180–187. doi: 10.1007/978-3-540-85990-1_22

Bells, S., Lefebvre, J., Longoni, G., Narayanan, S., Arnold, D. L., Yeh, E. A., et al. (2019). White matter plasticity and maturation in human cognition. *Glia* 67, 2020–2037. doi: 10.1002/glia.23661

Bloodgood, D. W., Sugam, J. A., Holmes, A., and Kash, T. L. (2018). Fear extinction requires infralimbic cortex projections to the basolateral amygdala. *Transl. Psychiatry* 8:60. doi: 10.1038/s41398-018-0106-x

Bonnefil, V., Dietz, K., Amatruda, M., Wentling, M., Aubry, A. V., Dupree, J. L., et al. (2019). Region-specific myelin differences define behavioral consequences of chronic social defeat stress in mice. *eLife* 8:e40855. doi: 10.7554/eLife.40855

Bukalo, O., Pinard, C. R., Silverstein, S., Brehm, C., Hartley, N. D., Whittle, N., et al. (2015). Prefrontal inputs to the amygdala instruct fear extinction memory formation. *Sci. Adv.* 1:e1500251. doi: 10.1126/sciadv.1500251

Buxton, R. B. (2009). *Introduction to Functional Magnetic Resonance Imaging: Principles and Techniques.* Cambridge: Cambridge University Press.

Buzsáki, G., and Wang, X.-J. (2012). Mechanisms of gamma oscillations. *Annu. Rev. Neurosci.* 35, 203–225. doi: 10.1146/annurev-neuro-062111-150444

Buzsáki, G., Logothetis, N., and Singer, W. (2013). Scaling brain size, keeping timing: evolutionary preservation of brain rhythms. *Neuron* 80, 751–764. doi: 10.1016/j.neuron.2013.10.002

Chiappelli, J., Rowland, L. M., Wijtenburg, S. A., Chen, H., Maudsley, A. A., Sheriff, S., et al. (2019). Cardiovascular risks impact human brain *N*-acetylaspartate in regionally specific patterns. *Proc. Natl. Acad. Sci. U S A* 116, 25243–25249. doi: 10.1073/pnas.1907730116

Ciocchi, S., Passecker, J., Malagon-Vina, H., Mikus, N., and Klausberger, T. (2015). Brain computation. Selective information routing by ventral hippocampal CA1 projection neurons. *Science* 348, 560–563. doi: 10.1126/science.aaa3245

Concina, G., Cambiaghi, M., Renna, A., and Sacchetti, B. (2018). Coherent activity between the prelimbic and auditory cortex in the slow-gamma band underlies fear discrimination. *J. Neurosci.* 38, 8313–8328. doi: 10.1523/JNEUROSCI.0540-18.2018

Courtin, J., Chaudun, F., Rozeske, R. R., Karalis, N., Gonzalez-Campo, C., Wurtz, H., et al. (2014). Prefrontal parvalbumin interneurons shape neuronal activity to drive fear expression. *Nature* 505, 92–96. doi: 10.1038/nature12755

Cressman, V. L., Balaban, J., Steinfeld, S., Shemyakin, A., Graham, P., Parisot, N., et al. (2010). Prefrontal cortical inputs to the basal amygdala undergo pruning during late adolescence in the rat. *J. Comp. Neurol.* 518, 2693–2709. doi: 10.1002/cne.22359

Davis, P., Zaki, Y., Maguire, J., and Reijmers, L. G. (2017). Cellular and oscillatory substrates of fear extinction learning. *Nat. Neurosci.* 20, 1624–1633. doi: 10.1038/nn.4651

Dimou, L., Simon, C., Kirchhoff, F., Takebayashi, H., and Gotz, M. (2008). Progeny of Olig2-expressing progenitors in the gray and white matter of the adult mouse cerebral cortex. *J. Neurosci.* 28, 10434–10442. doi: 10.1523/JNEUROSCI.2831-08.2008

Eluvathingal, T. J., Chugani, H. T., Behen, M. E., Juhasz, C., Muzik, O., Maqbool, M., et al. (2006). Abnormal brain connectivity in children after early severe socioemotional deprivation: a diffusion tensor imaging study. *Pediatrics* 117, 2093–2100. doi: 10.1542/peds.2005-1727

Fani, N., King, T. Z., Jovanovic, T., Glover, E. M., Bradley, B., Choi, K., et al. (2012). White matter integrity in highly traumatized adults with and without post-traumatic stress disorder. *Neuropsychopharmacology* 37, 2740–2746. doi: 10.1038/npp.2012.146

Fries, P. (2009). Neuronal gamma-band synchronization as a fundamental process in cortical computation. *Annu. Rev. Neurosci.* 32, 209–224. doi: 10.1146/annurev.neuro.051508.135603

Gee, D. G., Humphreys, K. L., Flannery, J., Goff, B., Telzer, E. H., Shapiro, M., et al. (2013). A developmental shift from positive to negative connectivity in human amygdala-prefrontal circuitry. *J. Neurosci.* 33, 4584–4593. doi: 10.1523/JNEUROSCI.3446-12.2013

Geraghty, A. C., Gibson, E. M., Ghanem, R. A., Greene, J. J., Ocampo, A., Goldstein, A. K., et al. (2019). Loss of adaptive myelination contributes to methotrexate chemotherapy-related cognitive impairment. *Neuron* 103, 250.e8–265.e8. doi: 10.1016/j.neuron.2019.04.032

Ghashghaei, H. T., Hilgetag, C. C., and Barbas, H. (2007). Sequence of information processing for emotions based on the anatomic dialogue between prefrontal cortex and amygdala. *NeuroImage* 34, 905–923. doi: 10.1016/j.neuroimage.2006.09.046

Gibson, E. M., Purger, D., Mount, C. W., Goldstein, A. K., Lin, G. L., Wood, L. S., et al. (2014). Neuronal activity promotes oligodendrogenesis and adaptive myelination in the mammalian brain. *Science* 344:1252304. doi: 10.1126/science.1252304

Headley, D. B., and Paré, D. (2013). In sync: gamma oscillations and emotional memory. *Front. Behav. Neurosci.* 7:170. doi: 10.3389/fnbeh.2013.00170

Hendry, D. P. (1967). Conditioned inhibition of conditioned suppression. *Psychon. Sci.* 9, 261–262. doi: 10.3758/bf03332212

Hill, R. A., Li, A. M., and Grutzendler, J. (2018). Lifelong cortical myelin plasticity and age-related degeneration in the live mammalian brain. *Nat. Neurosci.* 21, 683–695. doi: 10.1038/s41593-018-0120-6

Howe, W. M., Gritton, H. J., Lusk, N. A., Roberts, E. A., Hetrick, V. L., Berke, J. D., et al. (2017). Acetylcholine release in prefrontal cortex promotes gamma oscillations and theta-gamma coupling during cue detection. *J. Neurosci.* 37, 3215–3230. doi: 10.1523/JNEUROSCI.2737-16.2017

Hu, H., Gan, J., and Jonas, P. (2014). Interneurons. Fast-spiking, parvalbumin^{+} GABAergic interneurons: from cellular design to microcircuit function. *Science* 345:1255263. doi: 10.1126/science.1255263

Hughes, E. G., Orthmann-Murphy, J. L., Langseth, A. J., and Bergles, D. E. (2018). Myelin remodeling through experience-dependent oligodendrogenesis in the adult somatosensory cortex. *Nat. Neurosci.* 21, 696–706. doi: 10.1038/s41593-018-0121-5

Iadecola, C., Yaffe, K., Biller, J., Bratzke, L. C., Faraci, F. M., Gorelick, P. B., et al. (2016). Impact of hypertension on cognitive function: a scientific statement from the american heart association. *Hypertension* 68, e67–e94. doi: 10.1161/HYP.0000000000000053

Jackowski, A. P., Douglas-Palumberi, H., Jackowski, M., Win, L., Schultz, R. T., Staib, L. W., et al. (2008). Corpus callosum in maltreated children with posttraumatic stress disorder: a diffusion tensor imaging study. *Psychiatry Res.* 162, 256–261. doi: 10.1016/j.pscychresns.2007.08.006

Jovanovic, T., Kazama, A., Bachevalier, J., and Davis, M. (2012). Impaired safety signal learning may be a biomarker of PTSD. *Neuropharmacology* 62, 695–704. doi: 10.1016/j.neuropharm.2011.02.023

Jovanovic, T., Norrholm, S. D., Blanding, N. Q., Davis, M., Duncan, E., Bradley, B., et al. (2010). Impaired fear inhibition is a biomarker of PTSD but not depression. *Depress Anxiety* 27, 244–251. doi: 10.1002/da.20663

Karalis, N., Dejean, C., Chaudun, F., Khoder, S., Rozeske, R. R., Wurtz, H., et al. (2016). 4-Hz oscillations synchronize prefrontal-amygdala circuits during fear behavior. *Nat. Neurosci.* 19, 605–612. doi: 10.1038/nn.4251

Kim, M. J., and Whalen, P. J. (2009). The structural integrity of an amygdala-prefrontal pathway predicts trait anxiety. *J. Neurosci.* 29, 11614–11618. doi: 10.1523/JNEUROSCI.2335-09.2009

Kodama, Y., Kikusui, T., Takeuchi, Y., and Mori, Y. (2008). Effects of early weaning on anxiety and prefrontal cortical and hippocampal myelination in male and female Wistar rats. *Dev. Psychobiol.* 50, 332–342. doi: 10.1002/dev.20289

Larson, V. A., Mironova, Y., Vanderpool, K. G., Waisman, A., Rash, J. E., Agarwal, A., et al. (2018). Oligodendrocytes control potassium accumulation in white matter and seizure susceptibility. *eLife* 7:e34829. doi: 10.7554/eLife.34829

Lebel, C., and Beaulieu, C. (2011). Longitudinal development of human brain wiring continues from childhood into adulthood. *J. Neurosci.* 31, 10937–10947. doi: 10.1523/JNEUROSCI.5302-10.2011

Lesting, J., Narayanan, R. T., Kluge, C., Sangha, S., Seidenbecher, T., and Pape, H. C. (2011). Patterns of coupled theta activity in amygdala-hippocampal-prefrontal cortical circuits during fear extinction. *PLoS One* 6:e21714. doi: 10.1371/journal.pone.0021714

Li, H., Lin, X., Liu, L., Su, S., Zhu, X., Zheng, Y., et al. (2020). Disruption of the structural and functional connectivity of the frontoparietal network underlies symptomatic anxiety in late-life depression. *Neuroimage Clin.* 28:102398. doi: 10.1016/j.nicl.2020.102398

Likhtik, E., Stujenske, J. M., Topiwala, M. A., Harris, A. Z., and Gordon, J. A. (2014). Prefrontal entrainment of amygdala activity signals safety in learned fear and innate anxiety. *Nat. Neurosci.* 17, 106–113. doi: 10.1038/nn.3582

Lissek, S., Rabin, S. J., Mcdowell, D. J., Dvir, S., Bradford, D. E., Geraci, M., et al. (2009). Impaired discriminative fear-conditioning resulting from elevated fear responding to learned safety cues among individuals with panic disorder. *Behav. Res. Ther.* 47, 111–118. doi: 10.1016/j.brat.2008.10.017

Liu, J., Dietz, K., Deloyht, J. M., Pedre, X., Kelkar, D., Kaur, J., et al. (2012). Impaired adult myelination in the prefrontal cortex of socially isolated mice. *Nat. Neurosci.* 15, 1621–1623. doi: 10.1038/nn.3263

Liu, J., Dietz, K., Hodes, G. E., Russo, S. J., and Casaccia, P. (2018). Widespread transcriptional alternations in oligodendrocytes in the adult mouse brain following chronic stress. *Dev. Neurobiol.* 78, 152–162. doi: 10.1002/dneu.22533

Lu, M., Yang, C., Chu, T., and Wu, S. (2018). Cerebral white matter changes in young healthy individuals with high trait anxiety: a tract-based spatial statistics study. *Front. Neurol.* 9:704. doi: 10.3389/fneur.2018.00704

Luo, R., Uematsu, A., Weitemier, A., Aquili, L., Koivumaa, J., McHugh, T. J., et al. (2018). A dopaminergic switch for fear to safety transitions. *Nat. Commun.* 9:2483. doi: 10.1038/s41467-018-04784-7

Mabbott, D. J., Noseworthy, M., Bouffet, E., Laughlin, S., and Rockel, C. (2006). White matter growth as a mechanism of cognitive development in children. *NeuroImage* 33, 936–946. doi: 10.1016/j.neuroimage.2006.07.024

Makinodan, M., Rosen, K. M., Ito, S., and Corfas, G. (2012). A critical period for social experience-dependent oligodendrocyte maturation and myelination. *Science* 337, 1357–1360. doi: 10.1126/science.1220845

Mayer, D., Kahl, E., Uzuneser, T. C., and Fendt, M. (2018). Role of the mesolimbic dopamine system in relief learning. *Neuropsychopharmacology* 43, 1651–1659. doi: 10.1038/s41386-018-0020-1

Mckenzie, I. A., Ohayon, D., Li, H., De Faria, J. P., Emery, B., Tohyama, K., et al. (2014). Motor skill learning requires active central myelination. *Science* 346, 318–322. doi: 10.1126/science.1254960

Mehta, M. A., Golembo, N. I., Nosarti, C., Colvert, E., Mota, A., Williams, S. C., et al. (2009). Amygdala, hippocampal and corpus callosum size following severe early institutional deprivation: the English and Romanian Adoptees study pilot. *J. Child Psychol. Psychiatry* 50, 943–951. doi: 10.1111/j.1469-7610.2009.02084.x

Mitew, S., Gobius, I., Fenlon, L. R., Mcdougall, S. J., Hawkes, D., Xing, Y. L., et al. (2018). Pharmacogenetic stimulation of neuronal activity increases myelination in an axon-specific manner. *Nat. Commun.* 9:306. doi: 10.1038/s41467-017-02719-2

Nave, K. A. (2010). Myelination and support of axonal integrity by glia. *Nature* 468, 244–252. doi: 10.1038/nature09614

Ng, K. H., Pollock, M. W., Urbanczyk, P. J., and Sangha, S. (2018). Altering D1 receptor activity in the basolateral amygdala impairs fear suppression during a safety cue. *Neurobiol. Learn. Mem.* 147, 26–34. doi: 10.1016/j.nlm.2017.11.011

Noori, R., Park, D., Griffiths, J. D., Bells, S., Frankland, P. W., Mabbott, D., et al. (2020). Activity-dependent myelination: a glial mechanism of oscillatory self-organization in large-scale brain networks. *Proc. Natl. Acad. Sci. U S A* 117, 13227–13237. doi: 10.1073/pnas.1916646117

O'Muircheartaigh, J., Dean, D. C. III., Ginestet, C. E., Walker, L., Waskiewicz, N., Lehman, K., et al. (2014). White matter development and early cognition in babies and toddlers. *Hum. Brain Mapp.* 35, 4475–4487. doi: 10.1002/hbm.22488

Padilla-Coreano, N., Canetta, S., Mikofsky, R. M., Alway, E., Passecker, J., Myroshnychenko, M. V., et al. (2019). Hippocampal-prefrontal theta transmission regulates avoidance behavior. *Neuron* 104, 601.e4–610.e4. doi: 10.1016/j.neuron.2019.08.006

Pajevic, S., Basser, P. J., and Fields, R. D. (2014). Role of myelin plasticity in oscillations and synchrony of neuronal activity. *Neuroscience* 276, 135–147. doi: 10.1016/j.neuroscience.2013.11.007

Palotai, M., Mike, A., Cavallari, M., Strammer, E., Orsi, G., Healy, B. C., et al. (2018). Changes to the septo-fornical area might play a role in the pathogenesis of anxiety in multiple sclerosis. *Mult. Scler.* 24, 1105–1114. doi: 10.1177/1352458517711273

Pan, S., Mayoral, S. R., Choi, H. S., Chan, J. R., and Kheirbek, M. A. (2020). Preservation of a remote fear memory requires new myelin formation. *Nat. Neurosci.* 23, 487–499. doi: 10.1038/s41593-019-0582-1

Pavlov, I. P. (1927). *Conditioned Reflexes: An Investigation of the Physiological Activity of the Cerebral Cortex.* Oxford, England: Oxford University Press.

Pesaran, B., Vinck, M., Einevoll, G. T., Sirota, A., Fries, P., Siegel, M., et al. (2018). Investigating large-scale brain dynamics using field potential recordings: analysis and interpretation. *Nat. Neurosci.* 21, 903–919. doi: 10.1038/s41593-018-0171-8

Piantadosi, P. T., and Floresco, S. B. (2014). Prefrontal cortical GABA transmission modulates discrimination and latent inhibition of conditioned fear: relevance for schizophrenia. *Neuropsychopharmacology* 39, 2473–2484. doi: 10.1038/npp.2014.99

Rahman, M. M., Shukla, A., and Chattarji, S. (2018). Extinction recall of fear memories formed before stress is not affected despite higher theta activity in the amygdala. *eLife* 7:e35450. doi: 10.7554/eLife.35450

Rescorla, R. A. (1988). Pavlovian conditioning: it's not what you think it is. *Am. Psychol.* 43, 151–160. doi: 10.1037//0003-066x.43.3.151

Rogan, M. T., Leon, K. S., Perez, D. L., and Kandel, E. R. (2005). Distinct neural signatures for safety and danger in the amygdala and striatum of the mouse. *Neuron* 46, 309–320. doi: 10.1016/j.neuron.2005.02.017

Rosenkranz, J. A., and Grace, A. A. (2001). Dopamine attenuates prefrontal cortical suppression of sensory inputs to the basolateral amygdala of rats. *J. Neurosci.* 21, 4090–4103. doi: 10.1523/JNEUROSCI.21-11-04090.2001

Saab, A. S., and Nave, K. A. (2017). Myelin dynamics: protecting and shaping neuronal functions. *Curr. Opin. Neurobiol.* 47, 104–112. doi: 10.1016/j.conb.2017.09.013

Sakry, D., Neitz, A., Singh, J., Frischknecht, R., Marongiu, D., Biname, F., et al. (2014). Oligodendrocyte precursor cells modulate the neuronal network by activity-dependent ectodomain cleavage of glial NG2. *PLoS Biol.* 12:e1001993. doi: 10.1371/journal.pbio.1001993

Sampaio-Baptista, C., Khrapitchev, A. A., Foxley, S., Schlagheck, T., Scholz, J., Jbabdi, S., et al. (2013). Motor skill learning induces changes in white matter microstructure and myelination. *J. Neurosci.* 33, 19499–19503. doi: 10.1523/JNEUROSCI.3048-13.2013

Sangha, S., Chadick, J. Z., and Janak, P. H. (2013). Safety encoding in the basal amygdala. *J. Neurosci.* 33, 3744–3751. doi: 10.1523/JNEUROSCI.3302-12.2013

Sangha, S., Robinson, P. D., Greba, Q., Davies, D. A., and Howland, J. G. (2014). Alterations in reward, fear and safety cue discrimination after inactivation of the rat prelimbic and infralimbic cortices. *Neuropsychopharmacology* 39, 2405–2413. doi: 10.1038/npp.2014.89

Scantlebury, N., Cunningham, T., Dockstader, C., Laughlin, S., Gaetz, W., Rockel, C., et al. (2014). Relations between white matter maturation and reaction time in childhood. *J. Int. Neuropsychol. Soc.* 20, 99–112. doi: 10.1017/S1355617713001148

Schlegel, A. A., Rudelson, J. J., and Tse, P. U. (2012). White matter structure changes as adults learn a second language. *J. Cogn. Neurosci.* 24, 1664–1670. doi: 10.1162/jocn_a_00240

Scholz, J., Klein, M. C., Behrens, T. E., and Johansen-Berg, H. (2009). Training induces changes in white-matter architecture. *Nat. Neurosci.* 12, 1370–1371. doi: 10.1038/nn.2412

Sep, M. S. C., Steenmeijer, A., and Kennis, M. (2019). The relation between anxious personality traits and fear generalization in healthy subjects: a systematic review and meta-analysis. *Neurosci. Biobehav. Rev.* 107, 320–328. doi: 10.1016/j.neubiorev.2019.09.029

Sohal, V. S., Zhang, F., Yizhar, O., and Deisseroth, K. (2009). Parvalbumin neurons and gamma rhythms enhance cortical circuit performance. *Nature* 459, 698–702. doi: 10.1038/nature07991

Song, S.-K., Sun, S.-W., Ju, W.-K., Lin, S.-J., Cross, A. H., and Neufeld, A. H. (2003). Diffusion tensor imaging detects and differentiates axon and myelin degeneration in mouse optic nerve after retinal ischemia. *NeuroImage* 20, 1714–1722. doi: 10.1016/j.neuroimage.2003.07.005

Steadman, P. E., Xia, F., Ahmed, M., Mocle, A. J., Penning, A. R. A., Geraghty, A. C., et al. (2020). Disruption of oligodendrogenesis impairs memory consolidation in adult mice. *Neuron* 105, 150.e6–164.e6.doi: 10.1016/j.neuron.2019.10.013

Stedehouder, J., Brizee, D., Shpak, G., and Kushner, S. A. (2018). Activity-dependent myelination of parvalbumin interneurons mediated by axonal morphological plasticity. *J. Neurosci.* 38, 3631–3642. doi: 10.1523/JNEUROSCI.0074-18.2018

Stedehouder, J., Brizee, D., Slotman, J. A., Pascual-Garcia, M., Leyrer, M. L., Bouwen, B. L., et al. (2019). Local axonal morphology guides the topography of interneuron myelination in mouse and human neocortex. *eLife* 8:e48615. doi: 10.7554/eLife.48615

Stedehouder, J., and Kushner, S. A. (2017). Myelination of parvalbumin interneurons: a parsimonious locus of pathophysiological convergence in schizophrenia. *Mol. Psychiatry* 22, 4–12. doi: 10.1038/mp.2016.147

Steele, C. J., Bailey, J. A., Zatorre, R. J., and Penhune, V. B. (2013). Early musical training and white-matter plasticity in the corpus callosum: evidence for a sensitive period. *J. Neurosci.* 33, 1282–1290. doi: 10.1523/JNEUROSCI.3578-12.2013

Strobel, C., Marek, R., Gooch, H. M., Sullivan, R. K. P., and Sah, P. (2015). Prefrontal and auditory input to intercalated neurons of the amygdala. *Cell Rep.* 10, 1435–1442. doi: 10.1016/j.celrep.2015.02.008

Strüber, M., Jonas, P., and Bartos, M. (2015). Strength and duration of perisomatic GABAergic inhibition depend on distance between synaptically connected cells. *Proc. Natl. Acad. Sci. U S A* 112, 1220–1225. doi: 10.1073/pnas.1412996112

Stujenske, J. M., Likhtik, E., Topiwala, M. A., and Gordon, J. A. (2014). Fear and safety engage competing patterns of theta-gamma coupling in

the basolateral amygdala. *Neuron* 83, 919–933. doi: 10.1016/j.neuron.2014.07.026

Swire, M., Kotelevtsev, Y., Webb, D. J., Lyons, D. A., and Ffrench-Constant, C. (2019). Endothelin signalling mediates experience-dependent myelination in the CNS. *eLife* 8:e49493. doi: 10.7554/eLife.49493

Teicher, M. H., Dumont, N. L., Ito, Y., Vaituzis, C., Giedd, J. N., and Andersen, S. L. (2004). Childhood neglect is associated with reduced corpus callosum area. *Biol. Psychiatry* 56, 80–85. doi: 10.1016/j.biopsych.2004.03.016

Thomason, M. E., and Thompson, P. M. (2011). Diffusion imaging, white matter, and psychopathology. *Annu. Rev. Clin. Psychol.* 7, 63–85. doi: 10.1146/annurev-clinpsy-032210-104507

Tomassy, G. S., Berger, D. R., Chen, H. H., Kasthuri, N., Hayworth, K. J., Vercelli, A., et al. (2014). Distinct profiles of myelin distribution along single axons of pyramidal neurons in the neocortex. *Science* 344, 319–324. doi: 10.1126/science.1249766

Tomassy, G. S., Dershowitz, L. B., and Arlotta, P. (2016). Diversity matters: a revised guide to myelination. *Trends Cell Biol.* 26, 135–147. doi: 10.1016/j.tcb.2015.09.002

Traub, R. D., Whittington, M. A., Stanford, I. M., and Jefferys, J. G. (1996). A mechanism for generation of long-range synchronous fast oscillations in the cortex. *Nature* 383, 621–624. doi: 10.1038/383621a0

Tromp, D. P., Grupe, D. W., Oathes, D. J., Mcfarlin, D. R., Hernandez, P. J., Kral, T. R., et al. (2012). Reduced structural connectivity of a major frontolimbic pathway in generalized anxiety disorder. *Arch. Gen. Psychiatry* 69, 925–934. doi: 10.1001/archgenpsychiatry.2011.2178

Westlye, L. T., Bjørnebekk, A., Grydeland, H., Fjell, A. M., and Walhovd, K. B. (2011). Linking an anxiety-related personality trait to brain white matter microstructure: diffusion tensor imaging and harm avoidance. *Arch. Gen. Psychiatry* 68, 369–377. doi: 10.1001/archgenpsychiatry.2011.24

Yang, C., Zhang, Y., Lu, M., Ren, J., and Li, Z. (2019). White matter structural brain connectivity of young healthy individuals with high trait anxiety. *Front. Neurol.* 10:1421. doi: 10.3389/fneur.2019.01421

Yang, Y., Cheng, Z., Tang, H., Jiao, H., Sun, X., Cui, Q., et al. (2017). Neonatal maternal separation impairs prefrontal cortical myelination and cognitive functions in rats through activation of wnt signaling. *Cereb. Cortex* 27, 2871–2884. doi: 10.1093/cercor/bhw121

Yavas, E., Gonzalez, S., and Fanselow, M. S. (2019). Interactions between the hippocampus, prefrontal cortex and amygdala support complex learning and memory. *F1000Res.* 8:F1000. doi: 10.12688/f1000research.19317.1

Young, K. M., Psachoulia, K., Tripathi, R. B., Dunn, S. J., Cossell, L., Attwell, D., et al. (2013). Oligodendrocyte dynamics in the healthy adult CNS: evidence for myelin remodeling. *Neuron* 77, 873–885. doi: 10.1016/j.neuron.2013.01.006

Zhu, X., Hill, R. A., Dietrich, D., Komitova, M., Suzuki, R., and Nishiyama, A. (2011). Age-dependent fate and lineage restriction of single NG2 cells. *Development* 138, 745–753. doi: 10.1242/dev.047951

Conflict of Interest: The authors declare that the research was conducted in the absence of any commercial or financial relationships that could be construed as a potential conflict of interest.

frontiers in Cellular Neuroscience

MINI REVIEW
published: 23 February 2021
doi: 10.3389/fncel.2021.645240

Can Enhancing Neuronal Activity Improve Myelin Repair in Multiple Sclerosis?

Dorien A. Maas[1] and María Cecilia Angulo[1,2]*

[1] Université de Paris, Institute of Psychiatry and Neuroscience of Paris (IPNP), INSERM U1266, Paris, France, [2] GHU PARIS Psychiatrie et Neurosciences, Paris, France

Enhanced neuronal activity in the healthy brain can induce *de novo* myelination and behavioral changes. As neuronal activity can be achieved using non-invasive measures, it may be of interest to utilize the innate ability of neuronal activity to instruct myelination as a novel strategy for myelin repair in demyelinating disorders such as multiple sclerosis (MS). Preclinical studies indicate that stimulation of neuronal activity in demyelinated lesions indeed has the potential to improve remyelination and that the stimulation paradigm is an important determinant of success. However, future studies will need to reveal the most efficient stimulation protocols as well as the biological mechanisms implicated. Nonetheless, clinical studies have already explored non-invasive brain stimulation as an attractive therapeutic approach that ameliorates MS symptomatology. However, whether symptom improvement is due to improved myelin repair remains unclear. In this mini-review, we discuss the neurobiological basis and potential of enhancing neuronal activity as a novel therapeutic approach in MS.

Keywords: remyelination, neuronal activation, non-invasive brain stimulation, oligodendrocyte (OL) lineage cells, multiple sclerosis, adaptive myelination, neuron-oligodendroglia interactions

OPEN ACCESS

Edited by:
Maria Kukley,
Achucarro Basque Center for Neuroscience, Spain

Reviewed by:
Anna Williams,
University of Edinburgh, United Kingdom
Robert A. Hill,
Dartmouth College, United States

****Correspondence:***
Dorien A. Maas
dorothea.maas@inserm.fr

Specialty section:
This article was submitted to Non-Neuronal Cells, a section of the journal Frontiers in Cellular Neuroscience

Received: *22 December 2020*
Accepted: *01 February 2021*
Published: *23 February 2021*

Citation:
Maas DA and Angulo MC (2021) Can Enhancing Neuronal Activity Improve Myelin Repair in Multiple Sclerosis? Front. Cell. Neurosci. 15:645240. doi: 10.3389/fncel.2021.645240

INTRODUCTION

"Neuronal activity-dependent" or "adaptive" myelination is the process by which electrical activity of neuronal axons instructs oligodendroglial cells to myelinate these active axons, thereby increasing their conduction velocity. Increased myelination is often associated with improved brain function and this makes activity-driven myelination an attractive way to modulate neuronal circuit function and behavior. For example, learning to play the piano increases white matter integrity in the human brain, a measure associated with changes in white matter microstructures that include alterations of myelin sheaths (Han et al., 2009). Similarly, learning a complex motor task leads to increased myelination in motor brain areas in the mouse, while when this *de novo* myelination was blocked, motor learning did not occur to the same extent (McKenzie et al., 2014). Moreover, myelination defects of cortical parvalbumin interneurons results in a decreased inhibition and an excitation/inhibition imbalance that correlates with whisker-dependent texture discrimination impairments (Benamer et al., 2020). Neuronal activity-dependent myelination in animal models can be achieved in various ways including direct neuronal stimulation by optogenetics or

pharmacogenetics as well as indirect neuronal stimulation using behavioral paradigms or non-invasive brain stimulation like transcranial magnetic stimulation (TMS) and transcranial direct current stimulation (tDCS). The fact that neuronal activity can achieve *de novo* myelination in the healthy brain leads to the hypothesis that this is an innate biological mechanism that could be used to promote myelin regeneration under pathological conditions.

Despite the limited regenerative capacity of the CNS, myelin repair, or remyelination, can occur spontaneously in demyelinating diseases such as multiple sclerosis (MS). The most accepted mechanism of remyelination consists of both recruitment and proliferation of oligodendrocyte precursor cells (OPCs) as well as the differentiation of these new OPCs into mature myelinating oligodendrocytes (OLs) (**Figure 1**). However, recent studies in humans and rodents also support the idea that pre-existing OLs are a major source of myelin sheath regeneration (**Figure 1**; Jäkel et al., 2019; Yeung et al., 2019; Bacmeister et al., 2020). While remyelination is essential to prevent degradation of naked axons and restore axon potential conduction in neurons in the demyelinated lesion, remyelination failure is common in MS. Current therapies, mainly focused on the inflammatory component of the disease, are insufficient to prevent the consecutive neuronal loss that causes disabilities. Although recent clinical trials have tested the pro-remyelinating potential of several molecules, treatment strategies that effectively restore myelin in demyelinated lesions still need to be developed (Lubetzki et al., 2020). In this context, enhancing neuronal activity represents an attractive alternative strategy for remyelination in brain disorders where myelination is affected. In this minireview, we will address the potential of neuronal activity-enhanced remyelination as a novel therapeutic strategy in MS.

NEURONAL ACTIVITY-INDUCED MYELINATION IN THE HEALTHY BRAIN

Initial studies in the 90's demonstrated that neurons communicate with OL lineage cells at different stages of OL maturation, thereby modulating the myelination process (Barres and Raff, 1993; Demerens et al., 1996). From recent studies on adaptive myelination *in vivo*, it became clear that activation of neurons can stimulate the proliferation of OPCs as well as their differentiation into myelinating OLs. For example, optogenetic stimulation of layer V projection neurons leads to increased OPC proliferation and differentiation and an increase in myelin thickness (Gibson et al., 2014). Moreover, neuronal activity improved motor function. The use of DREADDs to pharmacogenetically enhance neuronal activity of somatosensory neurons in mice also leads to increased proliferation and differentiation of OPCs as well as a strong bias for newly differentiated OLs to myelinate activated axons (Mitew et al., 2018). When parvalbumin interneurons of the medial prefrontal cortex (mPFC) are activated using DREADDs, a significant increase in total length of myelination occurs (Stedehouder et al., 2018). Notably, increasing cortical activity by silencing parvalbumin interneurons using optogenetics in the anterior cingulate cortex results in an enhanced proliferation of OPCs, while decreasing cortical activity by optogenetically activating parvalbumin interneurons leads to decreased proliferation of OPCs (Piscopo et al., 2018). In this study, the number of newly generated myelinating OLs was increased in mice with increased cortical activity, but not altered in mice with reduced cortical activity. In line with this, activating parvalbumin interneurons with DREADDs, which should reduce the activity of neuronal networks, did not affect the number of myelinating OLs in the mPFC (Stedehouder et al., 2018). Taken together, these studies indicate that active axons receive increased myelination regardless of neuronal identity. They also suggest that the effect of neuronal activity on OPC proliferation and differentiation likely depends on the pattern of activity within neuronal networks. This is supported by a study showing that neuronal stimulation at various frequencies *in vivo* has different effects on OPC proliferation and differentiation (Nagy et al., 2017). Indirect measures of neuronal activation can also influence OLs and myelination. It has been demonstrated in mice that 14 or 28 days of repetitive TMS increased the survival of new OLs leading to a larger number of myelinating OLs and increased myelin internode length in the cortex (Cullen et al., 2019). This is interesting because TMS is a method with unknown biological mechanisms that has already been tested as a therapy for MS in clinical studies (Centonze et al., 2007; Hulst et al., 2017). It should be noted that the benefits of neuronal activity may not be solely attributed to effects on OL lineage cells and remyelination as neuronal activity is also known to affect neurons, astrocytes and microglial cells (Li et al., 2012; Hasel et al., 2017). As such, it remains unclear to what extent remyelination alone is necessary for the functional benefits of enhanced neuronal activity.

How electrically active axons communicate with OPCs and OLs to promote myelination remains unclear. However, there are multiple synaptic and non-synaptic signaling mechanisms that may play a role (Hines et al., 2015; Mensch et al., 2015; Wake et al., 2015; Hughes and Appel, 2019). Electrically active axons release potassium which depolarizes OPCs and leads to the opening of voltage-gated calcium channels on OPCs (Barron and Kim, 2019). Activated, unmyelinated axons release glutamate (Kukley et al., 2007; Ziskin et al., 2007) which activates AMPA (Barron and Kim, 2019), NMDA (Doyle et al., 2018) as well as metabotropic glutamate receptors (Wake et al., 2015) on oligodendroglia. Neuronal activity can also activate GABA and muscarinic receptors on OPCs (Paez and Lyons, 2020). In addition, purinergic receptors on oligodendroglia can be activated by activity-induced increases of extracellular ATP (Welsh and Kucenas, 2018). The activation of the above-mentioned receptors and transporters converges on an increase in the intracellular calcium level in oligodendroglia. Accordingly, calcium signaling in oligodendroglia increases OPC proliferation (Ohashi et al., 2018), OPC morphological maturation (Waggener et al., 2013), OL differentiation (Cheli et al., 2018), the expression of myelin-related transcription factors (Weider et al., 2018)

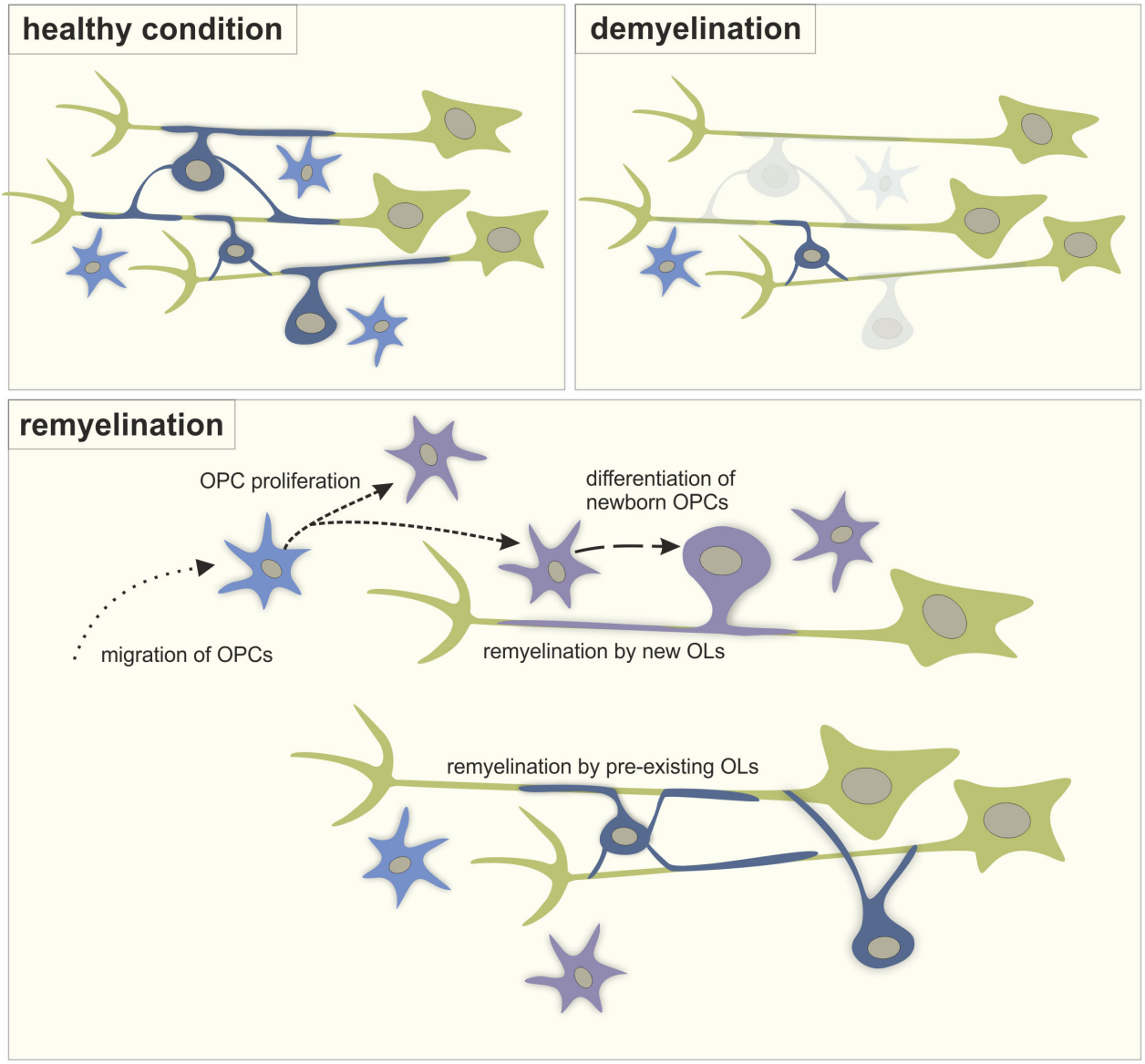

FIGURE 1 | The process of remyelination. A schematic representation of myelination in healthy condition, during demyelination and during the process of remyelination involving the migration of OPCs into the lesion from other brain regions, the proliferation of OPCs, the differentiation of new OPCs into myelinating OLs and the remyelination of naked axons by both newly differentiated OLs and pre-existing OLs. Green: neurons, light blue: OPCs, dark blue: mature OLs, purple: new-born cells.

and proteins (Cheli et al., 2018), as well as myelin sheath thickness (Waggener et al., 2013). Moreover, the frequency and amplitude of the calcium signals in OLs determine whether myelin sheaths grow or retract (Baraban et al., 2018; Krasnow et al., 2018). Alternatively, it has been proposed that activity-dependent myelination is mediated by the morphology of the to-be-myelinated axon (Stedehouder et al., 2019) or *via* mechanotransduction (Lourenço and Grãos, 2016). Taken together, in the healthy brain, communication between electrically active neurons and oligodendroglial cells affects OL proliferation and differentiation, and can initiate *de novo* myelination resulting in behavioral changes. Consequently, this makes stimulation of neuronal activity an interesting approach for myelin repair in demyelinating disorders such as MS.

MODULATION OF NEURONAL ACTIVITY DURING REMYELINATION

While activity-driven myelination is accepted as a key mechanism in the CNS, literature on the effect of neuronal activity on myelin repair is still scarce. Nevertheless, a limited number of studies have reported on the potency of manipulating neuronal activity as a remyelination strategy in animal models. The

intracerebral infusion of AMPA/kainate receptor antagonists and a voltage-dependent Na^+ channel blocker in demyelinated lesions induced by ethidium bromide showed a decreased differentiation of OPCs into myelinating OLs, an increased OL apoptosis and a reduced remyelination (Gautier et al., 2015). These results suggest that blocking neuronal activity negatively affects remyelination. The reverse experiment was also initially proposed in a model of contusive spinal cord injury in rats, associated with demyelination without axonal loss (Li et al., 2017). Several days of electrical stimulation in the motor cortex increased the number of OPCs and newly myelinating OLs as well as enhanced remyelination in the remote demyelinated region, the spinal cord. However, it was only recently that a positive effect of neuronal activity on remyelination was unequivocally demonstrated *in vivo* (Ortiz et al., 2019). Distinct neural stimulation paradigms applied directly at the injured site had particular effects on remyelination. On the one hand, in lysolecithin-induced demyelinated lesions of the mouse corpus callosum, a single 3 h session of 20 Hz optogenetic stimulation of callosal axons led to increased proliferation of OPCs in the lesion the day of the stimulation. However, this new pool of progenitors did not result in a larger number of myelinating OLs 1 week later. On the other hand, a 3 h 20 Hz optogenetic stimulation session every day during 1 week increased OL differentiation, enhanced the number of remyelinated axons and improved action potential conduction in the lesion (Ortiz et al., 2019). This study using direct neuronal stimulation indicates that neuronal activity may indeed promote remyelination in demyelinated lesions under specific stimulation paradigms.

Recent studies in animal models have addressed the effects of indirect methods of neuronal stimulation on remyelination. As indirect neuronal stimulation methods such as TMS, tDCS and behavioral training are readily applicable in the clinic, it is worthwhile to investigate different stimulation methods in rodents. Sixty Hz electromagnetic stimulation increases remyelination in toxin demyelinated lesions of the rat corpus callosum (Sherafat et al., 2012) and low frequency electromagnetic stimulation promotes the differentiation of OPCs and remyelination after spinal cord injury in rats (Li et al., 2019). Epidural electrical stimulation after spinal cord injury also enhanced remyelination and increased OL differentiation and survival (Li et al., 2020). Likewise, brain activation using 20 Hz ultrasound bursts increased remyelination after cuprizone demyelination in mice (Olmstead et al., 2018) and voluntary exercise immediately after lysolecithin lesions of the spinal cord white matter increased OPC proliferation, differentiation and remyelination (Jensen et al., 2018). Notably, pairing voluntary exercise with the pro-myelinating drug clemastine showed an additive effect in increasing myelin repair (Jensen et al., 2018). Although it is likely that in both studies utilizing physical exercise neuronal activity in the demyelinated lesion was enhanced, neither study provides evidence that this was indeed the case. Nevertheless, the results of OL differentiation and more efficient remyelination are in line with the observations made in studies employing direct neuronal stimulation. In addition to the above-mentioned studies, it is known that brain stimulation can influence myelination and oligodendroglial dynamics after brain damage or traumatic injury. For example, tDCS in rats after focal cerebral ischemia lead to a faster recovery of motor function and stimulated the migration of OPCs to the lesion (Braun et al., 2016). Moreover, oscillating field stimulation leads to increased OPC differentiation and enhances functional recovery after spinal cord injury in rats (Jing et al., 2015). This was confirmed in a second study where enhanced remyelination and increased protein expression of oligodendroglial marker Olig2 were found (Zhang et al., 2014). Collectively, indirect methods of neuronal activation can positively influence myelin repair.

Behavioral paradigms recruiting remyelinating brain regions might be able to accelerate the remyelination process, likely through increased neuronal activity. A recent study reported increased neuronal firing rates in the motor cortex following cuprizone demyelination that recovered to normal during the same period in which remyelination was completed, suggesting a correlation between the level of neuronal activity and remyelination (Bacmeister et al., 2020). Behavioral training that recruits the motor cortex during remyelination increased the number of myelinating OLs and the number of myelin sheaths produced by both pre-existing and newly formed OLs relative to untrained demyelinated mice (Bacmeister et al., 2020). Behavioral experiences can also improve myelin recovery in other forms of brain injury. For example, increased OPC numbers were found in ischemic lesions after environmental enrichment (Komitova et al., 2006). After both environmental enrichment and behavioral skilled reaching training, the number of OPCs was increased in a rat model for stroke (Keiner et al., 2008). Likewise, environmental enrichment increased the number of OPCs in a rat model with hypomyelination (Maas et al., 2020) and increased the OL differentiation and myelination in a model of perinatal brain injury (Forbes et al., 2020).

Although neuronal activity can be enhanced in a controlled manner to limit deleterious effects such as excitotoxicity, it cannot be excluded that apart from benefits for remyelination, enhanced neuronal activity may negatively affect the demyelinated neurons themselves. Indeed, Na^{2+} and Ca^{2+} channel blocking agents have been shown to reduce damage to neurons in demyelinating lesions by inhibiting a neuronal cell membrane depolarizing mechanism (Brand-Schieber and Werner, 2004). Further damage to demyelinated neurons complicates their remyelination and this might explain why during cuprizone demyelination in mice, enhancing neuronal activity by behavioral intervention had no positive effects on remyelination directly after demyelination, but only as remyelination had commenced (Bacmeister et al., 2020). Future studies into neuronal-activity dependent myelin repair should take this precise timing into account, or may follow an alternative route in which activity-dependent pathways in OLs are stimulated directly instead of *via* neuronal activity (Jung et al., 2020).

Although emerging lines of evidence point to a role of neuronal activity in modulating oligodendroglia dynamics in lesions, few papers have investigated the signaling mechanisms that underlie the communication between electrically active axons and oligodendroglia during remyelination. Since the frequency of calcium transients is increased during remyelination

(Battefeld et al., 2019), it is likely that OL calcium signaling pathways play a role, as occurs in adaptive myelination. However, whether intracellular calcium signaling has positive or negative effects on myelination under pathological conditions is unclear. For instance, ablation of the muscarinic M1 and M3 receptors that induce calcium responses in oligodendroglia enhances myelin repair, suggesting a negative role of muscarinic receptor-mediated calcium increases (Mei et al., 2016; Welliver et al., 2018). On the contrary, the removal of the inwardly rectifying calcium channel Cav1.2, which should reduce calcium activity, also impairs remyelination through decreases in OPC proliferation and maturation (Santiago González et al., 2017). While the activation of some receptors inducing calcium increases may have deleterious effects on myelin repair, specific intracellular calcium increases may be necessary to promote remyelination. In addition, it has been shown that in demyelinated lesions experimentally induced by the direct injection of gliotoxic agents, demyelinated axons make synaptic connections with OPCs that are positive for the glutamatergic synapse marker vGlut2, suggesting that axon-OPC synapses may play a role in remyelination (Etxeberria et al., 2010; Gautier et al., 2015; Sahel et al., 2015). Remarkably, an *in vitro* study has shown that magnetic field stimulation induces calcium influx in OPCs and enhances OPC differentiation and OL myelination (Prasad et al., 2017), suggesting that electrical stimulation *per se* may also induce direct effects on oligodendroglia in the absence of neuronal activity. Taken together, these findings suggest that complex mechanisms implicating calcium signals in OL lineage cells may be involved in neuronal activity-induced remyelination and that further research is necessary to unravel the associated signaling pathways.

METHODS OF NEURONAL STIMULATION AS NOVEL THERAPIES IN MS

As emerging evidence suggests that increased neuronal activity can aid remyelination, it is worthwhile to examine studies in which MS patients with demyelinating lesions undergo neuronal stimulation. Deep brain stimulation is the only direct stimulation method that has been tried in MS patients. Several studies have shown that thalamic deep brain stimulation significantly reduces tremor and improves quality of life in MS patients (Hooper et al., 2002; Berk et al., 2002; Bittar et al., 2005; Thevathasan et al., 2011; Brandmeir et al., 2020). However, it is unlikely that the positive effects of deep brain stimulation on tremor symptoms rely on increased remyelination as the effects are seen quickly after stimulation. Nevertheless, it would be interesting to assess whether long treatment periods or different deep brain stimulation protocols influence local remyelination in patients. Clinical studies have also already explored non-invasive brain stimulation as an attractive therapeutic approach that is easily applicable in the clinic and, in some cases,

TABLE 1 | Effects of direct and non-invasive neuronal stimulation on OPC proliferation, OPC differentiation, remyelination, and symptomatology in preclinical models and MS patients.

		Enhanced OPC proliferation in a lesion	Enhanced OPC differentiation in a lesion	Enhanced remyelination in a lesion	Improved symptomatology
Preclinical models	Direct stimulation	• Epidural electrical stimulation (Li et al., 2017) • Optogenetics (Ortiz et al., 2019)	• Epidural electrical stimulation (Li et al., 2017, 2020) • Optogenetics (Ortiz et al., 2019)	• Epidural electrical stimulation (Li et al., 2017, 2020) • Optogenetics (Ortiz et al., 2019)	• Epidural electrical stimulation (Li et al., 2017, 2020)
	Non-invasive stimulation	• Behavioral training (Bacmeister et al., 2020) • Voluntary exercise (Jensen et al., 2018)	• Behavioral training (Bacmeister et al., 2020) • Electromagnetic stimulation (Li et al., 2019)	• Behavioral training (Bacmeister et al., 2020) • Voluntary exercise (Jensen et al., 2018) • Electromagnetic stimulation (Sherafat et al., 2012) • Electromagnetic stimulation (Li et al., 2019) • Ultrasound burst stimulation (Olmstead et al., 2018)	• Electromagnetic stimulation (Li et al., 2019)
MS patients	Direct stimulation	NA	NA	NA	• Deep brain stimulation (Hooper et al., 2002; Berk et al., 2002; Bittar et al., 2005; Thevathasan et al., 2011)
	Non-invasive stimulation	NA	NA	NA	• High intensity exercise (Orban et al., 2019) • rTMS (Nielsen et al., 1996; Centonze et al., 2007; Hulst et al., 2017) • tDCS (Mattioli et al., 2016; Charvet et al., 2018)

NA, Not Available.

can be applied at home (Gough et al., 2020). Although the mechanisms behind the effects of non-invasive brain stimulation are yet to be explained and probably result from mixed effects on neurons and glia, non-invasive brain stimulation in MS patients has been shown to reduce motor symptoms including spasticity, fatigue, neuropathic pain, tactile sensory problems, as well as urinary tract difficulties (Leocani et al., 2019). Different stimulation methods and various stimulation patterns have successfully been tried. Using repetitive (r)TMS for example, stimulation twice daily for 7 days has been shown to reduce spasticity when applied to the spine in MS patients (Nielsen et al., 1996) and high as well as low frequency (r)TMS improve spasticity when applied to the motor cortex for 2 weeks (Centonze et al., 2007). Notably, non-invasive brain stimulation appears to improve cognition in MS patients, a symptom that is not improved by current MS medication (DeLuca et al., 2020). tDCS applied to the dorsolateral PFC during 10 sessions of cognitive therapy enhanced training effects on executive functioning and attention in MS patients (Mattioli et al., 2016). The positive effects of tDCS applied during cognitive therapy were replicated in a second study for complex attention in MS patients (Charvet et al., 2018). Similar results were found using rTMS over the dorsolateral PFC which improved accuracy during a working memory task (Hulst et al., 2017). Collectively, these studies point to beneficial effects of non-invasive brain stimulation on alleviating diverse MS symptoms, sometimes in the long term, and are therefore a promising treatment avenue. However, whether non-invasive brain stimulation constitutes a strategy to enhance remyelination in MS is still unclear. In stroke patients, tDCS increases white matter integrity, often considered as a proxy for myelin integrity, which correlates with improved motor skills (Zheng and Schlaug, 2015). Enhanced white matter integrity after TMS has also been observed in aphasia patients (Lu et al., 2014). However, both studies used magnetic resonance imaging measures to assess white matter integrity and this technique is not sensitive enough to measure myelination directly, but rather represents a mix of myelin and axonal-related correlates. Similar studies investigating the effects of non-invasive brain stimulation on the state of demyelinating lesions in MS patients are still lacking. Therefore, further studies are necessary to find out whether the positive effects of non-invasive brain stimulation on MS symptomatology are indeed caused by enhanced remyelination.

Other than non-invasive brain stimulation, exercise and behavioral paradigms have also been shown to positively affect MS symptoms and their effects might be mediated by enhanced neuronal activity. For example, 8 weeks of high intensity exercise improve clinical outcome (Orban et al., 2019) and both exercise and cognitive training are effective in reducing cognitive impairments in MS patients (DeLuca et al., 2020). It has even been suggested that exercise should be prescribed as a medicine in early MS stages (Dalgas et al., 2019). As for non-invasive brain stimulation, the neurobiological mechanisms underlying the positive effects of exercise and cognitive training remain unknown. However, white matter integrity is increased in MS patients that have a high cardiorespiratory fitness (Prakash et al., 2010) indicating that remyelination might play a role, but future studies are still necessary to correlate symptom improvements with remyelination. An important challenge for future MS research studies will be to distinguish the benefits of non-invasive brain stimulation caused by an increased remyelination from those generated by improved neuronal regeneration, effects on astrocytes and microglia, or even effects on motivation and activeness of patients.

CONCLUSION

Neuronal activity-dependent myelination can take place regardless of neuronal identity, but the effects of neuronal activity on oligodendroglial cells likely depend on the cumulative pattern of activity of a neuronal network. This means that both direct stimulation of neurons by for example optogenetics and indirect stimulation via non-invasive methods such as TMS and behavioral training can achieve *de novo* myelination in the healthy brain. The facts that neuronal activity can initiate myelination and that neuronal stimulation can be achieved relatively easily make activity-dependent myelination an attractive strategy for myelin repair in demyelinating disorders such as MS. Research into neuronal activity-dependent myelin repair is still scarce, however, the few *in vivo* preclinical studies that have been conducted suggest that enhanced neuronal activity in a demyelinated lesion indeed has the potential to improve remyelination (see **Table 1** for an overview of preclinical and clinical studies applying direct and indirect neuronal stimulation and their effects on remyelination). Notably, as during adaptive myelination in the healthy brain, the pattern and frequency of the neuronal stimulation are important determinants of its effect as a single stimulation session had no lasting effects on remyelination, while repeated stimulation sessions significantly improved remyelination in the demyelinated mouse corpus callosum (Ortiz et al., 2019). In rodents, both direct stimulation by optogenetics and indirect stimulation by non-invasive brain stimulation or using behavioral training paradigms have positive effects on myelin repair after injury. Non-invasive brain stimulation and behavioral training can be readily applied in the clinic and, in MS patients, it has been shown that rTMS, tDCS and physical exercise can ameliorate disease symptomatology. However, it is yet to be determined whether this improvement of symptoms is caused by enhanced myelin repair after neuronal stimulation or whether the benefits of neuronal activity could be attributed to effects on the neurons themselves or on other brain cells (**Table 1**).

It is known that electrically active axons can communicate with oligodendroglia cells via synaptic and non-synaptic sites involving a number of receptors and messenger molecules that often lead to a depolarization of oligodendroglia and subsequent intracellular calcium signals. The nature of the communication from neurons to oligodendroglia and the frequency and amplitude of intracellular calcium increases in oligodendroglia are thought to determine the OL response to neuronal activity. Future studies need to reveal the molecular pathways involved

in, and the calcium response characteristics of oligodendroglia to neuronal electrical activity.

In conclusion, the stimulation of neuronal activity is a promising strategy for myelin repair in demyelinating disorders such as MS and future research into the exact neurobiological mechanisms as well as clinical evaluation of changes in the brain after neuronal stimulation in patients will aid the development of this novel therapeutic approach to myelin repair.

AUTHOR CONTRIBUTIONS

DM and MCA wrote and corrected the manuscript. Both authors contributed to the article and approved the submitted version.

FUNDING

This work was supported by grants from a subaward agreement from the University of Connecticut with funds provided by Grant No. RG-1612-26501 from National Multiple Sclerosis Society (NMSS), Fondation pour l'aide à la recherche sur la Sclérose en Plaques (ARSEP), ANR under the frame of the European Joint Programme on Rare Diseases (EJP RD, project no. ANR-19-RAR4-008-03), ANR under the frame of Neuron Cofund (Era-Net Neuron, project no. ANR-18-Neur-0001-01). DM is recipient of a postodoctoral fellowship from Fondation pour la Recherche Médicale (FRM, project no. SPF202005011919). MCA is a CNRS (Centre National de la Recherche Scientifique) investigator.

REFERENCES

Bacmeister, C. M., Barr, H. J., McClain, C. R., Thornton, M. A., Nettles, D., Welle, C. G., et al. (2020). Motor learning promotes remyelination via new and surviving oligodendrocytes. *Nat. Neurosci.* 23, 819–831. doi: 10.1038/s41593-020-0637-3

Baraban, M., Koudelka, S., and Lyons, D. A. (2018). Ca (2+) activity signatures of myelin sheath formation and growth in vivo. *Nat. Neurosci.* 21, 19–23. doi: 10.1038/s41593-017-0040-x

Barres, B. A., and Raff, M. C. (1993). Proliferation of oligodendrocyte precursor cells depends on electrical activity in axons. *Nature* 361, 258–260. doi: 10.1038/361258a0

Barron, T., and Kim, J. H. (2019). Neuronal input triggers Ca(2+) influx through AMPA receptors and voltage-gated Ca(2+) channels in oligodendrocytes. *Glia* 67, 1922–1932. doi: 10.1002/glia.23670

Battefeld, A., Popovic, M. A., de Vries, S. I., and Kole, M. H. P. (2019). High-frequency microdomain Ca2+ transients and waves during early myelin internode remodeling. *Cell Rep.* 26, 182–191.e5. doi: 10.1016/j.celrep.2018.12.039

Benamer, N., Vidal, M., Balia, M., and Angulo, M. C. (2020). Myelination of parvalbumin interneurons shapes the function of cortical sensory inhibitory circuits. *Nat. Commun.* 11:5151. doi: 10.1038/s41467-020-18984-7

Berk, C., Carr, J., Sinden, M., Martzke, J., and Honey, C. R. (2002). Thalamic deep brain stimulation for the treatment of tremor due to multiple sclerosis: a prospective study of tremor and quality of life. *J. Neurosurg.* 97, 815–820. doi: 10.3171/jns.2002.97.4.0815

Bittar, R. G., Hyam, J., Nandi, D., Wang, S., Liu, X., Joint, C., et al. (2005). Thalamotomy versus thalamic stimulation for multiple sclerosis tremor. *J. Clin. Neurosci.* 12, 638–642. doi: 10.1016/j.jocn.2004.09.008

Brandmeir, N. J., Murray, A., Cheyuo, C., Ferari, C., and Rezai, A. R. (2020). Deep brain stimulation for multiple sclerosis tremor: a meta-analysis. *Neuromodulation* 23, 463–468. doi: 10.1111/ner.13063

Brand-Schieber, E., and Werner, P. (2004). Calcium channel blockers ameliorate disease in a mouse model of multiple sclerosis. *Exp. Neurol.* 189, 5–9. doi: 10.1016/j.expneurol.2004.05.023

Braun, R., Klein, R., Walter, H. L., Ohren, M., Freudenmacher, L., Getachew, K., et al. (2016). Transcranial direct current stimulation accelerates recovery of function, induces neurogenesis and recruits oligodendrocyte precursors in a rat model of stroke. *Exp. Neurol.* 279, 127–136. doi: 10.1016/j.expneurol.2016.02.018

Centonze, D., Koch, G., Versace, V., Mori, F., Rossi, S., Brusa, L., et al. (2007). Repetitive transcranial magnetic stimulation of the motor cortex ameliorates spasticity in multiple sclerosis. *Neurology* 68, 1045–1050. doi: 10.1212/01.wnl.0000257818.16952.62

Charvet, L., Shaw, M., Dobbs, B., Frontario, A., Sherman, K., Bikson, M., et al. (2018). Remotely supervised transcranial direct current stimulation increases the benefit of at-home cognitive training in multiple sclerosis. *Neuromodulation* 21, 383–389. doi: 10.1111/ner.12583

Cheli, V. T., Santiago González, D. A., Zamora, N. N., Lama, T. N., Spreuer, V., Rasmusson, R. L., et al. (2018). Enhanced oligodendrocyte maturation and myelination in a mouse model of timothy syndrome. *Glia* 66, 2324–2339. doi: 10.1002/glia.23468

Cullen, C. L., Senesi, M., Tang, A. D., Clutterbuck, M. T., Auderset, L., O'Rourke, M. E., et al. (2019). Low-intensity transcranial magnetic stimulation promotes the survival and maturation of newborn oligodendrocytes in the adult mouse brain. *Glia* 67, 1462–1477. doi: 10.1002/glia.23620

Dalgas, U., Langeskov-Christensen, M., Stenager, E., Riemenschneider, M., and Hvid, L. G. (2019). Exercise as medicine in multiple sclerosis-time for a paradigm shift: preventive, symptomatic, and disease-modifying aspects and perspectives. *Curr. Neurol. Neurosci. Rep.* 19:88. doi: 10.1007/s11910-019-1002-3

DeLuca, J., Chiaravalloti, N. D., and Sandroff, B. M. (2020). Treatment and management of cognitive dysfunction in patients with multiple sclerosis. *Nat. Rev. Neurol.* 16, 319–332.

Demerens, C., Stankoff, B., Logak, M., Anglade, P., Allinquant, B., Couraud, F., et al. (1996). Induction of myelination in the central nervous system by electrical activity. *Proc. Natl. Acad. Sci. U.S.A.* 93, 9887–9892. doi: 10.1073/pnas.93.18.9887

Doyle, S., Hansen, D. B., Vella, J., Bond, P., Harper, G., Zammit, C., et al. (2018). Vesicular glutamate release from central axons contributes to myelin damage. *Nat. Commun.* 9:1032. doi: 10.1038/s41467-018-03427-1

Etxeberria, A., Mangin, J. M., Aguirre, A., and Gallo, V. (2010). Adult-born SVZ progenitors receive transient synapses during remyelination in corpus callosum. *Nat. Neurosci.* 13, 287–289. doi: 10.1038/nn.2500

Forbes, T. A., Goldstein, E. Z., Dupree, J. L., Jablonska, B., Scafidi, J., Adams, K. L., et al. (2020). Environmental enrichment ameliorates perinatal brain injury and promotes functional white matter recovery. *Nat. Commun.* 11:964. doi: 10.1038/s41467-020-14762-7

Gautier, H. O. B., Evans, K. A., Volbracht, K., James, R., Sitnikov, S., Lundgaard, I., et al. (2015). Neuronal activity regulates remyelination via glutamate signalling to oligodendrocyte progenitors. *Nat. Commun.* 6:8518. doi: 10.1038/ncomms9518

Gibson, E. M., Purger, D., Mount, C. W., Goldstein, A. K., Lin, G. L., Wood, L. S., et al. (2014). Neuronal activity promotes oligodendrogenesis and adaptive myelination in the mammalian brain. *Science* 344:1252304. doi: 10.1126/science.1252304

Gough, N., Brkan, L., Subramaniam, P., Chiuccariello, L., De Petrillo, A., Mulsant, B. H., et al. (2020). Feasibility of remotely supervised transcranial direct current stimulation and cognitive remediation: a systematic review. *PloS One* 15:e0223029. doi: 10.1371/journal.pone.0223029

Han, Y., Yang, H., Lv, Y.-T., Zhu, C.-Z., He, Y., Tang, H.-H., et al. (2009). Gray matter density and white matter integrity in pianists' brain: a combined structural and diffusion tensor MRI study. *Neurosci. Lett.* 459, 3–6. doi: 10.1016/j.neulet.2008.07.056

Hasel, P., Dando, O., Jiwaji, Z., Baxter, P., Todd, A. C., Heron, S., et al. (2017). Neurons and neuronal activity control gene expression in astrocytes to regulate

their development and metabolism. *Nat. Commun.* 8:15132. doi: 10.1038/ncomms15132

Hines, J. H., Ravanelli, A. M., Schwindt, R., Scott, E. K., and Appel, B. (2015). Neuronal activity biases axon selection for myelination in vivo. *Nat. Neurosci.* 18, 683–689. doi: 10.1038/nn.3992

Hooper, J., Taylor, R., Pentland, B., and Whittle, I. R. A. (2002). Prospective study of thalamic deep brain stimulation for the treatment of movement disorders in multiple sclerosis. *Br. J. Neurosurg.* 16, 102–109. doi: 10.1080/02688690220131769

Hughes, A. N., and Appel, B. (2019). Oligodendrocytes express synaptic proteins that modulate myelin sheath formation. *Nat. Commun.* 10:4125. doi: 10.1038/s41467-019-12059-y

Hulst, H. E., Goldschmidt, T., Nitsche, M. A., de Wit, S. J., van den Heuvel, O. A., Barkhof, F., et al. (2017). rTMS affects working memory performance, brain activation and functional connectivity in patients with multiple sclerosis. *J. Neurol. Neurosurg. Psychiatry* 88, 386–394. doi: 10.1136/jnnp-2016-314224

Jäkel, S., Agirre, E., Mendanha Falcão, Q., van Bruggen, D., Lee, K. W., Knuesel, I., et al. (2019). Altered human oligodendrocyte heterogeneity in multiple sclerosis. *Nature* 566, 543–547. doi: 10.1038/s41586-019-0903-2

Jensen, S. K., Michaels, N. J., Ilyntskyy, S., Keough, M. B., Kovalchuk, O., and Yong, V. W. (2018). Multimodal enhancement of remyelination by exercise with a pivotal role for oligodendroglial PGC1α. *Cell Rep.* 24, 3167–3179. doi: 10.1016/j.celrep.2018.08.060

Jing, J.-H., Qian, J., Zhu, N., Chou, W.-B., and Huang, X.-J. (2015). Improved differentiation of oligodendrocyte precursor cells and neurological function after spinal cord injury in rats by oscillating field stimulation. *Neuroscience* 303, 346–351. doi: 10.1016/j.neuroscience.2015.07.017

Jung, K., Kim, H. N., Jeon, N. L., and Hyung, S. (2020). Comparison of the efficacy of optogenetic stimulation of glia versus neurons in myelination. *ACS Chem. Neurosci.* 11, 4280–4288. doi: 10.1021/acschemneuro.0c00542

Keiner, S., Wurm, F., Kunze, A., Witte, O. W., and Redecker, C. (2008). Rehabilitative therapies differentially alter proliferation and survival of glial cell populations in the perilesional zone of cortical infarcts. *Glia* 56, 516–527. doi: 10.1002/glia.20632

Komitova, M., Perfilieva, E., Mattsson, B., Eriksson, P. S., and Johansson, B. B. (2006). Enriched environment after focal cortical ischemia enhances the generation of astroglia and NG2 positive polydendrocytes in adult rat neocortex. *Exp. Neurol.* 199, 113–121. doi: 10.1016/j.expneurol.2005.12.007

Krasnow, A. M., Ford, M. C., Valdivia, L. E., Wilson, S. W., and Attwell, D. (2018). Regulation of developing myelin sheath elongation by oligodendrocyte calcium transients in vivo. *Nat. Neurosci.* 21, 24–28. doi: 10.1038/s41593-017-0031-y

Kukley, M., Capetillo-Zarate, E., and Dietrich, D. (2007). Vesicular glutamate release from axons in white matter. *Nat. Neurosci.* 10, 311–320. doi: 10.1038/nn1850

Leocani, L., Chieffo, R., Gentile, A., and Centonze, D. (2019). Beyond rehabilitation in MS: insights from non-invasive brain stimulation. *Mult. Scler.* 25, 1363–1371. doi: 10.1177/1352458519865734

Li, G., Fan, Z.-K., Gu, G.-F., Jia, Z.-Q., Zhang, Q.-Q., Dai, J.-Y., et al. (2020). Epidural spinal cord stimulation promotes motor functional recovery by enhancing oligodendrocyte survival and differentiation and by protecting myelin after spinal cord injury in rats. *Neurosci. Bull.* 36, 372–384. doi: 10.1007/s12264-019-00442-0

Li, Q., Houdayer, T., Liu, S., and Belegu, V. (2017). Induced neural activity promotes an oligodendroglia regenerative response in the injured spinal cord and improves motor function after spinal cord injury. *J. Neurotrauma* 34, 3351–3361. doi: 10.1089/neu.2016.4913

Li, Y., Du, X., Liu, C., Wen, Z., and Du, J. (2012). Reciprocal regulation between resting microglial dynamics and neuronal activity in vivo. *Dev. Cell* 23, 1189–1202. doi: 10.1016/j.devcel.2012.10.027

Li, Z., Yao, F., Cheng, L., Cheng, W., Qi, L., Yu, S., et al. (2019). Low frequency pulsed electromagnetic field promotes the recovery of neurological function after spinal cord injury in rats. *J.Orthop. Res.* 37, 449–456. doi: 10.1002/jor.24172

Lourenço, T., and Grãos, M. (2016). Modulation of oligodendrocyte differentiation by mechanotransduction. *Front. Cell. Neurosci.* 10:277. doi: 10.3389/fncel.2016.00277

Lu, H., Wu, H., Cheng, H., Wei, D., Wang, X., Fan, Y., et al. (2014). Improvement of white matter and functional connectivity abnormalities by repetitive transcranial magnetic stimulation in crossed aphasia in dextral. *Int. J. Clin. Exp. Med.* 7, 3659–3668.

Lubetzki, C., Zalc, B., Williams, A., Stadelmann, C., and Stankoff, B. (2020). Remyelination in multiple sclerosis: from basic science to clinical translation. *Lancet Neurol.* 19, 678–688. doi: 10.1016/S1474-4422(20)30140-X

Maas, D. A., Eijsink, V. D., Spoelder, M., van Hulten, J. A., De Weerd, P., Homberg, J. R., et al. (2020). Interneuron hypomyelination is associated with cognitive inflexibility in a rat model of schizophrenia. *Nat. Commun.* 11:2329. doi: 10.1038/s41467-020-16218-4

Mattioli, F., Bellomi, F., Stampatori, C., Capra, R., and Miniussi, C. (2016). Neuroenhancement through cognitive training and anodal tDCS in multiple sclerosis. *Mult. Scler.* 22, 222–230. doi: 10.1177/1352458515587597

McKenzie, I. A., Ohayon, D., Li, H., de Faria, J., Emery, B., Tohyama, K., et al. (2014). Motor skill learning requires active central myelination. *Science* 346:318–322. doi: 10.1126/science.1254960

Mei, F., Lehmann-Horn, K., Shen, Y.-A. A., Rankin, K. A., Stebbins, K. J., Lorrain, D. S., et al. (2016). Accelerated remyelination during inflammatory demyelination prevents axonal loss and improves functional recovery. *ELife* 5:e18246. doi: 10.7554/eLife.18246

Mensch, S., Baraban, M., Almeida, R., Czopka, T., Ausborn, J., El Manira, A., et al. (2015). Synaptic vesicle release regulates myelin sheath number of individual oligodendrocytes in vivo. *Nat. Neurosci.* 18, 628–630. doi: 10.1038/nn.3991

Mitew, S., Gobius, I., Fenlon, L. R., McDougall, S. J., Hawkes, D., Xing, Y. L., et al. (2018). Pharmacogenetic stimulation of neuronal activity increases myelination in an axon-specific manner. *Nat. Commun.* 9:306. doi: 10.1038/s41467-017-02719-2

Nagy, B., Hovhannisyan, A., Barzan, R., Chen, T.-J., and Kukley, M. (2017). Different patterns of neuronal activity trigger distinct responses of oligodendrocyte precursor cells in the corpus callosum. *PLoS Biol.* 15:e2001993. doi: 10.1371/journal.pbio.2001993

Nielsen, J. F., Sinkjaer, T., and Jakobsen, J. (1996). Treatment of spasticity with repetitive magnetic stimulation; a double-blind placebo-controlled study. *Mult. Scler.* 2, 227–232. doi: 10.1177/135245859600200503

Ohashi, K., Deyashiki, A., Miyake, T., Nagayasu, K., Shibasaki, K., Shirakawa, H., et al. (2018). TRPV4 is functionally expressed in oligodendrocyte precursor cells and increases their proliferation. *Pflügers Arch.* 470, 705–716. doi: 10.1007/s00424-018-2130-3

Olmstead, T. A., Chiarelli, P. A., Griggs, D. J., McClintic, A. M., Myroniv, A. N., and Mourad, P. D. (2018). Transcranial and pulsed focused ultrasound that activates brain can accelerate remyelination in a mouse model of multiple sclerosis. *J. Ther. Ultrasound* 6:11. doi: 10.1186/s40349-018-0119-1

Orban, A., Garg, B., Sammi, M. K., Bourdette, D. N., Rooney, W. D., Kuehl, K., et al. (2019). Effect of high-intensity exercise on multiple sclerosis function and phosphorous magnetic resonance spectroscopy outcomes. *Med. Sci. Sports Exercise* 51, 1380–1386. doi: 10.1249/MSS.0000000000001914

Ortiz, F. C., Habermacher, C., Graciarena, M., Houry, P.-Y., Nishiyama, A., Nait Oumesmar, B., et al. (2019). Neuronal activity in vivo enhances functional myelin repair. *JCI Insight* 5:e123434. doi: 10.1172/jci.insight.123434

Paez, P. M., and Lyons, D. A. (2020). Calcium signaling in the oligodendrocyte lineage: regulators and consequences. *Annu. Rev. Neurosci.* 43, 163–186. doi: 10.1146/annurev-neuro-100719-093305

Piscopo, D. M., Weible, A. P., Rothbart, M. K., Posner, M. I., and Niell, C. M. (2018). Changes in white matter in mice resulting from low-frequency brain stimulation. *Proc. Natl. Acad. Sci. U.S.A.* 115, E6339–E6346. doi: 10.1073/pnas.1802160115

Prakash, R. S., Snook, E. M., Motl, R. W., and Kramer, A. F. (2010). Aerobic fitness is associated with gray matter volume and white matter integrity in multiple sclerosis. *Brain Res.* 1341, 41–51. doi: 10.1016/j.brainres.2009.06.063

Prasad, A., Teh, D. B. L., Blasiak, A., Chai, C., Wu, Y., Gharibani, P. M., et al. (2017). Static magnetic field stimulation enhances oligodendrocyte differentiation and secretion of neurotrophic factors. *Sci. Rep.* 7:6743. doi: 10.1038/s41598-017-06331-8

Sahel, A., Ortiz, F. C., Kerninon, C., Maldonado, P. P., Angulo, M. C., and Nait-Oumesmar, B. (2015). Alteration of synaptic connectivity of oligodendrocyte precursor cells following demyelination. *Front. Cell. Neurosci.* 9:77. doi: 10.3389/fncel.2015.00077

Santiago González, D. A., Cheli, V. T., Zamora, N. N., Lama, T. N., Spreuer, V., Murphy, G. G., et al. (2017). Conditional deletion of the L-Type calcium channel Cav1.2 in NG2-positive cells impairs remyelination in mice. *J. Neurosci.* 37, 10038–10051. doi: 10.1523/JNEUROSCI.1787-17.2017

Sherafat, M. A., Heibatollahi, M., Mongabadi, S., Moradi, F., Javan, M., and Ahmadiani, A. (2012). Electromagnetic field stimulation potentiates endogenous myelin repair by recruiting subventricular neural stem cells in an experimental model of white matter demyelination. *J. Mol. Neurosci.* 48, 144–153. doi: 10.1007/s12031-012-9791-8

Stedehouder, J., Brizee, D., Shpak, G., and Kushner, S. A. (2018). Activity-dependent myelination of parvalbumin interneurons mediated by axonal morphological plasticity. *J. Neurosci.* 38, 3631–3642. doi: 10.1523/JNEUROSCI.0074-18.2018

Stedehouder, J., Brizee, D., Slotman, J. A., Pascual-Garcia, M., Leyrer, M. L., Bouwen, B. L., et al. (2019). Local axonal morphology guides the topography of interneuron myelination in mouse and human neocortex. *ELife* 8:e48615. doi: 10.7554/eLife.48615

Thevathasan, W., Schweder, P., Joint, C., Ray, N., Pretorius, P., Gregory, R., et al. (2011). Permanent tremor reduction during thalamic stimulation in multiple sclerosis. *J. Neurol. Neurosurg. Psychiatry* 82, 419–422. doi: 10.1136/jnnp.2010.213900

Waggener, C. T., Dupree, J. L., Elgersma, Y., and Fuss, B. (2013). CaMKII regulates oligodendrocyte maturation and CNS myelination. *J. Neurosci.* 33, 10453–10458. doi: 10.1523/JNEUROSCI.5875-12.2013

Wake, H., Ortiz, F. C., Woo, D. H., Lee, P. R., Angulo, M. C., and Fields, R. D. (2015). Nonsynaptic junctions on myelinating glia promote preferential myelination of electrically active axons. *Nat. Commun.* 6:7844. doi: 10.1038/ncomms8844

Weider, M., Starost, L. J., Groll, K., Küspert, M., Sock, E., Wedel, M., et al. (2018). Nfat/calcineurin signaling promotes oligodendrocyte differentiation and myelination by transcription factor network tuning. *Nat. Commun.* 9:899. doi: 10.1038/s41467-018-03336-3

Welliver, R. R., Polanco, J. J., Seidman, R. A., Sinha, A. K., O'Bara, M. A., Khaku, Z. M., et al. (2018). Muscarinic receptor M_3 R signaling prevents efficient remyelination by human and mouse oligodendrocyte progenitor cells. *J. Neurosci.* 38, 6921–6932. doi: 10.1523/JNEUROSCI.1862-17.2018

Welsh, T. G., and Kucenas, S. (2018). Purinergic signaling in oligodendrocyte development and function. *J. Neurochem.* 145, 6–18. doi: 10.1111/jnc.14315

Yeung, M. S. Y., Djelloul, M., Steiner, E., Bernard, S., Salehpour, M., Possnert, G., et al. (2019). Dynamics of oligodendrocyte generation in multiple sclerosis. *Nature* 566, 538–542. doi: 10.1038/s41586-018-0842-3

Zhang, C., Zhang, G., Rong, W., Wang, A., Wu, C., and Huo, X. (2014). Oscillating field stimulation promotes spinal cord remyelination by inducing differentiation of oligodendrocyte precursor cells after spinal cord injury. *Biomed. Mat. Eng.* 24, 3629–3636. doi: 10.3233/BME-141190

Zheng, X., and Schlaug, G. (2015). Structural white matter changes in descending motor tracts correlate with improvements in motor impairment after undergoing a treatment course of tDCS and physical therapy. *Front. Hum. Neurosci.* 9:229. doi: 10.3389/fnhum.2015.00229

Ziskin, J. L., Nishiyama, A., Rubio, M., Fukaya, M., and Bergles, D. E. (2007). Vesicular release of glutamate from unmyelinated axons in white matter. *Nat. Neurosci.* 10, 321–330. doi: 10.1038/nn1854

Conflict of Interest: The authors declare that the research was conducted in the absence of any commercial or financial relationships that could be construed as a potential conflict of interest.

frontiers in Cellular Neuroscience

ORIGINAL RESEARCH
published: 17 March 2021
doi: 10.3389/fncel.2021.576609

Deletion of the Thrombin Proteolytic Site in Neurofascin 155 Causes Disruption of Nodal and Paranodal Organization

Dipankar J. Dutta[1,2] *and R. Douglas Fields*[1]*

[1] Section on Nervous System Development and Plasticity, The Eunice Kennedy Shriver National Institute of Child Health and Human Development, National Institutes of Health, Bethesda, MD, United States, [2] The Henry M. Jackson Foundation for the Advancement of Military Medicine, Inc., Bethesda, MD, United States

In the central nervous system, myelin is attached to the axon in the paranodal region by a trimolecular complex of Neurofascin155 (NF155) in the myelin membrane, interacting with Caspr1 and Contactin1 on the axolemma. Alternative splicing of a single Neurofascin transcript generates several different Neurofascins expressed by several cell types, but NF155, which is expressed by oligodendrocytes, contains a domain in the third fibronectinIII-like region of the molecule that is unique. The immunoglobulin 5–6 domain of NF155 is essential for binding to Contactin1, but less is known about the functions of the NF155-unique third fibronectinIII-like domain. Mutations and autoantibodies to this region are associated with several neurodevelopmental and demyelinating nervous system disorders. Here we used Crispr-Cas9 gene editing to delete a 9 bp sequence of NF155 in this unique domain, which has recently been identified as a thrombin binding site and implicated in plasticity of the myelin sheath. This small deletion results in dysmyelination, eversion of paranodal loops of myelin, substantial enlargement of the nodal gap, a complete loss of paranodal septate junctions, and mislocalization of Caspr1 and nodal sodium channels. The animals exhibit tremor and ataxia, and biochemical and mass spectrometric analysis indicates that while NF155 is transcribed and spliced normally, the NF155 protein is subsequently degraded, resulting in loss of the full length 155 kDa native protein. These findings reveal that this 9 bp region of NF155 in its unique third fibronectinIII-like domain is essential for stability of the protein.

Keywords: Neurofascin155, thrombin, fibronectinIII-like, myelin, paranode, Crispr-Cas9, septate-like junctions, demyelination

OPEN ACCESS

Edited by:
Maria Kukley,
Achucarro Basque Center for Neuroscience, Spain

Reviewed by:
Yannick Poitelon,
Albany Medical College, United States
Jeffrey Dupree,
Virginia Commonwealth University, United States

***Correspondence:**
R. Douglas Fields
fieldsd@mail.nih.gov

Specialty section:
This article was submitted to Non-Neuronal Cells, a section of the journal Frontiers in Cellular Neuroscience

Received: *26 June 2020*
Accepted: *17 February 2021*
Published: *17 March 2021*

Citation:
Dutta DJ and Fields RD (2021) Deletion of the Thrombin Proteolytic Site in Neurofascin 155 Causes Disruption of Nodal and Paranodal Organization. Front. Cell. Neurosci. 15:576609. doi: 10.3389/fncel.2021.576609

INTRODUCTION

Neurofascins are a family of cell-surface proteins of the immunoglobulin superfamily generated by alternative splicing of a single Neurofascin (NF) transcript (Hassel et al., 1997). In the CNS, oligodendroglial Neurofascin 155 (NF155) interacts with the axonal Caspr1-Contactin1 complex to form septate-like cell-adhesion junctions that attach uncompacted loops of myelin to the paranodal axon. These junctions are essential for neural impulse conduction by securing the uncompacted

margin of myelin to the axon, thereby forming the paranodal loops, and maintaining separation of sodium channels in the node of Ranvier from potassium channels in the juxtaparanodal region (Banerjee et al., 2006). NF155 has a similar function in Schwann cells forming myelin on axons in the peripheral nervous system (Basak et al., 2007).

NF155 is a member of the L1-CAM family of cell adhesion molecules, with 6 immunoglobulin-like extracellular domains and four fibronectin type III-like (FNIII) extracellular regions anchored to the membrane by a short transmembrane segment (Hortsch, 1996). NF155 is produced by alternative splicing of *Neurofascin* into a NF186 form, expressed on neurons, and NF155, expressed by oligodendrocytes and localized to the paranodal region of myelinated axons (Davis et al., 1996). Binding of QKi to an RNA element (QRE2) in Nfasc intron 21 is required to promote inclusion of exons 21/22, which encodes the third FNIII-like domain that is unique to NF155 (Darbelli et al., 2016).

The biological functions of NF155 are well established and the functions of distinct domains comprising the macromolecule are being identified. Conditional deletion of NF155 in mice results in disruption of the paranodal junction and causes severe motor coordination defects and death at 16–17 days after birth (Pillai et al., 2009). Deletion of the immunoglobulin 5–6 domain in NF155, results in a truncated protein that is expressed normally. However, this domain is essential for binding of NF155 with Contactin1 and thus crucial for normal myelination. In mice with the immunoglobulin 5–6 domains deleted, the paranodal septate junctions are lost, resulting in diffusion of Caspr1 and Contactin1 from the paranodes and redistribution of the juxtaparanodal potassium channels toward the nodes (Thaxton et al., 2010).

Less is known of the functions of the unique third FNIII-like domain in NF155, but this region has been implicated in various CNS immune and neurodevelopmental disorders (Kira et al., 2018; Efthymiou et al., 2019). Homozygous mutations in the *NFASC* gene that introduces a STOP codon in AA846 (Arginine) within the unique third FNIII-like domain in NF155, results in a truncated NF155 protein, while sparing other members of the NF family including NF186. This mutation causes a severe neurodevelopmental disorder characterized by hypotonia, amimia, and areflexia (Smigiel et al., 2018).

Autoantibodies to NF155 have been detected in various central and peripheral autoimmune demyelinating pathologies including Multiple Sclerosis (MS), Guillane-Barre syndrome (GBS), Chronic Inflammatory Demyelinating Polyneuropathy (CIDP), and Combined Central and Peripheral Demyelination (CCPD) (Mathey et al., 2007; Kawamura et al., 2013; Yamasaki, 2013; Cortese et al., 2016; Burnor et al., 2018; Doppler et al., 2018). In CIDP, the NF155 autoantibodies have been traced to a domain that includes the unique third FNIII-like domain in NF155 (Ng et al., 2012). Several peripheral nerve neuropathological disorders, including GBS, CIDP, and others, are also associated with NF155 autoantibodies or genetic variants of NF155 (Ng et al., 2012).

Recent research has identified a thrombin binding site in this third FNIII-like domain of NF155 at AA924–926. Cleavage of NF155 at this site by thrombin results in detachment of paranodal loops of myelin from the axon, widening of the nodal gap, thinning of the myelin sheath, and a reduction in conduction velocity (Dutta et al., 2018). We used Crispr-Cas9 to delete the nine nucleotides corresponding to the three amino acids (AA924–926, Glycine-Arginine-Glycine) comprising the thrombin cleavage site of NF155. Surprisingly, this small deletion resulted in the complete loss of NF155 due to degradation of the proten post-synthesis, phenocopying the histological, ultrastructural, and functional outcome of complete and conditional NF155 knock outs (Sherman et al., 2005; Pillai et al., 2009). Thus this three amino acid site plays a crucial role in the stability of the NF155 protein.

MATERIALS AND METHODS

Transgenic Mouse Production and Maintenance

We generated a transgenic mouse line with Crispr-Cas9 mediated targeted deletion of 9 base pairs in chromosome 1: 132597812–132597821 corresponding to the thrombin cleavage site spanning AA 924–926 (Glycine—Arginine—Glycine) in the native Neurofascin 155 protein. The procedure was carried out by Chengyu Liu and his team in the transgenic core facility at the National Heart Lung and Blood Institute (NHLBI), National Institutes of Health (NIH), MD, United States. P90 mice of both sexes were used for all experimental analyses.

The NF155-Tdel mutant mouse line was generated using Crispr/Cas9 following standard protocols (Wang et al., 2013). Briefly, a sgRNA (TGGTCAATGGGAGAGGTGAC) was designed to cut around AA924–926, and was synthesized using ThermoFisher's custom *in vitro* transcription service. A single strand oligonucleotide ordered from IDT, which lacked the 9bp coding for AA924–926 (aagagacagcaggccagcttccctggtgaccgtccccggggcgtggtggcccgcctgt tc ccctacagtaactacaagctggagatggtggtggtcaat—gacgggcctcgaagtga aaccaaggaattcaccaccccagaaggag, in which the position of the deleted 9 bp is marked by a hyphen), was used as a donor for homology-mediated knockin. The sgRNA (20 ng/ul) was co-microinjected with the donor oligonucleotides (100 ng/ul) and Cas9 mRNA (50 ng/ul, ordered from Trilink BioTechnologies) into the cytoplasm of zygotes collected from C57BL/6N mice (Charles River Laboratories). Injected embryos were cultured in M16 medium (MilliporeSigma) overnight in a 37°C incubator with 6% CO_2. In the next morning, embryos that reached the 2-cell stage of development were implanted into the oviducts of pseudopregnant surrogate mothers (CD-1 strain purchased from Charles River Laboratories). Offspring born to the foster mothers were genotyped by PCR amplification using a primer pair (forward primer: CAGTCACTACCA CCACTAACC and reverse primer: CACTTTGGTGACGGTCATTCG) followed by Sanger sequencing using forward sequencing primer (CAACCTGCCTCTGTCTCAAAGG), or amplified using a PCR primer pair (forward primer: CAACCTGCCTCTGTCTCAAAGG and reverse primer: CTGCACAGATCTCTTGATAA C) followed by Sanger sequencing using a reverse primer (CACTTTGGTGAC

GGTCATTCG). Founder mice with the desired 9bp deletion were bred with wild type C57BL/6 for expanding the colonies. Results of studies on a total of 38 mice are reported.

Genotyping and Sanger Sequencing

Genotyping of the transgenic mice was carried out by PCR amplification of tail DNA followed by Sanger Sequencing of PCR amplified DNA by Macrogen, MD, United States. The PCR primer pair sequence is as follows:

NF155TDel_F1: CAA CCT GCC TCT GTC TCA AAG G

NF155TDel_R1: CTG CAC AGA TCT CTT GAT AAG C

After the sequences were obtained, it was aligned with the wild-type sequence using Multialin webserver (Corpet, 1988) to verify deletion of the intended 9 bp region in the genome.

Immunohistochemistry

Mice were anesthetized with Isoflurane and transcardially perfused with 4% Paraformaldehyde in 0.1M Phosphate buffer, pH 7.4. Optic nerves were collected, post-fixed in 4% Paraformaldehyde for 2 h on ice, embedded and frozen at –20°C for later longitudinal cryosectioning. Epitope retrieval was performed in Citrate buffer, pH 6.0 (Invitrogen, Camarillo, CA, United States), at 95°C for 10 min. Immunostaining with anti-pan Sodium channel (Cat#S6936, rabbit polyclonal IgG, 1:100, Sigma, Saint Louis, MO, United States) and anti-Caspr1 antibody (Cat#73-001, mouse monoclonal IgG, 1:50, NeuroMab, Davis, CA, United States) was conducted to visualize nodes of Ranvier in optic nerves. Images were captured by confocal laser microscopes (LSM510, LSM 780, LSM 710, Zeiss, Germany and Olympus Fluoview FV3000 Tokyo, Japan), using 20, 40, and 100X objective lenses and digital zoom up to 5X. Alexa fluor 488 and 594 dyes, used for immunohistochemistry in **Figure 2**, were excited at 500 and 590 nm respectively, and their emission were captured at 520 and 618 nm respectively. 20X imaging objective was used with a numerical aperture of 0.4 for this figure. Pinhole was set to 1 and the size of optical section was 1 micron. Results from 3 WT and 3 NF155-Tdel mice are reported.

Electron Microscopy

Mice were anesthetized and transcardially perfused with 2.5% Glutaraldehyde and 2% Paraformaldehyde in 0.13 M Sodium Cacodylate, pH 7.4. Optic nerves were immediately removed from animals, then post-fixed in the same solution for 2 h at room temperature. Samples were post-fixed for 2 h in 2% Osmium Tetroxide. Samples were washed six times in 0.13 M Sodium Cacodylate, pH 7.4, and stained with 1% Uranyl Acetate in 0.05 M Sodium Acetate, pH 5.0, for 2 h at 4°C. Samples were then dehydrated through a graded series of ethanol solutions and infiltrated with Epon. Ultrathin sections were cut with a diamond knife, stained with Uranyl Acetate and Lead Citrate and examined by transmission electron microscopy. TEM micrographs were generated via a paid contract with electron microscopists at Science Exchange Inc. Results from 3 WT and 3 NF155-Tdel mice are reported.

Immunoblotting

For detection of NF155, NF125, NF186, NSE, and Caspr1; freshly dissected optic nerve tissues were lysed in Tissue Protein Extraction Reagent (TPER) with protease inhibitors (Pierce, IL). The lysate was mixed with SDS-PAGE loading buffer (Thermo Fisher Scientific, MD) before electrophoresis.

Total protein was resolved by SDS-PAGE on 4–12% NuPAGE Bis-Tris gels (Life Technologies, Carlsbad, CA), transferred to PVDF membrane (Immobilon-P, Millipore, Bedford, MA) and blocked in Tris Buffer Solution (TBS, 10 Mm Tris-Cl, pH 7.5, 0.9% NaCl) containing 0.1% (v/v) Triton X-100 (TBST) and either 5% (w/v) non-fat milk or 5% (w/v) bovine serum albumin for 1 h at room temperature. Membranes were probed with appropriate antibodies in TBST and either 5% non-fat milk or 5% BSA overnight at 4°C. Primary antibodies were visualized with HRP-conjugated secondary antibodies (Amersham Pharmacia Biotech, Piscataway, NJ) at 1:5,000 dilution with either regular (picomolar sensitivity) or enhanced (femtomolar sensitivity) chemiluminescence (Life Technologies, Carlsbad, CA). The total protein loaded in the WT lane in **Figure 1C** was approximately 50% higher than that in the NF155T-del lane. Two identical trials were performed. Total protein loaded in all lanes in **Figure 1D** were equal. Two identical trials were performed. Results from 4 NF155-Tdel and 2 WT mice are reported. Primary antibodies used for immunoblotting: NF155 and NF125 polyclonal (Cat# ab15189, Millipore, Billerica, MA) used at 1:1,000, NF155 and NF125 monoclonal (Cat# 15035, Cell Signaling, Danvers, MA) used at 1:1,000, NF186 (Cat# ab31457, Abcam, Cambridge, MA) used at 1:1,000, NSE (Cat# ab53025, Abcam, Cambridge, MA) used at 1:2,000, and Caspr1 (Cat# ab34151, Abcam, Cambridge, MA) used at 1:1,000.

Antibodies Used for the Detection of NF155 Cleaved Fragments

Upon cleavage of NF155 by thrombin, its two cleaved fragments were detected in immunoblots with antibodies, polyclonal and monoclonal, whose epitopes are located N-terminal to the thrombin cleavage site in NF155 at AA 924. These antibodies (Polyclonal antibody, Cat# ab15189, Millipore, Billerica, MA; Monoclonal antibody, Cat# 15035, Cell Signaling, Danvers, MA) with the N-terminal epitopes detect the full-length NF155 protein as well as its longer 125 kDa thrombin-cleaved fragment, Neurofascin 125 (NF125).

Liquid Chromatography-Mass Spectrometry (LC-MS) Analyses

Liquid chromatography-mass spectrometry (LC-MS) was used to determine the presence of peptides corresponding to NF155 protein in immunoblots (**Figure 1E**) of NF155Tdel mice. Fresh optic nerve tissue lysates from NF155Tdel mice were run in a SDS-PAGE gel with size-appropriate protein ladders. Two bands on the gel corresponding to 250–150 and 150–100 kDa were excised and sent to the LC-MS facility at the National Institute of Neurological Disorders and Stroke (NINDS), NIH for protein identification analysis. Peptides identified by LC-MS as

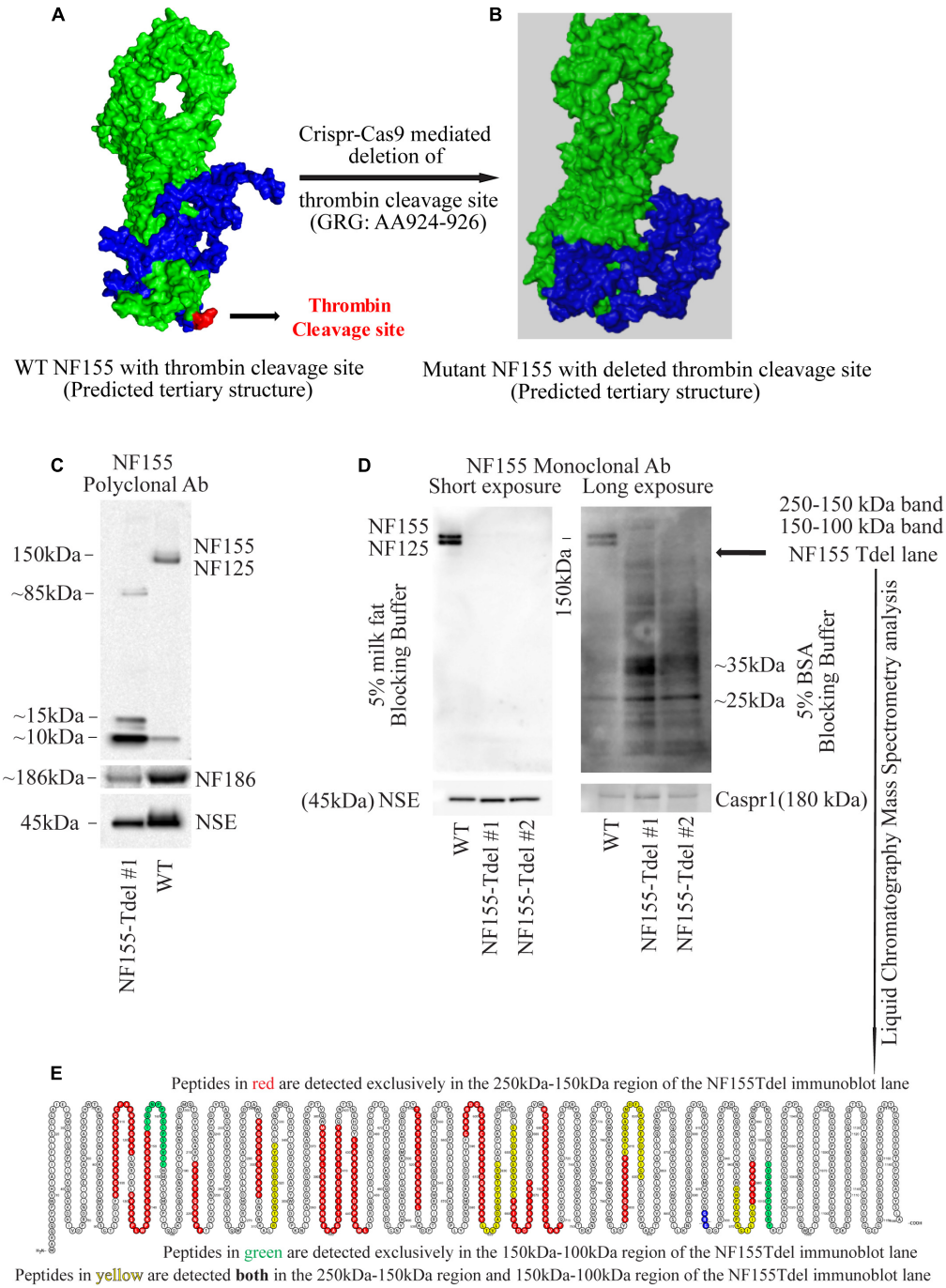

FIGURE 1 | Neurofascin 155 protein is degraded upon deletion of AA924–926 (GRG) in NF155Tdel mice. The predicted tertiary structure of wild type Neurofascin 155 **(A)** is overall similar to that of Neurofascin 155 with deleted thrombin binding site spanning AA924–926 **(B)**. Green = NF125, the region of NF155 protein N-terminal to the thrombin cleavage site. Blue = NF30, the region of the NF155 protein C-terminal to the thrombin cleavage site. Red = thrombin cleavage site. A polyclonal NF155 antibody could not detect the full length NF155 (155 kDa) and its longer thrombin cleaved fragment NF125 (125 kDa) in optic nerve samples from NF155Tdel mice **(C)**. Instead, it detected smaller sized fragments weighing; 10, 15, and 85 kDa; potentially belonging to degraded NF155 fragments **(C)**. Expression of NF186 was not affected in NF155del mice **(C)**. Neuron Specific Enolase (NSE) was used as loading control, and higher levels of protein were loaded in the WT condition as a more rigorous test of possible NF155 fragments also appearing in normal conditions, but no such fragmentation was detected in WT animals **(C)**. **(D)** Use of a monoclonal antibody with 5% BSA as blocking buffer and longer exposure showed a protein smear in two independent optic nerve samples from NF155Tdel mice, and no full length NF155 or its long thrombin cleaved fragment NF125 was observed, indicating degradation of the NF155 protein. Expression and stability of Caspr1, one of the other members of the paranodal septate-like junctions, was normal in NF155Tdel mice **(D)**. Protein loading, assessed via NSE expression, was equal in all immunoblot lanes in **(D)**. Liquid Chromatography—Mass Spectroscopy analysis confirmed the presence of peptides belonging to NF155 in the 250–100 kDa region of the smeared lanes from NF155Tdel mice **(E)**.

belonging to NF155 protein were rendered in a protein amino acid visualization tool, Protter (Omasits et al., 2014).

Protein Structure Prediction

The tertiary structure of native NF155 and its various putative mutant forms resulting from mutations and deletions in its thrombin cleavage site spanning AA924–926 were predicted using I-TASSER (Iterative Threading ASSEmbly Refinement), a state-of-the-art algorithm for protein structure and function prediction (Roy et al., 2010). The predicted structures were then rendered and annotated in Polyview-3D (Porollo and Meller, 2007).

Neurological Assessment of NF155Tdel Mice

NF155Tdel mice, beginning around 30 days after birth, exhibited sustained symptoms of ataxia which progressively got worse as the mice got older. We observed these mice regularly starting at their day of birth and until their death between 3 and 6 months of age. We observed them in their cages as well as outside their cages. The behavior of 20 mice was examined.

RESULTS

The neurofascin gene in mice is in chromosome 1: 132,564,690–132,741,797. All members of the neurofascin family of proteins, including NF155, are derived via alternative splicing of a single neurofascin gene transcript (Hassel et al., 1997). The thrombin cleavage site in NF155, located in the third Fibronectin-III like domain, is in a domain unique to NF155 among all other members of the Neurofascin family (Dutta et al., 2018). The 9 nucleotides corresponding to the 3 amino acid thrombin cleavage site in NF155 [Glycine (G, AA924)—Arginine (R, AA925)—Glycine (G, 926)] is located in chromosome 1: 132597812–132597821. Having determined the exact coordinates of the NF gene corresponding to the thrombin cleavage site in the NF155 protein, we proceeded to determine *in silico*, the putative effects of various mutations and deletions in this site to NF155 structure.

Predictive modeling of the NF155 protein structure suggested that this thrombin cleavage site is at the tip of a beta hairpin loop protruding away from the protein core (**Figure 1A**). Thrombin is capable of cleaving substrates with a wide range of amino acid sequences (Le Bonniec et al., 1996; Jenny et al., 2003). We introduced point mutations (**Supplementary Figures S1A–E**) and deletions (**Supplementary Figures S1F–H**) at and around AA924–926 region of NF155 *in silico*. Among all alternatives examined and shown in **Supplementary Figures S1A–H**, deletion of the three AA (GRG, AA924–926) corresponding to the entire thrombin cleavage site in NF155, yielded a predicted 3D structure that was most similar to the native NF155 tertiary structure (**Figures 1A,B**). Moreover, since these three AA are in a domain unique to NF155, this deletion would not have deleterious effects on other members of the Neurofascin family. We then performed Crispr-Cas9 mediated deletion of the 9 nucleotides, Chr1: 132597812–132597821, corresponding to AA924–926 in the NF155 protein, in C57Bl6 mice.

We confirmed that the mice, hereby referred to as NF155-Tdel, had the appropriate deletion by PCR amplification of the Neurofascin gene in the transgenic mice followed by Sanger sequencing of the amplified Neurofascin gene products (**Supplementary Figure S1I**).

Although we deleted only the three amino acids (GRG, AA924–926) corresponding to the thrombin cleavage site in the NF155-Tdel mice, we could not detect the full-length 155 kDa native protein in these mice by standard immunoblotting with an NF155 polyclonal antibody. Signs of protein degradation were evident (**Figure 1C**). These degraded fragments were not detected in the WT lane, even with higher protein loading in the WT lane. This implies that the bands in the NF155T-del lane in **Figure 1C** are indeed degraded protein fragments of NF155T-del protein, and are not non-specific protein bands. Use of a monoclonal NF155 antibody after prolonged exposure in the presence of a more sensitive chemiluminescent substrate, with and without 5% milk fat as blocking and incubation buffer, showed a protein smear where distinct protein bands should be, clearly indicating that the NF155 protein was severely degraded (**Figure 1D**). However, expression and stability of Caspr1 protein, one of the interacting partners of NF155 in paranodal septate-like junctions, was normal (**Figure 1D**). Neuron Specific Enolase (NSE) was used as protein loading controls.

We detected normal amounts and sizes of nodal Neurofascin186, the largest member of the family (Hassel et al., 1997), indicating that the alternative splicing of this neurofascin gene transcript is not affected by removal of the 9 nucleotides corresponding to the thrombin cleavage site in NF155. Since the thrombin cleavage site is located in a domain, the third Fibronectin III-like domain, which is unique to NF155, other members of the neurofascin family, as expected, were unaffected by removal of these 9 nucleotides from the neurofascin gene. NF186 was detected with a pan NF C-terminal antibody that does not detect full length NF155 as per the antibody product datasheet[1].

Both the polyclonal and the monoclonal NF155-specific antibodies detected residues in the third FNIII domain unique to NF155. Specifically, the NF155 polyclonal antibody detects the epitope spanning AA 886–903 of the full length NF155 protein, and the NF155 monoclonal antibody detects residues surrounding AA 881 of the full length NF155 protein. Since both these antibodies recognize denatured proteins in immunoblots, there is no reason to believe that any hypothetical change in tertiary structure of NF155 in NF155Tdel mice would preclude detection of the NF155 protein in immunoblots. These data support the conclusion that the smearing and absence of full-length NF155 protein detected in NF155Tdel immunoblots is the consequence of degradation of the NF155 protein in NF155Tdel mice.

For independent confirmation of the immunoblot data, we performed liquid chromatography mass spectrometry (LC-MS) analysis of two gel regions in the NF155Tdel immunoblot lane. We excised the gel region spanning 250–150 kDa to probe for the presence of NF155 protein weighing 155 kDa. We also

[1]https://www.abcam.com/neurofascin-antibody-ab31457.html

excised the gel region spanning 150–100 kDa to probe for the presence of NF125 protein weighing 125 kDa. The proteins in the excised gel regions were enzymatically digested, with Trypsin and Chymotrypsin, and the digested peptides were sequenced via LC-MS. Peptides from the 250 to 150 kDa region of the gel (red and yellow, **Figure 1E**), from full length NF155, mapped to both N-terminal and C-terminal to the thrombin cleavage site (blue, **Figure 1E**), as expected. However, surprisingly, 2 peptides from the 150–100 kDa region of the gel (green and yellow, **Figure 1E**) mapped C-terminal to the thrombin cleavage site (blue, **Figure 1E**). These two peptides do not belong to the NF125 protein, which is N-terminal to the thrombin cleavage site in NF155 (Dutta et al., 2018). Rather these two peptides belong to NF30, the small thrombin cleaved fragment of NF155 (Dutta et al., 2018), weighs 30 kDa, and therefore should not be present in the excised gel band spanning 150–100 kDa. In combination with the smeared NF155Tdel lanes seen in **Figure 1D**, this suggests that these two peptides are detected in a region they are not supposed to be detected because these peptides, in NF155Tdel mice, belong to randomly degraded fragments of NF155Tdel protein between 150 and 100 kDa in size. LC-MS detection of degraded fragments of the NF155 protein also indicates that the alternative splicing of the neurofascin transcript into NF155 transcript was unperturbed in the absence of the deleted 9 nucleotides, and that only the subsequent structural integrity of the mutated NF155 protein was affected.

Thus, the absence of the full length protein bands in sensitive immunoblots, smeared immunoblot lanes, and the presence of peptides corresponding to NF155 in the smeared immunoblot lane below 155 kDa in NF155Tdel immunoblot lanes, indicate that the NF155 protein was severely degraded in NF155Tdel mice. This indicates that the 3 AA (GRG), AA924–926, is essential for the structural integrity of the NF155 protein. In its absence, the NF155 protein is targeted for proteolytic degradation.

To corroborate our immunoblot results of degradation of NF155 in NF155Tdel mice (**Figures 1C,D**), we performed immunohistochemistry of optic nerve samples from WT and NF155Tdel mice (**Figure 2**). WT animals exhibited normal morphology of nodes of Ranvier with sodium channels flanked by Caspr1 in paranodes of optic nerves (**Figure 2A**). In contrast, Caspr1 and sodium channel expression were diffuse and disorganized in NF155 Tdel mice (**Figure 2B**). This implies disorganization of normal paranodal structure with loss of NF155 as previously reported (Pillai et al., 2009). Confocal microscopy confirmed that oligodendroglial Neurofascin 155 (green, **Figure 2C**) colocalized with its interacting axonal partner Caspr1 (red, **Figure 2D**) in WT mice (yellow, **Figure 2E**). However, no Neurofascin 155 expression was detected in the optic nerve of NF155 Tdel mice (**Figure 2F**). Caspr1 staining was weak and not localized into paranodal domains in NF155 Tdel mice (red, **Figures 2G,H**). These histological results are consistent with the known functions of NF155 in forming septate junctions that attach myelin to the axon in the perinodal region.

To examine the fine structure and predicted loss of septate junctions in NF155 Tdel mice, we performed transmission electron microscopy (TEM) of optic nerve of WT mice and NF155Tdel mice. In longitudinal sections, compared to WT mice (**Figure 3A**), the nodal gap was abnormally elongated in the NF155 Tdel mice (**Figure 3B**). In longitudinal sections, electron-dense septate-like intercellular junctions between paranodal loops of myelin and paranodal axon were present in WT mice (**Figures 3C,E**) and absent in NF155Tdel mice (**Figures 3D,F**). As expected, from the absence of septate-like junctions, the outermost paranodal myelin loops were frequently detached from the axon in NF155Tdel mice (**Figure 3D**) but were attached to the axon in WT mice (**Figure 3C**). Myelin sheath thickness appeared normal in both WT and NF155Tdel mice (**Figures 3G,H**). Normal thickness of the myelin sheath upon complete loss of NF155 has been described previously (Pillai et al., 2009). Myelin sheath morphology also appeared normal in NF155Tdel mice (**Figures 3G,H**). Normal myelin sheath morphology, upon complete loss of Nf155, has been described previously (Sherman et al., 2005; Pillai et al., 2009). However, we observed splitting of the myelin sheath in some cases in the NF155 Tdel mice (**Figure 3H**), giving a thicker appearance to those sheaths. Splitting of the myelin sheath in this way is one of the most common abnormalities in demyelinating conditions. With the attachments of myelin to the axon via the septate junctions missing, separation of the lamella that are no longer anchored is to be expected.

Behaviorally, the NF155Tdel mice had severe tremor and ataxia, which they started exhibiting around 1 month of age. This got worse with aging and most mice died within 3–6 months. NF155Tdel mice had abnormal gait and coordination, and exhibited sustained tremors, in comparison to their age and sex matched wild-type counterparts (Guyenet et al., 2010).

To assess their gait, we removed mice from their cages and placed them on a flat surface and observed the mice from behind while they walked. The WT mice moved normally, with body weight supported on all limbs, abdomen not touching the ground, and with both hindlimbs participating evenly. In contrast, the NF155Tdel mice exhibited tremor, appeared to limp with a lowered pelvis and feet pointing away from the body while walking ("duck feet"). These symptoms got progressively worse as the NF155Tdel mice aged and older mice had difficulty moving forward and/or dragged their abdomen on the ground while walking.

To assess their coordination, we performed the ledge test, where we lifted the mouse from their cage and placed it on the cage's ledge. WT mice would walk along the ledge without losing balance and then lower themselves into the cage using their paws. The NF155Tdel mice, in contrast, would lose their footing while walking along the ledge and simply fall into the cage headfirst instead of landing on their paws.

To conclude, deletion of the 3 AA in NF155 protein phenocopies a complete loss of the NF155 protein. As such, the properties of the nodal gap, myelin sheath and animal behavior are similar to mice with a complete deletion of NF155. In contrast, removal of much larger domains of NF155; i.e., Imuunoglobulin 5–6 domain, has resulted in the expression of a dysfunctional but truncated NF155 protein (Pillai et al., 2009). This suggest that the 3AA, GRG (AA924–926), is required for proper folding and structural integrity of the NF155 protein.

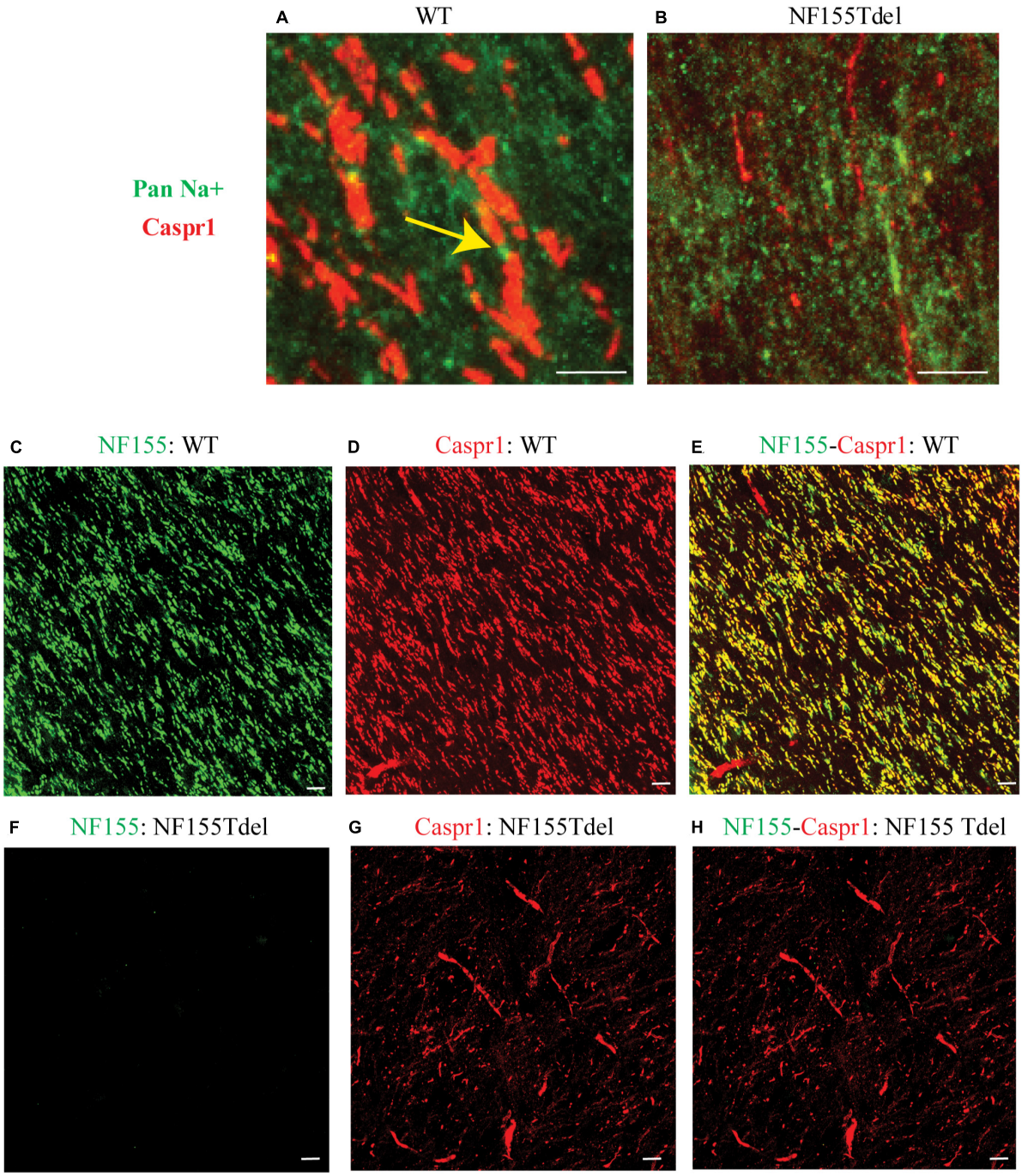

FIGURE 2 | Neurofascin 155 expression is lost and Caspr1 organization is disrupted in NF155Tdel mice. Nodes of Ranvier were severely disrupted in the optic nerves of NF155 Tdel mice, and NF155 protein could not be detected. The arrangement of nodal sodium channels and paranodal Caspr1, as shown in extreme high-magnification close-ups **(A,B)** showed the normal, regular arrangement of punctate Sodium channel (green) staining at the node flanked by tapering Caspr1 (red) staining at the paranode in wild-type animals (yellow arrow in **A**), but in contrast, these features were abnormal in the NF155Tdel mice **(B)**. Wider field images at lower magnification are provided in **(C–H)**, illustrate the marked contrast between nodal structure in WT and NF155del mice. In WT mice **(C–E)**, oligodendroglial Neurofascin 155 (green, **C**) colocalizedwith its axonal interacting partner Caspr1 (red, **D**) in paranodes (yellow, **E**). However, in NF155 Tdel mice **(F–H)**, NF155 could not be detected (green, **F**) and Caspr1 staining was week and diffuse (red, **G**). Optic nerves are oriented vertically in **(A,B)** and diagonally from the upper left to lower right of the other image panels **(C–H)**. Imaging conditions were maximized to detect the faint expression of these proteins in the NF155Tdel mice **(B)** where immunostaining for these proteins was diffuse and weak as a consequence of their mislocalization in the absence of NF155. Optic nerves were imaged in WT animals using the same settings on the confocal microscope, resulting in a somewhat oversaturated image **(A)**. Using microscopy settings optimized for imaging these proteins in WT animals, staining of these proteins in the NF155Tdel mice was too dim to detect. Non-specific labeling of blood vessels in **(C–H)** could be due to non-specific interaction of the primary antibodies used with immunoglobulins inside blood vessels. Scale bar = 5μm.

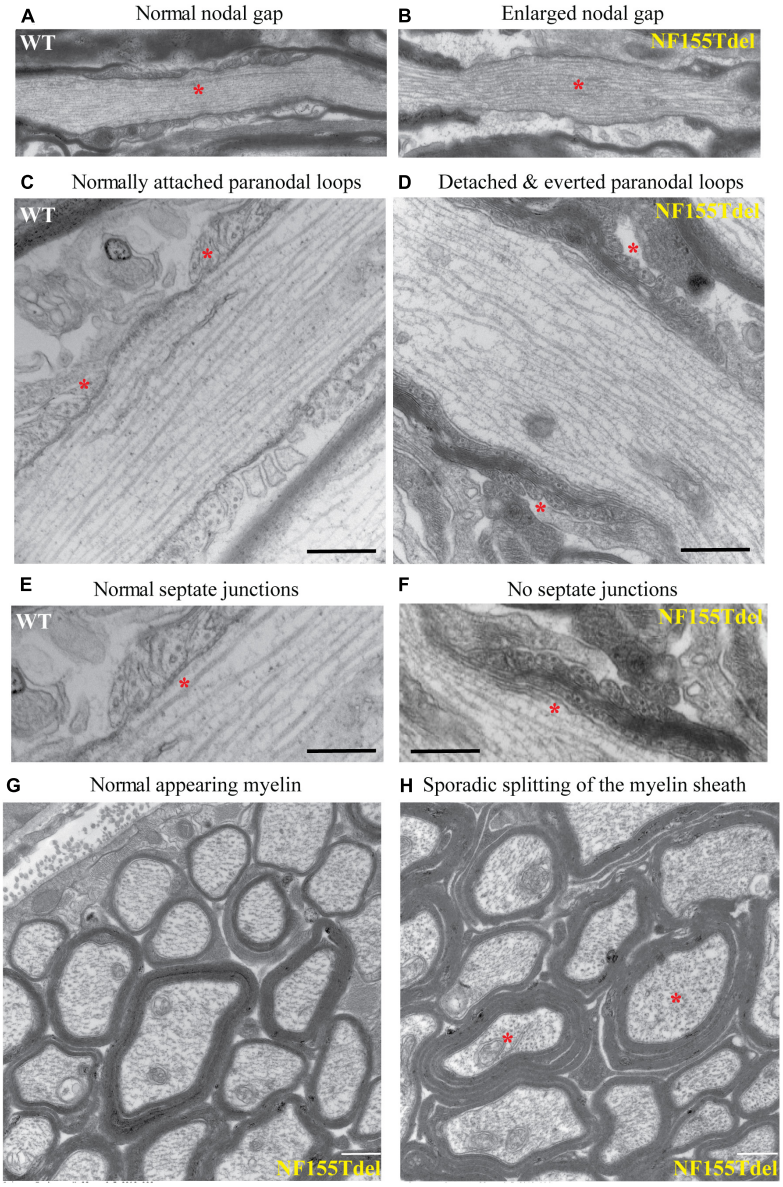

FIGURE 3 | Paranodal septate-like junctions are absent, and paranodal myelin attachment to the axon is disrupted in NF155Tdel mice. Transmission electron micrographs (TEM) of wild-type optic nerve showed normal nodal gap size **(A)**, and paranodal loops attached to either side of the node normally **(C)**, via transverse electron-dense sepatate-like junctions **(E)**. In stark contrast, nodal gap was greatly expanded in NF155Tdel mice **(B)**, and paranodal loops flanking the node were detached and in most cases everted **(D)**. Sepate-like junctions were absent in the NF155 Tdel mice **(F)**. **(E,F)** Are higher magnification close-ups of **(C,D)** to show the fine structure of septate junctions and their absence in NF155Tdel mice. Although, overall myelin morphology and thickness in NF155Tdel mice appeared normal **(G)**, there was sporadic evidence of splitting of the myelin sheath in NF155Tdel mice **(H)**. * = salient events described for each panel. Scale bars = 1 μm in **(A,B)** and 0.5 μm in the rest of the images.

DISCUSSION

Paranodal septate-like junctions are critical for proper saltatory action potential propagation in vertebrate myelinated axons (Cohen et al., 2020). Besides facilitating insulation by attaching the myelin sheath to the axon, they separate the nodal Na^+ channels from the juxtaparanodal K^+ channels and restrict the flow of ions between the node and the juxtaparanode (Brophy, 2001). Disruption in any of the three molecules that comprise the septate-like junctions results in similar dysmyelinating phenotypes with loss of the septate-like junctions culminating in abnormal organization of the nodal gap and the myelin sheath (Bhat et al., 2001; Boyle et al., 2001; Pillai et al., 2009). Because of the absence of a functional NF155 protein in our NF155-Tdel mice, they phenocopy mice with myelinating oligodendrocyte-specific NF155 null mutants (Charles et al., 2002; Sherman et al., 2005; Pillai et al., 2009). These mice also exhibit severe ataxia associated with everted paranodal loops, loss of paranodal

axoglial junctions and failure to maintain segregated axonal domains around the node. Similar phenotype is observed in the Caspr1 KO mice and the Contactin1 KO mice (Bhat et al., 2001; Boyle et al., 2001).

The Fibronectin III domain is an evolutionarily conserved protein domain found in a wide range of extracellular proteins (Campbell and Spitzfaden, 1994). It is on average 100 amino acids long and exhibits a beta-sandwich structure. These domains are commonly located between other protein domains and function as structural spacers, to optimally arrange other domains in space (Valk et al., 2017). The thrombin cleavage site in the third FNIII-like domain is at the tip of the beta-sandwich structure, in between two opposing antiparallel beta sheets. Given the unique and essential role of FNIII domains in organizing and stabilizing globular protein structure, it is evident that even slight changes to this sequence and/or structure can be detrimental to the structure and stability of the entire protein. This is possibly the reason why larger deletions in non-fibronectin domains of NF155; for example, deletion of the entire Contactin1-interacting Immunoglobulin 5–6 domains in NF155, result in a truncated but nevertheless stable protein (Thaxton et al., 2010).

Mutations in the third Fibronectin III-like domain, a 100 amino acid stretch of the NF155 protein (aa 839–938) have been clinically associated with demyelinating neuropathies (Efthymiou et al., 2019; Monfrini et al., 2019). These disorders are similar to those associated with Neurofascin155 autoantibodies in demyelinating neuropathies (Ng et al., 2012; Doppler et al., 2018). Whether mutations in NF155 can also lead to production of NF155 autoantibodies has not been directly investigated yet, but generation of fragments of myelin proteins can be immunogenic. Our study reveals the critical importance of this three amino acid sequence (AA924–926) in NF155 protein stability, and this finding may be important for our understanding of yet to be discovered human genetic disorders resulting from targeted mutations in this critical region.

DATA AVAILABILITY STATEMENT

The original contributions presented in the study are included in the article/**Supplementary Material**. Further inquiries can be directed to the corresponding author/s.

ETHICS STATEMENT

The animal study was reviewed and approved by the National Institutes of Health Animal Care and Use Committee, NICHD.

AUTHOR CONTRIBUTIONS

RDF and DJD conceived the project, designed experiments, analyzed data, interpreted results and prepared figures, and wrote the manuscript. DJD executed experiments and collected data. Both authors contributed to the article and approved the submitted version.

ACKNOWLEDGMENTS

We thank Chengyu Liu and his team at the transgenic core in the National Heart Lung and Blood Institute (NHLBI), NIH, for generating the transgenic mice via Crispr-Cas9 based gene editing. We are also thankful to Yan Li at the Protein/Peptide Sequencing Facility at the National Institute of Neurological Disorders and Stroke (NINDS), NIH for help with LC-MS analysis, and to William Huffman and Daniel Abebe for their assistance in maintaining the transgenic animal colony.

FUNDING

The research was supported by an intramural program of NICHD (Grant ZIAHD000713), and a Department of Defense grant (Grant 11162432) through the Henry M. Jackson Foundation for the Advancement of Military Medicine, Inc.

SUPPLEMENTARY MATERIAL

The Supplementary Material for this article can be found online at: https://www.frontiersin.org/articles/10.3389/fncel.2021.576609/full#supplementary-material

Supplementary Figure 1 | The adverse effects of various putative mutations in the thrombin binding site of NF155 on the predicted tertiary structure of NF155. Various theoretical amino acid substitutions **(A–E)** and deletions **(F–H)** in the thrombin binding site of NF155 spanning AA924–926 adversely affect the predicted tertiary structure of NF155. The predicted tertiary structure of wild type Neurofascin 155 (**Figure 1A**) is most similar to that of Neurofascin 155 with deleted thrombin binding site spanning AA924–926 (**Figure 1B**), among all potential thrombin-site mutated NF155 structures evaluated **(A–H)**. Confirmation of Crispr-Cas9 mediated deletion of the 9 nucleotides corresponding to AA924–926 in NF155Tdel mice via Sanger sequencing of PCR amplified tail DNA.

REFERENCES

Banerjee, S., Sousa, A. D., and Bhat, M. A. (2006). Organization and function of septate junctions: an evolutionary perspective. *Cell Biochem. Biophys.* 46, 65–77. doi: 10.1385/cbb:46:1:65

Basak, S., Raju, K., Babiarz, J., Kane-Goldsmith, N., Koticha, D., and Grumet, M. (2007). Differential expression and functions of neuronal and glial neurofascin isoforms and splice variants during PNS development. *Dev. Biol.* 311, 408–422. doi: 10.1016/j.ydbio.2007.08.045

Bhat, M. A., Rios, J. C., Lu, Y., Garcia-Fresco, G. P., Ching, W., St Martin, M., et al. (2001). Axon-glia interactions and the domain organization of myelinated axons requires neurexin IV/Caspr/Paranodin. *Neuron* 30, 369–383. doi: 10.1016/s0896-6273(01)00294-x

Boyle, M. E., Berglund, E. O., Murai, K. K., Weber, L., Peles, E., and Ranscht, B. (2001). Contactin orchestrates assembly of the septate-like junctions at the paranode in myelinated peripheral nerve. *Neuron* 30, 385–397.

Brophy, P. J. (2001). Axoglial junctions: separate the channels or scramble the message. *Curr. Biol.* 11, R555–R557. doi: 10.1016/S0960-9822(01)00341-4

Burnor, E., Yang, L., Zhou, H., Patterson, K. R., Quinn, C., Reilly, M. M., et al. (2018). Neurofascin antibodies in autoimmune, genetic, and idiopathic neuropathies. *Neurology* 90, e31–e38. doi: 10.1212/WNL.0000000000004773

Campbell, I. D., and Spitzfaden, C. (1994). Building proteins with fibronectin type III modules. *Structure* 2, 333–337. doi: 10.1016/S0969-2126(00)00034-4

Charles, P., Tait, S., Faivre-Sarrailh, C., Barbin, G., Gunn-Moore, F., Denisenko-Nehrbass, N., et al. (2002). Neurofascin is a glial receptor for the paranodin/Caspr-contactin axonal complex at the axoglial junction. *Curr. Biol.* 12, 217–220. doi: 10.1016/S0960-9822(01)00680-7

Cohen, C. C. H., Popovic, M. A., Klooster, J., Weil, M. T., Möbius, W., Nave, K. A., et al. (2020). Saltatory conduction along myelinated axons involves a periaxonal nanocircuit. *Cell* 180, 311–322.e15. doi: 10.1016/j.cell.2019.11.039

Corpet, F. (1988). Multiple sequence alignment with hierarchical clustering. *Nucleic Acids Res.* 16, 10881–10890. doi: 10.1093/nar/16.22.10881

Cortese, A., Devaux, J. J., Zardini, E., Manso, C., Taieb, G., Carra Dallière, C., et al. (2016). Neurofascin-155 as a putative antigen in combined central and peripheral demyelination. *Neurol. Neuroimmunol. Neuroinflamm.* 3:e238. doi: 10.1212/NXI.0000000000000238

Darbelli, L., Vogel, G., Almazan, G., and Richard, S. (2016). Quaking regulates neurofascin 155 expression for myelin and axoglial junction maintenance. *J. Neurosci.* 36, 4106–4120. doi: 10.1523/JNEUROSCI.3529-15.2016

Davis, J. Q., Lambert, S., and Bennett, V. (1996). Molecular composition of the node of Ranvier: identification of ankyrin-binding cell adhesion molecules neurofascin (mucin+/third FNIII domain-) and NrCAM at nodal axon segments. *J. Cell Biol.* 135, 1355–1367. doi: 10.1083/jcb.135.5.1355

Doppler, K., Stengel, H., Appeltshauser, L., Grosskreutz, J., Man Ng, J. K., Meinl, E., et al. (2018). Neurofascin-155 IgM autoantibodies in patients with inflammatory neuropathies. *J. Neurol. Neurosurg. Psychiatry* 89, 1145–1151. doi: 10.1136/jnnp-2018-318170

Dutta, D. J., Woo, D. H., Lee, P. R., Pajevic, S., Bukalo, O., Huffman, W. C., et al. (2018). Regulation of myelin structure and conduction velocity by perinodal astrocytes. *Proc. Natl. Acad. Sci. U.S.A.* 115, 11832–11837. doi: 10.1073/pnas.1811013115

Efthymiou, S., Salpietro, V., Malintan, N., Poncelet, M., Kriouile, Y., Fortuna, S., et al. (2019). Biallelic mutations in neurofascin cause neurodevelopmental impairment and peripheral demyelination. *Brain* 142, 2948–2964. doi: 10.1093/brain/awz248

Guyenet, S. J., Furrer, S. A., Damian, V. M., Baughan, T. D., La Spada, A. R., and Garden, G. A. (2010). A simple composite phenotype scoring system for evaluating mouse models of cerebellar ataxia. *J. Vis. Exp.* 39:1787. doi: 10.3791/1787

Hassel, B., Rathjen, F. G., and Volkmer, H. (1997). Organization of the neurofascin gene and analysis of developmentally regulated alternative splicing. .*J. Biol. Chem.* 272, 28742–28749. doi: 10.1074/jbc.272.45.28742

Hortsch, M. (1996). The L1 family of neural cell adhesion molecules: old proteins performing new tricks. *Neuron* 17, 587–593. doi: 10.1016/S0896-6273(00)80192-0

Jenny, R. J., Mann, K. G., and Lundblad, R. L. (2003). A critical review of the methods for cleavage of fusion proteins with thrombin and factor Xa. *Protein Expr. Purif.* 31, 1–11. doi: 10.1016/S1046-5928(03)00168-2

Kawamura, N., Yamasaki, R., Yonekawa, T., Matsushita, T., Kusunoki, S., Nagayama, S., et al. (2013). Anti-neurofascin antibody in patients with combined central and peripheral demyelination. *Neurology* 81, 714–722. doi: 10.1212/WNL.0b013e3182a1aa9c

Kira, J.-I., Yamasaki, R., and Ogata, H. (2018). Anti-neurofascin autoantibody and demyelination. *Neurochem. Int.* 130:104360. doi: 10.1016/j.neuint.2018.12.011

Le Bonniec, B. F., Myles, T., Johnson, T., Knight, C. G., Tapparelli, C., and Stone, S. R. (1996). Characterization of the P2' and P3' specificities of thrombin using fluorescence-quenched substrates and mapping of the subsites by mutagenesis. *Biochemistry* 35, 7114–7122. doi: 10.1021/bi952701s

Mathey, E. K., Derfuss, T., Storch, M. K., Williams, K. R., Hales, K, Woolley, D. R., et al. (2007). Neurofascin as a novel target for autoantibody-mediated axonal injury. *J. Exp. Med.* 204, 2363–2372. doi: 10.1084/jem.20071053

Monfrini, E., Straniero, L., Bonato, S., Monzio Compagnoni, G., Bordoni, A., Dilena, R., et al. (2019). Neurofascin (NFASC) gene mutation causes autosomal recessive ataxia with demyelinating neuropathy. *Parkinsonism Relat. Disord.* 63, 66–72. doi: 10.1016/j.parkreldis.2019.02.045

Ng, J. K. M., Malotka, J., Kawakami, N., Derfuss, T., Khademi, M., Olsson, T., et al. (2012). Neurofascin as a target for autoantibodies in peripheral neuropathies. *Neurology* 79, 2241–2248. doi: 10.1212/WNL.0b013e31827689ad

Omasits, U., Ahrens, C. H., Müller, S., and Wollscheid, B. (2014). Protter: interactive protein feature visualization and integration with experimental proteomic data. *Bioinformatics* 30, 884–886. doi: 10.1093/bioinformatics/btt607

Pillai, A. M., Thaxton, C., Pribisko, A. L., Cheng, J.-G., Dupree, J. L., and Bhat, M. A. (2009). Spatiotemporal ablation of myelinating glia-specific neurofascin (Nfasc NF155) in mice reveals gradual loss of paranodal axoglial junctions and concomitant disorganization of axonal domains. *J. Neurosci. Res.* 87, 1773–1793. doi: 10.1002/jnr.22015

Porollo, A., and Meller, J. (2007). Versatile annotation and publication quality visualization of protein complexes using POLYVIEW-3D. *BMC Bioinformatics* 8:316. doi: 10.1186/1471-2105-8-316

Roy, A., Kucukural, A., and Zhang, Y. (2010). I-TASSER: a unified platform for automated protein structure and function prediction. *Nat. Protoc.* 5, 725–738. doi: 10.1038/nprot.2010.5

Sherman, D. L., Tait, S., Melrose, S., Johnson, R., Zonta, B., Court, F. A., et al. (2005). Neurofascins are required to establish axonal domains for saltatory conduction. *Neuron* 48, 737–742. doi: 10.1016/j.neuron.2005.10.019

Smigiel, R., Sherman, D. L., Rydzanicz, M., Walczak, A., Mikolajkow, D., Krolak-Olejnik, B., et al. (2018). Homozygous mutation in the Neurofascin gene affecting the glial isoform of Neurofascin causes severe neurodevelopment disorder with hypotonia, amimia and areflexia. *Hum. Mol. Genet.* 27, 3669–3674. doi: 10.1093/hmg/ddy277

Thaxton, C., Pillai, A. M., Pribisko, A. L., Labasque, M., Dupree, J. L., Faivre-Sarrailh, C., et al. (2010). In vivo deletion of immunoglobulin domains 5 and 6 in neurofascin (Nfasc) reveals domain-specific requirements in myelinated axons. *J. Neurosci.* 30, 4868–4876. doi: 10.1523/JNEUROSCI.5951-09.2010

Valk, V., van der Kaaji, R. M., and Dijkhuizen, L. (2017). The evolutionary origin and possible functional roles of FNIII domains in two *Microbacterium aurum* B8.A granular starch degrading enzymes, and in other carbohydrate acting enzymes. *Amylase* 1, 1–11. doi: 10.1515/amylase-2017-0001

Wang, V., Yang, H., Shivalila, C. S., Dawlaty, M. M., Cheng, A. W., Zhang, F., et al. (2013). One-step generation of mice carrying mutations in multiple genes by CRISPR/Cas-mediated genome engineering. *Cell* 153, 910–918. doi: 10.1016/j.cell.2013.04.025

Yamasaki, R. (2013). Anti-neurofascin antibody in combined central and peripheral demyelination. *Clin. Exp. Neuroimmunol.* 4, 68–75. doi: 10.1111/cen3.12061

Conflict of Interest: The authors declare that the research was conducted in the absence of any commercial or financial relationships that could be construed as a potential conflict of interest. The United States Government applied for an international patent (US Patent PCT/US2016/027776) titled, "Methods of treating or preventing demyelination using thrombin inhibitors and methods of detecting demyelination using Neurofascin 155," on April 15, 2016, as the sole beneficiary. RF and DD are listed as inventors in the patent application.

frontiers in Cellular Neuroscience

REVIEW
published: 25 June 2021
doi: 10.3389/fncel.2021.685703

Altered Expression of Ion Channels in White Matter Lesions of Progressive Multiple Sclerosis: What Do We Know About Their Function?

Francesca Boscia[1]*, *Maria Louise Elkjaer*[2,3], *Zsolt Illes*[2,3,4] *and Maria Kukley*[5,6]*

[1] Division of Pharmacology, Department of Neuroscience, Reproductive and Dentistry Sciences, School of Medicine, University of Naples "Federico II", Naples, Italy, [2] Neurology Research Unit, Department of Clinical Research, University of Southern Denmark, Odense, Denmark, [3] Department of Neurobiology Research, Institute of Molecular Medicine, University of Southern Denmark, Odense, Denmark, [4] Department of Neurology, Odense University Hospital, Odense, Denmark, [5] Achucarro Basque Center for Neuroscience, Leioa, Spain, [6] Ikerbasque Basque Foundation for Science, Bilbao, Spain

OPEN ACCESS

Edited by:
Marta Fumagalli,
University of Milan, Italy

Reviewed by:
Elisabetta Coppi,
University of Florence, Italy
Domna Karagogeos,
University of Crete, Greece

***Correspondence:**
Francesca Boscia
boscia@unina.it
Maria Kukley
maria.kukley@achucarro.org

Specialty section:
This article was submitted to Non-Neuronal Cells, a section of the journal Frontiers in Cellular Neuroscience

Received: 13 March 2021
Accepted: 23 May 2021
Published: 25 June 2021

Citation:
Boscia F, Elkjaer ML, Illes Z and Kukley M (2021) Altered Expression of Ion Channels in White Matter Lesions of Progressive Multiple Sclerosis: What Do We Know About Their Function? Front. Cell. Neurosci. 15:685703. doi: 10.3389/fncel.2021.685703

Despite significant advances in our understanding of the pathophysiology of multiple sclerosis (MS), knowledge about contribution of individual ion channels to axonal impairment and remyelination failure in progressive MS remains incomplete. Ion channel families play a fundamental role in maintaining white matter (WM) integrity and in regulating WM activities in axons, interstitial neurons, glia, and vascular cells. Recently, transcriptomic studies have considerably increased insight into the gene expression changes that occur in diverse WM lesions and the gene expression fingerprint of specific WM cells associated with secondary progressive MS. Here, we review the ion channel genes encoding K^+, Ca^{2+}, Na^+, and Cl^- channels; ryanodine receptors; TRP channels; and others that are significantly and uniquely dysregulated in active, chronic active, inactive, remyelinating WM lesions, and normal-appearing WM of secondary progressive MS brain, based on recently published bulk and single-nuclei RNA-sequencing datasets. We discuss the current state of knowledge about the corresponding ion channels and their implication in the MS brain or in experimental models of MS. This comprehensive review suggests that the intense upregulation of voltage-gated Na^+ channel genes in WM lesions with ongoing tissue damage may reflect the imbalance of Na^+ homeostasis that is observed in progressive MS brain, while the upregulation of a large number of voltage-gated K^+ channel genes may be linked to a protective response to limit neuronal excitability. In addition, the altered chloride homeostasis, revealed by the significant downregulation of voltage-gated Cl^- channels in MS lesions, may contribute to an altered inhibitory neurotransmission and increased excitability.

Keywords: multiple sclerosis, progressive, white matter, lesions, ion channels, transcriptome

INTRODUCTION

Multiple sclerosis (MS) is an inflammatory demyelinating disease of the central nervous system (CNS) affecting more than 2 million people worldwide. MS lesions in CNS white matter (WM) are multiple focal areas of myelin loss accompanied by inflammation, gliosis, phagocytic activity, and axonal damage (Compston and Coles, 2008; Kuhlmann et al., 2017; Filippi et al., 2018; Rommer et al., 2019). Available MS therapies have little benefit for secondary-progressive MS (SPMS) patients, who develop progressive disability after a disease course characterized by inflammatory attacks. Therefore, promoting neuroprotection and remyelination are important therapeutic goals to prevent irreversible neurological deficits and permanent disability.

Ion channels play a fundamental role in maintaining WM integrity and regulating function of axons, interstitial neurons (Sedmak and Judas, 2021), glia, and vascular cells. Dysregulation of ionic homeostasis in the WM during demyelination is decisive for axonal damage and cell death and may interfere with tissue repair processes (Boscia et al., 2020). Furthermore, MS may involve an acquired channelopathy (Waxman, 2001; Schattling et al., 2014). Hence, selectively targeting ion channels in WM represents an attractive strategy to overcome axonal and glial impairment and prevent disease progression.

Recently, transcriptomic studies have considerably increased our insight into gene expression changes occurring in the MS brain (Elkjaer et al., 2019; Jakel et al., 2019; Schirmer et al., 2019). Aiming at identifying the ion channel genes governing WM dysfunction in SPMS brain, we analyzed the recent bulk RNA-sequencing (RNA-seq) datasets by using the MS-Atlas (Elkjaer et al., 2019; Frisch et al., 2020). We put a special emphasis on the distribution of shared and unique genes encoding ion channels in chronic active (CA), active (AL), inactive (IL), and remyelinating (RL) lesions, and normal-appearing white matter (NAWM) compared to control WM (**Figures 1A,B**, **Table 1**). We identified uniquely expressed ion channel genes: 34 genes in CA, 9 in IL, 1 in AL, as well as 2 genes in all lesions and NAWM (**Figures 1**, **2**, **Table 1**). The CA lesions displayed the highest number of upregulated ion channels genes while downregulated ion channels genes were more consistently found in ILs (**Figure 1C**). Next, we explored recent single-nuclei RNA-seq (snRNA-seq) datasets to identify the expression of dysregulated ion channel genes in cell clusters in the WM of control and SPMS brain (Jakel et al., 2019; **Tables 1**, **2**, **Figure 3**).

Abbreviations: AIS, axon initial segment; AL, active lesion; AP, action potential; CA, chronic active lesion; Ca^{2+}, calcium; Ca_V, voltage-gated calcium channels; ClC, chloride channels; CNS, central nervous system; COP, committed OPCs; Cx, connexin; EAE, experimental autoimmune encephalomyelitis; EAG, ether-àgo-go; ER, endoplasmic reticulum; GM, gray matter; HC, hemi-channel; IFN-γ, gamma-interferon; IL, inactive lesions; ImOLG, immune oligodendroglia; K2P, two-pore domain K^+ channels; K_{ir}, inward rectifier potassium channel; KO, knockout; K_V, voltage-gated K^+ channels; LPS, lipopolysaccharide; MS, multiple sclerosis; Na^+, sodium; Na_V, voltage-gated sodium channels; NAWM, normal-appearing white matter; NCX, sodium calcium exchanger; OPCs, oligodendrocyte precursor cells; Px, pannexin; RL, remyelinating lesion; RyR, ryanodine receptor; SCI, spinal cord injury; SPMS, secondary progressive multiple sclerosis; TRP, transient receptor potential; WM, white matter.

The goal of the present review is to discuss the current knowledge on the expression and function of ion channels that turned out to be significantly and uniquely dysregulated in WM lesions of SPMS brain. We summarize the information in the context of human MS and the related experimental models (**Tables 1**–**3**, **Figure 4**).

K^+ CHANNELS

Voltage-Gated K^+ Channels (K_v)

K_v channels are composed of four α-subunits that assemble as homo- or hetero-tetramers to form a membrane pore. Forty human genes encode for K_v α-subunits representing 12 families. K_V1–K_v4 (Shaker, Shab, Shaw, and Shal), K_V7 (KCNQ), and K_V10–K_V12 (eag, erg, and elk) α-subunits produce functional channels, while K_v5, K_v6, K_v8, and K_v9 fail to produce currents when expressed alone in heterologous expression system and are considered modulatory subunits for K_v2-subfamily. The diversity of K_v channels is further increased by the ability of α-subunits to combine with auxiliary subunits, which regulate gating properties.

$K_v1.1$, $K_v1.2$, and $K_v1.4$ (KCNA1, KCNA2, and KCNA4)

KCNA genes encode for low-threshold voltage-activated K_v1 ($K_v1.1$–1.8) channels, of which $K_v1.1$–$K_v1.6$ are expressed in the brain (Chittajallu et al., 2002; Vautier et al., 2004; Vacher et al., 2008; Rasmussen and Trimmer, 2019). K_v1 channels display little/no inactivation, resulting in sustained delayed rectifier K^+ currents, with the exception of $K_v1.4$, which underlies transient A-type K^+ current.

Neurons

$K_v1.1$ expression is highest in the brainstem, while $K_v1.4 > K_v1.2$ represent the main K_v1 subunits in the hippocampus (Trimmer, 2015). $K_v1.1$ channels, in association with $K_v1.2$, cluster in the juxtaparanodal regions of axons under the myelin sheath and regulate action potential (AP) propagation and neural excitability (Wang et al., 1993; Trimmer and Rhodes, 2004; Ovsepian et al., 2016). Mutations of K_v1 channels result in hyper-excitability, episodic ataxia, myokymia, and epilepsy (Allen et al., 2020).

Glia

Mouse astrocytes express low levels of $K_v1.1$, $K_v1.2$, and $K_v1.4$ transcripts (Smart et al., 1997), but $K_v1.2$ and $K_v1.4$ expression is high in reactive rat astrocytes (Akhtar et al., 1999). $K_v1.1$ transcripts and proteins are highly expressed in C6 glioma cells. Rodent oligodendrocyte precursor cells (OPCs) express $K_v1.1$, $K_v1.2$, and $K_v1.4$ transcripts (Attali et al., 1997; Chittajallu et al., 2002; Falcao et al., 2018; Batiuk et al., 2020) but only $K_v1.4$ and low level of $K_v1.2$ proteins (Attali et al., 1997; Schmidt et al., 1999). In OPCs and astrocytes, the K_v1 subunits regulate cell growth and cell cycle progression, e.g., $K_v1.4$ overexpression *in vitro* increases OPCs proliferation (Schmidt et al., 1999) while deletion decreases it (Gonzalez-Alvarado et al., 2020). Recent RNA-seq did not detect $K_v1.1$, $K_v1.2$, and $K_v1.4$ in mouse microglia (Hammond et al., 2019), but earlier studies found $K_v1.1$ and $K_v1.2$ mRNAs and/or proteins in BV2 microglia,

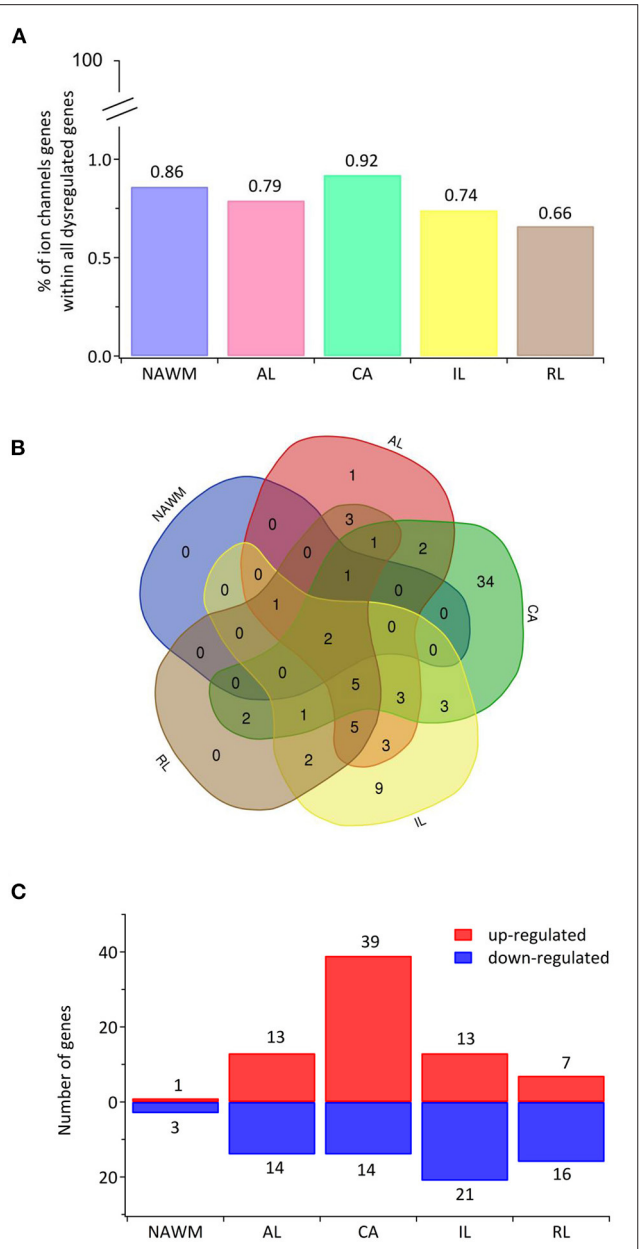

FIGURE 1 | The transcriptional landscape of ion channels in different types of white matter brain lesions from patients with secondary progressive multiple sclerosis. **(A)** The percentage of significantly differentially expressed genes coding for ion channels among all dysregulated genes and within each lesion type [chronic active (CA), active (AL), inactive (IL), and remyelinating (RL)] and normal-appearing white matter (NAWM) compared to control white matter are indicated. **(B)** The Venn diagram shows the number of lesion-specific differentially expressed genes coding for ion channels and the number of overlapping genes among the lesion types. **(C)** The number of significantly differentially upregulated (red) and downregulated (blue) genes in each type of while matter lesion and NAWM compared to control white matter are indicated.

rat cultured microglia, and amoeboid microglia within corpus callosum during development, but barely in resting microglia by P21 (Fordyce et al., 2005; Li F. et al., 2008; Wu et al., 2009). In microglia, $K_v1.1$ and $K_v1.2$ expression was linked to cell activation (Eder, 1998), and their upregulation induced by lipopolysaccharide (LPS), ATP, or hypoxia is involved in the release of pro-inflammatory cytokines and intracellular production of reactive oxygen species (ROS) and nitric oxide (NO) (Li F. et al., 2008; Wu et al., 2009).

Expression and Function in MS

Bulk RNA-seq found upregulation of $K_v1.1$, $K_v1.2$, and Kv1.4 transcripts in CA lesions (**Figure 2**, **Table 1**; Elkjaer et al., 2019; Frisch et al., 2020). The snRNA-seq detected significant $K_v1.2$ expression in neuronal clusters, slight increase of $K_v1.4$ transcripts in neuronal but not glial clusters, and no $K_v1.1$ transcript (**Tables 1**, **2**; Jakel et al., 2019).

The CA lesion is characterized by ongoing tissue damage and, functionally, $K_v1.2$ upregulation in CA lesions may be a hallmark of axonal damage. While recent data found that *KCNA1* gene is downregulated during demyelination in the cuprizone model (Martin et al., 2018), in animal models of MS, $K_v1.2$ (and also $K_v1.1$) ectopically redistributes to nodes and internodes of WM axons (McDonald and Sears, 1969; Wang et al., 1995; Sinha et al., 2006; Jukkola et al., 2012; Zoupi et al., 2013; Kastriti et al., 2015), while in human MS, the dislocation of $K_v1.2$ channels is associated with paranodal pathology, particularly in NAWM regions, and contributes to axonal dysfunction (Howell et al., 2010; Gallego-Delgado et al., 2020). The upregulated and redistributed $K_v1.2$ and $K_v1.1$ channels may hyperpolarize the axonal resting membrane potential (V_{rest}), elevate the amount of depolarization necessary for AP initiation, and impair AP conduction (Wang et al., 1995; Sinha et al., 2006; Jukkola et al., 2012). Pharmacological inhibition of $K_v1.1$ and $K_v1.2$ channels, e.g., with 4-aminopyridine, enhances axonal conduction and improves MS symptoms (Lugaresi, 2015).

It is difficult to speculate regarding $K_v1.4$ function in MS because data are not consistent. In animal models of MS and spinal cord injury (SCI), this developmentally restricted subunit re-appears/increases in OPCs, OLs, and astrocytic processes around lesion sites (Herrero-Herranz et al., 2007; Jukkola et al., 2012), but not in WM axons or microglia (Edwards et al., 2002; Jukkola et al., 2012). Mice lacking $K_v1.4$ exhibit reduced myelin loss in the spinal cord WM during EAE but no change of demyelination/remyelination in the corpus callosum in the cuprizone model (Gonzalez-Alvarado et al., 2020). However, it is unclear whether function of $K_v1.4$ subunits is relevant for glial cells in human MS because snRNA-seq barely detected $K_v1.4$ transcripts in glia clusters (**Table 2**).

Kv2.1 and Kv2.2 (KCNB1 and KCNB2)

K_v2 channels (encoded by *KCNB1* and *KCNB2* genes) mediate high-voltage-activated slowly inactivating delayed rectifier K^+ currents (Guan et al., 2007). $K_v2.1$ channels can assemble with electrically silent K_vS subunits, resulting in greater variability of K_v2 currents (Trimmer, 2015; Johnson et al., 2019).

Neurons

High-density clusters of $K_v2.1$ and $K_v2.2$ localize to soma, proximal dendrites, and axonal initial segment (AIS). K_v2

TABLE 1 | Expression and distribution of unique and overlapping genes coding for ion channels within SPMS lesions.

Protein	Gene	Bulk lesion[a]	Fold change Up (+)/down (–) regulated (compared to control WM)[a]	Current type/ conductance	Highly expressed in WM clusters of human brain[b]
K^+ channels					
K_v 1.1	KCNA1	CA	**+1.42**	Delayed rectifier	
K_v 1.2	KCNA2	CA	**+1.06**	Delayed rectifier	neuron2
K_v 1.3	KCNA3	AL, CA, IL	**+1.67 (AL); +1.35 (CA); +1.34 (IL)**	Delayed rectifier	
K_v 1.4	KCNA4	CA	**+1.34**	A-type	
K_v 1.5	KCNA5	AL, RL	**+0.86 (AL); +1.36 (RL)**	Delayed rectifier	
K_v 2.2	KCNB2	CA	**+1.56**	Delayed rectifier	Neuron1, 2, 3, 4, 5
K_v 2.1	KCNB1	CA	**+1.26**	Delayed rectifier	Neuron1, 2, 3
K_v 3.3	KCNC3	CA	**+0.87**	A-type	
K_v 3.4	KCNC4	AL, IL	**+0.81 (AL); +0.72 (IL)**	A-type	
K_v 4.2	KCND2	CA	**+0.95**	A-type	OPC, COP, neuron1,3
K_v 4.3	KCND3	AL, CA, IL	**+0.63 (AL); +0.86 (CA); +0.93 (IL)**	A-type	neuron1, 2, 3
K_v 6.1	KCNG1	AL, RL	**+2.72 (AL); +3.7 (RL)**	Modifier of Kv 2	
K_v 7.1	KCNQ1	AL, CA	**+0.91 (AL); +0.75 (CA)**	M-type	
K_v 7.2	KCNQ2	CA	**+0.75**	M-type	neuron1, 2
K_v 7.3	KCNQ3	CA	**+0.85**	M-type	ImOLGs, neuron1, 2, 3, 5, microglia/ macrophages
K_v 7.4	KCNQ4	AL, CA, IL, RL	**+1.19 (AL);+ 0.92 (CA); +1.36 (IL); +2.22 (RL)**	M-type	
K_v 7.5	KCNQ5	CA	**+1.69**	M-type	Neuron1, 2, 3, 5
K_v 8.1	KCNV1	CA	**+1.48**	Modifier of Kv 2	
K_v 9.2	KCNS2	CA	**+0.90**	Modifier of Kv 2	
K_v 9.3	KCNS3	AL, IL, RL, NAWM	−2.72 (AL); −1.5 (IL); −1.98 (RL); −0.71 (NAWM)	Modifier of Kv 2	
K_v 10.1/EAG1	KCNH1	CA, IL	**+0.81 (CA); +0.93 (IL)**	Delayed rectifier	Neuron1, 2, 3
K_v 10. 2/EAG2	KCNH5	CA	**+1.38**	Delayed rectifier	Neuron2
K_v 11.3/ERG3	KCNH7	CA	**+1.38**	Delayed rectifier	Neuron1, 2, 3, 5
K_v 12.1/ELK1	KCNH8	AL, CA, IL, RL, NAWM	−1.25 (AL); −1.4(CA); −2.05 (IL); −2.38 (RL); −0.62 (NAWM)	Delayed rectifier	Oligo3, Oligo4, Oligo6
TREK1	KCNK2	CA	**+1.03**	Leak, two pore	
TWIK2	KCNK6	AL, IL	**+1.57 (AL); +0.82 (IL)**	Leak, two pore	
TREK2	KCNK10	AL	−0.65	Leak, two pore	
K_{Ca}1.1	KCNMA1	AL, CA, IL	**+0.69 (AL); +0.87 (CA); +0.7 (IL)**	Calcium-Activated	OPC, neuron1, 2, 3, 5, microglia/macrophages
K_{Ca}2.3	KCNN3	IL	−0.7	Calcium-Activated	Astrocytes1
K_{Na}1.1	KCNT1	CA	**+1.24**	Sodium-Activated	
K_{Na}1.2	KCNT2	CA, IL	**+0.92 (CA); +1.15 (IL)**	Sodium-Activated	Neuron1, 2, 3, pericytes, vascular smooth cells
K_{ir}2.1	KCNJ2	AL, CA, IL, RL	−0.54 (AL); −0.48 (CA); −0.54 (IL); −0.92 (RL)	Inward rectifier	
K_{ir}3.4	KCNJ5	AL, CA, RL, NAWM	**+2.58 (AL); +1.56 (CA); +1.9 (RL); +1.53 (NAWM)**	Inward rectifier	
K_{ir}3.2	KCNJ6	CA	**+1.34**	Inward rectifier	Neuron1, 2, 3
K_{ir}6.1	KCNJ8	AL, IL	**+0.74 (AL); +0.71 (IL)**	Inward rectifier	
K_{ir}3.3	KCNJ9	CA, RL	−0.52 (CA); −0.9 (RL)	Inward rectifier	
K_{ir}4.1	KCNJ10	IL, RL	−1.06 (IL); −1.09 (RL)	Inward rectifier	Oligo5
K_{ir}5.1	KCNJ16	CA	**+1.27**	Inward rectifier	
Na^+ channels					
Na_v1.1	SCN1A	CA	**+1.12**	TTX-sensitive	OPC, COP, neuron1, 2, 3, 4, 5

(Continued)

TABLE 1 | Continued

Protein	Gene	Bulk lesion[a]	Fold change Up (+)/down (–) regulated (compared to control WM)[a]	Current type/ conductance	Highly expressed in WM clusters of human brain[b]
$Na_v1.2$	SCN2A	CA	**+1.1**	TTX-sensitive	Neuron1, 2, 3, 4, 5
$Na_v1.3$	SCN3A	CA	**+0.87**	TTX-sensitive	OPC, neuron1, 2, 3, 5
$Na_v1.6$	SCN8A	CA	**+1.15**	TTX-sensitive	Neuron1, 2, 3, 5
$Na_v1.9$	SCN11A	IL	−1.16	TTX-resistant	
Ca^{2+} channels					
$Ca_v1.2$	CACNA1C	CA	**+0.56**	L-type	Neuron1, 2, 3, 5, pericytes
$Ca_v1.3$	CACNA1D	CA	**+0.57**	L-type	Neuron1,3
$Ca_v2.1$	CACNA1A	CA	**+0.64**	P/Q-type	OPC, neuron1, 2
$Ca_v2.3$	CACNA1E	CA	**+0.97**	P/Q-type	Neuron1, 2, 5
$Ca_v3.1$	CACNA1G	IL	**+1.8**	T-type	
$Ca_v3.2$	CACNA1H	CA	**+1.12**	T-type	
$Ca_v3.3$	CACNA1I	CA	**+1.03**	T-type	
Ryanodine					
Ryr2	RYR2	CA	**+0.85**	Ca^{2+} Release channel	Neuron1, 2, 3
Ryr3	RYR3	IL	−0.76	Ca^{2+} Release channel	Astrocytes1
TRP channels					
TRPC1	TRPC1	AL, IL, RL	−0.5 (AL); −0.48 (IL); −0.85 (RL)	Ca^{2+}-permeable cation channel	
TRPM2	TRPM2	IL	**+0.92**	Ca^{2+}-permeable cation channel	
TRPM3	TRPM3	IL, RL	−1.09 (IL); −0.98 (RL)	Ca^{2+}-permeable cation channel	Astrocytes1, neuron1
TRPM6	TRPM6	CA, IL, RL	−0.99 (CA); −1.06 (IL); −1.08 (RL)	Ca^{2+}-permeable cation channel	
TRPP1	PKD2	IL	−0.48	Ca^{2+}-permeable cation channel	
TRPP3	PKD2L2	CA	−0.58	Ca^{2+}-permeable cation channel	
TRPV1	TRPV1	CA	−1.04	Ca^{2+}-permeable cation channel	
TRPV3	TRPV3	AL, CA, IL, RL	−0.51 (AL); −0.72 (CA); −0.5 (IL); −0.74 (RL)	Ca^{2+}-permeable cation channel	
TRPV5	TRPV5	AL, CA, IL, RL	−1.4 (AL); −1.67 (CA); −1.72 (IL); −2.02 (RL)	Ca^{2+}-permeable cation channel	
TRPV6	TRPV6	AL, CA, IL, RL, NAWM	−1.77 (AL); −1.97 (IL); −1.32 (CA); −2.23 (RL); 0.86 (NAWM)	Ca^{2+}-permeable cation channel	
Cl^- channels					
CLC-2	CLCN2	CA	−0.57	Inward rectification	
CLC-4	CLCN4	AL, IL, RL	−0.79 (AL); −0.73 (IL); −1.03 (RL)	Cl^-/H^+ antiporter	
CLC-7	CLCN7	CA	−0.72	Cl^-/H^+ antiporter	
Connexins and pannexins					
Cx43	GJA1	AL, CA, RL	**+1.53 (AL); +1.12 (CA); +1.19 (RL)**	Monovalent and divalent ions	Astrocytes1, astrocytes2
Cx32	GJB1	AL, CA, IL, RL	−1.6 (AL); −1.5 (CA); −1.85 (IL); −2.44 (RL)	Monovalent and divalent ions	Oligo5
CX37	GJA4	IL	**+1.19**	Monovalent and divalent ions	Pericytes
Cx47	GJC2	AL, CA	−1.62 (AL); −1.74 (CA)	Monovalent and divalent ions	

(Continued)

TABLE 1 | Continued

Protein	Gene	Bulk lesion[a]	Fold change Up (+)/down (–) regulated (compared to control WM)[a]	Current type/ conductance	Highly expressed in WM clusters of human brain[b]
Panx1	PX1	IL	**+0.56**	Monovalent and divalent ions	
Others					
Piezo2	PIEZO2	AL, CA, IL, RL	−0.92 (AL); −1.01 (CA); −0.93 (IL); −1.49 (RL)	Ca^{2+} -permeable	Oligo1, Oligo6
CFTR	CFTR	AL, CA, IL, RL	−1.22 (AL); −1.37 (CA); −1.77 (IL); −1.86 (RL)	Cl^--permeable	Oligo1
H_v1	HVCN1	CA, RL	**+0.71 (CA); +0.92 (RL)**	H^+-selective	
$Na_vi2.1$	NALCN	AL, IL, RL	−0.49 (AL); −0.73 (IL); −0.88 (RL)	Sodium leak channel, non-selective	
Orai3	ORAI3	AL, RL	**+0.87 (AL); +1.25 (RL)**	Store-Operated Ca^{2+} entry	
Aquaporin 1	AQP1	CA, IL	−1.03 (CA); −0.12 (IL)	Water, ammonia, H_20_2 permeability	Astrocytes1, astrocytes2
CATSPERG	CATSPERG	CA	**+0.7**	Ca^{2+} -permeable	
CATSPERE	CATSPERE	IL	−0.48	Ca^{2+} -permeable	

[a] *Expression and distribution of unique and overlapping genes coding for ion channels within chronic active (CA), active (AL), inactive (IL) remyelinating (RL) lesions, and normal-appearing white matter (NAWM). The information is based on the bulk-RNAseq (Elkjaer et al., 2019) and data are collected from the database available at www.msatlas.dk (Frisch et al., 2020).*
[b] *Cell type-specific clusters with significant expression of ion channels genes in human brain WM. The information is based on the snRNAseq from the WM of individuals with SPMS and non-neurological control subjects (Jakel et al., 2019), and data are collected from the database available at https://ki.se/mbb/oligointernodeen/ where the encoded subunits were listed according to the IUPHAR nomenclature. Fold changes of up-regulated genes are shown in bold.*

channels influence AP duration during high-frequency firing and regulate neuronal excitability (Guan et al., 2007). $K_v2.1$ mutations are associated with neonatal encephalopathy epilepsies and neurodevelopmental delays (Torkamani et al., 2014; Thiffault et al., 2015; de Kovel et al., 2017).

Glia

RNA-seq detected *KCNB1* gene in mouse OPC and microglia (Falcao et al., 2018; Hammond et al., 2019).

Expression and Function in MS

Bulk RNA-seq revealed upregulation of $K_v2.1$ and $K_v2.2$ transcripts in CA lesions of SPMS brain (**Figure 2**, **Table 1**; Elkjaer et al., 2019; Frisch et al., 2020), while snRNA-seq found $K_v2.1$ and $K_v2.2$ in neuronal clusters (**Tables 1**, **2**; Jakel et al., 2019). During EAE, $K_v2.1$ protein expression was downregulated in spinal cord motor neurons (Jukkola and Gu, 2015). Remarkably, $K_v2.1$ channels exist as freely dispersed conducting channels, or form electrically silent somatodendritic clusters (Schulien et al., 2020). Upregulated clustered $K_v2.1$ channels promote functional coupling of L-type Ca^{2+} channels in plasma membrane to ryanodine receptors (RyRs) of the endoplasmic reticulum (ER) (Deutsch et al., 2012; Kirmiz et al., 2018; Vierra et al., 2019) and may modulate intracellular Ca^{2+} level contributing to cell damage, while dispersal of $K_v2.1$-clusters blocks apoptogenic K^+ currents and provides neuroprotection (Sesti et al., 2014; Justice et al., 2017). Hence, to elucidate the functional role of K_v2 upregulation in MS (**Table 1**), it will be important to determine whether it reflects an increase in clustered or dispersed K_v2 channels.

$K_v3.3$ (KCNC3)

The *KCNC3* gene encodes for the $K_v3.3$ subunit, which, together with $K_v3.1$, $K_v3.2$, and $K_v3.4$, belongs to the K_v3 channel subfamily (Shaw). The $K_v3.3$ and $K_v3.4$ mediate transient A-type K^+ currents, while $K_v3.1$ and $K_v3.2$ mediate sustained K^+ currents.

Neurons

K_v3 channels localize to axonal and somatodendritic domains, and play a critical role in regulating AP firing at high frequency (Rasmussen and Trimmer, 2019). *KCNC3* mutations result in spinocerebellar ataxia type-13 and cerebellar neurodegeneration (Rasmussen and Trimmer, 2019).

Glia

Cortical and hippocampal astrocyte cultures express $K_v3.3$ and $K_v3.4$ mRNAs and proteins (Bekar et al., 2005; Boscia et al., 2017). *KCNC3* mRNA was detected in mouse OPCs and microglia (Larson et al., 2016; Falcao et al., 2018).

Expression and Function in MS

Bulk RNA-seq showed significant $K_v3.3$ upregulation in CA lesions (**Figure 2**, **Table 1**), while snRNA-seq revealed its predominant distribution in neuronal clusters (**Table 2**; Jakel et al., 2019). $K_v3.3$ may play a detrimental role in MS because it increases in injured WM axons during EAE progression in mice and in human MS lesions (Jukkola et al., 2017), and the deletion of $K_v3.1$, which forms hetero-tetramers with $K_v3.3$, reduced EAE severity in mice (Jukkola et al., 2017).

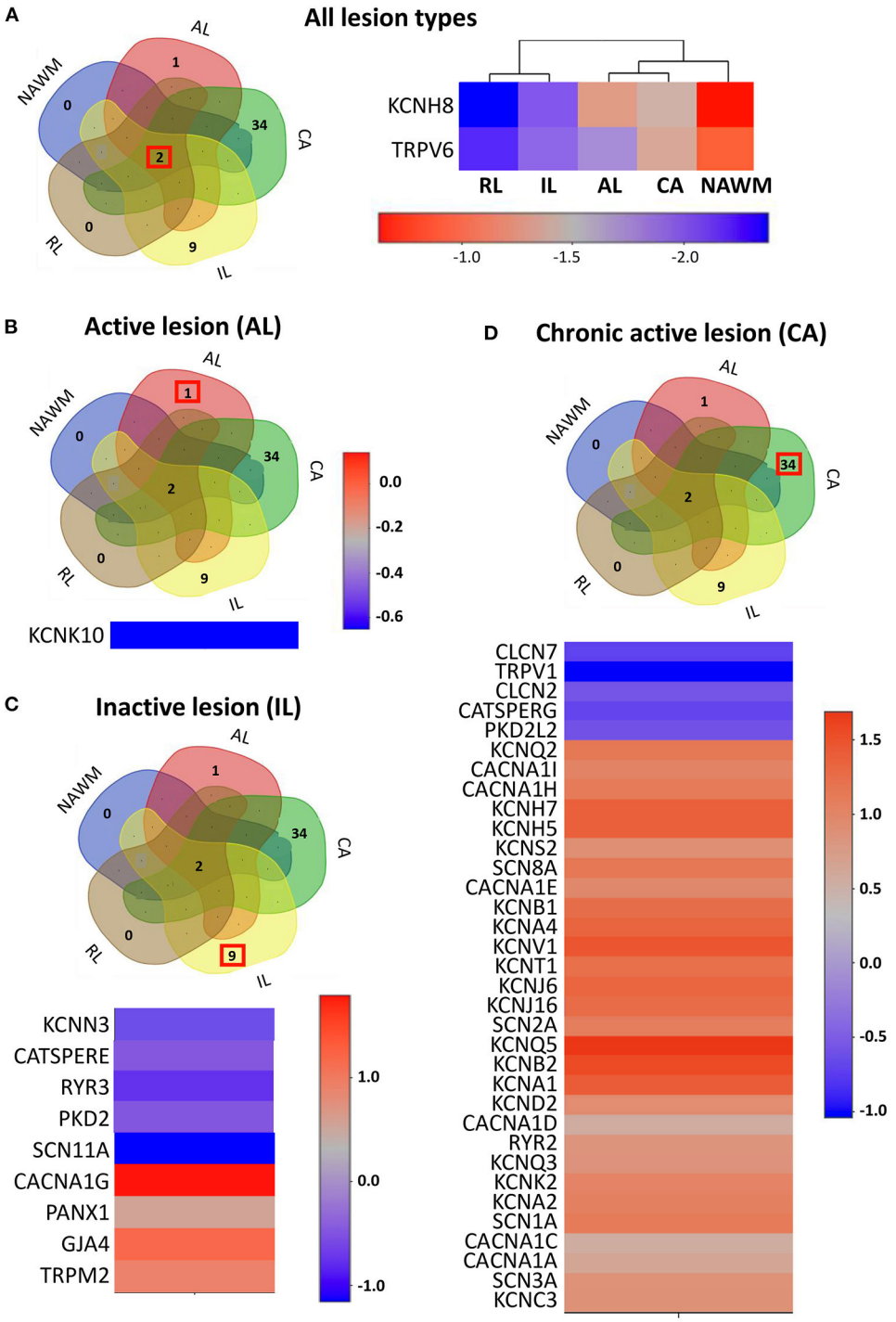

FIGURE 2 | The expression profile of the ion channel genes uniquely expressed in different lesion types. **(A)** Left panel: The Venn diagram represents the number of overlapping and lesion-specific differentially expressed genes coding for ion channels in chronic active (CA), active (AL), inactive (IL), and remyelinating (RL) lesions and in normal-appearing white matter (NAWM) compared to control white matter. Right panel: The heatmap shows two genes, coding for ion channels KCNH8 and TRPV6 that are significantly altered in all lesion types compared to control white matter. Scale bar indicates fold changes. **(B)** The Venn diagram, the heatmap, and the scale bar show the single ion channel gene, KCNK10, which is uniquely downregulated in active lesion (AL). **(C)** The Venn diagram, the heatmap, and the scale bar show the eight genes coding for ion channels that are uniquely significantly differentially dysregulated in inactive lesion (IL). **(D)** The Venn diagram, the heatmap, and the scale bar show the 33 genes coding for ion channels that are significantly and differentially dysregulated compared to control white matter in chronic active lesion (CA). The red box in Venn diagrams marks the genes that are specifically dysregulated in the corresponding type of lesion.

TABLE 2 | Profiling expression of unique gene in lesions in WM clusters of healthy and SPMS brain[a].

Protein	Gene	Neuron	Astrocyte	OPC	COP	ImOLG	Oligo	Microglia	Pericyte
K^+ channels									
Kv1.1	KCNA1	n.d	n.d	n.d	n.d	n.d	n.d	n.d	n.d
Kv1.2	KCNA2	+	+/–	+/–	+/–	–	+/–	–	–
Kv1.4	KCNA4	+/–	–	–	–	–	–	–	–
Kv2.1	KCNB1	+	+/–	+/–	+	+/–	+/–	–	+
Kv2.2	KCNB2	++	+/–	–	+/–	+/–	+/–	–	–
Kv3.3	KCNC3	+	+/–	–	+/–	+/–	+/–	+/–	–
Kv4.2	KCND2	+++	+	++++	+++	+	+/–	+/–	+/–
Kv7.2	KCNQ2	+	+/–	+	+	+/–	+/–	–	+/–
Kv7.3	KCNQ3	+++	+	+	+	++	+/–	+++	+/–
Kv7.5	KCNQ5	++++	+	+/–	+	+	+/–	+/–	+/–
Kv8.1	KCNV1	+	–	–	+/–	+/–	–	–	–
Kv9.2	KCNS2	+	–	–	+/–	–	–	–	–
Kv10. 2/EAG2	KCNH5	+	+/–	+/–	+	+/–	+/–	–	–
Kv11.3/ERG3	KCNH7	+++	+/–	–	+	+	+/–	–	–
Kv12.1/ELK1	KCNH8	+	+++	++	+++	++	+++	+/–	+/–
TREK1	KCNK2	+	+/–	+	+/–	–	–	–	–
TREK2	KCNK10	+	+/–	+/–	+	+/–	+/–	–	–
$K_{Ca}2.3$	KCNN3	+	++	+	+	+	+/–	+/–	+/–
KNa1.1	KCNT1	+	–	–	+/–	+/–	–	–	–
Kir3.2	KCNJ6	+	+/–	+	+	–	+	–	–
Kir5.1	KCNJ16	–	+/–	+	+	–	–	–	–
Na^+ channels									
Nav1.1	SCN1A	++	+	+++	++	+	+/–	–	–
Nav1.2	SCN2A	+++	+	+/–	+	+	+/–	–	+/–
Nav1.3	SCN3A	++	+/–	++	++	+	+	–	+/–
Nav1.6	SCN8A	n.d	n.d	n.d	n.d	n.d	n.d	n.d	n.d
Nav1.9	SCN11A	n.d	n.d	n.d	n.d	n.d	n.d	n.d	n.d
Ca^{2+} channels									
Cav1.2	CACNA1C	+++	+	+	+	+	+/–	–	+++
Cav1.3	CACNA1D	++	+/–	+	+	+	+/–	+	–
Cav2.1	CACNA1A	+++	+	+++	++	+	+/–	+	+/–
Cav2.3	CACNA1E	++	+/–	+/–	+	+	+/–	–	–
Cav3.1	CACNA1G	+	–	+/–	+/–	–	–	–	–
Cav3.2	CACNA1H	n.d	n.d	n.d	n.d	n.d	n.d	n.d	n.d
Cav3.3	CACNA1I	+	–	–	+/–	–	–	–	–
Ryanodine									
Ryr2	RYR2	++++	+	+/–	+	+	+	+/–	+
Ryr3	RYR3	+	+++	+	+	+	+/–	+/–	+/–
TRP channels									
TRPM2	TRPM2	+	+/–	–	+/–	+	–	+	+/–
TRPP1	PKD2	+	++	+	++	++	+	+	+
TRPP3	PKD2L2	n.d	n.d	n.d	n.d	n.d	n.d	n.d	n.d
TRPV1	TRPV1	+/–	+/–	–	+/–	–	+/–	–	–
TRPV6	TRPV6	n.d	n.d	n.d	n.d	n.d	n.d	n.d	n.d
Cl^- channels									
CLC–2	CLCN2	+/–	+/–	+/–	+/–	+/–	+	–	–
CLC–7	CLCN7	+	+	+	+	+	+	+	+/–
Connexins									
Cx37	GJA4	–	–	–	–	–	–	–	++

(Continued)

TABLE 2 | Continued

Protein	Gene	Neuron	Astrocyte	OPC	COP	ImOLG	Oligo	Microglia	Pericyte
Pannexin									
Px1	PANX1	n.d	n.d	n.d	n.d	n.d	n.d	n.d	n.d
Catsper									
CATSPERG	CATSPERG	+/–	+/–	–	+/–	+/–	+/–	–	–
CATSPERE	CATSPERE	n.d	n.d	n.d	n.d	n.d	n.d	n.d	n.d

[a]*sn-RNAseq from the white matter of individuals with SPMS and non-neurological controls. The information is based on the snRNAseq from the WM of individuals with SPMS and non-neurological control subjects (Jakel et al., 2019), and data are collected from the database available at https://ki.se/mbb/oligointernodeen/. Expression levels are based on the mean normalized expression counts (log-scale) per cluster.*

+/– (log scale > 0.01 ≤ 0.1); + (log scale > 0.1 ≤ 0.5); ++ (log scale > 0.6 ≤ 1); + + + (log scale >1.1≤ 1.5); + + ++ (log scale > 1.5); – (log scale 0); n.d., not detected; red (+), highly expressed gene in the cluster if compared to the rest of the clusters.

Note, that in the database, some of the clusters encompass both control and MS samples and, therefore, the mean can represent a combination of counts from control and MS brain.

Kv4.2 (KCND2)

The *KCND2* gene encodes for the $K_v4.2$ subunit that (together with $K_v4.1$ and $K_v4.3$) is a member of the K_v4 channel subfamily (Shal) and is highly expressed in the brain (Alfaro-Ruiz et al., 2019). K_v4 channels activate at subthreshold potentials and then inactivate and recover rapidly. They mediate transient A-type K^+ current (Bahring et al., 2001; Birnbaum et al., 2004).

Neurons

$K_v4.2$ subunits are highly expressed in soma and dendrites of hippocampal neurons and interneurons. They regulate the threshold for AP initiation and repolarization, frequency-dependent AP broadening, and AP back-propagation (Nerbonne et al., 2008). $K_v4.2$ mutations are associated with infant-onset epilepsy and autism.

Glia

$K_v4.2$-transcripts were found in mouse astrocytes (Bekar et al., 2005) and OPCs, but only at very low levels in microglia (Falcao et al., 2018; Hammond et al., 2019; Batiuk et al., 2020).

Expression and Function in MS

Bulk RNA-seq found significant $K_v4.2$ upregulation in CA lesions (**Figure 2**, **Table 1**; Elkjaer et al., 2019; Frisch et al., 2020). The snRNA-seq reported significant expression of $K_v4.2$ transcripts in neuronal, OPCs, and committed OPCs (COP) clusters (**Table 2**; Jakel et al., 2019). $K_v4.2$ subunit may contribute to oligodendrocyte dysfunction in SPMS brain because dysregulated *KCND2* transcripts are associated with oligodendrocyte dysfunction in mental illnesses (Vasistha et al., 2019).

$K_v7.2$, $K_v7.3$, and $K_v7.5$ (KCNQ2, KCNQ3, and KCNQ5)

The *KCNQ* genes encode for $K_v7.1$–$K_v7.5$ (*KCNQ1–KCNQ5*) family members that underlie a voltage-gated non-inactivating outward K^+ current, known as M current (I_M).

Neurons

The $K_v7.2/3$ or $K_v7.3/5$ hetero-tetramers represent the dominant subunit composition in neurons (Wang et al., 1998; Cooper et al., 2000; Kharkovets et al., 2000), while $K_v7.4/K_v7.5$ is dominant in vascular smooth muscles (Brueggemann et al., 2014). The $K_v7.2$- and $K_v7.3$ subunits co-cluster with Na_v channels at AIS and nodes of Ranvier in rodent somatosensory cortex and spinal cord WM and gray matter (GM) (Pan et al., 2006; Cooper, 2011; Battefeld et al., 2014). $K_v7.5$ localizes to soma and dendrites of cortical and hippocampal neurons and contributes to afterhyperpolarization currents (Tzingounis et al., 2010). The K_v7 channels stabilize V_{rest}, influence neuronal subthreshold excitability, and regulate spike generation (Jentsch, 2000; Miceli et al., 2008). By reducing the steady-state inactivation of nodal Na_v channels, the K_v7 channels increase the availability of transient Na_v currents at nodes of Ranvier, thereby accelerating the AP upstroke and elevating short-term axonal excitability (Hamada and Kole, 2015). In the perisomatic region, K_v7 channels counteract the persistent Na_v current and restrain repetitive firing (Pan et al., 2006; Cooper, 2011). Variants of *KCNQ2/KCNQ3* or *KCNQ4* genes cause developmental/epileptic disorders and hearing loss (Soldovieri et al., 2011; Miceli et al., 2013).

Glia

KCNQ3 gene is expressed in spinal cord WM astrocytes (Devaux et al., 2004), while *KCNQ5* is expressed in rat retinal astrocytes (Caminos et al., 2015). The *KCNQ2-5* mRNAs and proteins were detected in rat cortical OPCs and microglia cultures, while differentiated oligodendrocytes showed weak *KCNQ4* expression (Wang et al., 2011; Vay et al., 2020).

Expression and Function in MS

Bulk RNA-seq found upregulation of *KCNQ2-3-5* transcripts in CA lesions (**Figure 2**, **Table 1**; Elkjaer et al., 2019; Frisch et al., 2020). The snRNA-seq reported *KCNQ2-3-5* expression in neuronal clusters and *KCNQ3* expression in immune oligodendroglia (ImOLG) and microglia/macrophages clusters (**Tables 1**, **2**; Jakel et al., 2019). $K_v7.3$ upregulation may reflect increased necessity of the channels along the axons because $K_v7.3$ subunit extensively redistributes to internodes of acutely and chronically demyelinated GM axons in the cuprizone model (Hamada and Kole, 2015). It is tempting to speculate that K_v7 upregulation may be beneficial during MS. First, K_v7 channels may increase the availability of transient Na_v current *via* membrane hyperpolarization supporting AP conduction in demyelinated axons (Battefeld et al., 2014).

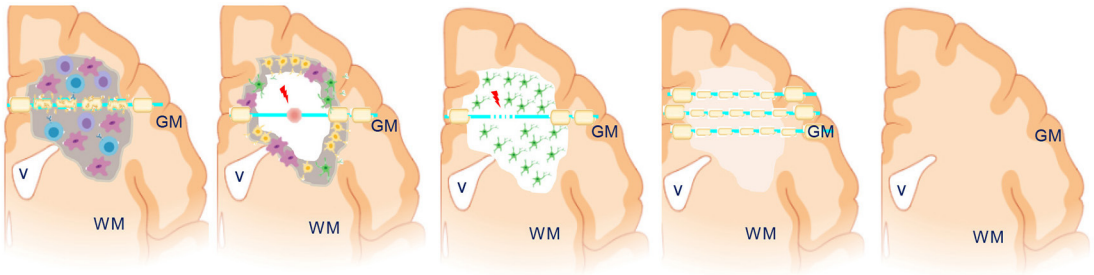

Lesion features	Active	Chronic Active	Inactive	Remyelinating	NAWM
	• inflammation • demyelination • axonal damage • glia activation • phagocytic activity	• demyelination • axonal damage • hypocellularity in the core • microglia/macrophages, OPCs, and astrocytes accumulation in the rim • remyelination failure	• demyelination • hypocellularity • axonal damage • glia scar • angiogenesis • remyelination failure	• OPC proliferation • OPC differentiation • axonal remyelination	• axonal abnormalities • myelin abnormalities • microglia activation
Clusters					
Neuronal		Kv1.1, Kv1.2, Kv1.4, Kv2.1, Kv2.2, Kv3.3, Kv4.2, KCNQ2, KCNQ3, KCNQ5, KCNV1, KCNS2, EAG2, ERG3,TREK1, KNa1.1, Kir3.2, Nav1.1, Nav1.2 , Nav1.3, Nav1.6, Cav1.2, Cav2.1, Cav2.3, Cav1.3, Cav3.2, Cav3.3, RYR2	Cav3.1 TRPM2		
OPC		Kv4.2, Kir5.1, TREK1, Nav1.1, Nav1.3, Cav2.1			
COP		Kv4.2, Nav1.1			
Oligo	ELK1	ELK1	ELK1	ELK1	ELK1
Microglia		KCNQ3	TRPM2		
ImOLG		KCNQ3	TRPM2		
Astrocyte			KCa2.3, RYR3		
Pericyte		Cav1.2	Cx37		
Unknown	TREK2, TRPV6	TRPV1, TRPV6, PKD2L2, CLC-2, CLC-7, CATSPERG	Px1, Nav1.9, TRPV6, PKD2, CATSPERE	TRPV6	TRPV6

FIGURE 3 | Distribution of uniquely dysregulated genes encoding ion channels in SPMS lesions. Schematic representation of active (AL), chronic active (CA), inactive (IL), and remyelinating (RL) lesions, and normal-appearing white matter (NAWM). Upregulated (blue) and downregulated (red) ion channels encoded by uniquely dysregulated genes are listed according to their expression in the lesions and in neuronal, oligodendrocyte precursor cells (OPCs), committed OPCs (COPs), oligodendrocytes (Oligo), microglia, immune oligo (ImOLG), astrocyte, pericyte, and unknown clusters. GM, gray matter; WM, white matter; v, brain ventricle. Gray areas indicate active inflammatory lesion, white areas indicate demyelinated inactive lesions, red spot indicates tissue damage, red arrow indicates axonal dysfunction. Source icon is from Biorender.com.

Second, K_v7 channels may mitigate inflammation-induced neuronal excitability because, following LPS exposure, the I_M inhibition underlies hyperexcitability of hippocampal neurons that is reversed by a nonselective K_v7-opener retigabine (Tzour et al., 2017). Although retigabine also exerts neuroprotective effects in several neurodegenerative conditions (Boscia et al., 2006; Nodera et al., 2011; Wainger et al., 2014; Bierbower et al., 2015; Li et al., 2019; Vigil et al., 2020; Wu et al., 2020), a clinical trial with retigabine analog flupirtine failed to demonstrate neuroprotective effects during MS (Dorr et al., 2018). Furthermore, blockade of K_v7 channels with XE-991 inhibited migration of LPS-treated pro-inflammatory microglia *in vitro* (Vay et al., 2020), suggesting that these channels may promote the pro-inflammatory role of microglia also during MS. Hence, neuronal and glial K_v7 channels may have diverse functions during MS.

TABLE 3 | Expression and role of unique dysregulated ion channels in experimental models of MS.

Gene/protein	Distribution, localization	Cellular functions during physiological conditions	WM in MS models	
			Alterations	**Role**
KCNA1/K_v1.1	JPN of myelinated axons	Regulate AP propagation and neural excitability	Redistribution to internodes and nodal segments, upregulation	Hyperpolarise axonal V_{rest}, affect AP threshold, impair AP conduction
	Microglia, astrocyte (t), OPCs (t)	Proliferation, cell activation		
KCNA2/K_v1.2	JPN of myelinated axons	Regulate AP propagation and neural excitability	Redistribution to internodes and nodal segments, upregulation	Hyperpolarise axonal V_{rest}, affect AP threshold, impair AP conduction
	Reactive astrocyte, microglia, OPC	Proliferation, cell activation		
KCNA4/K_v1.4	Axons (HP)	Regulate AP propagation and neural excitability	Upregulation in astrocytes and OPCs around EAE lesions	Deficiency ameliorated EAE course in KO mice, but have no effect on demyelination/ remyelination in the cuprizone model
	Reactive astrocyte, OPCs	Proliferation		
KCNB1/K_v2.1	Soma, proximal dendrites, AIS Microglia, OPCs (t)	Influence AP duration during high frequency firing, regulate neuronal excitability	Unknown in WM Downregulation in motor neurons of GM spinal cord during EAE	Unknown
KCNB2/ K_v2.2	Soma, proximal dendrites, AIS Not detected in glia	Influence AP duration during high frequency firing, regulate neuronal excitability	Unknown	Unknown
KCNC3/K_v3.3	Axons, somatodendritic compartment Astrocyte, microglia (t), OPCs (t)	Regulate AP firing at high frequency	Upregulation in some injured WM axons	Unknown
KCND2/K_v4.2	Soma, dendrites Astrocyte (t), OPCs (t), microglia (t)	Regulate threshold for AP initiation and repolarization, frequency-dependent AP broadening, AP back-propagation	Unknown	Unknown
KCNQ2/K_v7.2	AIS, nodes of Ranvier OPCs, microglia	Stabilize V_{rest}, regulate activity of Na_V-channels, accelerate AP upstroke, influence neuronal subthreshold excitability, regulate spike generation, and repetitive firing	Unknown	Unknown
KCNQ3/K_v7.3	AIS, nodes of Ranvier Microglia (pro-inflammatory), OPCs, astrocyte (t)	Stabilize V_{rest}, regulate activity of Na_V-channels, accelerate AP upstroke, influence neuronal subthreshold excitability, regulate spike generation and repetitive firing	Unknown in WM Upregulated in demyelinated neocortical axons of L5 pyramidal neurons in the cuprizone model.	Unknown in WM Ensure AP conduction in demyelinated GM axons, decrease excitability
KCNQ5/K_v7.5	Soma, dendrites Astrocyte, OPCs, microglia	Contributes to AHP currents in the HP	Unknown	Unknown
KCNV1/K_v8.1	Unknown Oligo lineage (t)	Co-assemble with K_v2.1, reduce K_v2.1 current density which may lead to AP broadening and hyper-synchronized high-frequency firing	Unknown	Unknown
KCNS2/K_v9.2	Unknown Oligo lineage (t)	Co-assemble with K_v2.1	Unknown	Unknown
KCNH5/EAG2	Unknown Astrocyte (t), OPCs (t)	Unknown	Unknown	Unknown
KCNH7/ERG3	Unknown Astrocyte (t), OPCs (t), microglia (t)	Dampen excitability, stabilize V_{rest}	Unknown	Unknown
KCNH8/ELK1	Unknown OPCs (t)	Unknown	Unknown	Unknown

(Continued)

TABLE 3 | Continued

Gene/protein	Distribution, localization	Cellular functions during physiological conditions	WM in MS models	
			Alterations	**Role**
KCNK2/ TREK1	Axons, and node of Ranviers in afferent myelinated nerve	Contribute to "leak" K^+-current, help establishing and maintaining V_{rest}, regulate neuronal excitability, ensure AP repolarization at nodes of Ranvier in afferent myelinated fibers	Unknown	Deficiency aggravates EAE course in KO mice Channel activation reduces CNS immune cell trafficking across BBB and attenuate EAE course
	Astrocyte, microglia (t) OPCs (t)	Contribute to passive membrane K^+ conductance, glutamate release		
KCNK10/ TREK2	Unknown	Contribute to "leak" K^+-current, help establishing and maintaining V_{rest}	Unknown	Unknown
	Astrocyte OPCs (t)	Contribute to K^+ buffering, glutamate clearance		
KCNT1/K_{Na}1.1	Soma, axons Astrocytes (t)	Regulate the generation of slow afterhyperpolarization, firing patterns, and setting and stabilizing the V_{rest}	Unknown	Unknown
KCNN3/ K_{Ca}2.3	Dendrites, AIS	Regulate AP propagation and neuronal excitability, contribute to maintaining Ca^{2+}-homeostasis	Unknown	Unknown
	Astrocyte, microglia, oligo lineage (t)	K^+ buffering in astrocytes Microglia proliferation and cytokines production		
KCNJ6/K_{ir}3.2	Somatodendritic compartment	K^+-homeostasis, maintenance of V_{rest}, hyperpolarization, control of AP firing and neuronal excitability, inhibition of excitatory neurotransmitter release	Unknown	Unknown
	Astrocyte, oligo lineage (t)			
KCNJ16/K_{ir}5.1	Somatodendritic compartment, dendritic spines	Silent channel when combined with K_{ir}2.1. When combined with K_{ir}4.1, build channels with larger conductance and greater pH-sensitivity. Plays a role in synaptic transmission	Unknown	Unknown
	Astrocyte, oligo lineage, microglia (t)	Chemoreception K^+ buffering		
SCN1A/ Na_v1.1	Somatodendritic compartment, AIS, nodes of Ranvier	Saltatory conduction, maintenance of sustained firing, control of excitability	Increase or no change; localize along the demyelinated regions	Unknown
	Microglia, astrocyte, OPCs (t)	Microglia phagocytosis, cytokine release		
SCN2A/ Na_v1.2	AIS, immature nodes of Ranvier, along the non-myelinated axons	Back-propagation of AP into the somatodendritic compartment, may support slow spike propagation	Increase of diffuse distribution along demyelinated axons in various mouse models; no change in myelin-deficient rat	Unclear. Suggested: preservation of AP propagation, or axonal damage
	Astrocyte, pre-oligodendrocytes	Oligo maturation	Upregulated in astrocytes during EAE	
SCN3A/ Na_v1.3	Somatodendritic compartment, along the axons including myelinated fibers Astrocyte oligo lineage (t)	AP initiation and propagation, proliferation and migration of cortical progenitors	No change in the optic nerve	Unknown
SCN8A/ Na_v1.6	AIS, nodes of Ranvier; low density on cell soma, dendritic shafts, synapses	AP initiation and propagation, neuronal excitability	Decrease at the nodes of Ranvier, increase of diffuse distribution along the damaged axons, no change at AIS	May trigger Na^+ increase in axoplasm, reversal of NCX, and intra-axonal Ca^{2+} overload. Deletion improves axonal health during EAE
	Astrocyte, microglia oligo (t)		Upregulated in microglia/ macrophages during EAE	
SCN11A/ Na_v1.9	Soma, proximal processes Negligible in all glial cells (t)	Regulate excitation, control activity-dependent axonal elongation, mediate sustained depolarizing current upon activation of muscarinic receptors	Unknown	Unknown

(Continued)

TABLE 3 | Continued

Gene/protein	Distribution, localization	Cellular functions during physiological conditions	WM in MS models	
			Alterations	**Role**
CACNA1C/ $Ca_V1.2$	Somatodendritic compartment (synaptically, extrasynaptically), axons, axonal terminals (extrasynaptically), pioneer axons during development Astrocyte, oligo lineage, reactive microglia	Synaptic modulation, propagation of dendritic Ca^{2+} spikes, regulation of glutamate receptor trafficking, CREB phosphorylation, coupling of excitation to nuclear gene transcription, modulation of long-term potentiation, neurites growth and axonal pathfinding during development Astrogliosis OPCs development and myelination	Unknown	Unknown. Suggested: Neurodegeneration because L-type VGCCs blockers attenuate mitochondrial pathology in nerve fibers and axonal loss Deletion in astrocyte- reduces cell activation and pro-inflammatory mediators release in the cuprizone model Deletion in OPCs reduced remyelination in the cuprizone model
CACNA1D/ $Ca_V1.3$	Somatodendritic compartment, axonal cylinders Astrocyte, microglia oligo lineage	Pacemaking activity, spontaneous firing, Ca^{2+}-dependent post-burst after-hyperpolarization, Ca^{2+}-dependent intracellular signaling pathways, regulation of morphology of dendritic spines and axonal arbores Oligodendrocyte-axon signaling, release of pro-inflammatory mediators by microglia	Unknown	Unknown. Suggested: neuroprotection because L-type VGCCs blockers attenuate mitochondrial pathology in nerve fibers and axonal loss
CACNA1A/ $Ca_V2.1$	Axonal synaptic terminals, axonal shafts in WM, somatodendritic compartment Reactive astrocyte OPCs, premyelinating oligo, microglia (t)	Neurotransmitter release at neuronal and neuron-glia synapses, regulation of BK and SK channels, control of neuronal firing, regulation of gene expression, local Ca^{2+} signaling, and cell survival Calcium influx in oligo upon neuronal activity	Unknown	Unknown
CACNA1E/ $Ca_V2.3$	Dendritic spines, axonal terminals Astrocyte, oligodendrocyte	Neurotransmitter release, synaptic plasticity, regulation of BK, SK, and $K_V4.2$ channels	Unknown	Unknown
CACNA1G/ $Ca_V3.1$	Somatodendritic compartment, AIS Astrocyte (t) oligo lineage	Generation and timing of APs, regulation of neuronal excitability, rhythmic AP bursts in thalamus, neuronal oscillations, neurotransmitter release	Unknown	T-cells from KO mice show decreased cytokine release Deficiency in KO mice inhibits the autoimmune response in the EAE model
CACNA1H/ $Ca_V3.2$	Somatodendritic compartment, AIS Astrocyte oligo lineage	Generation and timing of APs, regulation of neuronal excitability, rhythmic AP bursts in thalamus, neuronal oscillations, neurotransmitter release	Unknown	Unknown
CACNA1I/ $Ca_V3.3$	Somatodendritic compartment	Generation and timing of APs, regulation of neuronal excitability, rhythmic AP bursts in thalamus, neuronal oscillations, neurotransmitter release	Unknown	Unknown
RyR2	Along ER (also in axons) Astrocyte, oligo lineage	Ca^{2+} release from the ER into the cytoplasm, vesicle fusion, neurotransmitter release, synaptic plasticity, growth cone dynamics	Unknown	Unknown
RyR3	Along ER (also in axons) Astrocyte, OPCs, oligodendrocytes	Ca^{2+} release from the ER into the cytoplasm, vesicle fusion, neurotransmitter release, synaptic plasticity, growth cone dynamics Astrocyte motility OPCs development	Unknown	Unknown
TRPV1	Soma, post-synaptic dendritic spines, synaptic vesicles Astrocyte, microglia, oligodendrocytes	Regulation of Ca^{2+}-signaling, synaptic plasticity Astrocyte: migration, chemotaxis, activation during stress, inflammasome activation Microglia: migration, cytokine production, ROS generation, phagocytosis, polarization, cell death	Suggested a main role in regulating microglia inflammatory response	Both detrimental and beneficial effects have been described in EAE disease

(Continued)

TABLE 3 | Continued

Gene/protein	Distribution, localization	Cellular functions during physiological conditions	WM in MS models	
			Alterations	Role
TRPV6	Unknown Astrocyte (t)	Unknown	Unknown	Unknown
TRPM2	Soma and neurites in neuronal cultures Microglia, astrocyte (t), oligodendrocyte (t)	Contribute to synaptic plasticity and play an inhibitory role in neurite outgrowth Microglia activation and generation of proinflammatory mediators	Upregulated in monocyte-lineage cells	TRPM2 deficiency reduce monocyte infiltration in EAE
PKD2/TRPP1	ER, primary cilia, and plasma membrane Astrocyte (t), microglia (t), oligo lineage (t)	Maintenance of Ca^{2+}-homeostasis, cell proliferation	Unknown	Unknown
PKD2L2/ TRPP3	Unknown Astrocyte (t), microglia (t)	Unknown	Unknown	Unknown
CLCN2/CLC-2	Plasma membranes, intracellular membranes Astrocyte, OPCs, microglia	Maintenance of low intracellular Cl^- level, control of cell volume homeostasis, regulation of $GABA_AR$-mediated synaptic inputs, regulation of neuronal excitability Interacts with AQP4 in astrocytes, regulates OPCs differentiation, contribute to volume regulation and phagocytosis in microglia	Unknown	Unknown
CLCN7/CLC-7	Lysosomes Microglia, astrocyte (t), oligo lineage (t)	Suggested function in the neuronal endo-lysosomal pathway Regulate lysosomal acidification in activated microglia	Unknown	Unknown
GJA4/CX37	Largely expressed in vascular cells	Regulate vasomotor activity, endothelial permeability, and maintenance of body fluid balance	Unknown	Unknown
PANX1/Px1	Soma, dendrites, axons Astrocyte, OPCs microglia	Paracrine and autocrine signaling, ATP-sensitive ATP release in complex with $P2X_7Rs$, intercellular propagation of Ca^{2+}-waves, cell differentiation, migration, synaptic plasticity, memory	Unknown	Panx-1 induced ATP release and inflammasome activation contribute to WM damage during EAE Inhibition of Panx1 using pharmacology or gene disruption delays and attenuates disease course in EAE and cuprizone model
CATSPERG	Unknown Oligo lineage (t) Microglia (t)	Unknown	Unknown	Unknown
CATSPERE	Unknown	Unknown	Unknown	Unknown

AHP, afterhyperpolarization; AIS, axon initial segment; AP, action potential; BK, big-conductance Ca^{2+}-activated K^+-channels; ER, endoplasmatic reticulum; $GABA_AR$, ionotropic gamma aminobutyric acid A receptor; HP, hippocampus; JPN, juxtaparanodal regions; NCX, Na^+/Ca^{2+} exchanger; SCI, spinal cord injury; SK, small-conductance Ca^{2+}-activated K^+-channels; SSCx, somatosensory cortex; t, transcipts; V_{rest}, resting membrane potential.

K_v8.1 and K_v9.2 (KCNV1 and KCNS2)

Neurons

KCNV1 and *KCNS2* genes encode for electrically silent (K_vS) K_v8.1- and K_v9.2 subunits that assemble into hetero-tetrameric channels with K_v2 subunits (Bocksteins, 2016). A number of channelopathies is ascribed to K_vS subunits (Salinas et al., 1997a; Liu et al., 2016; Allen et al., 2020), pointing to their important physiological role.

Glia

KCNV1 and *KCNS2* transcripts were found in oligodendrocyte lineage cell (Marques et al., 2016).

Expression and Function in MS

Bulk RNA-seq showed upregulation of *KCNV1* and *KCNS2* genes in CA lesions (**Figure 2**, **Table 1**; Elkjaer et al., 2019; Frisch et al., 2020). The snRNA-seq detected *KCNV1* and *KCNS2* in neuronal clusters (**Table 2**; Jakel et al., 2019). Co-assembly between K_v8.1 and K_v2.1 reduces K_v2.1 current density (Hugnot et al., 1996; Castellano et al., 1997): the high stoichiometry of the K_v8.1 subunit suppresses surface expression and favors retention of heteromeric channels in the ER (Salinas et al., 1997b). Neurons with reduced K_v2.1-mediated currents demonstrate broadened APs (Du et al., 2000) underlying hyper-synchronized high-frequency firing observed during epilepsy. Hence, upregulated K_vS subunits in CA lesions may influence the localization of

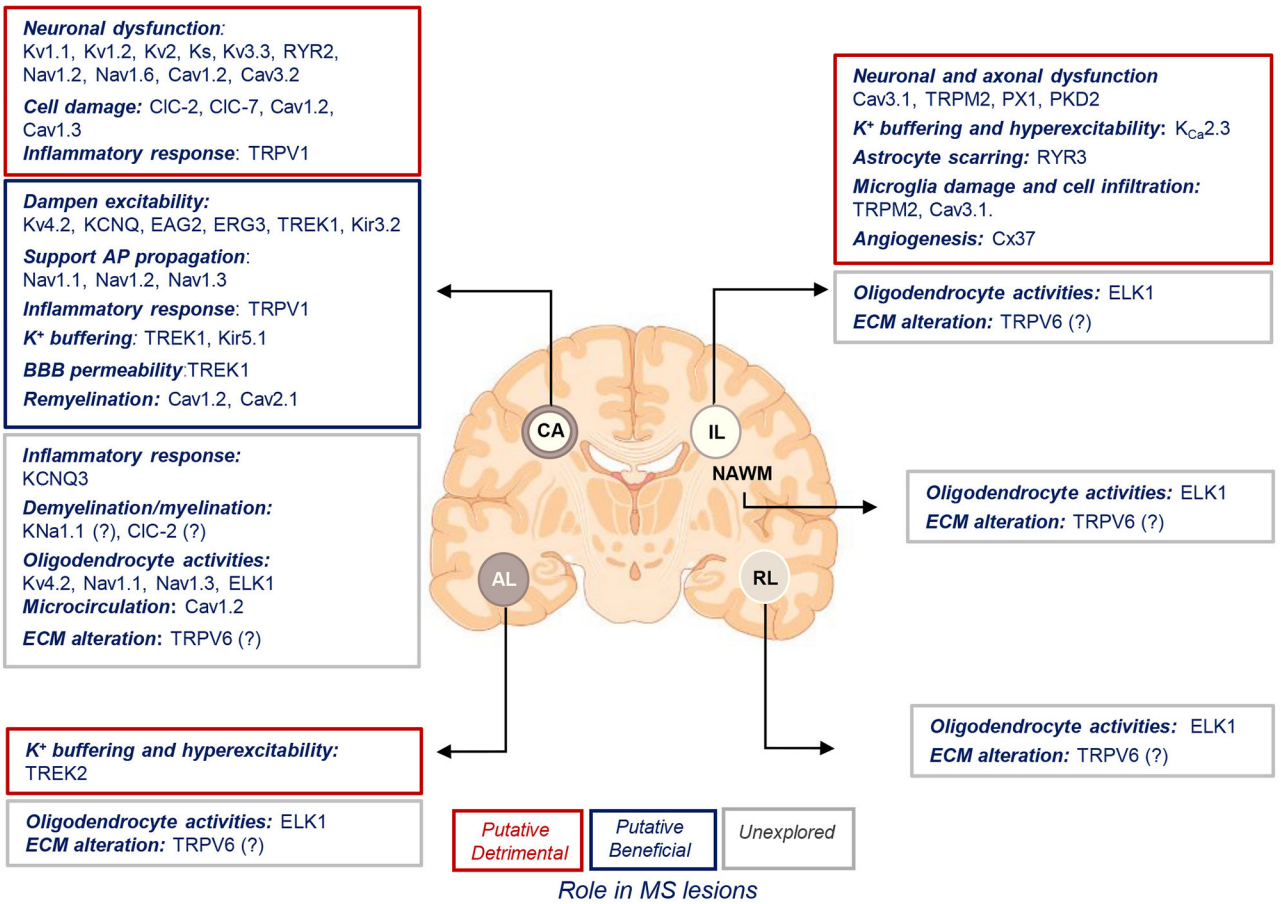

FIGURE 4 | Putative roles of ion channels encoded by uniquely dysregulated genes in SPMS lesions. Schematic illustration of the putative detrimental (red box), putative beneficial (blue box), and unexplored (gray box) functional roles of ion channel encoded by the uniquely dysregulated genes in active (AL), chronic active (CA), inactive (IL), and remyelinating (RL) lesions, and normal-appearing white matter (NAWM) of SPMS brain. Source icon is from Biorender.com.

clustered K_v2 subunits in SPMS brain and affect AP firing and/or propagation.

Eag2, erg3, and elk1 (KCNH5, KCNH7, and KCNH8)

KCNH genes encode for K_v10–K_v12 subfamilies, all orthologs of the Drosophila ether-àgo-go (EAG) channels. They include two eag (K_v10), three eag-related (erg/K_v11), and three eag-like (elk/K_v12) K^+ channels that can form heteromeric channels within each subfamily (Rasmussen and Trimmer, 2019).

Neurons

All EAG channels are expressed in the CNS neurons (Ludwig et al., 2000; Papa et al., 2003; Zou et al., 2003), but only erg-mediated currents have been verified using suitable blockers (Bauer and Schwarz, 2018).

Glia

RNA-seq detected *KCNH5*, *KCNH7*, and *KCNH8* expression in mouse OPCs (Falcao et al., 2018). *KCNH5* and *KCNH7* genes were found in astrocytes (Batiuk et al., 2020), while only the KCNH7 gene was detected in mouse microglia (Hammond et al., 2019). Erg-type currents were reported in neopallial microglia cultures (Zhou et al., 1998) and hippocampal astrocytes (Emmi et al., 2000; Papa et al., 2003).

Expression and Function in MS

Bulk RNA-seq detected increased *KCNH5(eag2)* and *KCNH7(erg3)* transcripts in CA lesions and downregulation of *KCNH8(elk1)* transcript in all lesions and NAWM (**Figure 2**, **Table 1**; Elkjaer et al., 2019; Frisch et al., 2020). The snRNA-seq found significant expression of *KCNH5* and *KCNH7* transcripts in neuronal clusters and *KCNH8* in mature oligodendrocyte clusters (**Tables 1**, **2**; Jakel et al., 2019). The functional role of *eag2, erg3,* and *elk1* during MS may be related to altered neuronal excitability. Indeed, human *eag1* and *eag2* gain-of-function mutations underlie severe neurological disorders associated with epileptic seizures (Allen et al., 2020). The *erg* channels that are active at subthreshold potentials stabilize the V_{rest} and dampen excitability (Fano et al., 2012). *Erg3* knockdown in mice increases intrinsic neuronal excitability and enhances seizure susceptibility, while treatment with *erg* activator reduces epileptogenesis (Xiao et al., 2018). *Erg3* expression is decreased

in the brain of epilepsy patients. Remarkably, association of *KCNH7(erg)* intronic polymorphisms with MS pathogenesis was speculated although never substantiated (Martinez et al., 2008; Couturier et al., 2009).

Two-Pore Domain K^+ Channels (K2P)

K2P K^+ channels are encoded by 15 *KCNK* genes, stratified into six subfamilies: TWIK, TASK (TWIK-related acid-sensitive), TREK (TWIK-related arachidonic acid activated), THIK (tandem pore domain halothane-inhibited), TALK (TWIK-related alkaline pH-activated), and TRESK (TWIK-related spinal cord) K^+ channels (Enyedi and Czirjak, 2010). K2P K^+ channels contribute to "leak" K^+ current, helping to establish and maintain V_{rest} (Enyedi and Czirjak, 2010).

TREK1 and TREK2 (KCNK2 and KCNK10)

Neurons and Glia

KCNK2 and *KCNK10* genes encode for TREK-1 and TREK-2 channels, which are expressed in neurons, astrocytes, and OPC (Hervieu et al., 2001; Talley et al., 2001; Falcao et al., 2018). Only TREK-1 transcripts were detected in microglia (Hammond et al., 2019). In astrocytes, TREK channels contribute to passive conductance and glutamate release (Zhou et al., 2009; Woo et al., 2012). TREK-1 and TREK-2 may be activated by a wide range of physiological and pathological stimuli reminiscent of inflammatory environment including membrane stretch, heat, intracellular acidosis, and cellular lipids (Ehling et al., 2015).

Expression and Function in MS

Bulk RNA-seq found upregulated TREK-1 transcripts in CA lesions, but a divergent modulation was observed for TREK-2 mRNAs in ALs (**Figure 2**, **Tables 1**, **2**; Elkjaer et al., 2019; Frisch et al., 2020). *KCNK2* and *KCNK10* transcripts were detected in neuronal and oligodendrocyte clusters, but scarcely observed in astrocytes (**Table 2**; Jakel et al., 2019). TREK-1 upregulation in CA lesions most likely reflects a protective response because TREK-1 plays a neuroprotective role during neurological diseases, including MS (Djillani et al., 2019). TREK-1 reduces neuronal excitability by hyperpolarizing the membrane potential (Honore, 2007) and is required for rapid AP repolarization at the node of Ranvier in mammalian afferent myelinated nerves, while TREK-1 loss-of-function retards nerve conduction and impairs sensory responses in animals (Kanda et al., 2019). Treatment of mice with TREK-1 activators, riluzole (Gilgun-Sherki et al., 2003), or alpha-linolenic acid attenuates EAE course (Blondeau et al., 2007), while these effects are reduced in TREK-$1^{-/-}$ mice (Bittner et al., 2014). TREK-1 function is also important for non-neuronal cells because aggravated EAE course in TREK-$1^{-/-}$ mice is associated with increased numbers of infiltrating T cells and higher endothelial expression of ICAM1 and VCAM1 (Bittner et al., 2013), and TREK-1 is reduced in the microvascular endothelium in inflammatory MS brain lesions (Bittner et al., 2013).

TREK-2 downregulation in AL, a lesion type characterized by myelin breakdown and infiltration by inflammatory cells (Elkjaer et al., 2019; Frisch et al., 2020), may contribute to reduced glutamate and K^+ buffering and neuronal over-excitation because TREK-2 helps maintain the membrane potential and low extracellular glutamate and K^+ level during ischemia (Gnatenco et al., 2002; Rivera-Pagan et al., 2015).

Na^+- and Ca^{2+}-Activated K^+ Channels

$K_{Na}1.1$ (KCNT1)

Neurons

The *KCNT1* and *KCNT2* genes encode for Slack and Slick K^+ channels that are activated by Na^+ influx (Bhattacharjee and Kaczmarek, 2005). They localize to soma and axons of neurons (Bhattacharjee et al., 2002; Brown et al., 2008; Rizzi et al., 2016) and are involved in the generation of slow after-hyperpolarization, regulation of firing patterns, and setting and stabilizing the V_{rest} (Franceschetti et al., 2003). Alterations in *KCNT1* and *KCNT2* genes are linked to early-onset epileptic encephalopathies and Fragile-X-syndrome (Kim and Kaczmarek, 2014).

Glia

RNA-seq detected *KCNT1* gene in mouse astrocytes (Batiuk et al., 2020).

Expression and Function in MS

Bulk RNA-seq showed $K_{Na}1.1$ upregulation in CA lesions (**Figure 2**, **Table 1**; Elkjaer et al., 2019; Frisch et al., 2020). SnRNA-seq detected *KCNT1* in neuronal clusters (**Table 2**). *KCNT1* function in MS may be related to myelination/demyelination because severely delayed myelination occurs in patients with *KCNT1* mutations (Vanderver et al., 2014). Furthermore, *KCNT1* is a causative gene in infants with hypomyelinating leukodystrophy showing WM alterations (Arai-Ichinoi et al., 2016), and *KCNT1* mutations occur in infant epilepsy associated with delayed myelination, thin corpus callosum, and WM hyper-intensity in MRI (McTague et al., 2013; Shang et al., 2016; Borlot et al., 2020).

$K_{Ca}2.3$, SK3 (KCNN3)

The *KCNN3* gene encodes for the SK3 subunit of small-conductance Ca^{2+}-activated K^+ channels (SK channels). They mediate Ca^{2+} gated K^+ current and thus couple the increase in intracellular Ca^{2+} concentration to hyperpolarization of the membrane potential.

Neurons

SK3 channels are found on dendrites and AIS (Abiraman et al., 2018). They play a role in AP propagation and regulation of neuronal excitability (Stocker, 2004). They protect against excitotoxicity by maintaining Ca^{2+} homeostasis after NMDA receptor activation (Dolga et al., 2011).

Glia

RNA-seq detected intense *KCNN3* expression in mouse astrocytes (Batiuk et al., 2020), confirming earlier studies, which showed labeling of $GFAP^+$ processes in the supraoptic nucleus for SK3 channels and suggested the role of SK3 in astrocytic K^+ buffering (Armstrong et al., 2005). Oligodendrocyte lineage cells express low levels of *KCNN3* mRNA (Falcao et al., 2018), while mouse microglia does not express *KCNN3* (Hammond

et al., 2019). However, rat microglia in culture expresses the SK3 subunit, which is increased upon microglia activation with LPS (Schlichter et al., 2010). SK3 activation inhibited microglia proliferation, inflammatory IL-6 production, and morphological transformation to macrophages, while blocking SK3 in microglia-reduced neurotoxicity (Dolga et al., 2012).

Expression and Function in MS

Bulk RNA-seq showed significant and unique downregulation of *KCNN3* in ILs (Elkjaer et al., 2019; Frisch et al., 2020). SnRNA-seq revealed high *KCNN3* expression in astrocyte clusters (**Figure 2**, **Table 1**; Jakel et al., 2019). ILs consist of large demyelinated areas devoid of macrophages but filled with scar-forming astrocytes showing reduced ability to buffer glutamate and K^+ (Compston and Coles, 2008; Kuhlmann et al., 2017; Filippi et al., 2018; Schirmer et al., 2018). Hence, *KCNN3* downregulation in MS may reflect altered function of astrocytes, e.g., K^+ buffering (Armstrong et al., 2005), contributing to axonal hyper-excitability and death.

Inward Rectifier K^+ Channels (K_{ir})

KCNJ gene family encodes K_{ir} channels and comprises 16 subunits of $K_{ir}1$–$K_{ir}7$ subfamilies categorized into four groups: (1) classical ($K_{ir}2.x$); (2) G-protein-gated ($K_{ir}3.x$); (3) ATP-sensitive ($K_{ir}6.x$); and (4) K^+-transport channels ($K_{ir}1.x$, $K_{ir}4.x$, $K_{ir}5.x$, $K_{ir}7.x$) (Hibino et al., 2010). At a comparable driving force, K_{ir} channels allow greater influx than efflux of K^+-ions. Their high open probability at negative transmembrane voltages makes them well-suited to set the V_{rest} and to control cell excitability.

Kir3.2 (KCNJ6)

KCNJ6 gene encodes for $K_{ir}3.2$ subunits, also known as G-protein-gated K_{ir} (GIRK2) channels that are effectors for $G_i/_o$-dependent signaling and mediate outward K^+ current.

Neurons

$K_{ir}3.1/K_{ir}3.2$ hetero-tetramers are found in the somatodendritic compartment of neurons. Activation of GIRK channels is mediated by G-protein-coupled receptors including muscarinic, metabotropic glutamate, somatostatin, dopamine, endorphins, endocannabinoids, etc. GIRK channels are important for K^+ homeostasis and maintenance of V_{rest} near the K^+ equilibrium potential. GIRK current hyperpolarizes neuronal membrane reducing spontaneous AP firing and inhibiting neurotransmitter release (Luscher and Slesinger, 2010). GIRK signaling contributes to learning/memory, reward, pain, anxiety, schizophrenia, addiction, and other processes (Mayfield et al., 2015). $K_{ir}3.2$ mutations in mice lead to a loss of K^+ selectivity and increased Na^+ permeability of the channel, resulting in the *weaver* phenotype (Liao et al., 1996; Surmeier et al., 1996).

Glia

Astrocytes and Müller cells express $K_{ir}3$ channels (Raap et al., 2002). $K_{ir}3.2$ transcripts were detected in the mouse optic nerve (Papanikolaou et al., 2020) and oligodendrocyte lineage (Falcao et al., 2018), but not in microglia (Hammond et al., 2019).

Expression and Function in MS

RNA-seq revealed *KCNJ6* upregulation in the CA lesions (Elkjaer et al., 2019; Frisch et al., 2020). The snRNA-seq predominantly found *KCNJ6* transcripts in neuronal clusters (Jakel et al., 2019; **Table 1**). The functional role of $K_{ir}3.2$ channels in MS may be related to membrane hyperpolarization and compensation of excessive neuronal excitability driving neurodegeneration.

Kir5.1 (KCNJ16)

KCNJ16 gene encodes for $K_{ir}5.1$ subunit, which forms an electrically silent channel when combined with $K_{ir}2.1$ (Derst et al., 2001; Pessia et al., 2001), but is functional when combined with $K_{ir}4.1$ (Konstas et al., 2003). Clustering of heteromeric $K_{ir}4.1/K_{ir}5.1$ and homomeric $K_{ir}5.1$ channels on plasmalemma involves the anchoring protein PSD-95 (Tanemoto et al., 2002; Brasko et al., 2017). Heteromeric $K_{ir}4.1/K_{ir}5.1$ channels exhibit larger channel conductance, greater pH sensitivity, and different expression patterns if compared to $K_{ir}4.1$ homomers (Tanemoto et al., 2000; Tucker et al., 2000; Pessia et al., 2001; Hibino et al., 2010).

Neurons

In cultures, $K_{ir}5.1$ immunoreactivity was detected in somatodendritic compartments where PSD-95 immunoreactivity was also localized. The $K_{ir}5.1$/PSD-95 complex may exist at dendritic spines *in vivo* and play a role in synaptic transmission (Tanemoto et al., 2002).

Glia

$K_{ir}5.1$ mRNA is two-fold higher in OPCs ($NG2^+$-glia) vs. astrocytes (Zhang et al., 2014), and mouse brain microglia expresses $K_{ir}5.1$ transcript too (Hammond et al., 2019). $K_{ir}5.1$ expression in oligodendrocytes and astrocytes depends on its association with $K_{ir}4.1$: loss of $K_{ir}4.1$ reduces $K_{ir}5.1$, suggesting that altered expression/distribution of $K_{ir}5.1$ may contribute to the phenotype of $K_{ir}4.1$ knockout mice (Brasko et al., 2017; Schirmer et al., 2018). The oligodendroglial $K_{ir}5.1/K_{ir}4.1$ channels are important for K^+ clearance (Poopalasundaram et al., 2000; Neusch et al., 2001), long-term maintenance of axonal function, and WM integrity (Kelley et al., 2018; Schirmer et al., 2018). In astrocytes, $K_{ir}5.1/K_{ir}4.1$ channels contribute to chemoreception, spatial K^+ buffering, and breathing control (Mulkey and Wenker, 2011).

Expression and Function in MS

Bulk RNA-seq revealed $K_{ir}5.1$ upregulation in CA lesions (**Table 1**; Elkjaer et al., 2019; Frisch et al., 2020). SnRNA-seq detected $K_{ir}5.1$ in OPCs clusters and scarcely in astrocytes. The *KCNJ16* gene is upregulated during demyelination and acute remyelination in mouse cuprizone model (Martin et al., 2018). Upregulation of $K_{ir}5.1$ may reflect the role of the oligodendroglial $K_{ir}4.1/K_{ir}5.1$ channels in K^+ clearance during MS and may represent a mechanism to compensate $K_{ir}4.1$ reduction in MS brain (Schirmer et al., 2014). Alternatively, $K_{ir}5.1$ upregulation may underlie reduced $K_{ir}4.1$ function in MS because presence of $K_{ir}5.1$ subunit confers loss of functional activity to $K_{ir}4.1/K_{ir}5.1$ channels under oxidative stress (Jin et al., 2012).

Voltage-Gated Na^+ Channels (Na_V)

In the mammalian brain, Na_V are composed of α-subunit (260 kDa) and one or several β-subunits (β1–β4, of 33–36 kDa) (Goldin et al., 2000). The α-subunit forms the channel pore and acts as a voltage sensor; β-subunits play a modulatory role and influence voltage dependence, gating kinetics, and surface expression of the channel (Goldin et al., 2000; Yu and Catterall, 2003; Namadurai et al., 2015). The nine $Na_V1.1$–$Na_V1.9$ α-subunits are encoded by the corresponding genes *SCN1A*–*SCN5A* and *SCN8A*–*SCN11A*. In addition, Na_X isoform was described,which is encoded by the *SCN6/7A* gene.

$Na_V1.1$ (SCN1A)

Neurons

$Na_V1.1$ channels localize to the somatodendritic compartment of principal neurons and AIS of GABAergic interneurons, spinal cord motor neurons, and retinal neurons (Ogiwara et al., 2007; Duflocq et al., 2008; Dumenieu et al., 2017). $Na_V1.1$ channels are also present at the nodes of Ranvier of the cerebellar WM, fimbria, corpus callosum, and spinal cord WM (Ogiwara et al., 2007; Duflocq et al., 2008; O'Malley et al., 2009). They play a role during saltatory conduction along myelinated axons and are essential for maintaining the sustained firing of GABAergic interneurons and Purkinje cells, thus controlling the excitability of neuronal networks (Duflocq et al., 2008; Dumenieu et al., 2017). Mutations in $Na_V1.1$ channels result in various types of epilepsy and reduced volume of brain GM and WM (Lee et al., 2017; Scheffer and Nabbout, 2019).

Glia

Human astrocytes show negligible immunolabelling for $Na_V1.1$ and no upregulation in the WM of MS patients (Black et al., 2010). Transcriptome analysis revealed low level of SCN1A in mouse cortical and hippocampal astrocytes (Batiuk et al., 2020). RNA-seq detected *SCN1A* in oligodendrocytes and OPCs throughout the CNS (Larson et al., 2016; Marques et al., 2016; Falcao et al., 2018). The functional role of $Na_V1.1$ channels in astrocytes and oligodendroglia remains unknown. Transcriptome studies have not detected *SCN1A* in microglia prepared from brain homogenates (Hammond et al., 2019), but $Na_V1.1$ protein was found in microglia derived from neonatal rat mixed glial cultures (Black et al., 2009). $Na_V1.1$ channels may be involved in regulation of phagocytosis and/or release of IL-1α, IL-β, and TNF-α from microglia (Black et al., 2009). The $Na_V1.1$ mRNA was detected in astrocytoma, oligodendroglioma, and glioblastoma samples from patients where these channels may contribute to the pathophysiology of brain tumors (Schrey et al., 2002).

Expression and Function in MS

Bulk RNA-seq detected *SCN1A* upregulation in CA lesions (**Figure 2**, **Table 1**; Elkjaer et al., 2019; Frisch et al., 2020). The snRNA-seq revealed significant expression of $Na_V1.1$ transcripts in neuronal, committed OPC, and OPC clusters (**Tables 1**, **2**; Jakel et al., 2019). Experimental models do not provide clues regarding the functional role of $Na_V1.1$ channels in MS: $Na_V1.1$ expression was increased or unaltered in the optic nerve during EAE (Craner et al., 2003; O'Malley et al., 2009), while in the spinal cord, these channels clustered at the nodes of Ranvier and localized along the demyelinated regions (O'Malley et al., 2009). *SCN1A* upregulation in human MS may reflect the necessity of the channel for redistribution along the demyelinated axons and support of AP propagation.

$Na_V1.2$ (SCN2A)

Neurons

The $Na_V1.2$ channels localize to the AIS, immature nodes of Ranvier, and in non-myelinated axons during early development. As nervous system matures, $Na_V1.2$ channels are replaced by $Na_V1.6$ channels (Boiko et al., 2001; Osorio et al., 2005; Dumenieu et al., 2017), although in some neurons, they remain into adulthood. $Na_V1.2$ channels of the AIS control back-propagation of APs into the somatodendritic compartment, while $Na_V1.6$ channels are being placed at distal parts of the AIS control initiation and propagation of AP into the axon (Boiko et al., 2003; Hu et al., 2009). $Na_V1.2$ channels are also diffusely distributed along non-myelinated axons in the adult CNS where they may support slow spike propagation (Arroyo et al., 2002; Dumenieu et al., 2017).

Glia

$Na_V1.2$ protein was found in rat astrocytes isolated from the spinal cord and optic nerve (Black et al., 1995), but only limited $Na_V1.2$ expression was observed in human astrocytes in control and MS tissue (Black et al., 2010). The RNA-seq detected *SCN2A* expression in oligodendrocytes and OPCs (Larson et al., 2016; Marques et al., 2016). Knockdown of $Na_V1.2$ in pre-oligodendrocytes of the auditory brainstem resulted in reduced number and length of cellular processes and decreased MBP level, indicating that $Na_V1.2$ channels are important for structural maturation of myelinating cells and myelination (Berret et al., 2017). Microglia expresses no/little functional $Na_V1.2$ channels (Black et al., 2009; Pappalardo et al., 2016; Hammond et al., 2019).

Expression and Function in MS

Bulk RNA-seq detected upregulation of *SCN2A* gene in CA lesions (**Figure 2**, **Table 1**; Elkjaer et al., 2019; Frisch et al., 2020), while snRNA-seq showed abundant *SCN2A* expression in neuronal clusters (**Tables 1**, **2**; Jakel et al., 2019). The upregulation may reflect re-expression of $Na_V1.2$ protein, in line with previous reports showing diffuse distribution of $Na_V1.2$ channels along the demyelinated axons in human MS lesions within optic nerve and spinal cord (Craner et al., 2004b). Axonal $Na_V1.2$ channels may contribute to preservation of AP propagation and re-establishment of myelin sheathes (Coman et al., 2006), as it occurs during development. On the other hand, $Na_V1.2$ channels may promote axonal damage by increasing the intracellular Na^+ concentration that triggers reversal of Na^+/Ca^{2+} exchanger (NCX) and Ca^{2+} overload in the axoplasm (Friese et al., 2014; Schattling et al., 2016). In line with this, human gain-of-function mutation in the mouse *SCN2A* gene triggers axonal damage, neurodegeneration, disability, and lethality in the mouse model of MS (Schattling et al., 2016). Expression of "developmental" $Na_V1.2$ channels in axons was also found in animal models of

MS, i.e., in adult *Shiverer* mice that lack myelin (Westenbroek et al., 1992; Boiko et al., 2001), in transgenic mice overexpressing proteolipid protein that initially have normal myelination but then lose myelin (Rasband et al., 2003), and in the demyelinated optic nerve and spinal cord during EAE (Craner et al., 2003, 2004a; Herrero-Herranz et al., 2008). However, other data showed that in chronic spinal cord MS lesions, $Na_V1.2$ channels localize on astrocytic processes surrounding the axons rather than on axons themselves (Black et al., 2007), and $Na_V1.2$ expression/distribution was unchanged in the spinal cord of myelin-deficient rats (Arroyo et al., 2002).

$Na_V1.3$ (SCN3A)

Neurons

$Na_V1.3$ channels are highly expressed in rodent and human CNS throughout the embryonic development (Black and Waxman, 2013). Some studies reported that their expression decreases during the first weeks after birth, while others found $Na_V1.3$ immunoreactivity in GM and/or WM of adult rat and human brain (Whitaker et al., 2001; Lindia and Abbadie, 2003; Thimmapaya et al., 2005; Cheah et al., 2013). $Na_V1.3$ channels mainly localize to the somatodendritic compartment of neurons but were also detected along the axons including myelinated fibers where they may contribute to initiation and propagation of APs (Whitaker et al., 2001; Lindia and Abbadie, 2003; Cheah et al., 2013; Wang et al., 2017). In the developing brain, $Na_V1.3$ channels regulate proliferation and migration of cortical progenitors that do not fire APs (Smith et al., 2018).

Glia

The mRNA and $Na_V1.3$ protein were detected in astrocytes (Black et al., 1995). RNA-seq demonstrated *SCN3A* expression in oligodendroglial cells and suggested higher expression in OPCs vs. mature oligodendrocytes (Larson et al., 2016; Marques et al., 2016). $Na_V1.3$ expression in microglia was negligible or absent (Black et al., 2009; Hammond et al., 2019). Heterogeneous expression (from weak to strong) of $Na_V1.3$ mRNA occurred in human astrocytoma, oligodendroglial tumors, and glioblastoma (Schrey et al., 2002). Functions of $Na_V1.3$ channels in glia remain unknown.

Expression and Function in MS

Bulk mRNA-seq reported upregulation of *SCN3A* gene in the CA lesions (Elkjaer et al., 2019; Frisch et al., 2020). The snRNA-seq found significant *SCN3A* expression in neuronal and OPCs clusters (Jakel et al., 2019; **Tables 1**, **2**). *SCN3A* upregulation during MS may reflect augmented expression of $Na_V1.3$ protein in axons that is necessary for supporting/re-establishment of AP propagation in injured WM, because increased $Na_V1.3$ levels are known to be associated with higher neuronal firing. For instance, mRNA and $Na_V1.3$ protein were upregulated in spontaneously epileptic rats (Guo et al., 2008), and expression in hippocampal neurons of a novel coding variant SCN3A-K354Q resulted in enhanced $Na_v1.3$ currents, spontaneous firing, and paroxysmal depolarizing shift-like depolarizations of the membrane potential (Estacion et al., 2010).

$Na_V1.6$ (SCN8A)

Neurons

$Na_V1.6$ channels cluster at high-density at the AIS and nodes of Ranvier of GM and WM axons, but can be also located on the soma, dendrites, and synapses although at a lower density (Caldwell et al., 2000; Dumenieu et al., 2017; Johnson et al., 2017; Eshed-Eisenbach and Peles, 2020). The expression level of $Na_V1.6$ channels is low during development, but significantly increases as the nervous system matures (Boiko et al., 2001; Osorio et al., 2005; Dumenieu et al., 2017). In the adult CNS, $Na_V1.6$ channels are the major Na^+ channels responsible for initiation and propagation of APs (Boiko et al., 2003; Hu et al., 2009). Loss of $Na_v1.6$ activity results in decreased neuronal excitability, while gain-of-function mutations potentiate excitability (O'Brien and Meisler, 2013). *SCN8A* mutations in mice result in ataxia, tremor, and dystonia; in humans, *SCN8A* haploinsufficiency is associated with intellectual disability, while hyperactivity can contribute to pathogenesis of epileptic encephalopathy (O'Brien and Meisler, 2013; Meisler, 2019).

Glia

RNA-seq detected *SCN8A* transcripts in mouse oligodendrocyte lineage (Marques et al., 2016), but they were negligible in microglia (Hammond et al., 2019). Immunoreactivity for $Na_V1.6$ was observed in cultured spinal cord astrocytes and in brain microglia *in vitro* and *in situ* (Reese and Caldwell, 1999; Black et al., 2009; Black and Waxman, 2012; Hossain et al., 2013), but their functional role is unknown.

Expression and Function in MS

Bulk mRNA-seq found upregulation of *SCN8A* gene in CA lesions (Elkjaer et al., 2019; Frisch et al., 2020), while snRNA-seq did not detect *SCN8A* transcripts (Jakel et al., 2019) (**Tables 1**, **2**). Upregulation of *SCN8A* may reflect increased diffuse distribution of the channels along the demyelinated axons; it may be important for remyelination but may also contribute to axonal damage. Re-distribution of $Na_V1.6$ channels, in parallel to their loss from the nodes of Ranvier, was reported previously in chronic, active, and inactive MS plaques within cerebral hemisphere, cerebellum, and spinal cord WM tissue from MS patients (Craner et al., 2004b; Black et al., 2007; Howell et al., 2010; Bouafia et al., 2014), as well as in several CNS regions affected by demyelination in animal models, including optic nerve and spinal cord WM (Craner et al., 2003, 2004a,b; Hassen et al., 2008; Howell et al., 2010). Expression of $Na_V1.6$ channels is disrupted at the nodes of Ranvier of WM axons in Shiverer mice that lack compact myelin (Boiko et al., 2001, 2003), and in transgenic mice overexpressing proteolipid protein that initially have normal myelination but then lose myelin (Rasband et al., 2003). During EAE in animals, $Na_V1.6$ co-localizes with NCX and may contribute to persistent Na^+ influx, increased Na^+ level in the axoplasm, reversal of NCX, and intra-axonal Ca^{2+} overload leading to axonal damage (Craner et al., 2004a). Interestingly, robust increase in $Na_V1.6$ expression was detected also in microglia/macrophages and was associated with microglia activation and phagocytosis in human MS brain and in the EAE model (Craner et al., 2005). *SCN8A* deletion resulted in reduced

inflammation and improved axonal health during EAE (Alrashdi et al., 2019). Hence, microglial $Na_V1.6$ may contribute to the pathophysiology of MS as well, yet, snRNA-seq did not detect *SCN8A* in WM glia clusters (**Tables 1**, **2**).

$Na_V1.9$ (SCN11A)

Neurons

Although $Na_V1.9$ channels are mainly expressed in sensory ganglia neurons (Wang et al., 2017), $Na_V1.9$ mRNA and/or protein were detected in soma and/or proximal processes of neurons in the olfactory bulb, hippocampus, cerebellar cortex, supraoptic nucleus, and spinal cord of rodents and humans (Jeong et al., 2000; Blum et al., 2002; Subramanian et al., 2012; Wetzel et al., 2013; Black et al., 2014; Kurowski et al., 2015). Information regarding axonal labeling for $Na_V1.9$ is lacking. $Na_V1.9$ channels regulate excitation in hippocampal neurons in concert with BDNF and TrkB, control activity-dependent axonal elongation in spinal cord motoneurons, and mediate sustained depolarizing current upon activation of M1 muscarinic receptors in cortical neurons (Blum et al., 2002; Subramanian et al., 2012; Kurowski et al., 2015). It is uncertain whether, similar to their role in the PNS (Cummins et al., 1999; Wang et al., 2017), $Na_V1.9$ channels contribute to the regulation of V_{rest} and AP threshold in the CNS neurons.

Glia

Very little expression of $Na_V1.9$ channels occurs in astrocytes, myelinating glia, and microglia (Marques et al., 2016; Pappalardo et al., 2016).

Expression and Function in MS

Bulk mRNA-seq showed *SCN11A* downregulation in ILs (Elkjaer et al., 2019; Frisch et al., 2020). By contrast, snRNA-seq did not detect *SCN11A* mRNA (Jakel et al., 2019; **Tables 1**, **2**). Functional consequence of *SCN11A* downregulation in MS is unknown.

Voltage-Gated Ca^{2+} Channels (VGCCs)

The VGCCs are composed of α1-, β-, α2/δ-, and γ-subunits (Catterall, 2011; Zamponi et al., 2015). The pore-forming α1-subunit determines channel activity, whereas other subunits are auxiliary and regulate function of α1-subunit. In mammalian cells, 10 different α1-subunits, encoded by different genes, classify into three subfamilies: Ca_V1, Ca_V2, and Ca_V3 (Catterall, 2011; Zamponi et al., 2015; Alves et al., 2019). Depending on the pharmacological properties and activation voltage of Ca^{2+} currents, five different types of VGCCs are distinguished: L-type, N-type, P/Q-type, R-type, and T-type.

L-Type VGCCs

The α1-subunit of L-type VGCCs is encoded by *CACNA1S* ($Ca_V1.1$), *CACNA1C* ($Ca_V1.2$), *CACNA1D* ($Ca_V1.3$), or *CACNA1F* ($Ca_V1.4$) genes. High sensitivity to dihydropyridine modulators distinguishes L-type Ca^{2+} channels from other types of VGCCs. In the CNS, mainly $Ca_V1.2$ and $Ca_V1.3$ subunits are expressed (Lipscombe et al., 2004; Zamponi et al., 2015), but $Ca_V1.1$ subunit was detected in human and rat basal ganglia where it is co-expressed with RyRs in GABAergic neurons (Takahashi et al., 2003).

$Ca_V1.2$ (CACNA1C)

Neurons

$Ca_V1.2$ channels account for 89% of all Ca^{2+} currents mediated by L-type VGCCs in the brain (Alves et al., 2019; Enders et al., 2020). In hippocampal neurons, $Ca_V1.2$ channels localize to somatodendritic compartment being placed at synapses or extra-synaptically (Joux et al., 2001; Hoogland and Saggau, 2004; Obermair et al., 2004; Tippens et al., 2008; Ortner and Striessnig, 2016), as well as to axons and/or extrasynaptic regions of axonal terminals (Tippens et al., 2008). Within the WM, $Ca_V1.2$ channels were identified in the developing rat pioneer axons and the follower axons projecting through the optic nerve, corpus callosum, anterior commissure, lateral olfactory tract, corticofugal fibers, thalamocortical axons, and the spinal cord (Ouardouz et al., 2003; Huang et al., 2012).

$Ca_V1.2$ channels open upon membrane depolarization beyond −30 mV, and mediate direct Ca^{2+} entry from the extracellular space into the cytoplasm. In addition, they may act as voltage sensors, transducing membrane depolarization to the RyRs activation and subsequent Ca^{2+} release from the ER *via* the mechanism of Ca^{2+-}induced Ca^{2+} release (CICR) (Ouardouz et al., 2003; Micu et al., 2016; Vierra et al., 2019). Clustering and functional coupling of plasmalemmal $Ca_V1.2$ channels to RyRs of the ER is mediated by the $K_V2.1$ channels (Vierra et al., 2019).

Neuronal $Ca_V1.2$ channels are involved in synaptic modulation, propagation of dendritic Ca^{2+} spikes, regulation of glutamate receptor trafficking, CREB phosphorylation, coupling of excitation to nuclear gene transcription, modulation of long-term potentiation, spatial learning, and fear response (Hofmann et al., 2014; Hopp, 2021). During brain development, spontaneous Ca^{2+} transients mediated by $Ca_V1.2$ channels regulate neurite growth and axonal pathfinding (Huang et al., 2012; Kamijo et al., 2018). Genetic variations in *CACNA1C* gene are associated with Timothy syndrome, Brugada syndrome, epilepsy, depression, schizophrenia, and autism spectrum disorders (Bhat et al., 2012; Bozarth et al., 2018).

Glia

$Ca_V1.2$ channels are expressed in cultured astrocytes and mediate Ca^{2+} transients upon direct Ca^{2+} entry and/or subsequent activation of RyRs (D'Ascenzo et al., 2004; Du et al., 2014; Cheli et al., 2016b). Ultrastructural studies found $Ca_V1.2$ proteins also in hippocampal astrocytes (Tippens et al., 2008). *In vitro*, $Ca_V1.2$ channels contribute to the mechanism of astrogliosis (Du et al., 2014; Cheli et al., 2016b), and in mouse models of Alzheimer's disease, they were detected in reactive astrocyte associated with Aβ-positive plaques (Willis et al., 2010; Daschil et al., 2013).

$Ca_V1.2$ mRNA and/or protein are expressed in oligodendrocytes and their progenitors (Agrawal et al., 2000; Paez et al., 2009, 2012; Fulton et al., 2010; Haberlandt et al., 2011; Cheli et al., 2016a; Larson et al., 2016; Marques et al., 2016; Santiago Gonzalez et al., 2017; Paez and Lyons, 2020; Pitman et al., 2020). $Ca_V1.2$ channels may regulate proliferation, migration, survival, or differentiation of OPCs, and myelination (Cheli et al., 2015, 2016a; Paez and Lyons, 2020; Pitman et al.,

2020). In human cultured OPCs, static magnetic stimulation augmented $Ca_V1.2$ mRNA expression, intracellular Ca^{2+} levels, and OPC differentiation (Prasad et al., 2017), suggesting a causal relationship between these processes.

Functional expression of $Ca_V1.2$ channels in microglia is still debated (Hopp, 2021). Sequencing data showed no/low CACNA1C expression in microglia (Hammond et al., 2019), and no $Ca_V1.2$ was found in cultured microglia even upon stimulation with TNF-α/IFN-γ (Schampel et al., 2017). However, increased immunolabelling for α1C-subunit of L-type VGCCs was observed in reactive microglia during excitotoxicity in rat hippocampus (Espinosa-Parrilla et al., 2015).

Expression and Function in MS

Bulk RNA-seq detected increased *CACNA1C* expression in CA lesions (**Figure 2**, **Table 1**; Elkjaer et al., 2019; Frisch et al., 2020). The snRNA-seq showed significant *CACNA1C* expression in neuronal and pericyte clusters (Jakel et al., 2019; **Tables 1**, **2**), while low expression in OPCs and astrocyte clusters. In mouse models of MS, application of L-type VGCCs blockers reduces brain and spinal cord WM damage, decreases mitochondrial pathology in nerve fibers, attenuates axonal loss, increases oligodendrocyte survival, and promotes remyelination (Brand-Schieber and Werner, 2004; Schampel et al., 2017; Ingwersen et al., 2018; Zamora et al., 2020). These findings suggest that $Ca_V1.2$ channels contribute to damage during MS. However, expression and activity of $Ca_V1.2$ channel increased in OPCs within the demyelinated lesions in the mouse corpus callosum after cuprizone treatment (Paez et al., 2012), and deletion of $Ca_V1.2$ specifically in OPCs resulted in reduced myelination and lower MBP and MOG expression (Santiago Gonzalez et al., 2017). Hence, activity of L-type channels in oligodendroglial lineage is crucial for remyelination in this MS model, but it is unclear whether oligodendroglial $Ca_V1.2$ channels also play a role during MS in humans. Upregulation of $Ca_V1.2$ channels in pericytes may reflect altered microcirculation in MS lesions, in analogy to the role of L-type VGCCs in pericytes outside the brain (Hashitani and Mitsui, 2019).

$Ca_V1.3$ (CACNA1D)

Neurons

$Ca_V1.3$ channels localize primarily in neuronal cell bodies and dendrites in GM (Hell et al., 1993; Zhang et al., 2005) but were also found in the developing rat optic nerve, corpus callosum (Huang et al., 2012), and axons in spinal dorsal columns of adult rats where they form clusters with RyR2s (Ouardouz et al., 2003). $Ca_V1.3$ channels activate at the membrane potential of −55 mV (Lipscombe et al., 2004) and are important players in generating the pacemaking activity and spontaneous firing (Zuccotti et al., 2011). $Ca_V1.3$ channels control Ca^{2+}-dependent post-burst after-hyperpolarization in CA1 pyramidal neurons, and their activity may trigger Ca^{2+}-dependent intracellular signaling pathways (Gamelli et al., 2011; Striessnig et al., 2014). $Ca_V1.3$ channels may contribute to the mechanisms of memory because their increased expression correlates with memory loss during aging while their inhibition improves age-related memory deficits (Veng et al., 2003). Deletion of $Ca_V1.3$ channels results in increased firing rates of amygdala neurons (probably caused by a reduced slow component of post-burst after-hyperpolarization) and underlies altered fear consolidation in $Ca_V1.3$ knockout mice (McKinney et al., 2009). $Ca_V1.3$ channels are important for formation of cellular architecture: their various splice variants regulate morphology of dendritic spines while their deletion results in reduced morphology of axonal arbors (Hirtz et al., 2012; Stanika et al., 2016).

Glia

$Ca_V1.3$ mRNA and/or protein were detected in cultured or freshly isolated rat brain astrocytes; $Ca_V1.3$ channels may mediate intracellular Ca^{2+} increase directly and *via* Ca^{2+}-mediated activation of RyRs (Latour et al., 2003; Yan et al., 2013; Du et al., 2014; Enders et al., 2020). $Ca_V1.3$ expression increases in reactive astrocytes after status epilepticus in mice, suggesting that role in initiation, maintenance, or spread of seizures (Xu J. H. et al., 2007). Yet, other studies have not found $Ca_V1.3$ channels in astrocytes (D'Ascenzo et al., 2004).

$Ca_V1.3$ channels are expressed in cortical and hippocampal OPCs where they, in concert with other Ca^{2+} channels, may mediate Ca^{2+} entry from the extracellular space and/or trigger CICR from the ER (Haberlandt et al., 2011; Cheli et al., 2015). Knockdown of $Ca_V1.3$ reduces Ca^{2+} influx but does not affect expression level of myelin proteins, proliferation, or morphological differentiation of OPCs (Cheli et al., 2015). In the adult rat spinal cord WM, $Ca_V1.3$ channels are expressed by APC-positive oligodendrocytes, may mediate oligodendrocyte-axon signaling, and/or contribute to Ca^{2+}-dependent injury following trauma (Sukiasyan et al., 2009). Static magnetic stimulation may alter $Ca_V1.3$ gene expression level in human cultured OPCs (Prasad et al., 2017), suggesting that external manipulations may be a useful approach to modulate L-type VGCCs in oligodendroglial cells during diseases.

RNA-seq detected *CACNA1D* gene (and its various splice variants) in microglia (Hammond et al., 2019), and its expression increased upon microglia activation (Espinosa-Parrilla et al., 2015). $Ca_V1.3$ channels regulate synthesis and release of pro-inflammatory substances from microglia, e.g., NO and TNF-α (Espinosa-Parrilla et al., 2015).

Expression and Function in MS

Bulk RNA-seq showed *CACNA1D* upregulation in CA lesions (Elkjaer et al., 2019; Frisch et al., 2020), while snRNA-seq detected significant expression of *CACNA1D* in neuronal clusters (Jakel et al., 2019; **Tables 1**, **2**). Administration of L-type VGCCs blockers resulted in multiple beneficial effects in animal MS models (see above), suggesting that $Ca_V1.3$ channels, perhaps in concert with $Ca_V1.2$ channels, contribute to tissue damage during MS.

P/Q-Type VGCCs

$Ca_V2.1$ (CACNA1A)

The *CACNA1A* gene encodes the pore-forming α1-subunit of P/Q-type ($Ca_V2.1$) VGCCs. Sensitivity to ω-Agatoxin distinguishes Ca^{2+} currents mediated by these channels.

Neurons

$Ca_V2.1$ channels localize on axonal synaptic terminals and play a fundamental role in neurotransmitter release: their direct interaction with the SNARE proteins and synaptotagmin is required for positioning the docked synaptic vesicles near the Ca^{2+} channels for fast vesicular exocytosis (Rettig et al., 1996; Zamponi et al., 2015; Mochida, 2019). $Ca_V2.1$ channels are also present at somatodendritic compartments of neurons (Catterall, 2000; Zamponi et al., 2015; Mochida, 2019) where they co-localize with BK and SK channels and provide Ca^{2+} for activation of these channels (Berkefeld et al., 2006; Indriati et al., 2013; Irie and Trussell, 2017). Ca^{2+} enters through the $Ca_V2.1$ channels and triggers further Ca^{2+} release from the intracellular stores upon activation of RyRs on the ER (Berkefeld et al., 2006; Indriati et al., 2013; Irie and Trussell, 2017). These mechanisms control neuronal firing even in the millisecond time scale (Irie and Trussell, 2017). Somatodendritic $Ca_V2.1$ channels regulate gene expression, local Ca^{2+} signaling, and cell survival (Pietrobon, 2010).

$Ca_V2.1$ channels are also present in the WM, i.e., corpus callosum and developing optic nerve (Alix et al., 2008; Nagy et al., 2017). In the optic nerve, $Ca_V2.1$ channels are transiently clustered in the axolemma at the sites where the underlying vesicular and tubular elements are fusing with the axonal membrane (Alix et al., 2008). Some of these sites later become nodes of Ranvier, and mutations of the α1A-subunit results in malformation of the nodes of Ranvier (Alix et al., 2008). In the corpus callosum, $Ca_V2.1$ channels mediate fast release of glutamatergic vesicles at axon-OPC synapses, and blockade of these channels in slices reduces release at axon-glia synapses by 88% (Nagy et al., 2017).

$Ca_V2.1$ channels may play a role in nociception because inflammatory and neuropathic pain is altered in mice with deletion of $Ca_V2.1$ channels (Pietrobon, 2010). Mutations in the *CACNA1A* gene underlie familial hemiplegic migraine type 1, spinocerebellar ataxia type 6, and episodic ataxia type 2, and may be associated with increased risk of epilepsy (Pietrobon, 2010; Rajakulendran et al., 2012; Izquierdo-Serra et al., 2020).

Glia

RT-PCR detected α1A-subunit in mouse cortical astrocytes in culture, but $Ca_V2.1$ channels did not mediate Ca^{2+} entry into astrocytes (Cheli et al., 2016b). Exposure of mouse primary astrocytes to β-Amyloid did not affect $Ca_V2.1$ transcript level (Daschil et al., 2014). However, increased expression of $Ca_V2.1$ channels was observed in reactive astrocytes after status epilepticus in mice, suggesting their role in initiation, maintenance, or spread of seizures (Xu J. H. et al., 2007). $Ca_V2.1$ channels are expressed in hippocampal OPCs, and in pre-myelinating oligodendrocytes of the brainstem (Haberlandt et al., 2011; Barron and Kim, 2019). In brainstem oligodendrocytes, opening of $Ca_V2.1$ channels is triggered upon depolarization mediated by glutamate (*via* AMPA receptors) or high K^+, as well as upon electrical stimulation of axons (Barron and Kim, 2019), suggesting that $Ca_V2.1$ channels mediate Ca^{2+} influx into the oligodendroglial cells upon neuronal activity *in vivo*. In this way, neuronal activity may trigger and/or modulate Ca^{2+}-dependent signaling in oligodendroglial cells. RNA-seq detected *CACNA1A* gene in microglia (Hammond et al., 2019). $Ca_V2.1$ channels may contribute to glioblastoma progression because their inhibition reduced proliferation of glioblastoma cells, although to a lesser extent than blockade of N-type channels (Nicoletti et al., 2017).

Expression and Function in MS

Bulk RNA-seq found *CACNA1A* upregulation in CA lesions (Elkjaer et al., 2019; Frisch et al., 2020). The snRNA-seq revealed significant expression of *CACNA1A* transcripts in neuronal and OPCs clusters (Jakel et al., 2019; **Tables 1**, **2**). *CACNA1A* upregulation in MS may reflect the necessity to build new nodes of Ranvier on demyelinated axons within the CA lesions. In oligodendroglial cells, Ca^{2+} entry through $Ca_V2.1$ channels may be required for activation of intracellular signaling pathways necessary for differentiation of OPCs and pre-myelinating oligodendrocytes.

$Ca_V2.3$ (CACNA1E), R-Type VGCCs

Neurons

$Ca_V2.3$ channels are localized to the dendritic spines and pre-synaptically (Parajuli et al., 2012). $Ca_V2.3$-mediated Ca^{2+} currents activate upon strong membrane depolarization and are distinguished by sensitivity to low $NiCl_2$ concentrations and SNX-482 toxin. Presynaptic R-type channels play a role in neurotransmitter release (Wu et al., 1999; Gasparini et al., 2001) and synaptic plasticity (Dietrich et al., 2003; Yasuda et al., 2003; Takahashi and Magee, 2009), but their efficiency in triggering neurotransmitter release may be lower compared to P/Q- or N-type VGCCs if they are placed distantly from vesicle release sites (Wu et al., 1999). Dendritic R-type channels are coupled to SK channels and provide Ca^{2+} influx for their activation during excitatory postsynaptic potentials and back-propagating APs (Bloodgood and Sabatini, 2008; Jones and Stuart, 2013). The capacity of dendritic SK channels to promote generation of dendritic Ca^{2+} spikes also depends on $Ca_V2.3$ activation (Bock et al., 2019). Besides, Ca^{2+} influx *via* $Ca_V2.3$ channels may be necessary for activation of $K_v4.2$ channels (Wang et al., 2014). The $Ca_V2.3$ channels also form complexes with BK channels, and this functional interaction modulates AP properties and short-term plasticity in hippocampal neurons (Gutzmann et al., 2019). Studies in KO mice revealed that $Ca_v2.3$ channels are involved in the mechanisms of sleep modulation, fear response, pain, and seizures (Saegusa et al., 2000; Lee et al., 2002; Weiergraber et al., 2007; Siwek et al., 2014; Zamponi et al., 2015; Wormuth et al., 2016). Deletion of $Ca_V2.3$ channels in mice resulted in larger infarct size after middle cerebral artery occlusion *in vivo* and larger Ca^{2+} entry into the cells upon oxygen-glucose deprivation in slices, suggesting that $Ca_V2.3$ channels are protective during ischemic tissue damage (Toriyama et al., 2002).

Glia

In primary astrocyte cultures, mRNA and $Ca_V2.3$ proteins were detected using RT-PCR, Western blotting, immunohistochemistry, and electrophysiological recordings (Latour et al., 2003; D'Ascenzo et al., 2004). During myelinogenesis, oligodendrocytes within WM of the brainstem,

cerebellum, and telencephalon transiently express $Ca_V2.3$ channels, but their expression strongly decreases into adulthood (Chen et al., 2000). Ultrastructural analysis demonstrated $Ca_V2.3$ immunoreactivity in soma and processes of oligodendrocytes, paranodal loops, and loose myelin sheaths (Chen et al., 2000). RNA-seq detected only negligible *CACNA1* expression in microglia (Hammond et al., 2019).

Expression and Function in MS

Bulk RNA-seq showed *CACNA1E* upregulation in CA lesions (Elkjaer et al., 2019; Frisch et al., 2020), while snRNA-seq found significant expression of *CACNA1E* transcripts in neuronal clusters (Jakel et al., 2019; **Tables 1**, **2**). The functional role of $Ca_V2.3$ channels in MS is unknown.

T-Type VGCCs

The T-type channels (Ca_v3) are low-voltage activated Ca^{2+} channels with α1-subunit being encoded by *CACNA1G* ($Ca_v3.1$), *CACNA1H* ($Ca_v3.2$), or *CACNA1I* ($Ca_v3.3$) gene. They are widely distributed in the brain, spinal cord, and DRGs. Ca_v3 channels activate around V_{rest}, show fast inactivation kinetics (Cav3.1 > Cav3.2 > Cav3.3), and mediate tiny Ca^{2+} currents (Perez-Reyes, 2003; Weiss and Zamponi, 2019). Ca_v3 channels regulate neuronal excitability and play a role during rhythmic AP bursts of thalamic relay neurons, which underlie generation of neuronal oscillations under physiological (sleep) and pathophysiological (epilepsy) conditions (Suzuki and Rogawski, 1989; Astori et al., 2011). Ca_v3 channels are involved in regulation of nociceptive pathways, sensory processing, hormone, and neurotransmitter release (Weiss and Zamponi, 2019). Mutations in Ca_v3 genes are linked to neurodevelopmental, neurological, and psychiatric diseases (Lory et al., 2020). Pharmacological non-selective T-type channel blockers are clinically used as antiepileptic drugs and also show anti-nociceptive effects (Zamponi et al., 2015).

Cav3.1, Ca3.2, and Ca3.3 (CACNA1G, CACNA1H, and CACNA1I)

Neurons

Ca_v3 isoforms display distinct distribution patterns with prominent somatodendritic expression in thalamic and hippocampal neurons (McKay et al., 2006). Ca^{2+} imaging and pharmacological experiments showed that $Ca_v3.2$ and $Ca_v3.3$ subtypes located in the AIS influence the generation and the timing of APs (Bender and Trussell, 2009; Kole and Stuart, 2012). In rodent WM, Ca_v3 transcripts were detected at low level (Aguado et al., 2016), and information on cellular distribution is lacking.

Glia

Some studies detected $Ca_v3.1$ transcripts and proteins in rat cortical astrocytic cultures (Latour et al., 2003), while others found only scarce $Ca_v3.1$ expression in cultured astrocytes (Cheli et al., 2016b; Kim et al., 2018). Divergent findings showed that $Ca_v3.2$ immunoreactivity was absent (Chen et al., 2015) or present (Li et al., 2017) in rat spinal cord astrocytes. $Ca_v3.1$ and $Ca_v3.2$ transcripts were detected in clonal oligodendroglial CG4 cell line (Rui et al., 2020) and in OPCs isolated from mouse cortex (Zhang et al., 2014) or hippocampal slices (Haberlandt et al., 2011). In microglia, RNA-seq did not detect the Ca_v3 isoforms (Hammond et al., 2019).

Expression and Function in MS

Bulk RNA-seq revealed upregulation of $Ca_v3.2$ and $Ca_v3.3$ genes in CA lesions and upregulation of $Ca_v3.1$ in ILs (Elkjaer et al., 2019; Frisch et al., 2020; **Table 1**). The snRNA-seq detected $Ca_v3.1$and $Ca_v3.3$ transcripts in neuronal clusters, while it did not detect the $Ca_v3.2$ (Jakel et al., 2019; **Tables 1**, **2**). Genome-wide sequencing identified significant association of a $Ca_v3.2$ mutation (*CACNA1Hp.R1871Q*) with patients suffering relapsing-remitting MS (Sadovnick et al., 2017). Ca_v3 upregulation in MS lesions may be triggered by inflammatory mediators and may contribute to axonal dysfunction. Indeed, prostanoids and hydrogen sulfide modulate $Ca_v3.2$ expression and function, and increased $Ca_v3.2$ channel activity and axonal accumulation is associated with inflammation and pain (Sadovnick et al., 2017; Chen et al., 2018). T-type currents contribute to Ca^{2+}-mediated injury of spinal cord WM axons triggered by anoxia (Imaizumi et al., 1999) and to peripheral nerve injury (Watanabe et al., 2015). L/T-type VGCC blocker lomerizine prevents retinal ganglion cell death after diffuse axonal injury (Karim et al., 2006).

Animal studies suggest that $Ca_v3.1$ upregulation in IL, a lesion type with complete demyelination and substantial axonal loss, may play a detrimental role. Specifically, the $Ca_v3.1$-deficient mice are markedly resistant to EAE induction, and this effect may be mediated by lower production of granulocyte–macrophage colony-stimulating factor (a cytokine implicated in EAE susceptibility) by CNS-infiltrating Th1 and Th17 cells (Wang et al., 2016). The $Ca_v3.1$ subunit is a functionally predominant T-type channel in $CD4^+$ T cells (Trebak and Kinet, 2019). The $Ca_v3.1$-mediated Ca^{2+} increase is critical for calcineurin-NFAT activation driving transcription of cytokines in T cells, and T cells from $Ca_v3.1$-deficient mice show decreased IL-17A, IL-17F, and IL-21 production. The development of isoform-specific modulators should help in establishing the differential role of Ca_v3 subtypes in MS lesions.

Ryanodine Receptors

RyRs encompass three mammalian isoforms, *RyR1–3*, which form homo-tetrameric channels on the ER. RyRs are highly conductive Ca^{2+} channels: they get activated by Ca^{2+} influx upon plasma membrane depolarization mediating CICR from the ER (Fill and Copello, 2002; Lanner et al., 2010). In the brain, the RyR2s show predominant expression, followed by RyR3s, and then RyR1s (McPherson and Campbell, 1990; Giannini et al., 1995).

RyR2 and RyR3

Neurons

RyRs localize along ER of neurons, including WM axons (Giannini et al., 1995). They play a role in vesicle fusion, neurotransmitter release, synaptic plasticity, and growth cone dynamics (Giannini et al., 1995; Kushnir et al., 2018). RyRs form

complexes with L-type Ca^{2+} channels: RyR1-$Ca_v1.2$ and RyR2-$Ca_v1.3$ (Ouardouz et al., 2003). WM axons transduce membrane depolarization to Ca^{2+} release from ER, whereby L-type VGCCs gate RyRs, analogous to "excitation–contraction coupling" in muscles (Ouardouz et al., 2003; Stirling and Stys, 2010). Genetic mutations or oxidative stress can render RyRs leaky to Ca^{2+} and promote defective signals as observed in neurodegenerative disorders, heart failure, and muscular dystrophy (Kushnir et al., 2018).

Glia

RYR2 and *RYR3* transcripts, but only RyR3 protein, were found in cultured astrocytes from mouse brain (Matyash et al., 2002; Kesherwani and Agrawal, 2012). *RyR2* transcripts and proteins were upregulated in spinal WM astrocytes after hypoxic injury (Kesherwani and Agrawal, 2012) and SCI (Liao et al., 2016; Pelisch et al., 2017). All *RYR*s subunits were found in rat optic nerve oligodendrocyte cultures (Ruiz et al., 2010), but *RYR3* was selectively expressed in rat cortical OPCs (Haak et al., 2001; Li T. et al., 2018). RyR3s amplify small inward Ca^{2+} currents in astrocytes and OPC, regulating behavior of these cells (Simpson et al., 1998; Matyash et al., 2002; Haberlandt et al., 2011). RyRs mediate stress response in oligodendrocytes, and RyR inhibition attenuated intracellular Ca^{2+} overload following AMPA excitotoxicity (Ruiz et al., 2010). RyR1 and RyR2 mRNAs were detected in adult human microglia, whereas only RyR3 was found in fetal microglia (Klegeris et al., 2007). RNA-seq did not detect *RYR2* and *RYR3* in mouse microglia (Hammond et al., 2019).

Expression and Function in MS

Bulk RNA-seq found upregulation of RyR2 transcripts in CA lesions and downregulation of RyR3 in ILs (**Table 1**; Elkjaer et al., 2019; Frisch et al., 2020). The snRNA-seq revealed significant expression of RyR2 in neuronal clusters and of RyR3 in the astrocyte1 cluster (**Table 1**; Jakel et al., 2019). RyR subunits probably play a differential role in perturbed intracellular Ca^{2+} homeostasis in WM cells of SPMS brain. RyR2 in CA lesions may contribute to axonal dysfunction because intra-axonal Ca^{2+} overload mediated by RyRs and IP3Rs activates the mitochondrial permeability transition pore and contributes to axonal dieback and degeneration following WM ischemic injury (Ouardouz et al., 2003; Stirling and Stys, 2010; Kesherwani and Agrawal, 2012) and SCI (Stirling et al., 2014; Liao et al., 2016). The RyRs inhibitor ryanodine significantly attenuates mitochondrial dysfunction (Villegas et al., 2014), axonal dieback, and secondary axonal degeneration in injured WM (Thorell et al., 2002; Stirling et al., 2014; Orem et al., 2017). In line, mice with RyR2 gain-of-function mutation exhibit more axonal damage than wild-type controls following SCI (Stirling et al., 2014), while RyR2 knockdown attenuates mitochondrial dysfunction and ER stress and improves functional recovery (Liao et al., 2016).

Functional RyR3s may contribute to astrocyte migration in response to injury, which is important for tissue remodeling and wound healing. In fact, RyR3s control astrocyte motility because astrocytes from RyR3 KO mice display reduced migratory activity (Matyash et al., 2002). Conversely, RyR3 downregulation in ILs may influence the formation of dense astrocytic scar imposing a major barrier to axonal and myelin regeneration. RyR3s also contribute to intracellular Ca^{2+} transients during OPCs differentiation, while RyR3 inhibition prevents OPCs development (Li T. et al., 2018). Interaction between RyRs and NCX in oligodendrocyte processes may represent an amplification mechanism to generate Ca^{2+} transients required for oligodendrocyte differentiation *in vitro* (Casamassa et al., 2016; Hammann et al., 2018; de Rosa et al., 2019; Boscia et al., 2020). However, it remains unclear whether these mechanisms play a role in human MS. The development of selective modulators will help to establish function of RyRs in MS.

TRP Channels

Transient receptor potential (TRP) channels are tetrameric non-selective cation channels which encompass 30 different types (Nilius and Owsianik, 2011). Upon TRP channel activation, the membrane potential depolarizes, leading to activation or inactivation of voltage-gated ion channels and regulation of Ca^{2+} signaling (Gees et al., 2010). Various intracellular or extracellular stimuli, including chemical and osmotic stress, can trigger activation of TRP channels (Clapham, 2003). TRP channels are involved in pain, regulation of neurotransmitter release, and immune functions. Vanilloid TRP channels (TRPV), melastatin TRP channels (TRPM), and polycystin TRP channels (TRPP) have been detected in WM lesions of patients with progressive MS.

TRPV1

Neurons

In the CNS, TRPV1 channels are mainly localized on cell bodies and dendritic spines, but also in synaptic vesicles (Goswami et al., 2010). TRPV1 channels are activated by exogenous (i.e., capsaicin) or endogenous (i.e., high temperatures, acid pH, anandamide, 2-arachidonoylglycerol, and lipid metabolites) stimuli (Van Der Stelt and Di Marzo, 2004). They play a role in weight, appetite, and energy homeostasis (Derbenev and Zsombok, 2016; Christie et al., 2018); synaptic plasticity (Gibson et al., 2008; Wang et al., 2020); neuropathic pain (Rivat et al., 2018); and regulation of inflammatory response (Kong et al., 2017).

Glia

TRPV1 channels are expressed in astrocytes (Ho et al., 2014), microglia (Sappington and Calkins, 2008), and, to a lesser extent, oligodendrocytes (Gonzalez-Reyes et al., 2013; Marques et al., 2016).

Expression and Function in MS

Bulk RNA-seq showed significant TRPV1 downregulation in CA lesions (**Figure 2**, **Table 1**; Elkjaer et al., 2019; Frisch et al., 2020), while snRNA-seq barely detected TRPV1 (**Table 2**; Jäkel and Williams, 2020). The downregulated TRPV1 in CA lesions may influence neural plasticity and glia response both in the hypocellular inactive demyelinated core and in the hypercellular rim filled with activated glia. However, it is unclear whether dysfunctional TRPV1 has pro- and anti-inflammatory roles,

and whether it favors or prevents CA lesion expansion and progression, because experimental findings are inconsistent. In rodents, administration of TRPV1 agonists reduced EAE severity (Tsuji et al., 2010), while the TRPV1 antagonist capsazepine, although ineffective for EAE severity (Paltser et al., 2013), reversed the beneficial effects of the endocannabinoid uptake inhibitor (Cabranes et al., 2005). Beneficial effects of TRPV1 may be mediated by its ability to promote micro-vesicle release from microglia, which enhances glutamatergic transmission in neurons (Marrone et al., 2017). However, on the other hand, TRPV1 stimulation induces the pro-inflammatory phenotype of microglia while downregulation promotes the anti-inflammatory phenotype (Hassan et al., 2014; Marrone et al., 2017). TRPV1 also regulates microglia migration, cytokine production, ROS generation, phagocytosis, and death (Kim et al., 2006; Schilling and Eder, 2009; Miyake et al., 2015). Furthermore, TRPV1 mediates migration and chemotaxis of astrocytes, their activation during stress and injury (Ho et al., 2014), and inflammasome activation. The picture becomes even more complex because TRPV1-KO mice show higher lethality during EAE peak but better recovery in the chronic stage (Musumeci et al., 2011). In addition, genetic deletion of TRPV1 in mice resulted in significant protection in the MOG-EAE model, and less severe breakdown of BBB (Paltser et al., 2013). Interestingly, patients with severe MS progression show over-representation of single-nucleotide polymorphisms (SNPs) in the TRPV1 gene (Paltser et al., 2013) that can affect the expression and activity of the channel and cortical excitability, and modulate pain (Xu H. et al., 2007; Mori et al., 2012; Stampanoni Bassi et al., 2019).

TRPV6

TRPV6 channels are distinguished by high Ca^{2+} selectivity (van de Graaf et al., 2006) and constitutive activity at low intracellular Ca^{2+} levels and V_{rest} (Vennekens et al., 2000). TRPV6 channels can form homo- or hetero-tetramers. TRPV5–6 are mainly expressed in epithelial and bone cells (Hoenderop et al., 2003).

Neurons and Glia

In the mouse brain, TRPV6 channels are expressed in neurons, while transcripts were detected in astrocytes by RNA-seq (Riccio et al., 2002; Nijenhuis et al., 2003; Batiuk et al., 2020).

Expression and Function in MS

Bulk RNA-seq found *TRPV6* downregulation in all MS lesion types and in NAWM (**Figure 2**, **Table 1**; Elkjaer et al., 2019; Frisch et al., 2020), but snRNA-seq failed to detect *TRPV6* transcripts (**Table 2**; Jakel et al., 2019). Little is known about the functional role of TRPV6 in brain cells. However, TRPV6 deletion in trophoblasts correlates with altered extracellular matrix (ECM) formation in the labyrinth during pregnancy (Winter et al., 2020). Hence, it will be important to investigate whether TRPV6 downregulation contributes to ECM alterations observed in SPMS lesions and believed to be a key remyelination-inhibiting factor.

TRPM2

Neurons

TRPM2 channels are found in cell bodies and neurites (Nagamine et al., 1998; Olah et al., 2009) and often co-localize with a marker of dopaminergic neurons (Bai and Lipski, 2010). They are Ca^{2+}-permeable sensors of various stimuli (Huang et al., 2020), contribute to synaptic plasticity, and inhibit neurite outgrowth (Sita et al., 2018).

Glia

TRPM2 transcripts are intensely expressed in mouse microglia (Malko et al., 2019), but only at lower levels in astrocytes and oligodendrocytes (Choi et al., 2015; Marques et al., 2016; Falcao et al., 2018; Batiuk et al., 2020; **Table 3**). TRPM2 plays a critical role in microglia activation and generation of pro-inflammatory mediators, thus contributing to neuropathic pain, brain damage due to chronic hypo-perfusion, neonatal hypoxia–ischemia, and amyloid-beta (Malko et al., 2019).

Expression and Function in MS

Bulk RNA-seq showed increased *TRPM2* expression in the ILs (**Table 1**; Elkjaer et al., 2019; Frisch et al., 2020). SnRNA-seq found *TRPM2* in neuronal, microglia, and ImOLG clusters. The functional role of TRPM2 channels in ILs, lesions that display reduced microglia density, axonal loss, and upregulation of stress response genes (Elkjaer et al., 2019; Frisch et al., 2020), may be related to neuronal and microglia damage. Indeed, TRPM2 channel is upregulated by diverse pathological stimuli (Malko et al., 2019) and is an important element during oxidative stress, mitochondrial dysfunction (Freestone et al., 2009), and neurodegenerative disorders (Chung et al., 2011). Constitutive TRPM2 activation is triggered by ROS and leads to pathological Ca^{2+} signaling and cell death (Eisfeld and Luckhoff, 2007; Naziroglu and Luckhoff, 2008). Knockout of *TRPM2* gene in mice, or blocking the channels with miconazole, improves pathological outcome in EAE and attenuates painful behavior (Melzer et al., 2012; So et al., 2015; Tsutsui et al., 2018). TRPM2-KO mice show reduction of CXCL2 chemokine production by CNS-infiltrating macrophages and suppressed neutrophil infiltration of the brain tissue (Tsutsui et al., 2018). These findings suggest that TRPM2 may represent a promising target in SPMS.

TRPP1 and TRPP3 (PKD2 and PKD2L2)

The TRPP(PKD2) channels are encoded by *TRPP1(PKD2)*, *TRPP2(PKD2L1),* and *TRPP3(PKD2L2)* genes (www.guidetopharmacology.org) and form Ca^{2+}-permeable non-selective cation channels. In the mouse brain, *PKD2* and *PKD2L2* transcripts are detected in neurons and glia (**Table 3**). TRPP1 is present on the ER, primary cilia, and plasma membrane, and TRPP3 is widely expressed in fetal tissues (Guo et al., 2000).

Expression and Function in MS

Bulk RNA-seq detected significant downregulation of PKD2 or PKD2L2 in ILs and CA lesions, respectively (Elkjaer et al., 2019; Frisch et al., 2020) (**Figure 2**, **Table 1**). SnRNA-seq detected PKD2 transcripts in neuronal and glia clusters but did not detect

PKD2L2 (**Table 2**). It is unclear whether TRPP downregulation in MS lesions is beneficial or detrimental. On one hand, it may be detrimental because TRPP1 and TRPP3 channels are important for maintaining Ca^{2+} homeostasis and contribute to cell proliferation (Xiao and Quarles, 2010; Xiao et al., 2010), while TRPP1 knockdown results in increased susceptibility to stress-induced cell death in kidney epithelial cells (Brill et al., 2020). On the other hand, overexpression of TRPP contributes to apoptosis (Xiao and Quarles, 2010; Xiao et al., 2010), and TRPP1 is upregulated as a direct consequence of ER and oxidative stress during pathological conditions.

Chloride Channels

ClC channels mediate voltage-dependent transmembrane transport of Cl^-. They are expressed in plasmalemma and intracellular membranes forming transmembrane dimers (Weinreich and Jentsch, 2001). ClC proteins can function as Cl^- channels or as Cl^-/H^+ exchangers. ClCs regulate V_{rest} in skeletal muscle, trans-epithelial Cl^- reabsorption in kidneys, and intracellular pH and Cl^- concentration through coupled Cl^-/H^+ exchange in several cell types including brain cells.

ClC-2 (CLCN2)

The *CLCN2* gene encodes a voltage- and volume-regulated ClC-2 channel (Chu et al., 1996), essential for efflux of accumulated Cl^- and control of cell volume homeostasis. ClC-2 is expressed in neurons and glia (Jentsch et al., 2005) and is upregulated at low osmolarity, cell swelling, and membrane hyperpolarization (Grunder et al., 1992; Clark et al., 1998).

Neurons

ClC-2 localizes on inhibitory interneurons and regulates $GABA_A$ receptor-mediated synaptic inputs from basket cells (Foldy et al., 2010). Cl^- extrusion by ClC-2 following hyperpolarization ensures the maintenance of low intracellular Cl^- concentration following synaptic inhibition (Foldy et al., 2010). The link of ClC-2 mutations with generalized epilepsies in humans suggests an important role of ClC-2 in regulating neuronal excitability (Kleefuss-Lie et al., 2009).

Glia

Astrocytes express ClC-2 that interacts with AQP4 to regulate Cl^- influx and efflux (Benfenati et al., 2007). ClC-2 is expressed in microglia and may regulate cell volume and phagocytosis (Ducharme et al., 2007). In oligodendrocyte lineage cells, ClC-2 positively regulates OPCs differentiation (Jentsch and Pusch, 2018) and transcription factors for myelin genes, thus contributing to myelin formation and WM integrity (Hou et al., 2018).

Expression and Function in MS

Bulk RNA-seq showed significant *CLCN2* downregulation in CA lesions (Elkjaer et al., 2019; Frisch et al., 2020; **Figure 2**, **Table 1**). SnRNA-seq detected *CLCN2* transcripts in oligodendrocyte clusters, while they were only faintly observed or absent in other clusters (**Table 2**). Several findings suggest that *CLCN2* downregulation in MS may reflect altered WM integrity and/or contribute to the mechanisms of myelin destruction: first, $ClCN2^{-/-}$ mice exhibit abnormal WM morphology (Blanz et al., 2007); second, loss-of-function *CLCN2* mutations lead to leukodystrophy; third, loss of cell adhesion molecule GlialCAM, which binds to ClC-2 in glia, is associated with leukodystrophy (Jeworutzki et al., 2012; Hoegg-Beiler et al., 2014). Of note, though, is a recent report showing that leukodystrophy fully develops only when ClC-2 is disrupted in both astrocytes and oligodendrocytes (Goppner et al., 2020). It remains to be investigated whether CLC-2 loss in glia contributes to the failure of myelin repair in human CA lesions.

ClC-7 (CLCN7)

The *CLCN7* gene encodes for the chloride-proton antiporter ClC-7 localized to lysosomes and crucial for function of osteoclasts and brain cells (Kornak et al., 2001; Jentsch and Pusch, 2018).

Neurons and Glia

In mice, neurons and microglia express ClC-7 protein (Kasper et al., 2005; Majumdar et al., 2011; Weinert et al., 2014), while transcripts were found in astrocytes and oligodendrocyte lineage (Falcao et al., 2018; Batiuk et al., 2020). Mutations in the human *CLCN7* gene are associated with osteopetrosis and neurodegeneration (Kornak et al., 2001).

Expression and Function in MS

Bulk RNA-seq detected significant *CLCN7* downregulation in CA lesions (Elkjaer et al., 2019; Frisch et al., 2020; **Figure 2**, **Table 1**). SnRNA-seq found *CLCN7* transcripts in neuronal and all glia clusters (**Table 2**). Functional role of ClC-7 under demyelinating conditions is unknown. In neurons, ClC-7 on lysosomes contributes to the function of the endosomal–lysosomal pathway (Poet et al., 2006; Bose et al., 2021). Lysosomal localization of CLC-7 increases during microglia activation, leading to increased lysosomal acidification and Aβ degradation (Majumdar et al., 2011). ClCN7-deficient mice display widespread WM atrophy, neuronal loss, microglia activation, astrocytosis, and accumulations of storage material in lysosomes (Kornak et al., 2001; Kasper et al., 2005; Pressey et al., 2010). In SPMS lesions, dysfunctional ClC-7 activity may directly affect the luminal pH and Cl^- concentrations and lysosomal protein degradation (Wartosch et al., 2009), which, in turn, may lead to neuronal and glial degeneration in the WM.

Connexins

Connexins (Cxs) are transmembrane proteins with channel and non-channel functions. Channel functions include the formation of gap junctions (GJs) and hemichannels (HCs) (Saez et al., 2003; Wang et al., 2013; Gajardo-Gomez et al., 2016), while non-channel functions involve adhesion properties and intracellular signaling (Zhou and Jiang, 2014; Leithe et al., 2018). More than 20 Cxs genes have been described in humans, and 11 of them are expressed in the brain (Willecke et al., 2002; Theis et al., 2005). Cxs are essential players in ionic homeostasis, intercellular Ca^{2+} signaling and Ca^{2+} waves propagation, gliotransmission, synaptic transmission and plasticity, brain metabolism, brain–blood barrier development and integrity, and myelination

(Takeuchi and Suzumura, 2014). In the WM, GJs are essential for K^+ buffering in response to neuronal activity, they facilitate transport of nutrients and ions from oligodendrocyte soma to myelin layers and from astrocytes to oligodendrocytes (Bradl and Lassmann, 2010). In the WM, HCs are involved in metabolic coupling and energy supply to neurons, and provide a major pathway for glucose entry into OPCs and oligodendrocytes (Niu et al., 2016).

Cx37 (GJA4)

Cx37, encoded by *GJA4* gene, predominantly builds heterotypic GJs with Cx40 and Cx43 in vascular cells and plays an essential role in vasomotor activity, endothelial permeability, and maintenance of body fluid balance (Falcao et al., 2018; Li et al., 2018).

Expression and Function in MS

Bulk RNA-seq revealed significant *GJA4* upregulation in ILs (Elkjaer et al., 2019; Frisch et al., 2020), while snRNA-seq showed high *GJA4* expression in pericyte cluster (Jakel et al., 2019; **Tables 1**, **2**). In chronically demyelinated axons, as those within ILs, hypoxia due to imbalance between increased energy demand and reduced ATP production because of mitochondrial dysfunction may drive angiogenesis. However, while providing trophic factors for tissue remodeling, angiogenesis may contribute to hypoperfusion and neurovascular uncoupling (Girolamo et al., 2014). Interestingly, Cx37 knockdown with siRNA in human umbilical vein endothelial cells diminishes capillary branching (Gartner et al., 2012), but $Cx37^{-/-}$ mice develop a more extensive vasculature under ischemic conditions and show enhanced recovery after hind limb ischemia (Fang et al., 2011). In the future, it will be important to investigate whether Cx37 protein contributes to aberrant cerebrovascular and angiogenic responses in human ILs during MS.

Pannexins

The Pannexin (Px) family consists of three members, encoded by *Panx1*, *Panx2,* and *Panx3* genes. Pannexins do not form GJ *in vivo* but operate as plasma membrane channels (pannexons) and participate in paracrine and autocrine signaling in brain GM and WM (Sosinsky et al., 2011; Sahu et al., 2014; Dahl, 2015).

Px1 (PANX1)

Px1 is permeable to anions, some negatively charged molecules (glutamate, aspartate, and ATP), and fluorescent dyes (Ma et al., 2012; Yeung et al., 2020). Opening of Px1 may be promoted by voltage, increased intracellular Ca^{2+}, mechanical stress, extracellular K^+, oxygen deprivation, caspases cleavage, ATP binding to P2Y or $P2X_7$ receptors, activation of α1-adrenergic, NMDA, and thromboxane receptors (Chiu et al., 2018; Dahl, 2018; Whyte-Fagundes and Zoidl, 2018).

Neurons and Glia

Px1 is distributed in GM and WM regions, including cerebellum, corpus callosum, and fimbria fornix of mice (Bruzzone et al., 2003) and rats (Vogt et al., 2005). Px1 is expressed in neurons, astrocytes, microglia, oligodendrocytes, vascular cells, and peripheral immune cells (Iglesias et al., 2009; Swayne et al., 2010; Orellana et al., 2013; Good et al., 2018; Lapato and Tiwari-Woodruff, 2018). In neurons, Px1 may be co-expressed with Px2 and is found in cell soma, dendrites, and axons (Cone et al., 2013).

Interaction between Px1 and purinergic signaling deserves special attention because Px1 forms complexes with $P2X_7$Rs (Taruno, 2018). Binding of ATP to $P2X_7$R triggers opening of Px1 channels with subsequent ATP release (Locovei et al., 2007; Iglesias et al., 2008; Pelegrin et al., 2008; Chiu et al., 2018). ATP signaling involving Px1 channels regulates neurite outgrowth and synaptic plasticity in neurons, while in glia, it underlies intercellular propagation of Ca^{2+} waves, cell differentiation, and migration (Giaume et al., 2021).

Expression and Function in MS

Bulk RNA-seq showed significant *PANX1* upregulation in ILs (**Table 1**; Elkjaer et al., 2019; Frisch et al., 2020), but snRNA-seq did not detect *PANX1* transcripts (Jakel et al., 2019). ILs are lesions with little/no inflammatory activity but with sharply demarcated hypocellular areas of demyelination and axonal degeneration. Px1 activation is known to enable ATP release, and ATP is a "find me" signal promoting chemotaxis of microglia/macrophages to the injury site for fast clearance of dead cells and a molecule important for myelination (Chekeni et al., 2010; Gajardo-Gomez et al., 2016). Hence, *PANX1* upregulation in ILs may be a compensatory mechanism that stimulates glial activity. On the other hand, upregulated Px1 mRNA expression in cerebellum and spinal cord in chronic EAE contributes to WM damage (Lutz et al., 2013). Uncontrolled opening of $P2X_7$R-Px1 complex in response to demyelination triggers excessive glutamate and ATP release, altered Ca^{2+} dynamics, excitotoxicity, damage of axons, and myelin (Orellana et al., 2011; Crespo Yanguas et al., 2017). Knockout or blockade of Px1 with probenecid in rodents restrains EAE symptoms and results in reduced inflammation and decreased oligodendrocyte damage (Hainz et al., 2017), suggesting that Px1 activity supports damage during MS. More studies are required to establish how Px1 should be modulated in order to halt neurodegeneration during MS.

CatSper Channels

Catsperg and Caspere

Cation channel of spermatozoa (CatSper) is a highly complex multi-subunit voltage-gated Ca^{2+}-permeable ion channel. Four distinct α-subunits (CatSper1–4) and several accessory subunits are encoded by *CATSPER* genes (Qi et al., 2007). The CatSper channel is essential for the activity of sperm flagellum and sperm fertility (Lishko and Mannowetz, 2018). RNA-seq detected only CATSPERG transcripts in mouse neurons, oligodendrocytes, and microglia (Marques et al., 2016; Hammond et al., 2019; Jakel et al., 2019).

Expression and Function in MS

Bulk RNA-seq found downregulation of the auxiliary subunit gamma (*CASPERG*) and epsilon (*CATSPERE*) in CA lesions and ILs, respectively (**Table 1**; Elkjaer et al., 2019; Frisch et al., 2020). SnRNA-seq did not find CATSPERE transcripts and barely detected CATSPERG in neuronal and glia clusters. It is difficult to

speculate on the role of CatSper channels in MS lesions because characterization of these subunits is limited to sperm cells, and no data on CatSper protein expression or function in the brain are available.

CONCLUSIONS

Understanding how distinct ion channels regulate CNS ionic homeostasis in WM neurons, axons, glia, and vascular cells under chronic demyelinating conditions is of critical importance for the development of novel therapeutic strategies to prevent neurodegeneration and disability progression and improve functional recovery and repair in MS. Recent Bulk RNA-seq (Elkjaer et al., 2019; Frisch et al., 2020) revealed a considerable number of ion channel genes that are altered in different types of WM lesions of the SPMS brain, particularly in WM CA lesions, a type of lesion that develops in MS patients despite disease-modifying therapy and predicts a more aggressive disease course (Absinta et al., 2019; Elliott et al., 2019). SnRNA-seq found that transcripts for dysregulated ion channels belong to the clusters of neurons, astrocytes, oligodendrocyte lineage, microglia/macrophages, and pericytes (Jakel et al., 2019). The dysregulation of ion channel genes in MS may be detrimental or beneficial for functions of neurons, including interstitial neurons. Intense upregulation of genes encoding voltage-gated Na^+ channels in CA lesions may reflect the imbalance of Na^+ homeostasis observed in SPMS brain (Inglese et al., 2010). Conversely, the upregulation of a large number of voltage-gated K^+ channel genes may be linked to a protective response to limit neuronal excitability. The altered Cl^- homeostasis, revealed by the significant downregulation of voltage-gated Cl^- channels in MS lesions, may contribute to an altered inhibitory neurotransmission and increased excitability. Depending on the type of alterations, dysregulated ion channels in MS may favor AP propagation and dampen neuronal hyperexcitability or, on the contrary, may contribute to axonal dysfunction and cell death. Altered expression and/or function of ion channels may also influence key properties of glia including proliferation, migration, spatial buffering, cytokine release, cell metabolism, myelin repair, angiogenesis, BBB permeability, and several other important functions.

We described the importance of uniquely dysregulated genes well-known to play a role in WM dysfunction in the MS brain (KCNA1, KCNA2, SCN2A, and SCN8A), or in experimental models of MS (KCNC3, KCNQ3, KCNK2, CACNA1C, CACNA1G, TRPV1, TRPM2, and PANX1). Furthermore, we highlighted the importance of ion channel genes that are uniquely dysregulated in SPMS lesions but have never been previously explored in MS brain. Those genes are expressed in OPC (KCND2, SCN1A, SCN3A, and CACNA1A), ImOLG (KCNQ3), mature oligodendrocyte (KCNH8), microglia (KCNQ3), astrocyte (KCNN3 and RYR3), and pericyte (GJA4 and CACNA1C) clusters of healthy and SPMS brain. It remains to be investigated whether and how the ionic imbalance in different glial cells, particularly oligodendroglia, contributes to impaired recovery and failure of myelin repair.

Several genes, including KCNA1, SCNA8, SCN11A, CACNA1H, PKD2L2 TRPV6, PANX1, and CATSPERE transcripts, were detected in bulk transcriptome (Elkjaer et al., 2019; Frisch et al., 2020), but were not found by snRNA-seq (Jakel et al., 2019). This discrepancy may be explained by several observations: (1) the transcriptional profiling may vary when lesions analyzed by different studies come from different WM regions (Jäkel and Williams, 2020); (2) snRNA-seq analysis lacks information on gene expression in WM axons that may also contain ion channel transcripts; and (3) snRNA-seq only includes RNA transcripts from the nucleus and may therefore lack RNA transcripts from cytoplasm.

Future experiments on dysregulated ion channels predicted by transcriptomic analysis are expected to provide a better understanding of the molecular mechanism of MS progression and may pave the way for the identification of new therapeutic targets to limit lesion expansion, reduce neurological impairment, and stimulate functional recovery.

AUTHOR CONTRIBUTIONS

FB, MK, ZI, and ME: writing-original draft preparation. FB and MK: writing-review and editing. FB, MK, and ZI: funding acquisition. All authors have read and agreed to the final version of the manuscript.

FUNDING

The work of FB was supported by grants from Fondazione Italiana Sclerosi Multipla FISM 2015/R/6 and by Italian Ministry for University and Research PRIN 2017, 20175SA5JJ. The work of MK was supported by Ikerbasque (Basque Foundation for Science), Spanish Ministry of Science and Innovation (Grant No. PID2019-110195RB-I00), and Basque Government. The work of ZI was supported by Lundbeckfonden R118-A11472, Scleroseforeningen R487-A33600-B15690, and R458-A31829-B15690.

ACKNOWLEDGMENTS

We thank Eneritz Agirre (Karolinska Institute, Stockholm, Sweden) for helpful discussions.

REFERENCES

Abiraman, K., Tzingounis, A. V., and Lykotrafitis, G. (2018). KCa2 channel localization and regulation in the axon initial segment. *FASEB J.* 32, 1794–1805. doi: 10.1096/fj.201700605R

Absinta, M., Sati, P., Masuzzo, F., Nair, G., Sethi, V., Kolb, H., et al. (2019). Association of chronic active multiple sclerosis lesions with disability *in vivo*. *JAMA Neurol.* 76, 1474–1483. doi: 10.1001/jamaneurol.2019.2399

Agrawal, S. K., Nashmi, R., and Fehlings, M. G. (2000). Role of L- and N-type calcium channels in the pathophysiology of traumatic spinal cord

white matter injury. *Neuroscience* 99, 179–188. doi: 10.1016/s0306-4522(00)00165-2

Aguado, C., Garcia-Madrona, S., Gil-Minguez, M., and Lujan, R. (2016). Ontogenic changes and differential localization of T-type Ca(2+) channel subunits Cav3.1 and Cav3.2 in mouse hippocampus and cerebellum. *Front. Neuroanat.* 10:83. doi: 10.3389/fnana.2016.00083

Akhtar, S., McIntosh, P., Bryan-Sisneros, A., Barratt, L., Robertson, B., and Dolly, J. O. (1999). A functional spliced-variant of beta 2 subunit of Kv1 channels in C6 glioma cells and reactive astrocytes from rat lesioned cerebellum. *Biochemistry* 38, 16984–16992. doi: 10.1021/bi992114x

Alfaro-Ruiz, R., Aguado, C., Martin-Belmonte, A., Moreno-Martinez, A. E., and Lujan, R. (2019). Expression, cellular and subcellular localisation of Kv4.2 and Kv4.3 channels in the rodent hippocampus. *Int. J. Mol. Sci.* 20:246. doi: 10.3390/ijms20020246

Alix, J. J., Dolphin, A. C., and Fern, R. (2008). Vesicular apparatus, including functional calcium channels, are present in developing rodent optic nerve axons and are required for normal node of ranvier formation. *J. Physiol.* 586, 4069–4089. doi: 10.1113/jphysiol.2008.155077

Allen, N. M., Weckhuysen, S., Gorman, K., King, M. D., and Lerche, H. (2020). Genetic potassium channel-associated epilepsies: clinical review of the Kv family. *Eur. J. Paediatr. Neurol.* 24, 105–116. doi: 10.1016/j.ejpn.2019.12.002

Alrashdi, B., Dawod, B., Schampel, A., Tacke, S., Kuerten, S., Marshall, J. S., et al. (2019). Nav1.6 promotes inflammation and neuronal degeneration in a mouse model of multiple sclerosis. *J. Neuroinflammation* 16:215. doi: 10.1186/s12974-019-1622-1

Alves, V. S., Alves-Silva, H. S., Orts, D. J. B., Ribeiro-Silva, L., Arcisio-Miranda, M., and Oliveira, F. A. (2019). Calcium signaling in neurons and glial cells: role of Cav1 channels. *Neuroscience* 421, 95–111. doi: 10.1016/j.neuroscience.2019.09.041

Arai-Ichinoi, N., Uematsu, M., Sato, R., Suzuki, T., Kudo, H., Kikuchi, A., et al. (2016). Genetic heterogeneity in 26 infants with a hypomyelinating leukodystrophy. *Hum. Genet.* 135, 89–98. doi: 10.1007/s00439-015-1617-7

Armstrong, W. E., Rubrum, A., Teruyama, R., Bond, C. T., and Adelman, J. P. (2005). Immunocytochemical localization of small-conductance, calcium-dependent potassium channels in astrocytes of the rat supraoptic nucleus. *J. Comp. Neurol.* 491, 175–185. doi: 10.1002/cne.20679

Arroyo, E. J., Xu, T., Grinspan, J., Lambert, S., Levinson, S. R., Brophy, P. J., et al. (2002). Genetic dysmyelination alters the molecular architecture of the nodal region. *J. Neurosci.* 22, 1726–1737. doi: 10.1523/JNEUROSCI.22-05-01726.2002

Astori, S., Wimmer, R. D., Prosser, H. M., Corti, C., Corsi, M., Liaudet, N., et al. (2011). The Ca(V)3.3 calcium channel is the major sleep spindle pacemaker in thalamus. *Proc. Natl. Acad. Sci. U.S.A.* 108, 13823–13828. doi: 10.1073/pnas.1105115108

Attali, B., Wang, N., Kolot, A., Sobko, A., Cherepanov, V., and Soliven, B. (1997). Characterization of delayed rectifier Kv channels in oligodendrocytes and progenitor cells. *J. Neurosci.* 17, 8234–8245. doi: 10.1523/JNEUROSCI.17-21-08234.1997

Bahring, R., Boland, L. M., Varghese, A., Gebauer, M., and Pongs, O. (2001). Kinetic analysis of open- and closed-state inactivation transitions in human Kv4.2 A-type potassium channels. *J. Physiol.* 535. (Pt. 1), 65–81. doi: 10.1111/j.1469-7793.2001.00065.x

Bai, J. Z., and Lipski, J. (2010). Differential expression of TRPM2 and TRPV4 channels and their potential role in oxidative stress-induced cell death in organotypic hippocampal culture. *Neurotoxicology* 31, 204–214. doi: 10.1016/j.neuro.2010.01.001

Barron, T., and Kim, J. H. (2019). Neuronal input triggers Ca(2+) influx through AMPA receptors and voltage-gated Ca(2+) channels in oligodendrocytes. *Glia* 67, 1922–1932. doi: 10.1002/glia.23670

Batiuk, M. Y., Martirosyan, A., Wahis, J., de Vin, F., Marneffe, C., Kusserow, C., et al. (2020). Identification of region-specific astrocyte subtypes at single cell resolution. *Nat. Commun.* 11:1220. doi: 10.1038/s41467-019-14198-8

Battefeld, A., Tran, B. T., Gavrilis, J., Cooper, E. C., and Kole, M. H. (2014). Heteromeric Kv7.2/7.3 channels differentially regulate action potential initiation and conduction in neocortical myelinated axons. *J. Neurosci.* 34, 3719–3732. doi: 10.1523/JNEUROSCI.4206-13.2014

Bauer, C. K., and Schwarz, J. R. (2018). Ether-a-go-go K(+) channels: effective modulators of neuronal excitability. *J. Physiol.* 596, 769–783. doi: 10.1113/JP275477

Bekar, L. K., Loewen, M. E., Cao, K., Sun, X., Leis, J., Wang, R., et al. (2005). Complex expression and localization of inactivating Kv channels in cultured hippocampal astrocytes. *J. Neurophysiol.* 93, 1699–1709. doi: 10.1152/jn.00850.2004

Bender, K. J., and Trussell, L. O. (2009). Axon initial segment Ca2+ channels influence action potential generation and timing. *Neuron* 61, 259–271. doi: 10.1016/j.neuron.2008.12.004

Benfenati, V., Nicchia, G. P., Svelto, M., Rapisarda, C., Frigeri, A., and Ferroni, S. (2007). Functional down-regulation of volume-regulated anion channels in AQP4 knockdown cultured rat cortical astrocytes. *J. Neurochem.* 100, 87–104. doi: 10.1111/j.1471-4159.2006.04164.x

Berkefeld, H., Sailer, C. A., Bildl, W., Rohde, V., Thumfart, J. O., Eble, S., et al. (2006). BKCa-Cav channel complexes mediate rapid and localized Ca2+-activated K+ signaling. *Science* 314, 615–620. doi: 10.1126/science.1132915

Berret, E., Barron, T., Xu, J., Debner, E., Kim, E. J., and Kim, J. H. (2017). Oligodendroglial excitability mediated by glutamatergic inputs and Nav1.2 activation. *Nat. Commun.* 8:557. doi: 10.1038/s41467-017-00688-0

Bhat, S., Dao, D. T., Terrillion, C. E., Arad, M., Smith, R. J., Soldatov, N. M., et al. (2012). CACNA1C (Cav1.2) in the pathophysiology of psychiatric disease. *Prog. Neurobiol.* 99, 1–14. doi: 10.1016/j.pneurobio.2012.06.001

Bhattacharjee, A., Gan, L., and Kaczmarek, L. K. (2002). Localization of the Slack potassium channel in the rat central nervous system. *J. Comp. Neurol.* 454, 241–254. doi: 10.1002/cne.10439

Bhattacharjee, A., and Kaczmarek, L. K. (2005). For K+ channels, Na+ is the new Ca2+. *Trends Neurosci.* 28, 422–428. doi: 10.1016/j.tins.2005.06.003

Bierbower, S. M., Choveau, F. S., Lechleiter, J. D., and Shapiro, M. S. (2015). Augmentation of M-type (KCNQ) potassium channels as a novel strategy to reduce stroke-induced brain injury. *J. Neurosci.* 35, 2101–2111. doi: 10.1523/JNEUROSCI.3805-14.2015

Birnbaum, S. G., Varga, A. W., Yuan, L. L., Anderson, A. E., Sweatt, J. D., and Schrader, L. A. (2004). Structure and function of Kv4-family transient potassium channels. *Physiol. Rev.* 84, 803–833. doi: 10.1152/physrev.00039.2003

Bittner, S., Ruck, T., Fernandez-Orth, J., and Meuth, S. G. (2014). TREK-king the blood-brain-barrier. *J. Neuroimmune Pharmacol.* 9, 293–301. doi: 10.1007/s11481-014-9530-8

Bittner, S., Ruck, T., Schuhmann, M. K., Herrmann, A. M., Moha ou Maati, H., Bobak, N., et al. (2013). Endothelial TWIK-related potassium channel-1 (TREK1) regulates immune-cell trafficking into the CNS. *Nat. Med.* 19, 1161–1165. doi: 10.1038/nm.3303

Black, J. A., Liu, S., and Waxman, S. G. (2009). Sodium channel activity modulates multiple functions in microglia. *Glia* 57, 1072–1081. doi: 10.1002/glia.20830

Black, J. A., Newcombe, J., Trapp, B. D., and Waxman, S. G. (2007). Sodium channel expression within chronic multiple sclerosis plaques. *J. Neuropathol. Exp. Neurol.* 66, 828–837. doi: 10.1097/nen.0b013e3181462841

Black, J. A., Newcombe, J., and Waxman, S. G. (2010). Astrocytes within multiple sclerosis lesions upregulate sodium channel Nav1.5. *Brain* 133 (Pt. 3), 835–846. doi: 10.1093/brain/awq003

Black, J. A., Vasylyev, D., Dib-Hajj, S. D., and Waxman, S. G. (2014). Nav1.9 expression in magnocellular neurosecretory cells of supraoptic nucleus. *Exp. Neurol.* 253, 174–179. doi: 10.1016/j.expneurol.2014.01.004

Black, J. A., and Waxman, S. G. (2012). Sodium channels and microglial function. *Exp. Neurol.* 234, 302–315. doi: 10.1016/j.expneurol.2011.09.030

Black, J. A., and Waxman, S. G. (2013). Noncanonical roles of voltage-gated sodium channels. *Neuron* 80, 280–291. doi: 10.1016/j.neuron.2013.09.012

Black, J. A., Westenbroek, R., Minturn, J. E., Ransom, B. R., Catterall, W. A., and Waxman, S. G. (1995). Isoform-specific expression of sodium channels in astrocytes *in vitro*: immunocytochemical observations. *Glia* 14, 133–144. doi: 10.1002/glia.440140208

Blanz, J., Schweizer, M., Auberson, M., Maier, H., Muenscher, A., Hubner, C. A., et al. (2007). Leukoencephalopathy upon disruption of the chloride channel ClC-2. *J. Neurosci.* 27, 6581–6589. doi: 10.1523/JNEUROSCI.0338-07.2007

Blondeau, N., Petrault, O., Manta, S., Giordanengo, V., Gounon, P., Bordet, R., et al. (2007). Polyunsaturated fatty acids are cerebral vasodilators via the TREK-1 potassium channel. *Circ. Res.* 101, 176–184. doi: 10.1161/CIRCRESAHA.107.154443

Bloodgood, B. L., and Sabatini, B. L. (2008). Regulation of synaptic signalling by postsynaptic, non-glutamate receptor ion channels. *J. Physiol.* 586, 1475–1480. doi: 10.1113/jphysiol.2007.148353

Blum, R., Kafitz, K. W., and Konnerth, A. (2002). Neurotrophin-evoked depolarization requires the sodium channel Na(V)1.9. *Nature* 419, 687–693. doi: 10.1038/nature01085

Bock, T., Honnuraiah, S., and Stuart, G. J. (2019). Paradoxical excitatory impact of SK channels on dendritic excitability. *J. Neurosci.* 39, 7826–7839. doi: 10.1523/JNEUROSCI.0105-19.2019

Bocksteins, E. (2016). Kv5, Kv6, Kv8, and Kv9 subunits: no simple silent bystanders. *J. Gen. Physiol.* 147, 105–125. doi: 10.1085/jgp.201511507

Boiko, T., Rasband, M. N., Levinson, S. R., Caldwell, J. H., Mandel, G., Trimmer, J. S., et al. (2001). Compact myelin dictates the differential targeting of two sodium channel isoforms in the same axon. *Neuron* 30, 91–104. doi: 10.1016/s0896-6273(01)00265-3

Boiko, T., Van Wart, A., Caldwell, J. H., Levinson, S. R., Trimmer, J. S., and Matthews, G. (2003). Functional specialization of the axon initial segment by isoform-specific sodium channel targeting. *J. Neurosci.* 23, 2306–2313. doi: 10.1523/JNEUROSCI.23-06-02306.2003

Borlot, F., Abushama, A., Morrison-Levy, N., Jain, P., Puthenveettil Vinayan, K., Abukhalid, M., et al. (2020). KCNT1-related epilepsy: an international multicenter cohort of 27 pediatric cases. *Epilepsia* 61, 679–692. doi: 10.1111/epi.16480

Boscia, F., Annunziato, L., and Taglialatela, M. (2006). Retigabine and flupirtine exert neuroprotective actions in organotypic hippocampal cultures. *Neuropharmacology* 51, 283–294. doi: 10.1016/j.neuropharm.2006.03.024

Boscia, F., de Rosa, V., Cammarota, M., Secondo, A., Pannaccione, A., and Annunziato, L. (2020). The Na(+)/Ca(2+) exchangers in demyelinating diseases. *Cell Calcium* 85:102130. doi: 10.1016/j.ceca.2019.102130

Boscia, F., Pannaccione, A., Ciccone, R., Casamassa, A., Franco, C., Piccialli, I., et al. (2017). The expression and activity of KV3.4 channel subunits are precociously upregulated in astrocytes exposed to abeta oligomers and in astrocytes of Alzheimer's disease Tg2576 mice. *Neurobiol. Aging* 54, 187–198. doi: 10.1016/j.neurobiolaging.2017.03.008

Bose, S., He, H., and Stauber, T. (2021). Neurodegeneration upon dysfunction of endosomal/lysosomal CLC chloride transporters. *Front. Cell Dev. Biol.* 9:639231. doi: 10.3389/fcell.2021.639231

Bouafia, A., Golmard, J. L., Thuries, V., Sazdovitch, V., Hauw, J. J., Fontaine, B., et al. (2014). Axonal expression of sodium channels and neuropathology of the plaques in multiple sclerosis. *Neuropathol. Appl. Neurobiol.* 40, 579–590. doi: 10.1111/nan.12059

Bozarth, X., Dines, J. N., Cong, Q., Mirzaa, G. M., Foss, K., Lawrence Merritt, J. 2nd, et al. (2018). Expanding clinical phenotype in CACNA1C related disorders: From neonatal onset severe epileptic encephalopathy to late-onset epilepsy. *Am. J. Med. Genet. A* 176, 2733–2739. doi: 10.1002/ajmg.a.40657

Bradl, M., and Lassmann, H. (2010). Oligodendrocytes: biology and pathology. *Acta Neuropathol.* 119, 37–53. doi: 10.1007/s00401-009-0601-5

Brand-Schieber, E., and Werner, P. (2004). Calcium channel blockers ameliorate disease in a mouse model of multiple sclerosis. *Exp. Neurol.* 189, 5–9. doi: 10.1016/j.expneurol.2004.05.023

Brasko, C., Hawkins, V., De La Rocha, I. C., and Butt, A. M. (2017). Expression of Kir4.1 and Kir5.1 inwardly rectifying potassium channels in oligodendrocytes, the myelinating cells of the CNS. *Brain Struct. Funct.* 222, 41–59. doi: 10.1007/s00429-016-1199-8

Brill, A. L., Fischer, T. T., Walters, J. M., Marlier, A., Sewanan, L. R., Wilson, P. C., et al. (2020). Polycystin 2 is increased in disease to protect against stress-induced cell death. *Sci. Rep.* 10:386. doi: 10.1038/s41598-019-57286-x

Brown, M. R., Kronengold, J., Gazula, V. R., Spilianakis, C. G., Flavell, R. A., von Hehn, C. A., et al. (2008). Amino-termini isoforms of the Slack K+ channel, regulated by alternative promoters, differentially modulate rhythmic firing and adaptation. *J. Physiol.* 586, 5161–5179. doi: 10.1113/jphysiol.2008.160861

Brueggemann, L. I., Mackie, A. R., Cribbs, L. L., Freda, J., Tripathi, A., Majetschak, M., et al. (2014). Differential protein kinase C-dependent modulation of Kv7.4 and Kv7.5 subunits of vascular Kv7 channels. *J. Biol. Chem.* 289, 2099–2111. doi: 10.1074/jbc.M113.527820

Bruzzone, R., Hormuzdi, S. G., Barbe, M. T., Herb, A., and Monyer, H. (2003). Pannexins, a family of gap junction proteins expressed in brain. *Proc. Natl. Acad. Sci. U.S.A.* 100, 13644–13649. doi: 10.1073/pnas.2233464100

Cabranes, A., Venderova, K., de Lago, E., Fezza, F., Sanchez, A., Mestre, L., et al. (2005). Decreased endocannabinoid levels in the brain and beneficial effects of agents activating cannabinoid and/or vanilloid receptors in a rat model of multiple sclerosis. *Neurobiol. Dis.* 20, 207–217. doi: 10.1016/j.nbd.2005.03.002

Caldwell, J. H., Schaller, K. L., Lasher, R. S., Peles, E., and Levinson, S. R. (2000). Sodium channel Na(v)1.6 is localized at nodes of ranvier, dendrites, and synapses. *Proc. Natl. Acad. Sci. U.S.A.* 97, 5616–5620. doi: 10.1073/pnas.090034797

Caminos, E., Vaquero, C. F., and Martinez-Galan, J. R. (2015). Relationship between rat retinal degeneration and potassium channel KCNQ5 expression. *Exp. Eye Res.* 131, 1–11. doi: 10.1016/j.exer.2014.12.009

Casamassa, A., La Rocca, C., Sokolow, S., Herchuelz, A., Matarese, G., Annunziato, L., et al. (2016). Ncx3 gene ablation impairs oligodendrocyte precursor response and increases susceptibility to experimental autoimmune encephalomyelitis. *Glia* 64, 1124–1137. doi: 10.1002/glia.22985

Castellano, A., Chiara, M. D., Mellstrom, B., Molina, A., Monje, F., Naranjo, J. R., et al. (1997). Identification and functional characterization of a K+ channel alpha-subunit with regulatory properties specific to brain. *J. Neurosci.* 17, 4652–4661.

Catterall, W. A. (2000). Structure and regulation of voltage-gated Ca2+ channels. *Annu. Rev. Cell. Dev. Biol.* 16, 521–555. doi: 10.1146/annurev.cellbio.16.1.521

Catterall, W. A. (2011). Voltage-gated calcium channels. *Cold Spring Harb. Perspect. Biol.* 3:a003947. doi: 10.1101/cshperspect.a003947

Cheah, C. S., Westenbroek, R. E., Roden, W. H., Kalume, F., Oakley, J. C., Jansen, L. A., et al. (2013). Correlations in timing of sodium channel expression, epilepsy, and sudden death in dravet syndrome. *Channels* 7, 468–472. doi: 10.4161/chan.26023

Chekeni, F. B., Elliott, M. R., Sandilos, J. K., Walk, S. F., Kinchen, J. M., Lazarowski, E. R., et al. (2010). Pannexin 1 channels mediate 'find-me' signal release and membrane permeability during apoptosis. *Nature* 467, 863–867. doi: 10.1038/nature09413

Cheli, V. T., Santiago Gonzalez, D. A., Namgyal Lama, T., Spreuer, V., Handley, V., Murphy, G. G., et al. (2016a). Conditional deletion of the l-type calcium channel Cav1.2 in oligodendrocyte progenitor cells affects postnatal myelination in mice. *J. Neurosci.* 36, 10853–10869. doi: 10.1523/JNEUROSCI.1770-16.2016

Cheli, V. T., Santiago Gonzalez, D. A., Smith, J., Spreuer, V., Murphy, G. G., and Paez, P. M. (2016b). L-type voltage-operated calcium channels contribute to astrocyte activation *in vitro*. *Glia* 64, 1396–1415. doi: 10.1002/glia.23013

Cheli, V. T., Santiago Gonzalez, D. A., Spreuer, V., and Paez, P. M. (2015). Voltage-gated Ca2+ entry promotes oligodendrocyte progenitor cell maturation and myelination *in vitro*. *Exp. Neurol.* 265, 69–83. doi: 10.1016/j.expneurol.2014.12.012

Chen, S., Ren, Y. Q., Bing, R., and Hillman, D. E. (2000). Alpha 1E subunit of the R-type calcium channel is associated with myelinogenesis. *J. Neurocytol.* 29, 719–728. doi: 10.1023/a:1010986303924

Chen, W., Chi, Y. N., Kang, X. J., Liu, Q. Y., Zhang, H. L., Li, Z. H., et al. (2018). Accumulation of Cav3.2 T-type calcium channels in the uninjured sural nerve contributes to neuropathic pain in rats with spared nerve injury. *Front. Mol. Neurosci.* 11:24. doi: 10.3389/fnmol.2018.00024

Chen, Y. L., Tsaur, M. L., Wang, S. W., Wang, T. Y., Hung, Y. C., Lin, C. S., et al. (2015). Chronic intrathecal infusion of mibefradil, ethosuximide and nickel attenuates nerve ligation-induced pain in rats. *Br. J. Anaesth.* 115, 105–111. doi: 10.1093/bja/aev198

Chittajallu, R., Chen, Y., Wang, H., Yuan, X., Ghiani, C. A., Heckman, T., et al. (2002). Regulation of Kv1 subunit expression in oligodendrocyte progenitor cells and their role in G1/S phase progression of the cell cycle. *Proc. Natl. Acad. Sci. U.S.A.* 99, 2350–2355. doi: 10.1073/pnas.042698399

Chiu, Y. H., Schappe, M. S., Desai, B. N., and Bayliss, D. A. (2018). Revisiting multimodal activation and channel properties of pannexin 1. *J. Gen. Physiol.* 150, 19–39. doi: 10.1085/jgp.201711888

Choi, H. J., Sun, D., and Jakobs, T. C. (2015). Astrocytes in the optic nerve head express putative mechanosensitive channels. *Mol. Vis.* 21, 749–766.

Christie, S., Wittert, G. A., Li, H., and Page, A. J. (2018). Involvement of TRPV1 Channels in energy homeostasis. *Front. Endocrinol.* 9:420. doi: 10.3389/fendo.2018.00420

Chu, S., Murray, C. B., Liu, M. M., and Zeitlin, P. L. (1996). A short CIC-2 mRNA transcript is produced by exon skipping. *Nucleic Acids Res*. 24, 3453–3457. doi: 10.1093/nar/24.17.3453

Chung, K. K., Freestone, P. S., and Lipski, J. (2011). Expression and functional properties of TRPM2 channels in dopaminergic neurons of the substantia nigra of the rat. *J. Neurophysiol* 106, 2865–2875. doi: 10.1152/jn.00994.2010

Clapham, D. E. (2003). TRP channels as cellular sensors. *Nature* 426, 517–524. doi: 10.1038/nature02196

Clark, S., Jordt, S. E., Jentsch, T. J., and Mathie, A. (1998). Characterization of the hyperpolarization-activated chloride current in dissociated rat sympathetic neurons. *J. Physiol.* 506 (Pt. 3), 665–678. doi: 10.1111/j.1469-7793.1998.665bv.x

Coman, I., Aigrot, M. S., Seilhean, D., Reynolds, R., Girault, J. A., Zalc, B., et al. (2006). Nodal, paranodal and juxtaparanodal axonal proteins during demyelination and remyelination in multiple sclerosis. *Brain* 129 (Pt. 12), 3186–3195. doi: 10.1093/brain/awl144

Compston, A., and Coles, A. (2008). Multiple sclerosis. *Lancet* 372, 1502–1517. doi: 10.1016/S0140-6736(08)61620-7

Cone, A. C., Ambrosi, C., Scemes, E., Martone, M. E., and Sosinsky, G. E. (2013). A comparative antibody analysis of pannexin1 expression in four rat brain regions reveals varying subcellular localizations. *Front. Pharmacol*. 4:6. doi: 10.3389/fphar.2013.00006

Cooper, E. C. (2011). Made for "anchorin": Kv7.2/7.3 (KCNQ2/KCNQ3) channels and the modulation of neuronal excitability in vertebrate axons. *Semin. Cell Dev. Biol*. 22, 185–192. doi: 10.1016/j.semcdb.2010.10.001

Cooper, E. C., Aldape, K. D., Abosch, A., Barbaro, N. M., Berger, M. S., Peacock, W. S., et al. (2000). Colocalization and coassembly of two human brain M-type potassium channel subunits that are mutated in epilepsy. *Proc. Natl. Acad. Sci. U.S.A*. 97, 4914–4919. doi: 10.1073/pnas.090092797

Couturier, N., Gourraud, P. A., Cournu-Rebeix, I., Gout, C., Bucciarelli, F., Edan, G., et al. (2009). IFIH1-GCA-KCNH7 locus is not associated with genetic susceptibility to multiple sclerosis in French patients. *Eur. J. Hum. Genet*. 17, 844–847. doi: 10.1038/ejhg.2008.259

Craner, M. J., Damarjian, T. G., Liu, S., Hains, B. C., Lo, A. C., Black, J. A., et al. (2005). Sodium channels contribute to microglia/macrophage activation and function in EAE and MS. *Glia* 49, 220–229. doi: 10.1002/glia.20112

Craner, M. J., Hains, B. C., Lo, A. C., Black, J. A., and Waxman, S. G. (2004a). Co-localization of sodium channel Nav1.6 and the sodium-calcium exchanger at sites of axonal injury in the spinal cord in EAE. *Brain* 127 (Pt. 2), 294–303. doi: 10.1093/brain/awh032

Craner, M. J., Lo, A. C., Black, J. A., and Waxman, S. G. (2003). Abnormal sodium channel distribution in optic nerve axons in a model of inflammatory demyelination. *Brain* 126 (Pt. 7), 1552–1561. doi: 10.1093/brain/awg153

Craner, M. J., Newcombe, J., Black, J. A., Hartle, C., Cuzner, M. L., and Waxman, S. G. (2004b). Molecular changes in neurons in multiple sclerosis: altered axonal expression of Nav1.2 and Nav1.6 sodium channels and Na+/Ca2+ exchanger. *Proc. Natl. Acad. Sci. U.S.A*. 101, 8168–8173. doi: 10.1073/pnas.0402765101

Crespo Yanguas, S., Willebrords, J., Johnstone, S. R., Maes, M., Decrock, E., De Bock, M., et al. (2017). Pannexin1 as mediator of inflammation and cell death. *Biochim. Biophys. Acta Mol. Cell Res*. 1864, 51–61. doi: 10.1016/j.bbamcr.2016.10.006

Cummins, T. R., Dib-Hajj, S. D., Black, J. A., Akopian, A. N., Wood, J. N., and Waxman, S. G. (1999). A novel persistent tetrodotoxin-resistant sodium current in SNS-null and wild-type small primary sensory neurons. *J. Neurosci*. 19:RC43

Dahl, G. (2015). ATP release through pannexon channels. *Philos. Trans. R. Soc. Lond. B Biol. Sci*. 370:20140191. doi: 10.1098/rstb.2014.0191

Dahl, G. (2018). The Pannexin1 membrane channel: distinct conformations and functions. *FEBS Lett*. 592, 3201–3209. doi: 10.1002/1873-3468.13115

D'Ascenzo, M., Vairano, M., Andreassi, C., Navarra, P., Azzena, G. B., and Grassi, C. (2004). Electrophysiological and molecular evidence of L-(Cav1), N-(Cav2.2), and R- (Cav2.3) type Ca2+ channels in rat cortical astrocytes. *Glia* 45, 354–363. doi: 10.1002/glia.10336

Daschil, N., Geisler, S., Obermair, G. J., and Humpel, C. (2014). Short- and long-term treatment of mouse cortical primary astrocytes with beta-amyloid differentially regulates the mRNA expression of L-type calcium channels. *Pharmacology* 93, 24–31. doi: 10.1159/000357383

Daschil, N., Obermair, G. J., Flucher, B. E., Stefanova, N., Hutter-Paier, B., Windisch, M., et al. (2013). CaV1.2 calcium channel expression in reactive astrocytes is associated with the formation of amyloid-beta plaques in an Alzheimer's disease mouse model. *J Alzheimers Dis*. 37, 439–451. doi: 10.3233/JAD-130560

de Kovel, C. G. F., Syrbe, S., Brilstra, E. H., Verbeek, N., Kerr, B., Dubbs, H., et al. (2017). Neurodevelopmental disorders caused by *de novo* variants in KCNB1 genotypes and phenotypes. *JAMA Neurol*. 74, 1228–1236. doi: 10.1001/jamaneurol.2017.1714

de Rosa, V., Secondo, A., Pannaccione, A., Ciccone, R., Formisano, L., Guida, N., et al. (2019). D-Aspartate treatment attenuates myelin damage and stimulates myelin repair. *EMBO Mol. Med*. 11:e9278. doi: 10.15252/emmm.201809278

Derbenev, A. V., and Zsombok, A. (2016). Potential therapeutic value of TRPV1 and TRPA1 in diabetes mellitus and obesity. *Semin. Immunopathol*. 38, 397–406. doi: 10.1007/s00281-015-0529-x

Derst, C., Karschin, C., Wischmeyer, E., Hirsch, J. R., Preisig-Muller, R., Rajan, S., et al. (2001). Genetic and functional linkage of Kir5.1 and Kir2.1 channel subunits. *FEBS Lett*. 491, 305–311. doi: 10.1016/s0014-5793(01)02202-5

Deutsch, E., Weigel, A. V., Akin, E. J., Fox, P., Hansen, G., Haberkorn, C. J., et al. (2012). Kv2.1 cell surface clusters are insertion platforms for ion channel delivery to the plasma membrane. *Mol. Biol. Cell* 23, 2917–2929. doi: 10.1091/mbc.E12-01-0047

Devaux, J. J., Kleopa, K. A., Cooper, E. C., and Scherer, S. S. (2004). KCNQ2 is a nodal K+ channel. *J. Neurosci*. 24, 1236–1244. doi: 10.1523/JNEUROSCI.4512-03.2004

Dietrich, D., Kirschstein, T., Kukley, M., Pereverzev, A., von der Brelie, C., Schneider, T., et al. (2003). Functional specialization of presynaptic Cav2.3 Ca2+ channels. *Neuron* 39, 483–496. doi: 10.1016/s0896-6273(03)00430-6

Djillani, A., Mazella, J., Heurteaux, C., and Borsotto, M. (2019). Role of TREK-1 in health and disease, focus on the central nervous system. *Front. Pharmacol*. 10:379. doi: 10.3389/fphar.2019.00379

Dolga, A. M., Letsche, T., Gold, M., Doti, N., Bacher, M., Chiamvimonvat, N., et al. (2012). Activation of KCNN3/SK3/K(Ca)2.3 channels attenuates enhanced calcium influx and inflammatory cytokine production in activated microglia. *Glia* 60, 2050–2064. doi: 10.1002/glia.22419

Dolga, A. M., Terpolilli, N., Kepura, F., Nijholt, I. M., Knaus, H. G., D'Orsi, B., et al. (2011). KCa2 channels activation prevents [Ca2+]i deregulation and reduces neuronal death following glutamate toxicity and cerebral ischemia. *Cell Death Dis*. 2:e147. doi: 10.1038/cddis.2011.30

Dorr, J., Wernecke, K. D., Wurfel, J., Bellmann-Strobl, J., Siffrin, V., Sattler, M. B., et al. (2018). Disease modification in multiple sclerosis by flupirtine-results of a randomized placebo controlled phase II trial. *Front. Neurol*. 9:842. doi: 10.3389/fneur.2018.00842

Du, J., Haak, L. L., Phillips-Tansey, E., Russell, J. T., and McBain, C. J. (2000). Frequency-dependent regulation of rat hippocampal somato-dendritic excitability by the K+ channel subunit Kv2.1. *J. Physiol.* 522 (Pt. 1), 19–31. doi: 10.1111/j.1469-7793.2000.t01-2-00019.xm

Du, T., Liang, C., Li, B., Hertz, L., and Peng, L. (2014). Chronic fluoxetine administration increases expression of the L-channel gene Cav1.2 in astrocytes from the brain of treated mice and in culture and augments K(+)-induced increase in [Ca(2+)]i. *Cell Calcium* 55, 166–174. doi: 10.1016/j.ceca.2014.01.002

Ducharme, G., Newell, E. W., Pinto, C., and Schlichter, L. C. (2007). Small-conductance Cl- channels contribute to volume regulation and phagocytosis in microglia. *Eur. J. Neurosci*. 26, 2119–2130. doi: 10.1111/j.1460-9568.2007.05802.x

Duflocq, A., Le Bras, B., Bullier, E., Couraud, F., and Davenne, M. (2008). Nav1.1 is predominantly expressed in nodes of ranvier and axon initial segments. *Mol. Cell Neurosci*. 39, 180–192. doi: 10.1016/j.mcn.2008.06.008

Dumenieu, M., Oule, M., Kreutz, M. R., and Lopez-Rojas, J. (2017). The segregated expression of voltage-gated potassium and sodium channels in neuronal membranes: functional implications and regulatory mechanisms. *Front. Cell Neurosci*. 11:115. doi: 10.3389/fncel.2017.00115

Eder, C. (1998). Ion channels in microglia (brain macrophages). *Am. J. Physiol*. 275, C327–342. doi: 10.1152/ajpcell.1998.275.2.C327

Edwards, L., Nashmi, R., Jones, O., Backx, P., Ackerley, C., Becker, L., et al. (2002). Upregulation of Kv 1.4 protein and gene expression after chronic spinal cord injury. *J Comp. Neurol*. 443, 154–167. doi: 10.1002/cne.10115

Ehling, P., Cerina, M., Budde, T., Meuth, S. G., and Bittner, S. (2015). The CNS under pathophysiologic attack–examining the role of K(2)p channels. *Pflugers Arch.* 467, 959–972. doi: 10.1007/s00424-014-1664-2

Eisfeld, J., and Luckhoff, A. (2007). Trpm2. *Handb. Exp. Pharmacol.* 237–252. doi: 10.1007/978-3-540-34891-7_14

Elkjaer, M. L., Frisch, T., Reynolds, R., Kacprowski, T., Burton, M., Kruse, T. A., et al. (2019). Molecular signature of different lesion types in the brain white matter of patients with progressive multiple sclerosis. *Acta Neuropathol. Commun.* 7:205. doi: 10.1186/s40478-019-0855-7

Elliott, C., Belachew, S., Wolinsky, J. S., Hauser, S. L., Kappos, L., Barkhof, F., et al. (2019). Chronic white matter lesion activity predicts clinical progression in primary progressive multiple sclerosis. *Brain* 142, 2787–2799. doi: 10.1093/brain/awz212

Emmi, A., Wenzel, H. J., Schwartzkroin, P. A., Taglialatela, M., Castaldo, P., Bianchi, L., et al. (2000). Do glia have heart? Expression and functional role for ether-a-go-go currents in hippocampal astrocytes. *J. Neurosci.* 20, 3915–3925. doi: 10.1523/JNEUROSCI.20-10-03915.2000

Enders, M., Heider, T., Ludwig, A., and Kuerten, S. (2020). Strategies for neuroprotection in multiple sclerosis and the role of calcium. *Int. J. Mol. Sci.* 21:1663. doi: 10.3390/ijms21051663

Enyedi, P., and Czirjak, G. (2010). Molecular background of leak K+ currents: two-pore domain potassium channels. *Physiol. Rev.* 90, 559–605. doi: 10.1152/physrev.00029.2009

Eshed-Eisenbach, Y., and Peles, E. (2020). The clustering of voltage-gated sodium channels in various excitable membranes. *Dev. Neurobiol.* 1–11. doi: 10.1002/dneu.2272

Espinosa-Parrilla, J. F., Martinez-Moreno, M., Gasull, X., Mahy, N., and Rodriguez, M. J. (2015). The L-type voltage-gated calcium channel modulates microglial pro-inflammatory activity. *Mol. Cell Neurosci.* 64, 104–115. doi: 10.1016/j.mcn.2014.12.004

Estacion, M., Gasser, A., Dib-Hajj, S. D., and Waxman, S. G. (2010). A sodium channel mutation linked to epilepsy increases ramp and persistent current of Nav1.3 and induces hyperexcitability in hippocampal neurons. *Exp. Neurol.* 224, 362–368. doi: 10.1016/j.expneurol.2010.04.012

Falcao, A. M., van Bruggen, D., Marques, S., Meijer, M., Jakel, S., Agirre, E., et al. (2018). Disease-specific oligodendrocyte lineage cells arise in multiple sclerosis. *Nat. Med.* 24, 1837–1844. doi: 10.1038/s41591-018-0236-y

Fang, J. S., Angelov, S. N., Simon, A. M., and Burt, J. M. (2011). Cx37 deletion enhances vascular growth and facilitates ischemic limb recovery. *Am. J. Physiol. Heart Circ. Physiol.* 301, H1872–1881. doi: 10.1152/ajpheart.00683.2011

Fano, S., Caliskan, G., and Heinemann, U. (2012). Differential effects of blockade of ERG channels on gamma oscillations and excitability in rat hippocampal slices. *Eur. J. Neurosci.* 36, 3628–3635. doi: 10.1111/ejn.12015

Filippi, M., Bar-Or, A., Piehl, F., Preziosa, P., Solari, A., Vukusic, S., et al. (2018). Multiple sclerosis. *Nat. Rev. Dis. Primers* 4:43. doi: 10.1038/s41572-018-0041-4

Fill, M., and Copello, J. A. (2002). Ryanodine receptor calcium release channels. *Physiol. Rev.* 82, 893–922. doi: 10.1152/physrev.00013.2002

Foldy, C., Lee, S. H., Morgan, R. J., and Soltesz, I. (2010). Regulation of fast-spiking basket cell synapses by the chloride channel ClC-2. *Nat. Neurosci.* 13, 1047–1049. doi: 10.1038/nn.2609

Fordyce, C. B., Jagasia, R., Zhu, X., and Schlichter, L. C. (2005). Microglia Kv1.3 channels contribute to their ability to kill neurons. *J. Neurosci.* 25, 7139–7149. doi: 10.1523/JNEUROSCI.1251-05.2005

Franceschetti, S., Lavazza, T., Curia, G., Aracri, P., Panzica, F., Sancini, G., et al. (2003). Na+-activated K+ current contributes to postexcitatory hyperpolarization in neocortical intrinsically bursting neurons. *J. Neurophysiol.* 89, 2101–2111. doi: 10.1152/jn.00695.2002

Freestone, P. S., Chung, K. K., Guatteo, E., Mercuri, N. B., Nicholson, L. F., and Lipski, J. (2009). Acute action of rotenone on nigral dopaminergic neurons–involvement of reactive oxygen species and disruption of Ca2+ homeostasis. *Eur. J. Neurosci.* 30, 1849–1859. doi: 10.1111/j.1460-9568.2009.06990.x

Friese, M. A., Schattling, B., and Fugger, L. (2014). Mechanisms of neurodegeneration and axonal dysfunction in multiple sclerosis. *Nat. Rev. Neurol.* 10, 225–238. doi: 10.1038/nrneurol.2014.37

Frisch, T., Elkjaer, M. L., Reynolds, R., Michel, T. M., Kacprowski, T., Burton, M., et al. (2020). Multiple sclerosis atlas: a molecular map of brain lesion stages in progressive multiple sclerosis. *Netw. Syst. Med.* 3, 122–129. doi: 10.1089/nsm.2020.0006

Fulton, D., Paez, P. M., Fisher, R., Handley, V., Colwell, C. S., and Campagnoni, A. T. (2010). Regulation of L-type Ca++ currents and process morphology in white matter oligodendrocyte precursor cells by golli-myelin proteins. *Glia* 58, 1292–1303. doi: 10.1002/glia.21008

Gajardo-Gomez, R., Labra, V. C., and Orellana, J. A. (2016). Connexins and pannexins: new insights into microglial functions and dysfunctions. *Front. Mol. Neurosci.* 9:86. doi: 10.3389/fnmol.2016.00086

Gallego-Delgado, P., James, R., Browne, E., Meng, J., Umashankar, S., Tan, L., et al. (2020). Neuroinflammation in the normal-appearing white matter (NAWM) of the multiple sclerosis brain causes abnormalities at the nodes of Ranvier. *PLoS Biol.* 18:e3001008. doi: 10.1371/journal.pbio.3001008

Gamelli, A. E., McKinney, B. C., White, J. A., and Murphy, G. G. (2011). Deletion of the L-type calcium channel Ca(V) 1.3 but not Ca(V) 1.2 results in a diminished sAHP in mouse CA1 pyramidal neurons. *Hippocampus* 21, 133–141. doi: 10.1002/hipo.20728

Gartner, C., Ziegelhoffer, B., Kostelka, M., Stepan, H., Mohr, F. W., and Dhein, S. (2012). Knock-down of endothelial connexins impairs angiogenesis. *Pharmacol. Res.* 65, 347–357. doi: 10.1016/j.phrs.2011.11.012

Gasparini, S., Kasyanov, A. M., Pietrobon, D., Voronin, L. L., and Cherubini, E. (2001). Presynaptic R-type calcium channels contribute to fast excitatory synaptic transmission in the rat hippocampus. *J. Neurosci.* 21, 8715–8721. doi: 10.1523/JNEUROSCI.21-22-08715.2001

Gees, M., Colsoul, B., and Nilius, B. (2010). The role of transient receptor potential cation channels in Ca2+ signaling. *Cold Spring Harb. Perspect. Biol.* 2:a003962. doi: 10.1101/cshperspect.a003962

Giannini, G., Conti, A., Mammarella, S., Scrobogna, M., and Sorrentino, V. (1995). The ryanodine receptor/calcium channel genes are widely and differentially expressed in murine brain and peripheral tissues. *J. CellBiol.* 128, 893–904. doi: 10.1083/jcb.128.5.893

Giaume, C., Naus, C. C., Saez, J. C., and Leybaert, L. (2021). Glial connexins and pannexins in the healthy and diseased brain. *Physiol. Rev.* 101, 93–145. doi: 10.1152/physrev.00043.2018

Gibson, H. E., Edwards, J. G., Page, R. S., Van Hook, M. J., and Kauer, J. A. (2008). TRPV1 channels mediate long-term depression at synapses on hippocampal interneurons. *Neuron* 57, 746–759. doi: 10.1016/j.neuron.2007.12.027

Gilgun-Sherki, Y., Panet, H., Melamed, E., and Offen, D. (2003). Riluzole suppresses experimental autoimmune encephalomyelitis: implications for the treatment of multiple sclerosis. *Brain Res.* 989, 196–204. doi: 10.1016/s0006-8993(03)03343-2

Girolamo, F., Coppola, C., Ribatti, D., and Trojano, M. (2014). Angiogenesis in multiple sclerosis and experimental autoimmune encephalomyelitis. *Acta Neuropathol. Commun.* 2:84. doi: 10.1186/s40478-014-0084-z

Gnatenco, C., Han, J., Snyder, A. K., and Kim, D. (2002). Functional expression of TREK-2 K+ channel in cultured rat brain astrocytes. *Brain Res.* 931, 56–67. doi: 10.1016/s0006-8993(02)02261-8

Goldin, A. L., Barchi, R. L., Caldwell, J. H., Hofmann, F., Howe, J. R., Hunter, J. C., et al. (2000). Nomenclature of voltage-gated sodium channels. *Neuron* 28, 365–368. doi: 10.1016/s0896-6273(00)00116-1

Gonzalez-Alvarado, M. N., Rotger, C., Berger, L., London, B., Haase, S., Kuhbandner, K., et al. (2020). Functional role of endogenous Kv1.4 in experimental demyelination. *J. Neuroimmunol.* 343:577227. doi: 10.1016/j.jneuroim.2020.577227

Gonzalez-Reyes, L. E., Ladas, T. P., Chiang, C. C., and Durand, D. M. (2013). TRPV1 antagonist capsazepine suppresses 4-AP-induced epileptiform activity *in vitro* and electrographic seizures *in vivo*. *Exp. Neurol.* 250, 321–332. doi: 10.1016/j.expneurol.2013.10.010

Good, M. E., Eucker, S. A., Li, J., Bacon, H. M., Lang, S. M., Butcher, J. T., et al. (2018). Endothelial cell pannexin1 modulates severity of ischemic stroke by regulating cerebral inflammation and myogenic tone. *JCI Insight* 3:e96272. doi: 10.1172/jci.insight.96272

Goppner, C., Soria, A. H., Hoegg-Beiler, M. B., and Jentsch, T. J. (2020). Cellular basis of ClC-2 Cl- channel-related brain and testis pathologies. *J. Biol. Chem.* 296:100074. doi: 10.1074/jbc.RA120.016031

Goswami, C., Rademacher, N., Smalla, K. H., Kalscheuer, V., Ropers, H. H., Gundelfinger, E. D., et al. (2010). TRPV1 acts as a synaptic protein and regulates vesicle recycling. *J. Cell Sci.* 123 (Pt. 12), 2045–2057. doi: 10.1242/jcs.065144

Grunder, S., Thiemann, A., Pusch, M., and Jentsch, T. J. (1992). Regions involved in the opening of CIC-2 chloride channel by voltage and cell volume. *Nature* 360, 759–762. doi: 10.1038/360759a0

Guan, D., Tkatch, T., Surmeier, D. J., Armstrong, W. E., and Foehring, R. C. (2007). Kv2 subunits underlie slowly inactivating potassium current in rat neocortical pyramidal neurons. *J. Physiol.* 581 (Pt. 3), 941–960. doi: 10.1113/jphysiol.2007.128454

Guo, F., Yu, N., Cai, J. Q., Quinn, T., Zong, Z. H., Zeng, Y. J., et al. (2008). Voltage-gated sodium channel Nav1.1, Nav1.3 and beta1 subunit were up-regulated in the hippocampus of spontaneously epileptic rat. *Brain Res. Bull.* 75, 179–187. doi: 10.1016/j.brainresbull.2007.10.005

Guo, L., Schreiber, T. H., Weremowicz, S., Morton, C. C., Lee, C., and Zhou, J. (2000). Identification and characterization of a novel polycystin family member, polycystin-L2, in mouse and human: sequence, expression, alternative splicing, and chromosomal localization. *Genomics* 64, 241–251. doi: 10.1006/geno.2000.6131

Gutzmann, J. J., Lin, L., and Hoffman, D. A. (2019). Functional coupling of Cav2.3 and BK potassium channels regulates action potential repolarization and short-term plasticity in the mouse hippocampus. *Front Cell Neurosci* 13, 27. doi: 10.3389/fncel.2019.00027

Haak, L. L., Song, L. S., Molinski, T. F., Pessah, I. N., Cheng, H., and Russell, J. T. (2001). Sparks and puffs in oligodendrocyte progenitors: cross talk between ryanodine receptors and inositol trisphosphate receptors. *J. Neurosci.* 21, 3860–3870. doi: 10.1523/JNEUROSCI.21-11-03860.2001

Haberlandt, C., Derouiche, A., Wyczynski, A., Haseleu, J., Pohle, J., Karram, K., et al. (2011). Gray matter NG2 cells display multiple Ca2+-signaling pathways and highly motile processes. *PLoS ONE* 6:e17575. doi: 10.1371/journal.pone.0017575

Hainz, N., Wolf, S., Beck, A., Wagenpfeil, S., Tschernig, T., and Meier, C. (2017). Probenecid arrests the progression of pronounced clinical symptoms in a mouse model of multiple sclerosis. *Sci. Rep.* 7:17214. doi: 10.1038/s41598-017-17517-5

Hamada, M. S., and Kole, M. H. (2015). Myelin loss and axonal ion channel adaptations associated with gray matter neuronal hyperexcitability. *J. Neurosci.* 35, 7272–7286. doi: 10.1523/JNEUROSCI.4747-14.2015

Hammann, J., Bassetti, D., White, R., Luhmann, H. J., and Kirischuk, S. (2018). alpha2 isoform of Na(+),K(+)-ATPase via Na(+),Ca(2+) exchanger modulates myelin basic protein synthesis in oligodendrocyte lineage cells *in vitro*. *Cell Calcium* 73, 1–10. doi: 10.1016/j.ceca.2018.03.003

Hammond, T. R., Dufort, C., Dissing-Olesen, L., Giera, S., Young, A., Wysoker, A., et al. (2019). Single-Cell rna sequencing of microglia throughout the mouse lifespan and in the injured brain reveals complex cell-state changes. *Immunity* 50, 253–271.e256. doi: 10.1016/j.immuni.2018.11.004

Hashitani, H., and Mitsui, R. (2019). Role of pericytes in the initiation and propagation of spontaneous activity in the microvasculature. *Adv. Exp. Med. Biol.* 1124, 329–356. doi: 10.1007/978-981-13-5895-1_14

Hassan, S., Eldeeb, K., Millns, P. J., Bennett, A. J., Alexander, S. P., and Kendall, D. A. (2014). Cannabidiol enhances microglial phagocytosis via transient receptor potential (TRP) channel activation. *Br. J. Pharmacol.* 171, 2426–2439. doi: 10.1111/bph.12615

Hassen, G. W., Feliberti, J., Kesner, L., Stracher, A., and Mokhtarian, F. (2008). Prevention of axonal injury using calpain inhibitor in chronic progressive experimental autoimmune encephalomyelitis. *Brain Res.* 1236, 206–215. doi: 10.1016/j.brainres.2008.07.124

Hell, J. W., Westenbroek, R. E., Warner, C., Ahlijanian, M. K., Prystay, W., Gilbert, M. M., et al. (1993). Identification and differential subcellular localization of the neuronal class C and class D L-type calcium channel alpha 1 subunits. *J. Cell Biol.* 123, 949–962. doi: 10.1083/jcb.123.4.949

Herrero-Herranz, E., Pardo, L. A., Bunt, G., Gold, R., Stuhmer, W., and Linker, R. A. (2007). Re-expression of a developmentally restricted potassium channel in autoimmune demyelination: Kv1.4 is implicated in oligodendroglial proliferation. *Am. J. Pathol.* 171, 589–598. doi: 10.2353/ajpath.2007.061241

Herrero-Herranz, E., Pardo, L. A., Gold, R., and Linker, R. A. (2008). Pattern of axonal injury in murine myelin oligodendrocyte glycoprotein induced experimental autoimmune encephalomyelitis: implications for multiple sclerosis. *Neurobiol. Dis.* 30, 162–173. doi: 10.1016/j.nbd.2008.01.001

Hervieu, G. J., Cluderay, J. E., Gray, C. W., Green, P. J., Ranson, J. L., Randall, A. D., et al. (2001). Distribution and expression of TREK-1, a two-pore-domain potassium channel, in the adult rat CNS. *Neuroscience* 103, 899–919. doi: 10.1016/s0306-4522(01)00030-6

Hibino, H., Inanobe, A., Furutani, K., Murakami, S., Findlay, I., and Kurachi, Y. (2010). Inwardly rectifying potassium channels: their structure, function, and physiological roles. *Physiol Rev.* 90, 291–366. doi: 10.1152/physrev.00021.2009

Hirtz, J. J., Braun, N., Griesemer, D., Hannes, C., Janz, K., Lohrke, S., et al. (2012). Synaptic refinement of an inhibitory topographic map in the auditory brainstem requires functional Cav1.3 calcium channels. *J. Neurosci.* 32, 14602–14616. doi: 10.1523/JNEUROSCI.0765-12.2012

Ho, K. W., Lambert, W. S., and Calkins, D. J. (2014). Activation of the TRPV1 cation channel contributes to stress-induced astrocyte migration. *Glia* 62, 1435–1451. doi: 10.1002/glia.22691

Hoegg-Beiler, M. B., Sirisi, S., Orozco, I. J., Ferrer, I., Hohensee, S., Auberson, M., et al. (2014). Disrupting MLC1 and GlialCAM and ClC-2 interactions in leukodystrophy entails glial chloride channel dysfunction. *Nat. Commun.* 5:3475. doi: 10.1038/ncomms4475

Hoenderop, J. G., Voets, T., Hoefs, S., Weidema, F., Prenen, J., Nilius, B., et al. (2003). Homo- and heterotetrameric architecture of the epithelial Ca2+ channels TRPV5 and TRPV6. *EMBO J.* 22, 776–785. doi: 10.1093/emboj/cdg080

Hofmann, F., Flockerzi, V., Kahl, S., and Wegener, J. W. (2014). L-type CaV1.2 calcium channels: from *in vitro* findings to *in vivo* function. *Physiol. Rev.* 94, 303–326. doi: 10.1152/physrev.00016.2013

Honore, E. (2007). The neuronal background K2P channels: focus on TREK1. *Nat. Rev. Neurosci.* 8, 251–261. doi: 10.1038/nrn2117

Hoogland, T. M., and Saggau, P. (2004). Facilitation of L-type Ca2+ channels in dendritic spines by activation of beta2 adrenergic receptors. *J. Neurosci.* 24, 8416–8427. doi: 10.1523/JNEUROSCI.1677-04.2004

Hopp, S. C. (2021). Targeting microglia L-type voltage-dependent calcium channels for the treatment of central nervous system disorders. *J. Neurosci. Res.* 99, 141–162. doi: 10.1002/jnr.24585

Hossain, M. M., Sonsalla, P. K., and Richardson, J. R. (2013). Coordinated role of voltage-gated sodium channels and the Na+/H+ exchanger in sustaining microglial activation during inflammation. *Toxicol. Appl. Pharmacol.* 273, 355–364. doi: 10.1016/j.taap.2013.09.011

Hou, X., Zhang, R., Wang, J., Li, Y., Li, F., Zhang, Y., et al. (2018). CLC-2 is a positive modulator of oligodendrocyte precursor cell differentiation and myelination. *Mol. Med. Rep.* 17, 4515–4523. doi: 10.3892/mmr.2018.8439

Howell, O. W., Rundle, J. L., Garg, A., Komada, M., Brophy, P. J., and Reynolds, R. (2010). Activated microglia mediate axoglial disruption that contributes to axonal injury in multiple sclerosis. *J. Neuropathol. Exp. Neurol.* 69, 1017–1033. doi: 10.1097/NEN.0b013e3181f3a5b1

Hu, W., Tian, C., Li, T., Yang, M., Hou, H., and Shu, Y. (2009). Distinct contributions of Na(v)1.6 and Na(v)1.2 in action potential initiation and backpropagation. *Nat. Neurosci.* 12, 996–1002. doi: 10.1038/nn.2359

Huang, C. Y., Chu, D., Hwang, W. C., and Tsaur, M. L. (2012). Coexpression of high-voltage-activated ion channels Kv3.4 and Cav1.2 in pioneer axons during pathfinding in the developing rat forebrain. *J. Comp. Neurol.* 520, 3650–3672. doi: 10.1002/cne.23119

Huang, Y., Fliegert, R., Guse, A. H., Lu, W., and Du, J. (2020). A structural overview of the ion channels of the TRPM family. *Cell Calcium* 85:102111. doi: 10.1016/j.ceca.2019.102111

Hugnot, J. P., Salinas, M., Lesage, F., Guillemare, E., de Weille, J., Heurteaux, C., et al. (1996). Kv8.1, a new neuronal potassium channel subunit with specific inhibitory properties towards shab and shaw channels. *EMBO J.* 15, 3322–3331.

Iglesias, R., Dahl, G., Qiu, F., Spray, D. C., and Scemes, E. (2009). Pannexin 1: the molecular substrate of astrocyte "hemichannels". *J. Neurosci.* 29, 7092–7097. doi: 10.1523/JNEUROSCI.6062-08.2009

Iglesias, R., Locovei, S., Roque, A., Alberto, A. P., Dahl, G., Spray, D. C., et al. (2008). P2X7 receptor-Pannexin1 complex: pharmacology and signaling. *Am. J. Physiol. Cell Physiol.* 295, C752–760. doi: 10.1152/ajpcell.00228.2008

Imaizumi, T., Kocsis, J. D., and Waxman, S. G. (1999). The role of voltage-gated Ca2+ channels in anoxic injury of spinal cord white matter. *Brain Res.* 817, 84–92. doi: 10.1016/s0006-8993(98)01214-1

Indriati, D. W., Kamasawa, N., Matsui, K., Meredith, A. L., Watanabe, M., and Shigemoto, R. (2013). Quantitative localization of Cav2.1 (P/Q-type) voltage-dependent calcium channels in Purkinje cells: somatodendritic gradient and distinct somatic coclustering with calcium-activated potassium channels. *J. Neurosci.* 33, 3668–3678. doi: 10.1523/JNEUROSCI.2921-12.2013

Inglese, M., Madelin, G., Oesingmann, N., Babb, J. S., Wu, W., Stoeckel, B., et al. (2010). Brain tissue sodium concentration in multiple sclerosis: a sodium imaging study at 3 tesla. *Brain* 133 (Pt. 3), 847–857. doi: 10.1093/brain/awp334

Ingwersen, J., De Santi, L., Wingerath, B., Graf, J., Koop, B., Schneider, R., et al. (2018). Nimodipine confers clinical improvement in two models of experimental autoimmune encephalomyelitis. *J. Neurochem.* 146, 86–98. doi: 10.1111/jnc.14324

Irie, T., and Trussell, L. O. (2017). Double-Nanodomain coupling of calcium channels, ryanodine receptors, and BK channels controls the generation of burst firing. *Neuron* 96, 856–870.e854. doi: 10.1016/j.neuron.2017.10.014

Izquierdo-Serra, M., Fernandez-Fernandez, J. M., and Serrano, M. (2020). Rare CACNA1A mutations leading to congenital ataxia. *Pflugers Arch.* 472, 791–809. doi: 10.1007/s00424-020-02396-z

Jakel, S., Agirre, E., Mendanha Falcao, A., van Bruggen, D., Lee, K. W., Knuesel, I., et al. (2019). Altered human oligodendrocyte heterogeneity in multiple sclerosis. *Nature* 566, 543–547. doi: 10.1038/s41586-019-0903-2

Jäkel, S., and Williams, A. (2020). What have advances in transcriptomic technologies taught us about human white matter pathologies? *Front. Cell Neurosci.* 14:238. doi: 10.3389/fncel.2020.00238

Jentsch, T. J. (2000). Neuronal KCNQ potassium channels: physiology and role in disease. *Nat. Rev. Neurosci.* 1, 21–30. doi: 10.1038/35036198

Jentsch, T. J., Maritzen, T., and Zdebik, A. A. (2005). Chloride channel diseases resulting from impaired transepithelial transport or vesicular function. *J. Clin. Invest.* 115, 2039–2046. doi: 10.1172/JCI25470

Jentsch, T. J., and Pusch, M. (2018). CLC chloride channels and transporters: structure, function, physiology, and disease. *Physiol. Rev.* 98, 1493–1590. doi: 10.1152/physrev.00047.2017

Jeong, S. Y., Goto, J., Hashida, H., Suzuki, T., Ogata, K., Masuda, N., et al. (2000). Identification of a novel human voltage-gated sodium channel alpha subunit gene, SCN12A. *Biochem. Biophys. Res. Commun.* 267, 262–270. doi: 10.1006/bbrc.1999.1916

Jeworutzki, E., Lopez-Hernandez, T., Capdevila-Nortes, X., Sirisi, S., Bengtsson, L., Montolio, M., et al. (2012). GlialCAM, a protein defective in a leukodystrophy, serves as a ClC-2 Cl(-) channel auxiliary subunit. *Neuron* 73, 951–961. doi: 10.1016/j.neuron.2011.12.039

Jin, X., Yu, L., Wu, Y., Zhang, S., Shi, Z., Chen, X., et al. (2012). S-Glutathionylation underscores the modulation of the heteromeric Kir4.1-Kir5.1 channel in oxidative stress. *J. Physiol.* 590, 5335–5348. doi: 10.1113/jphysiol.2012.236885

Johnson, B., Leek, A. N., and Tamkun, M. M. (2019). Kv2 channels create endoplasmic reticulum/plasma membrane junctions: a brief history of Kv2 channel subcellular localization. *Channels* 13, 88–101. doi: 10.1080/19336950.2019.1568824

Johnson, K. W., Herold, K. F., Milner, T. A., Hemmings, H. C. Jr., and Platholi, J. (2017). Sodium channel subtypes are differentially localized to pre- and post-synaptic sites in rat hippocampus. *J. Comp. Neurol.* 525, 3563–3578. doi: 10.1002/cne.24291

Jones, S. L., and Stuart, G. J. (2013). Different calcium sources control somatic versus dendritic SK channel activation during action potentials. *J. Neurosci.* 33, 19396–19405. doi: 10.1523/JNEUROSCI.2073-13.2013

Joux, N., Chevaleyre, V., Alonso, G., Boissin-Agasse, L., Moos, F. C., Desarmenien, M. G., et al. (2001). High voltage-activated Ca2+ currents in rat supraoptic neurones: biophysical properties and expression of the various channel alpha1 subunits. *J. Neuroendocrinol.* 13, 638–649. doi: 10.1046/j.1365-2826.2001.00679.x

Jukkola, P., and Gu, C. (2015). Regulation of neurovascular coupling in autoimmunity to water and ion channels. *Autoimmun. Rev.* 14, 258–267. doi: 10.1016/j.autrev.2014.11.010

Jukkola, P., Gu, Y., Lovett-Racke, A. E., and Gu, C. (2017). Suppression of inflammatory demyelinaton and axon degeneration through inhibiting Kv3 channels. *Front. Mol. Neurosci.* 10:344. doi: 10.3389/fnmol.2017.00344

Jukkola, P. I., Lovett-Racke, A. E., Zamvil, S. S., and Gu, C. (2012). K+ channel alterations in the progression of experimental autoimmune encephalomyelitis. *Neurobiol. Dis.* 47, 280–293. doi: 10.1016/j.nbd.2012.04.012

Justice, J. A., Schulien, A. J., He, K., Hartnett, K. A., Aizenman, E., and Shah, N. H. (2017). Disruption of KV2.1 somato-dendritic clusters prevents the apoptogenic increase of potassium currents. *Neuroscience* 354, 158–167. doi: 10.1016/j.neuroscience.2017.04.034

Kamijo, S., Ishii, Y., Horigane, S. I., Suzuki, K., Ohkura, M., Nakai, J., et al. (2018). A critical neurodevelopmental role for L-type voltage-gated calcium channels in neurite extension and radial migration. *J. Neurosci.* 38, 5551–5566. doi: 10.1523/JNEUROSCI.2357-17.2018

Kanda, H., Ling, J., Tonomura, S., Noguchi, K., Matalon, S., and Gu, J. G. (2019). TREK-1 and TRAAK are principal K(+) channels at the nodes of ranvier for rapid action potential conduction on mammalian myelinated afferent nerves. *Neuron* 104, 960–971.e967. doi: 10.1016/j.neuron.2019.08.042

Karim, Z., Sawada, A., Kawakami, H., Yamamoto, T., and Taniguchi, T. (2006). A new calcium channel antagonist, lomerizine, alleviates secondary retinal ganglion cell death after optic nerve injury in the rat. *Curr. Eye Res.* 31, 273–283. doi: 10.1080/02713680500536647

Kasper, D., Planells-Cases, R., Fuhrmann, J. C., Scheel, O., Zeitz, O., Ruether, K., et al. (2005). Loss of the chloride channel ClC-7 leads to lysosomal storage disease and neurodegeneration. *EMBO J.* 24, 1079–1091. doi: 10.1038/sj.emboj.7600576

Kastriti, M. E., Sargiannidou, I., Kleopa, K. A., and Karagogeos, D. (2015). Differential modulation of the juxtaparanodal complex in multiple sclerosis. *Mol. Cell Neurosci.* 67, 93–103. doi: 10.1016/j.mcn.2015.06.005

Kelley, K. W., Ben Haim, L., Schirmer, L., Tyzack, G. E., Tolman, M., Miller, J. G., et al. (2018). Kir4.1-dependent astrocyte-fast motor neuron interactions are required for peak strength. *Neuron* 98, 306–319.e307. doi: 10.1016/j.neuron.2018.03.010

Kesherwani, V., and Agrawal, S. K. (2012). Upregulation of RyR2 in hypoxic/reperfusion injury. *J. Neurotrauma* 29, 1255–1265. doi: 10.1089/neu.2011.1780

Kharkovets, T., Hardelin, J. P., Safieddine, S., Schweizer, M., El-Amraoui, A., Petit, C., et al. (2000). KCNQ4, a K+ channel mutated in a form of dominant deafness, is expressed in the inner ear and the central auditory pathway. *Proc. Natl. Acad. Sci. U.S.A.* 97, 4333–4338. doi: 10.1073/pnas.97.8.4333

Kim, G. E., and Kaczmarek, L. K. (2014). Emerging role of the KCNT1 Slack channel in intellectual disability. *Front. Cell Neurosci.* 8:209. doi: 10.3389/fncel.2014.00209

Kim, J. W., Oh, H. A., Lee, S. H., Kim, K. C., Eun, P. H., Ko, M. J., et al. (2018). T-Type calcium channels are required to maintain viability of neural progenitor cells. *Biomol. Ther.* 26, 439–445. doi: 10.4062/biomolther.2017.223

Kim, S. R., Kim, S. U., Oh, U., and Jin, B. K. (2006). Transient receptor potential vanilloid subtype 1 mediates microglial cell death *in vivo* and *in vitro* via Ca2+-mediated mitochondrial damage and cytochrome c release. *J. Immunol.* 177, 4322–4329. doi: 10.4049/jimmunol.177.7.4322

Kirmiz, M., Palacio, S., Thapa, P., King, A. N., Sack, J. T., and Trimmer, J. S. (2018). Remodeling neuronal ER-PM junctions is a conserved nonconducting function of Kv2 plasma membrane ion channels. *Mol. Biol. Cell* 29, 2410–2432. doi: 10.1091/mbc.E18-05-0337

Kleefuss-Lie, A., Friedl, W., Cichon, S., Haug, K., Warnstedt, M., Alekov, A., et al. (2009). CLCN2 variants in idiopathic generalized epilepsy. *Nat. Genet.* 41, 954–955. doi: 10.1038/ng0909-954

Klegeris, A., Choi, H. B., McLarnon, J. G., and McGeer, P. L. (2007). Functional ryanodine receptors are expressed by human microglia and THP-1 cells: their possible involvement in modulation of neurotoxicity. *J. Neurosci. Res.* 85, 2207–2215. doi: 10.1002/jnr.21361

Kole, M. H., and Stuart, G. J. (2012). Signal processing in the axon initial segment. *Neuron* 73, 235–247. doi: 10.1016/j.neuron.2012.01.007

Kong, W. L., Peng, Y. Y., and Peng, B. W. (2017). Modulation of neuroinflammation: role and therapeutic potential of TRPV1 in the neuro-immune axis. *Brain. Behav. Immun.* 64, 354–366. doi: 10.1016/j.bbi.2017.03.007

Konstas, A. A., Korbmacher, C., and Tucker, S. J. (2003). Identification of domains that control the heteromeric assembly of Kir5.1/Kir4.0 potassium channels. *Am. J. Physiol. Cell Physiol.* 284, C910–917. doi: 10.1152/ajpcell.00479.2002

Kornak, U., Kasper, D., Bosl, M. R., Kaiser, E., Schweizer, M., Schulz, A., et al. (2001). Loss of the ClC-7 chloride channel leads to osteopetrosis in mice and man. *Cell* 104, 205–215. doi: 10.1016/s0092-8674(01)00206-9

Kuhlmann, T., Ludwin, S., Prat, A., Antel, J., Bruck, W., and Lassmann, H. (2017). An updated histological classification system for multiple sclerosis lesions. *Acta Neuropathol.* 133, 13–24. doi: 10.1007/s00401-016-1653-y

Kurowski, P., Gawlak, M., and Szulczyk, P. (2015). Muscarinic receptor control of pyramidal neuron membrane potential in the medial prefrontal cortex (mPFC) in rats. *Neuroscience* 303, 474–488. doi: 10.1016/j.neuroscience.2015.07.023

Kushnir, A., Wajsberg, B., and Marks, A. R. (2018). Ryanodine receptor dysfunction in human disorders. *Biochim. Biophys. Acta. Mol. Cell Res.* 1865 (11 Pt. B), 1687–1697. doi: 10.1016/j.bbamcr.2018.07.011

Lanner, J. T., Georgiou, D. K., Joshi, A. D., and Hamilton, S. L. (2010). Ryanodine receptors: structure, expression, molecular details, and function in calcium release. *Cold Spring Harb. Perspect. Biol.* 2:a003996. doi: 10.1101/cshperspect.a003996

Lapato, A. S., and Tiwari-Woodruff, S. K. (2018). Connexins and pannexins: At the junction of neuro-glial homeostasis & disease. *J. Neurosci. Res.* 96, 31–44. doi: 10.1002/jnr.24088

Larson, V. A., Zhang, Y., and Bergles, D. E. (2016). Electrophysiological properties of NG2(+) cells: Matching physiological studies with gene expression profiles. *Brain Res.* 1638 (Pt. B):138–160. doi: 10.1016/j.brainres.2015.09.010

Latour, I., Hamid, J., Beedle, A. M., Zamponi, G. W., and Macvicar, B. A. (2003). Expression of voltage-gated Ca2+ channel subtypes in cultured astrocytes. *Glia* 41, 347–353. doi: 10.1002/glia.10162

Lee, S. C., Choi, S., Lee, T., Kim, H. L., Chin, H., and Shin, H. S. (2002). Molecular basis of R-type calcium channels in central amygdala neurons of the mouse. *Proc. Natl. Accad. Sci. U.S.A.* 99, 3276–3281. doi: 10.1073/pnas.052697799

Lee, Y. J., Yum, M. S., Kim, M. J., Shim, W. H., Yoon, H. M., Yoo, I. H., et al. (2017). Large-scale structural alteration of brain in epileptic children with SCN1A mutation. *Neuroimage Clin.* 15, 594–600. doi: 10.1016/j.nicl.2017.06.002

Leithe, E., Mesnil, M., and Aasen, T. (2018). The connexin 43 C-terminus: a tail of many tales. *Biochim. Biophys. Acta Biomembr.* 1860, 48–64. doi: 10.1016/j.bbamem.2017.05.008

Li, F., Lu, J., Wu, C. Y., Kaur, C., Sivakumar, V., Sun, J., et al. (2008). Expression of Kv1.2 in microglia and its putative roles in modulating production of proinflammatory cytokines and reactive oxygen species. *J. Neurochem.* 106, 2093–2105. doi: 10.1111/j.1471-4159.2008.05559.x

Li, L., Li, J., Zuo, Y., Dang, D., Frost, J. A., and Yang, Q. (2019). Activation of KCNQ channels prevents paclitaxel-induced peripheral neuropathy and associated neuropathic pain. *J. Pain* 20, 528–539. doi: 10.1016/j.jpain.2018.11.001

Li, T., Wang, L., Ma, T., Wang, S., Niu, J., Li, H., et al. (2018). Dynamic calcium release from endoplasmic reticulum mediated by ryanodine receptor 3 is crucial for oligodendroglial differentiation. *Front. Mol. Neurosci.* 11:162. doi: 10.3389/fnmol.2018.00162

Li, Y., Tatsui, C. E., Rhines, L. D., North, R. Y., Harrison, D. S., Cassidy, R. M., et al. (2017). Dorsal root ganglion neurons become hyperexcitable and increase expression of voltage-gated T-type calcium channels (Cav3.2) in paclitaxel-induced peripheral neuropathy. *Pain* 158, 417–429. doi: 10.1097/j.pain.0000000000000774

Li, Z., Zhang, S., Cao, L., Li, W., Ye, Y. C., Shi, Z. X., et al. (2018). Tanshinone IIA and Astragaloside IV promote the angiogenesis of mesenchymal stem cell-derived endothelial cell-like cells via upregulation of Cx37, Cx40 and Cx43. *Exp. Ther. Med.* 15, 1847–1854. doi: 10.3892/etm.2017.5636

Liao, B., Zhang, Y., Sun, H., Ma, B., and Qian, J. (2016). Ryanodine receptor 2 plays a critical role in spinal cord injury via induction of oxidative stress. *Cell Physiol. Biochem.* 38, 1129–1137. doi: 10.1159/000443063

Liao, Y. J., Jan, Y. N., and Jan, L. Y. (1996). Heteromultimerization of G-protein-gated inwardly rectifying K+ channel proteins GIRK1 and GIRK2 and their altered expression in weaver brain. *J. Neurosci.* 16, 7137–7150.

Lindia, J. A., and Abbadie, C. (2003). Distribution of the voltage gated sodium channel Na(v)1.3-like immunoreactivity in the adult rat central nervous system. *Brain Res.* 60, 132–141. doi: 10.1016/s0006-8993(02)03802-7

Lipscombe, D., Helton, T. D., and Xu, W. (2004). L-type calcium channels: the low down. *J. Neurophysiol.* 92, 2633–2641. doi: 10.1152/jn.00486.2004

Lishko, P. V., and Mannowetz, N. (2018). CatSper: a unique calcium channel of the sperm flagellum. *Curr. Opin. Physiol.* 2, 109–113. doi: 10.1016/j.cophys.2018.02.004

Liu, X., Hernandez, N., Kisselev, S., Floratos, A., Sawle, A., Ionita-Laza, I., et al. (2016). Identification of candidate genes for familial early-onset essential tremor. *Eur. J. Hum. Genet.* 24, 1009–1015. doi: 10.1038/ejhg.2015.228

Locovei, S., Scemes, E., Qiu, F., Spray, D. C., and Dahl, G. (2007). Pannexin1 is part of the pore forming unit of the P2X(7) receptor death complex. *FEBS Lett.* 581, 483–488. doi: 10.1016/j.febslet.2006.12.056

Lory, P., Nicole, S., and Monteil, A. (2020). Neuronal Cav3 channelopathies: recent progress and perspectives. *Pflugers Arch.* 472, 831–844. doi: 10.1007/s00424-020-02429-7

Ludwig, J., Weseloh, R., Karschin, C., Liu, Q., Netzer, R., Engeland, B., et al. (2000). Cloning and functional expression of rat eag2, a new member of the ether-a-go-go family of potassium channels and comparison of its distribution with that of eag1. *Mol. Cell Neurosci.* 16, 59–70. doi: 10.1006/mcne.2000.0851

Lugaresi, A. (2015). Pharmacology and clinical efficacy of dalfampridine for treating multiple sclerosis. *Expert. Opin. Drug Metab. Toxicol.* 11, 295–306. doi: 10.1517/17425255.2015.993315

Luscher, C., and Slesinger, P. A. (2010). Emerging roles for G protein-gated inwardly rectifying potassium (GIRK) channels in health and disease. *Nat. Rev. Neurosci.* 11, 301–315. doi: 10.1038/nrn2834

Lutz, S. E., Gonzalez-Fernandez, E., Ventura, J. C., Perez-Samartin, A., Tarassishin, L., Negoro, H., et al. (2013). Contribution of pannexin1 to experimental autoimmune encephalomyelitis. *PLoS ONE* 8:e66657. doi: 10.1371/journal.pone.0066657

Ma, W., Compan, V., Zheng, W., Martin, E., North, R. A., Verkhratsky, A., et al. (2012). Pannexin 1 forms an anion-selective channel. *Pflugers Arch.* 463, 585–592. doi: 10.1007/s00424-012-1077-z

Majumdar, A., Capetillo-Zarate, E., Cruz, D., Gouras, G. K., and Maxfield, F. R. (2011). Degradation of Alzheimer's amyloid fibrils by microglia requires delivery of ClC-7 to lysosomes. *Mol. Biol. Cell* 22, 1664–1676. doi: 10.1091/mbc.E10-09-0745

Malko, P., Syed Mortadza, S. A., McWilliam, J., and Jiang, L. H. (2019). TRPM2 channel in microglia as a new player in neuroinflammation associated with a spectrum of central nervous system pathologies. *Front. Pharmacol.* 10:239. doi: 10.3389/fphar.2019.00239

Marques, S., Zeisel, A., Codeluppi, S., van Bruggen, D., Mendanha Falcao, A., Xiao, L., et al. (2016). Oligodendrocyte heterogeneity in the mouse juvenile and adult central nervous system. *Science* 352, 1326–1329. doi: 10.1126/science.aaf6463

Marrone, M. C., Morabito, A., Giustizieri, M., Chiurchiu, V., Leuti, A., Mattioli, M., et al. (2017). TRPV1 channels are critical brain inflammation detectors and neuropathic pain biomarkers in mice. *Nat. Commun.* 8:15292. doi: 10.1038/ncomms15292

Martin, N. A., Nawrocki, A., Molnar, V., Elkjaer, M. L., Thygesen, E. K., Palkovits, M., et al. (2018). Orthologous proteins of experimental de- and remyelination are differentially regulated in the CSF proteome of multiple sclerosis subtypes. *PLoS ONE* 13:e0202530. doi: 10.1371/journal.pone.0202530

Martinez, A., Santiago, J. L., Cenit, M. C., de Las Heras, V., de la Calle, H., Fernandez-Arquero, M., et al. (2008). IFIH1-GCA-KCNH7 locus: influence on multiple sclerosis risk. *Eur. J. Hum. Genet.* 16, 861–864. doi: 10.1038/ejhg.2008.16

Matyash, M., Matyash, V., Nolte, C., Sorrentino, V., and Kettenmann, H. (2002). Requirement of functional ryanodine receptor type 3 for astrocyte migration. *FASEB J* 16, 84–86. doi: 10.1096/fj.01-0380fje

Mayfield, J., Blednov, Y. A., and Harris, R. A. (2015). Behavioral and genetic evidence for girk channels in the cns: role in physiology, pathophysiology, and drug addiction. *Int. Rev. Neurobiol.* 123, 279–313. doi: 10.1016/bs.irn.2015.05.016

McDonald, W. I., and Sears, T. A. (1969). Effect of demyelination on conduction in the central nervous system. *Nature*. 221, 182–183. doi: 10.1038/221182a0

McKay, B. E., McRory, J. E., Molineux, M. L., Hamid, J., Snutch, T. P., Zamponi, G. W., et al. (2006). Ca(V)3 T-type calcium channel isoforms differentially distribute to somatic and dendritic compartments in rat central neurons. *Eur. J. Neurosci.* 24, 2581–2594. doi: 10.1111/j.1460-9568.2006.05136.x

McKinney, B. C., Sze, W., Lee, B., and Murphy, G. G. (2009). Impaired long-term potentiation and enhanced neuronal excitability in the amygdala of Ca(V)1.3 knockout mice. *Neurobiol. Learn. Mem.* 92, 519–528. doi: 10.1016/j.nlm.2009.06.012

McPherson, P. S., and Campbell, K. P. (1990). Solubilization and biochemical characterization of the high affinity [3H]ryanodine receptor from rabbit brain membranes. *J. Biol. Chem.* 265, 18454–18460.

McTague, A., Appleton, R., Avula, S., Cross, J. H., King, M. D., Jacques, T. S., et al. (2013). Migrating partial seizures of infancy: expansion of the electroclinical, radiological and pathological disease spectrum. *Brain* 136 (Pt. 5), 1578–1591. doi: 10.1093/brain/awt073

Meisler, M. H. (2019). SCN8A encephalopathy: mechanisms and models. *Epilepsia* 60 (Suppl. 3), S86–S91. doi: 10.1111/epi.14703

Melzer, N., Hicking, G., Gobel, K., and Wiendl, H. (2012). TRPM2 cation channels modulate T cell effector functions and contribute to autoimmune CNS inflammation. *PLoS ONE* 7:e47617. doi: 10.1371/journal.pone.0047617

Miceli, F., Soldovieri, M. V., Ambrosino, P., Barrese, V., Migliore, M., Cilio, M. R., et al. (2013). Genotype-phenotype correlations in neonatal epilepsies caused by mutations in the voltage sensor of K(v)7.2 potassium channel subunits. *Proc. Natl. Acad. Sci. U.S.A.* 110, 4386–4391. doi: 10.1073/pnas.1216867110

Miceli, F., Soldovieri, M. V., Martire, M., and Taglialatela, M. (2008). Molecular pharmacology and therapeutic potential of neuronal Kv7-modulating drugs. *Curr. Opin. Pharmacol.* 8, 65–74. doi: 10.1016/j.coph.2007.10.003

Micu, I., Plemel, J. R., Lachance, C., Proft, J., Jansen, A. J., Cummins, K., et al. (2016). The molecular physiology of the axo-myelinic synapse. *Exp. Neurol.* 276, 41–50. doi: 10.1016/j.expneurol.2015.10.006

Miyake, T., Shirakawa, H., Nakagawa, T., and Kaneko, S. (2015). Activation of mitochondrial transient receptor potential vanilloid 1 channel contributes to microglial migration. *Glia* 63, 1870–1882. doi: 10.1002/glia.22854

Mochida, S. (2019). Presynaptic calcium channels. *Int. J. Mol. Sci.* 20:2217. doi: 10.3390/ijms20092217

Mori, F., Ribolsi, M., Kusayanagi, H., Monteleone, F., Mantovani, V., Buttari, F., et al. (2012). TRPV1 channels regulate cortical excitability in humans. *J. Neurosci.* 32, 873–879. doi: 10.1523/JNEUROSCI.2531-11.2012

Mulkey, D. K., and Wenker, I. C. (2011). Astrocyte chemoreceptors: mechanisms of H+ sensing by astrocytes in the retrotrapezoid nucleus and their possible contribution to respiratory drive. *Exp. Physiol.* 96, 400–406. doi: 10.1113/expphysiol.2010.053140

Musumeci, G., Grasselli, G., Rossi, S., De Chiara, V., Musella, A., Motta, C., et al. (2011). Transient receptor potential vanilloid 1 channels modulate the synaptic effects of TNF-alpha and of IL-1beta in experimental autoimmune encephalomyelitis. *Neurobiol. Dis.* 43, 669–677. doi: 10.1016/j.nbd.2011.05.018

Nagamine, K., Kudoh, J., Minoshima, S., Kawasaki, K., Asakawa, S., Ito, F., et al. (1998). Molecular cloning of a novel putative Ca2+ channel protein (TRPC7) highly expressed in brain. *Genomics* 54, 124–131. doi: 10.1006/geno.1998.5551

Nagy, B., Hovhannisyan, A., Barzan, R., Chen, T. J., and Kukley, M. (2017). Different patterns of neuronal activity trigger distinct responses of oligodendrocyte precursor cells in the corpus callosum. *PLoS Biol.* 15:e2001993. doi: 10.1371/journal.pbio.2001993

Namadurai, S., Yereddi, N. R., Cusdin, F. S., Huang, C. L., Chirgadze, D. Y., and Jackson, A. P. (2015). A new look at sodium channel beta subunits. *Open Biol.* 5:140192. doi: 10.1098/rsob.140192

Naziroglu, M., and Luckhoff, A. (2008). A calcium influx pathway regulated separately by oxidative stress and ADP-Ribose in TRPM2 channels: single channel events. *Neurochem. Res.* 33, 1256–1262. doi: 10.1007/s11064-007-9577-5

Nerbonne, J. M., Gerber, B. R., Norris, A., and Burkhalter, A. (2008). Electrical remodelling maintains firing properties in cortical pyramidal neurons lacking KCND2-encoded A-type K+ currents. *J. Physiol.* 586, 1565–1579. doi: 10.1113/jphysiol.2007.146597

Neusch, C., Rozengurt, N., Jacobs, R. E., Lester, H. A., and Kofuji, P. (2001). Kir4.1 potassium channel subunit is crucial for oligodendrocyte development and *in vivo* myelination. *J Neurosci* 21, 5429–5438

Nicoletti, N. F., Erig, T. C., Zanin, R. F., Roxo, M. R., Ferreira, N. P., Gomez, M. V., et al. (2017). Pre-clinical evaluation of voltage-gated calcium channel blockers derived from the spider *P. nigriventer* in glioma progression. *Toxicon* 129, 58–67. doi: 10.1016/j.toxicon.2017.02.001

Nijenhuis, T., Hoenderop, J. G., van der Kemp, A. W., and Bindels, R. J. (2003). Localization and regulation of the epithelial Ca2+ channel TRPV6 in the kidney. *J. Am. Soc. Nephrol.* 14, 2731–2740. doi: 10.1097/01.asn.0000094081.78893.e8

Nilius, B., and Owsianik, G. (2011). The transient receptor potential family of ion channels. *Genome Biol.* 12:218. doi: 10.1186/gb-2011-12-3-218

Niu, J., Li, T., Yi, C., Huang, N., Koulakoff, A., Weng, C., et al. (2016). Connexin-based channels contribute to metabolic pathways in the oligodendroglial lineage. *J. Cell Sci.* 129, 1902–1914. doi: 10.1242/jcs.178731

Nodera, H., Spieker, A., Sung, M., and Rutkove, S. (2011). Neuroprotective effects of Kv7 channel agonist, retigabine, for cisplatin-induced peripheral neuropathy. *Neurosci. Lett.* 505, 223–227. doi: 10.1016/j.neulet.2011.09.013

Obermair, G. J., Szabo, Z., Bourinet, E., and Flucher, B. E. (2004). Differential targeting of the L-type Ca2+ channel alpha 1C (CaV1.2) to synaptic and extrasynaptic compartments in hippocampal neurons. *Eur. J. Neurosci.* 19, 2109–2122. doi: 10.1111/j.0953-816X.2004.03272.x

O'Brien, J. E., and Meisler, M. H. (2013). Sodium channel SCN8A (Nav1.6): properties and *de novo* mutations in epileptic encephalopathy and intellectual disability. *Front. Genet.* 4, 213. doi: 10.3389/fgene.2013.00213

Ogiwara, I., Miyamoto, H., Morita, N., Atapour, N., Mazaki, E., Inoue, I., et al. (2007). Nav1.1 localizes to axons of parvalbumin-positive inhibitory interneurons: a circuit basis for epileptic seizures in mice carrying an Scn1a gene mutation. *J. Neurosci.* 27, 5903–5914. doi: 10.1523/JNEUROSCI.5270-06.2007

Olah, M. E., Jackson, M. F., Li, H., Perez, Y., Sun, H. S., Kiyonaka, S., et al. (2009). Ca2+-dependent induction of TRPM2 currents in hippocampal neurons. *J. Physiol.* 587 (Pt. 5), 965–979. doi: 10.1113/jphysiol.2008.162289

O'Malley, H. A., Shreiner, A. B., Chen, G. H., Huffnagle, G. B., and Isom, L. L. (2009). Loss of Na+ channel beta2 subunits is neuroprotective in a mouse model of multiple sclerosis. *Mol. Cell Neurosci.* 40, 143–155. doi: 10.1016/j.mcn.2008.10.001

Orellana, J. A., Froger, N., Ezan, P., Jiang, J. X., Bennett, M. V., Naus, C. C., et al. (2011). ATP and glutamate released via astroglial connexin 43 hemichannels mediate neuronal death through activation of pannexin 1 hemichannels. *J. Neurochem.* 118, 826–840. doi: 10.1111/j.1471-4159.2011.07210.x

Orellana, J. A., Montero, T. D., and von Bernhardi, R. (2013). Astrocytes inhibit nitric oxide-dependent Ca(2+) dynamics in activated microglia: involvement of ATP released via pannexin 1 channels. *Glia* 61, 2023–2037. doi: 10.1002/glia.22573

Orem, B. C., Pelisch, N., Williams, J., Nally, J. M., and Stirling, D. P. (2017). Intracellular calcium release through IP3R or RyR contributes to secondary axonal degeneration. *Neurobiol. Dis.* 106, 235–243. doi: 10.1016/j.nbd.2017.07.011

Ortner, N. J., and Striessnig, J. (2016). L-type calcium channels as drug targets in CNS disorders. *Channels* 10, 7–13. doi: 10.1080/19336950.2015.1048936

Osorio, N., Alcaraz, G., Padilla, F., Couraud, F., Delmas, P., and Crest, M. (2005). Differential targeting and functional specialization of sodium channels in cultured cerebellar granule cells. *J. Physiol.* 569 (Pt. 3), 801–816. doi: 10.1113/jphysiol.2005.097022

Ouardouz, M., Nikolaeva, M. A., Coderre, E., Zamponi, G. W., McRory, J. E., Trapp, B. D., et al. (2003). Depolarization-induced Ca2+ release in ischemic spinal cord white matter involves L-type Ca2+ channel activation of ryanodine receptors. *Neuron* 40, 53–63. doi: 10.1016/j.neuron.2003.08.016

Ovsepian, S. V., LeBerre, M., Steuber, V., O'Leary, V. B., Leibold, C., and Oliver Dolly, J. (2016). Distinctive role of KV1.1 subunit in the biology and functions of low threshold K(+) channels with implications for neurological disease. *Pharmacol. Ther.* 159, 93–101. doi: 10.1016/j.pharmthera.2016.01.005

Paez, P. M., Cheli, V. T., Ghiani, C. A., Spreuer, V., Handley, V. W., and Campagnoni, A. T. (2012). Golli myelin basic proteins stimulate oligodendrocyte progenitor cell proliferation and differentiation in remyelinating adult mouse brain. *Glia* 60, 1078–1093. doi: 10.1002/glia.22336

Paez, P. M., Fulton, D., Colwell, C. S., and Campagnoni, A. T. (2009). Voltage-operated Ca(2+) and Na(+) channels in the oligodendrocyte lineage. *J. Neurosci. Res.* 87, 3259–3266. doi: 10.1002/jnr.21938

Paez, P. M., and Lyons, D. A. (2020). Calcium signaling in the oligodendrocyte lineage: regulators and consequences. *Annu. Rev. Neurosci.* 43, 163–186. doi: 10.1146/annurev-neuro-100719-093305

Paltser, G., Liu, X. J., Yantha, J., Winer, S., Tsui, H., Wu, P., et al. (2013). TRPV1 gates tissue access and sustains pathogenicity in autoimmune encephalitis. *Mol. Med.* 19, 149–159. doi: 10.2119/molmed.2012.00329

Pan, Z., Kao, T., Horvath, Z., Lemos, J., Sul, J. Y., Cranstoun, S. D., et al. (2006). A common ankyrin-G-based mechanism retains KCNQ and NaV channels at electrically active domains of the axon. *J. Neurosci.* 26, 2599–2613. doi: 10.1523/JNEUROSCI.4314-05.2006

Papa, M., Boscia, F., Canitano, A., Castaldo, P., Sellitti, S., Annunziato, L., et al. (2003). Expression pattern of the ether-a-gogo-related (ERG) K+ channel-encoding genes ERG1, ERG2, and ERG3 in the adult rat central nervous system. *J Comp Neurol* 466, 119–135. doi: 10.1002/cne.10886

Papanikolaou, M., Butt, A. M., and Lewis, A. (2020). A critical role for the inward rectifying potassium channel Kir7.1 in oligodendrocytes of the mouse optic nerve. *Brain Struct. Funct*. 225, 925–934. doi: 10.1007/s00429-020-02043-4

Pappalardo, L. W., Black, J. A., and Waxman, S. G. (2016). Sodium channels in astroglia and microglia. *Glia* 64, 1628–1645. doi: 10.1002/glia.22967

Parajuli, L. K., Nakajima, C., Kulik, A., Matsui, K., Schneider, T., Shigemoto, R., et al. (2012). Quantitative regional and ultrastructural localization of the Ca(v)2.3 subunit of R-type calcium channel in mouse brain. *J. Neurosci*. 32, 13555–13567. doi: 10.1523/JNEUROSCI.1142-12.2012

Pelegrin, P., Barroso-Gutierrez, C., and Surprenant, A. (2008). P2X7 receptor differentially couples to distinct release pathways for IL-1beta in mouse macrophage. *J. Immunol*. 180, 7147–7157. doi: 10.4049/jimmunol.180.11.7147

Pelisch, N., Gomes, C., Nally, J. M., Petruska, J. C., and Stirling, D. P. (2017). Differential expression of ryanodine receptor isoforms after spinal cord injury. *Neurosci. Lett*. 660, 51–56. doi: 10.1016/j.neulet.2017.09.018

Perez-Reyes, E. (2003). Molecular physiology of low-voltage-activated t-type calcium channels. *Physiol. Rev*. 83, 117–161. doi: 10.1152/physrev.00018.2002

Pessia, M., Imbrici, P., D'Adamo, M. C., Salvatore, L., and Tucker, S. J. (2001). Differential pH sensitivity of Kir4.1 and Kir4.2 potassium channels and their modulation by heteropolymerisation with Kir5.1. *J. Physiol.* 532 (Pt. 2), 359–367. doi: 10.1111/j.1469-7793.2001.0359f.x

Pietrobon, D. (2010). CaV2.1 channelopathies. *Pflugers Arch*. 460, 375–393. doi: 10.1007/s00424-010-0802-8

Pitman, K. A., Ricci, R., Gasperini, R., Beasley, S., Pavez, M., Charlesworth, J., et al. (2020). The voltage-gated calcium channel CaV1.2 promotes adult oligodendrocyte progenitor cell survival in the mouse corpus callosum but not motor cortex. *Glia* 68, 376–392. doi: 10.1002/glia.23723

Poet, M., Kornak, U., Schweizer, M., Zdebik, A. A., Scheel, O., Hoelter, S., et al. (2006). Lysosomal storage disease upon disruption of the neuronal chloride transport protein ClC-6. *Proc. Natl. Acad. Sci. U.S.A*. 103, 13854–13859. doi: 10.1073/pnas.0606137103

Poopalasundaram, S., Knott, C., Shamotienko, O. G., Foran, P. G., Dolly, J. O., Ghiani, C. A., et al. (2000). Glial heterogeneity in expression of the inwardly rectifying K(+) channel, Kir4.1, in adult rat CNS. *Glia* 30, 362–372. doi: 10.1002/(sici)1098-1136(200006)30:4<362::aid-glia50>3.0.co;2-4

Prasad, A., Teh, D. B. L., Blasiak, A., Chai, C., Wu, Y., Gharibani, P. M., et al. (2017). Static magnetic field stimulation enhances oligodendrocyte differentiation and secretion of neurotrophic factors. *Sci. Rep*. 7:6743. doi: 10.1038/s41598-017-06331-8

Pressey, S. N., O'Donnell, K. J., Stauber, T., Fuhrmann, J. C., Tyynela, J., Jentsch, T. J., et al. (2010). Distinct neuropathologic phenotypes after disrupting the chloride transport proteins ClC-6 or ClC-7/Ostm1. *J. Neuropathol. Exp. Neurol*. 69, 1228–1246. doi: 10.1097/NEN.0b013e3181ffe742

Qi, H., Moran, M. M., Navarro, B., Chong, J. A., Krapivinsky, G., Krapivinsky, L., et al. (2007). All four CatSper ion channel proteins are required for male fertility and sperm cell hyperactivated motility. *Proc. Natl. Acad. Sci. U.S.A*. 104, 1219–1223. doi: 10.1073/pnas.0610286104

Raap, M., Biedermann, B., Braun, P., Milenkovic, I., Skatchkov, S. N., Bringmann, A., et al. (2002). Diversity of Kir channel subunit mRNA expressed by retinal glial cells of the guinea-pig. *Neuroreport* 13, 1037–1040. doi: 10.1097/00001756-200206120-00012

Rajakulendran, S., Kaski, D., and Hanna, M. G. (2012). Neuronal P/Q-type calcium channel dysfunction in inherited disorders of the CNS. *Nat. Rev. Neurol*. 8, 86–96. doi: 10.1038/nrneurol.2011.228

Rasband, M. N., Kagawa, T., Park, E. W., Ikenaka, K., and Trimmer, J. S. (2003). Dysregulation of axonal sodium channel isoforms after adult-onset chronic demyelination. *J. Neurosci. Res*. 73, 465–470. doi: 10.1002/jnr.10675

Rasmussen, H. B., and Trimmer, J. S. (2019). *The Voltage-Dependent K+ Channel Family*. Oxford: Oxford University Press.

Reese, K. A., and Caldwell, J. H. (1999). Immunocytochemical localization of NaCh6 in cultured spinal cord astrocytes. *Glia* 26, 92–96. doi: 10.1002/(sici)1098-1136(199903)26:1<92::aid-glia10>3.0.co;2-4

Rettig, J., Sheng, Z. H., Kim, D. K., Hodson, C. D., Snutch, T. P., and Catterall, W. A. (1996). Isoform-specific interaction of the alpha1A subunits of brain Ca2+ channels with the presynaptic proteins syntaxin and SNAP-25. *Proc. Natl. Acad. Sci. U.S.A*. 93, 7363–7368. doi: 10.1073/pnas.93.14.7363

Riccio, A., Medhurst, A. D., Mattei, C., Kelsell, R. E., Calver, A. R., Randall, A. D., et al. (2002). mRNA distribution analysis of human TRPC family in CNS and peripheral tissues. *Brain Res. Mol. Brain Res*. 109, 95–104. doi: 10.1016/s0169-328x(02)00527-2

Rivat, C., Sar, C., Mechaly, I., Leyris, J. P., Diouloufet, L., Sonrier, C., et al. (2018). Inhibition of neuronal FLT3 receptor tyrosine kinase alleviates peripheral neuropathic pain in mice. *Nat Commun* 9, 1042. doi: 10.1038/s41467-018-03496-2

Rivera-Pagan, A. F., Rivera-Aponte, D. E., Melnik-Martinez, K. V., Zayas-Santiago, A., Kucheryavykh, L. Y., Martins, A. H., et al. (2015). Up-regulation of TREK-2 potassium channels in cultured astrocytes requires *de novo* protein synthesis: relevance to localization of TREK-2 channels in astrocytes after transient cerebral ischemia. *PLoS ONE*. 10:e0125195. doi: 10.1371/journal.pone.0125195

Rizzi, S., Knaus, H. G., and Schwarzer, C. (2016). Differential distribution of the sodium-activated potassium channels slick and slack in mouse brain. *J. Comp. Neurol*. 524, 2093–2116. doi: 10.1002/cne.23934

Rommer, P. S., Milo, R., Han, M. H., Satyanarayan, S., Sellner, J., Hauer, L., et al. (2019). Immunological aspects of approved MS therapeutics. *Front. Immunol*. 10:1564. doi: 10.3389/fimmu.2019.01564

Rui, Y., Pollitt, S. L., Myers, K. R., Feng, Y., and Zheng, J. Q. (2020). Spontaneous local calcium transients regulate oligodendrocyte development in culture through store-operated Ca(2+) entry and release. *eNeuro* 7. doi: 10.1523/ENEURO.0347-19.2020

Ruiz, A., Matute, C., and Alberdi, E. (2010). Intracellular Ca2+ release through ryanodine receptors contributes to AMPA receptor-mediated mitochondrial dysfunction and ER stress in oligodendrocytes. *Cell Death Dis*. 1:e54. doi: 10.1038/cddis.2010.31

Sadovnick, A. D., Traboulsee, A. L., Zhao, Y., Bernales, C. Q., Encarnacion, M., Ross, J. P., et al. (2017). Genetic modifiers of multiple sclerosis progression, severity and onset. *Clin. Immunol*. 180, 100–105. doi: 10.1016/j.clim.2017.05.009

Saegusa, H., Kurihara, T., Zong, S., Minowa, O., Kazuno, A., Han, W., et al. (2000). Altered pain responses in mice lacking alpha 1E subunit of the voltage-dependent Ca2+ channel. *Proc. Natl. Acad. Sci. U.S.A*. 97, 6132–6137. doi: 10.1073/pnas.100124197

Saez, J. C., Berthoud, V. M., Branes, M. C., Martinez, A. D., and Beyer, E. C. (2003). Plasma membrane channels formed by connexins: their regulation and functions. *Physiol. Rev*. 83, 1359–1400. doi: 10.1152/physrev.00007.2003

Sahu, G., Sukumaran, S., and Bera, A. K. (2014). Pannexins form gap junctions with electrophysiological and pharmacological properties distinct from connexins. *Sci. Rep*. 4:4955. doi: 10.1038/srep04955

Salinas, M., de Weille, J., Guillemare, E., Lazdunski, M., and Hugnot, J. P. (1997a). Modes of regulation of shab K+ channel activity by the Kv8.1 subunit. *J. Biol. Chem*. 272, 8774–8780. doi: 10.1074/jbc.272.13.8774

Salinas, M., Duprat, F., Heurteaux, C., Hugnot, J. P., and Lazdunski, M. (1997b). New modulatory alpha subunits for mammalian Shab K+ channels. *J. Biol. Chem*. 272, 24371–24379. doi: 10.1074/jbc.272.39.24371

Santiago Gonzalez, D. A., Cheli, V. T., Zamora, N. N., Lama, T. N., Spreuer, V., Murphy, G. G., et al. (2017). Conditional deletion of the L-type calcium channel Cav1.2 in NG2-positive cells impairs remyelination in mice. *J. Neurosci*. 37, 10038–10051. doi: 10.1523/JNEUROSCI.1787-17.2017

Sappington, R. M., and Calkins, D. J. (2008). Contribution of TRPV1 to microglia-derived IL-6 and NFkappaB translocation with elevated hydrostatic pressure. *Invest Ophthalmol. Vis. Sci*. 49, 3004–3017. doi: 10.1167/iovs.07-1355

Schampel, A., Volovitch, O., Koeniger, T., Scholz, C. J., Jorg, S., Linker, R. A., et al. (2017). Nimodipine fosters remyelination in a mouse model of multiple sclerosis and induces microglia-specific apoptosis. *Proc. Natl. Acad. Sci. U.S.A*. 114, E3295–E3304. doi: 10.1073/pnas.1620052114

Schattling, B., Eggert, B., and Friese, M. A. (2014). Acquired channelopathies as contributors to development and progression of multiple sclerosis. *Exp. Neurol*. 262 (Pt. A), 28–36. doi: 10.1016/j.expneurol.2013.12.006

Schattling, B., Fazeli, W., Engeland, B., Liu, Y., Lerche, H., Isbrandt, D., et al. (2016). Activity of NaV1.2 promotes neurodegeneration in an animal model of multiple sclerosis. *JCI Insight* 1:e89810. doi: 10.1172/jci.insight.89810

Scheffer, I. E., and Nabbout, R. (2019). SCN1A-related phenotypes: epilepsy and beyond. *Epilepsia* 60 (Suppl. 3), S17–S24. doi: 10.1111/epi.16386

Schilling, T., and Eder, C. (2009). Importance of the non-selective cation channel TRPV1 for microglial reactive oxygen species generation. *J. Neuroimmunol.* 216, 118–121. doi: 10.1016/j.jneuroim.2009.07.008

Schirmer, L., Mobius, W., Zhao, C., Cruz-Herranz, A., Ben Haim, L., Cordano, C., et al. (2018). Oligodendrocyte-encoded Kir4.1 function is required for axonal integrity. *Elife* 7:e36428. doi: 10.7554/eLife.36428

Schirmer, L., Srivastava, R., Kalluri, S. R., Bottinger, S., Herwerth, M., Carassiti, D., et al. (2014). Differential loss of KIR4.1 immunoreactivity in multiple sclerosis lesions. *Ann. Neurol.* 75, 810–828. doi: 10.1002/ana.24168

Schirmer, L., Velmeshev, D., Holmqvist, S., Kaufmann, M., Werneburg, S., Jung, D., et al. (2019). Neuronal vulnerability and multilineage diversity in multiple sclerosis. *Nature* 573, 75–82. doi: 10.1038/s41586-019-1404-z

Schlichter, L. C., Kaushal, V., Moxon-Emre, I., Sivagnanam, V., and Vincent, C. (2010). The Ca2+ activated SK3 channel is expressed in microglia in the rat striatum and contributes to microglia-mediated neurotoxicity *in vitro*. *J. Neuroinflammation* 7:4. doi: 10.1186/1742-2094-7-4

Schmidt, K., Eulitz, D., Veh, R. W., Kettenmann, H., and Kirchhoff, F. (1999). Heterogeneous expression of voltage-gated potassium channels of the shaker family (Kv1) in oligodendrocyte progenitors. *Brain Res.* 843, 145–160. doi: 10.1016/s0006-8993(99)01938-1

Schrey, M., Codina, C., Kraft, R., Beetz, C., Kalff, R., Wolfl, S., et al. (2002). Molecular characterization of voltage-gated sodium channels in human gliomas. *Neuroreport* 13, 2493–2498. doi: 10.1097/00001756-200212200-00023

Schulien, A. J., Yeh, C. Y., Orange, B. N., Pav, O. J., Hopkins, M. P., Moutal, A., et al. (2020). Targeted disruption of Kv2.1-VAPA association provides neuroprotection against ischemic stroke in mice by declustering Kv2.1 channels. *Sci. Adv.* 6:eaaz8110. doi: 10.1126/sciadv.aaz8110

Sedmak, G., and Judas, M. (2021). White matter interstitial neurons in the adult human brain: 3% of cortical neurons in quest for recognition. *Cells* 10:190. doi: 10.3390/cells10010190

Sesti, F., Wu, X., and Liu, S. (2014). Oxidation of KCNB1 K(+) channels in central nervous system and beyond. *World J. Biol. Chem.* 5, 85–92. doi: 10.4331/wjbc.v5.i2.85

Shang, K. W., Zhang, Y. H., Yang, X. L., Liu, A. J., Yang, Z. X., Liu, X. Y., et al. (2016). [Clinical features and gene mutations in epilepsy of infancy with migrating focal seizures]. *Zhonghua Er Ke Za Zhi* 54, 735–739. doi: 10.3760/cma.j.issn.0578-1310.2016.10.005

Simpson, P. B., Holtzclaw, L. A., Langley, D. B., and Russell, J. T. (1998). Characterization of ryanodine receptors in oligodendrocytes, type 2 astrocytes, and O-2A progenitors. *J Neurosci. Res.* 52, 468–482. doi: 10.1002/(SICI)1097-4547(19980515)52:4<468::AID-JNR11>3.0.CO;2-#

Sinha, K., Karimi-Abdolrezaee, S., Velumian, A. A., and Fehlings, M. G. (2006). Functional changes in genetically dysmyelinated spinal cord axons of shiverer mice: role of juxtaparanodal Kv1 family K+ channels. *J. Neurophysiol.* 95, 1683–1695. doi: 10.1152/jn.00899.2005

Sita, G., Hrelia, P., Graziosi, A., Ravegnini, G., and Morroni, F. (2018). TRPM2 in the brain: role in health and disease. *Cells* 7:82. doi: 10.3390/cells7070082

Siwek, M. E., Muller, R., Henseler, C., Broich, K., Papazoglou, A., and Weiergraber, M. (2014). The CaV2.3 R-type voltage-gated Ca2+ channel in mouse sleep architecture. *Sleep* 37, 881–892. doi: 10.5665/sleep.3652

Smart, S. L., Bosma, M. M., and Tempel, B. L. (1997). Identification of the delayed rectifier potassium channel, Kv1.6, in cultured astrocytes. *Glia* 20, 127–134. doi: 10.1002/(sici)1098-1136(199706)20:2<127::aid-glia4>3.0.co;2-6

Smith, R. S., Kenny, C. J., Ganesh, V., Jang, A., Borges-Monroy, R., Partlow, J. N., et al. (2018). Sodium channel SCN3A (NaV1.3) regulation of human cerebral cortical folding and oral motor development. *Neuron* 99, 905–913.e907. doi: 10.1016/j.neuron.2018.07.052

So, K., Haraguchi, K., Asakura, K., Isami, K., Sakimoto, S., Shirakawa, H., et al. (2015). Involvement of TRPM2 in a wide range of inflammatory and neuropathic pain mouse models. *J. Pharmacol. Sci.* 127, 237–243. doi: 10.1016/j.jphs.2014.10.003

Soldovieri, M. V., Miceli, F., and Taglialatela, M. (2011). Driving with no brakes: molecular pathophysiology of Kv7 potassium channels. *Physiology* 26, 365–376. doi: 10.1152/physiol.00009.2011

Sosinsky, G. E., Boassa, D., Dermietzel, R., Duffy, H. S., Laird, D. W., MacVicar, B., et al. (2011). Pannexin channels are not gap junction hemichannels. *Channels* 5, 193–197. doi: 10.4161/chan.5.3.15765

Stampanoni Bassi, M., Gentile, A., Iezzi, E., Zagaglia, S., Musella, A., Simonelli, I., et al. (2019). Transient receptor potential vanilloid 1 modulates central inflammation in multiple sclerosis. *Front. Neurol.* 10:30. doi: 10.3389/fneur.2019.00030

Stanika, R., Campiglio, M., Pinggera, A., Lee, A., Striessnig, J., Flucher, B. E., et al. (2016). Splice variants of the CaV1.3 L-type calcium channel regulate dendritic spine morphology. *Sci. Rep.* 6:34528. doi: 10.1038/srep34528

Stirling, D. P., Cummins, K., Wayne Chen, S. R., and Stys, P. (2014). Axoplasmic reticulum Ca(2+) release causes secondary degeneration of spinal axons. *Ann. Neurol.* 75, 220–229. doi: 10.1002/ana.24099

Stirling, D. P., and Stys, P. K. (2010). Mechanisms of axonal injury: internodal nanocomplexes and calcium deregulation. *Trends. Mol. Med.* 16, 160–170. doi: 10.1016/j.molmed.2010.02.002

Stocker, M. (2004). Ca(2+)-activated K+ channels: molecular determinants and function of the SK family. *Nat. Rev. Neurosci.* 5, 758–770. doi: 10.1038/nrn1516

Striessnig, J., Pinggera, A., Kaur, G., Bock, G., and Tuluc, P. (2014). L-type Ca(2+) channels in heart and brain. *Wiley Interdiscip. Rev. Membr. Transp. Signal* 3, 15–38. doi: 10.1002/wmts.102

Subramanian, N., Wetzel, A., Dombert, B., Yadav, P., Havlicek, S., Jablonka, S., et al. (2012). Role of Na(v)1.9 in activity-dependent axon growth in motoneurons. *Hum. Mol. Genet.* 21, 3655–3667. doi: 10.1093/hmg/dds195

Sukiasyan, N., Hultborn, H., and Zhang, M. (2009). Distribution of calcium channel Ca(V)1.3 immunoreactivity in the rat spinal cord and brain stem. *Neuroscience* 159, 217–235. doi: 10.1016/j.neuroscience.2008.12.011

Surmeier, D. J., Mermelstein, P. G., and Goldowitz, D. (1996). The weaver mutation of GIRK2 results in a loss of inwardly rectifying K+ current in cerebellar granule cells. *Proc. Natl. Acad. Sci. U.S.A.* 93, 11191–11195. doi: 10.1073/pnas.93.20.11191

Suzuki, S., and Rogawski, M. A. (1989). T-type calcium channels mediate the transition between tonic and phasic firing in thalamic neurons. *Proc. Natl. Acad. Sci. U.S.A.* 86, 7228–7232. doi: 10.1073/pnas.86.18.7228

Swayne, L. A., Sorbara, C. D., and Bennett, S. A. (2010). Pannexin 2 is expressed by postnatal hippocampal neural progenitors and modulates neuronal commitment. *J. Biol. Chem.* 285, 24977–24986. doi: 10.1074/jbc.M110.130054

Takahashi, H., and Magee, J. C. (2009). Pathway interactions and synaptic plasticity in the dendritic tuft regions of CA1 pyramidal neurons. *Neuron* 62, 102–111. doi: 10.1016/j.neuron.2009.03.007

Takahashi, Y., Jeong, S. Y., Ogata, K., Goto, J., Hashida, H., Isahara, K., et al. (2003). Human skeletal muscle calcium channel alpha1S is expressed in the basal ganglia: distinctive expression pattern among L-type Ca2+ channels. *Neurosci. Res.* 45, 129–137. doi: 10.1016/s0168-0102(02)00204-3

Takeuchi, H., and Suzumura, A. (2014). Gap junctions and hemichannels composed of connexins: potential therapeutic targets for neurodegenerative diseases. *Front. Cell Neurosci.* 8:189. doi: 10.3389/fncel.2014.00189

Talley, E. M., Solorzano, G., Lei, Q., Kim, D., and Bayliss, D. A. (2001). Cns distribution of members of the two-pore-domain (KCNK) potassium channel family. *J. Neurosci.* 21, 7491–7505. doi: 10.1523/JNEUROSCI.21-19-07491.2001

Tanemoto, M., Fujita, A., Higashi, K., and Kurachi, Y. (2002). PSD-95 mediates formation of a functional homomeric Kir5.1 channel in the brain. *Neuron* 34, 387–397. doi: 10.1016/s0896-6273(02)00675-x

Tanemoto, M., Kittaka, N., Inanobe, A., and Kurachi, Y. (2000). *In vivo* formation of a proton-sensitive K+ channel by heteromeric subunit assembly of Kir5.1 with Kir4.1. *J. Physiol.* 525 (Pt. 3), 587–592. doi: 10.1111/j.1469-7793.2000.00587.x

Taruno, A. (2018). ATP release channels. *Int. J. Mol. Sci.* 19:808. doi: 10.3390/ijms19030808

Theis, M., Sohl, G., Eiberger, J., and Willecke, K. (2005). Emerging complexities in identity and function of glial connexins. *Trends Neurosci.* 28, 188–195. doi: 10.1016/j.tins.2005.02.006

Thiffault, I., Speca, D. J., Austin, D. C., Cobb, M. M., Eum, K. S., Safina, N. P., et al. (2015). A novel epileptic encephalopathy mutation in KCNB1 disrupts Kv2.1 ion selectivity, expression, and localization. *J. Gen. Physiol.* 146, 399–410. doi: 10.1085/jgp.201511444

Thimmapaya, R., Neelands, T., Niforatos, W., Davis-Taber, R. A., Choi, W., Putman, C. B., et al. (2005). Distribution and functional

characterization of human Nav1.3 splice variants. *Eur. J. Neurosci.* 22, 1–9. doi: 10.1111/j.1460-9568.2005.04155.x

Thorell, W. E., Leibrock, L. G., and Agrawal, S. K. (2002). Role of RyRs and IP3 receptors after traumatic injury to spinal cord white matter. *J. Neurotrauma* 19, 335–342. doi: 10.1089/089771502753594909

Tippens, A. L., Pare, J. F., Langwieser, N., Moosmang, S., Milner, T. A., Smith, Y., et al. (2008). Ultrastructural evidence for pre- and postsynaptic localization of Cav1.2 L-type Ca2+ channels in the rat hippocampus. *J. Comp. Neurol.* 506, 569–583. doi: 10.1002/cne.21567

Toriyama, H., Wang, L., Saegusa, H., Zong, S., Osanai, M., Murakoshi, T., et al. (2002). Role of Ca(v) 2.3 (alpha1E) Ca2+ channel in ischemic neuronal injury. *Neuroreport* 13, 261–265. doi: 10.1097/00001756-200202110-00018

Torkamani, A., Bersell, K., Jorge, B. S., Bjork, R. L. Jr., Friedman, J. R., Bloss, C. S., et al. (2014). De novo KCNB1 mutations in epileptic encephalopathy. *Ann. Neurol.* 76, 529–540. doi: 10.1002/ana.24263

Trebak, M., and Kinet, J. P. (2019). Calcium signalling in T cells. *Nat. Rev. Immunol.* 19, 154–169. doi: 10.1038/s41577-018-0110-7

Trimmer, J. S. (2015). Subcellular localization of K+ channels in mammalian brain neurons: remarkable precision in the midst of extraordinary complexity. *Neuron* 85, 238–256. doi: 10.1016/j.neuron.2014.12.042

Trimmer, J. S., and Rhodes, K. J. (2004). Localization of voltage-gated ion channels in mammalian brain. *Annu. Rev. Physiol.* 66, 477–519. doi: 10.1146/annurev.physiol.66.032102.113328

Tsuji, F., Murai, M., Oki, K., Seki, I., Ueda, K., Inoue, H., et al. (2010). Transient receptor potential vanilloid 1 agonists as candidates for anti-inflammatory and immunomodulatory agents. *Eur. J. Pharmacol.* 627, 332–339. doi: 10.1016/j.ejphar.2009.10.044

Tsutsui, M., Hirase, R., Miyamura, S., Nagayasu, K., Nakagawa, T., Mori, Y., et al. (2018). TRPM2 exacerbates central nervous system inflammation in experimental autoimmune encephalomyelitis by increasing production of CXCL2 chemokines. *J. Neurosci.* 38, 8484–8495. doi: 10.1523/JNEUROSCI.2203-17.2018

Tucker, S. J., Imbrici, P., Salvatore, L., D'Adamo, M. C., and Pessia, M. (2000). pH dependence of the inwardly rectifying potassium channel, Kir5.1, and localization in renal tubular epithelia. *J. Biol. Chem.* 275, 16404–16407. doi: 10.1074/jbc.C000127200

Tzingounis, A. V., Heidenreich, M., Kharkovets, T., Spitzmaul, G., Jensen, H. S., Nicoll, R. A., et al. (2010). The KCNQ5 potassium channel mediates a component of the afterhyperpolarization current in mouse hippocampus. *Proc. Natl. Acad. Sci. U.S.A.* 107, 10232–10237. doi: 10.1073/pnas.1004644107

Tzour, A., Leibovich, H., Barkai, O., Biala, Y., Lev, S., Yaari, Y., et al. (2017). KV 7/M channels as targets for lipopolysaccharide-induced inflammatory neuronal hyperexcitability. *J. Physiol.* 595, 713–738. doi: 10.1113/JP272547

Vacher, H., Mohapatra, D. P., and Trimmer, J. S. (2008). Localization and targeting of voltage-dependent ion channels in mammalian central neurons. *Physiol. Rev.* 88, 1407–1447. doi: 10.1152/physrev.00002.2008

van de Graaf, S. F., Hoenderop, J. G., and Bindels, R. J. (2006). Regulation of TRPV5 and TRPV6 by associated proteins. *Am. J. Physiol. Renal Physiol.* 290, F1295–1302. doi: 10.1152/ajprenal.00443.2005

Van Der Stelt, M., and Di Marzo, V. (2004). Endovanilloids. Putative endogenous ligands of transient receptor potential vanilloid 1 channels. *Eur. J. Biochem.* 271, 1827–1834. doi: 10.1111/j.1432-1033.2004.04081.x

Vanderver, A., Simons, C., Schmidt, J. L., Pearl, P. L., Bloom, M., Lavenstein, B., et al. (2014). Identification of a novel *de novo* p.Phe932Ile KCNT1 mutation in a patient with leukoencephalopathy and severe epilepsy. *Pediatr. Neurol.* 50, 112–114. doi: 10.1016/j.pediatrneurol.2013.06.024

Vasistha, N. A., Johnstone, M., Barton, S. K., Mayerl, S. E., Thangaraj Selvaraj, B., Thomson, P. A., et al. (2019). Familial t(1;11) translocation is associated with disruption of white matter structural integrity and oligodendrocyte-myelin dysfunction. *Mol. Psychiatry* 24, 1641–1654. doi: 10.1038/s41380-019-0505-2

Vautier, F., Belachew, S., Chittajallu, R., and Gallo, V. (2004). Shaker-type potassium channel subunits differentially control oligodendrocyte progenitor proliferation. *Glia* 48, 337–345. doi: 10.1002/glia.20088

Vay, S. U., Flitsch, L. J., Rabenstein, M., Moniere, H., Jakovcevski, I., Andjus, P., et al. (2020). The impact of hyperpolarization-activated cyclic nucleotide-gated (HCN) and voltage-gated potassium KCNQ/Kv7 channels on primary microglia function. *J. Neuroinflammation* 17:100. doi: 10.1186/s12974-020-01779-4

Veng, L. M., Mesches, M. H., and Browning, M. D. (2003). Age-related working memory impairment is correlated with increases in the L-type calcium channel protein alpha1D (Cav1.3) in area CA1 of the hippocampus and both are ameliorated by chronic nimodipine treatment. *Brain Res. Mol. Brain Res.* 110, 193–202. doi: 10.1016/s0169-328x(02)00643-5

Vennekens, R., Hoenderop, J. G., Prenen, J., Stuiver, M., Willems, P. H., Droogmans, G., et al. (2000). Permeation and gating properties of the novel epithelial Ca(2+) channel. *J. Biol. Chem.* 275, 3963–3969. doi: 10.1074/jbc.275.6.3963

Vierra, N. C., Kirmiz, M., van der List, D., Santana, L. F., and Trimmer, J. S. (2019). Kv2.1 mediates spatial and functional coupling of L-type calcium channels and ryanodine receptors in mammalian neurons. *Elife* 8:e49953. doi: 10.7554/eLife.49953

Vigil, F. A., Bozdemir, E., Bugay, V., Chun, S. H., Hobbs, M., Sanchez, I., et al. (2020). Prevention of brain damage after traumatic brain injury by pharmacological enhancement of KCNQ (Kv7, "M-type") K(+) currents in neurons. *J. Cereb. Blood Flow Metab.* 40, 1256–1273. doi: 10.1177/0271678X19857818

Villegas, R., Martinez, N. W., Lillo, J., Pihan, P., Hernandez, D., Twiss, J. L., et al. (2014). Calcium release from intra-axonal endoplasmic reticulum leads to axon degeneration through mitochondrial dysfunction. *J. Neurosci.* 34, 7179–7189. doi: 10.1523/JNEUROSCI.4784-13.2014

Vogt, A., Hormuzdi, S. G., and Monyer, H. (2005). Pannexin1 and Pannexin2 expression in the developing and mature rat brain. *Brain Res. Mol. Brain Res.* 141, 113–120. doi: 10.1016/j.molbrainres.2005.08.002

Wainger, B. J., Kiskinis, E., Mellin, C., Wiskow, O., Han, S. S., Sandoe, J., et al. (2014). Intrinsic membrane hyperexcitability of amyotrophic lateral sclerosis patient-derived motor neurons. *Cell Rep.* 7, 1–11. doi: 10.1016/j.celrep.2014.03.019

Wang, H., Allen, M. L., Grigg, J. J., Noebels, J. L., and Tempel, B. L. (1995). Hypomyelination alters K+ channel expression in mouse mutants shiverer and Trembler. *Neuron* 15, 1337–1347. doi: 10.1016/0896-6273(95)90012-8

Wang, H., Kunkel, D. D., Martin, T. M., Schwartzkroin, P. A., and Tempel, B. L. (1993). Heteromultimeric K+ channels in terminal and juxtaparanodal regions of neurons. *Nature* 365, 75–79. doi: 10.1038/365075a0

Wang, H., Zhang, X., Xue, L., Xing, J., Jouvin, M. H., Putney, J. W., et al. (2016). Low-Voltage-Activated CaV3.1 calcium channels shape T helper cell cytokine profiles. *Immunity* 44, 782–794. doi: 10.1016/j.immuni.2016.01.015

Wang, H. S., Pan, Z., Shi, W., Brown, B. S., Wymore, R. S., Cohen, I. S., et al. (1998). KCNQ2 and KCNQ3 potassium channel subunits: molecular correlates of the M-channel. *Science* 282, 1890–1893. doi: 10.1126/science.282.5395.1890

Wang, J., Ou, S. W., and Wang, Y. J. (2017). Distribution and function of voltage-gated sodium channels in the nervous system. *Channels* 11, 534–554. doi: 10.1080/19336950.2017.1380758

Wang, K., Lin, M. T., Adelman, J. P., and Maylie, J. (2014). Distinct Ca2+ sources in dendritic spines of hippocampal CA1 neurons couple to SK and Kv4 channels. *Neuron* 81, 379–387. doi: 10.1016/j.neuron.2013.11.004

Wang, N., De Bock, M., Decrock, E., Bol, M., Gadicherla, A., Vinken, M., et al. (2013). Paracrine signaling through plasma membrane hemichannels. *Biochim. Biophys. Acta* 1828, 35–50. doi: 10.1016/j.bbamem.2012.07.002

Wang, R., Tu, S., Zhang, J., and Shao, A. (2020). Roles of TRP channels in neurological diseases. *Oxid. Med. Cell Longev.* 2020:7289194. doi: 10.1155/2020/7289194

Wang, W., Gao, X. F., Xiao, L., Xiang, Z. H., and He, C. (2011). K(V)7/KCNQ channels are functionally expressed in oligodendrocyte progenitor cells. *PLoS ONE* 6:e21792. doi: 10.1371/journal.pone.0021792

Wartosch, L., Fuhrmann, J. C., Schweizer, M., Stauber, T., and Jentsch, T. J. (2009). Lysosomal degradation of endocytosed proteins depends on the chloride transport protein ClC-7. *FASEB J.* 23, 4056–4068. doi: 10.1096/fj.09-130880

Watanabe, M., Ueda, T., Shibata, Y., Kumamoto, N., Shimada, S., and Ugawa, S. (2015). Expression and regulation of Cav3.2 T-Type calcium channels during inflammatory hyperalgesia in mouse dorsal root ganglion neurons. *PLoS ONE* 10:e0127572. doi: 10.1371/journal.pone.0127572

Waxman, S. G. (2001). Acquired channelopathies in nerve injury and MS. *Neurology* 56, 1621–1627. doi: 10.1212/wnl.56.12.1621

Weiergraber, M., Henry, M., Radhakrishnan, K., Hescheler, J., and Schneider, T. (2007). Hippocampal seizure resistance and reduced neuronal excitotoxicity

in mice lacking the Cav2.3 E/R-type voltage-gated calcium channel. *J. Neurophysiol.* 97, 3660–3669. doi: 10.1152/jn.01193.2006

Weinert, S., Jabs, S., Hohensee, S., Chan, W. L., Kornak, U., and Jentsch, T. J. (2014). Transport activity and presence of ClC-7/Ostm1 complex account for different cellular functions. *EMBO Rep.* 15, 784–791. doi: 10.15252/embr.201438553

Weinreich, F., and Jentsch, T. J. (2001). Pores formed by single subunits in mixed dimers of different CLC chloride channels. *J. Biol. Chem.* 276, 2347–2353. doi: 10.1074/jbc.M005733200

Weiss, N., and Zamponi, G. W. (2019). T-type calcium channels: from molecule to therapeutic opportunities. *Int. J. Biochem. Cell Biol.* 108, 34–39. doi: 10.1016/j.biocel.2019.01.008

Westenbroek, R. E., Noebels, J. L., and Catterall, W. A. (1992). Elevated expression of type II Na+ channels in hypomyelinated axons of shiverer mouse brain. *J. Neurosci.* 12, 2259–2267

Wetzel, A., Jablonka, S., and Blum, R. (2013). Cell-autonomous axon growth of young motoneurons is triggered by a voltage-gated sodium channel. *Channels* 7, 51–56. doi: 10.4161/chan.23153

Whitaker, W. R., Faull, R. L., Waldvogel, H. J., Plumpton, C. J., Emson, P. C., and Clare, J. J. (2001). Comparative distribution of voltage-gated sodium channel proteins in human brain. *Brain Res. Mol. Brain Res.* 88, 37–53. doi: 10.1016/s0169-328x(00)00289-8

Whyte-Fagundes, P., and Zoidl, G. (2018). Mechanisms of pannexin1 channel gating and regulation. *Biochim. Biophys. Acta Biomembr.* 1860, 65–71. doi: 10.1016/j.bbamem.2017.07.009

Willecke, K., Eiberger, J., Degen, J., Eckardt, D., Romualdi, A., Guldenagel, M., et al. (2002). Structural and functional diversity of connexin genes in the mouse and human genome. *Biol. Chem.* 383, 725–737. doi: 10.1515/BC.2002.076

Willis, M., Kaufmann, W. A., Wietzorrek, G., Hutter-Paier, B., Moosmang, S., Humpel, C., et al. (2010). L-type calcium channel CaV 1.2 in transgenic mice overexpressing human AbetaPP751 with the London (V717I) and Swedish (K670M/N671L) mutations. *J. Alzheimers Dis.* 20, 1167–1180. doi: 10.3233/JAD-2010-091117

Winter, M., Weissgerber, P., Klein, K., Lux, F., Yildiz, D., Wissenbach, U., et al. (2020). Transient receptor potential vanilloid 6 (TRPV6) proteins control the extracellular matrix structure of the placental labyrinth. *Int. J. Mol. Sci.* 21:9674. doi: 10.3390/ijms21249674

Woo, D. H., Han, K. S., Shim, J. W., Yoon, B. E., Kim, E., Bae, J. Y., et al. (2012). TREK-1 and Best1 channels mediate fast and slow glutamate release in astrocytes upon GPCR activation. *Cell* 151, 25–40. doi: 10.1016/j.cell.2012.09.005

Wormuth, C., Lundt, A., Henseler, C., Muller, R., Broich, K., Papazoglou, A., et al. (2016). Review: Cav2.3 R-type voltage-gated Ca(2+) channels - functional implications in convulsive and non-convulsive seizure activity. *Open Neurol. J.* 10, 99–126. doi: 10.2174/1874205X01610010099

Wu, C. Y., Kaur, C., Sivakumar, V., Lu, J., and Ling, E. A. (2009). Kv1.1 expression in microglia regulates production and release of proinflammatory cytokines, endothelins and nitric oxide. *Neuroscience* 158, 1500–1508. doi: 10.1016/j.neuroscience.2008.11.043

Wu, L. G., Westenbroek, R. E., Borst, J. G., Catterall, W. A., and Sakmann, B. (1999). Calcium channel types with distinct presynaptic localization couple differentially to transmitter release in single calyx-type synapses. *J. Neurosci.* 19, 726–736.

Wu, Z., Li, L., Xie, F., Xu, G., Dang, D., and Yang, Q. (2020). Enhancing KCNQ channel activity improves neurobehavioral recovery after spinal cord injury. *J. Pharmacol. Exp. Ther.* 373, 72–80. doi: 10.1124/jpet.119.264010

Xiao, K., Sun, Z., Jin, X., Ma, W., Song, Y., Lai, S., et al. (2018). ERG3 potassium channel-mediated suppression of neuronal intrinsic excitability and prevention of seizure generation in mice. *J. Physiol.* 596, 4729–4752. doi: 10.1113/JP275970

Xiao, Y., Lv, X., Cao, G., Bian, G., Duan, J., Ai, J., et al. (2010). Overexpression of Trpp5 contributes to cell proliferation and apoptosis probably through involving calcium homeostasis. *Mol. Cell Biochem.* 339, 155–161. doi: 10.1007/s11010-009-0379-8

Xiao, Z. S., and Quarles, L. D. (2010). Role of the polycytin-primary cilia complex in bone development and mechanosensing. *Ann. N. Y. Acad. Sic.* 1192, 410–421. doi: 10.1111/j.1749-6632.2009.05239.x

Xu, H., Tian, W., Fu, Y., Oyama, T. T., Anderson, S., and Cohen, D. M. (2007). Functional effects of nonsynonymous polymorphisms in the human TRPV1 gene. *Am. J. Physiol. Renal Physiol.* 293, F1865–1876. doi: 10.1152/ajprenal.00347.2007

Xu, J. H., Long, L., Tang, Y. C., Hu, H. T., and Tang, F. R. (2007). Ca(v)1.2, Ca(v)1.3, and Ca(v)2.1 in the mouse hippocampus during and after pilocarpine-induced status epilepticus. *Hippocampus* 17, 235–251. doi: 10.1002/hipo.20263

Yan, E., Li, B., Gu, L., Hertz, L., and Peng, L. (2013). Mechanisms for L-channel-mediated increase in [Ca(2+)]i and its reduction by anti-bipolar drugs in cultured astrocytes combined with its mRNA expression in freshly isolated cells support the importance of astrocytic L-channels. *Cell Calcium* 54, 335–342. doi: 10.1016/j.ceca.2013.08.002

Yasuda, R., Sabatini, B. L., and Svoboda, K. (2003). Plasticity of calcium channels in dendritic spines. *Nat. Neurosci.* 6, 948–955. doi: 10.1038/nn1112

Yeung, A. K., Patil, C. S., and Jackson, M. F. (2020). Pannexin-1 in the CNS: emerging concepts in health and disease. *J. Neurochem.* 154, 468–485. doi: 10.1111/jnc.15004

Yu, F. H., and Catterall, W. A. (2003). Overview of the voltage-gated sodium channel family. *Genome Biol.* 4:207. doi: 10.1186/gb-2003-4-3-207

Zamora, N. N., Cheli, V. T., Santiago Gonzalez, D. A., Wan, R., and Paez, P. M. (2020). Deletion of voltage-gated calcium channels in astrocytes during demyelination reduces brain inflammation and promotes myelin regeneration in mice. *J. Neurosci.* 40, 3332–3347. doi: 10.1523/JNEUROSCI.1644-19.2020

Zamponi, G. W., Striessnig, J., Koschak, A., and Dolphin, A. C. (2015). The physiology, pathology, and pharmacology of voltage-gated calcium channels and their future therapeutic potential. *Pharmacol. Rev.* 67, 821–870. doi: 10.1124/pr.114.009654

Zhang, H., Maximov, A., Fu, Y., Xu, F., Tang, T. S., Tkatch, T., et al. (2005). Association of CaV1.3 L-type calcium channels with shank. *J. Neurosci.* 25, 1037–1049. doi: 10.1523/JNEUROSCI.4554-04.2005

Zhang, Y., Chen, K., Sloan, S. A., Bennett, M. L., Scholze, A. R., O'Keeffe, S., et al. (2014). An RNA-sequencing transcriptome and splicing database of glia, neurons, and vascular cells of the cerebral cortex. *J. Neurosci.* 34, 11929–11947. doi: 10.1523/JNEUROSCI.1860-14.2014

Zhou, J. Z., and Jiang, J. X. (2014). Gap junction and hemichannel-independent actions of connexins on cell and tissue functions–an update. *FEBS Lett.* 588, 1186–1192. doi: 10.1016/j.febslet.2014.01.001

Zhou, M., Xu, G., Xie, M., Zhang, X., Schools, G. P., Ma, L., et al. (2009). TWIK-1 and TREK-1 are potassium channels contributing significantly to astrocyte passive conductance in rat hippocampal slices. *J. Neurosci.* 29, 8551–8564. doi: 10.1523/JNEUROSCI.5784-08.2009

Zhou, W., Cayabyab, F. S., Pennefather, P. S., Schlichter, L. C., and DeCoursey, T. E. (1998). HERG-like K+ channels in microglia. *J. Gen. Physiol.* 111, 781–794. doi: 10.1085/jgp.111.6.781

Zou, A., Lin, Z., Humble, M., Creech, C. D., Wagoner, P. K., Krafte, D., et al. (2003). Distribution and functional properties of human KCNH8 (Elk1) potassium channels. *Am. J. Physiol. Cell Physiol.* 285, C1356–1366. doi: 10.1152/ajpcell.00179.2003

Zoupi, L., Markoullis, K., Kleopa, K. A., and Karagogeos, D. (2013). Alterations of juxtaparanodal domains in two rodent models of CNS demyelination. *Glia* 61, 1236–1249. doi: 10.1002/glia.22511

Zuccotti, A., Clementi, S., Reinbothe, T., Torrente, A., Vandael, D. H., and Pirone, A. (2011). Structural and functional differences between L-type calcium channels: crucial issues for future selective targeting. *Trends Pharmacol. Sci.* 32, 366–375. doi: 10.1016/j.tips.2011.02.012

Conflict of Interest: The authors declare that the research was conducted in the absence of any commercial or financial relationships that could be construed as a potential conflict of interest.

frontiers in Cellular Neuroscience

ORIGINAL RESEARCH
published: 02 August 2021
doi: 10.3389/fncel.2021.685044

Tension Sensor Based on Fluorescence Resonance Energy Transfer Reveals Fiber Diameter-Dependent Mechanical Factors During Myelination

*Takeshi Shimizu[1], Hideji Murakoshi[2,3], Hidetoshi Matsumoto[4], Kota Ichino[4], Atsunori Hattori[1], Shinya Ueno[1], Akimasa Ishida[1], Naoki Tajiri[1] and Hideki Hida[1]**

[1] Department of Neurophysiology and Brain Science, Nagoya City University Graduate School of Medical Sciences, Nagoya, Japan, [2] Supportive Center for Brain Research, National Institute for Physiological Sciences, Okazaki, Japan, [3] Department of Physiological Sciences, The Graduate University for Advanced Studies, Okazaki, Japan, [4] Department of Materials Science and Engineering, Tokyo Institute of Technology, Meguro, Japan

OPEN ACCESS

Edited by:
Nicola B. Hamilton-Whitaker, King's College London, United Kingdom

Reviewed by:
Robert A. Hill, Dartmouth College, United States
Nathalie Sol-Foulon, INSERM U1127 Institut du Cerveau et de la Moelle épinière (ICM), France

***Correspondence:**
Hideki Hida
hhida@med.nagoya-cu.ac.jp

Specialty section:
This article was submitted to Non-Neuronal Cells, a section of the journal Frontiers in Cellular Neuroscience

Received: *24 March 2021*
Accepted: *13 July 2021*
Published: *02 August 2021*

Citation:
Shimizu T, Murakoshi H, Matsumoto H, Ichino K, Hattori A, Ueno S, Ishida A, Tajiri N and Hida H (2021) Tension Sensor Based on Fluorescence Resonance Energy Transfer Reveals Fiber Diameter-Dependent Mechanical Factors During Myelination. Front. Cell. Neurosci. 15:685044. doi: 10.3389/fncel.2021.685044

Oligodendrocytes (OLs) form a myelin sheath around neuronal axons to increase conduction velocity of action potential. Although both large and small diameter axons are intermingled in the central nervous system (CNS), the number of myelin wrapping is related to the axon diameter, such that the ratio of the diameter of the axon to that of the entire myelinated-axon unit is optimal for each axon, which is required for exerting higher brain functions. This indicates there are unknown axon diameter-dependent factors that control myelination. We tried to investigate physical factors to clarify the mechanisms underlying axon diameter-dependent myelination. To visualize OL-generating forces during myelination, a tension sensor based on fluorescence resonance energy transfer (FRET) was used. Polystyrene nanofibers with varying diameters similar to neuronal axons were prepared to investigate biophysical factors regulating the OL-axon interactions. We found that higher tension was generated at OL processes contacting larger diameter fibers compared with smaller diameter fibers. Additionally, OLs formed longer focal adhesions (FAs) on larger diameter axons and shorter FAs on smaller diameter axons. These results suggest that OLs respond to the fiber diameter and activate mechanotransduction initiated at FAs, which controls their cytoskeletal organization and myelin formation. This study leads to the novel and interesting idea that physical factors are involved in myelin formation in response to axon diameter.

Keywords: oligodendrocyte, myelination, tension sensor, mechanical factor, fluorescence resonance energy transfer

INTRODUCTION

In the central nervous system (CNS) white matter, large and small caliber axons are intermingled, and the diameter of myelin internodes is highly divergent (Weruaga-Prieto et al., 1996), especially in the spinal cord. Large diameter axons are more suitable for being myelinated than small diameter axons (Friede, 1972). Additionally, the ratio of [axon diameter] to [axon + myelin diameter]

(g-ratio) is adjusted to optimum values for each axon. Optimization of the g-ratio is important for higher brain functions. This indicates that myelin formation is tightly associated with the axon caliber, involving unknown diameter-dependent regulatory factors.

A previous study has reported that OLs can myelinate axons of paraformaldehyde-fixed dorsal root ganglion neurons similarly to live axons (Rosenberg et al., 2008). Lee et al. (2012) have previously reported that OL can ensheath a myelin membrane on artificial electrospinning nanofibers without living neurons. These reports indicate that molecular signaling activated by functional proteins on the axonal surface is not required for initiation of myelination, but rather there are permissive axonal cues that initiate myelination (Lee et al., 2012). They also investigated the effect of fiber diameter on myelination using varying nanofiber diameters (0.2–4.0 μm), revealing that larger diameter fibers (more than 0.4 μm) were preferentially ensheathed by OLs. However, the mechanisms underlying optimal myelination according to axon diameter have not been fully elucidated.

Câmara et al. (2009) have previously reported that β1 integrin plays important roles in axoglial interactions that sense axon size and initiate myelination. Reduction in β1 integrin function by its dominant negative form affects myelination of small-diameter axons but not large-diameter axons (Câmara et al., 2009). Integrin is one of the major proteins in the focal adhesion complex. Focal adhesions (FAs) mechanically link the extracellular matrix (ECM) to the cytoplasm and are assemblies for mechanotransduction, which transduce signals from the ECM to the actin stress fibers. Integrin and other FA proteins, such as focal adhesion kinase (FAK), paxillin and talin, play important roles in refining FA complexes in response to mechanical stimulation (Giannone and Sheetz, 2006; Schwartz and DeSimone, 2008; Geiger et al., 2009). Suzuki et al. (2012) have also reported that myelination of small-diameter axons was significantly impaired in the spinal cord of *teneurin-4* deficient mice. Furthermore, Teneurin-4 positively regulated FAK, an essential signaling molecule for myelin formation (Suzuki et al., 2012).

As mentioned above, because integrin is involved in OL-neuron interactions that sense axon size to initiate myelination and is one of the key players in FAs, it is interesting to investigate OL mechanical forces across FAs, which are key platforms for mechanical signal transduction initiated by integrin.

In this study, we thus tried to assess physical OL factors that depend on axon diameter. To visualize the mechanical force generated at OL processes during myelination, we used a previously reported tension sensor (Grashoff et al., 2010). The tension sensor consists of two fluorophores that sandwich a tension sensor module consisting of a 40-amino-acid-long elastic domain (Grashoff et al., 2010). Because fluorescence resonance energy transfer (FRET) enables monitoring protein-protein interactions of two fluorophores, the tension loading on this sensor can reduce FRET efficiency.

We investigated the FRET index of the tension sensor at OL processes contacting nanofibers with different diameters. We found that higher tension was generated at OL processes contacting larger diameter fibers compared with smaller diameter fibers. Additionally, OL formed longer FAs on larger diameter fibers and shorter FAs on smaller diameter fibers. Previous studies have reported that FAs act as mechanotransducers that transmit various signaling pathways (Geiger et al., 2009), which regulate cell morphogenesis and dynamics. These and our results indicate that physical factors are involved in myelin formation in response to axon caliber by activating mechanical signaling initiated at FAs.

MATERIALS AND METHODS

Animals

Neonatal P1 rats of Wistar ST genetic background were purchased from Japan SLC (Shizuoka, Japan). Animal experimental procedures were approved by the Committee of Animal Experimentation of Nagoya City University Medical School and were conducted in accordance with the animal care guidelines of Nagoya City University.

DNA Construction

The pcDNA3.1-CMV-VinculinTS-mTFP1-mVenus plasmid was a gift from Martin Schwartz (Addgene plasmid # 26019). Super-folder GFP with A206K monomeric mutation (msfGFP) (Zacharias et al., 2002; Pedelacq et al., 2006) was created by introducing mutations by using the QuikChange Site-Directed Mutagenesis kit (Agilent Technologies). The pcDNA3.1-CMV-TSmod-sfGFP/ShadowG plasmid was constructed by inserting msfGFP and ShadowG (Murakoshi et al., 2015) into the pcDNA3.1-CMV-VinculinTS-mTFP1-mVenus plasmid by replacing mTFP1 and mVenus.

Preparation of Nanofibers

Polymer fibers were prepared by electrospinning from polystyrene (average $M_w \sim 280{,}000$, Sigma-Aldrich, St. Louis, MO, United States) in solvent mixtures of tetrahydrofuran (THF, Fujifilm Wako, Osaka, Japan) and *N*, *N*-dimethylformamide (DMF, Fujifilm Wako, Osaka, Japan) (the volume ratio of THF and DMF is 1:1). The fluorescent dye, sulforhodamine 101 (Purity > 95.0%, Tokyo Chemical Industry Co., Ltd., Tokyo, Japan), was added to the solutions at a concentration of 0.0025% w/v for fluorescent labeling of fibers. The electrospinning device was the same as that previously described (Matsumoto et al., 2013). For the adjustment of fiber diameter, the solutions with various concentrations were used. Polystyrene fibers with diameters ranging from 0.55 to 4.0 μm were directly electrospun on glass coverslips (18 mm square, thickness of 0.13–0.17 mm, Matsunami Glass Ind., Ltd., Osaka, Japan) from 14 to 22 wt% polystyrene/THF-DMF solutions. The electrospinning conditions were set to keep stable jet formation for each solution: The applied voltage was 12 kV, the flow rate of spinning solution was 0.2–0.5 ml/h; and the distance between the nozzle tip and the collector was 100 mm. The duration of the spinning was 20 sec. The fiber-containing glass coverslips (18 mm square) were put onto the 35 mm culture dishes and applied with elastic adhesive (AX-176, CEMEDINE Co., Ltd., Tokyo Japan) on both edges of

the 18 mm coverslips (including both ends of the nanofibers), and then air-dried for at least 24 h. The nanofibers were sterilized for cell culture by placing the fiber-containing glass coverslips under the UV light for 20 min.

Oligodendrocyte Progenitor Cell (OPC) Culture

The cortices of postnatal day 1 neonatal rats were dissociated and trypsinized, and then cultured on poly-D-lysine (PDL, Sigma, P0899)-coated flasks in DMEM with 10% fetal calf serum (FCS). By 10 days *in vitro*, these cultures consisted of microglia and oligodendrocyte precursor cells growing on an astrocyte monolayer. Microglia were removed based on their differential adhesion to the surface of astrocytes by mechanical shaking at 180 rpm at 37°C for 30 min. Purified OPCs were then acquired by mechanically shaking from the surface of astrocytes at 200 rpm at 37°C overnight. Purified OPCs were seeded on poly-D-lysine (PDL)- or Laminin-coated dishes, and maintained in growth medium: DMEM supplemented with 1 × N2 supplement (Invitrogen, Carlsbad, CA, United States), 0.01% bovine serum albumin, FGF2 (10 ng/ml, R&D systems) and PDGF-AA (10 ng/ml, R&D systems). To induce the differentiation of OPCs, FGF2 and PDGF-AA were removed from the culture medium, and triiodothyronine (T3, 30 ng/ml) was applied. Cells were then maintained in the differentiation medium for 2–5 additional days and fixed with 4% paraformaldehyde.

Oligodendroglial-Nanofiber Cultures Following Transfection of the Tension Sensor

To coat the nanofiber-containing glass coverslips, we dropped 200 μl of poly-D-lysine solution (final concentration of 0.1 mg/ml) onto an area of the coverslips with nanofibers and incubated for 1 h at room temperature, and coverslips were washed by immersing them by sterile water 3 times and air-dried the coverslips. The fiber-containing glass coverslips were then coated with laminin solution (0.1 mg/ml) for 2 h at 37°C, following the poly-D-lysine coating. One day before transfection, purified OPCs (1.5×10^5 cells per coverslip) were seeded onto the laminin-coated coverslips with nanofibers. Plasmid construct was pcDNA3.1-CMV-TSmod-sfGFP/ShadowG. The cells were transfected with the plasmid using LipofectAMINE 2,000 reagent (Invitrogen). We diluted 2.5 μg of DNA in 50 μl Opti-MEM^{TM} medium (Invitrogen) and 3 μl of LipofectAMINE 2,000 in 50 μl Opti-MEM^{TM} medium (Invitrogen) without serum, and combined the diluted DNA and diluted LipofectAMINE 2,000 (total volume was 100 μl). The transfection complex (100 μl) was applied to each coverslip containing OPCs along with 300 μl of growth medium. After having kept the coverslips containing fibers and OPCs in small volumes of medium for 3 h of incubation, the medium was changed to 2 ml of growth medium and the cells were maintained overnight. On the next day, the medium was changed to 2 ml of myelinating culture medium: composed of 50:50 mixture of DMEM (Invitrogen) supplemented with 1x N2 supplement (Invitrogen) and 0.01% BSA: Neurobasal medium (Invitrogen) supplemented with 1x B27 supplement (Invitrogen) and 1x Gluta-MAX^{TM} (Thermo Fisher Scientific), containing penicillin-streptomycin (Invitrogen), N-acetyl cysteine (5 μg/ml; Sigma) and forskolin (10 μM; Sigma). The medium was changed every 3 days for the remainder of the culture period. The length of the culture period required for optimal FRET observation was 8∼10 days.

Two-Photon Fluorescence Lifetime Imaging

Details of the 2pFLIM-FRET imaging were described previously (Yasuda et al., 2006). Briefly, msfGFP in the FRET sensor was excited with a Ti-sapphire laser (Mai Tai; Spectra-Physics) tuned to 920 nm. The scanning mirror (6210H; Cambridge Technology) was controlled with a PCI board (PCI-6110; National Instruments) and ScanImage software (Pologruto et al., 2003). The green fluorescence photon signals were collected by an objective lens (60×, 0.9 NA; Olympus) and a photomultiplier tube (H7422-40p; Hamamatsu) placed after a dichroic mirror (565DCLP; Chroma) and emission filter (FF01-510/84 or FF03-510/20; Semrock). Measurement of fluorescence lifetime was carried out using a time-correlated single-photon counting board (SPC-150; Becker & Hickl) controlled with custom software (Yasuda et al., 2006). The construction of fluorescence lifetime image was described previously (Murakoshi, 2021). Briefly, we acquired the mean fluorescence lifetime in each pixel by calculating the mean photon arrival time $<t>$ using the following Equation (1).

$$< t >= \int tF(t)dt \div \int F(t)\ dt - t_0 \qquad (1)$$

where t_o is obtained by fitting the whole image with double exponential functions convolved with an instrument response function as described previously (Murakoshi, 2021). Subsequently, the mean fluorescence lifetime in each pixel was converted to the corresponding color to generate fluorescence lifetime images.

Evaluation of Fluorescence Lifetime Changes

Fluorescence lifetime changes to the control value were evaluated as follows. The control area was assigned to fluorescent positive OL processes that did not contact nanofibers, and the average fluorescence lifetime value of each pixel at the control area was then calculated for each picture field. If there were several processes that did not contact the nanofibers in a picture field, the fluorescence lifetime of the control value was averaged by those processes to normalize it. The histogram was made by the fluorescence lifetime obtained at each pixel. Color was assigned to the average value of each histogram to construct a fluorescence lifetime image. Since FRET is known to shorten the fluorescence lifetime of the donor fluorophore (Murakoshi, 2021), we measured the fluorescence lifetime changes at fluorescent positive OL processes contacting nanofibers compared to the control area.

Immunostaining

The cultured cells were fixed with 4% paraformaldehyde (PFA) in 0.1 M phosphate buffer (pH 7.4) and used for immunostaining. Fixed cells were blocked with 5% normal goat serum in phosphate-buffered saline and 0.1% Triton X-100 (PBST) and then incubated with primary antibodies overnight at 4°C. The primary antibodies used were as follows: rat anti-GFP antibody (1/500, Nacalai Tesque, 04404-84), monoclonal anti-α-tubulin antibody (1/500, Sigma, T9026), rat anti-myelin basic protein (MBP) antibody (Millipore, MAB386), monoclonal O4 antibody (1/300, R&D systems, MAB1326) and rabbit anti-paxillin antibody (1/250, abcam, ab32084, clone Y113). After being rinsed with PBST, the cells were incubated with secondary antibodies. The secondary antibodies used were Alexa 488- or 594-conjugated goat anti-mouse, anti-rabbit and anti-rat IgG or goat anti-mouse IgM (Molecular Probes). Fluorescent signals were visualized using AX70 fluorescence microscope (Olympus, Tokyo) and A1Rsi confocal fluorescence microscope (Nikon, Tokyo). The number of OL primary processes was analyzed using "Analyze/Sholl" tool of Fiji software based on ImageJ (NIH).

Statistical Analyses

All results are expressed as the mean ± SEM. For comparison of two groups, a Student's *t*-test was used. *p*-values < 0.05 were considered significant. Data for multiple comparisons were analyzed by one-way ANOVA followed by a Tukey-Kramer *post hoc* test using the statistical program GraphPad InStat 3 (GraphPad Software, San Diego, CA, United States). A multiple comparison post-test was performed only if $p < 0.05$. The level of significance was $p < 0.05$.

RESULTS

Establishment of a New Assay System to Examine Fiber Diameter-Mediated Mechanical Forces During Myelination Using a Tension Sensor

A previous study has observed that myelinated axons have diameters ranging from 0.3 to 2 μm in the mammalian CNS (Remahl and Hildebrand, 1982). Another report has demonstrated that the threshold for minimum fiber diameter ensheathed by OLs was 0.4 μm (Lee et al., 2012). However, the mechanisms underlying myelination control by axon diameter are not well known.

To examine the correlation between axonal fiber diameter and mechanical forces generated at OL processes contacting the fibers, we used polystyrene nanofibers with different diameters. OPCs were seeded on small (0.55–0.9 μm), medium (1.5–1.7 μm), or large-diameter (2.5–4.0 μm) nanofibers (**Figures 1A–C**). We confirmed that OLs cultured on coverslips with nanofibers maintain their capacity to myelinate the fibers similarly to live axons (**Figures 1D,E**).

We next investigated the FRET index of the tension sensor at OL processes contacting each fiber group. The previously reported tension sensor has two fluorophores (mTFP1 and mVenus) with a tension sensor module comprising a 40-amino-acid-long elastic domain between them (Grashoff et al., 2010). The mechanical force loading on this sensor changes the FRET efficiency, because FRET can monitor the protein-protein interaction of two fluorophores. In this study, the two fluorophores (mTFP1 and mVenus) in the tension sensor were changed to the FRET pair of monomeric super-folder GFP (msfGFP)-ShadowG (Murakoshi et al., 2015). To quantitatively monitor the FRET index, we used fluorescence lifetime imaging microscopy (FLIM), which measures fluorescence lifetime changes of the donor fluorophore (Yasuda, 2006). The fluorescent proteins pair for the FLIM-FRET was msfGFP as the energy donor and ShadowG as the energy acceptor (Murakoshi et al., 2015).

At first, to examine whether transfection of the tension sensor itself does not affect OL properties and function, OPCs cultured on laminin-coated dishes were transfected with the tension sensor, and OL differentiation and the number of OL primary processes were examined. The tension sensor-transfected OPCs were transferred to culture medium without FGF2 and PDGF-AA to induce OL differentiation for 2 days. Transfection of the tension sensor did not affect the number of O4 + cells, a marker of immature and mature OLs differentiated from OPCs (**Figures 2A–C**). Additionally, the tension sensor did not affect the number of MBP + cells, a marker of mature OLs, which were maintained for 5 days in the differentiation medium (**Figures 2D–F**). We next examined the number of OL primary processes to assess OL morphology using immunocytochemistry with anti-α-tubulin antibody. Transfection of the tension sensor did not influence the number of OL primary processes (**Figures 2G–I**). Taken together, these results indicate that the tension sensor itself did not influence OL morphology or differentiation from OPCs to O4 + OLs.

Higher Tension Is Generated at OL Processes Contacting Large-Diameter Fibers

Next, we investigated the FRET index of the tension sensor at OL processes contacting small (0.55–0.9 μm), medium (1.5–1.7 μm), or large-diameter (2.5–4.0 μm) nanofibers. To quantitate the FRET index, FLIM was used to measure fluorescence lifetime changes of the donor fluorophore. The fluorescence lifetime is the time from when excitation light transits a fluorescent molecule to a high energy state, leading to the emission of a fluorescent photon. A histogram was made from the fluorescence lifetime obtained at each pixel. The average value of each histogram was then calculated, and color assignment was performed to construct a fluorescence lifetime image. FRET shortens the fluorescence lifetime of the donor fluorophore (Becker, 2012), hence it can be detected with FLIM. Using FLIM analysis, we found that OL processes contacting medium and large-diameter fibers showed longer average fluorescence lifetime, indicating higher tension, compared with small-diameter fibers (**Figures 3A–C**). These results suggest that higher tension is generated at OL processes contacting larger diameter axons, and physical factors influence myelin formation in response to axon caliber.

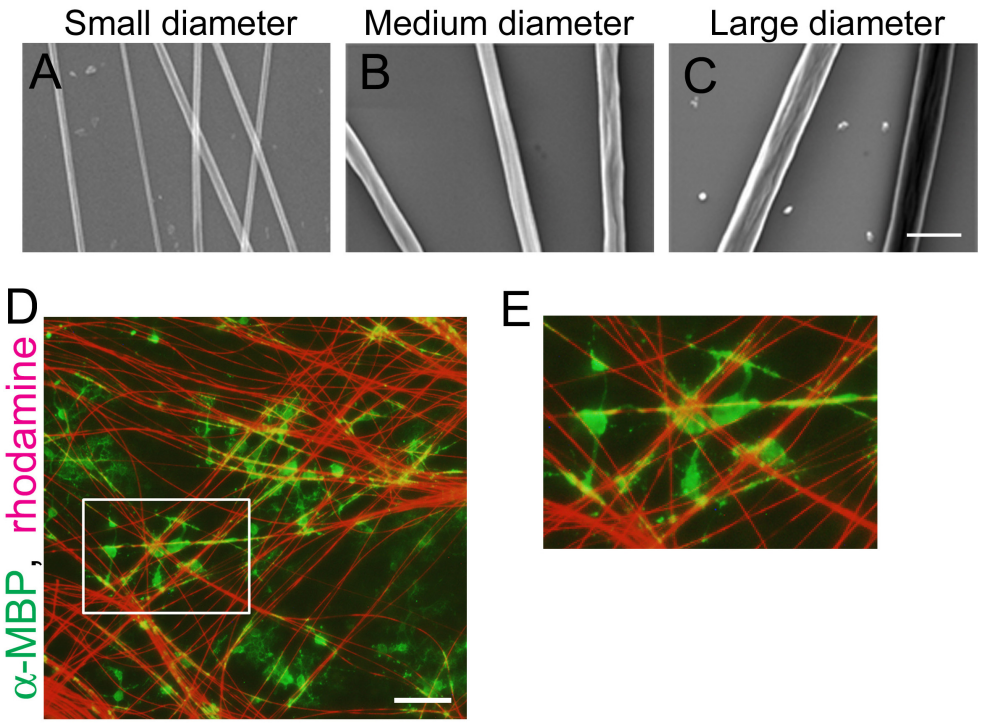

FIGURE 1 | OLs can ensheath polystyrene nanofibers similarly to live axons. **(A–C)** Phase contrast images of polystyrene nanofibers with diameters ranging 0.55–0.9 μm [**(A)**, small diameter], 1.5–1.7 μm [**(B)**, medium diameter] and 2.5–4.0 μm [**(C)**, large diameter]. Scale bar, 5 μm. **(D)** Fluorescent image of MBP (a mature OL marker, green) and sulforhodamine (red), labeling polystyrene nanofibers after 7 days *in vitro*. Scale bar, 100 μm. **(E)** Magnified images of **(D)**, showing OL cells ensheathing nanofibers.

To test whether the FRET index is actually related to the mechanical force generated in OLs, the cells were treated with cytochalasin D, which depolymerizes the F-actin network and inhibits actomyosin contractility (Brown and Spudich, 1979). Cytochalasin D application to OLs significantly decreased the average fluorescence lifetime, meaning decreased tension (**Figures 3D,E**). This result indicates that the FRET index of the tension sensor was truly dependent on a cytoskeleton-dependent intracellularly generated force.

We further examined whether different tensions can be detected in one OL that simultaneously extends processes to both smaller and larger diameter fibers. To this end, mixed nanofibers with both smaller and larger diameters on a culture dish were prepared. We observed that the tension generated by one OL on the smaller diameter fibers was lower than that on the larger diameter fibers (**Figures 3F,G**), indicating that the tension difference detected by the tension sensor is not likely to be caused by the maturation state of each OL, but rather is dependent on the different fiber diameters.

The Length of FAs Formed by OLs Positively Correlates With the Fiber Diameter

FA complexes are generated at the adhesion points and mechanically link the ECM to the cell, acting as key platforms for mechanotransduction. They consist of integrins, which bind to the ECM, adapter proteins, which link integrins to the cellular cytoskeleton, and cytoplasmic proteins, which are the downstream effectors of signaling pathways. A previous study has reported that the tension sensor was properly recruited to FAs where it was co-localized with paxillin, an FA protein (Grashoff et al., 2010). Hence, the tension sensor enables monitoring of the localization of FAs at OL processes. To test whether the GFP-positive tension sensor is actually localized at FAs in OLs, we performed double-immunostaining for GFP and paxillin, one of the typical FA markers. The GFP-positive tension sensor was co-localized with paxillin at the tip of OL processes on laminin-coated dishes (**Figure 4A**), indicating that the tension sensor was localized at FAs in OLs.

We next performed length measurements of the tension sensor-positive signals at OL processes contacting nanofibers with different diameters, which were supposed to be an indicator of FA sizes. We quantified the signal length of the tension sensor in each fiber group. OLs showed shorter tension sensor + signals on small-diameter fibers (0.55–0.9 μm), compared with those produced on medium (1.5–1.7 μm) and large-diameter (2.5–4.0 μm) fibers (**Figures 4B,C**). We further performed immunostaining of FAs in cultured OLs on nanofibers for 8 days. FAs on nanofibers were detected by anti-paxillin antibody and merged with sulforhodamine-positive nanofibers. FA immunostaining showed that longer FAs were formed on larger diameter fibers (**Figures 4D,E**), indicating that the length of FAs formed by OLs positively

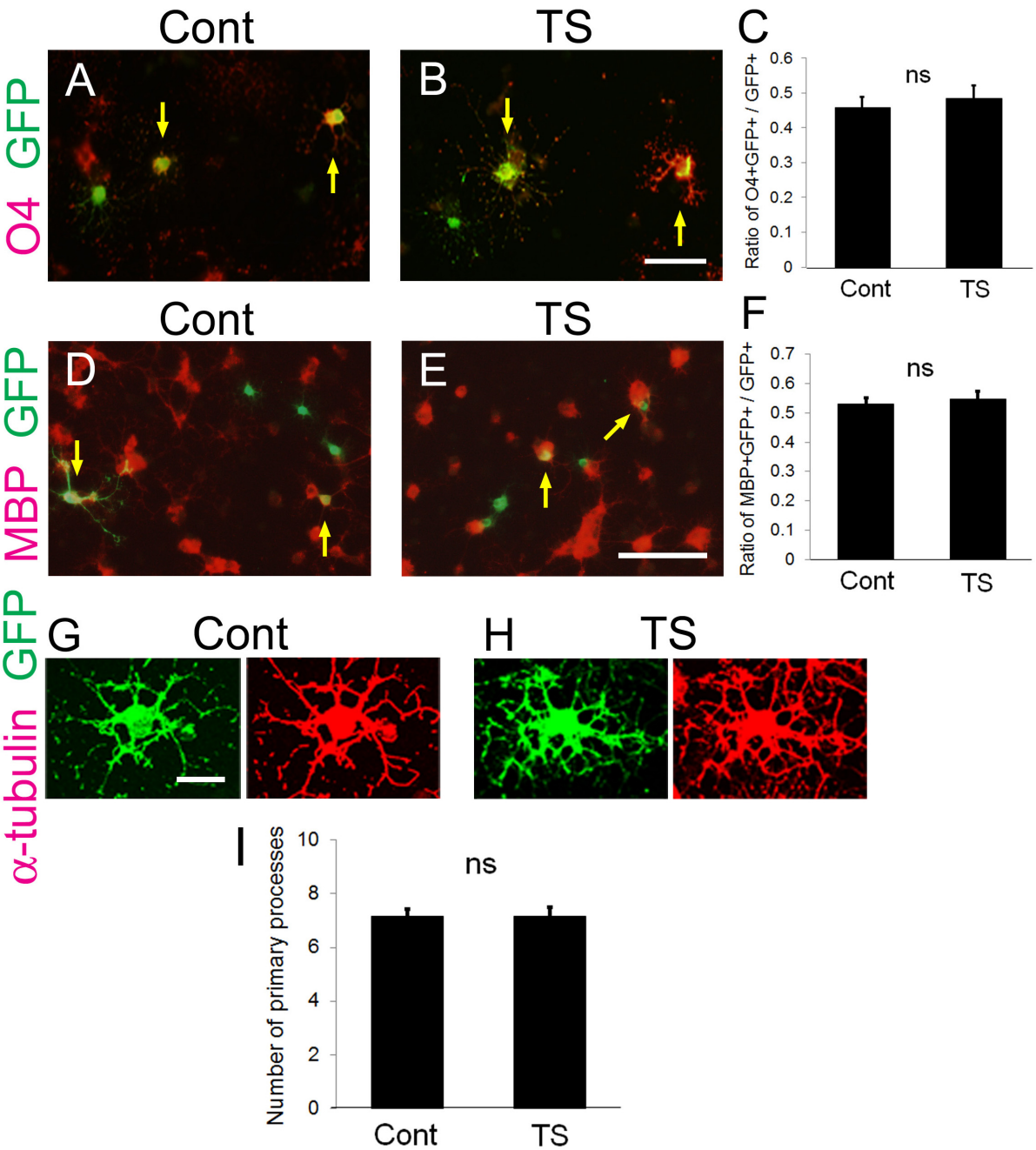

FIGURE 2 | Transfection of the tension sensor does not affect OL differentiation and morphogenesis. **(A–C)** The number of O4 + immature and mature OLs [red in **(A,B)**] among the GFP + tension sensor **(TS)**-expressing cells **(B)** was comparable to that in GFP-expressing control cells **(A)** on laminin-coated dishes. The transfected cells were detected by GFP expression (green). PDGF-AA and bFGF were removed from the culture medium 1 day after transfection, and triiodothyronine (T3, 30 ng/ml) was applied. Cells were maintained for 2 additional days, and then fixed for immunostaining with anti-O4 antibody. Arrows indicate O4-GFP double-positive cells. Scale bar, 50 μm. **(C)** The ratio of O4 + GFP + cells/GFP + cells was quantified (ns, no significant difference compared with control values, Student's *t*-test; n = 25 fields of view analyzed per condition, from three independently prepared cultures established on different days). **(D–F)** The number of MBP + mature OLs [red in **(D,E)**] among the GFP + tension sensor (TS)-expressing cells (E) was comparable to that in GFP-expressing control cells **(D)** on laminin-coated dishes. The transfected cells were detected by GFP expression (green). Cells were maintained for 5 days in the differentiation medium. Arrows indicate MBP-GFP double-positive cells. Scale bar, 100 μm. **(F)** The ratio of MBP + GFP + cells/GFP + cells was quantified (ns, no significant difference compared with control values, Student's *t*-test; *n* = 21 fields of view analyzed per condition, from four independently prepared cultures established on different days). **(G–I)** Transfection of the tension sensor did not affect the number of OL primary processes on laminin-coated dishes. Cells were maintained for 3 days after removal of PDGF-AA and bFGF from the culture medium. OL processes were visualized by immunostaining with an anti-α-tubulin antibody (red). Scale bar, 20 μm. **(I)** The number of primary processes per GFP + OL was quantified (ns, no significant difference compared with control values; Student's *t*-test, *n* = 27 cells analyzed per condition, from three independently prepared cultures established on different days).

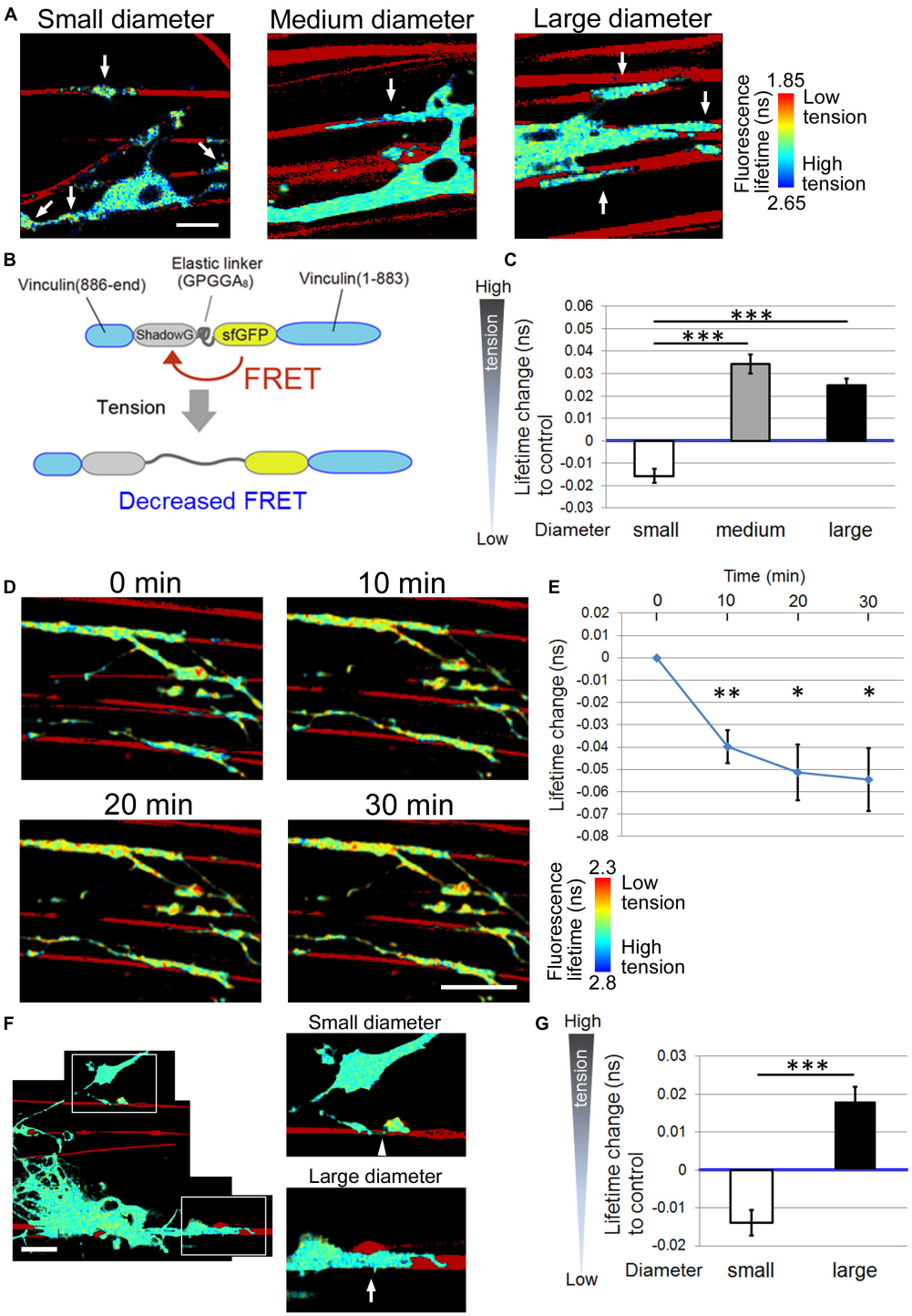

FIGURE 3 | Higher tension is generated at OL processes contacting larger diameter fibers. **(A)** Representative fluorescence lifetime images of the tension sensor-expressing OL contacting nanofibers with different diameters. Sulforhodamine (red) shows polystyrene nanofibers. Arrows indicate the fluorescence lifetime images on nanofibers. Scale bar, 10 μm. **(B)** A schematic drawing of a conformational change in the elastic domain of the tension sensor. The efficiency of FRET decreases when a mechanical force is applied on it, setting the two fluorophores apart from each other. **(C)** Quantification of average fluorescence lifetime changes relative to the control value in OLs contacting small-diameter (0.55–0.9 μm), medium-diameter (1.5–1.7 μm) and large-diameter (2.5–4.0 μm) nanofibers (***$P < 0.001$ by one-way ANOVA with a Tukey's *post hoc* test; $n = 58$ areas analyzed per condition, from five independently prepared cultures established on different days). **(D)** Fluorescence lifetime images of tension sensor-expressing OLs treated with cytochalasin D (1 μM). The images show OL processes before and after (10, 20, and 30 min) cytochalasin D treatment. Sulforhodamine (red) shows polystyrene nanofibers. Cytochalasin D application to OLs significantly decreased

(Continued)

FIGURE 3 | Continued
the fluorescence lifetime, meaning lowered tension. Scale bar, 20 μm. **(E)** The time course of average fluorescence lifetime changes in response to cytochalasin D (1 μM) application (**$P < 0.01$, *$P < 0.05$ compared with control values; Student's *t*-test, $n = 4$ independently prepared cultures established on different days). In the cytochalasin D experiments, the gross FRET index was analyzed in each field including OL processes both with and without nanofiber contacts, and compared with the values before cytochalasin D application. In OLs treated with cytochalasin D, the average fluorescence lifetime was getting significantly shorter (indicating lower tension) within the first 10 min of application. **(F)** A representative fluorescence lifetime image of the tension sensor-expressing OL contacting both small and large nanofibers simultaneously. The tension generated by one OL on the smaller diameter fiber was lower than that on the larger diameter fiber. Sulforhodamine (red) shows polystyrene nanofibers. The right pictures are higher magnification views of the boxed areas in the left picture. The arrow and arrowhead indicate the tension sensor + signals on larger or smaller diameter fibers, respectively. Scale bar, 20 μm. **(G)** Quantification of average fluorescence lifetime changes relative to the control value in OLs contacting smaller or larger diameter nanofibers on a culture dish (***$P < 0.001$ larger diameter values compared with smaller diameter values; Student's *t*-test, $n = 30$ cells analyzed from three independently prepared cultures established on different days).

correlates with the fiber diameter. Previous studies have reported that FAs act as mechanotransducers that transmit various intracellular signaling pathways (Geiger et al., 2009). Among the FA components, various signaling molecules including tyrosine kinases, tyrosine phosphatases and adaptor proteins have been identified (Geiger et al., 2009). The activity of these kinases and phosphatases triggers intracellular signaling pathways that control cell properties. These previous reports and our results suggest that OLs respond to the fiber diameter and activate mechanotransduction initiated by the FAs, which might control their cytoskeletal organization and myelin formation.

Finally, **Figure 5A** shows a representative image of the distal and proximal contact point to the OL process contacting nanofibers. Some OL processes exhibited unidirectional fiber coverage. We thus extracted the fiber coverage elongating unidirectionally and analyzed the FRET index in each fiber group. In the population that elongated unidirectionally, the tension sensor within the proximal contact points near the OL processes showed a longer average fluorescence lifetime, indicating high tension, whereas within the distal contact points far from the OL processes it showed a shorter average fluorescence lifetime, indicating low tension (**Figures 5A,B**). Previous reports have proposed a two-step model of myelination: (1) actin assembly drives OL process extension to ensheath axons, (2) local actin disassembly induces lateral spreading of the myelin membrane and its wrapping (Nawaz et al., 2015; Zuchero et al., 2015). These previous reports and our result showing lower tension within the distal contact points on nanofibers indicate that distal contact points exhibit a higher level of actin disassembly compared with proximal contact points, suggesting that more actin disassembly at the distal FAs on the axon fiber enables OL plasma membrane to lateral membrane flow for continuous myelin growth.

DISCUSSION

There are large and small-caliber axons in the CNS white matter. OLs ensheath various diameters of axons (Weruaga-Prieto et al., 1996). Large-diameter axons tend to be myelinated compared with small-diameter axons (Friede, 1972). Additionally, the ratio of [axon diameter] to [axon + myelin diameter] (g-ratio) is adjusted to optimum values for each axon, which is essential for exerting higher brain functions. This indicates that the axon diameter is associated with myelin formation, and there might be regulatory factors in response to the diameter. However, the mechanisms underlying axon diameter-dependent myelination have not been well clarified.

Câmara et al. (2009) have previously reported that β1 integrin is one of the factors that survey axon diameter and control myelination. They demonstrated that β1 integrin signaling is required for myelinating small-diameter axons. Integrin forms a signaling complex to initiate myelination by signal amplification. This signal amplification is necessary for triggering myelination of small-diameter axons, whereas large-diameter axons can be myelinated regardless of this amplification (Câmara et al., 2009). The axonal signal proportional to the diameter and above a certain threshold is required to initiate myelination. Integrin is one of the major FA proteins. FA is a central "hub" that transduces mechanically induced signaling from the ECM to the actin cytoskeleton. Expression of dominant-negative β1 integrin reduces this mechanical signaling, so that the signal initiated by some small axons will not be above the required threshold for myelination (Câmara et al., 2009). In the present study, we found that OLs formed shorter FAs on small-diameter axons (**Figure 4**), thereby providing less signals that were not above the threshold level. This is consistent with the fact that small-diameter axons in the CNS are unmyelinated in many cases. Furthermore, Suzuki et al. (2012) have reported that myelination of small-diameter axons was significantly affected in *teneurin-4*-deficient mice and that Teneurin-4 regulates integrin β1-FAK signaling. By contrast, OLs form longer FAs on large-diameter axons, which might generate signals at a level significantly higher than the threshold level, and thus not be canceled by a partial reduction in β1 integrin signaling by its dominant negative form.

Because the FA protein, integrin, has been reported to play important roles in OL-neuron interactions that regulate axon diameter-dependent myelination as mentioned above, we focused on mechanical forces generated at OL processes contacting axon fibers with different diameters. We found that large-diameter fibers induced a lower FRET index in OLs, indicating high tension, compared with small-diameter fibers (**Figure 3**). These results indicate that higher tension is generated at OL processes contacting larger diameter axons. We further examined whether different tensions can be detected in one OL that extends processes that contact both smaller and larger diameter fibers simultaneously (**Figures 3F,G**). The results suggest that the tension difference detected by the tension sensor is not caused by the maturation state of each OL. In the process of myelin formation, OLs must first extend their

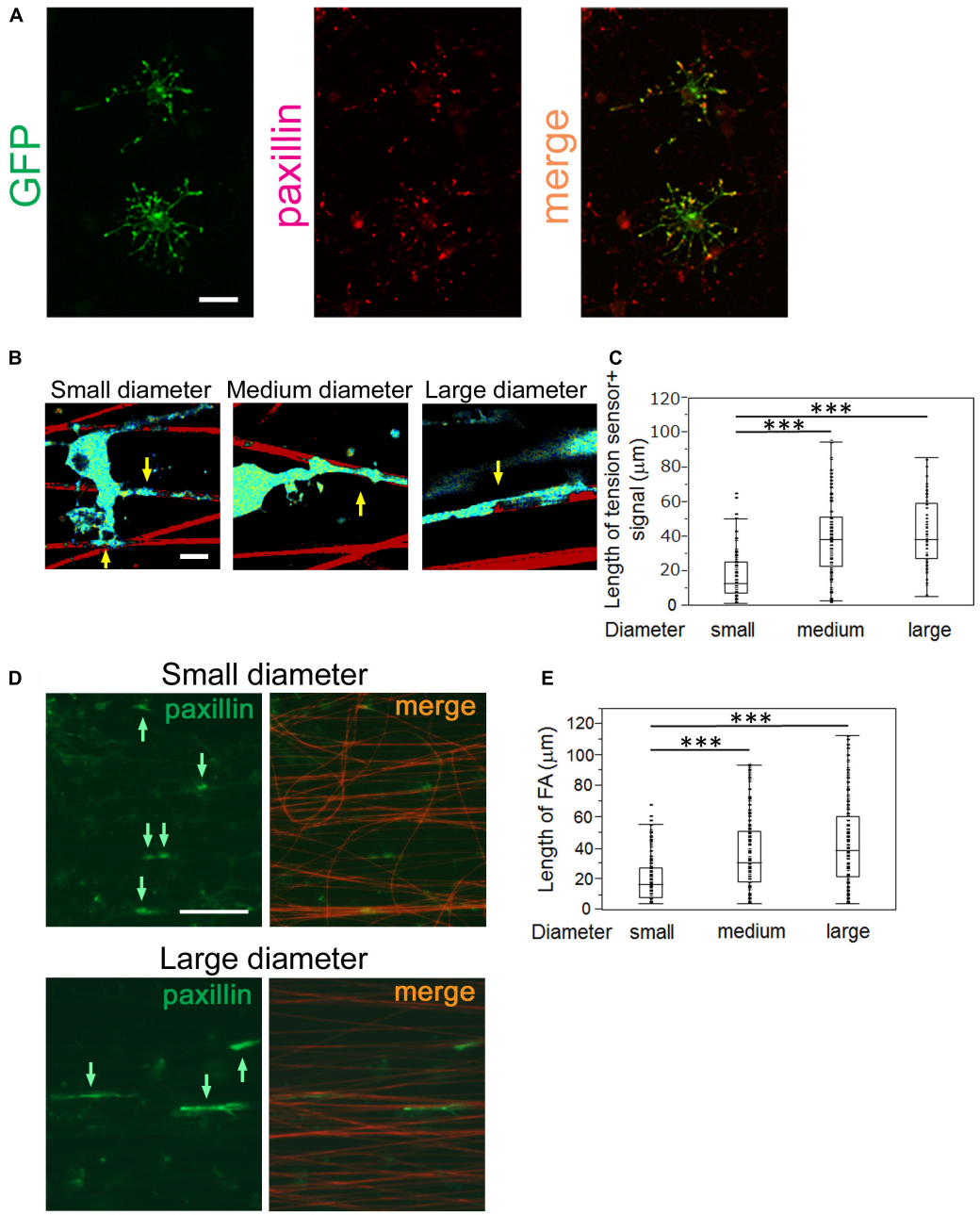

FIGURE 4 | OLs form longer FAs on larger diameter fibers and shorter FAs on smaller diameter fibers. **(A)** Double immunofluorescence of GFP + tension sensor (green) and paxillin (red), a typical FA marker, is shown. The GFP + tension sensor was co-localized with paxillin at the tip of OL processes. Scale bar, 20 μm. **(B)** A representative length image of the tension sensor + signals on small, medium and large- diameter fibers. The longer signals were observed on larger diameter fibers. Sulforhodamine (red) shows polystyrene nanofibers. Arrows indicate the tension sensor + signals on nanofibers. Scale bar, 10 μm. **(C)** The length of the tension sensor + signals was quantified in each fiber group. OLs formed shorter tension sensor + signals on small-diameter fibers (0.55–0.9 μm), compared with those produced on medium (1.5–1.7 μm) and large-diameter (2.5–4.0 μm) fibers (***$P < 0.001$ by one-way ANOVA with a Tukey's *post hoc* test; n = 81 areas analyzed per condition, from five independently prepared cultures established on different days). **(D)** Immunofluorescence of paxillin (an FA marker, green) is shown. Sulforhodamine (red) shows polystyrene nanofibers. The paxillin + FAs were observed on nanofibers with small or large diameters. Arrows indicate paxillin + FAs on nanofibers. Scale bar, 100 μm. **(E)** The size of paxillin + FAs on each fiber group was quantified. The shorter FAs were formed on small-diameter fibers (0.55–0.9 μm), whereas longer FAs were produced on medium (1.5–1.7 μm) and large-diameter fibers (2.5–4.0 μm) (***$P < 0.001$ by one-way ANOVA with a Tukey's *post hoc* test; $n = 96$ FAs analyzed per condition, from three independently prepared cultures established on different days).

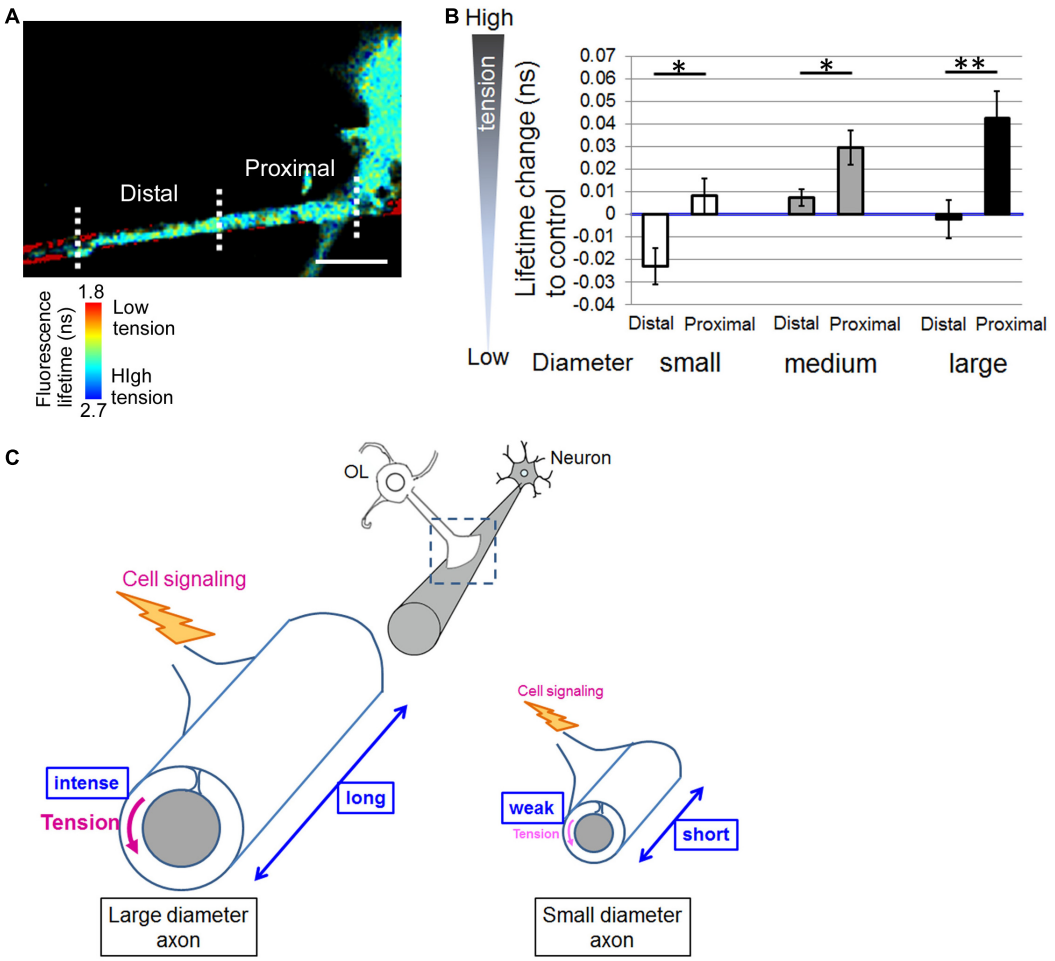

FIGURE 5 | Distal contact points on nanofibers far from the OL processes exhibit lowered tension generation. **(A)** A representative fluorescence lifetime image of the tension sensor + OL processes exhibiting fiber coverage elongating unidirectionally. Images of the distal contact point and proximal contact point to the OL process are also shown. The distal contact points far from the OL processes exhibited lower tension. Sulforhodamine (red) shows polystyrene nanofibers. Scale bar, 10 μm. **(B)** Quantification of average fluorescence lifetime changes relative to the control value in the distal contact points or proximal contact points to each OL process exhibiting unidirectional fiber coverage in small-diameter (0.55–0.9 μm), medium-diameter (1.5–1.7 μm) and large-diameter (2.5–4.0 μm) groups (**$P < 0.01$, *$P < 0.05$ proximal values compared with distal values; Student's *t*-test, $n = 7$ areas analyzed for small-diameter fibers, $n = 11$ areas analyzed for medium-diameter fibers, $n = 15$ areas analyzed for large-diameter fibers, from four independently prepared cultures established on different days). **(C)** Schematic drawing of mechanical force generated by OLs contacting neuronal axons with different diameters. Higher tension is generated at OL processes ensheathing larger diameter axons compared with smaller diameter axons, suggesting that physical factors influence myelin formation in response to axon caliber. Additionally, OLs form longer FAs on larger diameter axons and shorter FAs on smaller diameter axons. The proximal FAs near the OL processes showed higher tension, whereas the distal FAs far from the OL processes showed lower tension. This study suggests that intracellular signaling is initiated at FAs, whose size depends on axon diameter, and controls myelin formation involving actin assembly/disassembly.

processes to ensheath axons, which is driven by actin assembly. When OL processes contact neuronal axons, they form FAs at the contact foci. The larger the axon diameter is, the more the tip of OL processes must expand to surround it, therefore larger FA formation is required. When mechanical forces are loaded on FAs, the FAs connecting to the actin cytoskeleton are enlarged and thickened (Geiger et al., 2009). Taken together, larger FA formation at OL processes, which involves increased generation of mechanical forces, is recruited for larger diameter axons.

A previous study has reported that the tension sensor was properly recruited to FAs where the tension sensor was co-localized with paxillin, an FA protein (Grashoff et al., 2010). We confirmed that the GFP-positive tension sensor was co-localized with paxillin in OLs (**Figure 4**). Hence, the tension sensor is supposed to be an indicator of the localization of FAs at OL processes. Furthermore, in the previous report, mechanical force was measured in cells transiently expressing vinculin-GFP, which was specifically localized at FAs (Balaban et al., 2001). The expression of a vinculin-GFP fusion protein enables the visualization of individual adhesion sites in live cells and the quantification of their applied force by combination with the elasticity theory (Balaban et al., 2001). Moreover, fluorescent-tagged FA proteins, such as paxillin-GFP fusion protein or zyxin-GFP, was used to monitor adhesion turnover in

murine embryonic fibroblasts (Webb et al., 2004). Webb et al. (2004) have also shown that localization of zyxin-GFP to the dynamic adhesion points was due to inherent properties of the molecule. These reports demonstrated that fluorescent-tagged FA proteins can be used for monitoring FA properties and dynamics.

FAs act as a central "hub" that transduces various mechanical signaling pathways (Geiger et al., 2009). Several tyrosine phosphorylated proteins are activated in the transduction of FA-induced mechanical signaling pathways. For example, FAK activation is positively controlled by actomyosin activity and leads to upregulation of Src family kinases (Webb et al., 2004). FAK and Src family kinases are involved in myelination during its initial stages and OL morphogenesis, respectively (Forrest et al., 2009; Gonsior et al., 2014). We performed length measurements of tension sensor + signals on nanofibers and FA immunostaining with anti-paxillin antibody. Our results showed that longer FAs were formed on larger diameter fibers, while shorter FAs were formed on smaller diameter fibers, indicating the length of FAs positively correlates with the fiber diameter (**Figure 4**). These previous reports and our results suggest that OLs respond to fiber diameter and activate mechanotransduction initiated at FAs, which controls the cytoskeletal organization of OLs and thus myelin formation. The linkage between the actin cytoskeleton and the ECM is strengthened when force is applied to this linkage. Previous studies have reported that the size of FAs is tightly linked to the intensity of these applied forces (Balaban et al., 2001; Rape et al., 2011). Forces loaded on the actin cytoskeleton-adhesion complexes facilitate maturation of FAs in a positive feedback fashion. Maturation of FAs further activates intracellular signaling initiated at FAs (Seo et al., 2011; Gautrot et al., 2014). These previous reports and our data showing the linear dependence between mechanical force and the area of FAs in OLs indicate that larger FAs formed on larger diameter axons can facilitate more mechanical signals, such as FAK phosphorylation, compared with those on smaller diameter axons.

Our study showed that the tension sensor within proximal contact points on nanofibers near the OL processes exhibited longer fluorescence lifetime, indicating high tension, whereas within distal contact points far from the OL processes it exhibited shorter fluorescence lifetime, indicating low tension (**Figure 5**). Previous reports have proposed a two-step model of myelination. First, OL processes are extended to ensheath axons driven by actin assembly. Second, disassembly of actin filaments initiates membrane growth of OLs (Nawaz et al., 2015; Zuchero et al., 2015). The previous reports and our results indicate that distal contact points exhibit higher level of actin disassembly compared with proximal contact points. It is possible that intracellular cytoplasmic pressure can easily push the membrane forward at distal contact points, enabling lateral membrane flow and myelin wrapping.

CONCLUSION

We observed OL-generating forces during myelination in a manner dependent on fiber diameter using a FRET-based tension sensor. Higher tension was generated at OL processes contacting larger diameter fibers compared with smaller diameter fibers. Additionally, OLs formed longer FAs on larger diameter fibers, compared with shorter FAs on smaller diameter fibers. The proximal FAs near the OL processes showed higher tension, while the distal FAs far from the OL processes showed lower tension. These results suggest a novel and interesting idea that physical factors are involved in myelin formation in response to axon diameter. The present study suggests that intracellular signaling is initiated at FAs, whose size depends on axon diameter, which control actin assembly/disassembly and thus myelin formation.

DATA AVAILABILITY STATEMENT

The original contributions presented in the study are included in the article/supplementary material, further inquiries can be directed to the corresponding author/s.

ETHICS STATEMENT

The animal study was reviewed and approved by the Committee of Animal Experimentation of Nagoya City University Medical School and were conducted in accordance with the animal care guidelines of Nagoya City University.

AUTHOR CONTRIBUTIONS

TS, HMu, and HH designed the experiments. TS and HMu performed the experiments. TS and HMu analyzed the data. HMa and KI provided the materials. TS and HH wrote the manuscript. SU, AI, and NT advised the experimental processes. AH contributed to the revise experiments. All authors contributed to the article and approved the submitted version.

FUNDING

This study was supported by the Japan Society for the Promotion of Science Grants-in-Aid for Scientific Research (No. 18K07882 to HH, No. 21K07278 to TS, No. 18K10718 to AI, No. 18K10731 to NT), and by Grants-in-Aid for Scientific Research on Innovative Area ["Adaptive Circuit Shift," 15H01445 and 17H05574 to HH, "Advanced Bioimaging Support (ABiS)," JP16H06280 to TS] from the Ministry of Education, Culture, Sports, Science and Technology.

ACKNOWLEDGMENTS

We thank Terumi Sakurai for technical support. We thank Michal Bell from Edanz (https://jp.edanz.com/ac) for editing a draft of this manuscript.

REFERENCES

Balaban, N. Q., Schwarz, U. S., Riveline, D., Goichberg, P., Tzur, G., Sabanay, I., et al. (2001). Force and focal adhesion assembly: a close relationship studied using elastic micropatterned substrates. *Nat. Cell Biol.* 3, 466–472. doi: 10.1038/35074532

Becker, W. (2012). Fluorescence lifetime imaging–techniques and applications. *J. Microsc.* 247, 119–136. doi: 10.1111/j.1365-2818.2012.03618.x

Brown, S. S., and Spudich, J. A. (1979). Cytochalasin inhibits the rate of elongation of actin filament fragments. *J. Cell Biol.* 83, 657–662. doi: 10.1083/jcb.83.3.657

Câmara, J., Wang, Z., Nunes-Fonseca, C., Friedman, H. C., Grove, M., Sherman, D. L., et al. (2009). Integrin-mediated axoglial interactions initiate myelination in the central nervous system. *J. Cell Biol.* 185, 699–712. doi: 10.1083/jcb.200807010

Forrest, A. D., Beggs, H. E., Reichardt, L. F., Dupree, J. L., Colello, R. J., and Fuss, B. (2009). Focal adhesion kinase (FAK): a regulator of CNS myelination. *J. Neurosci. Res.* 87, 3456–3464. doi: 10.1002/jnr.22022

Friede, R. L. (1972). Control of myelin formation by axon caliber (with a model of the control mechanism). *J. Comp. Neurol.* 144, 233–252. doi: 10.1002/cne.901440207

Gautrot, J. E., Malmström, J., Sundh, M., Margadant, C., Sonnenberg, A., and Sutherland, D. S. (2014). The nanoscale geometrical maturation of focal adhesions controls stem cell differentiation and mechanotransduction. *Nano Lett.* 14, 3945–3952. doi: 10.1021/nl501248y

Geiger, B., Spatz, J. P., and Bershadsky, A. D. (2009). Environmental sensing through focal adhesions. *Nat. Rev. Mol. Cell Biol.* 10, 21–33. doi: 10.1038/nrm2593

Giannone, G., and Sheetz, M. P. (2006). Substrate rigidity and force define form through tyrosine phosphatase and kinase pathways. *Trends Cell Biol.* 16, 213–223. doi: 10.1016/j.tcb.2006.02.005

Gonsior, C., Binamé, F., Frühbeis, C., Bauer, N. M., Hoch-Kraft, P., Luhmann, H. J., et al. (2014). Oligodendroglial p130Cas is a target of Fyn kinase involved in process formation, cell migration and survival. *PLoS One* 9:e89423. doi: 10.1371/journal.pone.0089423

Grashoff, C., Hoffman, B. D., Brenner, M. D., Zhou, R., Parsons, M., Yang, M. T., et al. (2010). Measuring mechanical tension across vinculin reveals regulation of focal adhesion dynamics. *Nature* 466, 263–266. doi: 10.1038/nature09198

Lee, S., Leach, M. K., Redmond, S. A., Chong, S. Y., Mellon, S. H., Tuck, S. J., et al. (2012). A culture system to study oligodendrocyte myelination processes using engineered nanofibers. *Nat. Methods* 9, 917–922. doi: 10.1038/nmeth.2105

Matsumoto, H., Imaizumi, S., Konosu, Y., Ashizawa, M., Minagawa, M., Tanioka, A., et al. (2013). Electrospun composite nanofiber yarns containing oriented graphene nanoribbons. *ACS Appl. Mater. Interfaces* 5, 6225–6231. doi: 10.1021/am401161b

Murakoshi, H. (2021). Optogenetic imaging of protein activity using two-photon fluorescence lifetime imaging microscopy. *Adv. Exp. Med. Biol.* 1293, 295–308. doi: 10.1007/978-981-15-8763-4_18

Murakoshi, H., Shibata, A. C. E., Nakahata, Y., and Nabekura, J. (2015). A dark green fluorescent protein as an acceptor for measurement of Förster resonance energy transfer. *Sci. Rep.* 5:15334. doi: 10.1038/srep15334

Nawaz, S., Sánchez, P., Schmitt, S., Snaidero, N., Mitkovski, M., Velte, C., et al. (2015). Actin filament turnover drives leading edge growth during myelin sheath formation in the central nervous system. *Dev. Cell* 34, 139–151. doi: 10.1016/j.devcel.2015.05.013

Pedelacq, J. D., Cabantous, S., Tran, T., Terwilliger, T. C., and Waldo, G. S. (2006). Engineering and characterization of a superfolder green fluorescent protein. *Nat. Biotechnol.* 24, 79–88. doi: 10.1126/science.1068539

Pologruto, T. A., Sabatini, B. L., and Svoboda, K. (2003). ScanImage: flexible software for operating laser scanning microscopes. *Biomed. Eng. Online* 2:13.

Rape, A. D., Guo, W. H., and Wang, Y. L. (2011). The regulation of traction force in relation to cell shape and focal adhesions. *Biomaterials* 32, 2043–2051. doi: 10.1016/j.biomaterials.2010.11.044

Remahl, S., and Hildebrand, C. (1982). Changing relation between onset of myelination and axon diameter range in developing feline white matter. *J. Neurol. Sci.* 54, 33–45. doi: 10.1016/0022-510x(82)90216-7

Rosenberg, S. S., Kelland, E. E., Tokar, E., De la Torre, A. R., and Chan, J. R. (2008). The geometric and spatial constraints of the microenvironment induce oligodendrocyte differentiation. *Proc. Natl. Acad. Sci. U.S.A.* 105, 14662–14667. doi: 10.1073/pnas.0805640105

Schwartz, M. A., and DeSimone, D. W. (2008). Cell adhesion receptors in mechanotransduction. *Curr. Opin. Cell Biol.* 20, 551–556. doi: 10.1016/j.ceb.2008.05.005

Seo, C. H., Furukawa, K., Montagne, K., Jeong, H., and Ushida, T. (2011). The effect of substrate microtopography on focal adhesion maturation and actin organization via the RhoA/ROCK pathway. *Biomaterials* 32, 9568–9575. doi: 10.1016/j.biomaterials.2011.08.077

Suzuki, N., Fukushi, M., Kosaki, K., Doyle, A. D., de Vega, S., Yoshizaki, K., et al. (2012). Teneurin-4 is a novel regulator of oligodendrocyte differentiation and myelination of small-diameter axons in the CNS. *J. Neurosci.* 32, 11586–11599. doi: 10.1523/JNEUROSCI.2045-11.2012

Webb, D. J., Donais, K., Whitmore, L. A., Thomas, S. M., Turner, C. E., Parsons, J. T., et al. (2004). FAK-Src signalling through paxillin, ERK and MLCK regulates adhesion disassembly. *Nat. Cell Biol.* 6, 154–161. doi: 10.1038/ncb1094

Weruaga-Prieto, E., Eggli, P., and Celio, M. R. (1996). Rat brain oligodendrocytes do not interact selectively with axons expressing different calcium-binding proteins. *Glia* 16, 117–128. doi: 10.1002/(sici)1098-1136(199602)16:2<117::aid-glia4>3.0.co;2-0

Yasuda, R. (2006). Imaging spatiotemporal dynamics of neuronal signaling using fluorescence resonance energy transfer and fluorescence lifetime imaging microscopy. *Curr. Opin. Neurobiol.* 16, 551–561. doi: 10.1016/j.conb.2006.08.012

Yasuda, R., Harvey, C. D., Zhong, H., Sobczyk, A., van Aelst, L., and Svoboda, K. (2006). Supersensitive Ras activation in dendrites and spines revealed by two-photon fluorescence lifetime imaging. *Nat. Neurosci.* 9, 283–291. doi: 10.1038/nn1635

Zacharias, D. A., Violin, J. D., Newton, A. C., and Tsien, R. Y. (2002). Partitioning of lipid-modified monomeric GFPs into membrane microdomains of live cells. *Science* 296, 913–916. doi: 10.1126/science.1068539

Zuchero, J. B., Fu, M., Sloan, S. A., Ibrahim, A., Olson, A., Zaremba, A., et al. (2015). CNS myelin wrapping is driven by actin disassembly. *Dev. Cell* 34, 152–167. doi: 10.1016/j.devcel.2015.06.011

Conflict of Interest: The authors declare that the research was conducted in the absence of any commercial or financial relationships that could be construed as a potential conflict of interest.

Publisher's Note: All claims expressed in this article are solely those of the authors and do not necessarily represent those of their affiliated organizations, or those of the publisher, the editors and the reviewers. Any product that may be evaluated in this article, or claim that may be made by its manufacturer, is not guaranteed or endorsed by the publisher.

frontiers in Cellular Neuroscience

ORIGINAL RESEARCH
published: 17 November 2021
doi: 10.3389/fncel.2021.703431

Transmembrane Protein TMEM230, a Target of Glioblastoma Therapy

Cinzia Cocola[1,2†], Valerio Magnaghi[3†], Edoardo Abeni[1†], Paride Pelucchi[1‡], Valentina Martino[1‡], Laura Vilardo[1], Eleonora Piscitelli[1], Arianna Consiglio[1], Giorgio Grillo[1], Ettore Mosca[1], Roberta Gualtierotti[4], Daniela Mazzaccaro[5], Gina La Sala[6], Chiara Di Pietro[6], Mira Palizban[7], Sabino Liuni[1], Giuseppina DePedro[8], Stefano Morara[9], Giovanni Nano[5,10], James Kehler[11], Burkhard Greve[12], Alessio Noghero[13,14], Daniela Marazziti[6], Federico Bussolino[14,15], Gianfranco Bellipanni[16], Igea D'Agnano[1], Martin Götte[7], Ileana Zucchi[1] and Rolland Reinbold[1]**

[1] Institute for Biomedical Technologies, National Research Council, Milan, Italy, [2] Consorzio Italbiotec, Milan, Italy, [3] Department of Pharmacological and Biomolecular Sciences, University of Milan, Milan, Italy, [4] Department of Pathophysiology and Transplantation, Università degli Studi di Milano, Fondazione IRCCS Ca' Granda Ospedale Maggiore Policlinico, Milan, Italy, [5] Operative Unit of Vascular Surgery, IRCCS Policlinico San Donato, San Donato Milanese, Italy, [6] Institute of Biochemistry and Cell Biology, Italian National Research Council, Rome, Italy, [7] Department of Gynecology and Obstetrics, University Hospital of Münster, Münster, Germany, [8] Department of Molecular and Translational Medicine, University of Brescia, Brescia, Italy, [9] Institute of Neuroscience, Milan, Italy, [10] Department of Biomedical Sciences for Health, Università degli Studi di Milano, Milan, Italy, [11] National Institutes of Health, NIDDK, Laboratory of Cell and Molecular Biology, Bethesda, MD, United States, [12] Department of Radiation Therapy and Radiation Oncology, University Hospital of Münster, Münster, Germany, [13] Lovelace Biomedical Research Institute, Albuquerque, NM, United States, [14] Department of Oncology, University of Turin, Orbassano, Italy, [15] Laboratory of Vascular Oncology Candiolo Cancer Institute – IRCCS, Candiolo, Italy, [16] Department of Biology, Center for Biotechnology, Sbarro Institute for Cancer Research and Molecular Medicine, Temple University, Philadelphia, PA, United States

Glioblastomas (GBM) are the most aggressive tumors originating in the brain. Histopathologic features include circuitous, disorganized, and highly permeable blood vessels with intermittent blood flow. These features contribute to the inability to direct therapeutic agents to tumor cells. Known targets for anti-angiogenic therapies provide minimal or no effect in overall survival of 12–15 months following diagnosis. Identification of novel targets therefore remains an important goal for effective treatment of highly vascularized tumors such as GBM. We previously demonstrated in zebrafish that a balanced level of expression of the transmembrane protein TMEM230/C20ORF30 was required to maintain normal blood vessel structural integrity and promote proper vessel network formation. To investigate whether TMEM230 has a role in the pathogenesis of GBM, we analyzed its prognostic value in patient tumor gene expression datasets and performed cell functional analysis. TMEM230 was found necessary for growth of U87-MG cells, a model of human GBM. Downregulation of TMEM230 resulted in loss of U87 migration, substratum adhesion, and re-passaging capacity. Conditioned media from U87 expressing endogenous TMEM230 induced sprouting and tubule-like structure formation of HUVECs. Moreover, TMEM230 promoted vascular mimicry-like behavior of U87 cells. Gene expression analysis of 702 patients identified that TMEM230 expression levels distinguished high from low grade gliomas. Transcriptomic analysis of patients with gliomas revealed molecular pathways consistent with properties observed in U87 cell assays. Within low grade gliomas, elevated TMEM230 expression levels correlated with reduced overall survival independent from tumor subtype. Highest level of TMEM230 correlated with glioblastoma and ATP-dependent microtubule

OPEN ACCESS

Edited by:
Maria Kukley, Achucarro Basque Center for Neuroscience, Spain

Reviewed by:
Wanli W. Smith, Johns Hopkins University, United States
Susan L. Campbell, Virginia Tech, United States
Alison Colquhoun, University of São Paulo, Brazil

***Correspondence:**
Ileana Zucchi
ileana.zucchi@itb.cnr.it
Rolland Reinbold
rolland.reinbold@itb.cnr.it

† These authors share first authorship

‡ These authors have contributed equally to this work

Specialty section:
This article was submitted to Cellular Neurophysiology, a section of the journal Frontiers in Cellular Neuroscience

Received: *30 April 2021*
Accepted: *12 October 2021*
Published: *17 November 2021*

Citation:
Cocola C, Magnaghi V, Abeni E, Pelucchi P, Martino V, Vilardo L, Piscitelli E, Consiglio A, Grillo G, Mosca E, Gualtierotti R, Mazzaccaro D, La Sala G, Di Pietro C, Palizban M, Liuni S, DePedro G, Morara S, Nano G, Kehler J, Greve B, Noghero A, Marazziti D, Bussolino F, Bellipanni G, D'Agnano I, Götte M, Zucchi I and Reinbold R (2021) Transmembrane Protein TMEM230, a Target of Glioblastoma Therapy. Front. Cell. Neurosci. 15:703431. doi: 10.3389/fncel.2021.703431

kinesin motor activity, providing a direction for future therapeutic intervention. Our studies support that TMEM230 has both glial tumor and endothelial cell intracellular and extracellular functions. Elevated levels of TMEM230 promote glial tumor cell migration, extracellular scaffold remodeling, and hypervascularization and abnormal formation of blood vessels. Downregulation of TMEM230 expression may inhibit both low grade glioma and glioblastoma tumor progression and promote normalization of abnormally formed blood vessels. TMEM230 therefore is both a promising anticancer and antiangiogenic therapeutic target for inhibiting GBM tumor cells and tumor-driven angiogenesis.

Keywords: cargo vesicle transport, angiogenesis and normalization of vascular network, tumor cell migration and adhesion, anticancer and antiangiogenic therapy, glioma, kinesin motor proteins

INTRODUCTION

Glioblastoma (GBM) is the most malignant of brain tumors, representing 15% of all tumors within the brain. Glioblastoma is characterized by extensive vascularization, invasion and tissue remodeling with few patients surviving beyond 2 years (Ushio, 1991; Puzzilli et al., 1998; Karpati et al., 1999; Ohgaki and Kleihues, 2005; Brandes et al., 2008; Birk et al., 2017; PolivkaJr., Polivka et al., 2017; Gusyatiner and Hegi, 2018; Kang et al., 2020; Widodo et al., 2021). These pathological features contribute to GBM being highly untreatable and associated with the tumor recurring following therapeutic intervention. Studies suggest that while blood vessels of the tumor microenvironment are supportive to tumor cells, existing and newly generated tumor vasculature are often permeable, making targetability of antitumor agents ineffective (Visted et al., 2003; Tate and Aghi, 2009; Thomas et al., 2014; Trevisan et al., 2014; Vartanian et al., 2014; Weathers and De Groot, 2014, 2015; Wang et al., 2016; Wirsching et al., 2016; Touat et al., 2017; Zhou et al., 2020). Anti-angiogenic therapies while effective in certain types of tumors, have proven ineffective to normalize existing and newly generated tumor vasculature or block angiogenesis for treatment in GBM patients. Why antiangiogenic treatments are not efficacious in the highly vascularized GBM remains unknown (Jain, 2013; Arrillaga-Romany and Norden, 2014; Bartolotti et al., 2014; Redzic et al., 2014; Aldape et al., 2015; Masui et al., 2016; Montano et al., 2016; Ludwig and Kornblum, 2017; Jo and Wen, 2018; Jovcevska, 2018; Gately et al., 2019; Uddin et al., 2020; Jones et al., 2021; Lopes Abath Neto and Aldape, 2021). No specific mutations and chromatin lesions linked with GBM explain the ineffectiveness of anti-angiogenic strategies. Therefore, epigenomic components of the GBM tumor environment and interactions of different cell types likely contribute to the lack of effectiveness of current therapies (Nagarajan and Costello, 2009; Kondo et al., 2014; Romani et al., 2018). The model of tumor associated angiogenic switch supports that tumor cells remodel extracellular matrix tension or secrete factors or vesicles that promote vascularization of the tumor environment (Sogno et al., 2009; Xu et al., 2016; Groblewska et al., 2020). Of particular interest is whether tumor cells with angiogenic potential or tumor associated endothelial cells induced to have aberrant angiogenic features share genes in common that have pleiotropic like properties. Recently, we identified the transmembrane protein, TMEM230 as a novel regulator of normal development associated angiogenesis in zebrafish (Carra et al., 2018). Modulation of TMEM230 expression was sufficient to affect the activities of components of the VEGF and Delta/Notch signaling pathways and induce new blood vessel formation and structural remodeling of existing blood vessels *in vivo* (Carra et al., 2018). This suggested that TMEM230 promotes aspects of angiogenesis in parallel or independently of the Delta/Notch and VEGF signaling pathways. TMEM230 has the properties of being a novel master regulator in angiogenesis. Depending on the expression level, TMEM230 could induce or recover aberrant number of endothelial cells and inhibit or promote the normal function and structural properties of blood vessels. Additionally, TMEM230 could recuperate normal function and 3D structural properties of aberrantly formed blood vessels such as induced in disease or cancer development. Therefore, precise regulated levels of TMEM230 expression may determine its role in normal or disease associated angiogenesis. Search of published and open access research on microarray, sequencing and proteomic expression analysis did not uncover any datasets to ascertain at a preliminary level whether TMEM230 was differentially expressed specifically between non-malignant glial cells and glial cells from low- or high-grade gliomas. As *TMEM230* sequence is conserved in human and zebrafish, we investigated whether *TMEM230* is expressed in human tumors and may represent a promising novel drug target for antiangiogenic or antitumor therapy to restrict GBM tumor cell properties and tumor cell promoted angiogenesis.

In this study we demonstrated that TMEM230 represents a novel pleiotropic acting gene with both intracellular and extracellular tumor and vascularization in the form of vascular mimicry and angiogenic promoting capacities. Conditioned media from U87 cells expressing TMEM230 promoted human endothelial cells to sprout and form tubule-like structures. Intracellular expression of TMEM230 in U87-MG promoted cells to migrate and organize into endothelial vessel-like structures, a process described as vascular mimicry as vascular mimicry (VM). The vascular mimicry was inhibited in U87 cells when TMEM230 was down regulated. Our new study supported that the TMEM230 expressing U87 cells may secrete extracellular components and modulate their tumor microenvironment to

promote tumor cell induced VM or endothelial associated angiogenesis. Our previous research supports that proper levels of TMEM230 are necessary for normal endothelial cell sprouting and maintaining the structural integrity of blood vessels. Here we propose that aberrantly elevated levels of TMEM230 promote abnormal vascularization by driving endothelial cells to generate an abundance of defective blood vessels or glial tumor cells to form vessel like structures through VM. Moreover, TMEM230 drives glial tumor cells to promote abnormal tissue and existing blood vessel remodeling. TMEM230 therefore functions in two different cell types (glial and endothelial) to promote in tumor formation, tissue destruction and hypervascularization, and destabilization of existing normal blood vessels. Judicious and precise use of levels of TMEM230 for therapy may inhibit these tumor properties and also help to normalize blood vessel function in GBM. Human TMEM230 emerges as a promising novel target for antiangiogenic and antitumor therapies due to its pleiotropic like regulatory role in tumor associated angiogenesis and invasive and vascular mimicry properties in U87 tumor cells.

MATERIALS AND METHODS

Patient Data Collection

mRNAseq datasets of GBM and LGG brain tumors and corresponding patient clinical data were obtained from The Cancer Genome Atlas (TCGA) (Cancer Genome Atlas Research Network, Weinstein et al., 2013), analyzed using R package TCGA2STAT (Wan et al., 2016), and normalized with RSEM (Li and Dewey, 2011). GBM and LGG datasets used for TMEM230 expression included 172 brain samples from patients with high grade (G3, G4) GlioBlastoma Multiforme (GBM) and 530 brain samples from patients with low grade gliomas that include 198 oligodendroglioma, 134 oligoastrocytoma, 197 astrocytoma. Grades 3 and 4 tumors were defined according to the American Joint Committee on Cancer AJCC. For gene expression analysis we excluded the samples of unknown grading.

Patient RNA-Seq Gene Expression Analysis

Differential gene expression analysis was performed using DESEQ2 with a p-Value cut-off <0.0001 and an absolute log2 fold change cut-off >0.58 (Love et al., 2014). Functional enrichment analysis was performed using DAVID (6.8) (Huang da et al., 2009). Only terms with a corrected p-Value (Benjamini) < 0.05 were considered. The expression data related to the TCGA repository of LGG samples were downloaded using the TCGA2STAT R package (2) and gene expression analysis was performed using the DESEQ2 R package (version 1.30.1[1]).

Correlation and Heatmap Analysis of TMEM230 Expression From Patient Data

Correlation of TMEM230 gene expression levels on overall survival (OS) in astrocytoma, oligoastrocytoma and oligodendroglioma patients was performed using the Kaplan-Meier plotter online tool, GRAPHPAD PRISM. For each glioma subtype, analytical groups were generated based on the median of the RSEM normalized gene expression of TMEM230. The difference in survival between groups was calculated using the software R unpaired t-test. The Heatmap on the 100 most variable expressed genes was generated using the R "pheatmap" package. The functional enrichment analysis of the differential expressed genes was performed with DAVID 6.8.

RNA Isolation and RT PCR

RNA was isolated from U87 cells in which TMEM230 was down regulated or control cells using TRIzol Reagent (Thermo Fisher Scientific, 15596026) and reverse transcribed using High-Capacity cDNA Reverse Transcription Kit (Thermo Fisher Scientific, 4368813) following manufacturer's instructions. Quantitative real-time PCR (qRT-PCR) was performed with a 7500 Real-Time PCR System (Applied Biosystem, 4345241) in total volumes of 20 uL per reaction with TMEM230 specific primers (TMEM230_FW: 5′-GATTGGCGCCTTTCTCATTATT-3′ and TMEM230_RV: 5′- CTGCCCCCCCTTTGCT-3′) and HPRT1 primers as endogenous control (HPRT1_FW: 5′-TTTGCTGACCTGCTGGATTACA-3′ and HPRT1_RV: 5′-GGTCATTACAATAGCTCTTCAGTCTGAT-3′) using the SYBR Select Master Mix (Thermo Fisher Scientific, 4472918). All reactions were performed in triplicates 3 times. $\Delta\Delta$Ct analysis was used to determine the relative gene expression levels after normalization with the housekeeping gene HPRT1.

Generation and Cloning of the Endogenous TMEM230 Variant 2 (ISOFORM 2) Transcript

The TMEM230 coding sequence was amplified from cDNA obtained from U87 cDNA using primers T230infFw: 5′-gagctagcgaattcgaaTGTTATGATGCCGTCCCGTA-3′ T230infRv and 5′-atccgatttaaattcgaaCTATGGGGTGGGTGCTA-3′. Capital letters represent the nucleotide sequence that anneal with the endogenous TMEM230 transcript. Small letters are the docking sequences of the vector with the restriction sites underlined. The destination plasmid pCDH-CMV-MCS-EF1-copGFP (SBI CD511B-1) was linearized using the *Bst*BI restriction enzyme. Plasmid insert cloning was completed using In-fusion Cloning Plus (Clontech TAKARA 638920) following manufacturer's instructions. The U87 cDNA sequence was compared to the wild-type sequence on non-malignant human patient cells to confirm that U87 cells do not contain a mutated or aberrant sequence of TMEM230.

Cloning of Lentiviral System-Based Construct for Inhibiting TMEM230 Protein Expression

The shTMEM230 sequence (for down regulation of endogenous TMEM230) was cloned into pcDNA^{TM}6.2-GW/EmGFP using the BLOCK-iT^{TM} Pol II miR RNAi Expression Vector Kit with EmGFP (Thermo Fisher Scientific K493600) following the manufacturer's instruction. The following sequences were annealed to generate double stranded oligonucleotides:

[1]https://bioconductor.org/packages/release/bioc/html/DESeq2.html

TOP:5′-TGCTGTGTAGGTTCACTTAACATCTTgttttggccact gactgacAAGATGTTGTGAACCTACA-3′ and

BOTTOM:5′-cctgTGTAGGTTCACAACATCTTgtcagtcagtgg ccaaaacAAGATGTTAAGTGAACCTACAC-3′. Capital letters represent the sense and anti-sense sequences of the small hairpin RNA to be expressed for targeting the endogenous TMEM230 transcript. Small letters are the sequence forming the loop of the hairpin structure. The expression cassette of the resulting plasmid and the control vector provided in the kit (pcDNA^{TM}6.2-GW/EmGFP-miR-neg Control) were amplified by PCR using the following primers: FW 5′-GGCATGGACGAGCTGTACAA-3′ and RVNotI 5′-GTGCGGCCGCATCTGGGCCATTT-3′ (which added a *Not*I restriction site). The PCR product was cloned into the destination lentiviral vector pCDH-CMV-MCS-EF1-copGFP (SBI CD511B1), between *Bam*HI and *Not*I restriction sites.

Lentivirus Production

Lentiviral particles were produced in HEK293T cells by transfecting pCDH or pLENTI vectors together with psPAX2 and pMD2.G (gift from Didier Trono, Addgene plasmids #12260 and #12259) as helper vectors for 2nd generation viral packaging (with a ratio 4:3:1, respectively) using the Lipofectamine^{TM} 2000 Transfection Reagent (Thermo Fisher Scientific 11668027) following manufacturer's instructions. Cell culture supernatants containing the lentiviral particles were harvested after 48 and 72 h, concentrated by ultracentrifugation at 120,000 rcf for 3 h and stored at –80°C for later use.

Adherent Cell Cultures

The human brain glioblastoma U87-MG cell line was recently obtained from the ATTC and maintained in DMEM (Euroclone, ECB7501L) supplemented with 10% fetal bovine serum (FBS, Sigma, F7524), 1% Glutamine (Cambrex, BE17-605E) and 1% penicillin/streptomycin (Life Technology, 15140-122) in a humidified atmosphere of 5% CO_2 at 37°C. Cells were cultured to an 80% level of confluence. Transduction was performed on adherent cells using lentiviral vectors (shSCR-GFP, used as control and shTMEM230-GFP for downregulating endogenous TMEM230). Cells were allowed to recover for 1 day following transduction in transduction culture medium and then culture was continued with DMEM supplemented with 10% FBS or 10% KnockOut Serum Replacement (SR, Life Technologies, 10828-028), 1% Glutamine and 1% penicillin/streptomycin, depending on the assay to be performed. Human umbilical vein endothelial cells (HUVECs) were grown in EGM2 medium consisting of Ham's F12/DMEM-Glutamax (Life Technologies, 21765-029:31966-021) at a ratio of 1:1 supplemented with additional factors [Eurogene: (CC-4176), heparin (CC-4396A), hydrocortisone (CC-4112A), epidermal growth factor (CC-4317A), human basic fibroblast growth factor (CC-4113A), vascular endothelial growth factor (CC-4114A), ascorbic acid (CC-4116A), FBS (CC-4101A), gentamicin (CC-4381A), and R^3 Insulin-like growth factor (R^3IGF1, CC-4115A)]. Human umbilical vein endothelial cell were cultured in a humidified atmosphere of 5% CO_2 at 37°C to an 80% level of confluence and medium replaced twice a week.

Conditioned Medium Collection From U87-MG Grown With Fetal Bovine Serum or Serum Replacement Containing Medium

Conditioned media was collected from cells transduced with shSCR or shTMEM230 viral constructs cultured with 10% FBS or 10% SR, centrifuged at 2,000 × *g* for 5 min to clear supernatant of cells and cell debris and stored at –20°C for using in co-culture experiments.

U87-MG Tubulogenesis Assay

20,000 shSCR or shTMEM230 lentivirus transduced U87-MG cells were cultured in growth factor reduced Matrigel (BD Biosciences, 356231) in 48-well plates (Greiner, Twin-Helix, 677180) using U87 (tumor) or HUVEC (vascular) medium as described in the text. Structure formation was monitored for 24, 48, and 96 h by fluorescence microscope.

Human Umbilical Vein Endothelial Cell Angiogenesis Assays

For tubulogenesis assay, 20,000 HUVEC were plated in growth factor reduced Matrigel (BD Biosciences, 356231) in 48-well plates (Greiner, Twin-Helix, 677180) for 24 h. Tubuli forming media used were conditioned media obtained from U87shSCR cultured with FBS; U87shTMEM230 cultured with FBS; U87shSCR cultured with SR, or U87shTMEM230 cultured with SR.

For spheroid outgrowth assay, 16,000 HUVEC were suspended in 100 μl of 20% HUVEC medium containing 2% methylcellulose solution (Sigma, M7027) in 96 well plates. Spheroids were collected the day after and embedded in 60% methylcellulose containing 40% FBS and Collagen R (SERVA, Euroclone, SE4725401) at a ratio 1:1 and then layered onto a solidified bed of rat collagen in 96-well plates. After the methylcellulose-collagen mixture solidified, 100 μl of medium with or without angiogenic promoting factors were added. Angiogenetic factors used were 300 ng/ml Angiopoietin I (Sigma, Merck, SRP300) and 30 ng/ml VEGF (Sigma, Merck, V7259). Spheroids formed within 24 h from control cells with angiogenic factors. Five distinct culture conditions were examined: EGM2 (HUVEC medium) + or − angiogenic factors; condition media from U87shSCR grown in FBS + or − angiogenic factors; U87shTMEM230 in FBS + or − angiogenic factors; U87shSCR in SR + or − angiogenic factors; and U87shTMEM230 in SR + or − angiogenic factors. Spheroids from all experimental conditions were compared to spheroids generated from control cells cultured in fresh EGM2. Control spheroids contained of approximately 800 cells within 24 h.

Adherent Co-cultures of Human Umbilical Vein Endothelial Cells and U87-MG Cells

Drops of 50 μl containing 20,000 HUVEC were plated with shSCR or shTMEM230 transduced U87 cells at two opposite ends of a well in a 12 well-plate. U87 cells were distinguished

from HUVEC because of their green fluorescence. Following cell attachment at 37°C and 5% CO2, culture media was added to immerse the adherent cells. A combination of U87 + EGM2 media at a ratio of 1:1 was used. Cell migration capacities of U87 and HUVEC were monitored for more than 10 days. Half of media was replaced with fresh media every 3 days.

Western Blotting Analysis

For TMEM230 expression analysis proteins were prepared from conditioned media precipitated with Trichloroacetic acid (TCA, Sigma, T0699) followed by wash of methanol (412532, Carlo Erba) or U87 cells lysed on ice using Laemmli buffer (100 mM TRIS pH 7, 200 mM DTT, 20% glycerol, 4% SDS). About 10 μg and 100 μg of total protein for each sample derived from cells or conditioned media were mixed with a 6x loading dye buffer (0.375M Tris pH 6.8, 12% SDS, 60% glycerol, 0.6M DTT, 0.06% bromophenol blue) and loaded onto 10% SDS denaturing poly-acrylamide gels. After transferring proteins to a PVDF membrane (GE-Biotechnology, Euroclone, 10600021), the membrane was stained with 0.1% Ponceau S (Sigma, P3504) in 5% acetic acid (Thermo Fisher Scientific, A/0400/PB17), washed, blocked with 5% fat-dried milk (Euroclone, EMR180001) and incubated with primary antibodies. Antibodies used were polyclonal rabbit anit-C20ORF30 (TMEM230, 1:1,000, Santa Cruz, sc-85410), monoclonal mouse anti-MOESIN (1:200, Santa Cruz, sc-58806), polyclonal rabbit anti-CD138 (Syndecan-1, 1:250, Thermo Fisher Scientific, 36-2900), anti-HCAM (CD44, 1:1,000, Santa Cruz, sc-9960) and polyclonal goat anit-β-ACTIN (1:2,000, Santa Cruz, sc-1615, used as endogenous control). Donkey anti-rabbit (1:20,000, Amersham, NA934V), sheep anti-mouse (1:10,000, Amersham, NA931V), and donkey anti-goat (1:15,000, Santa Cruz, sc-2020) were used as secondary antibodies.

Coomassie Staining

Electrophoresis gels were fixed for 30 mins in fixing solution (7% glacial acetic acid in 40% methanol) and placed in a staining solution of 0.1% Coomassie Brilliant Blue (Sigma, B0149), 7% glacial acetic acid in 40% methanol for 1 h. Gels were washed in a de-staining solution (10% acetic acid in 15% methanol), rinsed and de-stained with 25% methanol for 24 h.

Immunofluorescence Analysis

U87 control and shTMEM230 cells were fixed with 4% Paraformaldehyde (Sigma) in 1× PBS for 10 min at room temperature (RT). Cells were incubated with a blocking buffer of 5% normal goat serum in 1× PBS. The primary antibodies used were anti-FIBRONECTIN (1:200 dilution, Chemicon International, AB2033), anti-CAVEOLIN-1 (1:100 dilution, Santa Cruz, sc-7875) and anti-phalloidin-TRITC conjugated (1:2,000, Sigma, P1951), all incubated for 2 hours at RT. Both were incubated for 2 h at RT. The cells were washed with 1× PBS and incubated with a secondary antibody of goat anti-rabbit Alexafluor-555 (1:500 dilution, A21429, Life Technologies) for 1 h at RT. Nuclei were visualized with 4′,6′-diamidino-2-phenylindole (DAPI) staining.

RESULTS

Analysis of *TMEM230* Gene Expression in Human Glioma Tumors From the Cancer Genome Atlas Datasets Revealed That Human Glioblastoma Multiforme Expresses Higher Levels of *TMEM230* Compared to Lower Grade Gliomas

We recently showed that TMEM230, a transmembrane protein conserved in vertebrates and highly expressed in the vascular compartments, modulates endothelial cell sprouting and migration in Zebrafish early development (Carra et al., 2018). As the formation of new blood vessels is necessary for tumor expansion, the expression level of *TMEM230* was evaluated in several types of human glial tumors to establish whether *TMEM230* expression discriminates glioblastoma multiforme (GBM) from lower grade glial (LGG) tumors. A cohort of 530 patient samples with low grade gliomas (LGG) and a cohort of 172 patient samples with GBM from The Cancer Genome Atlas (TCGA) RNA sequencing (RNAseq) database were analyzed for *TMEM230* expression level (The Cancer Genome Atlas Research Network[2]) (Cancer Genome Atlas Research Network, Weinstein et al., 2013). *TMEM230* was significantly higher in GBM compared with brain LGG with a *P*-value $^{***}P < 0.0001$ using the unpaired *t*-test (**Figure 1A**).

TMEM230 Low Expression Is Associated With Improved Overall Survival Rate

To investigate whether a correlation existed between *TMEM230* expression and overall survival rate, RNAseq expression datasets and clinical data of glial tumor affected patients were analyzed. The patient clinical features are summarized in **Supplementary Table 1** and include gender, age, tumor size, and *TMEM230* transcript expression level.

The cohort of 530 LGG patient samples was classified according to each tumor type and the expression level of *TMEM230*. RNA sequencing data and clinical data of 198 oligodendroglioma, 134 oligoastrocytoma, 197 astrocytoma, were analyzed using the TCGA2STAT R package (Wan et al., 2016). We then investigated whether *TMEM230* expression correlated with patient prognosis using Kaplan-Meier survival analysis that determined a relationship between lower expression of *TMEM230* and increased overall survival of patients in all types of LGG (**Figure 1B**). Additionally, we evaluated whether *TMEM230* expression correlated the specific glioma tumor subtypes, astrocytoma (top), oligoastrocytoma (middle) and oligodendroglioma (bottom). Higher *TMEM230* was associated with worse prognosis (**Figure 1C**). Moreover, it was observed that a higher percentage of patients died more rapidly compared to patients with lower expression of *TMEM230* (**Figures 1B,C**). Our previous work demonstrated that TMEM230 regulates endothelial cell sprouting and migration associated with angiogenesis in early Zebrafish development (Carra et al., 2018)

[2]http://www.cancergenome.nih.gov/

and TMEM230 protein was reported to be a component of vesicle trafficking and turnover (Kim et al., 2017; Mandemakers et al., 2017; Conedera et al., 2018; Deng et al., 2018; Wang et al., 2021). A functional enrichment analysis of the differentially expressed genes in patient derived LGG with low and high expression level TMEM230 was then performed with DAVID 6.8 and only the terms with a corrected *p*-value (Benjamini, Bonferroni or FDR) <0.05 were considered. Molecular pathways,

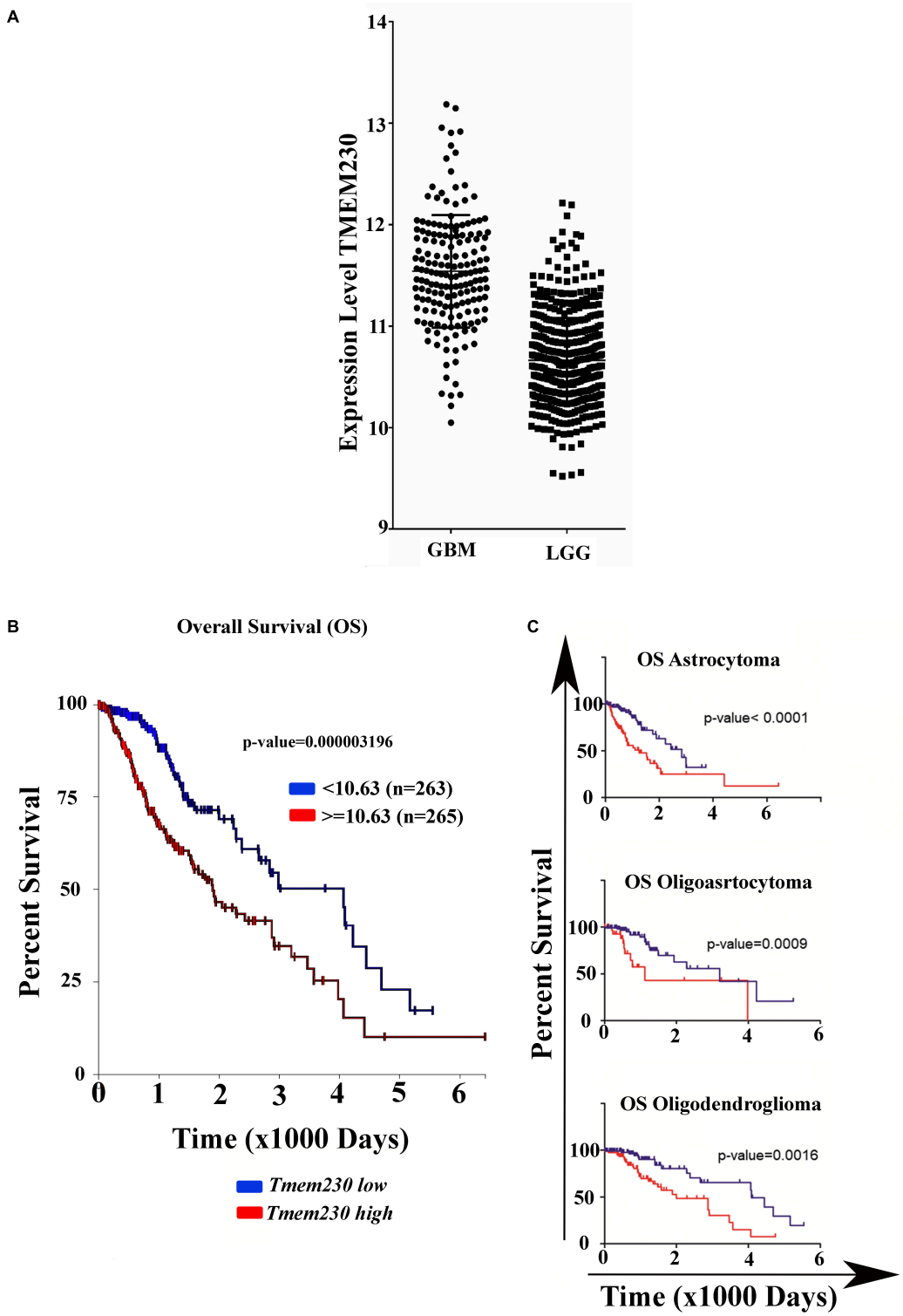

FIGURE 1 | (Continued)

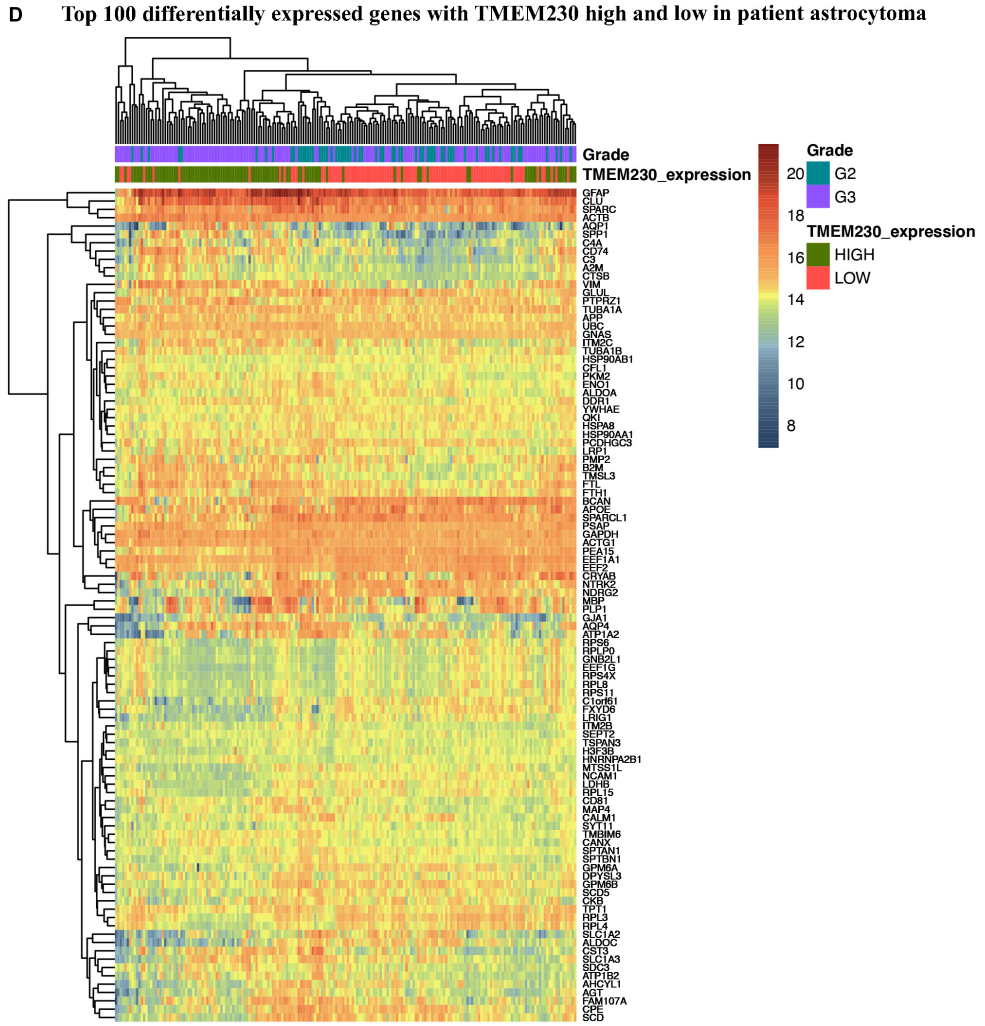

FIGURE 1 | Expression of *TMEM230* in brain Glioblastoma Multiforme (GBM) and Low-Grade Gliomas (LGG) analyzed from The Cancer Genome Atlas. **(A)** Glioblastoma multiforme tumors showed significantly elevated level of *TMEM230* mRNA compared to low-grade gliomas (unpaired *t*-test $p < 0.0001$). Low-grade gliomas consist of astrocytoma, oligoastrocytoma and oligodendroglioma patient samples. **(B)** Poor prognosis was correlated with high *TMEM230 in* low-grade gliomas. **(C)** Poor prognosis was correlated with high *TMEM230* in astrocytoma (top), oligoastrocytoma (middle) and oligodendroglioma (bottom). Relationship between *TMEM230* expression levels and prognosis of low-grade gliomas affected patients indicated that lower expression of *TMEM230* was associated with increased overall survival. Each glioma subtype is indicated by the median of gene expression of *TMEM230*. B and C analyses were generated from the Kaplan-Meier test based on the expression of medium *TMEM230*. **(D)** Representative heatmap displaying the most variable expressed genes for astrocytoma using the R with "pheatmap" package for which functional enrichment was generated with DAVID program.

keywords and diseases correlated with high or low levels of TMEM230 in patient gliomas derived from the functional enrichment are shown in **Supplementary Tables 2-12**. The analysis of genes and pathways differentially expressed support that TMEM230 has both intracellular and extracellular roles. In particular, the intracellular role is in cell membrane and extracellular matrix regulation and cell adhesion. An extracellular role was identified associated with cell cargo and exosome trafficking in all the types of gliomas analyzed from patients (**Supplementary Tables 2-12**, see red arrow, yellow and green highlighted terms). A representative heatmap indicates the most variable expressed genes in patient astrocytoma using the R with the "pheatmap" package (**Figure 1D**). To investigate the intracellular and extracellular role of TMEM230 in GBM, the U87 glioblastoma cell line that expresses TMEM230 and recapitulates the GBM invasive and proangiogenic tumor cell properties was chosen for functional analysis.

Constitutive Inhibition of Endogenous TMEM230 Expression in U87-MG Cells

Lentiviral constructs to constitutively upregulate and downregulate *TMEM230* mRNA and protein expression were generated. U87-MG cells were transduced with a dual promoter containing lentiviral construct expressing the copGFP reporter and *TMEM230* mRNA (for TMEM230 upregulation), with copGFP and a short hairpin sequence designed to

downregulate *TMEM230* (U87shTMEM230) or with copGFP alone and copGFP with a scrambled short hairpin sequence (U87shSCR), both used as control. The effectiveness of the shTMEM230 construct in down regulating TMEM230 protein in U87 cells was verified by comparison with the U87 control cells (**Figures 2A,B**). Potential unwanted off-site effects of the sh-mediated downregulation of endogenous TMEM230 were previously evaluated and not observed with Tmem230 specific morpholino oligos in zebrafish (Carra et al., 2018). Fetal bovine serum (FBS) may contain bovine generated TMEM230 protein or extracellular vesicles associated with TMEM230 protein (Guida et al., 2020). Therefore, the role of the human endogenous TMEM230 protein and endogenous TMEM230 generated vesicles in U87 cells was evaluated using 2 different tissue culture conditions, in which the culture media was identical except for containing serum replacement (SR) or extracellular vesicle depleted FBS. The use of SR ensured that the assays in which TMEM230 was downregulated in U87 did not contain and was not compensated by TMEM230 protein and TMEM230 associated vesicles exogenously derived from bovine serum. Use of FBS prepared by removing extracellular vesicles also guaranteed that there were no TMEM230 associated vesicles exogenously derived from the bovine serum in the culture assays. An additional purpose of using SR containing culture conditions was to determine whether the function of TMEM230 was dependent or modified by known or unknown soluble sera components such as cytokines, growth factors and inflammation modulating factors present in FBS.

Since serum replacement, unlike FBS is composed by defined proteins artificially derived and contains no animal protein or vesicles, as expected, TMEM230 protein was not detected in SR (**Figure 2C**, top panel lane 2, SR). TMEM230 protein was also not detected in vesicle depleted FBS (**Figure 2C** top panel lane 3, FBS). While TMEM230 protein was not detected, Ponceau S staining panel (bottom) shows the considerable amount of protein loaded for each condition. While TMEM230 protein was not detected in conditioned media generated by U87 cells cultured in SR or vesicle-deplete FBS conditions (**Figure 2C**, top panel lanes 4 and 5), in conditioned media from cells in which TMEM230 was upregulated using a lentiviral system, increased detection of CD81 (extracellular vesicle associated marker) was observed (**Figure 2D**, lane 3, TMEM230), suggesting that TMEM230 is associated with vesicle generation, turnover and/or secretion (**Figure 2D**). Coomassie staining, bottom panel verifies equal protein loading was performed (Caby et al., 2005; Haqqani et al., 2013; Jeppesen et al., 2014).

Constitutive Downregulation of Endogenous TMEM230 Promoted Morphological Remodeling of Cell and Cytoplasm, Cell Detachment, and Reduction in U87-MG Re-passaging Capacity

Time course experiments in which TMEM230 was constitutively down regulated revealed that U87-MG cells cultured in media containing vesicle depleted FBS (**Figure 3**) or SR (**Figure 4**) showed over time a rapid change in cell and cytoplasm morphology and a decrease in the number of cells anchored to tissue culture plates. U87shTMEM230 cell cytoplasm contracted within 24 hr in vesicle depleted FBS conditions (**Figure 3**, panels 3,4) or in SR conditions (**Figure 4**, panels 7,8) compared to control cells (**Figure 3**, panels 1-2, **Figure 4**, panels 5-6). Onset of the GFP reporter expression is at 0 hr. These results suggest loss of normal cytoskeleton structure and loss of cell membrane interaction with the extracellular scaffold with downregulation of endogenous TMEM230 protein. Change in cell morphology and fragmentation of cytoplasmic invadopodium like extensions were correlated with the loss of the anchorage ability of the cells, as observed with less cells attached to the culture plates over time see 0-72 h. See P0 for FBS (**Figure 3**, panels 1-13) and 0-192 h for SR (**Figure 4**, panels 1-16). Cells in which TMEM230 was downregulated also displayed significantly less ability to reattach with subsequent re-passaging (P1) compared to control cells expressing TMEM230 in vesicle depleted FBS. Compare 72 h in P0, **Figure 3**, panels 12-13, and panels 16-17. Second passage (P2) U87shTMEM230 cells in FBS displayed almost no adhesion capacity when attempts were made to generate a third passage on tissue culture plates (data not shown). In contrast, indefinite re-passaging was possible for U87shSCR control cells cultured in FBS (not shown). Green fluorescent protein control cells expressing endogenous TMEM230 cultured in SR containing media appeared more stressed (in terms of cell morphology, fragmentation of cytoplasmic extensions and substratum attachment capacity) compared to control cells cultured in FBS conditions. See SR conditions, **Figure 4**, panels 13, 14 at initial plating and FBS conditions, **Figure 3**, panels 18, 19 at P1. This was likely due to SR lacking essential factors necessary for maintaining the metabolic and growth demands of tumor cells. This suggested that TMEM230 may protect tumor cells in conditions in which essential extracellular growth factors are reduced or absent as in the case of SR media conditions. SR conditions may therefore recapitulate deficient conditions associated *in vivo* with a rapidly proliferating tumor cells in an insufficient vascularized and rapidly expanding or large tumor mass. Collectively, these analyses support that TMEM230 is necessary for U87 cells to maintain anchorage capacity to extracellular scaffolds/substratum or proper cytoskeleton function and structure. Additionally, TMEM230 may protect cells in stressful environments or conditions, such as those associated with growth factor deficiency and/or hypoxic tumor cores.

It is reported that TMEM230 is associated with vesicle generation, trafficking and turnover (Deng et al., 2016, 2018), in agreement our data suggested that increased expression of TMEM230 correlated with extracellular vesicle release (**Figure 2D**). We therefore evaluated both the intracellular and extracellular roles of TMEM230 in promoting 3D sprouting and migration in U87 cells, features that may recapitulate tumor cell aggressive properties associated with GBM, such as invasion and vascular mimicry. Additionally, we investigated the extracellular role of TMEM230 in promoting sprouting and migration of human umbilical vein endothelial cells (HUVECs), cultured in

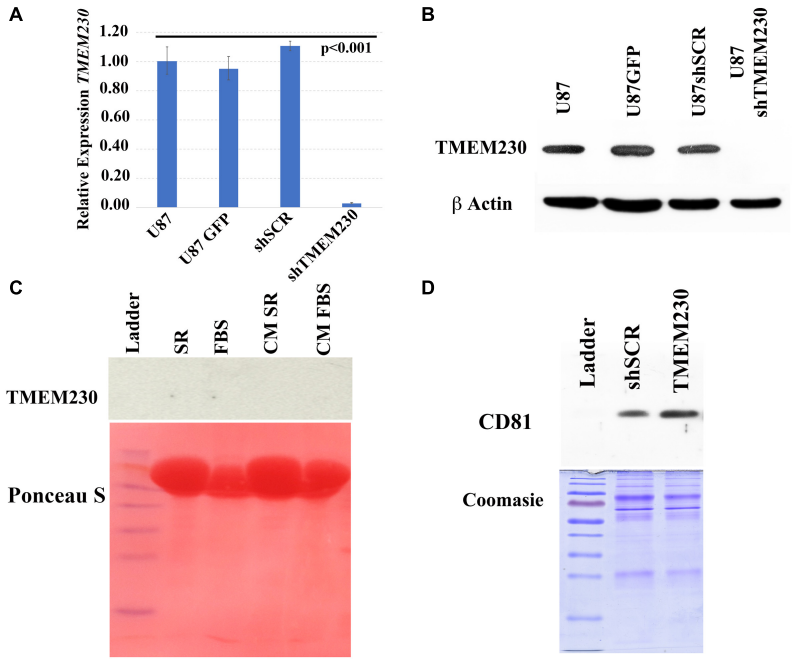

FIGURE 2 | Validation of endogenous and lentivirus downregulation of *TMEM230* mRNA and protein expression in U87-MG cells. **(A)** Validation of constitutive downregulation of endogenous *TMEM230* transcript expression with lentiviral system. Endogenous control: HPRT, Error bars represent 95% confidence interval. **(B)** Validation of constitutive downregulation of endogenous TMEM230 protein expression with the lentiviral system. Endogenous control: β-actin. **(C)** Western blot analysis (top panel) showed TMEM230 protein was not detected in fetal bovine serum (FBS), serum replacement (SR) or conditioned media (CM) containing serum replacement or FBS (CM SR and CM FBS) obtained from endogenous TMEM230 expressing U87 cells. Ponceau S staining (lower panel) showed an abundance of protein was loaded. **(D)** Coomassie blue staining showed an increase of expression of extracellular vesicle membrane protein, CD81 in conditioned media of U87 cells constitutively over-expressing TMEM230 with respect to conditioned media collected from control cells (U87GFP and U87shSCR). Detection of CD81 **(D)** but lack of detection of TMEM230 protein in culture media **(C)** supports that the TMEM230 protein regulates extracellular vesicle generation or secretion but is not itself a component of extracellular vesicles.

conditioned media generated by TMEM230 expressing U87 cells or by U87 cells in which TMEM230 was downregulated.

TMEM230 Expressing U87-MG Cells Promote Human Umbilical Vein Endothelial Cell Sprouting, Motility and Tubule-Like Structure Formation

To determine whether extracellular components associated with expression of TMEM230 promote blood vessel cell sprouting, HUVECs were cultured in conditioned media obtained from U87 control cells (U87shSCR) expressing endogenous TMEM230 or U87 cells in which endogenous TMEM230 expression was constitutively downregulated (U87shTMEM230). The culture media conditioned by the U87 cells was added to HUVEC plated as separated spots of confluent cells or as a 3D body formed by cell hanging drops in methylcellulose and collagen. These conditions recapitulate sprouting, migration and blood vessel formation (Nakatsu et al., 2003; Crampton et al., 2007; Nakatsu and Hughes, 2008; Heiss et al., 2015). When cultured with media conditioned by U87 cells in which TMEM230 was expressed in the absence of proangiogenic factors, HUVEC cells seeded in Matrigel formed tubule-like structures (**Figure 5**, panels 2,4). When cultured with media conditioned by U87 cells in which TMEM230 was downregulated, tubule structures where not observed (**Figure 5** panels 1-3, compare to HUVEC cultured with conditioned media by TMEM230 U87 expressing cells, panels 2,4). Similarly, HUVEC bodies seeded in 3D (in FBS or SR media) conditioned by U87 cells in which TMEM230 was downregulated failed to display cell sprouting (**Figure 5**, panels 7,8) compared to HUVEC cells cultured with media conditioned by endogenous TMEM230 U87 expressing cells (**Figure 5**, panels 5,6).

Results support that U87 tumor cells expressing TMEM230 recapitulate blood vessel sprouting or the early steps in vessel formation without direct contact with HUVECs. Significantly less sprouting was observed in the assay in which media not conditioned by U87 was used (**Figure 5**, panel 9) compared to culture media conditioned by TMEM230 expressing U87 (**Figure 5**, panels 5,6) or when proangiogenic factors were present (**Figure 5**, panel 15). Surprisingly, sprouting was initiated in HUVEC cultured in conditioned media obtained from TMEM230 expressing U87 cells, regardless if proangiogenic factors were present (**Figure 5**, panels 11,12) or not (**Figure 5**, panels 5-6).

Collectively, these results support that angiogenic like behavior was initiated in HUVEC by extracellular vesicles or factors generated from U87 cells expressing endogenous TMEM230 rather than components derived from FBS or SR.

TMEM230 Promotes U87-MG Cell Migration, Tumor and Endothelial Cell Interaction, and Displacement of Endothelial Cells

The ability of TMEM230 to promote tumor cell migration and displacement of endothelial cell to cell contacts as an early step in blood vessel disruption was accessed by determining whether TMEM230 expressing U87 cells can invade into endothelial cells, displace endothelial cell-cell contacts and cell-ECM scaffold interactions, using co-culture assays of U87 and HUVEC cells. U87shSCR cells or U87shTMEM230 cells in parallel culture assays were plated as a confluent mass equidistant from a confluent mass of HUVECs (**Figure 6A**, low magnification shows assay set up). As previously observed, both peripheral and core U87shTMEM230 confluent cells showed rapid onset of aberrations in their morphologies (**Figures 3**, **6B**). Downregulation of TMEM230 in U87 cells was associated with a cytoplasm of reduced mass, disrupted cytoplasmic invadopodium like extensions, decreased cell anchorage and reduced contacts among initially confluent plated cells (**Figure 6B**). Migration of U87shSCR cells or U87shTMEM230 was evaluated over time (9 days) relative to the HUVECs. U87 cells with reduced TMEM230 expression as observed in **Figure 3**, displayed reduced anchorage capacity and lack of motility compared to control cells (**Figures 6B,C**). In contrast, U87 control cells displayed extensive cell to cell contacts and motility capacity. U87 cells migrated from their initial seeding site into the core mass of non-GFP expressing HUVECs (**Figure 6D-F**). HUVECs, in both U87 control and U87shTMEM230 conditioned media, displayed little migration capacity for the entire time span of the assays. Contact and displacement of the confluent HUVECs were observed when U87 control cells infiltrated into the HUVEC mass, a behavior that is associated with the first step of intussusceptive induced blood vessel branching (**Figures 6D-F**; Djonov et al., 2003; Burri et al., 2004). The U87 assays demonstrated TMEM230 expression was necessary for tumor cell motility and infiltration-like behavior and supported that aberrant elevated levels of TMEM230 expression promote intravasation and blood vessel branching in the GBM tumor.

Collectively, contact and displacement of HUVECs observed with TMEM230 expressing U87 therefore support that TMEM230 in addition to having a role in infiltrating and remodeling tumor tissue, may also have an equally important role in tumor colonization through contact and intravasation of tumor cells into blood vessels.

TMEM230 Dependent U87-MG Migration and Tubule Like Structure Formation Mimic Blood Vessel Formation Through Vascular Mimicry

Vascular Mimicry (VM) is a not completely characterized process in which tumor cells recapitulate vascularization of tumor tissue by generating microchannels or by attaching themselves to blood vessels and following their 3D structure for oxygen and nutrient effusion. VM has been identified with GBM (Arbab et al., 2015; Ahsan et al., 2017; Angara et al., 2017). Formation of blood vessel like structures by tumor cells themselves, may allow uniting tumor cell vessels with existing endothelial blood vessels to augment tissue perfusion and promote conditions suitable for metastasis formation. To evaluate whether vascular mimicry is also a property associated with TMEM230, U87 cells where plated in 3D Matrigel. In contrast to cells in which TMEM230 was downregulated, U87 cells expressing endogenous TMEM230 displayed collective movement and cell to cell contact, cell sprouting and invasion in Matrigel, generating structures reminiscent of lumen containing tubules (**Figures 7A,B**). These structures wholly generated and containing only tumor cells may represent the early steps of the vascular mimicry associated with GBM. Generation of 3D like vessel structures provided an additional role of TMEM230 for promoting perfusion of a tumor mass, necessary for continued aggressive tumor expansion and infiltration into tissue.

The collective results of our study support that TMEM230 promotes anchorage, motility, sprouting and branching like behavior in two diverse cell types found in GBM, tumor glial cells and resident tumor blood vessel cells, as demonstrated in U87 and HUVEC assays (**Figures 3**-**7**). Increase in expression of CD81, a marker associated with extracellular vesicles detected from conditioned media of TMEM230 expressing cells (**Figure 2D**), suggests that TMEM230 has both intercellular and extracellular functions and the extracellular activities are achieved through extracellular vesicles and/or secreted factors.

RNA Sequence Analysis of Glioblastoma and Lower Grade Glial Patient Samples From the TGCA Dataset

To evaluate whether the changes in the cellular properties observed in U87 cell assays in which TMEM230 was downregulated, correlated with molecular pathways associated with patient glioma properties, differential gene expression analysis was performed from LGG subtypes and GBM tumors based on TMEM230 expression levels by comparing RNA-seq datasets. Functional enrichments with a p-Value (Benjamini) < 0.05 derived from the most variable expressed genes revealed 335 (oligodendrogliomas **Supplementary Table 2**), 107 (oligoastrocytoma **Supplementary Table 3**), 438 (astrocytoma **Supplementary Table 4**), and 67 (glioblastoma **Supplementary Table 5**) molecular pathways correlated with high and low levels of TMEM230 in LGG and GBM (**Supplementary Figures 1**-**4** and **Supplementary Tables 2**-**5**). When gene expression analysis was performed comparing high-grade gliomas (GBM) with all low-grade glioma (LGG) subtypes combined and independent of the level of TMEM230 (**Supplementary Figure 5** and **Supplementary Table 6**), pathways identified with high and low TMEM230 (**Supplementary Figures 1**-**4**) were a subset, as expected. Genes and pathways different between high grade (GBM) and low-grade gliomas (LGG) (**Supplementary Figures 1**-**5**) may provide insight into which pathways are correlated with lower overall patient survival based on tumor grading (**Figure 1** and **Supplementary Figures 7**-**9**). To determine whether TMEM230

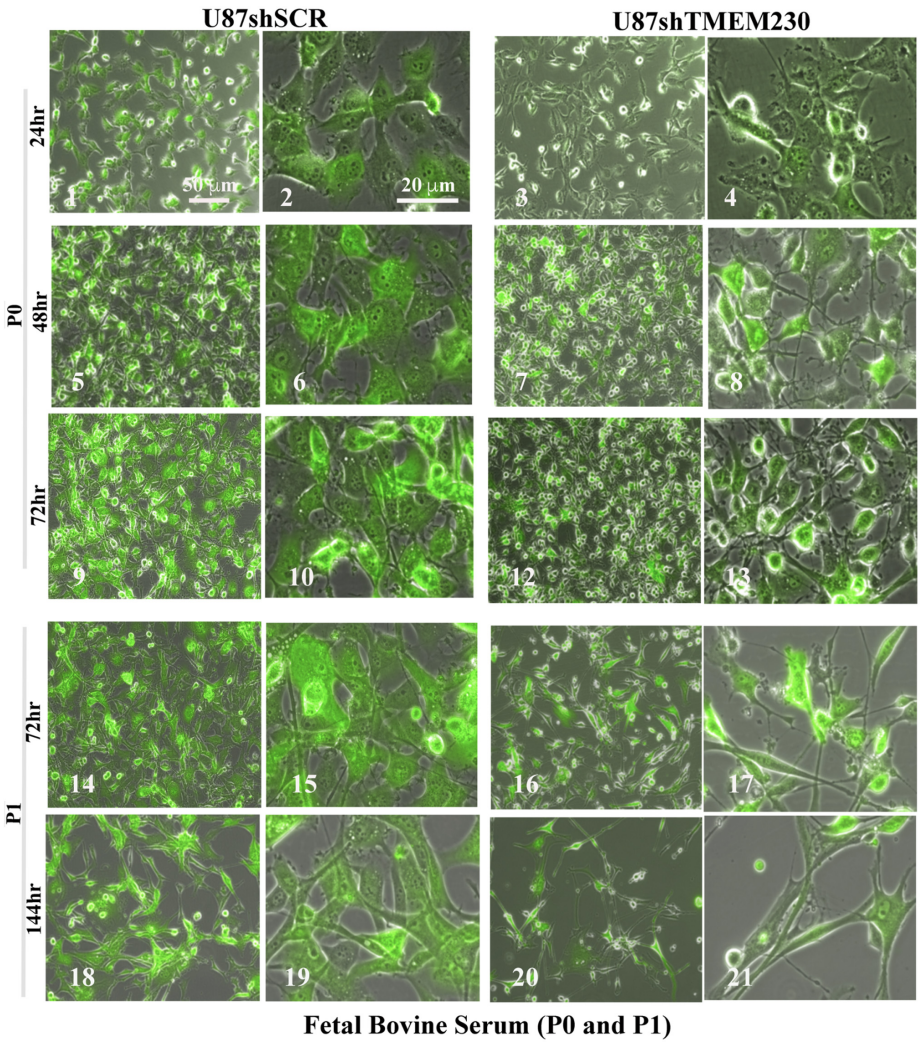

FIGURE 3 | Downregulation of TMEM230 was sufficient to promote loss of U87-MG substratum adhesion capacity in fetal bovine serum containing media. Control (U87shSCR) and U87 cells in which TMEM230 was constitutively downregulated (U87shTMEM230) were cultured in extracellular vesicle depleted FBS (Fetal Bovine Serum) containing culture media. Equal number of control cells and cells in which endogenous TMEM230 was downregulated were plated (P0) in vesicle depleted FBS containing culture media and monitored over 72 h, starting from when green fluorescent protein (GFP) expression was first observed (0 h, not shown). Cells in which TMEM230 were downregulated displayed decrease in cytoplasm dimensions and disrupted cytoplasmic invadopodium like extensions. Cells were re-passaged (P1) and monitored for additional 144 h. Re-passaged cells (P1) displayed a more limited capacity for cell adhesion, supporting that TMEM230 is necessary for scaffold attachment of cells.

may be a master regulator in development of diverse low-grade gliomas, expression analysis was performed to identify pathways that correlated with different TMEM230 expression levels in all LGG tumors (**Supplementary Figure 6** and **Supplementary Table 7**). Pathways were found in common in the different LGG suggesting that TMEM230 may regulate similar pathways. Candidate pathways may include signaling, extracellular matrix, cell membrane and adhesion regulation and extracellular exosome function (**Supplementary Figure 6**). Analysis was also performed to identify specific pathways correlated with different expression levels of *TMEM230* in low grade (G2) and high grade (G3) astrocytoma (**Supplementary Figures 8**, **9** and **Supplementary Tables 9**, **10**) and high grade GBM and astrocytoma independently of the level of TMEM230 (**Supplementary Figure 7** and **Supplementary Table 8**) and in GBM and astrocytoma, oligoastrocytoma and oligodendroglioma (**Figures 8A-C** and **Supplementary Tables 11**, **12**).

Collectively, the pathways correlated with different *TMEM230* expression levels identified from LGG patient and high-grade glioma GBM support the functional cellular behavior observed in the U87 cell assays in which TMEM230 expression was modulated. In particular, downregulation of TMEM230 in LGG was associated with repression of cellular activities regulating cell membrane and extracellular matrix function and organization, cell secretion and specifically exosome activity and angiogenesis (see **Figure 8A**). These analyses provide strong support that

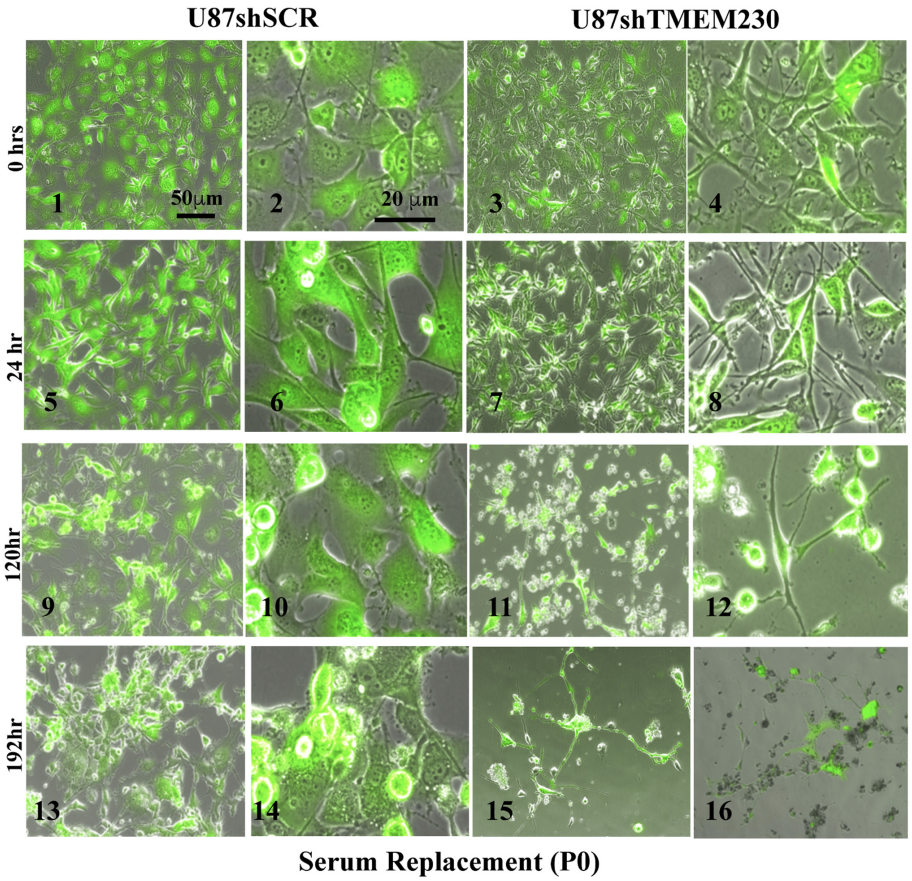

FIGURE 4 | Downregulation of endogenous TMEM230 was sufficient to promote loss of U87-MG substratum adhesion capacity in serum replacement containing media. Control (U87shSCR) and U87 cells in which TMEM230 was constitutively downregulated (U87shTMEM230) were cultured in serum replacement (SR) containing media (P0). Equal number of control cells and cells in which TMEM230 was downregulated were plated in SR containing culture media and monitored over 192 h, starting from when GFP expression was first observed (0 h).

TMEM230 function uncovered in U87 regulate the tumor processes of cell attachment, migration and secretion in glioma formation and progression. There was also a clear transition in changes in glial tumor cellular activity with increasing levels of TMEM230 as shown with GBM and LGG pathways being different except for exosome and extracellular matrix pathways (**Figures 1A**, **8B,C** and **Supplementary Table 12**).

As the transition in gene and pathways profiles correlated with the levels of TMEM230 expression, our results support that TMEM230 is a novel clinical marker that may differentiate GBM from LGG tumor properties for application in patient diagnostics and prognosis. Surprisingly, GBM tumors with highest TMEM230 expression indicated that TMEM230 activity was associated with cellular properties correlated with the regulation of cargo transport or vesicle trafficking via ATP hydrolysis of motor proteins of the kinesin family. Collectively, expression analysis of GBM and LGG identified candidate pathways regulated by TMEM230 in glial tumor formation. These pathways include cell adhesion and migration, secretion and membrane regulation, angiogenesis, response to hypoxia, endocytic vesicle membrane, exosome vesicle regulation, lysosome and phagosome functions. Validation of candidate targets of TMEM230 activity was performed by determining whether genes identified differentially expressed in gliomas were modulated with downregulation of TMEM230 in U87 cells (**Supplementary Figure 10**). Representative differentially expressed genes in patient gliomas were selected for expression analysis in U87 cells (**Figure 8** and **Supplementary Tables 1**-**12**). Western blot analysis indicated that SYNDECAN-1, CD44, and MOESIN proteins were downregulated with the inhibition of TMEM230 in U87 cells (U87shTMEM230) (**Supplementary Figure 10A**). SYNDECAN-1, CD44, and MOESIN all have roles in cytoskeleton (such as the actin family of proteins) regulation, cell adhesion and migration and tumor tissue remodeling. That TMEM230 may have a role in actin polymerization and cytoskeleton regulation was supported by immunofluorescence staining of phalloidin showing that U87 cells in which TMEM230 was downregulated displayed a decrease in long multistrand structures of actin (**Supplementary Figure 10B**). Immunofluorescence also showed that cell migration and scaffold regulating protein, CAVEOLIN-1 was also downregulated in U87 in which

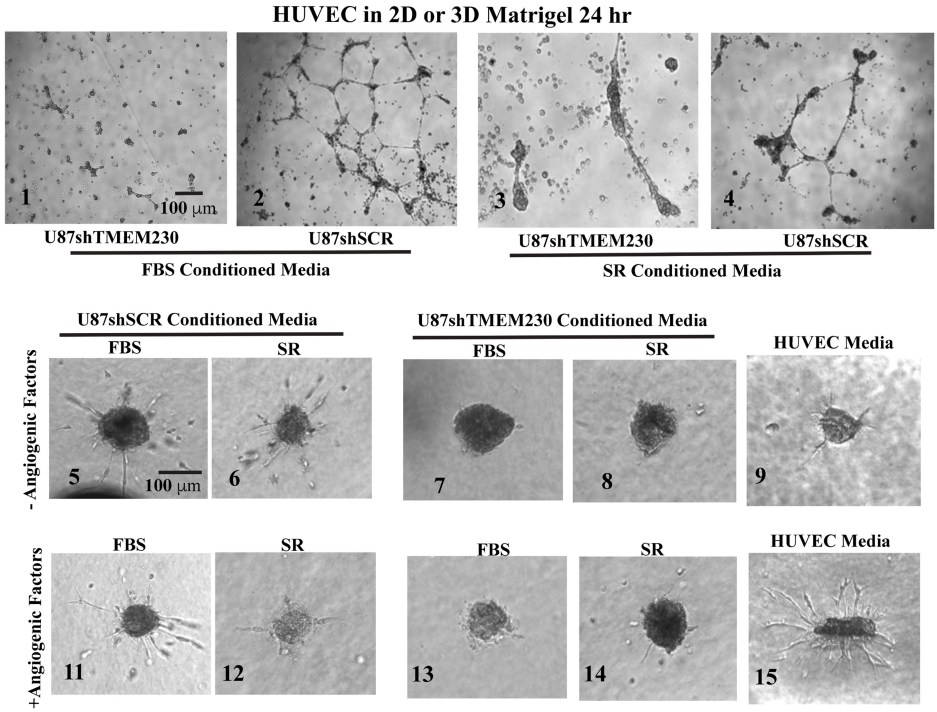

FIGURE 5 | Human umbilical vein endothelial cells cultured in FBS and serum replacement containing conditioned media from U87-MG cells expressing endogenous TMEM230 promoted angiogenic behavior. **(1–4)** Representative images at 24 h of human umbilical vein endothelial cells (HUVEC) in Matrigel treated with conditioned media obtained from 3 days cultures of U87 control (U87shSCR) and U87 in which TMEM230 was down regulated (U87shTMEM230). **(5–15)** Human umbilical vein endothelial cells in 3D treated with conditioned media obtained from 3 days cultures of U87 control and U87 which TMEM230 was down regulated shown for without **(5–9)** and with angiogenic factors **(11–14)**. U87 cells were cultured in media containing fetal bovine serum (FBS) or serum replacement (SR).

TMEM230 was downregulated (**Supplementary Figure 10B**). Other candidate proteins tested, such as FIBRONECTIN did not show a predicted change in expression with TMEM230 downregulation suggesting that additional genes influence glioma tumor formation and progression (**Supplementary Figure 10C**).

The collective analyses provide insight into how TMEM230 may regulate cellular activities in tumor tissue remodeling and aberrant vascularization in tumor development and progression. TMEM230 may be a novel candidate gene target to repress both tumor cell properties and tumor driven angiogenesis and consequently in the improvement of patient overall survival, not just for patients with high-grade glioblastoma and low-grade gliomas but also other types of abnormally vascularized tumors.

DISCUSSION

Tumor associated angiogenic switch is an event driven by the interactions of the tumor micro-environment and tumor cells that may lead to aggressive tumor properties and significant increase of probability tumor recurrence, subsequent to therapeutic intervention and patient mortality (Brown and Giavazzi, 1995; Bissell, 1999; Chintala et al., 1999; Bello et al., 2004; Box et al., 2010; Brooks et al., 2010; Alves et al., 2011; Belotti et al., 2011; Hielscher and Gerecht, 2012; Catalano et al., 2013; Ahir et al., 2020). While various known stimuli such as oxygen deprivation, inflammation and mechanical stress are inducers of angiogenic switch, key molecular components of the process are still not fully known. For instance, it is unclear if angiogenic switch utilizes similar genes and pathways in diverse tumors. Comprehensive characterization of tumor promoting angiogenic and extracellular matrix remodeling factors will contribute to identifying novel therapeutic targets for anticancer therapy, especially considering that existing antiangiogenic therapies based on canonical factors such as VEGF and VEGFR have proven often ineffective in certain tumors, such as GBM (Achen and Stacker, 1998; Fischer et al., 2005; Bergers and Hanahan, 2008; Argyriou et al., 2009; Crawford and Ferrara, 2009; Jo et al., 2012; Chowdhary and Chamberlain, 2013; de Groot et al., 2013; Arrillaga-Romany and Norden, 2014; Bartolotti et al., 2014; Curry et al., 2015; Ghiaseddin and Peters, 2015; Ameratunga et al., 2018; Jo and Wen, 2018; Anthony et al., 2019; Ceci et al., 2020; Funakoshi et al., 2020). Search of published and open access research on microarray, sequencing and proteomic expression analyses did not uncover any datasets to evaluate whether TMEM230 was differentially expressed specifically between non-malignant glial cells and glial cells from low- or high-grade gliomas. Surprisingly, also no patient study was available that allowed for directly comparing expression of any gene in non-malignant glial cells and glial cells from low- or high-grade gliomas. Existing gene expression studies only allowed

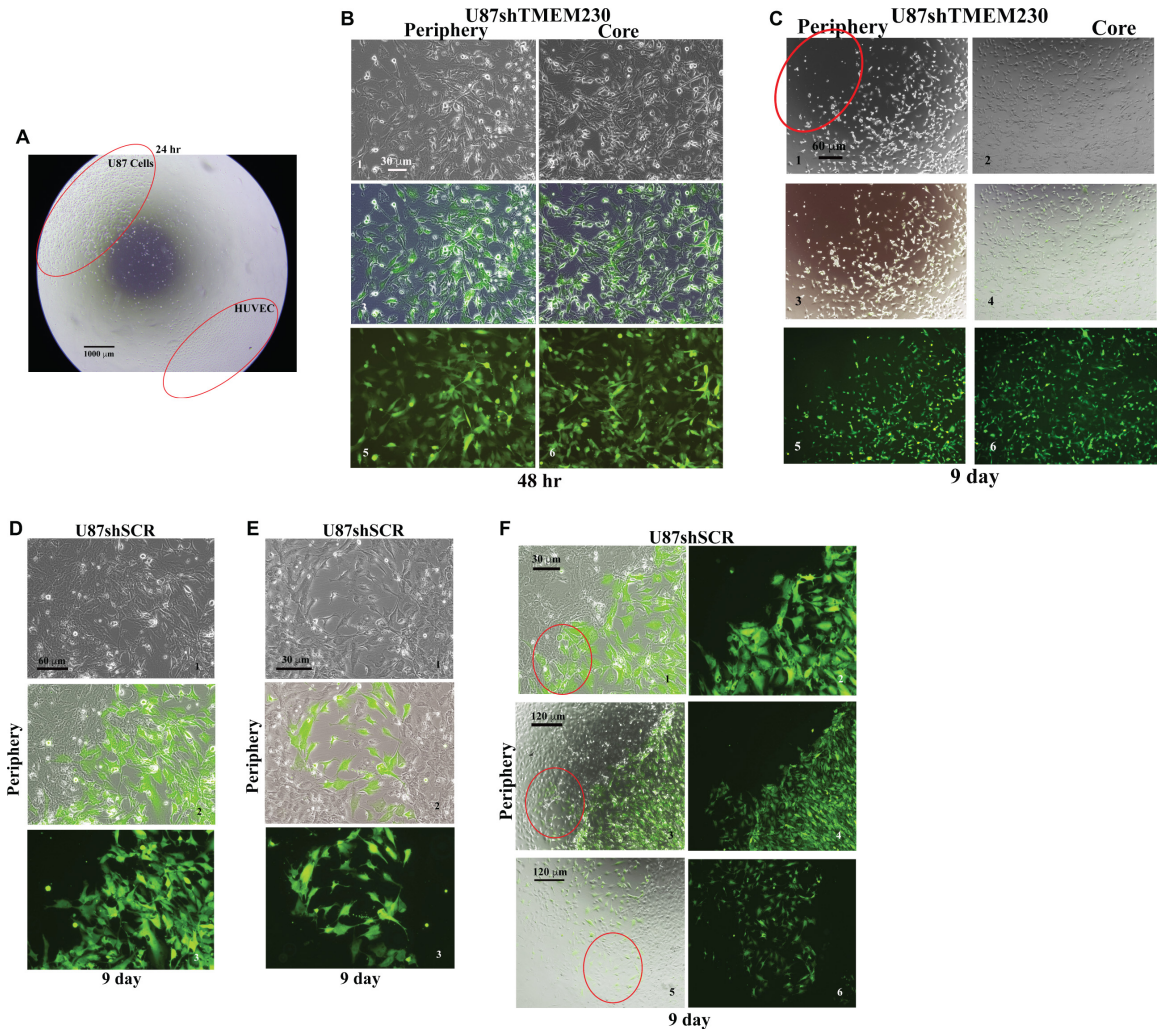

FIGURE 6 | Endogenous TMEM230 promoted U87-MG cell migration, tumor-endothelial cell contact and displacement in co-culture assays. **(A)** Low magnification shows the co-culture assay set up. **(B)** Representative images showing the periphery (outgrowth) and core (initial location of cell plating) of U87shTMEM230 cells at 48 h. Downregulation of TMEM230 in U87 cells was associated with cytoplasm of reduced mass, disrupted cytoplasmic invadopodium like extensions, decreased cell anchorage and reduced contacts among initially confluent plated cells. **(C)** Representative images of U87shTMEM230 cells at periphery and core at 9 days. U87 cells with reduced TMEM230 expression displayed reduced anchorage capacity and motility (see red circle at periphery of initial site of plating of the confluent cells) compared to control cells. **(D–F)** Displacement of the confluent human umbilical vein endothelial cells by U87 control cells (U87shSCR) expressing endogenous TMEM230 through infiltration into the confluent mass of human umbilical vein endothelial cells (see red circles), a behavior that is associated with the first step of intussusceptive induced blood vessel branching.

comparing glial cells from non-malignant tissue with tumor brain tissue in toto, or specific cell types but without the non-malignant counter-part cell from single cell sequencing data (Darmanis et al., 2015, 2017; Batiuk et al., 2017, 2020; Bayraktar et al., 2020). While studies do not allow a direct comparison of *TMEM230* between non-malignant and malignant specific cell types of the brain, they support that *TMEM230* is ubiquitously expressed in most cell types from the human non-malignant or malignant brain of patients, including glial cell lineages (see **Supplementary Figure 11**).

Our study here supported that TMEM230 promoted angiogenesis by inducing sprouting and tubule-like structures in HUVECs and vessel like structures by tumor cells themselves through a process described as vascular mimicry. Additionally, when TMEM230 was down regulated in tumor cells, the tumor cells lost the ability for substratum adhesion and consequently, substrate dependent motility. Control tumor cells expressing endogenous TMEM230 displayed significant migration capacity and when confronted with endothelial cells in their path, infiltrated, enveloped or displaced confluent colonies of endothelial cells, suggestive of the intussusceptive structural remodeling of blood vessels, leading to new vessel branching. TMEM230 appears to have the capacity to augment tissue vascularization by 3 known mechanisms that promote oxygen and nutrient diffusion of tissue. One is migration and homing like behavior of tumor cells to existing blood vessels.

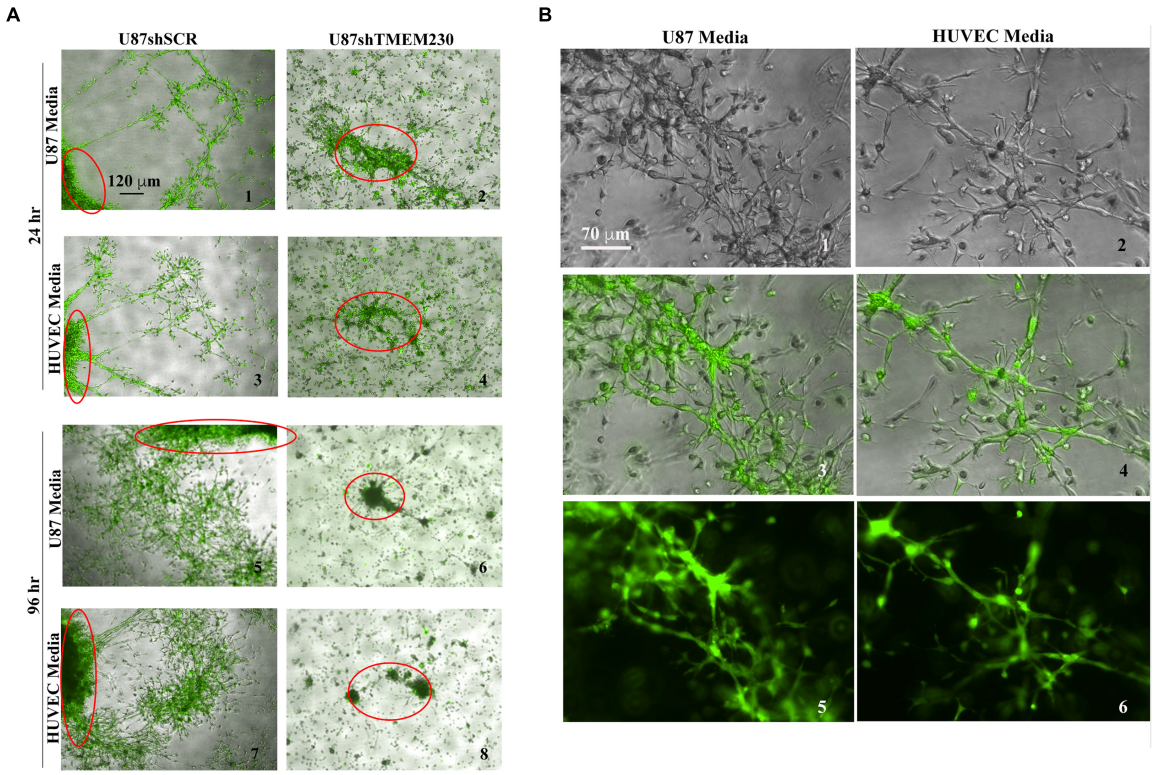

FIGURE 7 | Endogenous expression of TMEM230 promoted U87-MG migration and tubule like structure formation recapitulating a vascular mimicry like behavior. **(A)** Representative 3D bodies or structures (only the borders of a larger 3D body of U87shSCR or a complete body of U87shTMEM230 cells are shown by red circles) of U87 cells expressing endogenous TMEM230 displayed vascular mimicry, cell sprouting, collective cell movement, and invasion in 3D Matrigel. U87 cells in which endogenous TMEM230 was downregulated did not generate 3D bodies of significant size in agreement that TMEM230 was required for U87 cell growth. Two different media were used for generating VM like structures from U87 cells, media used for culturing adherent U87 tumor cells or HUVEC shown in **Figures 3**, **5** (top panel), respectively. **(B)** Higher magnification of control cells.

These properties allow tumor cells to home to, infiltrate and displace endothelial cells resulting in the generation of new branching structures by intussusceptive structural remodeling of existing blood vessels (**Figure 6**). Another is tumor cells expressing proangiogenic paracrine factors or secreting vesicles that co-opt epigenomic mechanisms of endothelial cells. The secreted factors induce new sprouting and vessel like structure formation of endothelial cells (**Figure 5**). The last mechanism is tumor cells remodeling the microenvironment to generate microchannels or vessel like structures that recapitulate lumen formation, a process described as VM (**Figure 7**). The 3 different models of tissue vascularization are well characterized in glioblastoma tumors. These models are described in diverse vascularized tumors (Burri et al., 2004; Djonov and Makanya, 2005; Dome et al., 2007; Hillen and Griffioen, 2007; Makanya et al., 2009; Sacewicz et al., 2009; Hlushchuk et al., 2011; Axnick and Lammert, 2012; De Spiegelaere et al., 2012; Ribatti and Crivellato, 2012; Ribatti and Djonov, 2012; Mentzer and Konerding, 2014; Bugyik et al., 2016; Krishna Priya et al., 2016; Nowak-Sliwinska et al., 2018; Diaz-Flores et al., 2020; Saravanan et al., 2020; Ribatti and Pezzella, 2021). Tumor cells generating microchannels through degradation and remodeling of the tumor extracellular matrix recapitulates lumen formation associated with neovascularization. Microchannels allow tumor cells to directly interact with existing and distant blood vessels. Consequently, the microchannels allow for increased passive oxygen and nutrient diffusion. Tumor cells may also follow along the blood vessels, whereby the blood vessel structures act as guides, allowing tumor cells to spread both internally into and externally around existing blood vessels (Ge and Luo, 2018; Zavyalova et al., 2019; Fathi Maroufi et al., 2020; Mei et al., 2020; Wechman et al., 2020; Zhang et al., 2020; Majidpoor and Mortezaee, 2021; Ribatti and Pezzella, 2021; Treps et al., 2021; Wei et al., 2021).

Insight into the molecular components of these 3 mechanisms is provided by gene expression analysis obtained from patients with glial tumors (Supplementary Figures and Tables) and the observation that expression of TMEM230 in GBM is positively correlated with increased expression of genes and pathways associated with extracellular vesicles, angiogenesis, cell adhesion and motility. While the TMEM230 expression profile of patient GBM was due to the contribution of diverse cell types comprising the tumor, we demonstrated that TMEM230 promoted anchorage, motility, sprouting and branching like behavior in two diverse cell types found in GBM, the tumor glial cells and resident tumor blood vessel cells, as demonstrated in

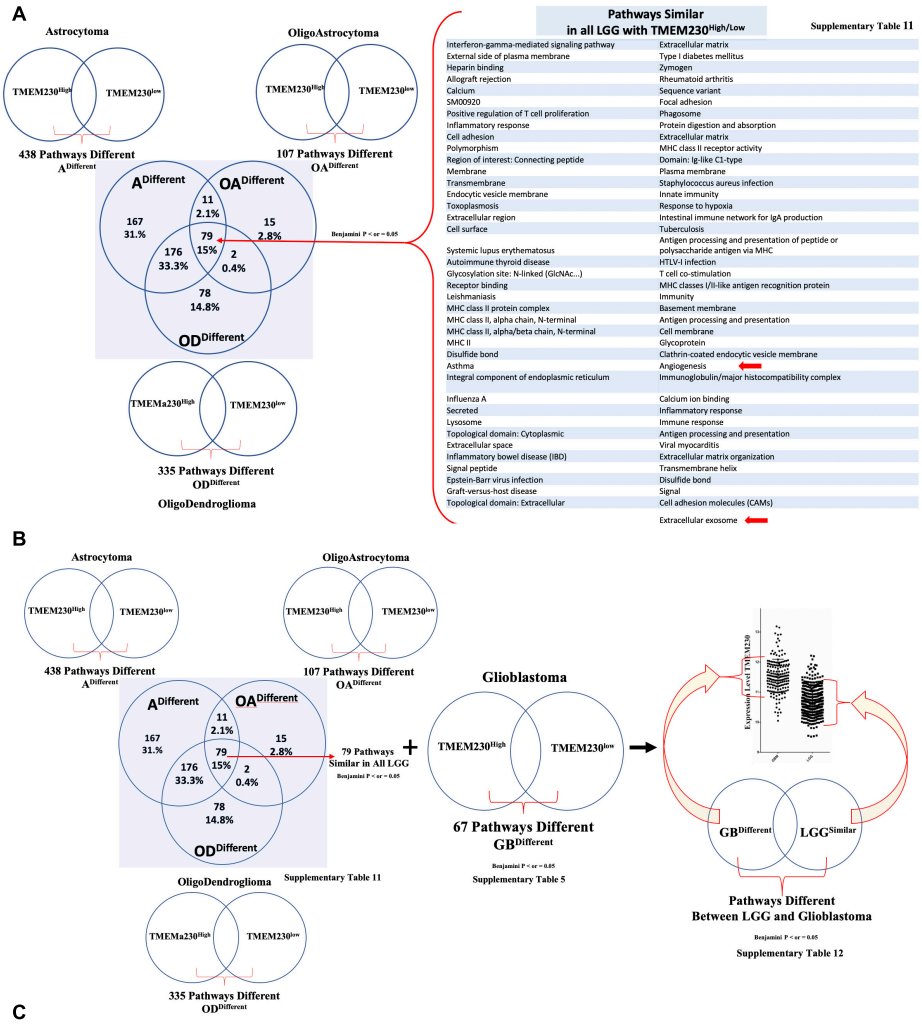

Pathways Similar in all LGG with TMEM230High/Low	
Interferon-gamma-mediated signaling pathway	Extracellular matrix
External side of plasma membrane	Type I diabetes mellitus
Heparin binding	Zymogen
Allograft rejection	Rheumatoid arthritis
Calcium	Sequence variant
SM00920	Focal adhesion
Positive regulation of T cell proliferation	Phagosome
Inflammatory response	Protein digestion and absorption
Cell adhesion	Extracellular matrix
Polymorphism	MHC class II receptor activity
Region of interest: Connecting peptide	Domain: Ig-like C1-type
Membrane	Plasma membrane
Transmembrane	Staphylococcus aureus infection
Endocytic vesicle membrane	Innate immunity
Toxoplasmosis	Response to hypoxia
Extracellular region	Intestinal immune network for IgA production
Cell surface	Tuberculosis
Systemic lupus erythematosus	Antigen processing and presentation of peptide or polysaccharide antigen via MHC
Autoimmune thyroid disease	HTLV-I infection
Glycosylation site: N-linked (GlcNAc...)	T cell co-stimulation
Receptor binding	MHC classes I/II-like antigen recognition protein
Leishmaniasis	Immunity
MHC class II protein complex	Basement membrane
MHC class II, alpha chain, N-terminal	Antigen processing and presentation
MHC class II, alpha/beta chain, N-terminal	Cell membrane
MHC II	Glycoprotein
Disulfide bond	Clathrin-coated endocytic vesicle membrane
Asthma	Angiogenesis
Integral component of endoplasmic reticulum	Immunoglobulin/major histocompatibility complex
Influenza A	Calcium ion binding
Secreted	Inflammatory response
Lysosome	Immune response
Topological domain: Cytoplasmic	Antigen processing and presentation
Extracellular space	Viral myocarditis
Inflammatory bowel disease (IBD)	Extracellular matrix organization
Signal peptide	Transmembrane helix
Epstein-Barr virus infection	Disulfide bond
Graft-versus-host disease	Signal
Topological domain: Extracellular	Cell adhesion molecules (CAMs)
	Extracellular exosome

GBM	
Oxidative phosphorylation	Kinesin, motor domain
Ribosome	Kinesin, motor region, conserved site
Ribosomal protein	Extracellular matrix
Alzheimer's disease	Mitochondrial proton-transporting ATP synthase complex, coupling factor F(o)
Huntington's disease	Cytosolic large ribosomal subunit
Parkinson's disease	CF(0)
Ribosome	Microtubule
Ribonucleoprotein	Phosphoprotein
Structural constituent of ribosome	Microtubule motor activity
Respiratory chain	ATP biosynthetic process
Mitochondrion inner membrane	Microtubule-based movement
SRP-dependent cotranslational protein	Hydrogen ion transmembrane transporter
Non-alcoholic fatty liver disease (NAFLD)	Microtubule binding
Mitochondrial inner membrane	Ubiquinone
Electron transport	Mitochondrion
Viral transcription	Acetylation
Mitochondrial respiratory chain complex I	Small ribosomal subunit
Nuclear-transcribed mRNA catabolic process, nonsense-mediated decay	ATP-dependent microtubule motor activity
Translation	Proton-transporting ATP synthase activity
Cytosolic small ribosomal subunit	Transport
Mitochondrial electron transport, NADH to ubiquinone	ATP synthesis coupled proton transport
rRNA processing	ATPase activity
Translational initiation	ATP synthesis
NADH dehydrogenase (ubiquinone) activity	Cytoplasm
Mitochondrial proton-transporting ATP synthase complex	Ion transport
Extracellular exosome	Cardiac muscle contraction
Hydrogen ion transport	Cytoskeleton
Mitochondrial respiratory chain complex I assembly	Ion channel
Mitochondrion	Mental retardation
KISc	Neurogenesis
Kinesin complex	Cytochrome-c oxidase activity
Mitochondrial ATP synthesis coupled proton transport	Meckel syndrome
Motor protein	Voltage-gated channel
Domain: Kinesin-motor	

LGG	
External side of plasma membrane	Lysosome
Cell adhesion	Topological domain: Cytoplasmic
Membrane	Inflammatory bowel disease (IBD)
Transmembrane	Signal peptide
Endocytic vesicle membrane	Epstein-Barr virus infection
Extracellular region	Graft-versus-host disease
Cell surface	Type I diabetes mellitus
Receptor binding	Zymogen
Extracellular space	Rheumatoid arthritis
Topological domain: Extracellular	Sequence variant
Extracellular matrix	Phagosome
Focal adhesion	Protein digestion and absorption
Extracellular matrix	MHC class II receptor activity
Plasma membrane	Domain: Ig-like C1-type
Basement membrane	Staphylococcus aureus infection
Cell membrane	Innate immunity
Extracellular matrix organization	Response to hypoxia
Extracellular exosome	Intestinal immune network for IgA production
Interferon-gamma-mediated signaling pathway	Tuberculosis
Heparin binding	Antigen processing and presentation of antigen via MHC
Allograft rejection	HTLV-I infection
Calcium	T cell co-stimulation
SM00920	MHC classes I/II-like antigen recognition protein
Positive regulation of T cell proliferation	Immunity
Inflammatory response	Antigen processing and presentation
Polymorphism	Glycoprotein
Region of interest: Connecting peptide	Clathrin-coated endocytic vesicle membrane
Toxoplasmosis	Angiogenesis
Systemic lupus erythematosus	Immunoglobulin/major histocompatibility complex
Autoimmune thyroid disease	Calcium ion binding
Glycosylation site: N-linked (GlcNAc...)	Inflammatory response
Leishmaniasis	Immune response
MHC class II protein complex	Antigen processing and presentation
MHC class II, alpha chain, N-terminal	Viral myocarditis
MHC class II, alpha/beta chain, N-terminal	Transmembrane helix
MHC II	Disulfide bond
Disulfide bond	Signal
Asthma	Cell adhesion molecules (CAMs)
Integral component of endoplasmic reticulum membrane	Secreted
Influenza A	

FIGURE 8 | All enriched pathways identified with high or low TMEM230 expression in diverse patient glioma tumors. **(A)** Enriched pathways identified common between high or low *TMEM230* expression in all LGG of patient. **(B)** Scheme for identifying different pathways between high or low *TMEM230* expression in LGG and glioblastomas. **(C)** Enriched pathways identified different between high or low *TMEM230* expression in LGG and glioblastoma. See corresponding **Supplementary Table 12**.

U87 and HUVEC assays. Therefore, the pathways enriched in GBM in which TMEM230 expression was elevated indicated that angiogenic switch associated with GBM was a process driven by the physical interactions of different cell types and scaffold or soluble factors present in the tumor environment. This is in agreement with the identification that TMEM230 has both intracellular and extracellular activity in tumor development and tumor driven angiogenesis. As our previous results showed that TMEM230 was expressed in diverse human tumor cell lines and patient tumor cells, this was suggestive that different tumors may utilize similar TMEM230 modulated genes and pathways for promoting tumor associated angiogenic switch. As extracellular vesicles such as exosomes are known to induce angiogenesis and modulate remodeling of the tumor microenvironment, future study will need to be performed to validate the role of TMEM230 in exosome activity in angiogenesis and determine whether exosomes are from diverse TMEM230 expressing cells in GBM.

Cell adhesion molecules such as integrins and other membrane proteins, are essential for cell attachment to basement membrane and extracellular matrix components to allow migration and remodeling of the microenvironment of both tumor cells and endothelial cells (Balkwill, 2003; Levin, 2005; Mackay, 2008; Alves et al., 2011; Lechertier and Hodivala-Dilke, 2012; Armento et al., 2017; Angelopoulou and Piperi, 2018; Lefranc et al., 2018). In this study, we demonstrated that downregulation of TMEM230 inhibited the adherence of U87 tumor cells both to the basement membrane like scaffold (Matrigel, cellulose or collagen) and to polystyrene surface of tissue culture plates. Cellular migration is dependent on the transfer of force from the cytoskeleton scaffold to the ECM. Loss of adherence is correlated with inability of the tumor cells to migrate and interact with HUVECs, conditions necessary for intussusceptive structural remodeling of blood vessels and for vascular mimicry. Gene expression analysis of patients supported that expression of genes associated with integrin mediated signaling and binding, focal adhesion complex formation, extracellular and transmembrane protein turnover are well represented and correlated with increased expression of TMEM230. Gene expression analysis of patients further suggested that TMEM230 played a role maintaining tumor cell adherence to the extracellular scaffold, necessary for tumor cell motility and invasion. In agreement, endogenous inhibitors of angiogenesis are often associated with extracellular matrix or basement membrane proteins which function to interfere with endothelial cell sprouting, migration and tube morphogenesis and down regulate genes expressed in endothelial cells (Pozzi and Zent, 2009; Box et al., 2010; Simon-Assmann et al., 2011).

Gene expression analysis uncovered specific pathways associated with the increase of TMEM230 expression in LGG and glioblastoma from patients (**Figure 8C** and **Supplementary Table 12**). These pathways involved: cell adhesion, secretion and membrane regulation, angiogenesis, response to hypoxia, endocytic vesicle membrane and exosome vesicle regulation and lysosome and phagosome activities. Highest levels of TMEM230 were correlated in glioblastoma with ribosome generation, mitochondria ATP synthesis, kinesin motor proteins, ATP synthesis and ATP dependent microtubule motor activity. Kinesins are motor proteins that move large proteins, vesicles, structures and organelles such as mitochondria with ATP dependent hydrolysis along microtubules (Ali and Yang, 2020; Furnish and Caino, 2020; Konjikusic et al., 2021). Most kinesins regulate transport from intracellular locations toward the cell periphery such as membrane components for cell membrane homeostasis, turnover and recycling. These intracellular cargos in turn can be derived from phagosomes and destined for lysosome activity. Formation of large multicomponent structures such as ribosomes require motor proteins to be transported to sites of assembly. Extracellular secretion of signaling products and extracellular matrix remodeling factors such as metalloproteinases are also regulated by kinesins in normal and disease development. This activity is also coordinated with actin for cell migration and 3D structure sprouting via membrane component turnover and regeneration (Feiguin et al., 1994; Langford, 1995; Oosawa, 1995; Hehnly and Stamnes, 2007). Therefore, the results of our analysis suggest that further investigations of kinesins and additional ATP-dependent cytoskeletal regulators may be worthwhile in the context of TMEM230 function.

In conclusion, the tumor properties associated with glioma patients are supportive of the functional tumor role of TMEM230 demonstrated in the U87 and HUVEC assays performed in this study. Higher levels of TMEM230 promoted aggressive tumor behavior, remodeling and increased endothelial and tumor cell (vascular mimicry) based vascularization of 3D scaffolds through intracellular and extracellular activities of TMEM230. All evidence supports that TMEM230 may be a novel target gene for both anticancer and anti-angiogenesis for certain highly vascularized tumors that are currently intransigent to therapeutic interventions. Moreover, molecular tumor and angiogenic pathways identified with TMEM230 may help develop novel therapeutic strategies for inhibiting migration, abnormal tumor microenvironment and blood vessel remodeling of tumor glial cells, and tumor driven angiogenesis of glioblastoma cells. Moreover, this study combined with our previous research supports that precision regulation of TMEM230 epxression levels in patients may likely promote normalization of tumor formed abnormal blood vessels to allow for better delivery of antitumor therapeutic drugs.

Inhibition of endogenous angiogenic promoting factors, such as TMEM230, are attractive targets for cancer therapy and tumor associated angiogenesis, as they may be less toxic and less likely to lead to drug resistance than exogenous inhibitors. Since we have previously demonstrated that TMEM230 appears to be a master regulator of angiogenesis, independent and in parral to the VEGF and NOTCH signaling pathways, our study presents a novel strategy and alternative target for inhibiting the VEGF dependent angiogenic pathway. This is especially relevant in clinical cases where VEGF specific targeted or antibodies therapies do not function. Modulation of TMEM230 may have applications in addition to cancer treatment, for instance disorders in which unregulated angiogenesis results in unwanted new blood vessel formation such as in macular degeneration.

DATA AVAILABILITY STATEMENT

The raw data supporting the conclusions of this article will be made available by the authors, without undue reservation.

AUTHOR CONTRIBUTIONS

CC performed all the U87 and HUVEC experiments, acquired the microscope images, and analyzed all the data. VMg conceived and designed experiments, provided guidance, and analyzed all the data. EA performed all the bioinformatics analysis of the TCAC and TACG data for glioblastomas and lower grade glial tumors. PP, VMr, and LV generated lentiviral construct for TMEM230 modulation. PP performed RNA extraction and expression analysis from U87. EP, RG, DMz, and MP contributed ideas. AC, GG, EM, and SL contributed to image analysis. CD, GL, and GD contributed with different tools. SM, GN, JK, and BG contributed ideas and tools. AN, DMr, and FB provided valuable guidance. GB and ID'A made critical observations. MG was a major contributor in revision of the manuscript. IZ and RR conceived, designed, optimized, jointly supervised all of the biological experiments of the project and analyzed all the data, and wrote and revised the manuscript. All authors contributed to the article and approved the submitted version.

FUNDING

This study was funded in part by the Consiglio Nazionale delle Ricerche and Italian Ministry of Education, University and Research CNR-MIUR Flagship Interomics. Funding for CC Fellowship is endowed by the Tiziano Oggionni, Walkjria Ferri and by the Academia Servorum Scientiae. "Progetto di Eccellenza" from the Ministry of Research to VMg; CNR-MIUR Flagship Projects Epigen and Interomics to IZ and RR.

ACKNOWLEDGMENTS

The authors would like to thank Loredana Ansalone from the ITB Unit for administrative support. Giorgio Zucchi for clinical guidance and patient data analysis.

SUPPLEMENTARY MATERIAL

The Supplementary Material for this article can be found online at: https://www.frontiersin.org/articles/10.3389/fncel.2021.703431/full#supplementary-material

Supplementary Figure 1 | Representative enriched pathways identified from differentially expressed Genes in patient derived oligoastrocytoma with high and low *TMEM230* expression.

Supplementary Figure 2 | Representative enriched pathways identified different between high or low *TMEM230* expression from differentially expressed genes (DEG) in patient samples of oligoastrocytoma.

Supplementary Figure 3 | Representative enriched pathways identified different between high or low *TMEM230* expression from differentially expressed genes (DEG) in patient samples of astrocytoma.

Supplementary Figure 4 | Representative enriched pathways identified different between high or low *TMEM230* expression from differentially expressed genes (DEG) in patient samples of glioblastoma.

Supplementary Figure 5 | Representative enriched pathways identified different between glioblastoma and LGG from DEG.

Supplementary Figure 6 | Representative enriched pathways identified different between high or low *TMEM230* expression from DEG in LGG.

Supplementary Figure 7 | Representative enriched pathways identified different between high or low *TMEM230* expression from DEG in GBM and astrocytoma.

Supplementary Figure 8 | Representative enriched pathways identified different between high or low *TMEM230* expression from DEG in low grade (G2) astrocytoma.

Supplementary Figure 9 | Representative enriched pathways identified different between high or low *TMEM230* expression from DEG in high grade (G3) astrocytoma.

Supplementary Figure 10 | Protein validation of TMEM230 candidate responding genes in U87-MG. **(A)** Western blot analysis for SYNDECAN-1, CD44, and MOESIN proteins in U87 control cells (U87shSCR) and in U87 cells in which TMEM230 was down regulated (U87shTMEM230). Endogenous control: β-ACTIN. **(B)** Immunofluorescence analysis for CAVEOLIN-1 and ACTIN through phalloidin interaction in U87 control and shTMEM230 transduced cells (GFP staining). Nuclei are visualized with DAPI. That TMEM230 may have a role in actin polymerization and cytoskeleton regulation is supported by immunofluorescence staining of PHALLOIDIN showing that U87 cells in which TMEM230 was downregulated was associated with decrease in the number and quality in the long multistrand structures of actin. **(C)** Immunofluorescence analysis for FIBRONECTIN in U87 control and shTMEM230 transduced cells (GFP staining). Nuclei are visualized with DAPI. Expression analysis of patient samples suggests that *Fibronectin* is differentially expressed between gliomas and non-malignant glial cells. Immunofluorescence analysis supports that FIBRONECTIN is not differentially expressed in U87 control and shTMEM230 transduced cells, and therefore TMEM230 does not regulate FIBRONECTIN expression.

Supplementary Figure 11 | TMEM230 expression in diverse cell types from non-malignant and malignant human brain. **(A)** Distribution of TMEM230 transcripts in different non-malignant cell populations from human brain according to the study of Darmanis (2015) (Accession: GSE67835, survey of human brain transcriptome diversity at the single cell level). Candidate cell populations were identified representative of the major neuronal, glial and vascular cell types according to published candidate gene markers. The distribution is represented by a boxplot with a minimum, the first quartile, the sample median, the third quartile and the maximum of the expression for each cell population, from the bottom to the top. The distribution profiles support that TMEM230 is expressed in most non-malignant cells at relatively equal but low levels. **(B–D)** Expression analysis of Tmem230 from Single-Cell Rna-Seq Analysis of Infiltrating Neoplastic Cells at the Migrating Front of Human Glioblastoma. **(B)** 2D-tSne representation of all single cells included from the study of Darmanis (2017) with a sample size of n = 3,589. Cell clusters are differentially colored and identified as distinct cell classes. **(C)** Expression of characteristic cell-type-specific genes overlaid on the 2D-tSne space. **(D)** Quantification of Tmem230-positive cells of distinct cell classes.

Supplementary Table1 | Patient clinical features include gender, age, tumor size in cm^3 and *TMEM230* expression level.

Supplementary Table 2 | All enriched pathways identified different between high or low TMEM230 from differentially expressed genes (DEG) in patient samples of oligodendrogliomas A).

Supplementary Table 3 | All enriched pathways identified different between high or low TMEM230 expression in oligoastrocytoma of patients from DEG.

Supplementary Table 4 | All enriched pathways identified different between high or low TMEM230 expression in astrocytoma of patients from DEG.

Supplementary Table 5 | All enriched pathways identified different between high or low TMEM230 expression in glioblastoma of patients from DEG.

Supplementary Table 6 | All enriched pathways identified different between glioblastoma and LGG from DEG.

Supplementary Table 7 | All enriched pathways identified different between high or low TMEM230 expression in LGG from DEG.

Supplementary Table 8 | All enriched pathways identified different between high or low TMEM230 expression in GBM and astrocytes from DEG.

Supplementary Table 9 | All enriched pathways identified different between high or low TMEM230 expression in low grade (G2) astrocytoma of patients from DEG.

Supplementary Table 10 | All enriched pathways identified different between high or low TMEM230 expression in high grade (G3) astrocytoma of patients from DEG.

Supplementary Table 11 | All pathways identified common between high or low TMEM230 expression in all LGG of patients from DEG.

Supplementary Table 12 | All pathways identified different between high or low TMEM230 expression in LGG and glioblastomas from DEG.

REFERENCES

Achen, M. G., and Stacker, S. A. (1998). The vascular endothelial growth factor family; proteins which guide the development of the vasculature. *Int. J. Exp. Pathol.* 79, 255–265.

Ahir, B. K., Engelhard, H. H., and Lakka, S. S. (2020). Tumor Development and Angiogenesis in Adult Brain Tumor: glioblastoma. *Mol. Neurobiol.* 57, 2461–2478. doi: 10.1007/s12035-020-01892-8

Ahsan, R., Baisiwala, S., and Ahmed, A. U. (2017). Rogue one: another faction of the Wnt empire implicated in assisting GBM progression. *Transl. Cancer Res.* 6, S321–S327. doi: 10.21037/tcr.2017.03.29

Aldape, K., Zadeh, G., Mansouri, S., Reifenberger, G., and Von Deimling, A. (2015). Glioblastoma: pathology, molecular mechanisms and markers. *Acta Neuropathol.* 129, 829–848.

Ali, I., and Yang, W. C. (2020). The functions of kinesin and kinesin-related proteins in eukaryotes. *Cell Adh. Migr.* 14, 139–152.

Alves, T. R., Lima, F. R., Kahn, S. A., Lobo, D., Dubois, L. G., Soletti, R., et al. (2011). Glioblastoma cells: a heterogeneous and fatal tumor interacting with the parenchyma. *Life Sci.* 89, 532–539. doi: 10.1016/j.lfs.2011.04.022

Ameratunga, M., Pavlakis, N., Wheeler, H., Grant, R., Simes, J., and Khasraw, M. (2018). Anti-angiogenic therapy for high-grade glioma. *Cochrane Database Syst. Rev.* 11:CD008218.

Angara, K., Borin, T. F., and Arbab, A. S. (2017). Vascular Mimicry: a Novel Neovascularization Mechanism Driving Anti-Angiogenic Therapy (AAT) Resistance in Glioblastoma. *Transl. Oncol.* 10, 650–660. doi: 10.1016/j.tranon.2017.04.007

Angelopoulou, E., and Piperi, C. (2018). Emerging role of plexins signaling in glioma progression and therapy. *Cancer Lett.* 414, 81–87. doi: 10.1016/j.canlet.2017.11.010

Anthony, C., Mladkova-Suchy, N., and Adamson, D. C. (2019). The evolving role of antiangiogenic therapies in glioblastoma multiforme: current clinical significance and future potential. *Expert Opin. Investig. Drugs* 28, 787–797. doi: 10.1080/13543784.2019.1650019

Arbab, A. S., Jain, M., and Achyut, B. R. (2015). Vascular Mimicry: the Next Big Glioblastoma Target. *Biochem. Physiol.* 4:e410. doi: 10.4172/2168-9652.1000e140

Argyriou, A. A., Giannopoulou, E., and Kalofonos, H. P. (2009). Angiogenesis and anti-angiogenic molecularly targeted therapies in malignant gliomas. *Oncology* 77, 1–11. doi: 10.1159/000218165

Armento, A., Ehlers, J., Schotterl, S., and Naumann, U. (2017). "Molecular Mechanisms of Glioma Cell Motility," in *Glioblastoma*, ed. S. De Vleeschouwer (Brisbane (AU)): Codon Publications).

Arrillaga-Romany, I., and Norden, A. D. (2014). Antiangiogenic therapies for glioblastoma. *CNS Oncol.* 3, 349–358. doi: 10.2217/cns.14.31

Axnick, J., and Lammert, E. (2012). Vascular lumen formation. *Curr. Opin. Hematol.* 19, 192–198. doi: 10.1097/moh.0b013e3283523ebc

Balkwill, F. (2003). Chemokine biology in cancer. *Semin. Immunol.* 15, 49–55. doi: 10.1016/s1044-5323(02)00127-6

Bartolotti, M., Franceschi, E., Poggi, R., Tosoni, A., Di Battista, M., and Brandes, A. A. (2014). Resistance to antiangiogenic therapies. *Future Oncol.* 10, 1417–1425.

Batiuk, M. Y., De Vin, F., Duque, S. I., Li, C., Saito, T., Saido, T., et al. (2017). An immunoaffinity-based method for isolating ultrapure adult astrocytes based on ATP1B2 targeting by the ACSA-2 antibody. *J. Biol. Chem.* 292, 8874–8891. doi: 10.1074/jbc.M116.765313

Batiuk, M. Y., Martirosyan, A., Wahis, J., De Vin, F., Marneffe, C., Kusserow, C., et al. (2020). Identification of region-specific astrocyte subtypes at single cell resolution. *Nat. Commun.* 11:1220. doi: 10.1038/s41467-019-14198-8

Bayraktar, O. A., Bartels, T., Holmqvist, S., Kleshchevnikov, V., Martirosyan, A., Polioudakis, D., et al. (2020). Astrocyte layers in the mammalian cerebral cortex revealed by a single-cell in situ transcriptomic map. *Nat. Neurosci.* 23, 500–509. doi: 10.1038/s41593-020-0602-1

Bello, L., Giussani, C., Carrabba, G., Pluderi, M., Costa, F., and Bikfalvi, A. (2004). Angiogenesis and invasion in gliomas. *Cancer Treat. Res.* 117, 263–284. doi: 10.1007/978-1-4419-8871-3_16

Belotti, D., Foglieni, C., Resovi, A., Giavazzi, R., and Taraboletti, G. (2011). Targeting angiogenesis with compounds from the extracellular matrix. *Int. J. Biochem. Cell Biol.* 43, 1674–1685. doi: 10.1016/j.biocel.2011.08.012

Bergers, G., and Hanahan, D. (2008). Modes of resistance to anti-angiogenic therapy. *Nat. Rev. Cancer* 8, 592–603. doi: 10.1038/nrc2442

Birk, H. S., Han, S. J., and Butowski, N. A. (2017). Treatment options for recurrent high-grade gliomas. *CNS Oncol.* 6, 61–70. doi: 10.2217/cns-2016-0013

Bissell, M. J. (1999). Tumor plasticity allows vasculogenic mimicry, a novel form of angiogenic switch. A rose by any other name? *Am. J. Pathol.* 155, 675–679. doi: 10.1016/S0002-9440(10)65164-4

Box, C., Rogers, S. J., Mendiola, M., and Eccles, S. A. (2010). Tumour-microenvironmental interactions: paths to progression and targets for treatment. *Semin. Cancer Biol.* 20, 128–138. doi: 10.1016/j.semcancer.2010.06.004

Brandes, A. A., Tosoni, A., Franceschi, E., Reni, M., Gatta, G., and Vecht, C. (2008). Glioblastoma in adults. *Crit. Rev. Oncol. Hematol.* 67, 139–152.

Brooks, S. A., Lomax-Browne, H. J., Carter, T. M., Kinch, C. E., and Hall, D. M. (2010). Molecular interactions in cancer cell metastasis. *Acta Histochem.* 112, 3–25.

Brown, P. D., and Giavazzi, R. (1995). Matrix metalloproteinase inhibition: a review of anti-tumour activity. *Ann. Oncol.* 6, 967–974.

Bugyik, E., Renyi-Vamos, F., Szabo, V., Dezso, K., Ecker, N., Rokusz, A., et al. (2016). Mechanisms of vascularization in murine models of primary and metastatic tumor growth. *Chin. J. Cancer* 35:19.

Burri, P. H., Hlushchuk, R., and Djonov, V. (2004). Intussusceptive angiogenesis: its emergence, its characteristics, and its significance. *Dev. Dyn.* 231, 474–488. doi: 10.1002/dvdy.20184

Caby, M. P., Lankar, D., Vincendeau-Scherrer, C., Raposo, G., and Bonnerot, C. (2005). Exosomal-like vesicles are present in human blood plasma. *Int. Immunol.* 17, 879–887.

Cancer Genome Atlas Research Network, Weinstein, J. N., Collisson, E. A., Mills, G. B., Shaw, K. R., Ozenberger, B. A., et al. (2013). The Cancer Genome Atlas Pan-Cancer analysis project. *Nat. Genet.* 45, 1113–1120.

Carra, S., Sangiorgio, L., Pelucchi, P., Cermenati, S., Mezzelani, A., Martino, V., et al. (2018). Zebrafish Tmem230a cooperates with the Delta/Notch signaling pathway to modulate endothelial cell number in angiogenic vessels. *J. Cell. Physiol.* 233, 1455–1467. doi: 10.1002/jcp.26032

Catalano, V., Turdo, A., Di Franco, S., Dieli, F., Todaro, M., and Stassi, G. (2013). Tumor and its microenvironment: a synergistic interplay. *Semin. Cancer Biol.* 23, 522–532. doi: 10.1016/j.semcancer.2013.08.007

Ceci, C., Atzori, M. G., Lacal, P. M., and Graziani, G. (2020). Role of VEGFs/VEGFR-1 Signaling and its Inhibition in Modulating Tumor Invasion: experimental Evidence in Different Metastatic Cancer Models. *Int. J. Mol. Sci.* 21:1388. doi: 10.3390/ijms21041388

Chintala, S. K., Tonn, J. C., and Rao, J. S. (1999). Matrix metalloproteinases and their biological function in human gliomas. *Int. J. Dev. Neurosci.* 17, 495–502.

Chowdhary, S., and Chamberlain, M. (2013). Bevacizumab for the treatment of glioblastoma. *Expert Rev. Neurother.* 13, 937–949.

Conedera, S. A., Li, Y., Funayama, M., Yoshino, H., Nishioka, K., and Hattori, N. (2018). Genetic analysis of TMEM230 in Japanese patients with familial Parkinson's disease. *Parkinsonism Relat. Disord.* 48, 107–108. doi: 10.1016/j.parkreldis.2017.12.020

Crampton, S. P., Davis, J., and Hughes, C. C. (2007). Isolation of human umbilical vein endothelial cells (HUVEC). *J. Vis. Exp.* 2007:183.

Crawford, Y., and Ferrara, N. (2009). VEGF inhibition: insights from preclinical and clinical studies. *Cell Tissue Res.* 335, 261–269. doi: 10.1007/s00441-008-0675-8

Curry, R. C., Dahiya, S., Alva Venur, V., Raizer, J. J., and Ahluwalia, M. S. (2015). Bevacizumab in high-grade gliomas: past, present, and future. *Expert Rev. Anticancer Ther.* 15, 387–397. doi: 10.1586/14737140.2015.1028376

Darmanis, S., Sloan, S. A., Croote, D., Mignardi, M., Chernikova, S., Samghababi, P., et al. (2017). Single-Cell RNA-Seq Analysis of Infiltrating Neoplastic Cells at the Migrating Front of Human Glioblastoma. *Cell Rep.* 21, 1399–1410. doi: 10.1016/j.celrep.2017.10.030

Darmanis, S., Sloan, S. A., Zhang, Y., Enge, M., Caneda, C., Shuer, L. M., et al. (2015). A survey of human brain transcriptome diversity at the single cell level. *Proc. Natl. Acad. Sci. U. S. A.* 112, 7285–7290. doi: 10.1073/pnas.1507125112

de Groot, J., Reardon, D. A., and Batchelor, T. T. (2013). Antiangiogenic therapy for glioblastoma: the challenge of translating response rate into efficacy. *Am. Soc. Clin. Oncol. Educ. Book* 33. doi: 10.1200/EdBook_AM.2013.33.e71

De Spiegelaere, W., Casteleyn, C., Van Den Broeck, W., Plendl, J., Bahramsoltani, M., Simoens, P., et al. (2012). Intussusceptive angiogenesis: a biologically relevant form of angiogenesis. *J. Vasc. Res.* 49, 390–404. doi: 10.1159/000338278

Deng, H., Fan, K., and Jankovic, J. (2018). The Role of TMEM230 Gene in Parkinson's Disease. *J. Parkinsons Dis.* 8, 469–477.

Deng, H. X., Shi, Y., Yang, Y., Ahmeti, K. B., Miller, N., Huang, C., et al. (2016). Identification of TMEM230 mutations in familial Parkinson's disease. *Nat. Genet.* 48, 733–739. doi: 10.1038/ng.3589

Diaz-Flores, L., Gutierrez, R., Gayoso, S., Garcia, M. P., Gonzalez-Gomez, M., Diaz-Flores, L. Jr., et al. (2020). Intussusceptive angiogenesis and its counterpart intussusceptive lymphangiogenesis. *Histol. Histopathol.* 35, 1083–1103. doi: 10.14670/HH-18-222

Djonov, V., Baum, O., and Burri, P. H. (2003). Vascular remodeling by intussusceptive angiogenesis. *Cell Tissue Res.* 314, 107–117. doi: 10.1007/s00441-003-0784-3

Djonov, V., and Makanya, A. N. (2005). New insights into intussusceptive angiogenesis. *EXS* 94, 17–33.

Dome, B., Hendrix, M. J., Paku, S., Tovari, J., and Timar, J. (2007). Alternative vascularization mechanisms in cancer: pathology and therapeutic implications. *Am. J. Pathol.* 170, 1–15. doi: 10.2353/ajpath.2007.060302

Fathi Maroufi, N., Taefehshokr, S., Rashidi, M. R., Taefehshokr, N., Khoshakhlagh, M., Isazadeh, A., et al. (2020). Vascular mimicry: changing the therapeutic paradigms in cancer. *Mol. Biol. Rep.* 47, 4749–4765. doi: 10.1007/s11033-020-05515-2

Feiguin, F., Ferreira, A., Kosik, K. S., and Caceres, A. (1994). Kinesin-mediated organelle translocation revealed by specific cellular manipulations. *J. Cell Biol.* 127, 1021–1039. doi: 10.1083/jcb.127.4.1021

Fischer, I., Gagner, J. P., Law, M., Newcomb, E. W., and Zagzag, D. (2005). Angiogenesis in gliomas: biology and molecular pathophysiology. *Brain Pathol.* 15, 297–310. doi: 10.1111/j.1750-3639.2005.tb00115.x

Funakoshi, Y., Hata, N., Kuga, D., Hatae, R., Sangatsuda, Y., Fujioka, Y., et al. (2020). Update on Chemotherapeutic Approaches and Management of Bevacizumab Usage for Glioblastoma. *Pharmaceuticals* 13:470. doi: 10.3390/ph13120470

Furnish, M., and Caino, M. C. (2020). Altered mitochondrial trafficking as a novel mechanism of cancer metastasis. *Cancer Rep.* 3:e1157. doi: 10.1002/cnr2.1157

Gately, L., Mclachlan, S. A., Philip, J., Rathi, V., and Dowling, A. (2019). Molecular profile of long-term survivors of glioblastoma: a scoping review of the literature. *J. Clin. Neurosci.* 68, 1–8. doi: 10.1016/j.jocn.2019.08.017

Ge, H., and Luo, H. (2018). Overview of advances in vasculogenic mimicry - a potential target for tumor therapy. *Cancer Manag. Res.* 10, 2429–2437. doi: 10.2147/CMAR.S164675

Ghiaseddin, A., and Peters, K. B. (2015). Use of bevacizumab in recurrent glioblastoma. *CNS Oncol.* 4, 157–169. doi: 10.2217/cns.15.8

Groblewska, M., Litman-Zawadzka, A., and Mroczko, B. (2020). The Role of Selected Chemokines and Their Receptors in the Development of Gliomas. *Int. J. Mol. Sci.* 21:3704. doi: 10.3390/ijms21103704

Guida, P., Piscitelli, E., Marrese, M., Martino, V., Cirillo, V., Guarino, V., et al. (2020). Integrating Microstructured Electrospun Scaffolds in an Open Microfluidic System for in Vitro Studies of Human Patient-Derived Primary Cells. *ACS Biomater. Sci. Eng.* 6, 3649–3663. doi: 10.1021/acsbiomaterials.0c00352

Gusyatiner, O., and Hegi, M. E. (2018). Glioma epigenetics: from subclassification to novel treatment options. *Semin. Cancer Biol.* 51, 50–58. doi: 10.1016/j.semcancer.2017.11.010

Haqqani, A. S., Delaney, C. E., Tremblay, T. L., Sodja, C., Sandhu, J. K., and Stanimirovic, D. B. (2013). Method for isolation and molecular characterization of extracellular microvesicles released from brain endothelial cells. *Fluids Barriers CNS* 10:4. doi: 10.1186/2045-8118-10-4

Hehnly, H., and Stamnes, M. (2007). Regulating cytoskeleton-based vesicle motility. *FEBS Lett.* 581, 2112–2118. doi: 10.1016/j.febslet.2007.01.094

Heiss, M., Hellstrom, M., Kalen, M., May, T., Weber, H., Hecker, M., et al. (2015). Endothelial cell spheroids as a versatile tool to study angiogenesis in vitro. *FASEB J.* 29, 3076–3084. doi: 10.1096/fj.14-267633

Hielscher, A. C., and Gerecht, S. (2012). Engineering approaches for investigating tumor angiogenesis: exploiting the role of the extracellular matrix. *Cancer Res.* 72, 6089–6096. doi: 10.1158/0008-5472.CAN-12-2773

Hillen, F., and Griffioen, A. W. (2007). Tumour vascularization: sprouting angiogenesis and beyond. *Cancer Metastasis Rev.* 26, 489–502.

Hlushchuk, R., Makanya, A. N., and Djonov, V. (2011). Escape mechanisms after antiangiogenic treatment, or why are the tumors growing again? *Int. J. Dev. Biol.* 55, 563–567. doi: 10.1387/ijdb.103231rh

Huang da, W., Sherman, B. T., and Lempicki, R. A. (2009). Systematic and integrative analysis of large gene lists using DAVID bioinformatics resources. *Nat. Protoc.* 4, 44–57.

Jain, R. K. (2013). Normalizing tumor microenvironment to treat cancer: bench to bedside to biomarkers. *J. Clin. Oncol.* 31, 2205–2218. doi: 10.1200/jco.2012.46.3653

Jeppesen, D. K., Hvam, M. L., Primdahl-Bengtson, B., Boysen, A. T., Whitehead, B., Dyrskjot, L., et al. (2014). Comparative analysis of discrete exosome fractions obtained by differential centrifugation. *J. Extracell. Vesicles* 3:25011. doi: 10.3402/jev.v3.25011

Jo, J., Schiff, D., and Purow, B. (2012). Angiogenic inhibition in high-grade gliomas: past, present and future. *Expert Rev. Neurother.* 12, 733–747. doi: 10.1586/ern.12.53

Jo, J., and Wen, P. Y. (2018). Antiangiogenic Therapy of High-Grade Gliomas. *Prog. Neurol. Surg.* 31, 180–199.

Jones, J., Nguyen, H., Drummond, K., and Morokoff, A. (2021). Circulating Biomarkers for Glioma: a Review. *Neurosurgery* 88, E221–E230.

Jovcevska, I. (2018). Sequencing the next generation of glioblastomas. *Crit. Rev. Clin. Lab. Sci.* 55, 264–282.

Kang, X., Zheng, Y., Hong, W., Chen, X., Li, H., Huang, B., et al. (2020). Recent Advances in Immune Cell Therapy for Glioblastoma. *Front. Immunol.* 11:544563. doi: 10.3389/fimmu.2020.544563

Karpati, G., Li, H., and Nalbantoglu, J. (1999). Molecular therapy for glioblastoma. *Curr. Opin. Mol. Ther.* 1, 545–552.

Kim, M. J., Deng, H. X., Wong, Y. C., Siddique, T., and Krainc, D. (2017). The Parkinson's disease-linked protein TMEM230 is required for Rab8a-mediated secretory vesicle trafficking and retromer trafficking. *Hum. Mol. Genet.* 26, 729–741. doi: 10.1093/hmg/ddw413

Kondo, Y., Katsushima, K., Ohka, F., Natsume, A., and Shinjo, K. (2014). Epigenetic dysregulation in glioma. *Cancer Sci.* 105, 363–369.

Konjikusic, M. J., Gray, R. S., and Wallingford, J. B. (2021). The developmental biology of kinesins. *Dev. Biol.* 469, 26–36.

Krishna Priya, S., Nagare, R. P., Sneha, V. S., Sidhanth, C., Bindhya, S., Manasa, P., et al. (2016). Tumour angiogenesis-Origin of blood vessels. *Int. J. Cancer* 139, 729–735. doi: 10.1002/ijc.30067

Langford, G. M. (1995). Actin- and microtubule-dependent organelle motors: interrelationships between the two motility systems. *Curr. Opin. Cell Biol.* 7, 82–88. doi: 10.1016/0955-0674(95)80048-4

Lechertier, T., and Hodivala-Dilke, K. (2012). Focal adhesion kinase and tumour angiogenesis. *J. Pathol.* 226, 404–412.

Lefranc, F., Le Rhun, E., Kiss, R., and Weller, M. (2018). Glioblastoma quo vadis: will migration and invasiveness reemerge as therapeutic targets? *Cancer Treat. Rev.* 68, 145–154. doi: 10.1016/j.ctrv.2018.06.017

Levin, E. G. (2005). Cancer therapy through control of cell migration. *Curr. Cancer Drug Targets* 5, 505–518. doi: 10.2174/156800905774574048

Li, B., and Dewey, C. N. (2011). RSEM: accurate transcript quantification from RNA-Seq data with or without a reference genome. *BMC Bioinformatics* 12:323. doi: 10.1186/1471-2105-12-323

Lopes Abath Neto, O., and Aldape, K. (2021). Morphologic and Molecular Aspects of Glioblastomas. *Neurosurg. Clin. N. Am.* 32, 149–158.

Love, M. I., Huber, W., and Anders, S. (2014). Moderated estimation of fold change and dispersion for RNA-seq data with DESeq2. *Genome Biol.* 15:550. doi: 10.1186/s13059-014-0550-8

Ludwig, K., and Kornblum, H. I. (2017). Molecular markers in glioma. *J. Neurooncol.* 134, 505–512.

Mackay, C. R. (2008). Moving targets: cell migration inhibitors as new anti-inflammatory therapies. *Nat. Immunol.* 9, 988–998. doi: 10.1038/ni.f.210

Majidpoor, J., and Mortezaee, K. (2021). Angiogenesis as a hallmark of solid tumors - clinical perspectives. *Cell. Oncol.* 44, 715–737. doi: 10.1007/s13402-021-00602-3

Makanya, A. N., Hlushchuk, R., and Djonov, V. G. (2009). Intussusceptive angiogenesis and its role in vascular morphogenesis, patterning, and remodeling. *Angiogenesis* 12, 113–123. doi: 10.1007/s10456-009-9129-5

Mandemakers, W., Quadri, M., Stamelou, M., and Bonifati, V. (2017). TMEM230: how does it fit in the etiology and pathogenesis of Parkinson's disease? *Mov. Disord.* 32, 1159–1162. doi: 10.1002/mds.27061

Masui, K., Mischel, P. S., and Reifenberger, G. (2016). Molecular classification of gliomas. *Handb. Clin. Neurol.* 134, 97–120. doi: 10.1016/b978-0-12-802997-8.00006-2

Mei, X., Chen, Y. S., Zhang, Q. P., Chen, F. R., Xi, S. Y., Long, Y. K., et al. (2020). Association between glioblastoma cell-derived vessels and poor prognosis of the patients. *Cancer Commun.* 40, 211–221. doi: 10.1002/cac2.12026

Mentzer, S. J., and Konerding, M. A. (2014). Intussusceptive angiogenesis: expansion and remodeling of microvascular networks. *Angiogenesis* 17, 499–509. doi: 10.1007/s10456-014-9428-3

Montano, N., D'alessandris, Q. G., Izzo, A., Fernandez, E., and Pallini, R. (2016). Biomarkers for glioblastoma multiforme: status quo. *J. Clin. Transl. Res.* 2, 3–10.

Nagarajan, R. P., and Costello, J. F. (2009). Epigenetic mechanisms in glioblastoma multiforme. *Semin. Cancer Biol.* 19, 188–197.

Nakatsu, M. N., and Hughes, C. C. (2008). An optimized three-dimensional in vitro model for the analysis of angiogenesis. *Methods Enzymol.* 443, 65–82.

Nakatsu, M. N., Sainson, R. C., Aoto, J. N., Taylor, K. L., Aitkenhead, M., Perez-Del-Pulgar, S., et al. (2003). Angiogenic sprouting and capillary lumen formation modeled by human umbilical vein endothelial cells (HUVEC) in fibrin gels: the role of fibroblasts and Angiopoietin-1. *Microvasc. Res.* 66, 102–112. doi: 10.1016/s0026-2862(03)00045-1

Nowak-Sliwinska, P., Alitalo, K., Allen, E., Anisimov, A., Aplin, A. C., Auerbach, R., et al. (2018). Consensus guidelines for the use and interpretation of angiogenesis assays. *Angiogenesis* 21, 425–532.

Ohgaki, H., and Kleihues, P. (2005). Epidemiology and etiology of gliomas. *Acta Neuropathol.* 109, 93–108.

Oosawa, F. (1995). Sliding and ATPase. *J. Biochem.* 118, 863–870. doi: 10.1093/jb/118.5.863

Polivka, J. Jr., Polivka, J., Holubec, L., Kubikova, T., Priban, V., Hes, O., et al. (2017). Advances in Experimental Targeted Therapy and Immunotherapy for Patients with Glioblastoma Multiforme. *Anticancer Res.* 37, 21–33.

Pozzi, A., and Zent, R. (2009). Regulation of endothelial cell functions by basement membrane- and arachidonic acid-derived products. *Wiley Interdiscip. Rev. Syst. Biol. Med.* 1, 254–272. doi: 10.1002/wsbm.7

Puzzilli, F., Ruggeri, A., Mastronardi, L., Di Stefano, D., and Lunardi, P. (1998). Long-term survival in cerebral glioblastoma. Case report and critical review of the literature. *Tumori* 84, 69–74.

Redzic, J. S., Ung, T. H., and Graner, M. W. (2014). Glioblastoma extracellular vesicles: reservoirs of potential biomarkers. *Pharmgenomics Pers. Med.* 7, 65–77.

Ribatti, D., and Crivellato, E. (2012). "Sprouting angiogenesis", a reappraisal. *Dev. Biol.* 372, 157–165. doi: 10.1016/j.ydbio.2012.09.018

Ribatti, D., and Djonov, V. (2012). Intussusceptive microvascular growth in tumors. *Cancer Lett.* 316, 126–131. doi: 10.1016/j.canlet.2011.10.040

Ribatti, D., and Pezzella, F. (2021). Overview on the Different Patterns of Tumor Vascularization. *Cells* 10:639. doi: 10.3390/cells10030639

Romani, M., Pistillo, M. P., and Banelli, B. (2018). Epigenetic Targeting of Glioblastoma. *Front. Oncol.* 8:448. doi: 10.3389/fonc.2018.00448

Sacewicz, I., Wiktorska, M., Wysocki, T., and Niewiarowska, J. (2009). [Mechanisms of cancer angiogenesis]. *Postepy Hig. Med. Dosw.* 63, 159–168.

Saravanan, S., Vimalraj, S., Pavani, K., Nikarika, R., and Sumantran, V. N. (2020). Intussusceptive angiogenesis as a key therapeutic target for cancer therapy. *Life Sci.* 252:117670. doi: 10.1016/j.lfs.2020.117670

Simon-Assmann, P., Orend, G., Mammadova-Bach, E., Spenle, C., and Lefebvre, O. (2011). Role of laminins in physiological and pathological angiogenesis. *Int. J. Dev. Biol.* 55, 455–465. doi: 10.1387/ijdb.103223ps

Sogno, I., Vene, R., Sapienza, C., Ferrari, N., Tosetti, F., and Albini, A. (2009). Anti-angiogenic properties of chemopreventive drugs: fenretinide as a prototype. *Recent Results Cancer Res.* 181, 71–76. doi: 10.1007/978-3-540-69297-3_8

Tate, M. C., and Aghi, M. K. (2009). Biology of angiogenesis and invasion in glioma. *Neurotherapeutics* 6, 447–457.

Thomas, A. A., Brennan, C. W., Deangelis, L. M., and Omuro, A. M. (2014). Emerging therapies for glioblastoma. *JAMA Neurol.* 71, 1437–1444. doi: 10.1001/jamaneurol.2014.1701

Touat, M., Idbaih, A., Sanson, M., and Ligon, K. L. (2017). Glioblastoma targeted therapy: updated approaches from recent biological insights. *Ann. Oncol.* 28, 1457–1472. doi: 10.1093/annonc/mdx106

Treps, L., Faure, S., and Clere, N. (2021). Vasculogenic mimicry, a complex and devious process favoring tumorigenesis - Interest in making it a therapeutic target. *Pharmacol. Ther.* 223:107805. doi: 10.1016/j.pharmthera.2021.107805

Trevisan, E., Bertero, L., Bosa, C., Magistrello, M., Pellerino, A., Ruda, R., et al. (2014). Antiangiogenic therapy of brain tumors: the role of bevacizumab. *Neurol. Sci.* 35, 507–514.

Uddin, M. S., Mamun, A. A., Alghamdi, B. S., Tewari, D., Jeandet, P., Sarwar, M. S., et al. (2020). Epigenetics of glioblastoma multiforme: from molecular mechanisms to therapeutic approaches. *Semin. Cancer Biol.* [Epub Online ahead of print]. doi: 10.1016/j.semcancer.2020.12.015

Ushio, Y. (1991). Treatment of gliomas in adults. *Curr. Opin. Oncol.* 3, 467–475.

Vartanian, A., Singh, S. K., Agnihotri, S., Jalali, S., Burrell, K., Aldape, K. D., et al. (2014). GBM's multifaceted landscape: highlighting regional and microenvironmental heterogeneity. *Neuro Oncol.* 16, 1167–1175. doi: 10.1093/neuonc/nou035

Visted, T., Enger, P. O., Lund-Johansen, M., and Bjerkvig, R. (2003). Mechanisms of tumor cell invasion and angiogenesis in the central nervous system. *Front. Biosci.* 8:e289–e304. doi: 10.2741/1026

Wan, Y. W., Allen, G. I., and Liu, Z. (2016). TCGA2STAT: simple TCGA data access for integrated statistical analysis in R. *Bioinformatics* 32, 952–954. doi: 10.1093/bioinformatics/btv677

Wang, X., Whelan, E., Liu, Z., Liu, C. F., and Smith, W. W. (2021). Controversy of TMEM230 Associated with Parkinson's Disease. *Neuroscience* 453, 280–286. doi: 10.1016/j.neuroscience.2020.11.004

Wang, Y., Xing, D., Zhao, M., Wang, J., and Yang, Y. (2016). The Role of a Single Angiogenesis Inhibitor in the Treatment of Recurrent Glioblastoma Multiforme: a Meta-Analysis and Systematic Review. *PLoS One* 11:e0152170. doi: 10.1371/journal.pone.0152170

Weathers, S. P., and De Groot, J. (2014). Resistance to antiangiogenic therapy. *Curr. Neurol. Neurosci. Rep.* 14:443.

Weathers, S. P., and De Groot, J. (2015). VEGF Manipulation in Glioblastoma. *Oncology* 29, 720–727.

Wechman, S. L., Emdad, L., Sarkar, D., Das, S. K., and Fisher, P. B. (2020). Vascular mimicry: triggers, molecular interactions and in vivo

models. *Adv. Cancer Res.* 148, 27–67. doi: 10.1016/bs.acr.2020.06.001

Wei, X., Chen, Y., Jiang, X., Peng, M., Liu, Y., Mo, Y., et al. (2021). Mechanisms of vasculogenic mimicry in hypoxic tumor microenvironments. *Mol. Cancer* 20:7.

Widodo, S. S., Hutchinson, R. A., Fang, Y., Mangiola, S., Neeson, P. J., Darcy, P. K., et al. (2021). Toward precision immunotherapy using multiplex immunohistochemistry and in silico methods to define the tumor immune microenvironment. *Cancer Immunol. Immunother.* 70, 1811–1820. doi: 10.1007/s00262-020-02801-7

Wirsching, H. G., Galanis, E., and Weller, M. (2016). Glioblastoma. *Handb. Clin. Neurol.* 134, 381–397.

Xu, R., Pisapia, D., and Greenfield, J. P. (2016). Malignant Transformation in Glioma Steered by an Angiogenic Switch: defining a Role for Bone Marrow-Derived Cells. *Cureus* 8:e471. doi: 10.7759/cureus.471

Zavyalova, M. V., Denisov, E. V., Tashireva, L. A., Savelieva, O. E., Kaigorodova, E. V., Krakhmal, N. V., et al. (2019). Intravasation as a Key Step in Cancer Metastasis. *Biochemistry* 84, 762–772. doi: 10.1134/s0006297919070071

Zhang, Y., Wang, S., and Dudley, A. C. (2020). Models and molecular mechanisms of blood vessel co-option by cancer cells. *Angiogenesis* 23, 17–25. doi: 10.1007/s10456-019-09684-y

Zhou, Y., Wu, W., Bi, H., Yang, D., and Zhang, C. (2020). Glioblastoma precision therapy: from the bench to the clinic. *Cancer Lett.* 475, 79–91. doi: 10.1016/j.canlet.2020.01.027

Conflict of Interest: IZ and RR have a patent accepted concerning the use of Agents that modulate TMEM230 in tumor associated angiogenesis. Patent Application International Publication number: 20200247882. Agents that modulate TMEM230 as angiogenesis regulators and that detect TMEM230 AS markers of metastasis.

The remaining authors declare that the research was conducted in the absence of any commercial or financial relationships that could be construed as a potential conflict of interest.

Publisher's Note: All claims expressed in this article are solely those of the authors and do not necessarily represent those of their affiliated organizations, or those of the publisher, the editors and the reviewers. Any product that may be evaluated in this article, or claim that may be made by its manufacturer, is not guaranteed or endorsed by the publisher.

Advantages of publishing in Frontiers

OPEN ACCESS
Articles are free to read for greatest visibility and readership

FAST PUBLICATION
Around 90 days from submission to decision

HIGH QUALITY PEER-REVIEW
Rigorous, collaborative, and constructive peer-review

TRANSPARENT PEER-REVIEW
Editors and reviewers acknowledged by name on published articles

Frontiers
Avenue du Tribunal-Fédéral 34
1005 Lausanne | Switzerland

Visit us: www.frontiersin.org
Contact us: frontiersin.org/about/contact

REPRODUCIBILITY OF RESEARCH
Support open data and methods to enhance research reproducibility

DIGITAL PUBLISHING
Articles designed for optimal readership across devices

FOLLOW US
@frontiersin

IMPACT METRICS
Advanced article metrics track visibility across digital media

EXTENSIVE PROMOTION
Marketing and promotion of impactful research

LOOP RESEARCH NETWORK
Our network increases your article's readership